Faculty of Biology

University of Gdańsk

Morgane Dromby, MSc

Adaptive skull shape changes in bottlenose dolphins (*Tursiops* spp.): inference from 3D morphological analyses

Adaptacyjne zmiany kształtu czaszki u delfinów butlonosych (*Tursiops* spp.): wnioskowanie na podstawie analiz morfologicznych 3D

PhD thesis presented to The Scientific Council of Biological Sciences of the University of Gdańsk in order to obtain a doctoral degree in the field of exact and natural sciences in the discipline of biological sciences

This thesis was funded by the NCN PRELUDIUM-Bis research program, as part of the project number 2019/35/O/NZ8/03900

Supervisor: dr. hab. Andre E. Moura

Department of Genetics and Biosystematics

GDAŃSK 2025

Acknowledgement

I am profoundly grateful for the journey that has led to the completion of this thesis. What once began as a youthful aspiration has now transformed into the reality of a researcher's path. This achievement stands not as an individual endeavor but as a testament to the unwavering support, wisdom, and generosity of many individuals and institutions, without whom it would not have been possible.

Among them, I extend my deepest gratitude to my supervisor, Dr. Moura, for granting me this transformative opportunity. His insightful guidance, expertise, and patience have been instrumental not only in shaping this work but also in helping me through the challenges inherent in this journey. This PhD experience has been far more than an academic pursuit, it has broadened my perspective, instilled in me enduring convictions, and fostered a mindset that will guide me throughout my life.

I am also profoundly grateful to my co-authors for their invaluable contributions, which have significantly enriched this research. In particular, I extend my heartfelt thanks to Dr. McGowen, Dr. Ellen Coombs, and Mary Faith Flores for their inspiring mentorship and for the extraordinary experience I had at the Smithsonian Institution. Their passion for discovery and their generosity in sharing their vast knowledge made my time there not only intellectually rewarding but also personally unforgettable.

I gratefully acknowledge the financial support provided by the National Science Centre (NCN) through the NCN PRELUDIUM-Bis research program, as part of the project number 2019/35/O/NZ8/03900, and the Polish National Agency for Academic Exchange (NAWA) under grant number PPN/STA/2021/1/00045 for the financial support for the internship at the Smithsonian Institution.

J'aimerais exprimer ma plus profonde et sincère gratitude à mon père, dont l'amour indéfectible, les encouragements au fil des années, et la conviction en mon potentiel, malgré mon choix d'un chemin peu conventionnel, ont été des piliers tout au long de ce chemin. Sa droiture, sa force et son dévouement, sont une source d'inspiration constante, et c'est avec une immense fierté que je lui dédie cette thèse aujourd'hui. Je tiens également à remercier de tout cœur ma belle-maman, dont l'amour inconditionnel et le soutien bienveillant m'ont offert une précieuse source de réconfort.

À mes sœurs, dont les accomplissements, tant personnels que professionnels, m'inspirent chaque jour, je veux exprimer mon admiration et ma reconnaissance. Enfin, à mon petit frère, dont la résilience, la détermination et l'intelligence sont une source de fierté et

d’émerveillement : sache que ton courage m’inspire autant que j’espère pouvoir t’inspirer en retour.

Sarò per sempre grata a Simone Gonella, che è stato al mio fianco durante tutto il percorso del dottorato, dalla stesura del mio curriculum vitae fino a questo momento. Nonostante la distanza, il suo sostegno e il suo amore sono stati una fonte di forza sia nei momenti di trionfo che di difficoltà. La sua pazienza e il suo spirito mi hanno aiutato a diventare la persona che sono oggi. Le sarò per sempre grata per la sua constante fiducia nella mia capacità di successo. E come non menzionare la sua famiglia, alla quale sono profondamente grata per la loro calorosa accoglienza e per avermi fatto sentire come una di loro. Condividere la loro cultura e il loro stile di vita sono stati una boccata d'aria fresca durante le sfide di questo dottorato.

To my dear colleagues and friends, Roya, Karolina, Francelly, Milomir, Alejandro, and Marketa, thank you for transforming even the most challenging days into moments of joy, filled with laughter and camaraderie. Your presence has been a source of light throughout this journey, and I will forever cherish the memories of our time together in Poland.

I wish to express my deepest gratitude to my dearest friends, Anaïs, Tim, Estelle, Basia, Charlotte, and Victoria for their friendship. Your remarkable journeys, strength, and determination serve as a perpetual source of motivation. Your presence in my life is a gift beyond measure, and I am profoundly grateful for the bond we share.

Adaptacyjne zmiany kształtu czaszki u delfinów butlonosych (*Tursiops* spp.): wnioskowanie na podstawie analiz morfologicznych 3D

Streszczenie

Morfometria geometryczna (GM) jest potężnym narzędziem do analizowania zmienności kształtu, oferującym wgląd w relacje ewolucyjne, procesy ekologiczne oraz zmiany rozwojowe. Postępy w obliczeniach komputerowych i obrazowaniu 3D rozszerzyły zastosowania GM, umożliwiając badanie skomplikowanych struktur i subtelnych wariacji w większym szczególe. Aby analizować zmienność kształtu czaszki, badacze często używają trójwymiarowej morfometrii geometrycznej (3DGM), która uchwyca skomplikowane kształty i zależności przestrzenne z modeli 3D. Dzięki temu zmniejszają się błędy związane z uchwyceniem obrazu 2D, takie jak perspektywa i zniekształcenia obiektywu, a także poprawia się umiejscowienie punktów charakterystycznych, zachowując cechy powierzchniowe, takie jak kontury i krzywe, które giną w projekcjach 2D. Umożliwia to dokładniejszą analizę kształtu oraz zwiększa zdolność wykrywania subtelnych wariacji kształtu, co jest szczególnie przydatne w porównaniach wewnątrzgatunkowych. Ponadto dane GM mogą być integrowane z danymi biologicznymi i środowiskowymi, dodając kontekst ekologiczny i funkcjonalny do analizy kształtu. Ta integracja z kolei zapewnia bardziej kompleksowe zrozumienie relacji między zmiennością kształtu, funkcją, adaptacją i historią ewolucyjną.

Różnorodne siedliska zajmowane przez odontocety, od rzek po otwarte oceany, sprawiają, że są one odpowiednim modelem do badania morfologicznych kształtów, ponieważ ta różnorodność napędza rozwój unikalnych cech morfologicznych u różnych gatunków. Na przykład kształt czaszki u odontocetów jest ściśle związany z różnicami w czasie rozwoju, szczególnie z różnicami w szybkości wzrostu między gatunkami, co uważa się za czynnik napędzający dywersyfikację i zmiany kształtu w obrębie kladu. U delfinów drapieżnych szybszy wzrost rostrum prowadzi do odmiennych morfologii dorosłych osobników w porównaniu do ssaków żywiących się ssaniem. Podobny wzór obserwuje się w środowiskach rzecznych, gdzie przyspieszony wzrost twarzy i rostrum (prowadzący do wydłużenia tych struktur) może być związany z adaptacjami żywieniowymi w płytkich wodach. Badania morfologiczne zidentyfikowały związek między zmiennością kształtu czaszki a strukturami zaangażowanymi w kluczowe funkcje życia odontocetów, w tym w karmieniu, echolokacji, oddychaniu oraz zachowaniach pływackich i nurkowych. Na przykład zmiany w rostrum, kościach skroniowych, ciemieniowych i jarzmowych są związane z mięśniami szczęki, co może ułatwiać mechanikę żuchwy związaną z określonymi strategiami żywieniowymi. Podobnie,

zmiany w asymetrii czaszki, wklęsłości regionu czołowego i kształcie rostrum są związane ze strukturami echolokacyjnymi, sugerując, że mogą one wpływać na właściwości echolokacji. Na koniec, ogólny profil czaszki (smukły versus masywny) oraz orientacja otworu potylicznego i rostrum są związane z mechanicznymi i efektywnościowymi aspektami pływania.

Ponadto badania z użyciem 3DGM zidentyfikowały także dimorfizm płciowy (SD) w kształcie czaszki u niektórych gatunków, w tym u delfina butlonosego. SD wydaje się być wynikiem różnic w szybkościach wzrostu i czasach trwania, odzwierciedlając różnice w lokalnych warunkach ekologicznych. Sugeruje to, że stopień i natura SD w kształcie czaszki mogą różnić się pomiędzy różnymi populacjami tego samego gatunku. Zmienność ta może początkowo wynikać z plastyczności fenotypowej w odpowiedzi na lokalne warunki środowiskowe, często przejawiającej się różnicami w zależnościach skalowania rozmiaru. Pomimo postępów w zrozumieniu ewolucji odontocetów na poziomie gatunku, czynniki napędzające zmienność kształtu czaszki wewnątrzgatunkowej pozostają stosunkowo niedostatecznie zbadane. Jednak badanie zmienności kształtu czaszki wewnątrzgatunkowej mogłoby ujawnić ukryte procesy ekologiczne i ewolucyjne, które są niezbędne do zrozumienia dywersyfikacji gatunków delfinów. Rodzaj *Tursiops*, dobrze zbadany członek rodziny Delphinidae, obejmuje trzy odrębne gatunki: delfina butlonosego pospolitego (*Tursiops truncatus*), delfina butlonosego Indo-Pacyficznego (*Tursiops aduncus*) oraz delfina Tamamenda (*Tursiops erebennus*). Szczególnie *T. truncatus* wykazuje znaczną zmienność wewnątrzgatunkową, co czyni go cennym modelem do badania kształtu czaszki. Ta zmienność jest związana z szerokim rozmieszczeniem gatunku, obejmującym różnorodne siedliska i szereg cech ekologicznych oraz behawioralnych. Powszechnym wzorem jest rozróżnienie między regionami przybrzeżnymi a morskim, obserwowane w różnych regionach na całym świecie. Delfiny z regionów przybrzeżnych zwykle zamieszkują płytkie obszary bogate w ofiary, podczas gdy delfiny morskie żyją w głębszych wodach o mniejszej bioróżnorodności. Sugeruje się, że te różnice w siedliskach wprowadzają różne presje selekcyjne, które przyczyniają się do zaobserwowanej regionalnej dyferencjacji. Wiele badań zidentyfikowało genetycznie unikalne populacje delfinów butlonosych pospolitych o wyraźnych kształtach czaszek, co w niektórych przypadkach doprowadziło do wyodrębnienia podgatunków, mianowicie *Tursiops truncatus gephyreus* na wybrzeżu Atlantyku w Ameryce Południowej oraz *Tursiops truncatus ponticus* w Morzu Czarnym. Ta kombinacja różnorodności ekologicznej, genetycznej i morfologicznej sprawia, że *Tursiops* jest idealnym systemem do badania sił ewolucyjnych kształtujących morfologię czaszki, szczególnie umożliwiając porównania między dobrze zdefiniowanymi jednostkami operacyjnymi taksonomicznymi.

Zmienności kształtu czaszki zdają się odzwierciedlać zróżnicowanie populacyjne w obrębie rodzaju, a kilka jednostek przybrzeżnych zostało zasugerowanych. Jednakże konieczne są dalsze badania, aby określić dokładne procesy napędzające te różnice w kształcie czaszki między jednostkami przybrzeżnymi i morskim.

Mianowicie, nie jest jasne, czy te różnice odzwierciedlają spójny wzór adaptacji do środowiska przybrzeżnego, czy też obserwowane wariacje są unikalne dla poszczególnych jednostek. Jeśli zmienności są unikalne dla konkretnych jednostek, sugeruje to, że inne procesy ewolucyjne, takie jak dryf genetyczny lub inne formy selekcji, mogą również napędzać obserwowane różnice. Kluczową przeszkodą w zrozumieniu czynników napędzających zmienność kształtu czaszki wewnątrzgatunkowej są wyzwania metodologiczne, w tym niespójne metody oznaczania punktów charakterystycznych, które zmniejszają porównywalność i powtarzalność. Ponadto, ręczne umieszczanie punktów charakterystycznych jest czasochłonne, co utrudnia analizowanie dużych zbiorów danych i skomplikowanych struktur. Na koniec, wciąż występują trudności w powiązaniu danych o kształcie czaszki z czynnikami środowiskowymi (np. głębokość, temperatura wody), co utrudnia wyciąganie wniosków na temat potencjalnych czynników napędzających lub testowanie związanych z tym implikacji funkcjonalnych.

Niniejsza praca stanowi pierwszy krok w badaniu globalnych trendów w zmienności kształtu czaszki delfinów butlonosych z wykorzystaniem 3DGM. Zastosowanie automatycznego oznaczania punktów charakterystycznych na powierzchni, badanie to łączy kształt czaszki z danymi środowiskowymi i bada związane z tym wzorce allometryczne na małą skalę geograficzną. Celem tego podejścia jest określenie, czy rozbieżność kształtu czaszki jest zjawiskiem globalnym, czy też specyficznym dla regionów, co pozwoli na lepsze zrozumienie adaptacyjnej natury zmian kształtu czaszki u cetaceów, mechanizmów napędzających dywersyfikację czaszki u delfinów butlonosych oraz potencjalne zidentyfikowanie nowych przybrzeżnych jednostek operacyjnych. Konkretnie, badania te badają, czy zmiany kształtu czaszki są wynikiem lokalnej adaptacji, zdarzeń stochastycznych lub historii biogeograficznej. Odpowiedź na te pytania pozwoli uzyskać wgląd w czynniki inicjujące dywersyfikację i ujawni implikacje funkcjonalne związane z procesami ekologicznymi w obrębie kladu.

Badanie to obejmuje cztery główne cele: 1) Określenie różnic w kształcie czaszki 3D między dobrze opisanymi jednostkami przybrzeżnymi i morskim delfinów butlonosych w skali światowej. 2) Zbadanie korelacji między tymi kształtami czaszek a zmiennymi środowiskowymi. 3) Zbadanie zmienności kształtu czaszki na małą skalę geograficzną w obrębie jednostki operacyjnej zamieszkującej zachodnią część Północnego Atlantyku (WNA).

4) Zbadanie wzorców allometrycznych związanych z różnymi populacjami na małą skalę regionalną (WNA).

Aby osiągnąć te cele, rozdział 2 przedstawia opracowanie ustandaryzowanego protokołu tworzenia modeli 3D z wykorzystaniem fotogrametrii. Protokół ten zawiera szczegółowe wytyczne dotyczące konstruowania dokładnych i powtarzalnych modeli 3D, które będą wykorzystywane w analizie morfometrii geometrycznej (GM).

W rozdziale 3 przetestowano techniki Surface Semi-Landmarking (SSL), aby rozwiązać ograniczenia związane z ręcznym oznaczaniem punktów charakterystycznych, porównując kształty czaszek populacji przybrzeżnych z Zatoki Guayaquil (Ekwador) i Morza Śródziemnego z kształtami czaszek próbek z wód morskich. Wyniki pokazują, że SSL jest skuteczne w wykazywaniu, że obie populacje przybrzeżne wykazują odrębne wzory kształtu, które różnią się nie tylko od ekotypu morskiego, ale także między sobą. W porównaniu z ręcznym oznaczaniem punktów charakterystycznych, SSL zapewnia lepsze pokrycie powierzchni, co poprawia dokładność i wydajność analizy kształtu czaszki. Te postępy umożliwiają bardziej solidne porównania wewnątrzgatunkowe i pozwalają na efektywniejszą analizę dużych zbiorów danych.

W rozdziale 4 zrealizowano pierwszy cel, porównując kształty czaszek 10 regionów przybrzeżnych z ich odpowiednikami w wodach morskich na skali światowej. Choć zmienność kształtu czaszki między jednostkami przybrzeżnymi a morskimi jest dobrze udokumentowana, żadne wcześniejsze badania 3DGM nie porównywały bezpośrednio wielu jednostek przybrzeżnych z próbkami morskim. Chociaż warunki ekologiczne były sugerowane jako potencjalne czynniki napędzające te zmiany, hipoteza ta nie była szeroko testowana przy użyciu danych środowiskowych. W związku z tym w tym badaniu zbadano związek między kształtem czaszki a tymi zmiennymi środowiskowymi, aby określić, które czynniki najlepiej korelują z kształtem czaszki. Wyniki ujawniają spójne wzorce różnicowania kształtu czaszki między jednostkami przybrzeżnymi, przy czym ekotyp morski pełni rolę średniego kształtu czaszki. Kształt czaszki okazał się korelować z kilkoma zmiennymi środowiskowymi, które odzwierciedlają cechy siedlisk przybrzeżnych i morskich. Rozdział ten wnosi nowe spostrzeżenia dotyczące różnorodności fenotypowej delfinów butlonosych, identyfikuje czynniki napędzające zmienność fenotypową i poprawia nasze zrozumienie procesów ewolucyjnych i ekologicznych kształtujących różnorodność w tym gatunku.

W rozdziale 5 zrealizowano cele trzeci i czwarty, przeprowadzając szczegółową analizę zmienności kształtu czaszki w WNA, badając potencjalne wzorce allometryczne związane z kształtem czaszki. Chociaż podział genetyczny zaobserwowano wśród kilku populacji

przybrzeżnych wzdłuż wybrzeża USA oraz w Zatoce Meksykańskiej i na Karaibach, zmienność kształtu czaszki w tych populacjach pozostaje niedostatecznie zbadana. Ponadto, choć zidentyfikowano szerokozasięgowe wzorce allometryczne między delfinami butlonosymi z wód morskich i przybrzeżnych, brakuje szczegółowych analiz geograficznych tych wzorców. Wyniki ujawniają wyraźne wzory kształtu czaszki w różnych lokalizacjach, z diagnostycznymi kształtami czaszek z Florydy, Zatoki Meksykańskiej i Delaware Bay.

Ponadto, zmienność kształtu czaszki obserwowana w różnych lokalizacjach została powiązana z różnicami allometrycznymi, co sugeruje, że plastyczność ekologiczna częściowo odpowiada za zaobserwowane różnice w kształcie. W związku z tym zarówno zmienność kształtu, jak i statyczna allometria są skutecznymi kryteriami do rozróżniania populacji delfinów butlonosych. Dodatkowo nasza analiza allometryczna ujawnia wyraźne wzorce płciowe w niektórych populacjach, co sugeruje, że lokalne warunki środowiskowe mogą wpływać na zmienność kształtu i dymorfizm płciowy u delfinów. Różnice te mogą wynikać z różnych potrzeb ekologicznych samców i samic w tych populacjach.

Rozdział 6 podsumowuje kluczowe wyniki niniejszych badań doktoranckich. Przybrzeżne jednostki delfinów butlonosych wykazują wyraźnie różne kształty czaszek związane z lokalnymi środowiskami, podczas gdy delfiny morskie wykazują bardziej jednorodne kształty czaszek, prawdopodobnie z powodu selekcji stabilizującej. Zatem zmienność kształtu czaszki u delfinów przybrzeżnych prawdopodobnie odzwierciedla także procesy nieadaptacyjne, takie jak dryf genetyczny, wydarzenia historyczne, takie jak cykle glacjalne, a także potencjalnie plastyczność fenotypowa. Niektóre zmiany kształtu czaszki u delfinów butlonosych odzwierciedlają te, które występują w obrębie rodziny Delphinidae, i które często korelują z lokalnymi cechami środowiskowymi. Ponadto, zmienność morfologiczna często zachodzi w cechach czaszki, które mogą być związane z odżywianiem, komunikacją i oddychaniem. Prawdopodobnie odzwierciedla to funkcjonalne wymagania lokalnych siedlisk, z potencjalnymi kompromisami wynikającymi z strukturalnej integracji różnych cech czaszki. Podział nisz, napędzany konkurencją o zasoby pokarmowe, sugeruje również, że jest ważnym czynnikiem napędzającym zmienność kształtu czaszki u delfinów butlonosych, możliwie wzmocnionym przez zachowania społeczne. Na koniec wyniki badania wspierają klasyfikację znanych gatunków/podgatunków (*T. aduncus, T. erebennus, T. t. gephyreus*) i sugerują możliwość istnienia dodatkowych, odrębnych przybrzeżnych jednostek operacyjnych w Morzu Północnym, Japonii, Zachodniej Afryce i Zachodniej Ameryce Południowej. Szczególnie silna różnicowanie populacji występuje w Południowo-Wschodnim Pacyfiku, prawdopodobnie napędzane przez większą heterogeniczność ekologiczną i efekty założycielskie.

Summary

Geometric morphometrics (GM) is a powerful tool for analysing shape variation, offering insights into evolutionary relationships, ecological processes, and developmental changes. Advancements in computing and 3D imaging have broadened GM's applications, allowing complex structures and subtle variations to be studied in greater detail. To analyse skull shape variations, researchers often use three-dimensional geometric morphometrics (3DGM), which captures complex shapes and spatial relationships from 3D models. This mitigates biases associated with 2D image capture, such as perspective and lens distortion, and improves landmark placement by preserving surface features such as contours and curves that are lost in 2D projections. This enables more accurate shape analysis and enhances the ability to detect subtle shape variations, which is particularly useful in intraspecific comparisons. Additionally, GM data can be integrated with biological and environmental datasets, adding ecological and functional context to shape analysis. This integration, in turn, provides a more comprehensive understanding of the relationships between shape variation, function, adaptation, and evolutionary history.

The diverse habitats occupied by odontocetes, ranging from rivers to open oceans, makes them a suitable model for studying morphological shape, as this diversity drives the development of unique morphological features across different species. For example, skull shape in odontocetes is closely related to differences in developmental timing, especially differences in growth rates between species, which is thought to drive diversification and shape changes across the clade. In raptorial dolphins, faster growth of the rostrum results in distinct adult morphologies compared to suction feeders. A similar pattern is observed in riverine environments, where accelerated growth of the face and rostrum (leading to elongation of these structures) may be associated with feeding adaptations in shallow waters. Morphological studies identified an association between skull shape variations in structures involved in key functional aspects of odontocete life, including feeding, echolocation, breathing and swimming or diving behaviours. For example, variations in the rostrum, squamosal, parietal and zygomatic bones are associated with jaw musculature, which may facilitate jaw mechanics associated with specific feeding strategies. Similarly, variation in skull asymmetry, concavity of the frontal region and rostrum shape are associated with echolocating structures, suggesting they may influence echolocation properties. Finally, the overall skull profile (slender versus stout) and the orientation of the foramen magnum and rostrum are associated with swimming mechanics and efficiency.

Furthermore, studies using 3DGM have also identified skull shape sexual dimorphism (SD) in some species, including the bottlenose dolphin. SD appears to be influenced by differences in growth rates and durations, reflecting differences in local ecological conditions. This suggests that the degree and nature of SD in skull shape can vary between different populations of the same species. This variation may initially arise from phenotypic plasticity in response to local environmental conditions, often manifested through differences in size scaling relationships. Despite advances in understanding odontocete evolution at the species level, the drivers of intraspecific skull shape variation remain relatively understudied. However, investigating intraspecific skull shape variation could reveal underlying ecological and evolutionary processes essential for understanding dolphin species' diversification. The genus *Tursiops,* a well studied member of the family Delphinidae, comprises three distinct species: the common bottlenose dolphin *(Tursiops truncatus),* the Indo-Pacific bottlenose dolphin (*Tursiops aduncus*) and the Tamamend's dolphin (*Tursiops erebennus*). *T. truncatus* in particular, exhibits substantial intraspecific variation, making it a valuable model for studying skull shape. This variation is associated with the species' wide distribution, including diverse habitats and a range of ecological and behavioural characteristics. A common pattern is a coastal versus offshore differentiation, observed in multiple regions worldwide. Dolphins in coastal regions typically inhabit shallow, prey-rich areas, while offshore dolphins live in deeper waters with lower biodiversity. These habitat differences were suggested to provide distinct selective pressures, which contribute to observed regional differentiation. Multiple studies have identified genetically unique populations of common bottlenose dolphins with distinct cranial shapes, which in some cases led to the denomination of subspecies, namely *Tursiops truncatus gephyreus* in the Atlantic coast of South America, and *Tursiops truncatus ponticus* in the Black Sea. This combination of ecological, genetic, and morphological diversity makes *Tursiops* an ideal system for investigating the evolutionary forces shaping skull morphology, particularly by allowing comparisons across well defined operational taxonomic units.

Skull shape variations appear to reflect population differentiation within the genus, and several coastal operational units have been suggested. However, further research is needed to determine the exact processes driving these coastal versus offshore skull differences. Namely, it is unclear whether these differences reflect a consistent pattern of adaptation to a coastal environment, or if the observed variations are unique to individual units. If the variations are unique to specific units, it suggests other evolutionary processes, such as genetic drift or other forms of selection, are also likely driving the observed differences. A key obstacle to understanding the drivers of intraspecific skull shape variation relate to methodological

challenges, including inconsistent landmarking methods, which reduce comparability and replicability. Additionally, placing landmarks manually is time-consuming, hindering the analysis of large datasets and complex structures. Finally, challenges persist in linking skull shape data to environmental factors (e.g., depth, water temperature), making it difficult to infer potential drivers or test associated functional implications.

This thesis represents the first effort towards investigating worldwide trends in bottlenose dolphins' skull shape variation using 3DGM. Employing automated surface semi-landmarking, this study links skull shape to environmental data and explores associated allometric patterns at fine geographical scale. This approach aims to determine whether skull shape divergence is a global phenomenon or region-specific, enhancing our understanding of the adaptive nature of cetacean skull changes, the mechanisms driving cranial diversification in bottlenose dolphins, and the potential identification of new coastal operational units. Specifically, this research investigates whether skull shape variations are driven by local adaptation, stochastic events, or biogeographic history. Addressing these questions will provide insights into the factors initiating diversification and reveal functional implications associated with ecological processes within the clade.

This study addresses four key objectives: 1) Quantify 3D skull shape differences between well-described coastal and offshore operational units of bottlenose dolphins in a worldwide context. 2) Investigate the correlation between these skull shapes and environmental variables. 3) Investigate fine-scale skull shape variations within the operational unit inhabiting the Western North Atlantic (WNA). 4) Investigate allometric patterns associated with different populations on a fine regional scale (WNA).

To achieve these objectives, Chapter 2 presents the development of a standardized protocol for creating 3D models using photogrammetry. This protocol provides step-by-step guidelines for constructing accurate and replicable 3D models, to be used in geometric morphometric (GM) analysis.

In Chapter 3, Surface Semi-Landmarking (SSL) techniques are tested to address the limitations associated with manual landmarking, by comparing the skull shapes of coastal populations from the Gulf of Guayaquil (Ecuador) and the Mediterranean Sea with those of offshore specimens. The results show that SSL can be effective at showing that both coastal populations exhibit distinct shape patterns, which not only differ from the offshore ecotype but also from each other. In comparison to manual landmarking, SSL provides enhanced surface coverage, thereby improving the accuracy and efficiency of skull shape analysis. These

advancements facilitate more robust intraspecific comparisons and enable the analysis of large-scale datasets with greater efficiency.

In Chapter 4 the first objective was addressed by comparing the skull shapes of 10 coastal regions with their offshore counterparts at a worldwide scale. While skull shape variations between coastal and offshore operational units are well documented, no previous 3DGM studies have directly compared multiple coastal units to offshore specimens. While ecological conditions have been proposed as potential drivers of these variations, this hypothesis has not been extensively tested using environmental data. Therefore, in this study, the relationship between skull shape and these environmental variables was tested to identify which factors best correlate with skull shape. The results revealed consistent patterns of skull shape differentiation between the coastal units, with the offshore ecotype standing as an average skull shape. Skull shape was found to correlate with several environmental variables which represented characteristics of coastal and offshore habitats. This chapter provides new insights into the bottlenose dolphin phenotypic diversity, identifies the drivers of phenotypic variation and improves our understanding of the evolutionary and ecological processes shaping diversity in this species

In Chapter 5, objectives three and four were addressed by performing a fine-scale analysis of skull shape variations in the WNA, investigating potential allometric patterns related to skull shape. While genetic partitioning has been observed between several coastal populations along the U.S. coast and in the Gulf of Mexico and the Caribbean, skull shape variation across these populations remains underexplored. Additionally, although broad-scale allometric patterns between offshore and coastal bottlenose dolphins have been identified, fine-scale geographic analyses of these patterns are lacking. The results reveal distinct skull shape patterns between locations, with diagnostic skull shapes identified in Florida, the Gulf of Mexico and Delaware Bay. Furthermore, skull shape variations observed across different locations were found to be associated with allometric differences, suggesting that ecological plasticity partially accounts for the observed shape differences. As such, both shape variations and static allometry are effective criteria for distinguishing between bottlenose dolphin populations. Additionally, our allometric analysis reveals distinct male and female patterns in some populations, suggesting that local environmental conditions may influence shape variation and sexual dimorphism in dolphins. These differences may arise due to the varying ecological needs of males and females in these populations.

Chapter 6 summarises the key findings of this PhD research. Coastal bottlenose dolphin units exhibit distinct skull shapes associated with local environments, while offshore dolphins show

more consistent skull shapes, likely due to stabilising selection. Therefore, coastal skull variations also likely reflect non-adaptive processes such as genetic drift, historical events such as glacial cycles, and possibly phenotypic plasticity. Some skull shape variations in bottlenose dolphins mirror those seen across Delphinidae, which often correlate with local environmental characteristics. Furthermore, morphological variation often occurs in skull traits that can be related to feeding, communication, and respiration. This likely reflects local habitat functional demands, with potential trade-offs due to the structural integration of the various skull features. Niche partitioning, driven by competition for food resources is also suggested to be an important driver of skull shape variation in bottlenose dolphins, possibly reinforced by social behaviours. Finally, the study findings support known species/sub-species classification (*T. aduncus, T. erebennus, T. t. gephyreus*) and suggest the potential for additional distinct coastal operational taxonomic units in the North Sea, Japan, West Africa, and Western South America. The Southeast Pacific shows especially strong population differentiation, likely driven by greater ecological heterogeneity and historical founder effects.

Table of Contents

List of Figures

List of Tables

Abbreviations

Abbreviation	Expansion
2b-PLS	Two-block Partial Least Squares
2D	Two-dimensional
3D	Three-dimensional
3DGM	3 Dimensional Geometric Morphometrics
AC	Agglomerative Coefficient
AMMM	Adductor Mandibular Muscle Mass
ANOVA	Analysis of Variance
BSE	Bays, Sounds, and Estuaries
CI	Confidence Interval
CREA	Craniofacial Evolutionary Allometry
CT	Computed Tomography
CVA	Canonical Variate Analysis
EV	Exposure Value
GM	Geometric Morphometric
GPA	Generalized Procrustes Analysis
HCA	Hierarchical Cluster Analysis
HL	Homologous Landmarks
LGM	Last Glacial Maximum
MANOVA	Multivariate Analysis of Variance
MLD	Mixed Layer Depth
MRI	Magnetic Resonance Imaging
NEA	North East Atlantic
NIR	No Information Rate
OOB	Out-of-Bag
OTU	Operational Taxonomic Unit
PC	Principal Component
PCA	Principal Component Analysis
PERMANOVA	Permutational Multivariate Analysis of Variance
RDA	Redundancy Analysis
RF	Random Forest
RMSE	Root Mean Square Error
SD	Sexual Dimorphism
SEP	Southeast Pacific
SfM	Structure from Motion
SIFT	Scale-Invariant Feature Transform
SSL	Surface Semi Landmark
TPS	Thin-plate spline
WNA	Western North Atlantic

Chapter 1 – Main Introduction

Morphological shape is considered a core element in biological research, offering insights into the diversity and evolution of organisms. Morphological shape refers to the geometric configuration of a structure, excluding its size, position, and orientation (Dryden & Kanti, 2016; Klingenberg, 2016). It varies considerably between species, geographic regions, sexes and age, due to both biological and/or ecological processes, resulting in the high morphological diversity observed in the wild (Foote, 1997). In morphological studies, comparisons of shape between taxa, species, and populations or between different life stages, are commonly performed at a single point in time or over time. These comparisons help understand evolutionary processes such as adaptation and speciation, as well as developmental pathways.

Shape analysis is therefore important in fields including taxonomy for classifying organisms (e.g. Ferreira-Cardoso et al., 2020; Machado & Teta, 2020; Noftz & Calede, 2023), functional biology to understand the evolutionary changes in body parts related to functions such as movement or feeding (Thomson & Motani, 2021; Giacomini et al., 2022), and in ecology for investigating how organisms adapt to specific ecological niches (e.g. Law, 2021). In this context, Geometric Morphometric (GM) has been established as a powerful tool, enabling precise and quantitative analysis of shape variations. It has facilitated the exploration of evolutionary relationships and classification (Pretorius et al., 2000), environmental influences on shapes (Fadda & Corti, 2001) and development changes related to functional adaptations (i.e., ontogenetic studies; Monteiro, 2000). In palaeontology, GM applied to comparative anatomy has facilitated the study of evolutionary changes over time (Marugán-Lobón & Buscalioni, 2004).

For morphological studies, GM provides precise shape descriptions based on individual ‘landmarks’, which can be adjusted to fit individual research questions (Rohlf & Slice, 1990; Rohlf & Marcus, 1993; Bookstein, 1997). These ’landmarks’ are usually selected for their structural, developmental, or biomechanical significance, and help ensure consistency and replicability across specimens and studies. Landmarks are typically categorized into three types. Type I, are defined as anatomically homologous points that are clearly identifiable across all specimens. They are located where different structures meet or where certain features are anatomically consistent (e.g. joining bones, and nerve foramen). Type II landmarks are defined by geometric criteria rather than strict anatomical homology. They are often placed at points of maximum curvature, points equidistant from others, or at the extremities of structures (e.g. tips or notches in a bone; Bookstein, 1991; Richtsmeier et al., 2002)., Type III landmarks are points

placed along a curve or surface where exact homology is difficult to establish (e.g. endpoints of the longest diameter of an element, the intersection of inter-landmark segments; Bookstein, 1991; Richtsmeier et al., 2002). The coordinates of these landmarks can be used to convert complex, multidimensional shape data into numerical formats suitable for statistical analysis. After the landmarks are aligned through Generalized Procrustes Analysis (GPA), multivariate statistics, such as Principal Component Analysis (PCA), Canonical Variate Analysis (CVA), and Multivariate Analysis of Variance (MANOVA) can be used to identify and quantify shape variations across groups (Rohlf & Marcus, 1993). Importantly, GM data can be integrated with other biological and environmental datasets to provide a comprehensive understanding of the relationships between shape variation, function, adaptation, and evolutionary history (Frost et al., 2003; Van Heteren et al., 2014).

Since its inception, the use of GM has steadily increased, including the development of dedicated software. These tools have allowed researchers across fields such as evolutionary biology, ecology, and functional morphology to explore shape changes in greater detail, leading to significant insights into developmental processes, species evolution, and functional adaptations (Morgan, 2009; Figueirido & Soibelzon, 2010; Prevosti et al., 2012). Advancements in 3D imaging technologies, including CT scanning, MRI, and laser surface scanning, have further expanded GM's scope, enabling the analysis of complex, three-dimensional structures. Moreover, GM is now used in combination with other methodologies, enhancing its applicability across disciplines. For example, its combination with biomechanics has facilitated studies of functional adaptations (e.g. Polly et al., 2016; O'Higgins et al., 2019), and its integration with quantitative genetics has provided insights into the heritability and evolution of morphological traits (e.g. Pavličev et al., 2016; Baab, 2018). Similarly, GM's integration with molecular and developmental biology has advanced our understanding of the genetic and developmental underpinnings of shape variation (e.g. Martínez-Abadiás et al., 2016; Buchberger et al., 2021; Marchini et al., 2021).

Geometric morphometric has been widely used to study morphological variation across a wide array of organisms, ranging from insects and amphibians to reptiles and mammals. For example, in anuran species, GM has shown that skull diversity is associated with adaptation to ecological niches, revealing an association between skull shape and specific microhabitats (e.g. fossorial vs. aquatic) or feeding strategies (e.g. vertebrate vs. myrmecophagous diets; Paluh et al., 2020). Additionally, it has revealed a relationship between hyperossification and dietary specializations as well as defensive behaviours (e.g. phragmosis), demonstrating how structural changes enhance survival through specialized functions (Paluh et al., 2020). This shows that

morphological evolution is tightly linked to behavioural strategies, with form and function evolving together to optimize environmental interactions. Similarly, GM proved valuable in capturing subtle and complex variations in skull shape within other species, such as grey seals across different regions, sexes, and age groups (Galatius et al., 2022).

Dolphins are a good model for studying shape, providing valuable insights into ecological and evolutionary questions. Odontocetes' adaptation to aquatic environments has resulted in substantial modifications of their body and skull structures relative to their terrestrial ancestors (Fordyce & Barnes, 1994). For example, their skulls underwent telescoping, where the premaxillary and maxillary bones have been extended over the frontal region of the neurocranium (Miller et al., 1923). Furthermore, odontocetes display a reduced zygomatic bone and a "secondary zygomatic arch", adaptations associated with their loss of masticatory function, as they swallow prey whole (Oelschläger, 2000). Odontocetes are also ecologically diverse and adapted to various habitats from rivers to open oceans, leading to unique morphological features in different dolphin species. For example, the Amazon River Dolphin (*Inia geoffrensis*) has developed a highly flexible neck due to unfused cervical vertebrae and a long, slender beak (Da Silva et al., 2023). Similarly, the Ganges River Dolphin (*Platanista gangetica*) with its nearly-blind small eyes, relies on echolocation to navigate and forage in the murky waters of the Ganges and Brahmaputra rivers (Sinha et al., 2014). Intraspecific variations have also been documented between different populations, such as the bottlenose dolphin (Mead & Potter, 1995; Perrin et al., 2011; Costa et al., 2022), killer whales (Pitman et al., 2003) and common dolphins (Ngqulana et al., 2019). Some differences in rostrum size, squamosal expansion, occipital contraction, and premaxillae depression are thought to be influenced by specific environmental pressures. For instance, mammal-eating killer whales have wider, more robust rostra and larger teeth compared to fish-eating populations, likely for capturing and processing larger prey (Fung, 2016).

1.1. Systematic Literature Review

A systematic review of the literature was conducted to investigate how GM has contributed to understanding the diversity of skull shapes in odontocetes The academic search engines Web of Science, ScienceDirect, Scopus, Ingenta Connect, and Semantic Scholar were used, as they are well-respected databases for scientific peer-reviewed articles, with the keywords “Geometric morphometric,” “skull shape,” “odontocete,” and “delphinid.” Articles published between 1990 and March 2021 were searched, as the term “Geometric morphometric” was first

introduced in 1993 (Rohlf & Marcus, 1993). Then, the references cited in each identified publication were reviewed to ensure comprehensive coverage of relevant studies. To focus the review on advancements in GM related to delphinid skull shape evolution, only peer-reviewed studies that investigated skull shape variations using 2D or 3D GM were included. Studies employing non-GM methods or focusing on marine mammal clades other than odontocetes (e.g. mysticetes, pinnipeds) or structures other than skulls were excluded. For each study, the main research area, geographical scope, taxonomic family and targeted genus were identified. The factors considered in the main studies are summarized in Table 1.1 and illustrated in Figures 1.2, 1.3 and 1.4.

Table 1.1. Classification of reviewed articles into field studies

Field Study	Criteria of selection
Taxonomy & Phylogeny	Studies investigating taxonomic or phylogenetic relationships between delphinids.
Intraspecific variation	Studies investigating skull shape changes within the same species.
Interspecific variation	Studies investigating skull shape changes between species.
Evolutionary ecology	Studies investigating the ecological drivers of skull shape changes in delphinids.
Ontogeny	Studies investigating differences in shape between foetal, young, and adult delphinids of the same genus.
Sexual dimorphism	Studies investigating differences in shape between sexes of the same delphinid genus.
Functional morphology	Studies investigating the relationship between anatomy of the skull and its function.
Population Structure	Studies investigating population structure within a delphinid genus, based on skull differences.

Thirty-two relevant studies were identified (see details in supplementary information Table S1.2.1). Since the first studies in 2002 (De Araujo Monteiro-Filho et al., 2002; Higa et al., 2002), 3DGM research has grown steadily, particularly between 2015 and 2021 which accounts for over half of the studies conducted by 2021 (Figure 1.1). Therefore, although the number of GM studies in odontocetes has grown steadily, it is still an early stage of growth.

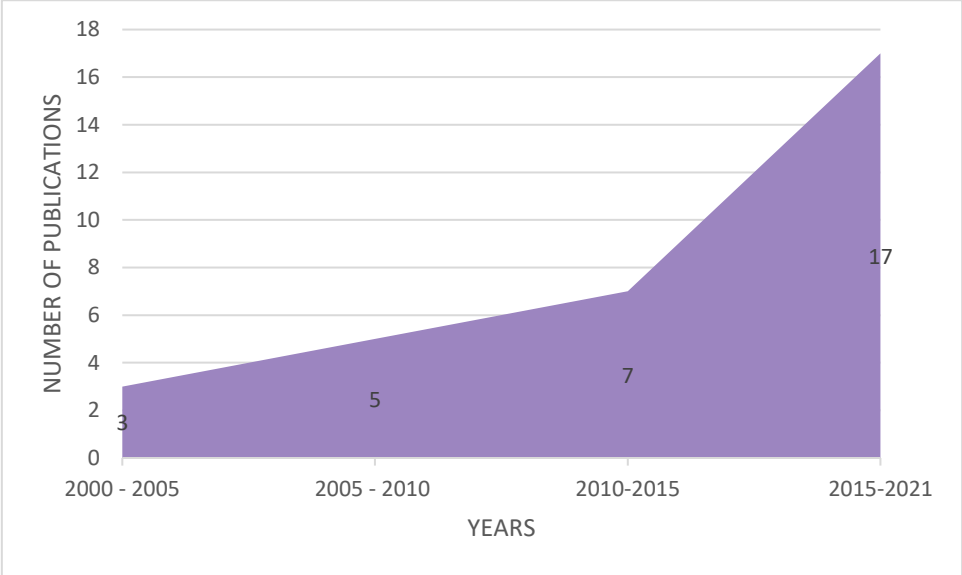

Figure 1.1 Number of publications that used geometric morphometrics to study the skull shape of Odontocetes from 2002 to March 2021.

Across the 32 studies, 5 families and 14 genera were investigated. The families Delphinidae, Iniidae, Phocoenidae, and Pontoporidae were the most studied (Figure 1.2). Among these, the genera *Tursiops, Delphinus, Stenella,* and *Phocoena* were the most frequently studied, each featuring in eight or more articles. These findings reflect, in part, that delphinids constitute the largest odontocete family and are more commonly represented in museum collections, especially for the bottlenose dolphin (*Tursiops truncatus*) and the common dolphin (*Delphinus delphis*). Also, smaller species were studied more often, likely because digital images of these species are easier to obtain compared to those of larger species.

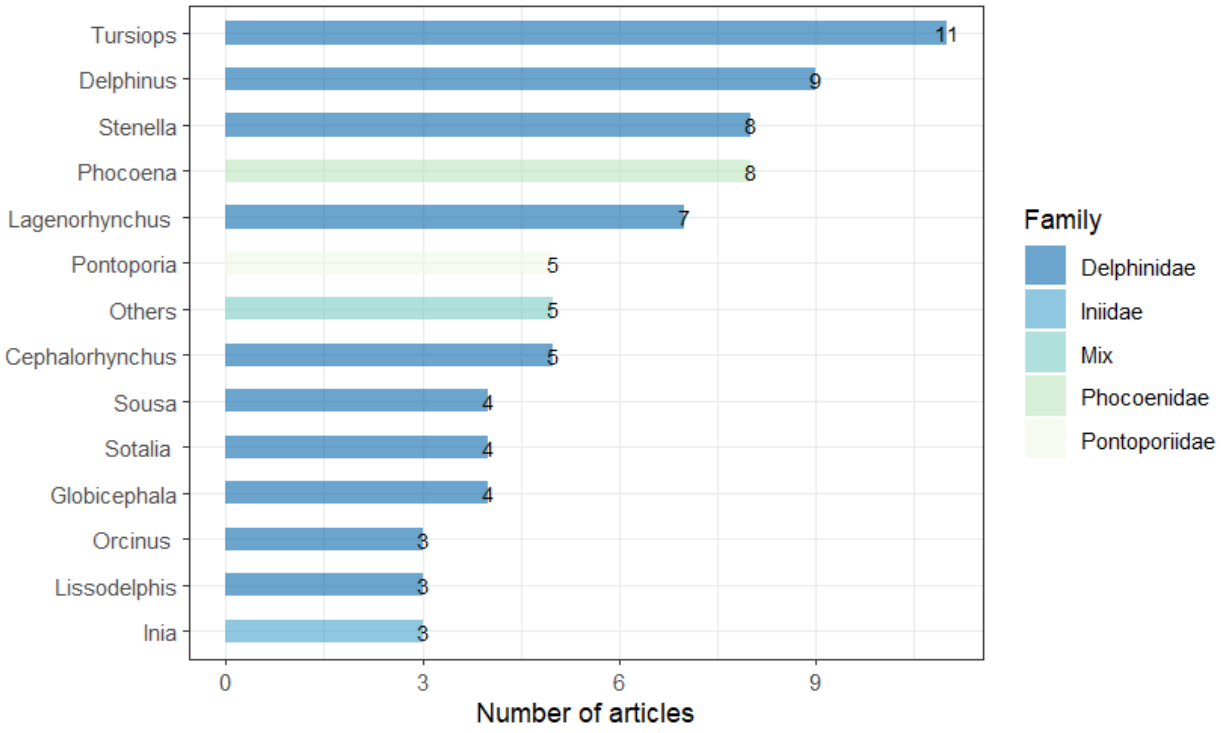

Figure 1.2 Barplot showing the number of GM publications targeting different genera of Odontocetes. The colour of the bars indicates the family to which the genus belongs. The figure was generated with the package ggplot2 (Wickham, 2009).

The studies encompassed nine distinct geographical areas, with most including specimens from multiple regions across the world, reflecting the comparative nature of GM analyses. However, a clear bias was observed toward the North Atlantic (9) and contiguous regions, including the Mediterranean (7) and the North Sea (11) followed by the South Pacific (13) and South Atlantic oceans (11), and the Indian Ocean (11) (Figure 1.3). Other regions included the North Pacific Oceans (4), Black Sea (4), the Amazon River (6), the Baltic Sea (4) and other less commonly studied regions (6) (Figure 1.3). Additionally, species-specific regions were found more frequently in the literature. For example, studies on *Phocoena* were notably prevalent in the Black and Baltic seas, although not exclusively (Galatius & Gol'din, 2011; Gol'din & Vishnyakova, 2015, 2016), while research on the genus *Sotalia* and the Amazon River dolphin was only possible in Brazil (De Araujo Monteiro-Filho et al., 2002; Cunha et al., 2005; Del Castillo et al., 2014).

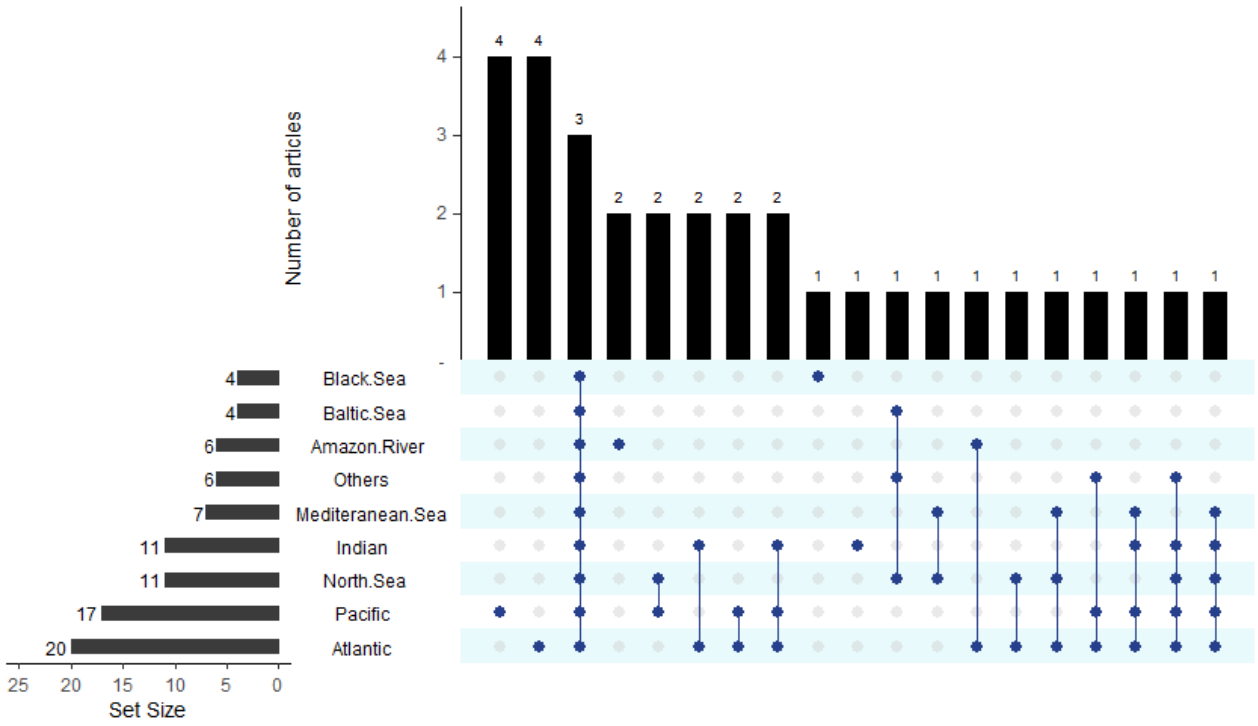

Figure 1.3. UpSet diagram showing geographic focus for studies of skull shape variation in Odontocetes using GM. The figure was generated with the package UPsetR (Lex et al., 2014; Conway et al., 2017) in R (R Core Team, 2018).

Six primary research areas were investigated by the studies: evolutionary ecology, ontogeny, sexual dimorphism, taxonomy and phylogeny, functional morphology, and population structure (Figure 1.4A & 1.4B.). A common approach in 27 out of the 32 studies was the comparison of skull structures either between different species (interspecific) or within the same species across different populations (intraspecific) reflecting the comparative nature of most GM analyses. Hence, these studies largely fell within the scope of evolutionary ecology, attempting to establish connections between evolutionary patterns and ecological processes. The remaining studies explored patterns of ontogenetic development, species classifications, sexual dimorphism and functional morphology.

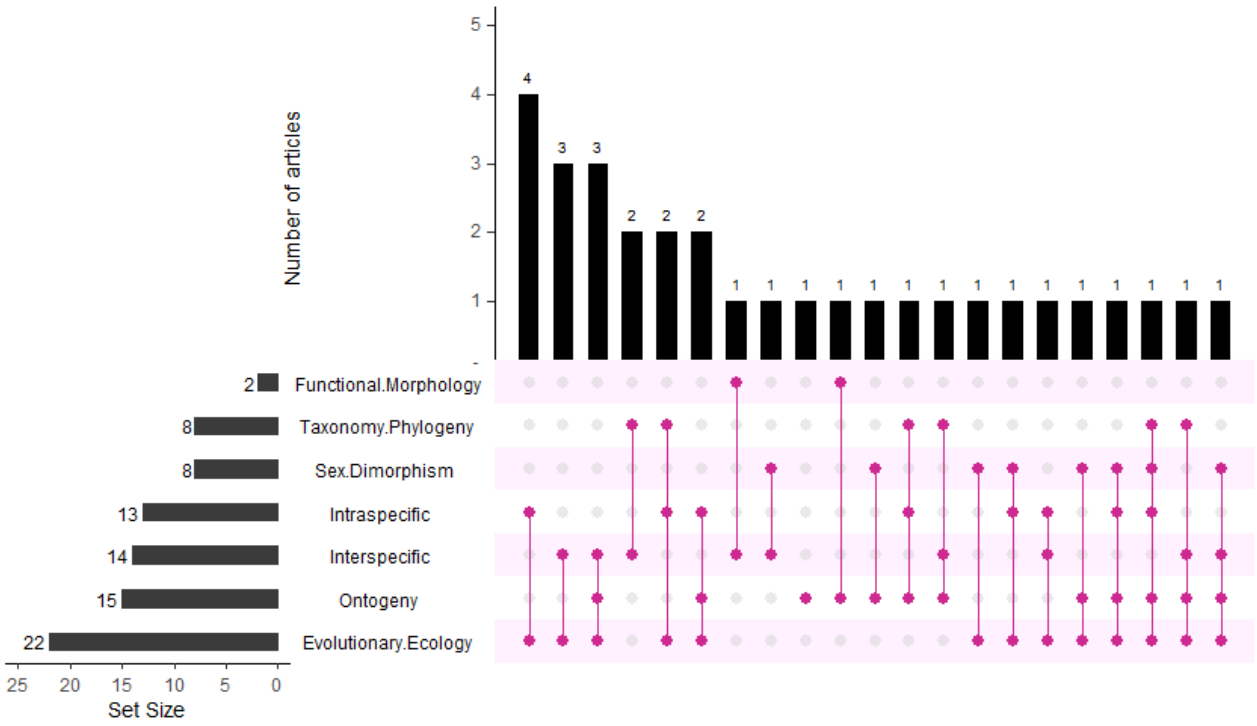

Figure 1.4A. UpSet diagram showing the scientific fields represented by all odontocete GM skull studies presented in this review. The figure was generated with the package UPsetR (Lex et al., 2014; Conway et al., 2017) in R (R Core Team, 2018).

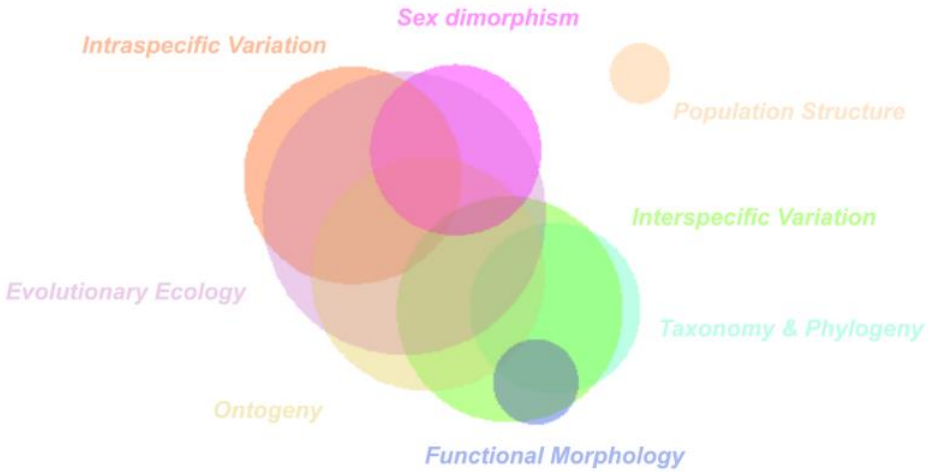

Figure 1.4B. Venn Diagram showing the scientific fields targeted by all the skull GM studies in odontocetes, found in this review. The figure was generated with the packages Venneuler, (Wilkinson & Urbanek, 2011) in R (R Core Team, 2018).

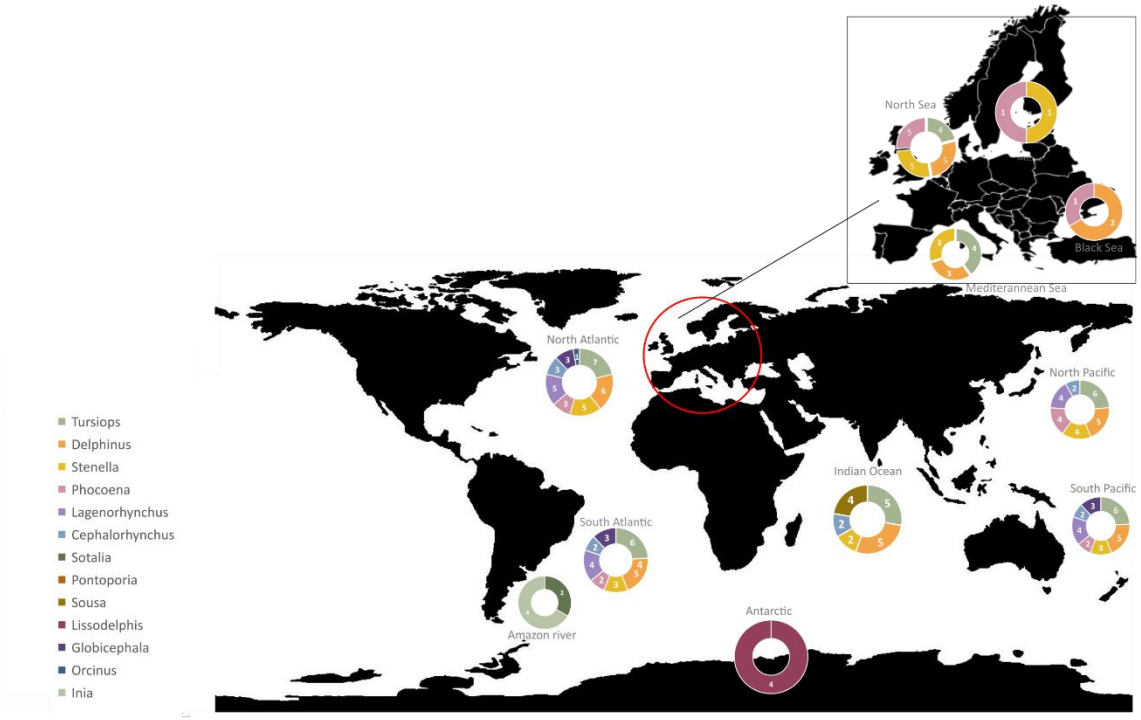

Figure 1.5. Composite image overlaying the frequency of studies focused on different Odontocete species skull shape variation using GM, with the geographical location on those studies. Worldmap sourced from Clipart Library. https://clipart-library.com/clip-art/world-map-silhouette-vector-1.htm, accessed in 2021.

1.2. Inference From Odontocete Skull GM Studies

In this review, ontogenetic studies were identified as a prominent application of GM. Because it standardises morphological data by removing the effect of size, it enables researchers to study evolutionary changes and developmental mechanisms without the confounding influence of overall growth. Consequently, many studies have investigated how morphological traits change over an organism's lifetime and compared these changes between groups (Nicolosi & Loy, 2010; Sydney et al., 2012; Del Castillo et al., 2014; De Francesco et al., 2016).

In Delphinidae, differences in skull shape have been closely related to variations in developmental timing, the rate and stages at which different skull features mature during an individual's growth. Comparison of skull shapes between life stages in several Delphinidae species has revealed that young dolphins, initially have a more compressed neurocranium, with the rostrum lengthening and telescoping as they mature (Sydney et al., 2012; Del Castillo et al., 2014; De Francesco et al., 2016). For example, in *Sotalia guianensis*, the facial region and neurocranium were found to grow at different rates, with the face reaching adult size and shape relatively quickly, while the neurocranium shows slower shape changes that persist into

adulthood (e.g. Sydney et al., 2012). Heterochrony, defined as a change in the timing or rate of developmental events (Gould, 1988), has been suggested to promote diversification in the clade. For example, the evolutionary divergence between marine and riverine species of *Sotalia* has been attributed to differences in developmental timing, induced by different ecological demands (Sydney et al., 2012). Specifically, faster facial and rostral growth in riverine environments is potentially associated with feeding mechanisms in shallow waters. Similarly, heterochrony can be involved in shape changes across species, such as accelerated rostral growth in raptorial dolphins compared to suction feeders, resulting in distinct adult rostrum morphologies (Frainer et al., 2021).

GM was also commonly used to investigating sexual dimorphism (SD). It has been found that skull shape SD is established early in development, influenced by differences in growth rates and durations (De Francesco et al., 2016). For example, in franciscana dolphins, females exhibit faster growth in certain traits compared to males, which retain more juvenile characteristics (Del Castillo et al., 2014). These variations arise from both non-allometric and allometric processes (changes in shape depending on size; De Francesco et al., 2016; Nicolosi & Loy, 2019) and have often involved structures related to feeding, vocalizing and breathing (Frandsen & Galatius, 2013; Del Castillo et al., 2014; De Francesco et al., 2016). Therefore, SD in skull shape appears to be closely associated with local ecological conditions and has been suggested to represent population-dependent adaptations to varying environmental pressures. For example, strong interspecific competition has been suggested as a driver of SD in harbour porpoise, potentially related to niche partitioning (Galatius & Gol'din, 2011). Alternatively, SD has been proposed to result from the development of specialized features in males for mating competition (Frandsen & Galatius, 2013).

Furthermore, GM has been applied to the investigation of phylogenetic relationships, providing insight into morphological evolution relative to genetic lineages. Often, GM analysis of skull shape corroborate molecular-based trees across families, species, or genera (Amaral et al., 2009; Galatius & Goodall, 2016). For example, skull shape has been shown to reflect the molecular phylogeny of the subfamily Lissodelphininae (e.g. Galatius & Goodall, 2016). In cases where genetically similar lineages have been difficult to differentiate, GM effectively helped distinguish species (Kurihara & Oda, 2007; Amaral et al., 2009; Hohl et al., 2020; Jedensjö et al., 2020). This has been particularly relevant in dolphin lineages, where incomplete lineage sorting from recent divergence, can result in shared genetic material making species difficult to differentiate. In addition, sympatric populations may hybridize, producing intermediate individuals, further complicating genetic distinction (Amaral et al., 2009). In such

cases, GM can differentiate species based on cranial shape even when genetic data overlap, reflecting ecological adaptations like feeding strategies, echolocation, or social structures (Kurihara & Oda, 2007; Hohl et al., 2020; Jedensjö et al., 2020).

While clear genetic distinctions between populations or closely related species can be identified through molecular data, ecological and functional context is provided by GM, showing how factors like feeding strategies or habitat preferences, influence morphological evolution. Integrating GM and molecular data provides a more comprehensive view of evolutionary trajectories. When evolutionary pathways cannot be fully explained by molecular data and adult skull shape analysis alone, especially when genetically divergent species have similar adult skull shapes, further insights can be provided by GM through the investigation of skull shape differences during various developmental stages. This approach can reveal diagnostic features apparent only in specific developmental phases. For example, despite similar adult skull shapes (basic shape and overall form), different developmental trajectories (ontogeny), particularly in rostrum development have been observed in *Cephalorhynchus commersonii* and *Lagenorhynchus albirostris (*Galatius & Goodall, 2016). *Cephalorhynchus commersonii* is associated with coastal environments, feeding on a variety of small fish and squid, while *Lagenorhynchus albirostris* inhabits more open, pelagic waters, potentially foraging in deeper marine environments. Therefore, such ontogenetic variations have been suggested to reflect distinct ecological niches and evolutionary paths.

Intraspecific studies have also benefit from GM's precise shape information, as subtle shape variations often overlooked by other methods can be detected. Skull shapes between populations from distinct environments, such as different oceans, seas, or coastal vs. offshore areas have been compared to identify shape variations (De Araujo Monteiro-Filho et al., 2002; Kurihara & Oda, 2007; Galatius & Gol'din, 2011; Loy et al., 2011; Gol'din & Vishnyakova, 2015; Fung, 2016; Marina et al., 2018; Ngqulana et al., 2019; Hohl et al., 2020; Jedensjö et al., 2020). These patterns were suggested to reflect dolphins' adaptation to their specific ecological niches. Variations in skull traits such as the length and width of the rostrum, palatine area, and braincase, are often observed in dolphins and are thought to reflect adaptations to specific feeding strategies (Kurihara & Oda, 2007; Galatius & Gol'din, 2011b; Loy et al., 2011; Marina et al., 2018; Ngqulana et al., 2019). For example, rostrum shape can affect prey capture techniques, while the size and shape of the palatine area can affect tooth arrangement and function. Similarly, variations in the width of the temporal fossae and the length of the zygomatic process suggest adaptations in jaw musculature and mechanics, which may facilitate different feeding modes (Galatius & Gol'din, 2011; Marina et al., 2018). On the other hand,

variations in the bones forming the nasal cavity and the position and size of the orbits suggest adaptations for respiratory efficiency and visual acuity (Galatius & Gol'din, 2011; Marina et al., 2018).

Skull shape variations in Delphinidae, are also related to feeding modes. In raptorial-like species, finer features, such as narrower skulls, rostrums and palates, along with elongated rostrums are often found in coastal specimens (Loy et al., 2011; Ngqulana et al., 2019; Hohl et al., 2020). However, these variations are not always consistent, especially in species with wide geographic distributions. For example, bottlenose dolphins in Australia have smaller skulls with longer and narrower rostrums compared to their offshore counterparts (Jedensjö et al., 2020). In contrast, bottlenose dolphins in California, show larger skulls with stouter rostrums and temporal fossae (Perrin et al., 2011). Collectively, these variations suggest an important influence of local environmental pressures, such as prey availability or habitat conditions on skull shape.

Rounder, more robust skulls, with shorter temporal fossae (the depressions on the skull where the jaw muscles attach) are typically observed in suction feeders (Galatius et al., 2020). This may support a larger, more powerful oral cavity, enabling the dolphin to create a stronger negative pressure when opening its mouth, which facilitates effective suction feeding. They also often have shorter and wider rostrums, potentially enhancing their grip on larger or tougher prey, such as octopus and large pelagic fish (Galatius & Gol'din, 2011; Marina et al., 2018). In contrast, narrower skulls and more elongated rostrums are typically exhibited by ram feeders (Galatius et al., 2020), reducing drag for faster swimming, and enabling fast and forceful jaw movements for capturing elusive fish. Wider and shorter rostrums, along with enlarged temporal fossae, are found in marine mammal feeders such as *Orcinus orca*, likely indicating an association with larger jaw muscles for increased bite force to depredate on larger prey (Galatius et al., 2020). Ontogenetic studies have also revealed that skull morphology changes as individuals age, potentially impacting feeding strategies and prey preferences. For example, in bottlenose dolphins, more pronounced temporal fossae are developed by adults, supporting larger muscles for greater bite force and faster mouth-clapping movements. This allows adults to consume larger and more challenging prey compared to juveniles (De Francesco et al., 2016).

Beyond feeding adaptations, skull shape variations in Delphinidae have also been found to be closely associated with differences in communication and echolocation abilities. GM studies have revealed that Delphinidae with more asymmetrical skulls tend to produce more directional and powerful sound beams (Frainer et al., 2021; Laeta et al., 2021). Asymmetry in Delphinidae is characterized by a leftward shift in nasal bones and the right premaxilla, along with an

enlargement of the right premaxilla and maxilla (Laeta et al., 2021). This likely reflects the degree of asymmetry found in sound-producing organs, like the nasal apparatus and melon. Notably, this asymmetry is more pronounced in species foraging in deep waters, like monodontids and globicephalines, suggesting an adaptation to their ecological niches where efficient echolocation is crucial (Laeta et al., 2021). Within species, variations in the concavity of the frontal region have also been linked to habitat differences, with phocoenids having a more offshore lifestyle displaying deeper facial regions compared to those having a more coastal lifestyle (Galatius et al., 2011). Furthermore, the shape of the rostrum also affects sound production, with elongated rostra enhancing directionality and creating more effective sound (Frainer et al., 2021). Interestingly, GM studies have also identified SD in skull shapes, particularly in the premaxillary bones and nasal openings. Females, for example, exhibit modifications in the ear bones (Del Castillo et al., 2014), which may influence the morphology of soft tissues responsible for vocalisation, such as the nasal plugs. These variations may reflect differences in how vocalisations are used by males and females, especially in social and competitive contexts.

Slender skulls and longer rostrums are typically exhibited by dolphins inhabiting shallow riverine or coastal environments, with these traits thought to be associated with their feeding strategies and the type of prey available in these habitats (McCurry et al., 2017a). In these environments, dolphins often use sweep feeding a technique involving lateral head movements to catch agile prey, such as small fish. Drag is reduced by elongated rostrums, which maximizes swiping speed and enhancing hydrodynamic efficiency facilitating the capture fast-moving prey. Additionally, certain populations, such as the Black Sea porpoises exhibit distinct alignments of the rostrum and the occipital condyle (the part of the skull connecting to the vertebral column), with a more downward orientation of the foramen magnum and rostrum compared to porpoises from other regions (Galatius & Gol'din, 2011). This morphology is thought to provide greater lateral flexibility and to distribute the mechanical forces generated during feeding, such as shaking or biting prey, thus reducing strain on the skull and neck joints. Such adaptations have been observed in species living in riverine environments and is suggested to reflect the specific ecological demands of these habitats (De Araujo Monteiro-Filho et al., 2002; McCurry et al., 2017c)

1.3. Thesis Objectives

Several knowledge gaps in the current research on odontocetes skull shape diversity, particularly in relation to the application of GM have been identified in this literature review. Among these gaps, a lack of standardized landmarking methods across studies is noticeable. Inconsistent landmarking methods, such as the use of varying landmark sets, prevent comparability, replicability, and meta-analyses. This inconsistency can lead to misleading comparisons and prevent the identification of subtle yet biologically significant trends in skull shape variation. This is especially problematic in intraspecific studies, where precise and accurate landmarking is essential for detecting the subtle differences inherent to this kind of analysis. Moreover, the inability to reuse data forces each research group to invest considerable time and resources, often resampling the same individuals. Therefore, the development of standardised landmarking methods is suggested as a means of providing a uniform framework for recording and analysing skull shapes, facilitating meta-analyses and large-scale comparative studies, essential for reliable phylogenetic and functional morphology analysis.

Manual landmarking has been essential in advancing studies of evolutionary biology, comparative anatomy, and functional morphology within Delphinidae, uncovering important insights into taxonomic relationships, ontogenetic development, and the impact of environmental factors and functional demands, such as feeding and echolocation. While effective for general shape patterns, through predefined single points, it has limitations in describing more intricate structures. To address these limitations, high-density surface semi-landmarks can be used, to capture more continuous shape variations. This method improves the ability to represent complex structures, by incorporating information from entire surfaces rather than isolated points. These approaches complement traditional landmarking by providing a more detailed and comprehensive description of shape, enabling researchers to address increasingly complex questions in the study of morphology and evolution (Gao et al., 2019).

Dolphin skull shape variations are often studied by comparing populations from different ocean basins with distinct environmental conditions (e.g. Loy et al., 2011; Galatius & Gol'din, 2011; Galatius & Goodall, 2016; Marina et al., 2018). However, most comparisons are geographically limited with only one comprehensive study on the bottlenose dolphin covering nine marine regions (Nicolosi & Loy, 2019). This study revealed distinct regional morphotypes, population-specific sexual dimorphism, and the substantial influence of allometric growth on shape variation (Nicolosi & Loy, 2019). These findings suggest that processes such as local adaptation as well as phenotypic plasticity might be driving shape variation. However, this

study identified broad patterns, without delving into the specific changes between these populations, partly due to limited use of landmarks.

A worldwide perspective on skull shape variation within a single species could provide deeper insights into the drivers of skull shape variations, helping to distinguish between broad evolutionary trends and local adaptations. Relating shape data to environmental conditions (e.g. salinity, water temperature) or mechanistic properties (e.g. bite force) is essential for inferring drivers and testing functional implications. To the best of our knowledge, only one study has clearly demonstrated how feeding ecology significantly influences skull shape by correlating it with prey size (McCurry, et al., 2017b). This study also showed the roles of different feeding modes (e.g. suction feeding vs. raptorial feeding) in shaping skull morphology. However, it emphasizes that feeding ecology is complex and often involves many factors that are difficult to account for collectively, make it challenging to draw definitive conclusions. By combining shape data with ecological variables, such as habitat type, water depth, prey type and availability, a better understanding of how environmental pressures drive morphological changes can be achieved, especially in coastal versus offshore contexts.

This thesis is focused on the bottlenose dolphin (genus *Tursiops*). The genus *Tursiops* is a well-known cosmopolitan member of the Delphinidae family, which is comprised of three distinct species: the common bottlenose dolphin *(Tursiops truncatus)*, the Indo-Pacific bottlenose dolphin (*Tursiops aduncus*) and the Tamamend's bottlenose dolphin (*Tursiops erebennus*). These species have been differentiated through genetic studies (Möller & Beheregaray, 2001; Costa et al., 2022) and form independent clades in phylogenetic analyses (Leduc et al., 1999; Kingston & Rosel, 2004). Extensive research has focused on the genetic and morphological diversity within *Tursiops*, showing the occurrence of multiple operational taxonomic units (OTUs), with strong differentiation between coastal and offshore habitats (Hersh & Duffield, 1990; Kenney, 1990; Mead & Potter, 1995; Tezanos-Pinto et al., 2009; Perrin et al., 2011; Costa et al., 2022; Dromby et al., 2023).

This diversity has caused some inconsistency in the way clades within *Tursiops* have been named, particularly given that different clades have often been classified at different taxonomic levels. For example, some groups have been designated as subspecies while others are considered distinct species. Therefore, in this thesis the term 'Operational Taxonomic Unit' (OTU) is adopted as a unifying term to refer to the distinct groups within the genus exhibiting distinct characteristics based on diverse criteria (e.g. ecological, morphological or genetic). This is preferred to the term 'ecotype' (commonly used in the literature) because the same ecotype (e.g. coastal) might include further differentiation based on other criteria.

These variations are often attributed to different selective pressures, with coastal OTUs inhabiting shallow, prey-rich areas, while offshore dolphins live in deeper waters with lower biodiversity. Studies have shown that these operational units differentiate in skeletal structures (Costa et al., 2016), social behaviours (Costa et al., 2015), parasite loads (Walker, 1981), haematological profiles (Duffield et al., 1983), colouration, body proportions (Ross & Cockcroft, 1990) and fin shapes (Félix et al., 2018). Consequently, various studies have documented that such operational units are genetically unique and exhibit cranial differentiation, leading them to be classified as different subspecies, such as *Tursiops truncatus gephyreus* in Southeast America (Wickert et al., 2016), *Tursiops truncatus ponticus* in the Black Sea. These distinctions demonstrate that skull shape variations reflect, to some extent, population differentiation within the genus, indicating how ecological specialization drives this process. However, a worldwide perspective on skull shape variation is lacking. Investigation of these variations worldwide could test for repeated patterns of coastal versus offshore differentiation, potentially revealing whether morphological divergence between these habitats is global or region-specific. Such a worldwide perspective would improve the understanding of the adaptive nature of cetacean skull changes, the mechanisms driving cranial diversification in bottlenose dolphins, and the identification of potential new coastal morphotypes. This thesis is the first attempt to investigate worldwide trends in skull shape variation within bottlenose dolphins using 3DGM, linking skull shape with several environmental data and exploring associated allometric patterns. The main objectives of this research are:

1) Quantify 3D skull shape differences between well-described coastal and offshore OTUs of bottlenose dolphins in a worldwide context.

2) Investigate the correlation between these skull shapes and environmental variables.

3) Investigate the occurrence of fine-scale skull shape variations within individual OTUs .

4) Investigate allometric patterns associated with different populations.

In Chapter 2, the development of a standardized protocol for creating 3D models using photogrammetry is presented. This protocol ensures replicability and consistency across different sampling environments. In Chapter 3, the application of Surface Semi Landmark (SSL) techniques with automatic landmarking was explored and further refined in chapter 4 and 5. These techniques have enabled the capture of shape information with greater accuracy and efficiency. In Chapter 3, the first objective was addressed by comparing skull shapes from coastal operational units in the Gulf of Guayaquil and the Mediterranean Sea to those of offshore specimens, identifying key morphological differences. In Chapter 4, objectives one and two were assessed by performing a worldwide analysis of skull shape variation across 10

different coastal OTUs and their offshore counterparts. Here, skull shape data were integrated with environmental variables to investigate how environmental factors may drive morphological changes. In Chapter 5, objectives three and four were addressed by performing a fine-scale analysis of skull shape variations in the western north Atlantic (WNA) and investigating potential allometric patterns related to skull shape. Finally, in chapter 6, the findings from this PhD research are summarized and discussed in their broader implications for evolutionary biology within the Delphinidae family.

1.4. Bibliography

Amaral, A. R., Coelho, M. M., Marugán-Lobón, J., & James Rohlf, F. (2009). Cranial shape differentiation in three closely related delphinid cetacean species: insights into evolutionary history. *Zoology*, *112*(1), 38–47. doi: 10.1016/j.zool.2008.03.001

Baab, K. L. (2018). Evolvability and craniofacial diversification in genus *Homo*. *Evolution*, *72*(12), 2781–2791. doi: 10.1111/evo.13637

Bookstein, F. L. (1997). Landmark methods for forms without landmarks: morphometrics of group differences in outline shape. *Medical Image Analysis*, *1*(3), 225–243. doi: 10.1016/S1361-8415(97)85012-8

Bookstein, FL. (1991). Morphometric tools for landmark data: geometry and biology (Issue 10). Cambridge University Press.

Buchberger, E., Bilen, A., Ayaz, S., Salamanca, D., Matas De Las Heras, C., Niksic, A., Almudi, I., Torres-Oliva, M., Casares, F., & Posnien, N. (2021). Variation in pleiotropic Hub gene expression is associated with interspecific differences in head shape and eye size in *Drosophila*. *Molecular Biology and Evolution*, *38*(5), 1924–1942. doi: 10.1093/molbev/msaa335

Conway, J. R., Lex, A., & Gehlenborg, N. (2017). UpSetR: an R package for the visualization of intersecting sets and their properties. *Bioinformatics*, *33*(18), 2938–2940. doi: 10.1093/bioinformatics/btx364

Costa, A. A., Mcfee, W., Wilcox, L. A., Archer, F. I., & Rosel, P. E. (2022). The common bottlenose dolphin (*Tursiops truncatus*) ecotypes of the western North Atlantic revisited: an integrative taxonomic investigation supports the presence of distinct species. *Zoological Journal of the Linnean Society*, 196, 1608–1636. doi: 10.1093/zoolinnean/zlac025

Costa, A. P. B., Fruet, P., Daura-Jorge, F. G., Simões-Lopes, P. C., Ott, P. H., Valiati, V. H., Oliveira, L. R. de, Costa, A. P. B., Fruet, P., Daura-Jorge, F. G., Simões-Lopes, P. C., Ott, P. H., Valiati, V. H., & Oliveira, L. R. de. (2015). Bottlenose dolphin communities from the southern Brazilian coast: do they exchange genes or are they just neighbours? *Marine and Freshwater Research*, *66*(12), 1201–1210. doi: 10.1071/mf14007

Costa, A., Rosel, P., Daura-Jorge, F., & Simões-Lopes, P. (2016). Offshore and coastal common bottlenose dolphins of the western South Atlantic face-to-face: what the skull and the spine can tell us. *Marine Mammal Science*, *32*(4), 1433–1457. doi: 10.1111/mms.12342

Cunha, H. A. A., Da Silva, V. M. F. M. F., Lailson-Brito, J., Santos, M. C. O. C. O., Flores, P. A. C. A. C., Martin, A. R. R., Azevedo, A. F. F., Fragoso, A. B. L. B. L., Zanelatto, R. C. C., & Solé-Cava, A. M. M. (2005). Riverine and marine ecotypes of *Sotalia* dolphins are different species. *Marine Biology*, *148*(2), 449–457. doi: 10.1007/S00227-005-0078-2

Da Silva, V. M., Brum, S. M., de Mello, D. M. D., de Souza Amaral, R., Gravena, W., Campbell, E., ... & Mintzer, V. (2023). The Amazon River dolphin, *Inia geoffrensis*: what have we learned in the last

two decades of research? *Latin American Journal of Aquatic Mammals*, *18*(1), 139-157. doi: 10.5597/lajam00298

De Araujo Monteiro-Filho, E. L., Monteiro, L. R., & Dos Reis, S. F. (2002). Skull shape and size divergence in dolphins of the genus *Sotalia*: a tridimensional morphometric analysis. *Journal of Mammalogy*, *83*(1), 125–134. doi: 10.1644/1545-1542(2002)083<0125:SSASDI>2.0.CO;2

De Francesco, M. C., Loy, A., Francesco, M. C. de, & Loy, A. (2016). Intra- and interspecific interactions as proximate determinants of sexual dimorphism and allometric trajectories in the bottlenose dolphin *Tursiops truncatus* (Cetacea, Odontoceti, Delphinidae). *PLoS ONE*, *11*(10), e0164287. doi: 10.1371/journal.pone.0164287

Del Castillo, D. L., Flores, D. A., & Cappozzo, H. L. (2014). Ontogenetic development and sexual dimorphism of *franciscana* dolphin skull: a 3D geometric morphometric approach. *Journal of Morphology*, *275*(12), 1366–1375. doi: 10.1002/jmor.20309

Dromby, M., Félix, F., Haase, B., Simões-Lopes, P. C., Costa, A. P. B., Lalis, A., Bens, C., Podestà, M., Doria, G., & Moura, A. E. (2023). Cranial variation between coastal and offshore bottlenose dolphins, Tursiops truncatus (Cetacea: Delphinidae) in Ecuador and the Mediterranean: a three-dimensional geometric morphometric study. *Zoological Journal of the Linnean Society*, *199*(1), 83–96. doi: 10.1093/zoolinnean/zlad022

Duffield, D. A., Ridgway, S. H., & Cornell, L. H. (1983). Hematology distinguishes coastal and offshore forms of dolphins (*Tursiops*). *Canadian Journal of Zoology*, *61*(4), 930–933. doi: 10.1139/Z83-123

Fadda, C., & Corti, M. (2001). Three-dimensional geometric morphometrics of *Arvicanthis*: Implications for systematics and taxonomy. *Journal of Zoological Systematics and Evolutionary Research*, *39*(4), 235–245. doi: 10.1046/j.1439-0469.2001.00169.x

Félix, F., Centeno, R., Romero, J., Zavala, M., & Vásconez, Ó. (2018). Prevalence of scars of anthropogenic origin in coastal bottlenose dolphin in Ecuador. *Journal of the Marine Biological Association of the United Kingdom*, *98*(5), 1177–1186. doi: 10.1017/S0025315417000686

Ferreira-Cardoso, S., Billet, G., Gaubert, P., Delsuc, F., & Hautier, L. (2020). Skull shape variation in extant pangolins (Pholidota: Manidae): allometric patterns and systematic implications. *Zoological Journal of the Linnean Society*, *188*, 255–275.

Figueirido, B., & Soibelzon, L. H. (2010). Inferring palaeoecology in extinct tremarctine bears (Carnivora, Ursidae) using geometric morphometrics. *Lethaia*, *43*(2), 209–222. doi: 10.1111/J.1502-3931.2009.00184.X

Foote, M. (1997). The evolution of morphological diversity. *Annual Review of Ecology and Systematics*, (28) 129–152. doi: 10.1146/annurev.ecolsys.28.1.129

Fordyce, R. E. , & Barnes, L. G. (1994). The evolutionary history of whales and dolphins. *Annual Review Of Earth And Planetary Sciences*, *22*, 419–455. doi: 10.1146/annurev.ea.22.050194.002223

Frainer, G., Huggenberger, S., Moreno, I. B., Plön, S., & Galatius, A. (2021). Head adaptation for sound production and feeding strategy in dolphins (Odontoceti: Delphinida). *Journal of Anatomy*, *238*(5), 1070–1081. doi: 10.1111/joa.13364

Frandsen, M. S., & Galatius, A. (2013). Sexual dimorphism of Dall's porpoise and harbor porpoise skulls. *Mammalian Biology 78*(2), 153–156. doi: 10.1016/j.mambio.2012.04.005

Frost, S. R., Marcus, L. F., Bookstein, F. L., Reddy, D. P., & Delson, E. (2003). Cranial allometry, phylogeography, and systematics of large-bodied papionins (primates: Cercopithecinae) inferred from geometric morphometric analysis of landmark data. *The Anatomical Record Part A: Discoveries in Molecular, Cellular, and Evolutionary Biology*, *275A*(2), 1048–1072. doi: 10.1002/ar.a.10112

Fung, C. W. (2016). Cranial shape correlates with diet specialization in Northeast Pacific killer whale (*Orcinus orca*) ecotypes. [MSc thesis]. doi: 10.14288/1.0314137

Galatius, A., Berta, A., Frandsen, M. S., & Goodall, R. N. P. (2011). Interspecific variation of ontogeny and skull shape among porpoises (Phocoenidae). *Journal of Morphology*, *272*(2), 136–148. doi: 10.1002/jmor.10900

Galatius, A., & Gol'din, P. E. (2011). Geographic variation of skeletal ontogeny and skull shape in the harbour porpoise (*Phocoena phocoena*). *Canadian Journal of Zoology*, *89*(9), 869–879. doi: 10.1139/z11-059

Galatius, A., & Goodall, R. N. P. (2016). Skull shapes of the Lissodelphininae: radiation, adaptation and asymmetry. *Journal of Morphology*, *277*(6), 776–785. doi: 10.1002/jmor.20535

Galatius, A., Racicot, R., McGowen, M., & Olsen, M. T. (2020). Evolution and diversification of delphinid skull shapes. *IScience*, *23*(10), 101543. doi: 10.1016/j.isci.2020.101543

Galatius, A., Svendsen, M. S., Messer, D., Valtonen, M., McGowen, M., Sabin, R., Dahl, V. A., Dahl, A. B., & Olsen, M. T. (2022). Range-wide variation in grey seal (*Halichoerus grypus*) skull morphology. *Zoology*, *153*, 126023. doi: 10.1016/j.zool.2022.126023

Gao, T., Kovalsky, S. Z., Boyer, D. M., & Daubechies, I. (2019). Gaussian process landmarking for three-dimensional geometric morphometrics. *SIAM Journal on Mathematics of Data Science*, *1*(1), 237–267. doi: 10.1137/18M1203481

Giacomini, G., Herrel, A., Chaverri, G., Brown, R., Russo, D., Scaravelli, D., & Meloro, C. (2022). Functional correlates of skull shape in Chiroptera: feeding and echolocation adaptations. *Integrative Zoology*, *17*(3), 430–442. doi: 10.1111/1749-4877.12564

Gol'din, P. E., & Vishnyakova, K. A. (2015). Differences in skull size of harbour porpoises, *Phocoena phocoena* (Cetacea), in the sea of azov and the black sea: Evidence for different morphotypes and populations. *Vestnik Zoologii*, *49*(2), 171–180. doi: 10.1515/vzoo-2015-0017

Gol'din, P., & Vishnyakova, K. (2016). Habitat shapes skull profile of small cetaceans: evidence from geographical variation in Black Sea harbour porpoises (*Phocoena phocoena*). *Zoomorphology*, *135*(3), 387–393. doi: 10.1007/s00435-016-0311-1

Gould, S. J. (1988). *The Uses of Heterochrony*. Pp. 1–13, *in* M. L. McKinney (ed.), Heterochrony in evolution: a multidisciplinary approach. Plenum Press, New York. doi: 10.1007/978-1-4899-0795-0_1

Hersh S. L. Duffield, D. A. (1990). Distinction between northwest Atlantic offshore and coastal bottlenose dolphins based on hemoglobin profile and morphometry. In S. P. Leatherwood & R. R. Reeves (Eds.), *The bottlenose dolphin* (pp. 155–164). Academic Press. San Diego, CA.

Higa, A., Hingst-Zaher, E., & Vivo, M. (2002). Size and shape variability in the skull of *Pontoporia blainvillei* (Cetacea: Pontoporiidae) from the Brazilian coast. *Latin American Journal of Aquatic Mammals*, *1*(1), 145–152. doi: 10.5597/lajam00018

Hohl, L. S. L., Sicuro, F. L., Wickert, J. C., Moreno, I. B., Rocha-Barbosa, O., & Barreto, A. S. (2020). Skull morphology of bottlenose dolphins from different ocean populations with emphasis on South America. *Journal of Morphology*, *281*(6), 564–577. doi: 10.1002/jmor.21121

Dryden, I.L., Mardia. K. V. (2016). Statistical shape analysis: with applications in R. John Wiley & Sons.

Jedensjö, M., Kemper, C. M. M., Milella, M., Willems, E. P. P., & Krützen, M. (2020). Taxonomy and distribution of bottlenose dolphins (genus *Tursiops*) in Australian waters: an osteological clarification. *Canadian Journal of Zoology*, *98*(7), 461–479. doi: 10.1139/cjz-2018-0270

Kenney, R.D. (1990). Bottlenose dolphins off the northeastern United States. In S. Leatherwood & R. R. Reeves (Eds.), *The bottlenose dolphin* (pp. 369–386). Academic Press, San Diego, CA.

Kingston, S. E., & Rosel, P. E. (2004). Genetic Differentiation among recently diverged delphinid taxa determined using AFLP markers. *Journal of Heredity*, *95*(1), 1–10. doi: 10.1093/jhered/esh010

Klingenberg, C. P. (2016). Size, shape, and form: concepts of allometry in geometric morphometrics. *Development Genes and Evolution*, *226*(3), 113–137. doi: 10.1007/S00427-016-0539-2

Kurihara, N., & Oda, S. (2007). Cranial variation in bottlenose dolphins *Tursiops spp*. from the Indian and western Pacific Oceans: additional evidence for two species. *Acta Theriologica*, *52*(4), 403–418. doi: 10.1007/bf03194238

Laeta, M., Ruenes, G. F., Siciliano, S., Oliveira, J. A., & Galatius, A. (2021). Variation in cranial asymmetry among the Delphinoidea. *Biological Journal of the Linnean Society*, *132*(2), 414–430. doi: 10.1093/biolinnean/blaa161

Law, C. J. (2021). Ecological drivers of carnivoran body shape evolution. *The American Naturalist*, *198*(3), 406-420. doi: 10.1086/715588

Leduc, R. G., Perrin, W. F., & Dizon, A. E. (1999). Phylogenetic relationships among the delphinid cetaceans based on full Cytochrome B sequences. *Marine Mammal Science*, *15*(3), 619–648. doi: 10.1111/j.1748-7692.1999.tb00833.x

Lex, A., Gehlenborg, N., Strobelt, H., Vuillemot, R., & Pfister, H. (2014). UpSet: visualization of intersecting sets. *IEEE Transactions on Visualization and Computer Graphics*, *20*(12), 1983–1992. doi: 10.1109/tvcg.2014.2346248

Loy, A., Tamburelli, A., Carlini, R., & Slice, D. E. (2011). Craniometric variation of some Mediterranean and Atlantic populations of *Stenella coeruleoalba* (Mammalia, Delphinidae): a three-dimensional geometric morphometric analysis. *Marine Mammal Science*, *27*(2), E65–E78. doi: 10.1111/j.1748-7692.2010.00431.x

Machado, F. A., & Teta, P. (2020). Morphometric analysis of skull shape reveals unprecedented diversity of African Canidae. *Journal of Mammalogy*, *101*(2), 349–360. doi: 10.1093/jmammal/gyz214

Marchini, M., Hu, D., Lo Vercio, L., Young, N. M., Forkert, N. D., Hallgrímsson, B., & Marcucio, R. (2021). Wnt signaling drives correlated changes in facial morphology and brain shape. *Frontiers in Cell and Developmental Biology*, *9*, 644099. doi: 10.3389/fcell.2021.644099/bibtex

Marina, T. I., Marchesi, M. C., & Goodall, R. N. P. (2018). Long-finned pilot whale (*Globicephala melas*, Traill 1809) subspecies in the Atlantic Ocean: are there differences in their skulls? *Marine Mammal Science*, *35*(2), 660–676. doi: 10.1111/mms.12548

Martínez-Abadiás, N., Mateu, R., Niksic, M., Russo, L., & Sharpe, J. (2016). Geometric morphometrics on gene expression patterns within phenotypes: a case example on limb development. *Systematic Biology*, *65*(2), 194–211. doi: 10.1093/sysbio/syv067

Marugán-Lobón, J., & Buscalioni, Á. D. (2004). Geometric morphometrics in macroevolution: morphological diversity of the skull in modern avian forms in contrast to some theropod dinosaurs. *Morphometrics*, 157–173. doi: 10.1007/978-3-662-08865-4_12

McCurry, M. R., Evans, A. R., Fitzgerald, E. M. G., Adams, J. W., Clausen, P. D., & McHenry, C. R. (2017). The remarkable convergence of skull shape in crocodilians and toothed whales. *Proceedings of the Royal Society B: Biological Sciences*, *284*(1850), 20162348. doi: 10.1098/rspb.2016.2348

McCurry, M. R., Fitzgerald, E. M. G., Evans, A. R., Adams, J. W., & McHenry, C. R. (2017). Skull shape reflects prey size niche in toothed whales. *Biological Journal of the Linnean Society*, *121*(4), 936–946. doi: 10.1093/biolinnean/blx032

McCurry, M. R., Walmsley, C. W., Fitzgerald, E. M. G., & McHenry, C. R. (2017). The biomechanical consequences of longirostry in crocodilians and odontocetes. *Journal of Biomechanics*, *56*, 61–70. doi: 10.1016/j.jbiomech.2017.03.003

Mead, J., & Potter, C. (1995). Recognizing two populations of the bottlenose dolphin (*Tursiops truncatus*) of the Atlantic coast of North America morphologic and ecologic considerations. *IBI Reports*, *5*, 51–44.

Miller, G. S. (1923). The telescoping of the cetacean skull (with eight plates). *Smithsonian Miscellaneous Collections*, *76*, 1-70.

Möller, L. M., & Beheregaray, L. B. (2001). Coastal bottlenose dolphins from Southeastern Australia are *Tursiops aduncus* according to sequences of the mitochondrial DNA control region. *Marine Mammal Science*, *17*(2), 249–263. doi: 10.1111/J.1748-7692.2001.tb01269.X

Monteiro, L. R. (2000). Geometric morphometrics and the development of complex structures: ontogenetic changes in scapular shape of dasypodid armadillos. *Hystrix, the Italian Journal of Mammalogy*, *11*(1). doi: 10.4404/hystrix-11.1-4138

Morgan, C. C. (2009). Geometric morphometrics of the scapula of South American caviomorph rodents (Rodentia: Hystricognathi): form, function and phylogeny. *Mammalian Biology*, *74*(6), 497–506. doi: 10.1016/j.mambio.2008.09.006

Ngqulana, S. G., Plön, S., Galatius, A., Pistorius, P., & Hofmeyr, G. J. G. (2019). Cranial variation in common dolphins *Delphinus* spp. off South Africa, with the inclusion of information from the holotype of *Delphinus capensis*. *African Journal of Marine Science*, *41*(3), 247–260. doi: 10.2989/1814232X.2019.1648318

Nicolosi, P., & Loy, A. (2010). Landmark based morphometric variation in common dolphin (*Delphinus delphis* L.,1758). Pages 263–268 in P. L. Nimis and R. Vignes Lebbe, eds. *Tools for identifying biodiversity: Progress and problems.* Proceedings of the International Congress, Paris, 20–22 September 2010, EUT Edizioni Universita di Trieste, Trieste, Italy.

Nicolosi, P., & Loy, A. (2019). Geometric morphometric methods as complementary tools to investigate variability in common dolphins (*Delphinus* sp.) using museum specimens. *Aquatic Conservation: Marine and Freshwater Ecosystems*, *31*, 22–35. doi: 10.1002/aqc.3042

Noftz, L. A., & Calede, J. J. M. (2023). Multivariate analyses of skull morphology inform the taxonomy and evolution of geomyoid rodents. *Current Zoology*, *69*(4), 456–474. doi: 10.1093/cz/zoac055

O'Higgins, P., Fitton, L. C., & Godinho, R. M. (2019). Geometric morphometrics and finite elements analysis: assessing the functional implications of differences in craniofacial form in the hominin fossil record. *Journal of Archaeological Science*, *101*, 159–168. doi: 10.1016/j.jas.2017.09.011

Paluh, D. J., Stanley, E. L., & Blackburn, D. C. (2020). Evolution of hyperossification expands skull diversity in frogs. *Proceedings of the National Academy of Sciences of the United States of America*, *117*(15), 8554–8562. doi: 10.1073/pnas.2000872117

Pavličev, M., Mitteroecker, P., Gonzalez, P. M., Rolian, C., Jamniczky, H., Villena, F. P. M., Marcucio, R., Spritz, R., & Hallgrimsson, B. (2016). Development shapes a consistent inbreeding effect in mouse crania of different line crosses. *Journal of Experimental Zoology Part B: Molecular and Developmental Evolution*, *326*(8), 474–488. doi: 10.1002/jez.b.22722

Perrin, W. F., Thieleking, J. L., Walker, W. A., Archer, F. I., & Robertson, K. M. (2011). Common bottlenose dolphins (*Tursiops truncatus*) in California waters: cranial differentiation of coastal and offshore ecotypes. *Marine Mammal Science*, *27*(4), 769–792. doi: 10.1111/j.1748-7692.2010.00442.x

Pitman, R. L., & Ensor, P. (2003). Three forms of killer whales (*Orcinus orca*) in Antarctic waters. *Journal of Cetacean Research and Management*, *5*(2), 131-139. doi: 10.47536/jcrm.v5i2.813

Polly, P. D., Stayton, C. T., Dumont, E. R., Pierce, S. E., Rayfield, E. J., & Angielczyk, K. D. (2016). Combining geometric morphometrics and finite element analysis with evolutionary modeling: towards a synthesis. *Journal of Vertebrate Paleontology*, *36*(4). doi: 10.1080/02724634.2016.1111225

Pretorius, E., Philips, T. K., & Scholtz, C. (2000). Geometric morphometrics, the metendosternite and its use in phylogenetics of the Scarabaeinae (Coleoptera). *Elytron*, *14*, 125-148. Downloaded from https://www.researchgate.net/publication/236057529

Prevosti, F. J., Turazzini, G. F., Ercoli, M. D., & Hingst-Zaher, E. (2012). Mandible shape in marsupial and placental carnivorous mammals: a morphological comparative study using geometric morphometrics. *Zoological Journal of the Linnean Society*, *164*(4), 836–855. doi: 10.1111/J.1096-3642.2011.00785.X

Richtsmeier, J. T., DeLeon, V. Burke., & Lele, S. R. (2002). The promise of geometric morphometrics. *Yearbook of Physical Anthropology*, *45*(35), 63–91. doi: 10.1002/ajpa.10174

Rohlf, F. J., & Slice, D. (1990). Extensions of the Procrustes Method for the Optimal Superimposition of Landmarks. *Systematic Biology*, *39*(1), 40–59. doi: 10.2307/2992207

Rohlf, F., & Marcus, L. (1993). A revolution morphometrics. *Trends in Ecology and Evolution*, *8*(4), 129–132. doi: 10.1016/0169-5347(93)90024-J

Ross, G. J. B., & Cockcroft, V. G. (1990). Observations on the early development of a captive bottlenose dolphin calf. In S. Leatherwood & R. R. Reeves (Eds.), *The bottlenose dolphin* (pp. 461–478). Academic Press.

Sinha, R. K., & Kannan, K. (2014). Ganges River dolphin: an overview of biology, ecology, and conservation status in India. *Ambio*, *43*, 1029-1046. doi.org/10.1007/s13280-014-0534-7

Sydney, N. V., Machado, F. A., & Hingst-Zaher, E. (2012). Timing of ontogenetic changes of two cranial regions in *Sotalia guianensis* (Delphinidae). *Mammalian Biology*, *77*(6), 397–403. doi: 10.1016/j.mambio.2012.04.007

Tezanos-Pinto, G., Baker, C. S., Russell, K., Martien, K., Baird, R. W., Hutt, A., ... & Garrigue, C. (2009). A worldwide perspective on the population structure and genetic diversity of bottlenose dolphins (*Tursiops truncatus*) in New Zealand. *Journal of Heredity*, *100*(1), 11–24. doi: 10.1093/jhered/esn039

Thomson, T. J., & Motani, R. (2021). Functional morphology of vertebrate claws investigated using functionally based categories and multiple morphological metrics. *Journal of Morphology*, *282*(3), 449–471. doi: 10.1002/jmor.21317

Van Heteren, A. H., MacLarnon, A., Soligo, C., & Rae, T. C. (2014). Functional morphology of the cave bear (*Ursus spelaeus*) cranium: a three-dimensional geometric morphometric analysis. *Quaternary International*, *339*, 209–216. doi: 10.1016/j.quaint.2013.10.056

Walker, W. A. (1981). Geographical variation in morphology and biology of Bottlenose dolphins (*Tursiops*) in the eastern north Pacific. NOAA Administrative Report LJ-81-03C.

Wickert, J. C., Von Eye, S. M., Oliveira, L. R., & Moreno, I. B. (2016). Revalidation of *Tursiops gephyreus* Lahille, 1908 (Cetartiodactyla: Delphinidae) from the southwestern Atlantic Ocean. *Journal of Mammalogy*, *97*(6), 1728–1737. doi: 10.1093/jmammal/gyw139

Wickham, H. (2009). Ggplot2 : elegant graphics for data analysis, (pp. 9–26). Springer, New York, 2016.

Wilkinson, L., & Urbanek, S. (2011). Venneuler: venn and euler diagrams (*R package version 1.1-0)* Retrieved from http://CRAN. R-project. org/package= venneuler.

Chapter 2 – Workflow for 3D Skull Reconstruction of Dolphin Skeletal Specimens, for Geometric Morphometric Analysis.

2.1. Introduction to 3D modelling and photogrammetry

Three-dimensional modelling is the process by which precise 3D digital representations of physical objects are created, based on the geometric relationships between points on the object's surface, known as “point clouds” (Leberl et al., 2010; Aharchi & Ait Kbir, 2020). Point cloud data are commonly collected through techniques such as laser scanning and photogrammetry (Barber et al., 2002; Remondino et al., 2005; Otero et al., 2020). Three-dimensional models are then constructed from these point clouds using three core geometric elements: vertices (points in 3D space), edges (lines connecting vertices) and faces (surfaces defined by edges), which together define the model’s structure and forms (i.e., topology; Kettner, 1999; Botsch et al., 2007). These geometric elements are combined using algorithms that interpolate the positions between vertices to create 3D surfaces and volumes to create a wireframe model (Aharchi & Ait Kbir, 2020). Then, the model is textured and rendered to produce the final 3D representation. The model detail is dependent on point cloud density and geometric precision.

3D modelling is applied in a diversity of fields including media to create films and video games (e.g. Statham, 2018), architecture and design to visualize buildings or products (e.g. Kazi et al., 2020) and cultural heritage to preserve sites or artwork (e.g. Smith et al., 2019). In medicine, 3D modelling is also used for anatomical visualisation, surgical planning, and the design of implants and prostheses (Burnard et al., 2020; Robb et al., 2022). One significant application of 3D modelling is in the field of morphometrics, where it is used to investigate shape and size variations in biological structures across populations, species, individuals, and sexes (Elewa, 2004; Ferreira-Cardoso et al., 2020; Meloro & Tamagnini, 2022; Viacava et al., 2022). By using robust mathematical and statistical techniques (Rohlf & Slice, 1990; Bookstein, 1991; Rohlf & Marcus, 1993; Adams et al., 2004; Mitteroecker & Bookstein, 2011; Zelditch et al., 2012), variations in structures such as bones and shells, can be quantified to infer evolutionary and developmental processes. Morphometrics was initially based on direct linear measurements of biological specimens, including distances, angles and ratios (Rohlf et al., 1990). However, the field progressed with geometric morphometrics (GM; Bookstein, 1991; Rohlf & Marcus, 1993), where sets of two-dimensional (2D) Cartesian coordinates (x, y) are mapped onto digital images whose spatial relationships are compared between groups to quantify shape variation, usually after removing size effects. Landmarks in GM are selected

based on their biological relevance and their ability to be reliably and consistently identified across individuals (Bookstein, 1991). These are classified into three types: type I landmarks which consist of points at intersections of biological structures; type II landmarks, consisting of points along curves or outlines; and type III landmarks, often derived from geometric properties such as the furthest points from inter-landmark segments, and therefore defined with less precision (Bookstein, 1991; Palci & Lee, 2019).

GM can also be expanded to three-dimensional analysis (3DGM; Rohlf & Marcus, 1993). This approach often relies on 3D digital models, with 3D cartesian coordinates used to capture complex shapes and spatial relationships. Three-dimensionality offers several benefits over traditional 2D methods. Crucially, it mitigates bias associated with photographic setups, such as feature obscuration, perspective distortion and lens distortion caused by projecting a 3D object onto a 2D plane (Cardini, 2014; Buser et al., 2018). Additionally, 3D models can be handled in virtual environments, facilitating the landmarking process (Adams & Otárola-Castillo, 2013). Consequently, 3DGM preserves surface features such as contours and curves that would otherwise be lost in 2D projection (Álvarez & Perez, 2013; Cardini, 2014), which is especially beneficial when working with complex structures.

Overall, 3DGM improves the identification of subtle shape variations while contributing to increased uniformity within the field of morphometrics. Development in 3D modelling software and algorithms have increased its application in geometric morphometrics (Mitteroecker & Schaefer, 2022) across fields such as palaeontology, anthropology, and biology (e.g. Curran, 2018; Morley et al., 2022; Viacava et al., 2022). 3DGM facilitates anatomical comparisons among and between taxa, within the context of their phylogenetic relationships (Bertrand et al., 2019; Dunn & Avery, 2021), and the effect of external variables affecting shapes such as ontogeny, allometry, environment and diet (e.g. Bertrand et al., 2019; Viacava et al., 2020; Lang et al., 2022). Additionally, shape covariation, integration, and modularity can be investigated (Klingenberg & Marugán-Lobón, 2013; Püschel et al., 2020). Consistent 3D modelling protocols and methods facilitate the integration of automated tools into geometric morphometric (GM) workflows, streamlining data collection and improving efficiency. This is particularly beneficial for comparative studies, where the processing of hundreds of specimens from various sources, such as biological collections distributed worldwide, is often required (e.g. Lang et al., 2022). Furthermore, digital 3D models can be stored and reused for future comparative studies investigating biological questions of interest.

Digital photogrammetry is a technique used to generate 3D models of an object, from several overlapping photographs (Linder, 2009; 2013). Perspective and positional changes between

individual photographs are analysed by photogrammetry software to reconstruct an object's spatial characteristics, such as shape, size and position. Initially, photogrammetry was used to study landscapes and geological features (e.g. Bitelli et al., 2004; Ferrari et al., 2021), but has since been adopted in archaeology, palaeontology (Pavlidis et al., 2007; Magnani et al., 2020) and evolutionary ecology studies across diverse species (Postma et al., 2015; Giacomini et al., 2019). Unlike scanning, by which 3D coordinates of points are directly captured on an object's surface, photogrammetry extracts 3D information from overlapping 2D images taken from different viewpoints using consumer digital cameras (Remondino et al., 2005; Linder, 2009; 2013). This overlapping ensures that each point on the object is captured by multiple images, each providing different perspectives. Common points are identified by photogrammetry software, and their 3D positions are then calculated using triangulation (Aharchi & Ait Kbir, 2020), resulting in the creation of a dense point cloud on the object's surface. A polygonal mesh representing the object's surface is then created by dedicated algorithms, which is textured with colour information from the original photos for a realistic 3D model (Meshroom, 2021).

Photogrammetry offers several benefits for comparative studies of wide-ranging species. First, it enables data collection from specimens scattered over geographically distant collections due to its use of consumer digital cameras, which are easily carried and whose setups can be adjusted to suit varying local conditions. Moreover, standardized photographic protocols can be implemented (e.g. James et al., 2019; De Oliveira et al., 2023), facilitating reliable data collection across museums by local staff. This way, the logistics associated with data collection can be greatly simplified, by reducing the need to travel to distant locations and reducing the need to carry specialised equipment when travel is unavoidable. Second, the resulting 3D models can be stored in digital format, enabling future use and continuous supplementation over time. These models can be accessed without physically handling the skulls in museums, facilitating data sharing between institutions (Boyer et al., 2016; Jacobs, 2022). They can also provide a digital backup of the museum specimens, ensuring that the morphological information can be protected from accidental damage to the physical specimens. Finally, photogrammetry benefits from the availability of open-source 3D modelling software (e.g. Cignoni et al., 2019; Griwodz et al., 2021), which improves workflow transparency, through documenting specific algorithms and methodologies used. This accessibility fosters more comprehensive comparative studies and the addition of new data following standardized protocols.

Photogrammetry has become an invaluable tool in 3D geometric morphometrics (3DGM), finding applications across a wide range of species (e.g. Durão et al., 2018; Giacomini et al., 2019; Tsuboi et al., 2020; Rainha et al., 2021; Brassard et al., 2023). It has been used to capture

body, head, and facial shapes, as well as structures like teeth, skulls, limbs, and antlers, from museum collections. The method has been useful in identifying species and subtle skull shape differences (Evin et al., 2016; Gabelaia et al., 2018; Brassard et al., 2023). It is particularly effective for studying large species, like marine mammals (e.g. Moshobane, 2014; Fahlke & Hampe, 2015; Vicari et al., 2023), due to its capability to photograph objects of various sizes. For example, skull shapes and sizes of different odontocete species have been compared using 3DGM (Vicari et al., 2023). It was suggested that at an interspecific level, prey size and peak vocalisation frequency are the main drivers of skull shape differentiation between species, which are largely size-related. Photogrammetry's ability to create accurate 3D models of complex biological features is crucial for the present study, as intraspecific shape variations are generally subtle (e.g. Maestri et al., 2016; Hošková et al., 2021). To ensure data comparability, consistency in photographic setups and 3D reconstruction models across museums must be maintained. However, detailed protocols for 3D model reconstruction for cetaceans are scarce in the literature, as large-scale photogrammetry studies are still relatively uncommon. Therefore, a standardised workflow was developed in this thesis to ensure replicability across museum collections and photographic setups.

2.2. On-site Image Acquisition

Equipment used for image capture

The photographic equipment consisted of a high-resolution DSLR camera (> 8 Megapixels) with APS-C sized sensors. The camera was mounted on a tripod with adjustable legs and a pivoting central column, allowing the skulls to be photographed from various vertical perspectives. The skull was positioned in the centre of a motorized turntable, with adjustable rotation angle, speed, and stopping points of the turntable. Therefore, the turntable could be set to stop at specific angles or intervals during rotation to synchronize it with the camera shots. Synchronization was achieved using a remote camera trigger attached to the camera, whose timing between consecutive shots was set to match the turntable rotation. This ensured coordination between image capture and skull rotation. An external flash unit was attached to the camera when necessary.

Setup used for image capture

The setup was arranged by covering the wall, floor, and surface of the motorized turntable with black sheets to create a high-contrast background and therefore minimise light reflection

and isolate the skull from the background. Each section followed a standard photographing set-up protocol to avoid systematic errors related to equipment and image distortion. The skull was placed in the centre of the turntable, its rostrum facing the camera. The tripod supporting the camera was placed at a distance from the turntable, so the skull was centred and framed in the camera, leaving enough space around the object. Following framing and focusing on the object, the turntable was set to rotate by 20 degrees every 4 seconds after the object had stopped to rotate (rotation time lasting up to 1.5 seconds), until completing a full rotation. The camera was connected to a remote camera trigger, which was timed to take photos every 6 seconds. This was synchronized with the turntable's pauses to ensure optimal photo overlap. Skulls were captured from ventral and dorsal perspectives, with the tripod set at a 0-degree angle relative to the floor. Additional photos were captured from elevated angles of 25, 50, and 75 degrees above the floor (Figure 2.1). The angles were selected based on preliminary tests that indicated these perspectives would capture the entirety of the skull' surface details. The process took 45 to 60 minutes per individual.

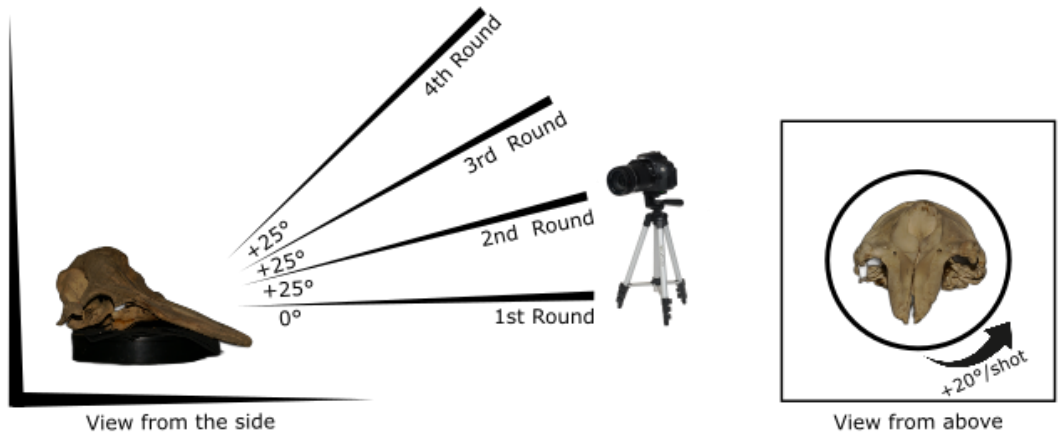

Figure 2.1. Schematic representation of the photogrammetry protocol setup.

Camera settings and lighting conditions

A fixed focal length was used throughout each photography session for all specimens to maintain consistency in image scale and perspective. The ISO was set to 200 to reduce digital noise and improve overall image quality by reducing noise. Sharpness and depth of field were optimized by balancing the smallest aperture with the highest shutter speed possible, maintaining consistency in these parameters across shots taken on the same day. Suitable room lighting conditions were prioritised, because light, shadows, and reflections can impact image

accuracy. Whenever possible, the natural light from windows was used, avoiding direct sunlight to minimize shadows. In environments lacking natural light, artificial lighting alongside an external flash and diffuser was used, with various setups tested to establish optimal conditions for accurate morphometric analysis.

The photographs were saved in full-resolution JPG files with the lowest compression level available. File size is substantially reduced through compression in JPG format while maintaining good image details, thus facilitating the storage of a larger number of images (required for photogrammetry of each specimen). This file format enables fast image processing and transfer between media, therefore reducing the computational workload associated with the processing and manipulation of a large number of files. Additionally, the JPG format is broadly compatible with most software, eliminating the need for image post-processing before use (Triantaphillidou & Allen, 2012; Kropscot, 2016). Image data can also be saved in RAW format by most consumer digital cameras, which provide the highest quality images due to the lack of compression. As a result, details and colours, especially in highlights and shadows recovery, are preserved. However, RAW files are larger in size requiring substantial storage space, which results in lengthy data transfer and backup procedures. In addition, the RAW format is specific to each camera model and requires dedicated software for processing before use in many downstream analyses. Therefore, despite the better photo quality offered by the RAW format, it poses challenges in handling and transferring images during the 3D reconstruction step (Triantaphillidou & Allen, 2012; Kropscot, 2016). Although JPEG is an 8-bit format and inevitably results in some loss of detail through compression, it still provides a good balance between photo quality, storage, time efficiency and compatibility (Cardaci et al., 2022). This balance is particularly important for studies requiring the collection of hundreds of images from a large number of specimens. Furthermore, preliminary tests carried out showed no discernible differences in the models produced from JPG files relative to RAW files in the resulting 3D model.

2.3. 3D Reconstruction Workflow

Image processing and photo editing protocol

Each museum had unique lighting conditions, such as different intensities and colour temperatures of light, which can affect the appearance of colours and shadows in photographs. Additionally, the unique characteristics each skull had (e.g. colour, texture), influenced how light was reflected on their surfaces. Therefore, variation in image characteristics like brightness and contrast was often observed between specimens. However, when photographing a single

specimen, lighting conditions remained consistent. Thus, batch-editing of images was performed using the open-source software Darktable v.3.2.1 (https://www.darktable.org). The best results were obtained by increasing local contrast while reducing global contrast, because this caused the details on the surface of the skull to become more uniformly visible. For this purpose, a workflow was developed that consistently improved 3D reconstruction (Table 2.1). Key adjustments were made within Darktable's "Darkroom" module, by referring to the luminance spectrum in the darkroom section of Darktable. The luminance spectrum illustrates the distribution of brightness for each pixel in the image. On the horizontal axis, the spectrum depicts the range of luminance values, from pure black (0) on the left to pure white (255 or 100%) on the right. The vertical axis indicates the frequency or number of pixels at each luminance level. Therefore, if the histogram showed a prominent peak toward the left, indicating a lot of dark tone in the image, or a peak toward the right suggesting that the image contained a lot of bright highlights; manual adjustments of the sliders were applied to several parameters to balance the tonal distribution. Overall, adjustments aimed at enhancing image sharpness and maintaining uniform lighting across the luminance spectrum within individual images. Within each darkroom session, the following adjustments were applied in the presented order:

1) The parameter “Black level correction” within the module “basic adjustment” was adjusted. This parameter adjusts the cutoff for dark grey values, turning them to pure black. Lowering it keeps more dark details visible while increasing it raises contrast in areas with low brightness. Subtle adjustments were made within a range of -0.015 to 0.050 to fine-tune the threshold and enhance local contrast in areas with dark values. High parameter values were avoided, to preserve dark details across the image.

2) The local contrast was adjusted using the module "local contrast". This module controls the visibility of fine details in specific regions of the photo by changing the contrast between pixels on a local level. Increasing the “details” value enhances local contrast, resulting in a more detailed image. Furthermore, the “highlights” slider was adjusted to either increase or decrease the contrast in the highlights. Increasing the highlights made the brighter areas of the image more detailed, while decreasing the highlights brought them closer in tone to the midtones and shadows, effectively reducing the overall contrast between the bright and dark areas of the image. The same principle was applied to the “shadows” slider, and the "midtone" slider. These adjustments were kept subtle to avoid increasing global contrast excessively. Additionally, the "detail" parameter was kept between 125% and 175% to prevent undesirable halo effects.

3) The module "Shadows and highlights" was used, which independently modifies the tonal range of shadows and highlights within an image. This allows the amount of contrast across the entire image to be controlled, by modifying the intensity of dark and light areas. This tool was used to reduce global contrast by increasing the shadows levels and decreasing the highlight levels to avoid increasing global contrast. This may create unwanted effects, like halos or blue tints in dark areas. Therefore, the parameter "shadows" was kept between +50 and +25 and the parameter "highlights" between -50 and +25 to avoid artefacts.

4) The module "tone equalizer" was used, to edit the photo so that each pixel with similar brightness was modified in the same way. This tool enables the adjustment of brightness in specific predetermined brightness zones, achieving a more balanced overall contrast across the entire image. The brightness and contrast were adjusted across different brightness zones (EV) sliding the settings between -0.25 and +0.25 to keep the effect subtle. To check that the image had no under or over-exposed area, the "toggle over/underexposed" was used.

5) The module "contrast equalizer" was used by adjusting the luminance contrast (parameter "luma"). This module divides the photo into different detail levels, from fine to coarse details. By adjusting the predetermined sliders on the module graph, contrast at specific levels of detail can be increased or decreased as needed. For each photograph a typical S-shaped curve was applied, by raising contrast on finer details (increasing local contrast) while lowering contrast on the coarser details (decreasing global contrast).

6) The module "sharpen" was used to enhance the contrast between adjacent pixels, and therefore adjust the fine-scale contrast of the image. However, excessive sharpening may create halos around the pixel edges, and therefore adjustments at this step should remain subtle. All adjustments were based on visual assessment of the results, although the parameter "radius" was kept low (1.20-2.00), while the parameter "amount" was kept below approximately 0.7 to avoid artificial halos.

For some specimens, it was found that removing the background before image processing improved the model. Therefore, before editing the photographs, the background was removed from all images using the Python script REMBG (Gatis, 2020). REMBG uses machine learning algorithms to identify and isolate the foreground object in each picture. Once the object is detected, the background is then removed, leaving an isolated image of the foreground specimen. REMBG was used with the settings: rembg p -a. The "p" option enabled batch processing, removing the background from all photos within a folder. The "-a" option used alpha matting, which generates precise alpha masks for each pixel of the foreground object.

This creates detailed boundaries around the foreground object, ensuring that only the object remains visible while the background is completely removed.

Table 2.1. List of parameters modified during the image editing workflow.

Parameters	Modifications	Range
1) Basic adjustment	Black level correction	Between -0.015 and 0.050
2) Local contrast	Detail	Between 125% and 175%
3) Shadows and Highlights	Shadows; Highlights	Between +25 and +50 Between -50 and +25
4) Tone equalizer	Each tone value adjusted depending on the luminance histogram	Variable; avoid extreme values.
5) Contrast equalizer	Luma	Variable; avoid extreme values.
6) Sharpen	Radius; Amount	Between 1.20 and 2.00 Below 0.7

3D modelling software

Several software options are available for 3D reconstruction using photogrammetry, including Agisoft Metashape, Autodesk, Bundler, and Meshroom (Bartoš et al., 2014; Kingsland, 2020). For this study, Meshroom v.2019.2.0 (Alice vision 2019; https://alicevision.org) was chosen, due to its open-source nature and intuitive interface, supporting multiple image file formats. This makes it suitable for various research groups (Carrière & Tallman, 2024), even with limited budgets, and researchers with varying levels of technical expertise. It is built around a modular structure, with each step including its own module, allowing connections to be formed between modules to create complex workflows. Moreover, all resulting files are automatically saved into dedicated folders, making it easier to track progress and revisit specific stages of the reconstruction if needed. The workflow can thus be adapted to follow the development of a given project requirements. This set of characteristics also facilitates the replicability of the workflow, which is especially beneficial for comparative analyses.

Meshroom uses the Structure from Motion (SfM) algorithm to construct 3D models from a series of photos, generating high-resolution point clouds (Carrivick et al., 2016; Eltner et al., 2016). Key features are identified and matched across successive images, and analysed to measure distances between their positions in 3D space. SfM then uses triangulation to determine where each point is located in the 3D space. During this process, straight lines are derived from the camera lens through a specific point on the object for each photo taken. These

multiple lines, obtained from different camera positions, will intersect at a same point in space, representing the 3D position of that specific point on the object. Additionally, the position and orientation of the camera for each individual photograph are calculated (referred to as "bundle adjustment"; Triggs et al., 2000). Once the camera positions and orientations have been determined, SfM generates a dense point cloud, comprising a collection of 3D points that represent the object's surface from which a detailed 3D surface model can be reconstructed.

The Meshroom workflow begins by importing photos of the object into the software. Distinctive features are then extracted from each image (“FeatureExtraction”), and matched across images (“FeatureMatching”), while the SFM algorithm estimates camera positions, orientations, and scene 3D structure (“StructureFromMotion”). Based on this information, a sparse point cloud is constructed, where each point is recognised and matched across images, to represent the object's 3D structure ("PrepareDenseScene”). Following this, refinements are applied to both camera parameters and 3D point positions, before the point cloud density is increased by filling in areas sparse in points. Subsequently, a polygonal mesh is constructed from the dense point cloud, to represent the object's surface geometry (“Meshing” and “MeshFiltering”). Finally, the original images are projected onto the mesh to apply textures, resulting in a realistic representation of the reconstructed object ("Texturing”). Settings in certain steps of the Meshroom workflow can be critical for the accuracy of the final 3D model. For example, during ‘FeatureExtraction’, an increased number of identified features across images can lead to a more accurate 3D reconstruction (Meshroom, 2021).

3D reconstruction parameters

For dolphin skulls, capturing between 200 to 500 photos per specimen using the above setup, was sufficient to generate high-quality models. For the default reconstruction, features were identified in the ”Feature Extraction” step using the default “Sift” algorithm (Scale-Invariant Feature Transformation; (Otero & Delbracio, 2014) and the “SIFT_float” algorithm to produce a 3D model of the entire skull that could be fully rotated. In the “Feature matching” step, camera recognition was increased by implementing a second stage in the matching procedure using ‘Guided matching’. The ‘Use rig constraint’ in the “StructureFromMotion” step was disabled since the camera position changed during the photographing session. In the “DepthMap” step, the 'Depth Map' node was set to downscale=1, as this produced the most detailed model surfaces. Some specimens from Guayaquil were exceptions as models with similar levels of detail and polygon count were produced when downscale=2 was applied.

For some specimens, limited museum time and suboptimal lighting conditions resulted in fewer usable photographs. With fewer than 300 photographs, the software identified less features, causing gaps or inaccuracies in the resulting model. Therefore, adjustments were required in several Meshroom settings to optimize reconstruction quality. To increase the number of features identified in the 'FeatureExtraction' step, several parameters were optimized. First, the 'Akaze' algorithm (Alcantarilla et al., 2011) was used in addition to the "Sift" and "SIFT_float" algorithms. When combined with other algorithms, Akaze contributes to the detection of additional feature types that might otherwise be missed, increasing the total number of matched points across images. Additionally, the prescriber preset was set to 'High' in the 'FeatureExtraction' module, which increased the sensitivity and density of feature detection algorithms (i.e., Akaze and Sift).

Additionally, the parameters for 'Max Descriptors' and 'Number of matches' were set to 0, removing a hard limit on the number of feature descriptors retained for each image or the number of matches between images. This setting maximized the number of data points available for reconstruction. Moreover, the values for "minimum consistency camera" and "minimum consistency camera similarity" were lowered to 2 and 3, respectively. The "minimum consistency camera" determines how many cameras must agree on the position of a feature before it is considered valid for triangulation. By setting it to 2, a feature must be detected in at least two different camera views to be used for building the 3D model. Similarly, "minimum consistency camera similarity" defines the minimum level of similarity between camera views for a feature to be considered consistent and valid for triangulation. The higher the value, the stricter the algorithm is in accepting features as valid. Lowering it from 4 to 3 allowed a greater number of features to be included in the triangulation process.

2.4. Common Causes Of Sub-optimal Reconstructions And Mitigation Strategies

During model optimisation, 'Feature Extraction' was identified as a critical step for the final 3D model's accurate reconstruction. Sub-optimal reconstruction was primarily caused by the software's inability to evenly identify enough features across the skull compared to those in the background. As a result, 3D models could be incomplete, include portions of the background, or be reconstructed with irregular textures and/or small holes in the meshes. These issues were addressed through a combination of image pre-processing, and adjustments to the reconstruction settings, as described below.

For some specimens, features were identified in the photo's background, leading to the unwanted inclusion of background elements in the 3D model. These elements were difficult to remove during post-processing, without compromising the accuracy of the final models. Therefore, the background was removed from these pictures using the python script REMBG (https://github.com/danielgatis/rembg). REMBG is a machine learning tool, trained to differentiate primary objects (such as skulls in this study) from background elements by analysing colour, texture and spatial relationships within the image. The foreground elements were isolated from the background and placed onto a transparent background while preserving their original shape. Through this process, the number of background features identified by the software was significantly reduced, therefore improving the 3D reconstruction of the skulls.

For specimens with a lower number of pictures, the software had difficulties in identifying enough details to accurately represent both ventral and dorsal perspectives in the same model. As a result, one of the perspectives, particularly the ventral area, was often reconstructed incompletely, blurred or darkened. To address this problem, the most effective strategy involved capturing more photographs. However, in some cases, optimising the reconstruction parameters was also necessary to achieve satisfactory results. In the „FeatureExtraction" step, selecting the 'Akaze' algorithm with a "High" "Describer Preset", helped identify a higher number of features, particularly in high contract areas. In the "ImageMatching" step, decreasing the 'Max Descriptors' and 'Nb Matches', facilitated an overall more complete reconstruction of the skull. However, this change also led to a sparser point cloud, which could potentially result in a less detailed surface reconstruction. Further improvements were achieved by decreasing the 'Min Consistency Cameras', and 'Min Consistent Camera Bad Similarity' parameters in the "DepthMapFilter" step. These changes allowed for the inclusion of more data points in the model, although they also relaxed the standards used to evaluate how well data from different images align with each other, potentially compromising detail accuracy in the final 3D model. For details on parameter adjustments refer to Table 2.2.

In areas like the premaxilla or the occipital region, the mesh surface was often reconstructed with considerable irregularities and small artificial holes. These structures are especially important in recognizing between different species in the bottlenose dolphin. For example, the premaxillae are wider and more robust in *T. truncatus* compared to *T. aduncus* (Jedensjö et al., 2020). To prevent this problem, the photo editing workflow was optimized by enhancing image sharpness, increasing local contrast and reducing global contrast (photo editing described in section 2.3.).

To improve surface textures, adjustments were made in the "Meshing" step by reducing "Max input points," "Max points," and "Max points per voxel" by 50% to 20% from their default values. “Max input points” was reduced to limit the number of input points used for meshing, while “Max points” was decreased to control the maximum number of points used to generate the mesh. By reducing these values, the software prioritised higher-quality points, thereby reducing overall point density. Similarly, “Max points per voxel” controls the number of points within each voxel, and therefore lowering it prevents the clustering of points which can lead to uneven or rough textures. These adjustments helped regulate point density and quality in the meshing process, resulting in smoother surface textures, and reducing irregularities and/or artificial holes (particularly noticeable in the occipital and premaxillae areas). However, this often resulted in the loss of surface details in the reconstructed object. For details on parameter adjustments refer to Table 2.2.

Table 2.2. Description of the parameters used for the 3D modelling in Meshroom.

Settings	Parameters	Effects	Related issues
Feature Extraction	Sift_float + Akaze Preset = high	Increased the number of feature extraction and feature identification.	Low number of pictures
Image matching	Max descriptor = 0 Number of matches = 0	Maximized number of descriptors used for reconstruction Kept all matches recovered for downstream processing.	Low number of pictures
Depth map	Downscale = 1 Min consistency camera = 2 Min consistency camera similarity = 3	Higher triangulation Optimize mesh completeness	None Low number of pictures
Meshing	Max input point = 25000000 or 10000000 Max points = 2500000 or 1000000 Max points per voxel = 500000 or 200000	Reduced the number of point cloud data used to generate the model. Therefore, simplified the mesh and smoothed the surface.	Models could be reconstructed with a rough texture.

Finally, a strategy to balance completeness and surface detail was required. A more complete mesh was better able to capture the overall shape but often lacked the fine details necessary for morphological analyses. Conversely, a highly detailed mesh might accurately represent surface features but miss parts of the object, leading to an incomplete model. In some cases, optimal results were achieved by merging 2 to 3 meshes created using different settings. By merging meshes optimised for completeness with those optimised for mesh details, the strengths of both approaches were leveraged to ensure the best quality in the final reconstructed model. Using Meshlab (Cignoni et al., 2019), an open-source software for editing, cleaning, inspecting, and

converting large 3D meshes, the selected meshes were merged using the feature "flatten visible layers". This feature merged and integrated the vertices, edges and faces from the multiple meshes into a single mesh, resulting in higher mesh density and improved accuracy, as it combines the best aspects of each individual mesh. However, differing vertex densities from the original meshes due to the different parameters used during their construction, caused intersecting faces in the merged mesh. To address this issue, a Screened Poisson surface reconstruction was applied (Kazhdan et al., 2006). This method reconstructed the merged mesh, removing intersecting faces, redundant vertices and edges, therefore resulting in a more uniform surface. Key settings such as "reconstruction depth" were set to 13 and "interpolation weight" to 0 to optimize the reconstruction process.

2.5. Preparing Final Mesh Files

For some specimens, the final model included skull features not commonly present in other skulls. Typically, this consisted of segments of the zygomatic bone, which is notoriously thin in dolphins and is therefore missing in many museum specimens. Furthermore, most models failed to accurately reconstruct this bone, resulting in only partial reconstruction. Earlier tests with the automatic landmarking procedure (see details in later chapters) showed that the presence of these features caused some landmarks to be placed in the zygomatic, causing bias in the shape analyses. Therefore, those structures were manually removed whenever present. The bisection tool was used in the open-source software Blender v.5.2.2 (Blender Development Team, 2022). This tool allows for precise cuts along a specified plane, minimizing the introduction of shape information resulting from the model editing process.

Given the different parameters used for model reconstruction, the resulting meshes had different polygon counts. Higher polygon counts increase computational time without necessarily enhancing resolution. Therefore, to standardise mesh resolution and reduce the computational requirements of downstream analyses, a simplification step was performed. The meshes were simplified to 1 000 000 faces using the "Simplification: Quadric Edge Collapse Decimation" feature in Meshlab (Cignoni et al., 2008). This method was applied iteratively, with mesh edges collapsed based on a quadric error metric, preserving the overall shape and features of the model. As a result, we obtained models that could be processed further with reasonable computational times, while still retaining the necessary details for morphometric analysis.

Finally, all files were aligned to a standard orientation to maintain consistency with the approach applied throughout the study. Each specimen was imported into the open-source 3D editing software Blender and used its transformation tools to move and rotate the skulls. First, the skull origins were aligned to their centre of mass, and the centre of mass moved to the midpoint of the 3-coordinate axis. Then the skulls were rotated to be oriented in lateral view with the rostrum oriented along the x-axis. In dorsal view, the x-axis passed through the middle of the two maxillae. The skull was then rotated on the y-axis so the axis would pass vertically through the middle of the occipital condyle when viewed from the occipital perspective. Throughout this process, the Z-axis was left untouched.

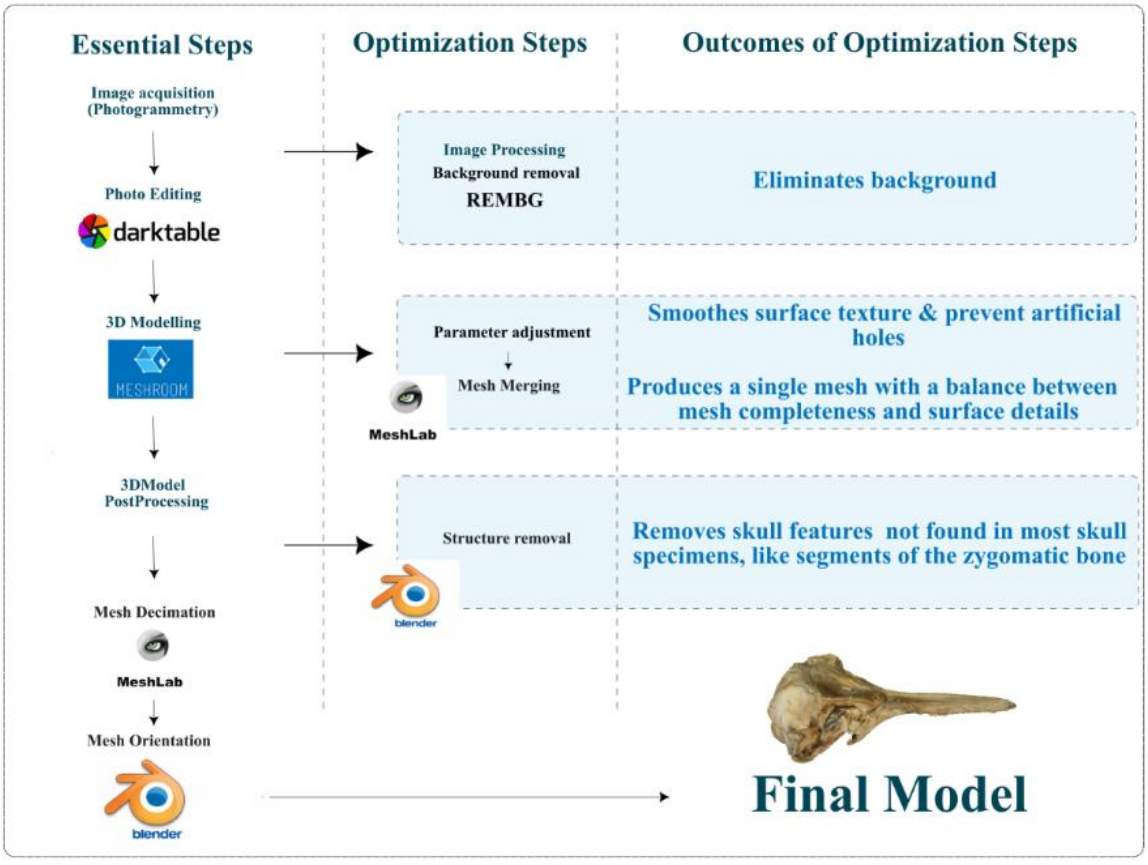

Figure 2.2. Workflow of the 3D modelling protocol using photogrammetry.

2.6. Discussion

This chapter establishes a protocol for creating accurate 3D dolphin skull models suitable for geometric morphometric analysis. The protocol is based on the open-source 3D modelling software Meshroom, whose interface was found to be particularly useful in a research context where optimisation of the 3D reconstruction process is required. The protocol designed here

was found to be effective, successfully reconstructing 296 models from a total of 314 photographed skulls, which were suitable for subsequent geometric morphometric analysis. Notably, high-quality models were created, even when the initial photograph quality was sub-optimal, or the number of photographs was low. Therefore, several common challenges in producing 3D models are identified in this chapter, and practical solutions are provided, enabling reproducible datasets to be created for collaborative and downstream comparative studies.

Although the skulls were photographed from different museums with varying local conditions, photogrammetry's flexibility to adjust photographic set-up allowed for good quality photographs to be taken across sites and skulls to be generated with comparable accuracy, independently of the environmental conditions. The production of high-quality photographs is therefore a critical step of the protocol. To achieve complete and accurate 3D dolphin skull models, a minimum of 300 photographs, taken with a tripod-mounted camera and diffuse lightning, is typically required. This ensures the presence of multiple consistent angles, reduces motion blur, and minimizes shadows and reflections that can interfere with feature detection. Models derived from fewer images often resulted in incomplete skulls, with coarse and/or patchy surfaces due to insufficient data for robust feature matching. Guidance on best practices for photographing objects for 3D geometric morphometrics (3DGM), is provided in section "2.2 - On-site image acquisition".

Certain inherent characteristics of dolphin skulls, mostly related to low contrast or the reflective properties of certain structures (e.g. the premaxilla), can impair the identification of sufficient features for accurate reconstruction. While it is also difficult to scan those features, the work done here identified an image editing workflow for processing images before photogrammetric reconstruction (Table 2.1), offers a solution to this challenge. By relying on the open-source software Darktable v.3.2.1, batch editing for consistent adjustments across high-volume images of the same individual can be achieved in a reasonable processing time. Specifically, increasing local contrast while reducing global contrast results in sharper images with uniform lighting across the image's luminance spectrum. This process was further improved by background removal using the REMBG Python script, a process that was facilitated considerably by using a photography setup that reduces the background information of the pictures.

At the 3D reconstruction stage in Meshroom, the "feature extraction" settings were identified as critical. Insufficient or indistinct features (e.g. due to low image quality or repetitive textures) can lead to unreliable image matching, negatively impacting downstream steps and resulting in

incomplete or noisy 3D reconstructions with coarse and patchy textures. Setting the prescriber preset to "High" had the highest impact in increasing the density of feature detection (see Section “2.3 - 3D reconstruction workflow” for further details). Additionally, the number of features detected was increased by incorporating the "AKAZE" algorithm, in addition to the standard "SIFT" and "SIFT_float" algorithms. However, it was less effective in placing them in areas where other algorithms missed.

Alternatively, when optimising Meshroom's settings was insufficient, suitable post-processing solutions are provided by the protocol, such as merging multiple models generated by Meshroom using alternative settings (particularly at the “Meshing” stage). This involves creating several reconstructions of the same skull, each capturing different aspects or details, and then combining them into a single, more complete model. Detailed information about this merging process can be found in section “2.4 – Common causes of sub-optimal reconstructions and mitigation strategies”. This approach is particularly beneficial because it allows the reuse of existing photos instead of taking new ones.

While Meshroom was found to be effective in reconstructing models, particularly those that were initially difficult to process, a small number of models could not be fully reconstructed. In some cases, this was attributed to the software's difficulty in capturing fine skull details. Considering this aspect, further investigation into the optimization of feature extraction parameters is suggested to improve performance and increase the success rate of reconstructions. Furthermore, while Meshroom performed well with dolphin skulls, which are generally large and exhibit minimal damage due to their robust structure, the protocol may require further changes for smaller objects with intricate structures and low contrast. In such cases, closer or higher-resolution imaging, or the incorporation of structured light techniques, may be necessary to enhance the capture of fine details.

The methods described in this chapter provide a robust approach for creating accurate 3D models for morphometric analyses, contributing to reliable results and supporting collaborative research in evolutionary biology. The 3D models produced can be digitally stored, shared, and reused. This enables the creation of landmarking strategies suitable for specific research questions or the use of landmarking from previous research groups, therefore facilitating collaborative and longitudinal studies while reducing the physical handling of specimens. This, in turn, reduces the need for travel to remote locations and the transportation of specialized equipment for data collection. Additionally, these 3D models can be used as training tools for students and early-career researchers, expanding access to advanced morphometric techniques. The detailed documentation of the algorithms and methods described here contributes to the

reproducibility, consistency, and compatibility with future technologies, further supporting the ongoing advancement of geometric morphometric research.

2.7. Bibliography

Adams, D. C., & Otárola-Castillo, E. (2013). Geomorph: an r package for the collection and analysis of geometric morphometric shape data. *Methods in Ecology and Evolution*, *4*(4), 393–399. doi: 10.1111/2041-210X.12035

Adams, D. C., Rohlf, F. J., & Slice, D. E. (2004). Geometric morphometrics: ten years of progress following the 'revolution.' *Italian Journal of Zoology*, *71*(1), 5–16. doi: 10.1080/11250000409356545

Aharchi, M., & Ait Kbir, M. (2020). A review on 3D reconstruction techniques from 2D images. *Lecture Notes in Intelligent Transportation and Infrastructure*, *Part F1409*, 510–522. doi: 10.1007/978-3-030-37629-1_37

Alcantarilla, P., Nuevo, J., & Bartoli, A. (2011). Fast explicit diffusion for accelerated features in nonlinear scale spaces. *IEEE Transactions on Pattern Analysis and Machine Intelligence*, *34*(7), 1281–1298. doi: bmvc/2013/Papers/paper0013

Álvarez, A., & Perez, S. I. (2013). Two-versus three-dimensional morphometric approaches in macroevolution: insight from the mandible of caviomorph rodents. *Evolutionary Biology*, *40*(1), 150–157. doi: 10.1007/S11692-012-9194-3

Barber, D., Mills, J., & Bryan, P. (2002). Laser scanning and photogrammetry - 21th century metrology. *International Archives of Photogrammetry Remote Sensing and Spatial Information Sciences*, *34*, 360–366. Available at: www.isprs.org/proceedings/xxxiv/5-c7/pdf/2001-08-db01.pdf

Bartoš, K., Pukanska, K., Sabová, J., & Pukanská, K. (2014). Overview of available open-source photogrammetric software, its use and analysis. *International Journal for Innovation Education and Research*, *2*(04). doi: 10.31686/ijier.vol2.iss4.170

Bertrand, O. C., San Martin-Flores, G., & Silcox, M. T. (2019). Endocranial shape variation in the squirrel-related clade and their fossil relatives using 3D geometric morphometrics: contributions of locomotion and phylogeny to brain shape. *Journal of Zoology*, *308*(3), 197–211. doi: 10.1111/jzo.12665

Bitelli, G., Dubbini, M., & Zanutta, A. (2004). Terrestrial laser scanning and digital photogrammetry techniques to monitor landslide bodies. *International Archives of Photogrammetry, Remote Sensing and Spatial Information Sciences*, *35*, 246–251.

Blanco, M. V. F., Cassini, G. H., & Bona, P. (2023). A three-dimensional geometric morphometric analysis of the morphological transformation of Caiman lower jaw during post-hatching ontogeny. *PeerJ*, *11*, e15548. doi: 10.7717/Peerj.15548

Bookstein, FL. (1991). Morphometric tools for landmark data: geometry and biology. Cambridge University Press.

Botsch, M., Pauly, M., Kobbelt, L., Alliez, P., Lévy, B., Bischoff, S., & Röossl, C. (2007). Mesh data Structure. In *Geometric Modeling Based on Polygonal Meshes (*pp. 8-20*)*. Max-Planck-Institut für Informatik.

Boyer, D. M., Gunnell, G. F., Kaufman, S., & McGeary, T. M. (2016). Morphosource: archiving and sharing 3-D digital specimen data. *The Paleontological Society Papers*, *22*, 157–181. doi: 10.1017/SCS.2017.13

Brassard, C., Evin, A., Ameen, C., Curth, S., Michaud, M., Tamagnini, D., Dobney, K., Guintard, C., Porcier, S., & Jerbi, H. (2023). Wild or domestic? A 3D approach applied to crania to revisit the identification of mummified canids from ancient Egypt. *Archaeological and Anthropological Sciences*, *15*(5), 1–20. doi: 10.1007/S12520-023-01760-1

Bright, J. A., Marugán-Lobón, J., Rayfield, E. J., & Cobb, S. N. (2019). The multifactorial nature of beak and skull shape evolution in parrots and cockatoos (Psittaciformes). *BMC Evolutionary Biology*, *19*(1), 1–9. doi: 10.1186/S12862-019-1432-1

Burnard, J. L., Parr, W. C. H., Choy, W. J., Walsh, W. R., & Mobbs, R. J. (2020). 3D-printed spine surgery implants: a systematic review of the efficacy and clinical safety profile of patient-specific and off-the-shelf devices. *European Spine Journal*, *29*(6), 1248–1260. doi: 10.1007/S00586-019-06236-2

Buser, T. J., Sidlauskas, B. L., & Summers, A. P. (2018). 2D or Not 2D? Testing the utility of 2D Vs. 3D landmark data in geometric morphometrics of the Sculpin subfamily Oligocottinae (Pisces; Cottoidea). *The Anatomical Record*, *301*(5), 806–818. doi: 10.1002/AR.23752

Cardaci, A., Azzola, P., Bianchessi, M., Folli, R., & Rapelli, S. (2022). Comparative analysis among photogrammetric 3D models RAW data vs RGB images. *Communications in Computer and Information Science*, *1507 CCIS*, 271–282. doi: 10.1007/978-3-030-94426-1_20

Cardini, A. (2014). Missing the third dimension in geometric morphometrics: how to assess if 2D images really are a good proxy for 3D structures? *HYSTRIX*, *25*(2), 73–81. doi: 10.4404/Hystrix-25.2-10993

Carrière, C., & Tallman, S. D. (2024). Assessing the utility of 3D modeling with photogrammetry in assigned sex estimation from the greater sciatic notch. *Forensic Imaging*, *36*, 200576. doi: 10.1016/J.FRI.2023.200576

Carrivick, J. L., Smith, M. W., & Quincey, D. J. (2016). *Structure from motion in the geosciences*. John Wiley & Sons. doi: 10.1002/9781118895818.

Cignoni, P., Ranzuglia, G., Callieri, M., Corsini, M., Ganovelli, F., Pietroni, N., & Tarini, M. (2008). MeshLab: an open-source mesh processing tool. *Sixth Eurographics Italian Chapter Conference*, 129–136. doi: 10.2312/LocalChapterEvents/ItalChap/ItalianChapConf2008/129-136

Curran, S. C. (2018). Three-dimensional geometric morphometrics in Paleoecology. In: Croft, D., Su, D., Simpson, S. (eds) *Methods in Paleoecology. Vertebrate Paleobiology and Paleoanthropology. Springer, Cham.*, 319–337. doi: 10.1007/978-3-319-94265-0_14

De Oliveira, A. de S. B., Leonel, L. C. P. C., LaHood, E. R., Hallak, H., Link, M. J., Maleszewski, J. J., Pinheiro-Neto, C. D., Morris, J. M., & Peris-Celda, M. (2023). Foundations and guidelines for high-quality three-dimensional models using photogrammetry: a technical note on the future of neuroanatomy education. *Anatomical Sciences Education*, *16*(5), 870–883. doi: 10.1002/ASE.2274

Dromby, M., Félix, F., Haase, B., Simões-Lopes, P. C., Costa, A. P. B., Lalis, A., Bens, C., Podestà, M., Doria, G., & Moura, A. E. (2023). Cranial variation between coastal and offshore bottlenose dolphins, *Tursiops truncatus* (Cetacea: Delphinidae) in Ecuador and the Mediterranean: a three-dimensional geometric morphometric study. *Zoological Journal of the Linnean Society*, *199*(1), 83–96. doi: 10.1093/Zoolinnean/zlad022

Dunn, R. H., & Avery, J. E. (2021). Ecomorphological variation in artiodactyl calcanei using 3D geometric morphometrics. *The Anatomical Record*, *304*(7), 1529–1540. doi: 10.1002/AR.24544

Durão, A. F., Muñoz, F., & Ventura, J. (2018). Obtaining three-dimensional models of limb long bones from small mammals: a photogrammetric approach. In C. Rissech, L. Lloveras, J. Nadal, & J. M. Fullola (Eds.), *MONOGRAFIES 14. Geometric morphometrics. Trends in biology, paleobiology and archaeology*. Barcelona: Seminari d'Estudis i Recerques Prehistòriques.

Elewa, A. M., Ed. (2004). *Morphometrics: Applications in Biology and Paleontology*. Springer-Verlag.

Eltner, A., Kaiser, A., Castillo, C., Rock, G., Neugirg, F., & Abellán, A. (2016). Image-based surface reconstruction in geomorphometry-merits, limits and developments. *Earth Surface Dynamics*, *4*(2), 359–389. doi: 10.5194/esurf-4-359-2016

Evin, A., Souter, T., Hulme-Beaman, A., Ameen, C., Allen, R., Viacava, P., Larson, G., Cucchi, T., & Dobney, K. (2016). The use of close-range photogrammetry in zooarchaeology: creating accurate 3D models of wolf crania to study dog domestication. *Journal of Archaeological Science: Reports*, *9*, 87–93. doi: 10.1016/j.jasrep.2016.06.028

Fahlke, J. M., & Hampe, O. (2015). Cranial symmetry in baleen whales (Cetacea, Mysticeti) and the occurrence of cranial asymmetry throughout cetacean evolution. *Science of Nature*, *102*(9), 1–16. doi: 10.1007/S00114-015-1309-0

Fernandez Blanco, M. V., Cassini, G. H., & Bona, P. (2018). Skull ontogeny of extant caimans: a three-dimensional geometric morphometric approach. *Zoology*, *129*, 69–81. doi: 10.1016/j.zool.2018.06.003

Ferrari, R., Lachs, L., Pygas, D. R., Humanes, A., Sommer, B., Figueira, W. F., Edwards, A. J., Bythell, J. C., & Guest, J. R. (2021). Photogrammetry as a tool to improve ecosystem restoration. *Trends in Ecology and Evolution*, *36*(12), 1093–1101. doi: 10.1016/j.tree.2021.07.004

Ferreira-Cardoso, S., Billet, G., Gaubert, P., Delsuc, F., & Hautier, L. (2020). Skull shape variation in extant pangolins (Pholidota: Manidae): allometric patterns and systematic implications. *Zoological Journal of the Linnean Society*, *188*, 255–275. doi: 10.1093/zoolinnean/zlz096

Gabelaia, M., Tarkhnishvili, D., & Adriaens, D. (2018). Use of three-dimensional geometric morphometrics for the identification of closely related species of Caucasian rock lizards (Lacertidae: Darevskia). *Biological Journal of the Linnean Society*, *125*(4), 709–717. doi: 10.1093/biolinnean/bly143

Gatis, D. (2020). *REMBG - A tool to remove images backgrounds*. Downloaded from https://github.com/danielgatis/rembg

Giacomini, G., Scaravelli, D., Herrel, A., Veneziano, A., Russo, D., Brown, R. P., & Meloro, C. (2019). 3D photogrammetry of bat Skulls: perspectives for macro-evolutionary Analyses. *Evolutionary Biology*, *46:3*, *46*(3), 249–259. doi: 10.1007/S11692-019-09478-6

Griwodz, C., Gasparini, S., Calvet, L., Gurdjos, P., Castan, F., Maujean, B., Lanthony, Y., & De Lillo, G. (2021). AliceVision Meshroom: an open-source 3D reconstruction pipeline. *In Proceedings of the 12th ACM Multimedia Systems Conference*, 241–247. doi: 10.1145/3458305.3478443

Gunz, P., & Freidline, S. E. (2022). Cranial form of the hofmeyr skull: comparative 3D geometric morphometrics. *Vertebrate Paleobiology and Paleoanthropology*, 143–150. doi: 10.1007/978-3-031-07426-4_8

Hošková, K., Pokorná, A., Neustupa, J., & Pokorný, P. (2021). Inter- and intraspecific variation in grass phytolith shape and size: a geometric morphometrics perspective. *Annals of Botany*, *127*(2), 191–201. doi: 10.1093/aob/mcaa102

Jacobs, H. L. (2022). SketchUp and Sketchfab: tools for teaching with 3D. *Journal of the Society of Architectural Historians*, *81*(2), 256–259. doi: 10.1525/jsah.2022.81.2.256

James, M. R., Chandler, J. H., Eltner, A., Fraser, C., Miller, P. E., Mills, J. P., Noble, T., Robson, S., & Lane, S. N. (2019). Guidelines on the use of structure-from-motion photogrammetry in geomorphic research. *Earth Surface Processes and Landforms*, *44*(10), 2081–2084. doi: 10.1002/ESP.4637

Jedensjö, M., Kemper, C. M. M., Milella, M., Willems, E. P. P., & Krützen, M. (2020). Taxonomy and distribution of bottlenose dolphins (genus *Tursiops*) in Australian waters: an osteological clarification. *Canadian Journal of Zoology*, *98*(7), 461–479. doi: 10.1139/CJZ-2018-0270

Kazhdan, M., Bolitho, M., & Hoppe, H. (2006). Poisson surface reconstruction. *In Proceedings of the fourth Eurographics symposium on Geometry processing* (7, No. 4).

Kazi, A., Sausthanmath, A., Meena, S. M., Gurlahosur, S. V., & Kulkarni, U. (2020). Detection of holes in 3D architectural models using shape classification based Bubblegum algorithm. *Procedia Computer Science*, *167*, 1684–1695. doi: 10.1016/j.Procs.2020.03.379

Kettner, L. (1999). Using generic programming for designing a data structure for polyhedral surfaces. *Computational Geometry*, *13*, 65–90. doi: 10.1016/S0925-7721(99)00007-3

Kingsland, K. (2020). Comparative analysis of digital photogrammetry software for cultural heritage. *Digital Applications in Archaeology and Cultural Heritage*, *18*, e00157. doi: 10.1016/j.daach.2020.e00157

Klingenberg, C. P., & Marugán-Lobón, J. (2013). Evolutionary covariation in geometric morphometric data: analyzing integration, modularity, and allometry in a phylogenetic context. *Systematic Biology*, *62*(4), 591–610. doi: 10.1093/sysbio/syt025

Kropscot, C. (2016). Basics of photo file formats, Part 2-RAW. *PSA Journal*, *82*(10), 8–9.

Lang, A. J., Engler, T., & Martin, T. (2022). Dental topographic and three-dimensional geometric morphometric analysis of carnassialization in different clades of carnivorous mammals (Dasyuromorphia, Carnivora, Hyaenodonta). *Journal of Morphology*, *283*(1), 91–108. doi: 10.1002/jmor.21429

Leberl, F., Irschara, A., Pock, T., Meixner, P., Gruber, M., Scholz, S., & Wiechert, A. (2010). Point clouds. *Photogrammetric Engineering and Remote Sensing*, *76*(10), 1123–1134. doi: 10.14358/PERS.76.10.1123

Linder, W. (2009). *Digital photogrammetry: a practical course*. Springer Berlin Heidelberg. doi: 10.1007/978-3-540-92725-9

Linder, W. (2013). *Digital Photogrammetry: Theory and Applications*. Springer Berlin Heidelberg. doi: 10.1007/978-3-662-06725-3

Maestri, R., Fornel, R., Gonçalves, G. L., Geise, L., de Freitas, T. R. O., & Carnaval, A. C. (2016). Predictors of intraspecific morphological variability in a tropical hotspot: comparing the influence of random and non-random factors. *Journal of Biogeography*, *43*(11), 2160–2172. doi: 10.1111/JBI.12815

Meloro, C., & Tamagnini, D. (2022). Macroevolutionary ecomorphology of the Carnivora skull: adaptations and constraints in the extant species. *Zoological Journal of the Linnean Society*, *196*(3), 1054–1068. doi: 10.1093/zoolinnean/zlab075. doi: 10.1093/zoolinnean/zlab075

Mitteroecker, P., & Bookstein, F. (2011). Linear discrimination, ordination, and the visualization of selection gradients in modern morphometrics. *Evolutionary Biology*, *38*(1), 100–114. doi: 10.1007/S11692-011-9109-8

Mitteroecker, P., & Schaefer, K. (2022). Thirty years of geometric morphometrics: achievements, challenges, and the ongoing quest for biological meaningfulness. *American Journal of Biological Anthropology*, *178*(74), 181–210. doi: 10.1002/ajpa.24531

Morley, J., Bucchi, A., Lorenzo, C., & Püschel, T. A. (2022). Characterizing the body morphology of the first metacarpal in the Homininae using 3D geometric morphometrics. *American Journal of Biological Anthropology*, *177*(4), 748–759. doi: 10.1002/ajpa.24473

Moshobane, M. C. (2014). Inter-population craniometrics of adult male Subantarctic fur seals (*Arctocephalus tropicalis*) [Master's thesis]. University of Pretoria (South Africa).

Otero, A., Moreno, A. P., Falkingham, P. L., Cassini, G., Ruella, A., Militello, M., & Toledo, N. (2020). Three-dimensional image surface acquisition in vertebrate paleontology: a review of principal techniques. *Publicacion Electronica de La Asociacion Paleontologica Argentina*, *20*(1), 1–14. doi: 10.5710/peapa.04.04.2020.310

Otero, I. R., & Delbracio, M. (2014). Anatomy of the SIFT method, image processing. *Image Processing On Line*, *4*, 370–396. doi: 10 5201/-pol 2014.82

Palci, A., & Lee, M. S. Y. (2019). Geometric morphometrics, homology and cladistics: review and recommendations. *Cladistics*, *35*(2), 230–242. doi: 10.1111/cla.12340

Postma, M., Tordiffe, A. S. W., Hofmeyr, M. S., Reisinger, R. R., Bester, L. C., Buss, P. E., & De Bruyn, P. J. N. (2015). Terrestrial mammal three-dimensional photogrammetry: multispecies mass estimation. *Ecosphere*, *6*(12), 1–16. doi: 10.1890/ES15-00368.1

Püschel, T. A., Friess, M., & Manríquez, G. (2020). Morphological consequences of artificial cranial deformation: Modularity and integration. *PLOS ONE*, *15*(1), e0227362. doi: 10.1371/journal.pone.0227362

Rainha, R. N., Martinez, P. A., Moraes, L. J. C. L., Castro, K. M. S. A., Réjaud, A., Fouquet, A., Leite, R. N., Rodrigues, M. T., & Werneck, F. P. (2021). Subtle environmental variation affects phenotypic differentiation of shallow divergent treefrog lineages in Amazonia. *Biological Journal of the Linnean Society*, *134*(1), 177–197. doi: 10.1093/biolinnean/blab056

Remondino, F., Guarnieri, A., & Vettore, A. (2005). 3D modeling of close-range objects: photogrammetry or laser scanning? *5665*, 216–225. doi: 10.1117/12.586294

Robb, H., Scrimgeour, G., Boshier, P., Przedlacka, A., Balyasnikova, S., Brown, G., Bello, F., & Kontovounisios, C. (2022). The current and possible future role of 3D modelling within oesophagogastric surgery: a scoping review. *Surgical Endoscopy*, *36*(8), 5907–5920. doi: 10.1007/S00464-022-09176-Z

Rohlf, F. J., & Slice, D. (1990). Extensions of the Procrustes method for the optimal superimposition of landmarks. *Systematic Biology*, *39*(1), 40–59. doi: 10.2307/2992207

Rohlf, F., & Marcus, L. (1993). A revolution morphometrics. *Trends in Ecology and Evolution*, *8*(4), 129–132. doi: 10.1016/0169-5347(93)90024-J

Smith, M., Walford, N. S., & Jimenez-Bescos, C. (2019). Using 3D modelling and game engine technologies for interactive exploration of cultural heritage: an evaluation of four game engines in relation to roman archaeological heritage. *Digital Applications in Archaeology and Cultural Heritage*, *14*, e00113. doi: 10.1016/J.daach.2019.e00113

Statham, N. (2018). Use of photogrammetry in video games: a historical overview. *Games and Culture*, *15*(3), 289–307. doi: 10.1177/1555412018786415

Triantaphillidou, S., & Allen, E. (2012). Digital image file formats. In E. Allen & S. Triantaphillidou (Eds.). The Manual of Photography (pp. 315-328). Routledge. doi: 10.4324/9780080926803-17

Triggs, B., McLauchlan, P. F., Hartley, R. I., & Fitzgibbon, A. W. (2000). Bundle Adjustment — A Modern Synthesis. *Lecture Notes in Computer Science (Including Subseries Lecture Notes in Artificial Intelligence and Lecture Notes in Bioinformatics)*, 298–372. doi: 10.1007/3-540-44480-7_21

Tsuboi, M., Kopperud, B. T., Syrowatka, C., Grabowski, M., Voje, K. L., Pélabon, C., & Hansen, T. F. (2020). Measuring complex morphological traits with 3D photogrammetry: a case study with deer antlers. *Evolutionary Biology*, *47*(2), 175–186. doi: 10.1007/S11692-020-09496-9

Van Heteren, A. H., Germonpr, M., Van Heteren, E., Mammalogie, S., Staatssammlung, Z., & Unchen, M. (2023). Geometric morphometric assessment of the fossil bears of Namur, Belgium: allometry and ecomorphology. *Boreas*, *52*(4), 498–506. doi: 10.1111/bor.12629

Viacava, P., Baker, A. M., Blomberg, S. P., Phillips, M. J., & Weisbecker, V. (2022). Using 3D geometric morphometrics to aid taxonomic and ecological understanding of a recent speciation event within a small Australian marsupial (Antechinus: Dasyuridae). *Zoological Journal of the Linnean Society*, *196*(3), 963–978. doi: 10.1093/zoolinnean/zlab048

Viacava, P., Blomberg, S. P., Sansalone, G., Phillips, M. J., Guillerme, T., Cameron, S. F., Wilson, R. S., & Weisbecker, V. (2020). Skull shape of a widely distributed, endangered marsupial reveals little evidence of local adaptation between fragmented populations. *Ecology and Evolution*, *10*(18), 9707–9720. doi: 10.1002/ece3.6593

Vicari, D., McGowen, M. R., Lambert, O., Brown, R. P., Bianucci, G., Sabin, R. C., & Meloro, C. (2023). Ecomorphology of toothed whales (Cetacea, Odontoceti) as revealed by 3D skull geometry. *Journal of Mammalian Evolution*, *30*(2), 475–491. doi: 10.1007/S10914-022-09642-4

Vicari, D., Sabin, R. C., Brown, R. P., Lambert, O., Bianucci, G., & Meloro, C. (2022). Skull morphological variation in a British stranded population of false killer whale (*Pseudorca crassidens*): a three-dimensional geometric morphometric approach. *Canadian Journal of Zoology*, *100*(2), 119–132. doi: 10.1139/CJZ-2021-0112

Zelditch, M., Swiderski, D. L., & Sheets, H. (2012). *Geometric morphometrics for biologists : a primer*. Academic Press.

Chapter 3 – Cranial Variation Between Coastal and Offshore Bottlenose Dolphins, *Tursiops truncatus* (Cetacea: Delphinidae) in Ecuador and the Mediterranean: a Three-Dimensional Geometric Morphometric Study

This chapter has been published as: Dromby, M., Félix, F., Haase, B., Simões-Lopes, P. C., Costa, A. P., Lalis, A., Bens, C., Podestà, M., Doria, G., and Moura, A. E. (2023). Cranial variation between coastal and offshore bottlenose dolphins, *Tursiops truncatus* (Cetacea: Delphinidae) in Ecuador and the Mediterranean: a three-dimensional geometric morphometric study. *Zoological Journal of the Linnean Society, 199*(1), 83-96.

Zoological Journal of the Linnean Society, 2023, **199**, 83–96
https://doi.org/10.1093/zoolinnean/zlad022
Advance access publication 24 June 2023
Original Article

OXFORD

Original Article

Cranial variation between coastal and offshore bottlenose dolphins, *Tursiops truncatus* (Cetacea: Delphinidae) in Ecuador and the Mediterranean: a three-dimensional geometric morphometric study

Morgane Dromby[1], Fernando Félix[2,3], Ben Haase[3], Paulo C. Simões-Lopes[4], Ana P.B. Costa[4,5], Aude Lalis[6], Celine Bens[7], Michela Podestà[8], Giuliano Doria[9], Andre E. Moura[1,*]

[1]Museum and Institute of Zoology PAS, ul. Wilcza 64, 00-679 Warszawa, Poland
[2]Pontificia Universidad Católica del Ecuador (PUCE), Ave 12 de Octubre 1076, 170143 Quito, Ecuador
[3] Museo de Ballenas, Av. General Enríquez Gallo, entre calles 47 y 50, Salinas, Ecuador
[4]Federal University of Santa Catarina, R. Eng. Agronômico Andrei Cristian Ferreira, s/n - Trindade, 88040-900, Florianópolis, SC, Brazil
[5]Rosenstiel School of Marine, Atmospheric, and Earth Science, University of Miami, 1365 Memorial Drive, 33146, Coral Gables, Florida, USA
[6]Institut de Systématique, Évolution, Biodiversité (ISYEB), Muséum national d'Histoire naturelle, CNRS, Sorbonne Université, EPHE, Université des Antilles, CP51, 57 rue Cuvier, 75005 Paris, France
[7]Muséum National d'Histoire Naturelle, UMR CNRS 5202, 55 rue Buffon, 75000 Paris, France
[8]Museum of Natural History of Milan, corso Venezia 55, 20121 Milan, Italy
[9]Museo Civico di Storia Naturale 'Giacomo Doria', Via Brigata Liguria 9, I-16121 Genova, Italy

[*]Corresponding author. Ornithological Station (MIZ-PAS), ul. Nadwiślańska 108, 80-680 Gdańsk, Poland. E-mail: amoura@miiz.waw.pl

ABSTRACT

Skull shape analysis provides useful information on wildlife ecology and potential local adaptations. Common bottlenose dolphins (*Tursiops truncatus*) often differentiate between coastal and offshore populations worldwide, and skull shape analyses can be particularly useful in this context. Here we quantify skull shape variation between coastal populations from the Gulf of Guayaquil (Ecuador) and the Mediterranean Sea, compared to offshore specimens from multiple oceans. We analysed skull shape differences using 3D models from museum specimens through geometric morphometrics (3DGM). Two complementary landmark approaches included single-point semi-landmarks in homologous features, as well as pseudo-landmarks placed automatically. Results show skull shape distinction between both coastal populations and offshore specimens. Offshore specimens showed little differentiation between distinct locations. Skull shape patterns mostly diverged in the shape and length of rostrum, as well as the shape of the ascending processes of the maxilla, pterygoids, and occipital bones. However, both coastal populations differed in the patterns and direction of change of those features and were also morphologically distinct. Our results are consistent with local data on site fidelity and social structure in the coastal populations. Skull shape changes suggest divergent feeding and sound production patterns are potential drivers, probably specific to the local environment of each community.

Keywords: 3DGM; ecotypes; morphology; photogrammetry; skull shape

INTRODUCTION

Mammals are ecologically diverse animals, and their highly variable skull shape can provide a wealth of information regarding the ecology, evolutionary history, and taxonomy of the animals (e.g. Smith 2006; Costa *et al.* 2016; Machado 2020). Therefore, analyses of skull variation and its geographical structure can provide an important contribution to our understanding of the evolutionary ecology and biogeography of wild animals, particularly in taxa where other data are challenging to acquire.

The bottlenose dolphin (*Tursiops truncatus* Montagu, 1821) is a cosmopolitan, polymorphic, and widely recognized dolphin

Received 7 September 2022; revised 24 January 2023; accepted 6 March 2023

species. Throughout its range, researchers have described a distinction between coastal and offshore ecotypes based on multiple criteria. Cranial features, in particular, can be used to distinguish many coastal bottlenose dolphin populations from offshore dolphins. For example, along the west coast of the United States, coastal specimens have narrower internal nares and palatine width, and a higher number of teeth (Perrin *et al.* 2011). Along the east coast of the United States, coastal dolphins can also be distinguished from offshore dolphins based on relative length of internal nares, condylobasal length, and zygomatic width (Kenney 1990; Mead and Potter 1995), while having a smaller skull on average (Mead and Potter 1995; Costa *et al.* 2022). They also have distinct physiological signatures and parasitological patterns when compared to their offshore counterparts (Hersh and Duffield 1990; Mead and Potter 1995; Costa *et al.* 2022). Differences in skull structures have also been found in specimens from the south-eastern Pacific with coastal specimens having shorter anteorbital processes, narrow palatine bones, wide and fragile pterygoids with a rounded apex, and broad separation between the occipital condyles (Van Waerebeek *et al.* 1990).

Coastal dolphins are often found in distinct shallow areas and often show high site fidelity to bays and estuaries, while offshore dolphins are thought to be part of a single unstructured population found in pelagic, nearshore and insular waters worldwide (e.g. Hoelzel *et al.* 1998; Natoli *et al.* 2004; Sellas *et al.* 2005; Parsons *et al.* 2006; Quérouil *et al.* 2007; Tezanos-Pinto *et al.* 2009; Costa *et al.* 2016, 2021, 2022; Simões-Lopes *et al.* 2019; Moura *et al.* 2020). This ecological distinction has been suggested to result from distinct foraging habits between coastal and offshore dolphins, as demonstrated by differences in tooth numbers/size (Perrin *et al.* 2011; Costa *et al.* 2016), stable isotopes (Fernández *et al.* 2011; Gibbs *et al.* 2011; Giménez *et al.* 2017; Díaz-Gamboa *et al.* 2018; Pereira *et al.* 2020; Borrell *et al.* 2021), and stomach contents (Barros and Wells 1998; Gannon and Waples 2004; McCabe *et al.* 2010; Gibbs *et al.* 2011; Giménez *et al.* 2017).

Studies on genetics, behaviour and social structure in the south-east Pacific have also identified coastal and offshore populations of bottlenose dolphins in the Gulf of Guayaquil, Ecuador (Félix *et al.* 2017, 2018; Bayas-Rea *et al.* 2018; Félix and Burneo 2020). The coastal population is hierarchically structured, with females grouping with each other and males forming alliances for reproductive purposes (Félix 1997). This population was also seen using specific foraging strategies such as fish stranding (Jimenez and Alava, 2015), in some areas. Studies on mtDNA variation showed that this coastal population is genetically distinct from other coastal and offshore populations living in the south-east Pacific (Bayas-Rea *et al.* 2018). Morphometric studies supported these findings when discerning skull shape between these same populations (e.g. Peru and Ecuador; Santillán *et al.* 2008). However, a comparison with bottlenose dolphins from locations outside the Pacific has not been carried out.

Genetic studies have suggested a similar division in the Mediterranean, with several communities showing high site fidelity to coastal areas with varying degrees of social segregation from dolphins elsewhere. Overall, Mediterranean bottlenose dolphins occupy most coastal waters of the basin and, to a lesser extent, offshore waters around islands and archipelagos (Bearzi *et al.* 2005, 2008). They can form groups of between 4 to 20 individuals, depending on the ecological conditions of specific regions (Forcada *et al.* 2004). Some social groupings were shown to be mostly unstable, regularly changing in composition and size (Bearzi *et al.* 2005), without apparent sexual segregation reported so far (Bearzi *et al.* 1997). However, stable social units have been described in some locations. Most notably, dolphins inhabiting the Ligurian sea have been shown to form two large and stable social units along the coasts of Italy and Corsica that do not often interact with dolphins from elsewhere (Gnone *et al.* 2011; Carnabuci *et al.* 2016). Although no fine-scale data exist for the Ligurian sea, genetic studies elsewhere also found evidence of genetic structure between geographically close regions (Natoli *et al.* 2005; Gaspari *et al.* 2015a, b; Brotons *et al.* 2019). Therefore, multiple studies have referred to the Mediterranean *Tursiops* as having a meta-population structure (Nichols *et al.* 2007; Gaspari *et al.* 2015b; Carnabuci *et al.* 2016), which could include animals with a more typical offshore ecology (Gaspari *et al.* 2015b). However, no information to date exists on potential morphological differentiation between coastal and offshore specimens in the Mediterranean.

In the study of morphological variation, geometric morphometrics (GM) has been shown to be a useful tool to detect potential adaptive skull shape patterns in several vertebrate species and infer their driving factors (Christiansen 2008; Adams 2011; Cooke 2011; Fabre *et al.* 2014; Forrest *et al.* 2018; Borgard *et al.* 2020). One main benefit is that it assesses shape changes in biological forms regardless of size, which can be highly plastic. The method is based on placing key landmarks (LMs) distributed over the structure of interest (Richtsmeier *et al.* 2002). Although traditionally based on two-dimensional (2D) images, increasingly the analyses of three-dimensional shapes are favoured when using GM. Three-dimensional geometric morphometrics (3DGM) limits errors related to distortion effects generated from photographing or translating a 3D object into a 2D image (Buser *et al.* 2018), allowing a more robust evolutionary interpretation of the morphological changes.

Geometric morphometrics has been used previously in the analyses of cetaceans, providing important insights into the patterns and processes determining skull shape changes in several species. This includes understanding of ontogenic patterns in porpoises (Galatius *et al.* 2011), identifying ecological drivers of skull shape evolution across cetaceans (Galatius and Goodall 2016; McCurry *et al.* 2017a, b; Galatius *et al.* 2020), and describing the geographical variation of skull shape within dolphin species (Loy *et al.* 2011; Ngqulana *et al.* 2019b; Nicolosi and Loy 2019). Geometric morphometrics has been used to analyse morphological differentiation in *Tursiops* (e.g. Indian Ocean: Jedensjö *et al.* 2017, 2020; Gray *et al.* 2022; Ngqulana *et al.* 2019a; Brazil: Hohl *et al.* 2020; Mexico: Esteves-Ponte *et al.* 2022), although 3DGM has not yet been used extensively to distinguish skull shape between coastal and offshore ecotypes of bottlenose dolphins. A recent study used 3DGM in combination with other morphological and genetic data to investigate the evolutionary distinction between the ecotypes of the north-west Atlantic, with results supporting distinct species (Costa *et al.* 2022). This shows the potential of 3DGM to identify morphological variation in cetacean skulls. In the south-east Pacific, only 2D morphometric studies exist (Santillán *et al.* 2008), and none was carried out in the Mediterranean region.

Figure 1. Map showing sample number of common bottlenose dolphin individuals per location. Offshore populations in dark red, coastal populations from Guayaquil (Ecuador) in purple, coastal populations from the Mediterranean Sea in orange.

In this study, we present the results of our 3DGM analysis on skulls of bottlenose dolphins to identify cranial variation that is congruent with differential habitat use, with a focus on the coastal populations from the Gulf of Guayaquil and the Mediterranean Sea relative to offshore specimens. We test the following hypotheses: is there a significant distinction in skull shape between dolphins showing an offshore vs. coastal ecology in these regions? If so, do the different coastal ecotypes differ in their skull shape depending on location, or do they converge to similar skull shapes due to ecological similarity? We also test if the observed 3D shape changes can be used to predict the potential ecological drivers. Previous studies suggest that feeding habits, communication systems, diving patterns and other environmental factors could be responsible for skull shape patterns in *Tursiops* (e.g. Mead and Potter 1995; Perrin *et al.* 2011; Costa *et al.* 2016), and skull shape changes observed in coastal populations will be interpreted in light of their relevant ecological characteristics.

MATERIAL AND METHODS

Data collection

We analysed physically mature skulls of common bottlenose dolphins (*Tursiops truncatus*) kept at the Museo de Ballenas in Salinas (Ecuador), the Museum d'Histoire Naturelle in Paris (France), the Federal University of Santa Catarina (Brazil), the Museum of Natural History of Milan (Italy), and the Museo Civico di Storia Naturale 'Giacomo Doria' in Genova (Italy). Physically immature specimens were not analysed, since skull shape changes considerably during early life stages in Delphinidae (Perrin and Heyning 1993).

The specimens originated from the south-east Pacific, the Mediterranean Sea, north-east and south-west Atlantic (Fig. 1), and included both putative coastal and confirmed offshore specimens. Putative coastal specimens included those originating from the inner estuary of the Guayaquil Gulf (Ecuador) and the Ligurian and Adriatic seas in the Mediterranean. Offshore specimens were from the coast of Brazil [confirmed as offshore by Costa *et al.* (2016)], and the French Atlantic coast (which, based on previous genetic analyses, are most likely to be of the offshore ecotype; Quérouil *et al.* 2007), and from the central coast of Ecuador north of the Gulf of Guayaquil [as defined by Bayas-Rea *et al.* (2018), based on genetic analysis]. Full details and accession numbers of the specimens used here can be found in the Supporting Information, Table S1. Details regarding habitat classification also available in the Supporting Information, Table S2.

Image acquisition and three-dimensional modelling

Three-dimensional (3D) models were created for all specimens, using photogrammetric techniques based on 250 to 500 high-resolution digital photographs covering the entire surface of the skull. A standard photographing set-up protocol was replicated for each session to avoid systematic errors related to the equipment and image distortion. Photographs were taken using

a high-resolution DSLR camera (> 8 Megapixel) and ensuring a minimum lateral overlap of 60% and frontal overlap of 80% between consecutive photographs. For each specimen, a fixed focal length was used and kept constant throughout the photography session. Camera shooting settings depended on the lighting conditions in the room and aimed to optimize image sharpness and depth of field by finding a balance between the smallest aperture combined with the highest shutter speed possible.

Three-dimensional reconstruction from digital photographs was done using the open-source photogrammetry software MESHROOM v.2019.2.0 (Griwodz *et al.* 2021). MESHROOM applies a variety of algorithms to identify notable features within each image, which can then be reliably matched between images. Feature matching is then used to identify the relative position of individual photographs in 3D space together with camera specific information, such as focal length. Before model reconstruction, images were edited to improve tonal contrast and sharpening, to isolate the skulls from the background, and to increase the number of notable features visible on the skulls. Features were identified using the SIFT method (Scale-Invariant Feature Transformation; Otero and Delbracio 2014). Because we aimed at producing a 3D model of the entire skull that could be fully rotated, the SIFT_float method was used. For the feature-matching step, we used the option 'Guided matching', which improves the number of recognized cameras by producing a second stage in the matching procedure. Because the camera positioning changed between photographs, we also disabled the 'Use rig constraint' option. For specimens with < 300 images, we also added the 'Akaze' algorithm for feature identification (Alcantarilla *et al.* 2013) and changed the prescriber preset to 'High' to increase the number of features extracted from the pictures. We also decreased the 'Max Descriptors' and 'Number of matches' to 0, as this maximizes the number of descriptors used for the reconstruction and kept all matches recovered for downstream processing. The Downscale level was set to 1 in the 'Depth Map' node to increase the precision of the modelling, and lowered the 'minimum consistency camera' and the 'minimum consistency camera similarity' to 2 and 3, respectively, to maximize the completeness of the meshes in the final models. Full details of the parameters used during 3D reconstruction can be found in the Supporting Information, Table S3.

Landmark placement for geometric morphometrics

We performed GM skull shape analyses on the 3D models of 58 adult skull specimens, using two different landmarking strategies: manual and automatic. Manual landmarking is based on the prior selection of multiple landmarks in homologous features that can be placed consistently in all individuals analysed (Richtsmeier *et al.* 2002). It has been used extensively in GM studies to identify variation in specific morphological structures and relate them to other mechanisms, such as ontogenic development, ecologic, taxonomic, or biomechanic differences (Mitteroecker and Gunz 2009; Lawing and Polly 2010; Cooke and Terhune 2015). However, the process requires high precision and is time-consuming. Furthermore, it is typically based on relatively sparse landmark configurations, which can lose important geometric information by missing morphological features of interest when comparing variation between predefined groups.

Alternatively, automatic landmarking can be used to compensate for the limitations of manual landmarking. It requires less processing time and minimizes errors related to observer subjectivity or natural variability occurring among individuals (Gao *et al.* 2019). Automatic landmarking generates pseudo-landmarks based on point cloud registration, distributed all over the target 3D surface without considering homology. Compared to manual landmarking, it increases the overall surface coverage, which enables the capturing of more biological information. This is especially useful in structures with poor geometric shapes, where homologous points are difficult to determine (Gao *et al.* 2019). However, such methods are 'blind' to biological information and, therefore, carry the risk of more noisy inference when comparing the ecological significance of differences in biological structures. Therefore, in this study the two approaches are used to complement each other.

Manual landmarking

We imported 3D models into the software IDAV Landmark v.3.0 (Wiley 2005), and digitized 71 single-point LMs in homologous skull features and 340 semi-landmarks based on eight line and three patch guides (Fig. 2; Supporting Information, Table S4). For skulls where some of the target structures were missing (due to post-mortem damage), we used the R-package 'geomorph' (v.3.2.0) to estimate 3D LMs by applying the function 'estimate.missing' with the option thin-plate spline. The technique estimates landmark locations using a thin-plate spline on specimens with missing landmarks by first aligning it with a complete reference individual based on their common set of landmarks (Mitteroecker and Gunz 2009).

Automatic landmarking

We carried out automatic landmarking in the software 3D SLICER (Rolfe *et al.* 2021) using the ALPACA extension (Porto *et al.* 2021). ALPACA requires the selection of a 3D reference mesh (source) from which it creates template point clouds through global registration steps (Rusu *et al.* 2009). We chose the 3D reference mesh based on the skull integrity, and its shape being close to the mean skull shape determined by a preliminary analysis. This preliminary analysis consisted of an initial automatic landmarking on all individuals, using a well-preserved skull as reference without consideration of its position in the morphospace. This was followed by a preliminary generalized Procrustes analysis (GPA) and subsequent principal component analysis (PCA) on the landmarked skulls (as described in more detail below), after which we could choose a skull positioned at the centre of the morphospace. For the registration steps, we set the point density at 0.5, which automatically defined 724 single-point pseudo-landmarks distributed over the entire 3D skull meshes (Fig. 3). Then, the software produced a deformable registration step on the source point cloud to match the coordinates of the floating surface to the coordinate of the target surface. This allowed corresponding landmarks between source and target meshes to be transferred to all target specimens.

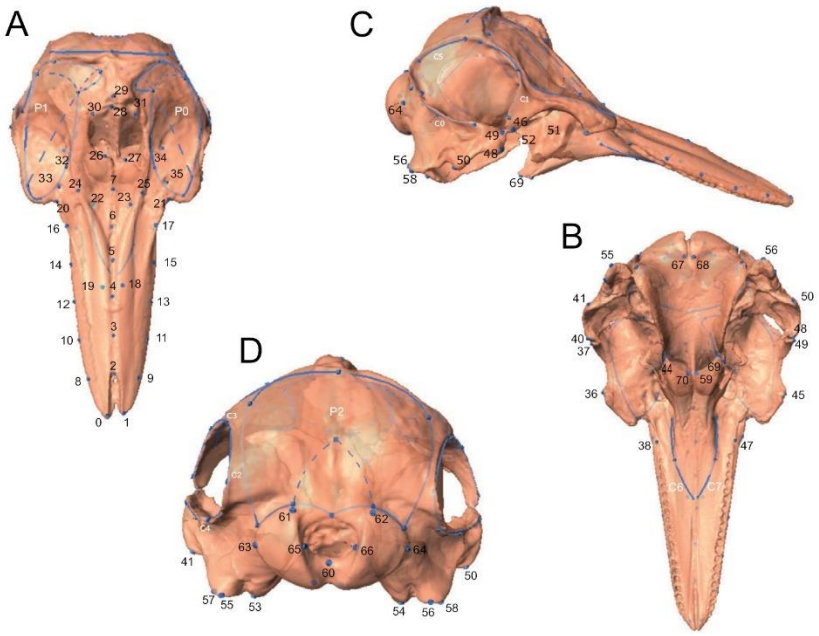

Figure 2. Three-dimensional landmarks used in this study, showed in dorsal (A), ventral (B), lateral (C), and occipital (D) aspects of the bottlenose dolphin skull.

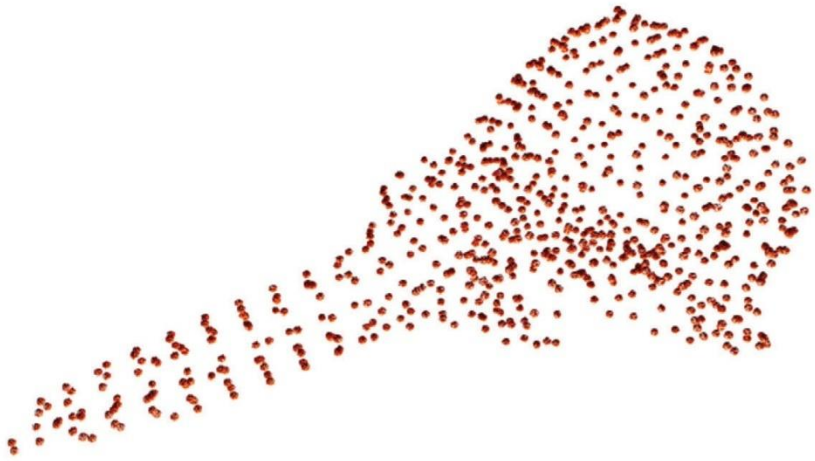

Figure 3. 3D LMs points generated from the automatic landmarking from the bottlenose dolphin skull reference template.

Geometric morphometric shape analysis

For both manual and automatic landmark datasets, we performed a GPA. It translated the centroids to a single origin, i.e. centred all shapes, scaled the LMs to the same centroid size, and rotated each shape around the centroid (Rohlf and Slice 1990). This produced a set of aligned Procrustes coordinates for each specimen, on which the effects of size, rotation, and translation were removed. Shape changes between specimens were identified by performing a PCA, which finds the axes of greatest variation in our dataset (principal components—PC), and groups specimens by similarity across each PC (Rohlf and Marcus 1993; Adams *et al.* 2004). GPA and PCA were performed independently for each of the landmark datasets produced earlier (manual and automatic) using the SLICER extension slicermorph (Rolfe *et al.* 2021). We visualized shape changes associated with PC axes using vector displacement graphs (also known broadly as a lollipop graphs) in slicermorph (Rolfe *et al.* 2021), and coloured each landmark according to their relative rate of change using the software PARAVIEW (Ahrens *et al.* 2005).

To test the differentiation in skull shape, we carried out multiple tests between *a priori* defined groups, which were implemented in the software PAST (Hammer *et al.* 2001). First, we determined five *a priori* groups distinguishing both habitat and geographic origin. The Guayaquil group consisted of specimens determined previously to belong to a resident population of the inner estuary of the Gulf of Guayaquil, based on behavioural, morphological, and genetic criteria (Félix 1997; Bayas-Rea *et al.* 2018; Félix *et al.* 2019). Individuals from Ecuador that were determined as not being part of this resident population were categorized as being offshore specimens from the south-east Pacific (OSEP). Further offshore groups included specimens sampled along the coast of Brazil, known to be taxonomically distinct from the local coastal ecotype (Costa *et al.* 2016; named Offshore South Atlantic—OSA), and specimens from the Atlantic coast of France (named Offshore North Atlantic—ONA). Finally, the Mediterranean group included specimens from the Mediterranean Sea along the Ligurian and Adriatic coasts. Since our tests showed no clear differentiation between the three *a priori* geographically distinct offshore groups (i.e. OSEP, OSA, ONA; see Results for more details, and Supporting Information Fig. S1), they were then clustered into a single *a priori* group consisting of offshore specimens.

All tests were based on the first 55 principal components (PC) scores as they represent approximately 95% of the total variance in our data. First, a non-parametric multivariate analysis of variance test (PERMANOVA) was performed on the PC scores. Additionally, we carried out a linear discriminant analysis (LDA) on the first 55 PC scores. This method carries a pairwise comparison between all defined groups to test how well individual specimens can be classified to their defined group according to their skull shapes. We considered groups to represent different morphotypes when results from the LDA specified that 90% or more of all specimens could be assigned to their respective groups.

We also carried out a hierarchical cluster analysis (HCA), which clusters the skulls based on their shape similarity defined by the first 55 PCs, without consideration of *a priori* groups. Ward's method was used as a clustering procedure.

Alveoli count

In addition to the landmarking, we also counted tooth alveoli numbers for both left and right upper tooth rows. When the rostrums were broken or tooth alveoli were undetectable, we did not include the individual in the analysis. Tests for differences in the alveoli counts between the *a priori* groups were carried out in the software PAST (Hammer *et al.* 2001). Normality tests for each *a priori* group were first carried out using the Shapiro–Wilk test, while homogeneity of variances was assessed through a Levene's test. Because data were not normally distributed and had unequal variances, differences in alveoli count were tested using a non-parametric Kruskal–Wallis test, with pairwise differences between groups assessed using the Dunn's post-hoc test.

RESULTS

The PCA morphospace results for the manual and automatic landmarking approaches are largely consistent in the patterns of shape differentiation between the samples analysed. However, there are differences in the resulting level of differentiation. Therefore, we present the PCA results from the automatic landmarking in the main text below, showing both results only when the downstream analyses are different. PCA and vector displacement graphs for manual landmarking are shown in the Supporting Information, Figs, S2, S4 and S6.

Shape variation between locations

The first three principal components together account for 24.9% of the total shape variation (PC1 = 10.6%, PC2 = 8.4%, PC3 = 5.9%) using the automatic landmarking. The PCA morphospace plot reveals that the strongest differentiation is between specimens from the Gulf of Guayaquil and specimens from the Mediterranean (Fig. 4). Both locations also separate well from confirmed offshore individuals, although there is more overlap between the Mediterranean and offshore specimens (Fig. 4). Visual analyses of the plot did not reveal any noticeable separation between offshore specimens from different regions (see Results further down for statistical testing results; Supporting Information, Fig. S1). PCA plot based on manual landmarking shown in Supporting Information, Fig. S2.

In terms of shape change, along PC1, a relative elongation of the rostrum is noticeable, with most changes occurring on the tip of the rostrum and the base of the rostrum, where elongation and narrowing of the palate are noticeable, with an accompanying expansion of the pterygoid bones. There is also a noticeable expansion of the supra-occipital region, causing an apparent contraction of the upper parietal bone. There is also a relative upward shift of the squamosal bone, which collectively would lead to a noticeable change in the shape of the temporal fossae (Fig. 4A; Supporting Information, Fig. S3). Along PC2, there is a noticeable lengthening of the rostrum, with an apparent narrowing and elongation of the upper part of the premaxillae. There is a pronounced contraction upward of the pterygoid bones, and a deepening of the ascending process of the maxilla is also visible (Fig. 4B; Supporting Information, Fig. S3). Along PC3, there is a shortening of the rostrum with an accompanying forward shift in the upper part of the premaxillae near the internal nares. There is also a visible extension backward of the lower edge of the temporal fossae, involving shifts of the frontal, squamosal, and temporal bones, accompanied by a compression of the occipital bone. Overall, specimens with positive PC3 values showed convex curving of the rostral area, with a more prominent rostral bump (Fig. 4C; Supporting Information, Fig. S3). Corresponding shape change plots based on manual landmarking available in Supporting Information, Fig. S4).

Overall, coastal specimens from the Mediterranean show a slender and longer skull, as revealed by the greater interlandmark distances in the rostrum, parietal, and pterygoid areas (Supporting Information, Fig. S5). Individuals from the Gulf of Guayaquil have stouter skulls than the offshore and coastal specimens from the Mediterranean, as revealed by the shortening of the frontal areas and a broadening of the exoccipital region (Fig. 4; Supporting Information, Fig. S5). Corresponding shape change plots based on manual landmarking, available in Supporting Information, Fig. S6.

In our dataset, three skulls showed considerable separation of the maxillary and premaxillary bones along the mid-palate

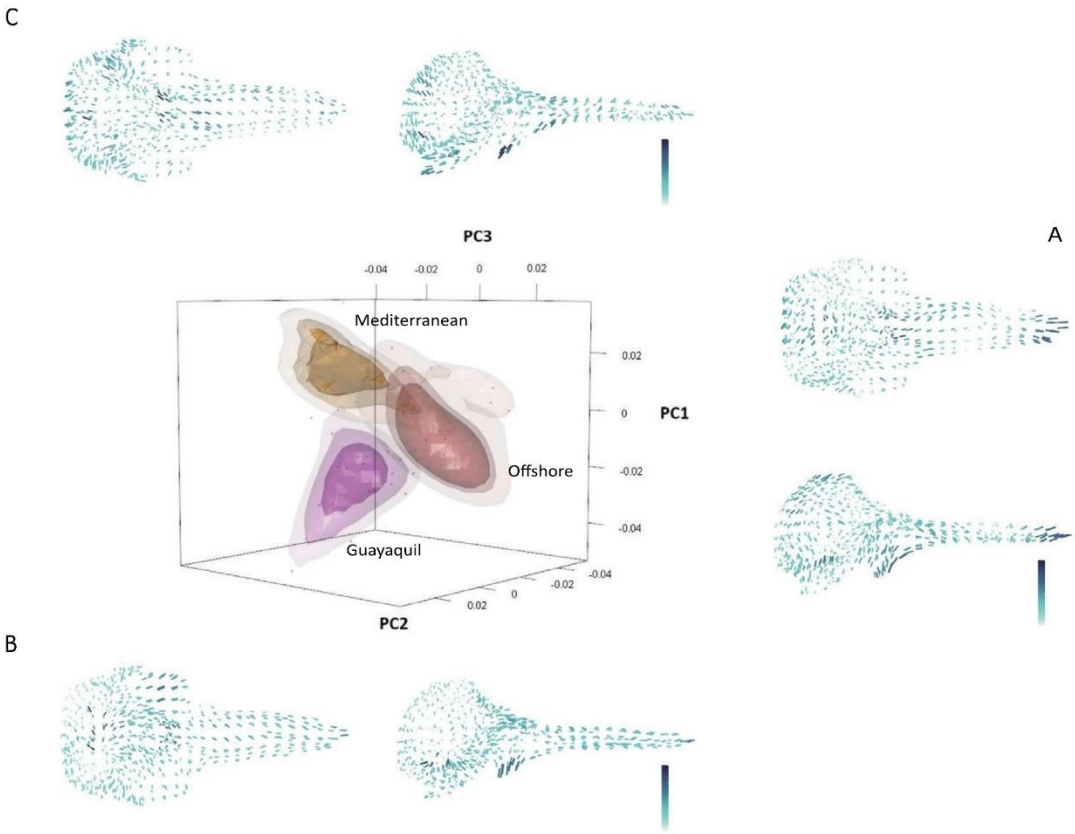

Figure 4. 3D PCA morphospace generated from the automatic landmarking procedure, with samples categorized by *a priori* groups. Shaded areas correspond to 90% kernel density clouds for each cluster, as calculated in the R package KS (Duong 2007). Line graphs around the PCA plot represent vector displacement graphs, which represent the difference in landmark position between the mean landmark configuration and specimens grouped along the positive PC1 (A), PC2 (B), and PC3 (C). Darker colour shows a higher rate of shape change for the corresponding landmark.

suture. This is a common modification in delphinid museum specimens resulting from drying of the bones over time, and it was not controlled for in our analyses. However, careful evaluation of the PCA plots revealed that the skulls containing this modification did not cluster together and were not ecotype-specific. This modification was also not shown in the shape deformation grids for the principal components explaining most of the variation. Therefore, although this deformation occurs in our dataset, it is unlikely to influence the conclusions regarding ecotype grouping. However, we cannot exclude other potential biases that might result from this issue in our dataset.

Statistical differentiation tests

Pairwise PERMANOVA analysis among the five a priori defined geographic groups found no significant differentiation in shape among the three a priori offshore groups (OSEP, OSA, ONA), but significant differentiation was observed between Gulf of Guayaquil and Mediterranean Sea with the other groups (Table 1). The significant differentiation between offshore and both Guayaquil and Mediterranean coastal groups was still present when all offshore specimens were pooled into a single group (Table 2). We should note that there was no difference in the statistical testing between the manual and the automatic landmarking datasets. The linear discriminant function analysis on the first 55 PC scores discriminating offshore (N = 18), Gulf of Guayaquil (N = 22), and the coastal Mediterranean (N = 18) specimens showed that all specimens could be correctly assigned to their respective groups when using both manual and automatic landmarking (Fig. 5).

The HCA shows some differences between the manual and automatic datasets. Both identify three main clusters among all specimens (Table 3), but the relationships estimated between those clusters change slightly (Fig. 6). When using automatic LMs, 77.3% of the Guayaquil specimens (Total N = 22) are assigned to cluster 1, whereas 38.9% of offshore specimens (Total N = 18) are assigned to cluster 2, and 88.9% of the Mediterranean specimens (Total N = 18) are assigned into cluster 3 (Table 3). Although more offshore individuals are assigned to cluster 3 than cluster 2, cluster 2 is still mostly represented by offshore specimens (63.6%) when compared to the other groups. When using manual LMs, 90.9% of the Guayaquil specimens (Total N = 22) are again assigned to cluster 1, whereas 77.8% of Mediterranean

specimens (Total $N = 18$) and 61.1% of the offshore specimens (Total $N = 18$) are now assigned to distinct clusters: cluster 2 and cluster 3, respectively (Table 3). Therefore, both datasets show good correspondence between clusters identified and our ecotype assignment, although the automatic landmarking groups more offshore specimens in the same cluster as the Mediterranean specimens. The two datasets also show different relationships in shape similarity between the three clusters. The automatic landmarking separates the Guayaquil specimens more clearly from both offshore and Mediterranean groups (Fig. 6A). However, the automatic landmarking places the offshore cluster closer to Guayaquil in shape similarity, with the Mediterranean being the most distinct (Fig. 6A). On the contrary, manual landmarking appears to place the Mediterranean cluster closer to the offshore one, but shows less cross-classification between both clusters (Fig. 6B).

Table 1. Pairwise PERMANOVA analysis on the first 55 PCs of principal component analysis (PCA) between *a priori* groups separating both habitat and geographical areas. Results are shown for both manual (regular text) and automatic (bold text) landmarks. *F*-values are shown above the empty diagonal cells, while *P*-values are shown below the empty diagonal cells. Significant comparisons are marked by an asterisk (*). Population abbreviations: OSEP—*Offshore Southeast Pacific*; ONA—*Offshore North Atlantic*; OSA—*Offshore South Atlantic*.

	Mediterranean	Guayaquil	OSEP	OSA	ONA
Mediterranean		9.208*/**4.614***	2.195*/**1.628***	3.277*/**1.968***	2.633*/**1.383**
Guayaquil	< 0.001*/< **0.001***		4.228*/**2.966***	2.425*/**2.754***	2.914*/**1.849***
OSEP	< 0.001*/**0.010***	< 0.001*/<**0.001***		1.406/**1.092**	1.329/**1.230**
OSA	< 0.001*/**0.002***	< 0.001*/<**0.001***	0.061/**0.284**		1.155/**1.332**
ONA	0.001*/**0.054**	< 0.001*/**0.002***	0.080/**0.122**	0.252/**0.120**	

Table 2. Pairwise PERMANOVA analysis on the first 55 PCs of principal component analysis (PCA), between *a priori* groups separating both coastal habitats from the offshore habitat using manual (regular text) and automatic (bold text) landmarks. *F*-values are shown above the empty diagonal cells, while *P*-values are shown below the empty diagonal cells. Significant comparisons are marked by an asterisk (*).

	Mediterranean	Guayaquil	Offshore
Mediterranean		9.208*/**4.614***	3.676*/**2.168***
Guayaquil	< 0.001*/< **0.001***		5.018*/**3.673***
Offshore	< 0.001*/< **0.001***	< 0.001*/< **0.001***	

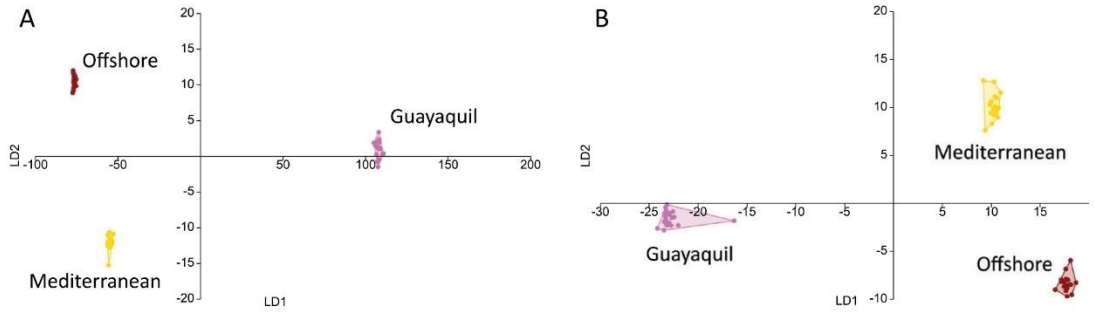

Figure 5. Linear discriminant analysis (LDA) on the first 55 PCs of principal component analysis (PCA) of the three *a priori* groups of bottlenose dolphins, generated from: A, manual landmarking; B, automatic landmarking.

Table 3. Distribution of bottlenose dolphin skulls over three clusters as inferred by the hierarchical cluster analyses (HCA). Results are shown for both automatic and manual landmarkings.

	Automatic			Manual		
	Cluster 1	**Cluster 2**	**Cluster 3**	**Cluster 1**	**Cluster 2**	**Cluster 3**
Offshore	0%	38.9%	61.1%	16.7 %	22.2 %	61.1 %
Mediterranean	0%	11.1 %	88.9%	5.5 %	77.8 %	16.7 %
Guayaquil	77.3%	9.1%	13.6%	90.9 %	0 %	9.1 %

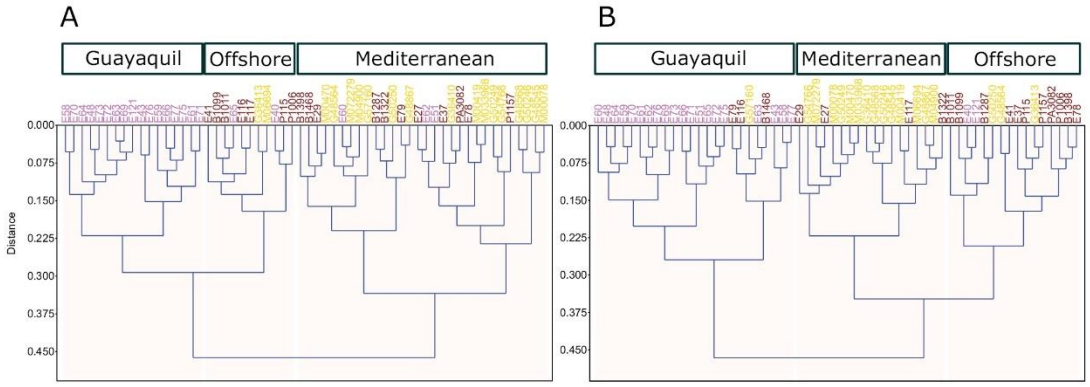

Figure 6. Ward's clustering analysis based on the first 55 PCs of principal component analysis (PCA) Euclidean distances: A, automatic landmarking; B, manual landmarking. Location shown indicates the origin of the majority of specimens within each cluster.

Alveoli counts

The Guayaquil dolphins have fewer alveoli than the Mediterranean and the offshore specimens. Guayaquil have a mean 18.9 alveoli on each tooth row of the maxillae (range 18–22), while the Mediterranean and the offshore specimens have mean 22.7 and 21.8 alveoli, respectively (range 20–25 and 20–23, respectively). Kruskal–Wallis test shows significant differences between the groups ($H = 29.89$; P-value = 2.3×10^{-8}). Pairwise Dunn's test shows significant differences between the Guayaquil and the other groups (all P-values <0.001), but no significant differences between the Mediterranean and the offshore groups (P-value = 0.82; Table 4). For some individuals, the alveoli of the first teeth at the tip of the rostrum were not visible. However, these were found in all groups equally, and therefore are unlikely to cause any bias.

Table 4. Pairwise Dunn's test results for comparison between *a priori* groups of teeth alveoli counts. P-values are shown above the empty diagonal cells, while Z-statistic is shown below the empty diagonal cells. Significant comparisons are marked by an asterisk (*).

	Offshore	Mediterranean	Guayaquil
Offshore		0.82	1.31×10^{-6}*
Mediterranean	0.23		2.36×10^{-7}*
Guayaquil	4.84*	5.17*	

DISCUSSION

Our GM study used a transoceanic approach to identify skull shape variations between coastal and offshore populations of bottlenose dolphins. Our results indicate that specimens from both the Gulf of Guayaquil (Ecuador) and the Mediterranean Sea differentiate well from offshore specimens originating from diverse ocean basins. However, the coastal populations from the Gulf of Guayaquil and the Mediterranean Sea are also clearly divergent from each other, meaning that each possess specific cranial morphological characteristics. There was an overlap observed in the morphospace between coastal and offshore specimens in both locations, although the overlap was more noticeable in specimens from the Mediterranean Sea.

Overall, coastal specimens differed from the offshores through the shape and length of their rostrum, the area surrounding the ascending processes of the maxilla, pterygoid bones and occipital regions. Results showed a relative shortening and broadening of Guayaquil dolphins' rostrums, a ventrodorsal contraction of the supraoccipital region, as well as lengthening downward of the pterygoid hamuli. These shape changes made the Guayaquil skulls appear generally stouter when compared to the offshore specimens (all changes refer to shape, as the analyses removed the effect of size). On the contrary, Mediterranean skulls displayed a slender shape, with a relative lengthening of their rostrums and occipital region relative to offshore specimens. Skull shape changes that appeared similar in both coastal populations relative to offshore include a broadening and lengthening of the upper part of the maxillae and premaxillae sac fossae, a frontward compression of the lower edge of the temporal fossae, a flattening of the lacrimal process (an exoccipital region further oriented toward the inside of the skull), and a lengthening of the posterior edge of the pterygoid hamulus. The pterygoid, though, was more aligned with the rest of the skull in the Mediterranean dolphins, while in Guayaquil individuals there was a more acute angle with the sagittal plane of the skull.

These results are consistent with previous morphometric studies on *Tursiops truncatus*, which found skull morphological differences between coastal and offshore environments around the world (Mead and Potter 1995; Turner and Worthy 2003; Santillán *et al.* 2008; Viaud-Martinez *et al.* 2008; Perrin *et al.* 2011; Costa *et al.* 2016; Hohl *et al.* 2020; Esteves-Ponte *et al.* 2022). Along the US Atlantic coast, coastal specimens could be differentiated from offshore by a combination of skull length and width, as well as width of the internal nares (Mead and Potter 1995), features that also distinguish coastal from offshore specimens in this study. In California, the shape of the temporal fossa was also found to differentiate between coastal and offshore specimens (Perrin *et al.* 2011). In this study, we found changes in several bones surrounding the mandibular joint, as well as changes in the supraoccipital, which would result in changes to the shape of the temporal fossa. In the coast of Brazil, another

feature that separated the coastal from offshore specimens was the shape of the premaxillary sac fossa and the prenarial triangle (Costa *et al.* 2016), which is also a feature identified in this study as being different between coastal and offshore specimens. These morphological traits were also found to separate coastal from offshore specimens in the Black Sea (Viaud-Martinez *et al.* 2008) and the Gulf of California (Esteves-Ponte *et al.* 2022). Previous studies with skulls from the south-east Pacific showed differences between coastal and offshore specimens at the anteorbital process, palatine, pterygoids, and form of occipital condyles (Van Waerebeek *et al.* 1990, 2017). Our study also detected changes in the areas involving the pterygoids, the orbital arches, and the basicranium. There were also changes detected in the palate region, associated with an overall shape change in the rostrum. However, our study showed that the magnitude of change was larger for the pterygoid bones and features associated with the shape of the rostrum.

Although our study identified diagnostic changes along common skull traits between coastal and offshore specimens, it shows that different coastal populations can also differ from each other. While previous studies did not always compare their coastal populations to the same offshore specimens, different relative patterns were sometimes reported. For example, while the coastals from the US Atlantic coast were reportedly smaller with a slender rostrum compared to offshores (Mead and Potter 1995; Costa *et al.* 2022), the California coastals appear overall more robust in their skull shapes (Perrin *et al.* 2011). The coastal specimens from Brazil were larger relative to offshore specimens (Costa *et al.* 2016). Our study compares both putative coastal animals against the same offshore specimens, which includes representatives from the Pacific and Atlantic Oceans, and our inference does also suggest that coastal animals from different locations display distinct skull shapes.

In this context, our use of two distinct landmarking strategies also provides insight regarding which context they might be most useful. While both effectively distinguished the two coastal populations, the automatic landmarking suggests that the Mediterranean differentiation is subtler compared to Guayaquil. This is not only consistent with the results obtained in the PCA morphospace, but also consistent with known ecological differences (as discussed below). Thus, while manual landmarking of known features might be more effective at identifying subtle differences in individual cases where differentiation is known to occur, automatic landmarking could be more suitable for the identification of relative patterns of differentiation in broader comparative studies.

Ecological data supporting local differentiation

The skull shape differentiation found in this study also matches other lines of evidence from those coastal areas. Previous studies on site fidelity and social behaviour in the Gulf of Guayaquil suggest a strong level of demographic independence between animals found frequently in the inner estuary of the Gulf, as opposed to the ones found outside the Gulf (Félix *et al.* 2019). Studies on mtDNA differentiation also show evidence of genetic differentiation, suggesting reduced gene flow between those two ecotypes (Bayas-Rea *et al.* 2018).

The Ligurian sea, where most of the specimens analysed in this study originated, was also suggested to include a localized social unit that is demographically independent of animals found in Sicily (Gnone *et al.* 2011; Carnabuci *et al.* 2016; Rossi *et al.* 2017; Terranova *et al.* 2021). In the Mediterranean Sea, genetic studies show population structuring from the Black Sea to the Atlantic, with genetic breaks matching environmental barriers (Natoli *et al.* 2005). The occurrence of individuals with a genetic profile typical of Atlantic offshore animals suggests the occurrence of the offshore ecotype within the Mediterranean (Gaspari *et al.* 2015b). Although bottlenose dolphins in the Mediterranean are more frequently sighted in nearshore waters (Bearzi *et al.* 2008; Gnone *et al.* 2011; Marini *et al.* 2015; Karamitros *et al.* 2020; ACCOBAMS 2021), the larger overlap in shape observed between the Mediterranean and offshore specimens suggests the occurrence of offshore animals in the Mediterranean and is consistent with a potential metapopulation dynamic in the region (Nichols *et al.* 2007; Gaspari *et al.* 2015b; Carnabuci *et al.* 2016).

Functional role of observed morphological changes

Our 3DGM approach allowed us to identify the main areas of skull shape change between these groups, showing that most changes involve rostrum shape, the concavity of the interorbital shield, and the shape of bones surrounding the mandibular joint. Those features naturally suggest roles for differences in feeding and sound production (as the interorbital shield accommodates the melon and associated musculature) (Harper *et al.* 2008).

Similar interpretations have been proposed by earlier studies, with suggestions that differences in prey size might be particularly relevant (McCurry *et al.* 2017a). In animals showing exaggerated extension of the rostrum (such as dolphins), the rostrum and the mandibular joint were shown to be areas of high mechanical strain (McCurry *et al.* 2017c). Longer and more robust rostrums with a higher number of teeth were often associated with dolphins' ability to capture large demersal prey living in coastal environments (Perrin *et al.* 2011; Costa *et al.* 2016). In addition, larger temporal fossae and maxillae in those individuals would permit the attachment of larger temporal muscles, allowing a more potent bite force when depredating larger prey (Perrin *et al.* 2011; Cozzi *et al.* 2016; Galatius *et al.* 2020).

Dolphins from the Gulf of Guayaquil have been reported to prey on demersal fish, such as sciaenids and small pelagic species (Félix 1994), but also a variety of other species including mullets, catfish, snooks, and carangids, as observed during feeding periods (Félix, **unpublished data**). They also often show strand-feeding behaviour, which is seen relatively rarely in this species (Jiménez and Alava 2015). There is no information on potential prey for offshore bottlenose in Ecuador, but studies elsewhere in the Pacific suggest a preference for small pelagic and mesopelagic fish (Walker *et al.* 1999; Van Waerebeek *et al.* 2017). Stomach content studies show that Mediterranean animals predominantly consume demersal fish, while offshore appear to feed on a mixture of pelagic fish and cephalopods (Martin 1986; Blanco *et al.* 2001; Santos *et al.* 2001; Bearzi *et al.* 2008). Differences in prey size have been suggested to be an important driver of skull shape changes in delphinids more broadly (Perrin *et al.* 2011; McCurry *et al.* 2017b) and, therefore, prey size differences could also be driving the skull shape differences described here.

Another important ecological difference that could be driving these skull differences is the behaviour required to exploit locally abundant prey. In Delphinids, the hamuli are directly involved in sound production (Cozzi *et al.* 2016), and a previous study suggested that thicker and longer hamuli in offshore specimens could facilitate tracking of smaller and more challenging prey via echolocation (Perrin *et al.* 2011). Similarly, modifications of the maxillae were associated with specific sound emission and reception, and some authors have argued that larger premaxillae and interorbital shields (maxillae and lacrimals involved) could act as a reflector in dolphins (Geisler *et al.* 2014). Coastal dolphins in the Gulf of Guayaquil live in an environment with poor visibility due to the sediment charge of rivers, which could demand more frequent use of echolocation compared to other environments with better visibility.

In this study, offshore specimens showed a more prominent rostral bump and more concave premaxillae at the interorbital shield region. This area corresponds to the melon attachment area (Harper *et al.* 2008). Previous studies identified divergences in whistle patterns between populations of bottlenose dolphins living in different Mediterranean basins (La Manna *et al.* 2020). Therefore, the changes in rostral bump found in the offshore specimens relative to those of the Mediterranean could be related to divergent acoustic requirements associated with their differing ecology. The higher concavity of the premaxillae suggests a potentially larger melon, although we lack concrete data to support this. A study comparing external morphology in Brazil concluded that offshore animals had a proportionally shorter rostrum relative to coastal, which translates into a noticeably larger melon, although no direct melon measurements were taken (Simões-Lopes *et al.* 2019).

It is common for the bottlenose dolphin to develop complex behaviours associated with specific foraging techniques. These foraging techniques can be habitat-specific and have, in some cases, been learned socially (Gazda *et al.* 2005; Pennino and Floris 2013; Whitehead and Rendell 2014). Therefore, we hypothesize that distinct environments could require different behavioural strategies for effective survival. The Mediterranean Sea is a large and heterogenous body of water, although it is generally oligotrophic with high oxygen and salt concentrations and low freshwater inputs (Bas 2009; Coll *et al.* 2010). The Ligurian Sea, from where most of the skull specimens used in this study originated from, is a relatively deep basin, with steep, narrow, continental shelf areas in nearby coastlines (Pinardi *et al.* 2006). It is characterized by the convergence of multiple main-water currents, leading to seasonal upwelling (Prieur *et al.* 2020). Conversely, the inner estuary of the Guayaquil Gulf is a small, semi-enclosed body of water, which records high fluctuations in saline composition due to variations in freshwater input yearly (Twilley *et al.* 2001). There is also a high tidal range (around 3 m) that produces strong currents (up to 100 cm/s). The two coastal environments are, therefore, divergent and may also require specific adaptive behaviours.

CONCLUSIONS

In this study, we show that 3DGM, using either manual or automatic landmarking, is a useful tool for identifying significant skull shape differences, not only between dolphins with differing ecologies but also between the coastal specimens of Guayaquil and the Mediterranean. Offshore specimens from different geographical locations showed considerable overlap in skull shape, even between geographically distant areas.

Contrastingly, there was comparatively little overlap between offshore specimens and both coastal populations, although this overlap was noticeably larger in the Mediterranean. Skulls of Guayaquil dolphins looked relatively more robust and had significantly lower tooth count than the offshore and the Mediterranean populations. Contrastingly, the Mediterranean skulls were longer and slenderer compared to others, but did not differentiate in tooth count from offshore specimens. The patterns of shape changes are consistent with previous suggestions that feeding (i.e. prey type and size) and sound production might be ecological drivers. We, therefore, hypothesize that skull differentiation between the two coastal environments may be a response to living in divergent local environments.

Future studies should aim to compare 3D skull shapes between other coastal and offshore ecotypes of bottlenose dolphins. This would improve our understanding of the cranium shape patterns in this clade by analysing the entire 3D surface of each specimen. In addition, more studies are needed on local differences in diets (i.e. stable isotopes or stomach contents), as well as acoustic and genomic composition, providing a deeper insight into the evolutionary ecology of this complex species.

SUPPLEMENTARY DATA

Supplementary data is available at *Zoological Journal of the Linnean* online.

Table S1. Accession numbers and details of the specimens used in the analysis.

Table S2. The number of individuals per geographical area and habitat type.

Table S3. Description of the parameters used for the 3D modelling in MESHROOM.

Table S4. Description of the manual LMs used in this study, as shown in Figure 2.

Figure S1. 2D PCA morphospace generated from the automatic landmarking procedure, with samples categorized by habitat and geographical area. Specimens from the Gulf of Guayaquil shown in magenta; Offshore from the Southeast Pacific in light blue (OSEP); Offshore from the South Atlantic in dark blue (OSA); Offshore from the North Atlantic in red (ONA); specimens from the Mediterranean Sea in orange.

Figure S2. 3D PCA morphospace and kernel density cloud generated from the manual landmarking procedure, with samples categorized by habitat. Offshore populations in red, coastal populations from Guayaquil (Ecuador) in magenta, and from the Mediterranean in orange.

Figure S3. Landmark vector displacement plots (Lollipops) between the three ecotypes from the automatic landmarking. Lines represent the difference in landmark position between the mean landmark configuration (black dots) and specimens grouped along the positive PC axis. PC1 is represented in red, PC2 in green and PC3 in blue.

Figure S4. Landmark vector displacement plots (Lollipops) between the three ecotypes from the manual landmarking. Lines

represent the difference in landmark position between the mean landmark configuration (black dots) and specimens grouped along the positive PC axis. PC1 is represented in red, PC2 in green and PC3 in blue.

Figure S5. 3D PCA morphospace and kernel density cloud generated from the automatic landmarking procedure, comparing Guayaquil vs. offshore specimens only (top), and Mediterranean vs. offshore specimens only (bottom). Landmark vector displacement plots (lollipops) represent the difference in landmark position between the mean landmark configuration and specimens grouped along the positive PC1 (A), PC2 (B), and PC3 (C).

Figure S6. Landmark vector displacement plots (lollipops) for manual landmarking between offshore and Guayaquil specimens (left, magenta), and between offshore and Mediterranean (right, orange). Lines represent the difference in landmark position between the mean landmark configuration and specimens grouped along the positive PC axis.

ACKNOWLEDGEMENTS

This project is funded by the Polish National Science Centre (NCN) Preludium-BIS research grant nr 2019/35/O/NZ8/03900, awarded to AEM, in support of M.D.'s Ph.D.. We would also like to thank Dr Kent Mori (National Museum of Nature and Science, Tokyo; The Museum on the Street) for his role in training our research group on the basics of 3D photogrammetry. We also acknowledge the work of all museum staff, who contributed to maintaining the museum collections over the years. A.E.M. was supported by the Polish National Science Centre (Sonata research grant 2018/31/D/NZ8/02835) and the Polish National Agency for Academic Exchange (NAWA Ulam programme PPN/ULM/2019/1/00162).

FUNDING

This research was funded by the Polish Narodowe Centrum Nauki (NCN), through the Preludium-BIS scholarship number 2019/35/O/NZ8/03900. AEM was further supported by the Narodowe Centrum Nauki (NCN) Sonata programme (nr 2018/31/D/NZ8/02835) and the Narodowa Agencja Wymiany Akademickiej (NAWA) Ulam programme (PPN/ULM/2019/1/00162).

DATA AVAILABILITY

Landmark data used in this publication are available as a Mendeley dataset, doi: 10.17632/ggkx4jwnmf.1

CONFLICT OF INTEREST

The authors declare no conflict of interests.

REFERENCES

ACCOBAMS. 2021. *Estimates of Abundance and Distribution of Cetaceans, Marine Mega-fauna and Marine Litter in the Mediterranean Sea from 2018–2019 Surveys*. Panigada S, Boisseau O, Canadas A, Lambert C, Laran S, McLanaghan R, Moscrop A (ed.). Monaco: ACCOBAMS Survey Initiative Project, 177.

Adams DC. Quantitative genetics and evolution of head shape in *Plethodon* salamanders. *Evol Biol* 2011;**38**:278–86.

Adams DC, Rohlf FJ, Slice DE. Geometric morphometrics: ten years of progress following the 'revolution'. *Ital J Zool* 2004;**71**:5–16.

Ahrens J, Geveci B, Law C. ParaView: an end-user tool for large data visualization. In: Hansen CD, Johnson CR (ed.), *The Visualization Handbook*. Amsterdam: Elsevier, 2005.

Alcantarilla P, Nuevo J, Bartoli A. Fast explicit diffusion for accelerated features in nonlinear scale spaces. In: Burghardt T, Damen D, Mayol-Cuevas W, Mirmehdi M (ed.), BMVC 2013—Electronic Proceedings of the British Machine Vision Conference 2013, 2013.

Barros NB, Wells RS, Barros NB. Prey and feeding patterns of resident bottlenose dolphins (*Tursiops truncatus*) in Sarasota bay, Florida. *J Mammal* 1998;**79**:1045–59.

Bas C. The Mediterranean: a synoptic overview. *Contributions Sci* 2009;**5**:25–39.

Bayas-Rea R, Félix F, Montufar R. Genetic divergence and fine scale population structure of the common bottlenose dolphin (*Tursiops truncatus*, Montagu) found in the Gulf of Guayaquil, Ecuador. *PeerJ* 2018;**6**:e4589.

Bearzi G, Notarbartolo-Di-Sciara G, Politi E. Social ecology of bottlenose dolphins in the Kvarneric (northern Adriatic Sea). *Mar Mamm Sci* 1997;**13**:650–68.

Bearzi G, Politi E, Agazzi S *et al.* Occurrence and present status of coastal dolphins (*Delphinus delphis* and *Tursiops truncatus*) in the Eastern Ionian Sea. *Aquat Conserv Mar Freshwater Ecosyst* 2005;**15**:243–57.

Bearzi G, Fortuna CM, Reeves RR. Ecology and conservation of common bottlenose dolphins *Tursiops truncatus* in the Mediterranean Sea. *Mammal Rev* 2008;**39**:92–123.

Blanco C, Salomón O, Raga JA. Diet of the bottlenose dolphin (*Tursiops truncatus*) in the Western Mediterranean Sea. *J Mar Biol Assoc U K* 2001;**81**:1053–8.

Borgard HL, Baab K, Pasch B *et al.* The shape of sound: a geometric morphometrics approach to laryngeal functional morphology. *J Mamm Evol* 2020;**27**:577–90.

Borrell A, Vighi M, Genov T *et al.* Feeding ecology of the highly threatened common bottlenose dolphin of the Gulf of Ambracia, Greece, through stable isotope analysis. *Mar Mamm Sci* 2021;**37**:98–110.

Brotons JM, Islas-Villanueva V, Alomar C *et al.* Genetics and stable isotopes reveal non-obvious population structure of bottlenose dolphins (*Tursiops truncatus*) around the Balearic Islands. *Hydrobiologia* 2019;**842**:233–47.

Buser TJ, Sidlauskas BL, Summers AP. 2D or not 2D? Testing the utility of 2D vs. 3D landmark data in geometric morphometrics of the sculpin subfamily Oligocottinae (Pisces; Cottoidea). *Anat Rec* 2018;**301**:806–18.

Carnabuci M, Schiavon G, Bellingeri M *et al.* Connectivity in the network macrostructure of *Tursiops truncatus* in the Pelagos sanctuary (NW Mediterranean Sea): does landscape matter? *Popul Ecol* 2016;**58**:249–64.

Christiansen P. Evolution of skull and mandible shape in cats (Carnivora: Felidae). *PLoS One* 2008;**3**:e2807.

Coll M, Piroddi C, Steenbeek J *et al.* The biodiversity of the Mediterranean Sea: estimates, patterns, and threats. *PLoS One* 2010;**5**:e11842.

Cooke SB. Paleodiet of extinct platyrrhines with emphasis on the Caribbean forms: three-dimensional geometric morphometrics of mandibular second molars. *Anat Rec* 2011;**294**:2073–91.

Cooke SB, Terhune CE. Form, function, and geometric morphometrics. *Anat Rec* 2015;**298**:5–28.

Costa A, Rosel P, Daura-Jorge F *et al.* Offshore and coastal common bottlenose dolphins of the western South Atlantic face-to-face: what the skull and the spine can tell us. *Mar Mamm Sci* 2016;**32**:1433–57.

Costa AP, Fruet PF, Secchi ER *et al.* Ecological divergence and speciation in common bottlenose dolphins in the Western South Atlantic. *J Evol Biol* 2021;**34**:16–32.

Costa APB, Mcfee W, Wilcox LA *et al.* The common bottlenose dolphin (*Tursiops truncatus*) ecotypes of the western North Atlantic revisited: an integrative taxonomic investigation supports the presence of distinct species. *Zool J Linn Soc* 2022;**196**:1608–36.

Cozzi B, Huggenberger S, Oelschläger H. Head and senses. In: Cozzi B, Huggenberger S, Oelschläger H (eds), *Anatomy of Dolphins: Insights into Body Structure and Function*. London: Academic Press, 2016, 133–196.

Díaz-Gamboa RE, Gendron D, Busquets-Vass G. Isotopic niche width differentiation between common bottlenose dolphin ecotypes and sperm whales in the Gulf of California. *Mar Mamm Sci* 2018;**34**:440–57.

Duong T. Ks: kernel density estimation and kernel discriminant analysis for multivariate data in R. *J Stat Softw* 2007;**21**:1–16.

Esteves-Ponte MA, Aurioles-Gamboa D, García-Rodríguez FJ. Skull morphometric variability related to offshore and inshore ecotypes of the common bottlenose dolphin (*Tursiops truncatus*) from northwestern Mexico. *Mar Mamm Sci* 2022;**38**:1088–103.

Fabre AC, Cornette R, Huyghe K *et al.* Linear versus geometric morphometric approaches for the analysis of head shape dimorphism in lizards. *J Morphol* 2014;**275**:1016–26.

Félix F. Ecology of the coastal bottlenose dolphin *Tursiops truncatus* in the Gulf of Guayaquil, Ecuador. *Investigations on Cetacea* 1994;**25**:235–56.

Félix F. Organization and social structure of the coastal bottlenose dolphin *Tursiops truncatus* in the Gulf de Guayaquil, Ecuador. *Aquat Mamm* 1997;**23**:1–16.

Félix F, Burneo S. Imminent risk of extirpation for two bottlenose dolphin communities in the Gulf of Guayaquil, Ecuador. *Front Mar Sci* 2020;**7**:1–17.

Félix F, Calderón A, Vintimilla M *et al.* Decreasing population trend in coastal bottlenose dolphin (*Tursiops truncatus*) from the Gulf of Guayaquil, Ecuador. *Aquat Conserv Mar Freshwater Ecosyst* 2017;**27**:856–66.

Félix F, Centeno R, Romero J *et al.* Prevalence of scars of anthropogenic origin in coastal bottlenose dolphin in Ecuador. *J Mar Biol Assoc U K* 2018;**98**:1177–86.

Félix F, Zavala M, Centeno R *et al.* Spatial distribution, social structure and conservation threats of a small community of bottlenose dolphins, *Tursiops truncatus* (Odontoceti: Delphinidae) in Ecuador. *Revista de Biología Tropical* 2019;**67**:1059–76.

Fernández R, García-Tiscar S, Santos MB *et al.* Stable isotope analysis in two sympatric populations of bottlenose dolphins *Tursiops truncatus*: evidence of resource partitioning? *Mar Biol* 2011;**158**:1043–55.

Forcada J, Gazo M, Aguilar A *et al.* Bottlenose dolphin abundance in the NW Mediterranean: addressing heterogeneity in distribution. *Mar Ecol Prog Ser* 2004;**275**:275–87.

Forrest FL, Plummer TW, Raaum RL. Ecomorphological analysis of bovid mandibles from Laetoli Tanzania using 3D geometric morphometrics: implications for hominin paleoenvironmental reconstruction. *J Hum Evol* 2018;**114**:20–34.

Galatius A, Goodall RNP. Skull shapes of the Lissodelphininae: radiation, adaptation and asymmetry. *J Morphol* 2016;**277**:776–85.

Galatius A, Berta A, Frandsen MS *et al.* Interspecific variation of ontogeny and skull shape among porpoises (Phocoenidae). *J Morphol* 2011;**272**:136–48.

Galatius A, Racicot R, McGowen M *et al.* Evolution and diversification of delphinid skull shapes. *iScience* 2020;**23**:101543.

Gannon DP, Waples DM. Diets of coastal bottlenose dolphins from the U.S. Mid-Atlantic coast differ by habitat. *Mar Mamm Sci* 2004;**20**:527–45.

Gao T, Kovalsky SZ, Boyer DM *et al.* Gaussian process landmarking for three-dimensional geometric morphometrics. *SIAM J Math Data Sci* 2019;**1**:237–67.

Gaspari S, Holcer D, Mackelworth P *et al.* Population genetic structure of common bottlenose dolphins (*Tursiops truncatus*) in the Adriatic Sea and contiguous regions: implications for international conservation. *Aquat Conserv Mar Freshwater Ecosyst* 2015a;**25**:212–22.

Gaspari S, Scheinin A, Holcer D *et al.* Drivers of population structure of the bottlenose dolphin (*Tursiops truncatus*) in the Eastern Mediterranean Sea. *Evol Biol* 2015b;**42**:177–90.

Gazda SK, Connor RC, Edgar RK *et al.* A division of labour with role specialization in group hunting bottlenose dolphins (*Tursiops truncatus*) off Cedar Key, Florida. *Proc R Soc B: Biol Sci* 2005;**272**:135–40.

Geisler JH, Colbert MW, Carew JL. A new fossil species supports an early origin for toothed whale echolocation. *Nature* 2014;**508**:383–6.

Gibbs SE, Harcourt RG, Kemper CM *et al.* Niche differentiation of bottlenose dolphin species in South Australia revealed by stable isotopes and stomach contents. *Wildl Res* 2011;**38**:261–70.

Giménez J, Marçalo A, Ramírez F *et al.* Diet of bottlenose dolphins (*Tursiops truncatus*) from the Gulf of Cadiz: insights from stomach content and stable isotope analyses. *PLoS One* 2017;**12**:e0184673.

Gnone G, Bellingeri M, Dhermain F *et al.* Distribution, abundance, and movements of the bottlenose dolphin (*Tursiops truncatus*) in the Pelagos Sanctuary MPA (northwest Mediterranean Sea). *Aquat Conserv Mar Freshwater Ecosyst* 2011;**21**:372–88.

Gray H, Van Waerebeek K, Owen J *et al.* Evolutionary drivers of morphological differentiation among three bottlenose dolphin lineages, *Tursiops spp.* (Delphinidae), in the Northwest Indian ocean utilizing linear and geometric morphometric techniques. *Biol J Linn Soc* 2022;**135**:610–29.

Griwodz C, Gasparini S, Calvet L, Gurdjos P, Castan F, Maujean B, Lillo GD, Gasparini S, Calvet L, Gurdjos P, Castan F, Maujean B, Lanthony Y, De Lillo G. AliceVision Meshroom: An open-source 3D reconstruction pipeline. *Proc. 12th ACM Multimed Syst Conf* 2021.

Hammer O, Harper DAT, Ryan PD. PAST: paleontological statistics software package for education and data analysis. *Palaeontol Electronica* 2001;**4**:1–9.

Harper CJJ, McLellan WAA, Rommel SAA *et al.* Morphology of the melon and its tendinous connections to the facial muscles in bottlenose dolphins (*Tursiops truncatus*). *J Morphol* 2008;**269**:820–39.

Hersh SL, Duffield DA. Distinction between northwest Atlantic offshore and coastal bottlenose dolphins based on hemoglobin profile and morphometry. In: Leatherwood S, Reeves RR (eds), *The Bottlenose Dolphin*. Amsterdam: Elsevier, Academic Press, 1990, 129–40.

Hoelzel AR, Potter CW, Best PB. Genetic differentiation between parapatric nearshore and offshore populations of the bottlenose dolphin. *Proc R Soc Lond Ser B: Biol Sci* 1998;**265**:1177–83.

Hohl LSL, Sicuro FL, Wickert JC *et al.* Skull morphology of bottlenose dolphins from different ocean populations with emphasis on South America. *J Morphol* 2020;**281**:564–77.

Jedensjö M, Kemper CM, Krützen M. Cranial morphology and taxonomic resolution of some dolphin taxa (Delphinidae) in Australian waters, with a focus on the genus *Tursiops*. *Mar Mamm Sci* 2017;**33**:187–205.

Jedensjö M, Kemper CM, Milella M *et al.* Taxonomy and distribution of bottlenose dolphins (genus *Tursiops*) in Australian waters: an osteological clarification. *Can J Zool* 2020;**98**:461–79.

Jiménez PJ, Alava JJ. Strand-feeding by coastal bottlenose dolphins (*Tursiops truncatus*) in the Gulf of Guayaquil, Ecuador. *Latin Am J Aquat Mamm* 2015;**10**:33–7.

Karamitros G, Gkafas GA, Giantsis IA *et al.* Model-based distribution and abundance of three delphinidae in the Mediterranean. *Animals* 2020;**10**:260.

Kenney RD. 1990. Bottlenose dolphins off the Northeastern United States. In: Leatherwood S, Reeves RR (eds), *The Bottlenose Dolphin*. Amsterdam: Elsevier, Academic Press, 369–86.

La Manna G, Rako-Gospić N, Sarà G *et al.* Whistle variation in Mediterranean common bottlenose dolphin: the role of geographical, anthropogenic, social, and behavioral factors. *Ecol Evol* 2020;**10**:1971–87.

Lawing AM, Polly PD. Geometric morphometrics: recent applications to the study of evolution and development. *J Zool* 2010;**280**:1–7.

Loy A, Tamburelli A, Carlini R *et al.* Craniometric variation of some Mediterranean and Atlantic populations of *Stenella coeruleoalba* (Mammalia, Delphinidae): a three-dimensional geometric morphometric analysis. *Mar Mamm Sci* 2011;**27**:E65–78.

Machado FA. Selection and constraints in the ecomorphological adaptive evolution of the skull of living canidae (Carnivora, mammalia). *Am Nat* 2020;**196**:197–215.

Marini C, Fossa F, Paoli C *et al.* Predicting bottlenose dolphin distribution along Liguria coast (northwestern Mediterranean Sea) through different modeling techniques and indirect predictors. *J Environ Manage* 2015;**150**:9–20.

Martin AR. Feeding association between dolphins and shearwaters around the Azores Islands. *Can J Zool* 1986;**64**:1372–4.

McCabe EJB, Gannon DP, Barros NB *et al.* Prey selection by resident common bottlenose dolphins (*Tursiops truncatus*) in Sarasota Bay, Florida. *Mar Biol* 2010;**157**:931–42.
McCurry MR, Evans AR, Fitzgerald EMGG *et al.* The remarkable convergence of skull shape in crocodilians and toothed whales. *Proc R Soc B: Biol Sci* 2017a;**284**:20162348.
McCurry MR, Fitzgerald EMG, Evans AR *et al.* Skull shape reflects prey size niche in toothed whales. *Biol J Linn Soc* 2017b;**121**:936–46.
McCurry MR, Walmsley CW, Fitzgerald EMG *et al.* The biomechanical consequences of longirostry in crocodilians and odontocetes. *J Biomech* 2017c;**56**:61–70.
Mead J, Potter C. Recognizing two populations of the bottlenose dolphin (*Tursiops truncatus*) of the Atlantic coast of North America-morphologic and ecologic considerations. *IBI Rep* 1995;**5**:31–44.
Mitteroecker P, Gunz P. Advances in geometric morphometrics. *Evol Biol* 2009;**36**:235–47.
Moura AE, Shreves K, Pilot M *et al.* Phylogenomics of the genus *Tursiops* and closely related Delphininae reveals extensive reticulation among lineages and provides inference about eco-evolutionary drivers. *Mol Phylogenet Evol* 2020;**146**:106756.
Natoli A, Peddemors VM, Rus Hoelzel A. Population structure and speciation in the genus *Tursiops* based on microsatellite and mitochondrial DNA analyses. *J Evol Biol* 2004;**17**:363–75.
Natoli A, Birkun A, Aguilar A *et al.* Habitat structure and the dispersal of male and female bottlenose dolphins (*Tursiops truncatus*). *Proc R Soc B: Biol Sci* 2005;**272**:1217–26.
Ngqulana SG, Pistorius P, Galatius A *et al.* Variation in cranial morphology of bottlenose dolphins (genus *Tursiops*) off South Africa. *Mar Mamm Sci* 2019a;**35**:617–36.
Ngqulana SG, Plön S, Galatius A *et al.* Cranial variation in common dolphins *Delphinus* spp. off South Africa, with the inclusion of information from the holotype of *Delphinus capensis*. *Afr J Mar Sci* 2019b;**41**:247–60.
Nichols C, Herman J, Gaggiotti OE *et al.* Genetic isolation of a now extinct population of bottlenose dolphins (*Tursiops truncatus*). *Proc R Soc B: Biol Sci* 2007;**274**:1611–6.
Nicolosi P, Loy A. Geometric morphometric methods as complementary tools to investigate variability in common dolphins (*Delphinus* sp.) using museum specimens. *Aquat Conserv Mar Freshwater Ecosyst* 2019;**31**:22–35.
Otero IR, Delbracio M. Anatomy of the SIFT method, image processing. *Image Process Line* 2014;**4**:370–96.
Parsons KM, Durban JW, Claridge DE *et al.* Population genetic structure of coastal bottlenose dolphins (*Tursiops truncatus*) in the northern Bahamas. *Mar Mamm Sci* 2006;**22**:276–98.
Pennino MG, Floris A. Assessing foraging tradition in wild bottlenose dolphins (*Tursiops truncatus*). *Aquat Mamm* 2013;**39**:282–9.
Pereira LB, Botta S, Teixeira CR *et al.* Feeding ecology of two subspecies of bottlenose dolphin: a tooth tale. *Aquat Ecol* 2020;**54**:941–55.
Perrin WF, Heyning JE. Rostral fusion as a criterion of cranial maturity in the common dolphin, *Delphinus delphis*. *Mar Mamm Sci* 1993;**9**:195–7.
Perrin WF, Thieleking JL, Walker WA *et al.* Common bottlenose dolphins (*Tursiops truncatus*) in California waters: cranial differentiation of coastal and offshore ecotypes. *Mar Mamm Sci* 2011;**27**:769–92.
Pinardi N, Arneri E, Crise A *et al.* The physical, sedimentary and ecological structure and variability of shelf areas in the Mediterranean sea. In: Robinson AR, Brink KH (eds), *The Sea: Ideas and Observations on Progress in the Study of the Seas*. Volume **14**: Interdisciplinary Regional Studies and Syntheses. Cambridge, MA: Harvard University Press, 2006, 1243–330.
Porto A, Rolfe S, Maga AM. ALPACA: a fast and accurate computer vision approach for automated landmarking of three-dimensional biological structures. *Methods Ecol Evol* 2021;**12**:2129–44.
Prieur L, D'Ortenzio F, Taillander V *et al.* Physical oceanography of the Ligurian Sea. In: Migon C, Nival P, Sciandra A (eds), *The Mediterranean Sea in the Era of Global Change 1: 30 Years of Multidisciplinary Study of the Ligurian Sea*. London: Wiley-ISTE, 2020, 49–78.
Quérouil S, Silva MA, Freitas L *et al.* High gene flow in oceanic bottlenose dolphins (*Tursiops truncatus*) of the North Atlantic. *Conserv Genet* 2007;**8**:1405–19.
Richtsmeier JT, Deleon VB, Lele SR. The promise of geometric morphometrics. *Am J Biol Antrhopol* 2002;**119**:63–91.
Rohlf JF, Marcus LF. A revolution morphometrics. *Trends Ecol Evol*1993;**8**:129–32.
Rohlf JF, Slice D. Extensions of the procrustes method for the optimal superimposition of landmarks. *Syst Zool* 1990;**39**:40–59.
Rolfe S, Pieper S, Porto A *et al.* SlicerMorph: an open and extensible platform to retrieve, visualize and analyse 3D morphology. *Methods Ecol Evol* 2021;**12**:1816–25.
Rossi A, Scordamaglia E, Bellingeri M *et al.* Demography of the bottlenose dolphin *Tursiops truncatus* (Mammalia: Delphinidae) in the eastern Ligurian Sea (NW Mediterranean): quantification of female reproductive parameters. *Eur Zool J* 2017;**84**:294–302.
Rusu RB, Blodow N, Beetz M. Fast point feature histograms (FPFH) for 3D registration. *Proc IEEE Int Conf Robot Autom* 2009:3212–7.
Santillán L, Félix F, Haase B. A preliminary morphological comparison of skulls of common bottlenose dolphins *Tursiops truncatus* from Peru and Ecuador. In: Document SC/60/SH10 presented to the Scientific Committee of the International Whaling Commission, Santiago, Chile, 2008.
Santos MB, Pierce GJ, Reid RJ *et al.* Stomach contents of bottlenose dolphins (*Tursiops truncatus*) in Scottish waters. *J Mar Biol Assoc U K* 2001;**81**:873–8.
Sellas AB, Wells RS, Rosel PE. Mitochondrial and nuclear DNA analyses reveal fine scale geographic structure in bottlenose dolphins (*Tursiops truncatus*) in the Gulf of Mexico. *Conserv Genet* 2005;**6**:715–28.
Simões-Lopes PC, Daura-Jorge FG, Lodi L *et al.* Bottlenose dolphin ecotypes of the western South Atlantic: the puzzle of dorsal fin shapes, colors and habitats. *Aquat Biol* 2019;**28**:101–11.
Smith KK. Craniofacial development in marsupial mammals: developmental origins of evolutionary change. *Dev Dyn* 2006;**235**:1181–93.
Terranova F, Gnone G, Friard O *et al.* Signature whistles of the demographic unit of bottlenose dolphins (*Tursiops truncatus*) inhabiting the Eastern Ligurian Sea: characterisation and comparison with the literature. *Eur Zool J* 2021;**88**:771–81.
Tezanos-Pinto G, Baker CS, Russell K *et al.* A worldwide perspective on the population structure and genetic diversity of bottlenose dolphins (*Tursiops truncatus*) in New Zealand. *J Hered* 2009;**100**:11–24.
Turner JP, Worthy GAJ. Skull morphometry of bottlenose dolphins (*Tursiops truncatus*) from the Gulf of Mexico. *J Mammal* 2003;**84**:665–72.
Twilley RR, Cárdenas W, Rivera-Monroy VH *et al.* The gulf of Guayaquil and the Guayas river estuary, Ecuador. In: Seeliger U, Kjerfve B (eds), *Coastal marine ecosystems of Latin America*. Berlin: Springer Science, 2001, 245–63.
Van Waerebeek K, Reyes JC, Read AJ *et al.* Preliminary observations of bottlenose dolphins from the Pacific coast of South America. Pages 143–154. In: Leatherwood S, Reeves RR (eds), *The Bottlenose Dolphin*. San Diego: Academic Press, 1990, 653.
Van Waerebeek K, Reyes JC, Sanino GP *et al.* Common bottlenose dolphins *Tursiops truncatus* of Pacific South America, a synoptic review of population identification data. In: IWC Scientific Committee Meeting, Bled, Slovenia, 2017.
Viaud-Martinez KA, Brownell RL, Komnenou A *et al.* Genetic isolation and morphological divergence of Black Sea bottlenose dolphins. *Biol Conserv* 2008;**141**:1600–11.
Walker JL, Potter CW, Macko SA. The diets of modern and historic bottlenose dolphin populations reflected through stable isotopes. *Mar Mamm Sci* 1999;**15**:335–50.
Whitehead H, Rendell L. *The Cultural Lives of Whales and Dolphins*. Chicago: University of Chicago Press, 2014.
Wiley DF. *Landmark Editor 3.0. IDAV*. Davis: University of California, 2005.

Chapter 4 – Worldwide Skull Shape Differentiation in Bottlenose Dolphins: Unveiling Geographic and Environmental Patterns Across Operational Taxonomic Units

4.1. Introduction

The skull is a complex bony structure that protects vertebrates' brains and sensory organs. Its shape, size, and bone arrangement vary substantially across species due to evolutionary pressures associated with feeding behaviours, sensory needs and other ecological demands (Hendges et al., 2016; Giacomini et al., 2022; Meloro & Tamagnini, 2022; Russo et al., 2022). Comparative studies of skull shape have provided valuable insights into evolutionary processes, particularly in identifying conserved anatomical features and adaptative modifications. For example, studies of skull shape in squamate reptiles have provided important insights into the ecological origins of snakes. The evolutionary transition from lizards to snakes involved gradual skull shape changes reflecting adaptations to a fossorial lifestyle, including small, encased, and inflexible skulls (Da Silva et al., 2018).

In mammals, skull shape is closely linked to functional specialisation, particularly regarding feeding, sensing, and moving (Dumont et al., 2016; Giacomini et al., 2022; Meloro & Tamagnini, 2022). Among Carnivora, skull shape and size are strongly influenced by food acquisition mechanisms and prey preference, partly driven by differences in jaw muscle development associated with specific masticatory stresses and bite force (Meloro & Tamagnini, 2022). Terrestrial mammals, with their diverse feeding strategies, exhibit greater skull morphological variation compared to aquatic carnivores, where functional constraints of aquatic life likely limit evolutionary changes (Meloro & Tamagnini, 2022). Other functional demands, such as echolocation, also influence skull morphology. In bats (Chiroptera), for example, cranial shape differences are more closely related to echolocation than to dietary habits (Arbour et al., 2019). Rostral flexion, a key feature related to echolocation, changes not only between echolocating and non-echolocating bats but also between different types of echolocation (e.g., nasal vs. oral; Arbour et al., 2019).

In the study of animal morphology, geometric morphometrics (GM) has become an invaluable and widely used tool (e.g. Mitteroecker & Schaefer, 2022). This method places landmarks on digital surfaces and analyses their Cartesian coordinates to quantify shape variations between pre-defined groups (e.g. species or populations) independently of size (Bookstein, 1986; Rohlf & Marcus, 1993; Adams et al., 2013; Manthey & Ousley, 2020). Its

application to three-dimensional models (3DGM) is particularly valuable for studying skull shape, especially in intraspecific studies where variations are subtle. Compared to linear measurements or 2D images, 3DGM captures the skull's complex shape more comprehensively, preserving details on contours, curvatures and surface morphology, that would otherwise be limited in either 2D images or individual linear measurements taken directly on the skull (Buser et al., 2018).

The bottlenose dolphin (*Tursiops truncatus*) is a particularly suitable model for studying intraspecific worldwide patterns of skull shape variation. The species is widely distributed and is found in diverse environments, including open oceans, coastal waters, and estuaries (Wells & Scott, 2009). This ecological diversity is accompanied by considerable behavioural variability, including feeding strategies (Krützen et al., 2005; Daura-Jorge et al., 2013; Ramos et al., 2022), social structures (Foley et al., 2010; Moreno & Acevedo-Gutierrez, 2016; Díaz López, 2020), and communication patterns (La Manna et al., 2020; Luís et al., 2021).

Comparative studies have consistently documented regional skull shape differences in bottlenose dolphins, with some populations having larger, more robust skulls, while others appear slender. Notable examples include the Black Sea (Viaud-Martinez et al., 2008), Brazil (Wickert et al., 2016; Hohl et al., 2020), the Gulf of Guayaquil in Ecuador (Dromby et al., 2023), the West North Atlantic (Costa et al., 2022) and the Gulf of California (Esteves-Ponte et al., 2022). These variations often involve specific cranial features, such as differences in the rostrum’s length and width, size of the temporal fossae, and palatine width (Viaud-Martinez et al., 2008; Perrin et al., 2011; Costa et al., 2016; Jedensjö et al., 2017; Hohl et al., 2020; Costa et al., 2022; Esteves-Ponte et al., 2022).

Bottlenose dolphins also exhibit widespread regional differentiation in behaviour, physiology and diet. For example, offshore dolphins along the United States East Coast have higher parasite loads (Walker, 1981) and unique haematological profiles (Duffield et al., 1983), potentially reflecting their deep-sea habitats. Conversely, dolphins occupying more coastal habitats, often display variations in colouration, body proportions (Hersh & Duffield, 1990) and fin shape (Félix et al., 2018). Coastal bottlenose dolphins also have different dietary preferences (e.g. Pereira et al, 2020) and typically demonstrate strong site fidelity and reduced dispersal (Urian et al., 2009; Giacomo & Ott, 2016; Sprogis et al., 2016; Passadore et al., 2018a) compared to offshore groups (Dinis et al., 2021).

These ecological differences are accompanied by substantial genetic differentiation across regions (e.g., Hoelzel, 1998; Natoli et al., 2004; Tezanos-Pinto et al., 2009; Moura et al., 2013; Louis et al., 2014; Fruet et al., 2017; Bayas-Rea et al., 2018; Nykänen et al., 2019). These

genetic studies have identified multiple operational taxonomic units (OTUs), with some units given formal taxonomic ranks. The most established distinction separates *Tursiops truncatus,* with a worldwide distribution, from *Tursiops aduncus* which is distributed along coastal waters of the Indian Ocean and southwestern Pacific (Committee on Taxonomy, 2023). More recently, the coastal population of the United States East Coast has been recognized as a third species (*Tursiops erebennus*) given multiple lines of evidence for its separation from other *Tursiops* (reviewed in Costa et al., 2022). Furthermore, subspecies status has been recognized in the Black Sea (*T. t. ponticus*; Viaud-Martinez et al., 2008) and along the southern coast of Brazil and Uruguay (*T. t. gephyreus*; Wickert et al., 2016). Beyond these formally described taxa, other genetically distinct units have been identified, but without formal taxonomic description. This includes units in the coast of California (USA; Lowther-Thieleking et al., 2015), the Gulf of Guayaquil (Ecuador; Bayas-Rea et al., 2018), the English Channel/North Sea (Louis et al., 2014) and in the Western North Pacific (Chen et al., 2017).

Morphometric studies have repeatedly documented skull shape differences between offshore bottlenose dolphins and the multiple coastal OTUs described above. However, these variations are not uniform across units but instead appear to vary regionally. For example, in the West North Atlantic, coastal dolphin skulls are smaller, with shorter rostrums and more contracted internal nares compared to offshore dolphins (Mead & Potter, 1995; Costa et al., 2022). In the Southeast Pacific (Ecuador), coastal dolphins have stouter skulls, with shorter broader rostrums and ventro-dorsal compression of the supraoccipital (Santillán et al., 2008; Dromby et al., 2023). In the Southwest Atlantic**,** coastal *T. t. gephyreus* have larger and more robust skulls, characterized by a slightly longer rostrum, falciform premaxillae, and more concave premaxilla and prenarial areas (Costa et al., 2016; Hohl et al., 2020). In the Northeast Pacific**,** skull shapes differ between dolphins inside and outside of the Gulf of California, with those from the outside having larger and more robust skulls, more teeth, stouter rostrum as well as narrower internal nares (Perrin et al., 2011; Costa et al., 2016).

These regionally distinct skull morphologies have been suggested to reflect adaptations to feeding strategies, echolocation, or swimming behaviour. For example, coastal specimens from the Southwest Atlantic (Brazil) have telescoped skulls (i.e., dorsal elongation of the skull; Costa et al., 2016), a feature that may improve swimming efficiency in shallower waters by reducing drag (McCurry et al., 2017). These specimens also have deeper and more concave prenarial triangles and maxillae, which are thought to be related to tissues involved in communication (Costa et al., 2016). In contrast, coastal specimens from California have larger teeth and robust

skulls, including an expanded temporal fossa, which were suggested to reflect a diet composed of tougher, larger prey (Perrin et al., 2011).

A major challenge in studying worldwide patterns of bottlenose dolphin skull morphology is collecting a geographically comprehensive sample set that adequately represents the worldwide distinction between coastal and offshore operational units. Worldwide analysis requires extensive travel to local museum collections for data gathering, which is both time-consuming and costly. In addition, many skulls in museum collections are fragile and require careful handling to avoid damage. As a result, they are not typically transported between institutions for collaborative research. Consequently, worldwide analyses are often limited, making it difficult to identify and accurately describe any consistent skull shape patterns between those units. For example, it remains unclear if each coastal operational unit exhibits unique traits consistently associated with a coastal environment and how these units may differ from one another (Oxford-Smith et al., 2024). Furthermore, the precise skull traits that exhibit the greatest variation remain undetermined. It is also unclear if offshore individuals are more similar to each other irrespective of their regional origin compared to coastal units, or if they also exhibit regional shape variations that have remained undetected.

Previous GM studies have relied on traditional manual landmarking, which relies on prior biological knowledge to place homologous landmarks (Adams et al., 2013). While providing valuable insights into morphological studies, it is time-consuming, particularly with large datasets with hundreds of specimens. Consequently, most studies limited their landmarking to a few points, which can overlook important geometric features and oversimplify skull shape descriptions (Rolfe et al., 2021). This limitation becomes particularly problematic when investigating intraspecific shape variations which are usually subtle, potentially leading to inaccurate identification of shape differences between units and biased biological interpretations. Furthermore, manual landmarking is dependent on researchers' subjective choice of landmarks and their placement (Fagertun et al., 2014), limiting reproducibility and comparability with future studies.

The role of environmental factors in shaping skull morphology also remains poorly understood. While some studies have correlated skull shape with ecological factors like foraging strategies (McCurry et al., 2017; Frainer et al., 2021) or vocalisation patterns (Del Castillo et al., 2016; Frainer et al., 2021; Laeta et al., 2023), this approach does not identify specific environmental features that may act as selective pressures. Furthermore, most studies focused on coastal vs pelagic differentiation within limited geographical areas, restricting our ability to infer broader patterns of repeated adaptation to coastal habitats.

The limitations associated with landmarking methodology can be mitigated by using automated pseudo-landmarking techniques. This approach uses algorithms to automate landmark placement on surfaces across multiple specimens, considerably reducing preprocessing time while ensuring consistent landmark placement across specimens (Porto et al., 2021). This method has been shown to produce comparable results to traditional techniques, and due to increased point density can even provide greater insight into shape variation (Porto et al., 2021; Rolfe et al., 2021). For example, a study investigating intraspecific shape variations in the genus *Tursiops* found that both automated pseudo-landmarking and manual landmarking inferred similar biological differentiation patterns, although with varying degrees of differentiation between units (Dromby et al., 2023). Furthermore, using the coordinates of landmarks generated by automated pseudo-landmarking techniques, the relationship between skull shape and a set of environmental variables extracted from satellite data can be tested. Multivariate statistics can then be used to identify the environmental variables most strongly correlated with skull shape differences (Van den Wollenberg, 1977; Rohlf & Corti, 2000). In this study, skull shape variations in bottlenose dolphins were assessed using 3D skull models from 234 individuals worldwide. This dataset encompassed six well-described coastal OTUs and their offshore counterparts, as well as four less-studied regional units, providing a broad worldwide geographic representation. 3DGM was used to overcome shape distortions inherent in two-dimensional analyses, together with 760 evenly spaced pseudo-landmarks to capture shapes with the detail required for intraspecific studies. Shape differences across geographical units were first explored using a Generalised Procrustes Analysis followed by multivariate statistics. These were combined with supervised and unsupervised classification methods to verify the consistency of identified clusters with the a priori defined operational unit.

Finally, using this diverse worldwide dataset, skull shape variations as represented by their Procrustes aligned coordinates, were correlated with a set of several environmental variables, to identify the factors that best explain observed patterns. This high-resolution 3DGM analysis of skull shape differences between several bottlenose dolphins worldwide OTUs (both coastal and offshore) and their association with several environmental variables provides new insights into bottlenose dolphin phenotypic diversity. This method helps identify the drivers of phenotypic variation and improves our understanding of the evolutionary and ecological processes that shape bottlenose dolphin diversity.

4.2. Material And Methods

Data collection

Data were collected from 234 skulls of bottlenose dolphins (*Tursiops* spp.) worldwide, deposited at the collections of the Federal University of Santa Catarina (Brazil), the Museo de Ballenas in Salinas (Ecuador), the musée d'Histoire Naturelle in Paris (France), the Staatliches Museum für Naturkunde in Stuttgart (Germany), the Museo di Storia Naturale in Milan (Italy), the Museo Civico di Storia Naturale 'Giacomo Doria' in Genova (Italy), the Naturalis Biodiversity Centre in Leiden (Netherlands), the Natural History Museum of Los Angeles County in Los Angeles (USA), and the Smithsonian National Museum of Natural History in Washington (USA). Only physically mature specimens were included, as skull shape undergoes significant changes during early life stages (Perrin & Heyning, 1993). Details and skull accession numbers are available in Supplementary Table S4.2.1.

Specimens were selected to represent differences between offshore and coastal Operational Taxonomic Units (OTUs) from multiple locations worldwide including: the California coast (USA; n= 19; Perrin et al., 2011); the coast of Ecuador, where specimens using the inner estuary of the Guayaquil Gulf were found to differ from the offshore (n= 17; Bayas-Rea et al., 2018); the Northeast coast of the USA (n= 28; recently described as *Tursiops erebennus* by Costa et al., 2022); the coast of Brazil (n= 16, corresponding to the subspecies *Tursiops truncatus gephyreus*; Wickert et al., 2016; Hohl et al., 2020). In addition, skulls were included from regions where a coastal vs offshore differentiation has been suggested but supported by less conclusive evidence, namely: the North Sea region (n= 14, represented here mostly by specimens from the Netherlands; Louis et al., 2014); the Mediterranean Sea (n= 18, represented by samples from Italy; Gaspari et al., 2015; Carnabuci et al., 2016); the coast of West Africa (n= 11; Van Waerebeek et al., 2016; Oxford-Smith et al., 2024); the coast of Japan (n= 14; Chen et al., 2017; Oxford-Smith et al., 2024); multiple locations along the Western coast of South America (n= 16; Santillán et al., 2008; Bayas-Rea et al., 2018; Félix et al., 2018). Finally, skulls of *Tursiops aduncus* from several locations in the Indian Ocean were also included (n= 28; Rice, 1998; Wang et al., 1999, 2000). These sample regions and their corresponding specimen counts are summarized in Table 4.1, and a map showing all specimens' approximate locations is provided in Figure 4.1.

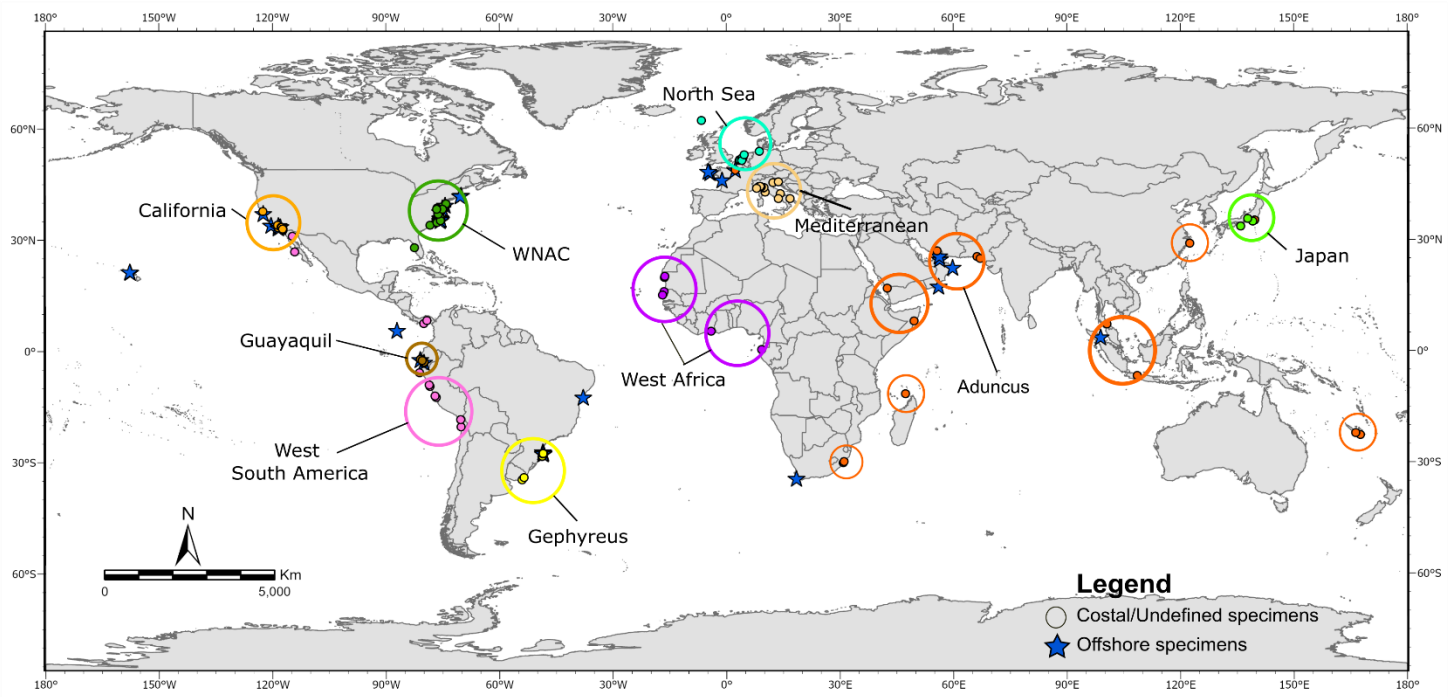

Figure 4.1 Map showing the approximate location of bottlenose dolphin specimens analysed in this study, with colours representing their a priori operational taxonomic unit classification. The world map was sourced from the GADM project (version 3.6, gadm.org).

Table 4.1. The number of individuals per geographical area and habitat type.

Geography	**Habitat**	**N**
Offshore	Offshore	53
Erebennus	Coastal	28
Aduncus	Coastal	28
Guayaquil	Coastal	17
California	Coastal	19
Mediterranean	Coastal	18
Gephyreus	Coastal	16
West South America	Coastal	16
North Sea	Coastal	14
Japan	Coastal	14
West Africa	Coastal	11
Total		234

Three-dimensional modelling

Three-dimensional (3D) models were created for each skull using digital photogrammetry with the software Meshroom v.2019.2.0 (Griwodz et al., 2021). For each specimen, 250 to 500 high-resolution digital photographs were captured, following a common protocol, using a high-resolution DSLR camera (> 8 Megapixels) with APS-C sized sensors, ensuring a minimum of 60% lateral overlap and 80% frontal overlap between successive images to cover the entire skull surface. The focal length was kept constant throughout each photographing session, and camera settings were set to balance between small apertures to ensure long depth of field, and fast shutter speeds to avoid motion blur. When possible, the camera was fixed on a tripod, while the skull was placed on a rotating turntable.

A draft 3D model was constructed for each skull to assess reconstruction quality. Based on a qualitative assessment of this draft reconstruction, pictures were digitally pre-processed to optimize the quality of the final model. First, the skull was isolated from the background using the software REMBG (Gatis, 2020). The resulting pictures were then edited to improve the clarity of surface skull features using the software Darktable (https://www.darktable.org), by increasing local contrast while reducing global contrast (details in Chapter 2 - Workflow for 3D Skull Reconstruction of Dolphin Skeletal Specimens, for Geometric Morphometric Analysis."). For the final 3D reconstruction, fully rotating 3D models were produced using the software Meshroom (Griwodz et al., 2021) with the following settings: "Feature Extraction" step, with the "Sift" (Scale-Invariant Feature Transformation (Otero & Delbracio, 2014) and "sift_float" algorithms, employing "Guided matching", for improved camera recognition; in the "StructureFromMotion" step, the 'Use rig constraint' was disabled, due to the changing relative camera position during the photographing session. In the "DepthMap" step the "Depth Map node" was set to downscale=1 for detailed model surfaces, with some Guayaquil specimens using downscale=2 to achieve similar detail and polygon count (See supplementary information Table S4.2.2).

For specimens with fewer photos, settings were adjusted to achieve comparably accurate models (See supplementary information Table S4.2.2). In the "Feature Extraction" step, the "Akaze" (Alcantarilla et al., 2011) algorithm was used alongside the default algorithm and the prescriber preset was set to 'High'. This increased the number of features identified in the photos, improving camera positioning during the subsequent 'StructurefromMotion' step. In the "image matching step", descriptors settings were optimized for mesh completeness, setting the 'Max Descriptors' and 'Number of matches' to 0 and "minimum consistency camera" and "minimum consistency camera similarity" to 2 and 3, respectively. The "Meshing" step

involved reducing, the "Max input points," "Max points," and "Max points per voxel," by 50% from their default value and sometimes by a fifth depending on the model. This produced meshes using less point cloud data, improving surface texture reconstruction at the expense of surface details in the reconstructed skulls. Therefore, in some models, 2 to 3 meshes corresponding to different meshing settings were merged to maximise both surface coverage and detail (details in Chapter 2 – Workflow for 3D Skull Reconstruction of Dolphin Skeletal Specimens, for Geometric Morphometric Analysis). Meshes were merged using the function “Flatten visible layers” in the software Meshlab (Cignoni et al., 2019), followed by a Poisson surface reconstruction (Kazhdan et al., 2006), with “reconstruction depth” set to 13 and “interpolation weight” set to 0. The final 3D models were then decimated to 1 000 000 faces, using the function "Simplification: Quadric Edge Collapse Decimation" in Meshlab. This step reduced the computational requirements of downstream analyses while preserving model details. Finally, models were trimmed to remove extra bone features that were not present in all skulls (e.g. the zygomatic arches), using the bisection tool in the open-source software Blender v.5.2.2 (Blender Development Team, 2022).

Landmarking

Skull shapes were analysed using a Surface Semi-Landmarks (SSL) approach (Bardua et al., 2019). This method uses a set of evenly spaced surface pseudo-landmarks, whose density can be adjusted to capture the desired level of detail. These landmarks are typically generated on a reference skull, representing the average shape of the dataset. Then, they are automatically transferred to other skulls, ensuring that the landmarks remain evenly spaced and consistently positioned on the target skull, thus preserving their relative geometry and spatial relationships.

This SSL approach has several benefits for comparative studies: it captures subtle shape variations due to its high coverage, reduces observer bias in landmark placement, and improves the time efficiency of the landmark placement workflow (Gunz et al., 2005; Bardua et al., 2019). However, SSL landmarks are not, by definition, placed on homologous anatomical features (although some might be landmarked by chance), and as a result, landmarks may not correspond to anatomical features directly related to the skull's ecological functions. Consequently, the observed shape differences may reflect artefacts of the alignment process rather than true biological variation (Gao et al., 2018; 2019). In addition, the high landmark density can result in more landmarks than specimens being analysed, presenting challenges for statistical analysis, including spurious correlations that do not reflect meaningful biological patterns. Collinearity

between nearby landmarks can also be introduced, complicating the identification of true shape variation without redundancy.

To mitigate these limitations, the SSL approach was complemented with point-only Homologous Landmarks (HL), which enabled the placing of landmarks in homologous points, chosen based on prior biological information (Adams et al., 2013). HL is typically more time-consuming for large datasets and can therefore overlook important geometric details because it limits the number of landmarks (Watanabe, 2018; Rolfe et al., 2021). Therefore, the process was made more efficient for our large dataset, by automating HL placement. Details of both landmarking pipelines are presented below.

Surface-Semi Landmarking (SSL)

Landmarks were generated using the module PseudoLMGenerator in the SlicerMorph extension (Rolfe et al., 2021). PseudoLMGenerator generates a set of evenly spaced landmarks on a reference skull's triangular mesh, which can then be projected onto the surfaces of other 3D skull models by aligning them through point registration. This ensures that the relative distances and positions of the landmarks remain consistent across the reference and target skulls, enabling a consistent representation of surface geometry.

A reference skull that best represented the average shape of our dataset was first selected. This was determined through a preliminary Generalized Procrustes Analysis (GPA) and Principal Component Analysis (PCA) using the geomorph package in R (Adams & Otárola-Castillo, 2013; Baken et al., 2021), identifying the skull closest to the mean using the function findMeanSpec().

Odontocete skulls are bilaterally asymmetric (Macleod et al., 2007) and failing to account for this asymmetry can introduce noise or bias in geometric morphometrics (GM) analysis, causing skulls to appear either more similar or more different than they are. In *Tursiops* in particular, previous research has shown that the asymmetric component is not related to ecotype differentiation (Oxford-Smith et al., 2024), thus overlooking asymmetry could lead to biased inference regarding ecological differentiation. Therefore, the landmarks were generated based on a bilateral central plane (explained below), allowing for the placement of pseudo-landmarks in bilateral pairs. This central plane was positioned to be as close as possible to the following 4 skull points: the middle of the two maxilla edges at the tip of the rostrum; the central point between the occipital condyles, the central suture between the two pterygoid bones; the central line between the external nares.

The PseudoLMGenerator was set to a "spacing tolerance" value of 2.5, resulting in a total of 838 pseudo-landmarks. These landmarks were used as templates for automatic landmark placement on the remaining skulls. In the ALPACA extension, we set the registration step to a point density of 0.5, with rigidity (alpha) set to 2 and motion coherence (beta) set to 2, keeping other parameters at their default values (See Supplementary Information Table S4.2.3). Due to damage or breakage in the pterygoid bone in over 24% of the skulls, 73 corresponding landmarks were excluded from further analysis. Additional outlier landmarks were identified and excluded using the "GPA" module in SlicerMorph. This resulted in a total of 760 pseudo-landmarks kept for subsequent analysis (Figure 4.2).

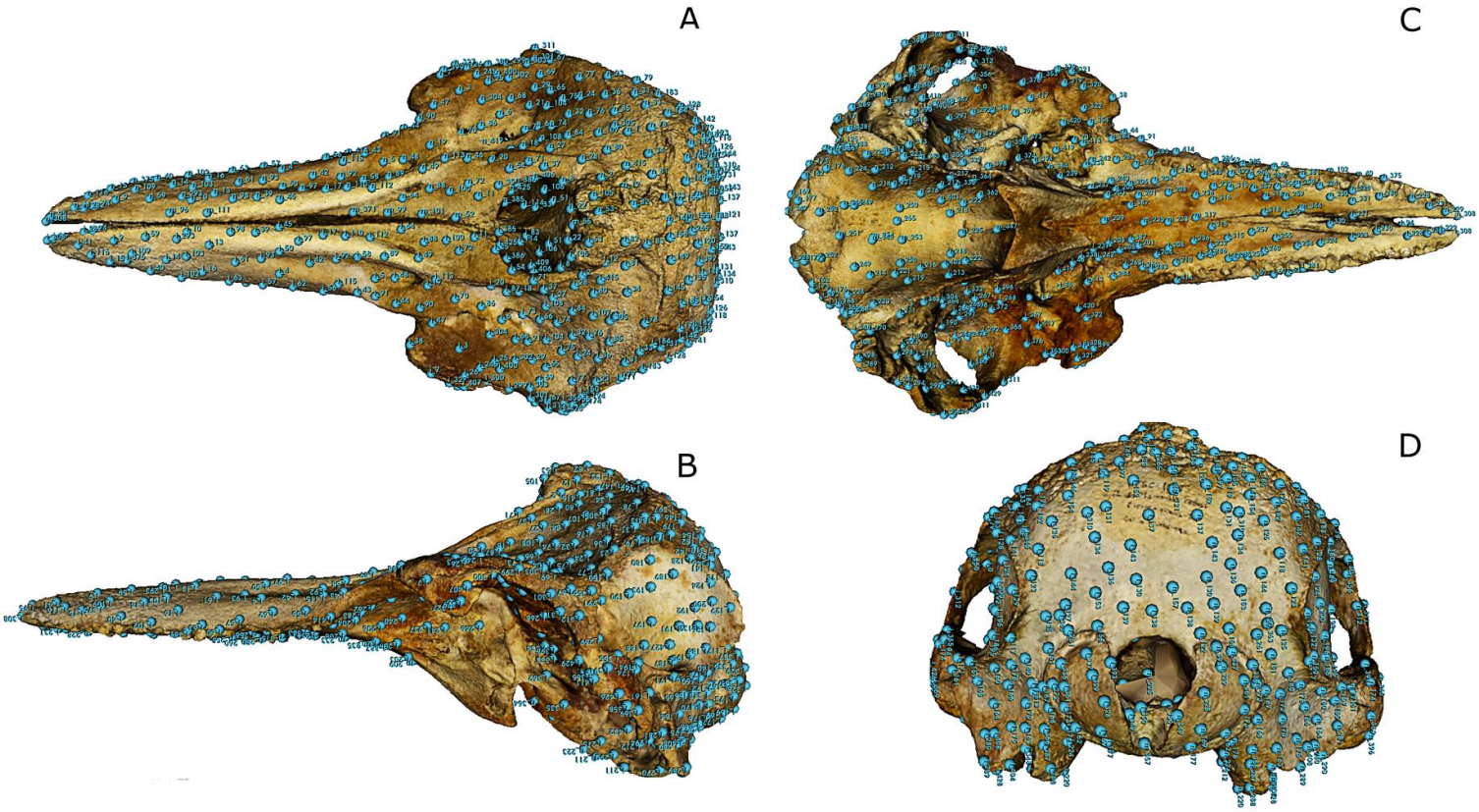

Figure 4.2. Three-dimensional landmarks used in this study and obtained from the automatic landmarking showed in dorsal (A), lateral (B), ventral (C), and occipital (D) aspects of the bottlenose dolphin skull.

Homologous landmarking (HL)

Twelve templates were landmarked with 76 manually placed homologous single-point landmarks using the software IDAV Landmark v.3.0 (Wiley 2005; details in Supplementary Table S4.2.4). Landmarks were selected based on the description in (Dromby et al., 2023)

excluding all patch and line landmarks to avoid redundancy with the SSL method, which already uses surface landmarks.

The MALPACA tool (Zhang et al., 2022) implemented in the SlicerMorph extension (Rolfe et al., 2021), was used to automate landmark placement on the remaining skulls. MALPACA uses the registration step in ALPACA to align multiple template models to each target specimen. For each landmark, MALPACA calculates the median of x, y, and z coordinates from all templates and uses it as the final landmark position for the target specimens. MALPACA effectively addresses the challenges with high shape variations between templates and target specimens, a common limitation of single-template registration methods (i.e., registration algorithms optimisation; Porto et al., 2021; Young & Maga, 2015). Templates were selected based on the morphospace generated by a preliminary analysis (described in the previous section), as well as the ecotype differentiation patterns identified in previous studies (Dromby et al 2023; Oxford-Smith et al., 2024). One to two non-damaged skulls were chosen per operational unit (details in Supplementary Information Figure S4.2.1), ensuring that they were free from anomalies such as breakage or holes on their surfaces.

These skulls were situated at the centre of their respective morphospace operational units' cloud, while also being sufficiently spaced apart to ensure they represented the average shape and covered the most shape diversity for each unit. In MALPACA, these templates were set as source models, and their corresponding landmarks were used as reference points. During the registration step, alpha, beta, and point density settings, which control registration accuracy, were tested iteratively. Alpha controls the rigidity of template model deformation to match the target specimen (higher alpha values reduce deformation), while Beta adjusts the smoothness of landmark displacement during registration (higher beta values result in a more coordinated motion), and point density determines the number of points used during registration (higher density captures more detailed surface).

The optimal settings were Alpha =2, Beta =2, and point density =1 (details in Supplementary Information Table S4.2.3), which led to the optimal landmark placements. Accuracy was assessed by visually inspecting if landmarks were in their expected locations and comparing root mean square error (RMSE) between original and registered landmarks for each specimen. RMSE measures the average deviation between original and registered landmark positions, with lower values indicating better accuracy in landmark placement (Zhang et al., 2022). Outlier landmarks and those on the pterygoid region (n=3) were then removed, resulting in 73 final landmarks used in subsequent analysis (Figure 4.3).

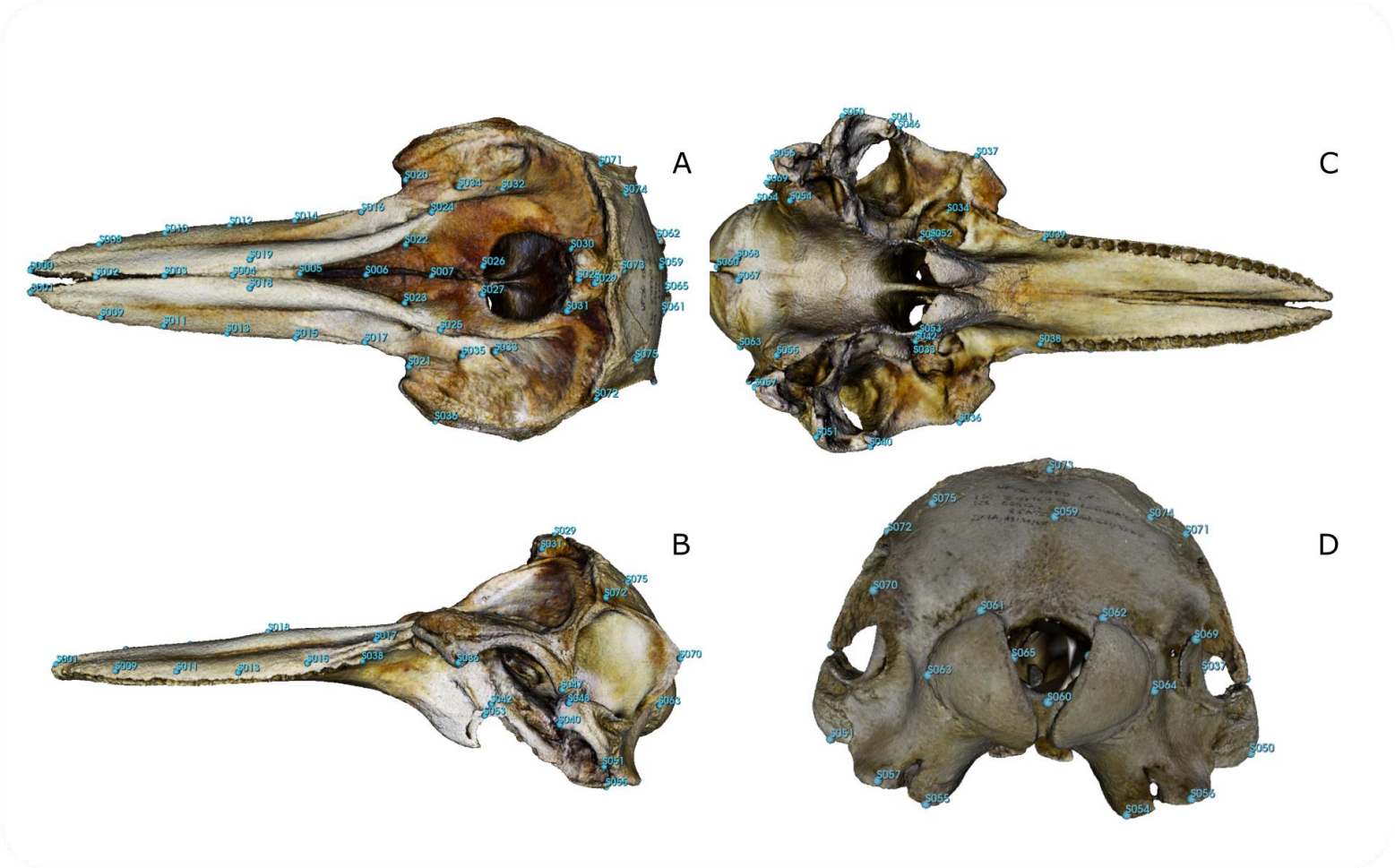

Figure 4.3. Three-dimensional landmarks used in this study and obtained from the semi-automatic homologous landmarking, showed in dorsal (A), lateral (B), ventral (C), and occipital (D) aspects of the bottlenose dolphin skull.

Geometric morphometric shape analysis

All analyses described below were performed using the R package Geomorph (Baken et al., 2021; Adams et al., 2023) unless stated otherwise. Generalized Procrustes Analysis (GPA; Goodall, 1991) was applied to the two sets of landmarks using the gpagen() function. GPA aligns the shapes of all specimens by translating, rotating, and scaling them to a common centroid size (i.e., Procrustes superimposition; Rohlf & Slice, 1990; Goodall, 1991), generating a set of Procrustes coordinates for each specimen for downstream shape comparisons. Since SSLs were placed automatically on the skull surface without considering feature homology, landmarks were not placed on the same biological feature between skulls (by definition). This issue was compounded when landmarks were automatically transferred between skulls, particularly in regions with high variability (Gunz & Mitteroecker, 2013; Rolfe et al., 2021). To address these biases, the Generalized Procrustes Analysis (GPA) was carried out using a sliding

landmark approach by minimizing bending energy (Perez et al., 2006; Mitteroecker & Schaefer, 2022). Minimization of bending energy allows landmarks to slide along their tangent planes while preserving relative distances between landmarks. This process ensured that landmarks placement between each specimen approximated true feature homology, and thus better represented the relative geometry of each skull (Bardua et al., 2019).

Since HLs were also automatically placed using MALPACA, landmarks were not strictly placed by the experimenter on homologous features for all specimens. Therefore, landmarks were also aligned during the GPA but using the Procrustes distance method, which calculates the Procrustes distance as the sum of squared differences between corresponding landmarks after superimposition (Perez et al., 2006; Mitteroecker & Schaefer, 2022). This method was considered more appropriate for the sparsely distributed HL landmarks because it does not consider the relative distance between points, which is not necessarily constant between homologous features. Asymmetry was identified using the function bilat.symmetry() in the Geomorph package. After identifying the asymmetric components, the function removed them by reflecting one side of the specimen onto the other, rotating and scaling the mirrored landmarks to optimally align with the original side. This process produced a symmetric shape component, which was then used for further analysis. Principal Component Analysis (PCA) was then performed on the symmetric component landmarks using the function gm.prcomp() in the Geomorph package.

To test the significance of skull shape differentiation between the a priori defined OTUs, a non-parametric multivariate analysis of variance test (PERMANOVA) was performed on the complete set of PC scores using the software PAST (Hammer et al., 2001). The distance matrix was calculated using the Euclidean method, with statistical significance determined using 10 000 permutations. The Bonferroni correction method was applied to adjust for multiple comparisons.

The shape changes associated with the PC axis were illustrated using vector displacement graphs using the function plotRefToTarget (method =c(„vector")) in the package geomorph. Additionally, warped meshes were created for each a priori OTU individually. First, specimens that best represented each operational unit shape characteristics were selected. These were specimens found at the periphery of their specific unit in the morphospace. Then, the mean specimen in the dataset was identified using the function findMeanSpec() and its mesh was used as a reference for warping other meshes. Subsequently, a thin-plate spline (TPS) deformation of the reference mesh relative to skulls typical of each OTU, was implemented via

the warpRefMesh() function to achieve point-to-point correspondence with the discrete surface representation of each target specimen

The transformed meshes were visualised using the function plotRefToTarget(mesh=wmesh, method=c("surface")) and exported in PLY format. Afterwards, the PLYs were imported into Meshlab to further illustrate the shape characteristics of each unit. The "Distance from Reference Mesh", was calculated to quantify how much each specimen differs from the mean specimen shape based on the vertex positions, using Euclidean metrics. Then, the "Quality Mapper" was used to colour-code these differences, helping to visually illustrate the degree of difference from the mean shape.

Classification by machine learning approach

Random Forest

Random forest (RF; Breiman, 2001) is a machine learning algorithm used for classification tasks. Patterns and relationships within data are learned by constructing several decision trees during training and combining their results to make predictions random subset of the training data is used to train each decision tree and a random subset of corresponding features at each split is evaluated. This process continues recursively until each tree forms a structure that best separates the data. Class labels (the defined OTUs) are then predicted for individual instances by each tree. After predictions have been made by all trees, the final prediction is determined by a majority vote among all trees (Biau & Scornet, 2016). To assess the accuracy and effectiveness of the RF models in classifying skulls based solely on their shape characteristics, the predicted OTUs were compared with the actual predefined operational unit from a testing set, using the R package randomforest (Liaw & Wiener, 2002). Several RF models were trained using a subset of the total dataset, with skull shape data serving as predictors and the predefined operational unit associated with each skull as the target variable for classification.

For the training set, 6 to 8 individuals were selected from each unit (n = 86). Specimens that were clearly differentiated from other units and within the mean range of their respective unit in a morphospace plot were chosen. This morphospace plot was based on the first three principal components (PCs) of aligned Procrustes landmarks adjusted for symmetry (as described in the "Geometric Morphometric Shape Analysis" section; Figure S4.2.1; Table S4.2.5).

The RF algorithm requires tuning two main parameters: the number of unpruned trees (ntree) and the number of features considered at each split (mtry). First, the optimal number of trees was determined by incrementally increasing ntree from 8 000 to 25 000, in steps of 1 000. For each increment, the Out-of-Bag (OOB) error, which estimates how well the RF model

generalises to unseen data, was evaluated. The OOB error at each step was assessed and the error against the number of trees was plotted. The OOB error was considered to be “stable and relatively low” when there was no significant reduction in the error after successive increments and when the error approached a plateau. After evaluating the OOB error for each increment, the error stabilised and reached a lower value at ntree = 12 000, indicating that further increases in the number of trees did not result in substantial improvements in model performance. Therefore, this value was selected as optimal for the RF model. Then, the mtry parameter was optimized using the function tuneRF(), which automates the process of finding the best number of features considered at each split in the trees, thereby improving the RF model's robustness and predictive accuracy. Through this process, the ideal mtry value was found to be 56. The optimized RF model was then used to predict the OTU assignment probabilities for the remaining skulls in the dataset (234 skulls). The results from the classification were summarised with a classification matrix and visualised with a heatmap to provide a detailed overview of the model's performance, showing the number of correctly and incorrectly classified instances for each operational unit.

Hierarchical Cluster Analysis

Hierarchical Cluster Analysis (HCA; Köhn & Hubert, 2015) is an unsupervised machine learning algorithm used to classify objects into a hierarchical tree structure based on their similarities. To assess the congruence between skull clustering based on shape similarities and the predefined OTU designations, an HCA was applied without prior knowledge of operational unit information during the clustering process. HCA was performed using the complete set of Procrustes landmarks from our dataset as the classification criteria. First, the data were scaled to ensure that all landmarks were on a comparable scale before calculating the Euclidian pairwise distances between the Procrustes landmarks of all specimens (Yim & Ramdeen, 2015). The "Ward.d2" clustering linkage method was applied because it showed better performance compared to other methods. This was evaluated using the agnes() function in R, which performs different agglomerative hierarchical clustering methods (Ward, single, complete), and after clustering assesses their agglomerative coefficient (AC) to assess the fit of the data to the clustering structure. In addition, the "Ward.d2" method is generally more robust to outliers than other methods, because it focuses on minimising variance between clusters rather than measuring distance between points only (Murtagh & Legendre, 2011).

To determine the optimal number of clusters, the gap statistic method was used with the function clusGap() in R. This method computes the gap statistic for various numbers of clusters

and compares it to expected dispersion under a null reference distribution. When the number of clusters stabilises, it indicates that adding more clusters does not significantly reduce variance within the clusters or improve the overall fit of the model to the data, indicating that the chosen number of clusters effectively represents the inherent groupings. A range of bootstrap values (50-400) was tested to estimate the optimal number of clusters. Based on recommendations in the literature, the number of clusters typically remains constant with bootstrap values exceeding 500 (Maechler et al., 2013). In this study, the number of clusters was stabilized with 200 bootstrap iterations, thus this value was selected for the analyses.

A dendrogram was then constructed using the function hclust(). The clustering results were summarised by assigning each cluster to predefined OTUs and creating a classification matrix to compare the clustering outcomes with the a priori-defined units.

Alveoli Count

For each specimen, the left and right upper tooth alveoli were independently counted twice by three different observers. The small teeth located at the distal end of the rostrum were excluded from the count because they were less identifiable, making accurate quantification uncertain. Their presence and number vary greatly between individuals, potentially because they are initially absent or lost postmortem, leaving no evidence of their presence. Including these teeth would have potentially introduced inconsistency in the counting process. A systematic counting and verification procedure was applied. Specifically, if all observer counts were consistent, those numbers were designated as "Unanimous" and used as the final count. If two observers agreed but not all, the count was labelled as "Majority." In cases of disagreement, a careful recount was done and checked for consistency with previous counts. If no consistency could be found between observers and recounts, then the specimen was excluded from the analyses.

The Shapiro-Wilk test was used to determine if the data had a normal distribution. Since the data were not normally distributed, a non-parametric Kruskal-Wallis test was used to compare alveoli count between the different OTUs, followed by a Dunn's post-hoc test to carry out pairwise comparisons. All analyses and plots were conducted in PAST (Hammer et al., 2001), and tests were corrected using Bonferroni correction.

Environmental analysis

Two-block Partial Least square (2b-PLS; Rohlf & Corti, 2000) and Redundancy analysis (RDA; Peres-Neto et al., 2006) were performed to investigate the relationship between cranial shape variation and environmental factors. Specifically, this test aimed to determine: 1) whether

distinct OTUs, defined by their distinct cranial shapes, also occupied distinct ecological niches; and 2) which environmental variables showed the strongest correlations with cranial shape, and which operational units were associated with these variables.

Habitat characterisation

To categorise the habitats representative of each OTU, polygons defining the most likely core geographic areas associated with each unit were created using the software ArcGIS PRO version 3.2. The geographic extent of each polygon was determined using data on unit distribution, as described in the available literature. For coastal operational units like Guayaquil and Erebennus, polygons were designed to encompass, respectively, the inner estuary of the Gulf of Guayaquil (Felix 1994; 2017) and the coastline spanning from New York to Florida. For Erebennus, the polygon boundary was limited to 34 km from the shoreline (Torres et al., 2003).

For other coastal units, the polygons were extended to the edge of the continental platform encompassing an area where most specimens were collected. For some coastal units (California, West South America, Gephyreus, Mediterranean and Aduncus), this meant creating multiple polygons to reflect the discontinuous distribution of the skull's collection locations. For the different populations of the offshore operational unit, the polygons were placed in open waters with edges outside the continental platform. The radius of these polygons ranged from 395 nautical miles (Hawaii) to 563 nautical miles (Northwest Atlantic), based on known dispersal ranges of offshore bottlenose dolphins.

In total, 38 Polygons were created as a single layer in ArcGIS (See Supplementary Information Table S4.2.6; Figure S4.2.2). Then, data for 18 environmental variables were obtained (Table 4.2), and used to characterise the local habitats in each polygon. Each variable global rasters were downloaded from Bio-ORACLE v.3.0 (Tyberghein et al., 2012; Assis et al., 2024), representing the surface layer averaged for the years 2000 to 2010 at 0.05 degrees resolution. The mean represented the average of the yearly maxima and minima values for a specific variable over a decade, while the range represented the average absolute difference between the maximum and minimum records per year (Assis et al., 2024).

In ArcGIS, a model was created to batch-calculate the mean raster values of each environmental variable within the boundaries of each polygon (See Supplementary Information Figure S4.2.3.A**).** To automate the process, in the Spatial Analyst toolbox, the "Iterate Raster" tool was used to process all raster files sequentially. For each raster, the "Zonal Statistics as Table" then calculated the mean value of raster cells that fell within the boundaries of each

polygon. The “ignore no data in calculation” option was selected to exclude any missing values within the polygons.

The initial output tables used a generic field name "MEAN", that did not specify which environmental variable the mean values corresponded to. This ambiguity hindered later analysis and table merging because the identity (environmental variable) of each mean value would be unclear. Therefore, a second model was created to replace the generic field name "MEAN" with the correct variable names for each output table (See Supplementary Information Figure S4.2.3.B). This model used the “Iterate Table” tool to process each output table sequentially and the “Alter Field” tool to update the field names in each table. Since raster files were named after their corresponding environmental variables, the model automatically renamed the 'MEAN' field in each table to match the corresponding raster’s name (e.g., bathymetry, ocean temperature, etc.).

In the final step, a third model was created to combine all individual tables into a single common table (See Supplementary Information Figure S4.2.3.C). First, a template table was created containing the unique identifiers for each polygon. Then the **“**Iterate Table” tool was used to loop through each of the individual output tables, using the 'Add Join' tool. Each table was therefore added to the template table based on the common polygon identifier. This process merged the environmental variable data into the template table, thus creating a unified dataset.

Finally, this table was imported into R and merged with the individual specimen dataset, which included the a priori OTU classification and the corresponding polygon name, using the merge() function. The merge was performed based on the “Polygon” field, ensuring that the environmental data corresponded to the correct polygons in the specimen dataset. The resulting merged dataset, now containing both the environmental and specimen data, was then used for further analysis (See script in Appendix).

Table 4.2. Environmental layers used to test the correlation between shapes and environments.

Variables (Unit)	Description	References using the variable in the literature.
Aspect (-)	Aspect refers to the compass direction (e.g., north, south, east, west) that an underwater slope faces.	(Paradell et al., 2019; La Manna et al., 2020)
Slope (-)	Slope reflects the rate of depth change over a horizontal distance. It is derived from bathymetric data and indicates the steepness of the seafloor	(Paradell et al., 2019; La Manna et al., 2020; Correia et al., 2021; Milani et al., 2021; Muckenhirn et al., 2021)
Terrain ruggedness index (-)	Terrain Ruggedness Index quantifies the variability or roughness of the seafloor by measuring the difference in depth between adjacent cells. Higher values indicate more rugged terrain.	Na

Topographic Position Index (-)	Topographic Position Index compares the depth of a specific seafloor location (focal cell) to the average depth of its surrounding area (adjacent focal cells), identifying whether the location is a ridge, valley, or flat terrain.	Na
Bathymetry (m)	Bathymetry refers to the depth of the seafloor at a given location (each focal cell).	(Passadore et al., 2018b; Paradell et al., 2019; Milani et al., 2021; Muckenhirn et al., 2021; Torreblanca et al., 2022)
Chlorophyll (mmol . m-3)	Chlorophyll represents the concentration of chlorophyll-a in seawater. This variable serves as an indicator of phytoplankton biomass and primary productivity.	(Paradell et al., 2019; La Manna et al., 2020; Correia et al., 2021; Lambert et al., 2022; Torreblanca et al., 2022)
Current direction (degree) Current velocity (m.s-1)	Current direction refers to the angle at which ocean currents flow relative to true north (e.g., 0° for north, 90° for east). Current velocity refers to the speed of ocean water movement.	(Milani et al., 2021; Torreblanca et al., 2022)
DissolvedO2 (mmol.m-3)	Dissolved O2 refers to the concentration of oxygen dissolved in seawater.	Na
Iron, Nitrate, Phosphate, Silicate (mmol.m-3)	Refer to the concentration of these essential nutrients in seawater.	(Muckenhirn et al., 2021)
Ocean temperature (ºC)	Ocean temperature refers to the temperature of seawater.	(Passadore et al., 2018b; Paradell et al., 2019; La Manna et al., 2020; Milani et al., 2021; Muckenhirn et al., 2021; Lambert et al., 2022; Torreblanca et al., 2022)
Salinity (-)	Salinity refers to the concentration of dissolved salts in seawater.	(Hornsby et al., 2017; Passadore et al., 2018b; Paradell et al., 2019; Milani et al., 2021; Muckenhirn et al., 2021; Lambert et al., 2022; Torreblanca et al., 2022)
Primary productivity (mmol.m-3)	Primary productivity refers to the rate at which phytoplankton and other photosynthetic organisms produce organic matter through photosynthesis.	(Lambert et al., 2022)
Mixed Layer Depth (MLD)	MLD refers to the depth of the ocean's upper layer where water is well mixed due to wind and wave action.	(Lambert et al., 2022)
PH	PH Indicates the acidity or alkalinity of seawater on a scale from 0 (acidic) to 14 (alkaline).	(Passadore et al., 2018b)

Two-Block Partial Least square (2b-PLS) & Redundancy analysis (RDA)

A two-block Partial Least Square (2b-PLS) analysis was performed using the two.b.pls() function from the geomorph package, along with redundancy analysis (RDA) using the rda() function from the vegan package. Both analyses were conducted with 999 permutations at a significance level of 0.05 to explore patterns of covariation between shape data (Block 1) and environmental variables (Block 2).

The Procrustes Coordinates (from the analysis described above) were used as the shape data. However, individuals P199 and P208 were excluded from the analysis due to unknown

stranding locations, preventing their classification into any specific polygon. The environmental variables (Block 2) were selected from the previously obtained set of variables after assessing them for multicollinearity. For this, the cor() function in R was used to compute a correlation matrix. This matrix was then used to identify highly correlated variables, which in ecological data are considered when greater than 70% (Dormann et al., 2013). For variables with correlations above this threshold, one variable from each correlated pair was removed (See Supplementary Information Table S4.2.7).

If the correlation was between the mean and range of the same variable, the mean was retained and the range was removed, as the range was often highly correlated with other variables. Furthermore, some variables were biologically associated, meaning they likely reflected similar environmental processes or functions. To avoid redundancy, only one variable from each correlated pair was kept. The iron variables were also excluded due to high correlations with several other variables, including silicate mean, temperature range, pH range, and bathymetry mean. The final dataset contained 17 environmental variables. To ensure comparability across these variables, they were standardized to have a mean of zero and a standard deviation of one using the function scale() in R.

For the 2b-PLS, the relationships between shape and environmental variables were visualised using the function plot(). Additionally, a histogram of the environmental loadings was generated using the function barplot(), to illustrate the relative contribution of each environmental variable to the identified axes of covariation. These loadings measure how strongly each variable influences shape variation.

For the RDA, a 3D biplot displaying the main axes of correlation between the two data blocks, was generated using the function ordiplot3d() in the package vegan3D. The significance of the RDA model was assessed using several ANOVA tests using the anova.cca function from the vegan package in R. This included testing the overall relationship between environmental variables and shape, to assess if the environmental variables explained a significant amount of variation in the shape data. To identify the specific environmental variables most strongly correlated with shape, the significance of each environmental variable was further tested using the function anova.cca(by = "terms"). This test identified which individual environmental variables were significantly correlated with shape variation. Finally, the significance of each RDA axis was tested using the function anova.cca(by = "axes"). This test showed which axes in the multivariate space (representing the combined effect of environmental variables) were most correlated with shape variation.

4.3. Results

Principal Component Analysis

The first three principal components account for 53.91 % of the total shape variation (PC1 = 27.6%, PC2 = 17.7%, PC3 = 8.61%). Offshore specimens cluster at the centre of the morphospace, while the coastal operational units occupy distinct regions around the offshore cluster, with varying degrees of overlap (PERMANOVA - *F*-values ranging from 2.70 to 28 and *p*-values ranging from 0.006 to 0.193; Table 4.3; Figure 4.4). The coastal operational units were also separate from each other to varying degrees, with some statistically significant differences (PERMANOVA - *F*-values ranging from 2.46 to 32.5 and *p*-values ranging from 0.006 to 0.506; Table 4.3; Figure 4.4). Visually, the operational units corresponding to the well described coastal species/sub-species of *T. aduncus* and *T. t. gephyreus* were clearly separate from other coastal units (PERMANOVA - *F*-values ranging from 7.7 to 32.5 and *p*-values = 0.006, Table 4.3; Figure 4.4). Coastal specimens from the Western North Atlantic, recently described as *T. erebennus*, while distinct from the other operational taxonomic units (OTUs), overlapped visually with specimens from elsewhere in the American continent, including Guayaquil, West South America and California (although remaining significantly different; PERMANOVA - *F*-values ranging from 5.6 and 7.94 and *p*-values = 0.006; Table 4.3; Figure 4.4). Comparatively, specimens from California and the Mediterranean were found to each overlap considerably with the offshore OTU and clustered closely with other coastal units from nearby regions. California also overlaps closely with West South America (PERMANOVA - *F*-values = 2.5 and *p*-values = 0.506; Table 4.3; Figure 4.4), while the Mediterranean shows some overlap with West Africa (PERMANOVA - *F*-values = 3.39 and *p*-values = 0.473; Table 4.3; Figure 4.4). Specimens from West Africa show an interesting differentiation pattern in the morphospace, with some specimens occupying a fairly distinct position in the morphospace, while other specimens' group closely with other operational units. This overlap is visually more noticeable with the offshores (PERMANOVA - *F*-values = 5.43 *and p*-values = 0.006; Table 4.3; Figure 4.4) and show no significant difference from Japan (PERMANOVA - *F*-values = 4.49 and *p*-value = 0.149; Table 4.3; Figure 4.4). Finally, specimens from Japan and the North Sea show some visual overlap with the offshore OTU (PERMANOVA - *F*-values = 2.70 and 6.01 and *p*-values = 0.006 and 0.193, Table 4.3; Figure 4.4, respectively) as well as with each other (PERMANOVA - *F*-values = 2.46 and *p*-value = 0.204; Table 4.3; Figure 4.4), despite being geographically distant.

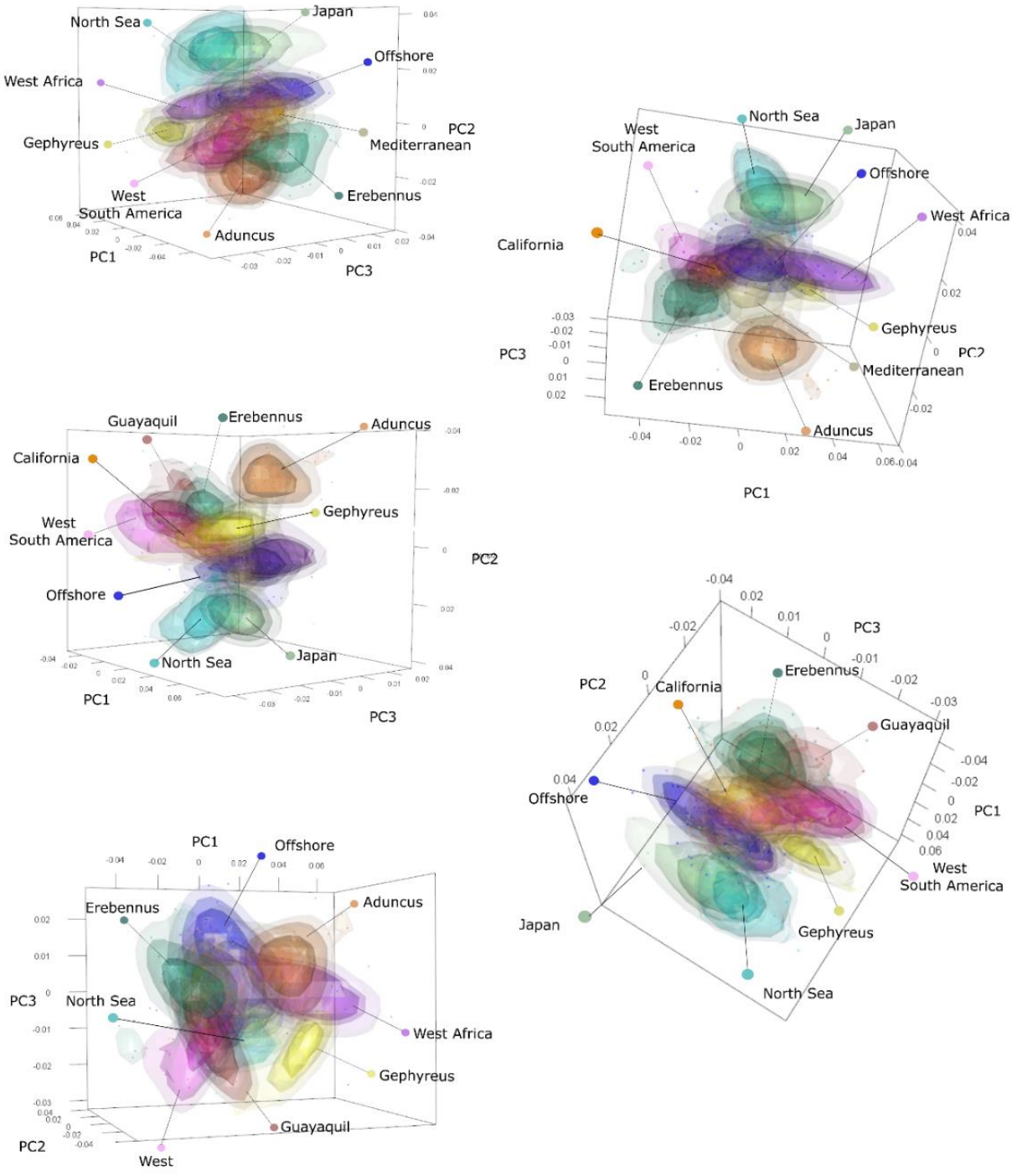

Figure 4.4 3D PCA morphospace displaying the three most important principal components, from five different perspectives, with OTUs distinguished by colours. Kernel discriminant analysis clouds are calculated in the R package KS (Duong, 2007).

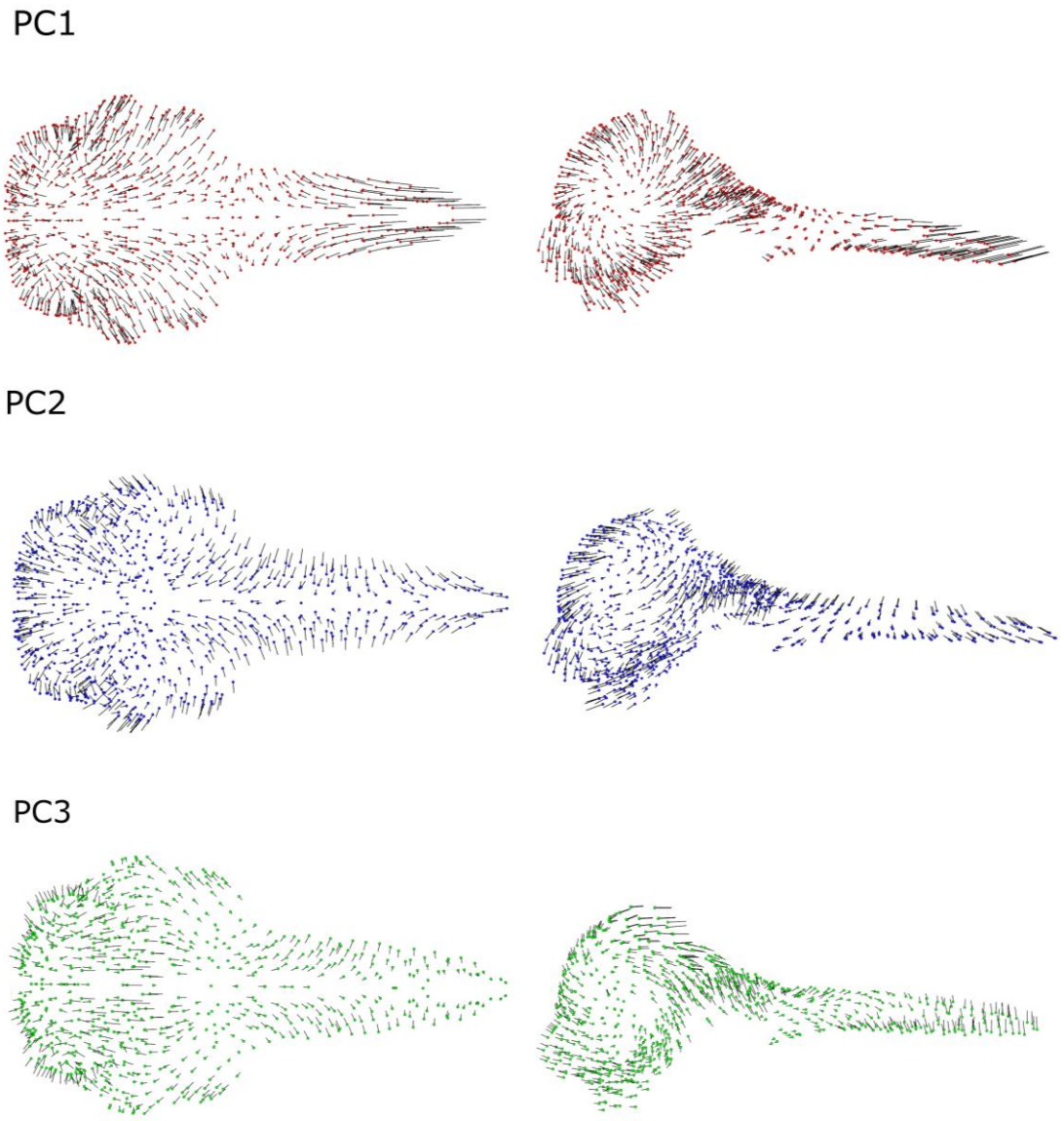

Figure 4.5. Vector displacement graph representing differences in landmark position between the mean landmark configuration and specimens along the positive PC1, PC2 and PC3 axes from the PCA produced in Figure 4.4.

Table 4.3. Results from Pairwise PERMANOVA tests on all Principal components retained from the PCA analysis shown in Figure 4.4. p-values are shown above the empty diagonal cells, while F-values are shown below the empty diagonal cells. Significant comparisons are marked in bold.

	Aduncus	California	Gephyreus	Guayaquil	Japan	Mediterranean	North Sea	Offshore	West Africa	Erebennus	Wsouth America
Aduncus (N = 28)		**0.006**	**0.006**	**0.006**	**0.006**	**0.006**	**0.006**	**0.006**	**0.006**	**0.006**	**0.006**
California (N = 19)	20.9		**0.006**	**0.006**	**0.006**	**0.006**	**0.006**	**0.006**	**0.006**	**0.006**	0.506
Gephyreus (N = 16)	15.9	18.7		**0.006**	**0.006**	**0.006**	**0.006**	**0.006**	**0.006**	**0.006**	**0.006**
Guayaquil (N = 17)	26.8	6.6	29.2		**0.006**	**0.006**	**0.006**	**0.006**	**0.006**	**0.006**	**0.011**
Japan (N = 14)	22.4	6.5	14.3	17.6		**0.006**	0.204	0.193	0.149	**0.006**	**0.033**
Mediterranean (N = 18)	10.8	3.9	12.0	10.1	5.73		**0.006**	**0.022**	0.473	**0.006**	**0.011**
North Sea (N = 14)	26.1	9.0	12.2	19.6	2.46	7.77		**0.006**	**0.017**	**0.006**	**0.006**
Offshore (N = 53)	28.0	5.8	18.4	17.3	2.70	3.76	6.01		**0.006**	**0.006**	**0.011**
West Africa (N = 11)	7.7	8.8	8.2	16.4	4.49	3.39	6.11	5.43		**0.006**	**0.022**
Erebennus (N = 28)	32.4	7.6	32.5	5.6	20.3	13.8	23.2	25.5	21.8		**0.006**
Wsouth America (N = 16)	21.4	2.5	16.2	4.8	5.07	4.46	5.80	4.79	7.97	7.94	

Distinct regions of the morphospace are occupied by each a priori OTU, as reflected by their different distributions across the first three PCs, each showing unique patterns of shape change. The main directions and magnitudes of shape change for each operational unit along the first 3 PCs are illustrated by the vector displacement plots (Figure 4.5). On PC1, shape changes relate to an elongation of the anterior half of the rostrum, extending from the mid-section to the anterior end of the rostrum. This elongation is accompanied by a slight shift upward towards the dorsal side, resulting in an apparently straighter rostrum with a less pronounced rostral bump. There is also a medial contraction of the maxillae, along with a deepening of the ascending processes of the maxilla at the base of the rostrum (near the external nares), resulting in a narrower and more concave profile at the skull features surrounding the prenarial triangle area. Finally, there is an upward displacement of both the squamosal arch and the occipital condyles, contributing to a greater ventro-dorsal compression of the basioccipital, as well as a slight contraction of the supraoccipital region (Figure 4.5).

On PC2, shape changes related to an elevation of the mid-rostrum region, resulting in the formation of a noticeable rostral bump. Additionally, there is a widening of the exterior margins of the maxillae and a depression of the craniofacial junction, which appears noticeably more concave. There is also a posterior expansion of the paraoccipital process and the squamosal arch, which combined with a contraction of the supraoccipital region, results in a noticeable change in the overall cranium shape (Figure 4.5).

On PC3, shape changes, although more subtle, reflect a medial contraction of the posterior half of the rostrum, while the anterior part shifts slightly upward. This results in a straighter

rostrum with a less prominent rostral bump. Additionally, there is a forward shift of the nasal bones and surrounding structures and a slight posterior expansion of the ascending process of the squamosal and the occipital condyles (Figure 4.5).

While an overview of the changes associated with the landmarks used to characterise skull shape variation between operational units are provided by vector displacement plots, they are less effective at capturing region-specific changes, given that coastal areas in particular are widely spread through the 3D morphospace. For this purpose, a clearer three-dimensional representation of skull shapes for each unit can be provided by warped meshes (Figures 4.6 & 4.7). The mean specimen, P198, identified using the function findMeanSpec(), was used as the reference skull to produce the warp meshes. This was an offshore specimen from the European seas, which is expected given the central position of offshore specimens in the morphospace. Therefore, all skull shape variations identified in the subsequent section are compared to this offshore "mean shape", meaning that the changes described will be subtler in the offshore OTU compared to those described in coastal units.

The *T. aduncus* skulls appear slender and more streamlined compared to the average skull. The anterior end of the rostrum is slightly longer, while the posterior margins of the premaxillae are contracted towards the sagittal plane. Additionally, the facial fossa (concave surface of the ascending process of the maxilla) is more expanded, the lateral side of the pterygoid is more compressed, and the ventral condyloid fossa together with the posterior part of the basioccipital is more expanded (Figures 4.6 & 4.7).

Some similar patterns of shape change are observed in skulls from the American continent, namely a general contraction of the rostrum and expansion of the ascending processes of the maxillae. However, there are also notable differences specific to each OTU. Guayaquil skulls have a more rounded supra-occipital region, accompanied by a more constricted parietal area, resulting in an apparent narrowing of the skull behind the frontal crest. Skulls from West South America show an enlargement of the posterior half of the rostrum, which combined with the enlargement of the ascending processes of the maxilla, makes the rostrum noticeably wider at the base. In Erebennus the area of the skull encompassing the basioccipital, squamosal, parietal, and frontal is wider with all these features expanding considerably. As a result, the skull looks broader in the region near the temples with a wider cranial width between the temporal bones. In addition, the exterior margins of the premaxillae are more contracted, and the occipital condyle is ventrally displaced. In California, wider cranial width between the temporal bones with an expansion of the temporal fossae and frontal area is observed. Additionally, a downward expansion of the pterygoid bone and a widening of the palatal surface are noticeable (Figures

4.6 & 4.7). In contrast, Gephyreus skulls have a broader posterior section of the rostral premaxillae, which seems to be related to the point of melon attachment. Additionally, the ascending process of the maxillae is expanded, while the region encompassing the parieto-supraoccipital contracts (Figures 4.6 & 4.7).

The skulls from Japan and the North Sea appear stouter and larger. They have wider rostrums relative to the mean, particularly at the posterior half of the rostrum, and the regions surrounding the nasal fossae are more expanded. In addition, the temporal arches and frontal bones are expanded, giving the cranium a wider appearance in the dorsal view and a more expanded occipital region. In Japan, the nuchal plane is contracted, and the tip of the pterygoid bone expands, while in the North Sea, the entirety of the occipital region, including the occipital condyle contracts, while the base of the pterygoid expands (Figures 4.6 & 4.7).

The Mediterranean skulls have a narrower orbital margin, which results in a less pronounced antorbital process. Additionally, the posterior part of the temporal fossae edge is expanded, making the skull appear broader and more robust in its posterior view. West African skulls appear overall more elongated and narrower, with a prominent extended rostrum and a rounder occipital region of the cranium. Most variations are characterised by the anterior half of the rostrum elongating into a thin tip, while the posterior half also elongates but widens slightly at the base of the rostrum. Additionally, the temporal fossae were more contracted, leading to a noticeably smaller occipital region (Figures 4.6 & 4.7).

Finally, the offshores show a contraction of the maxillae at the anteorbital process, resulting in a more concave appearance in this area. Additionally, they have more prominent nasal bones, a slight expansion at the parietal edges and the dorsal part of the occipital condyle, and an elongation of the pterygoid area (Figure 4.6). However, it should be noted that those changes are comparatively smaller because the mean reference skull is itself an offshore specimen.

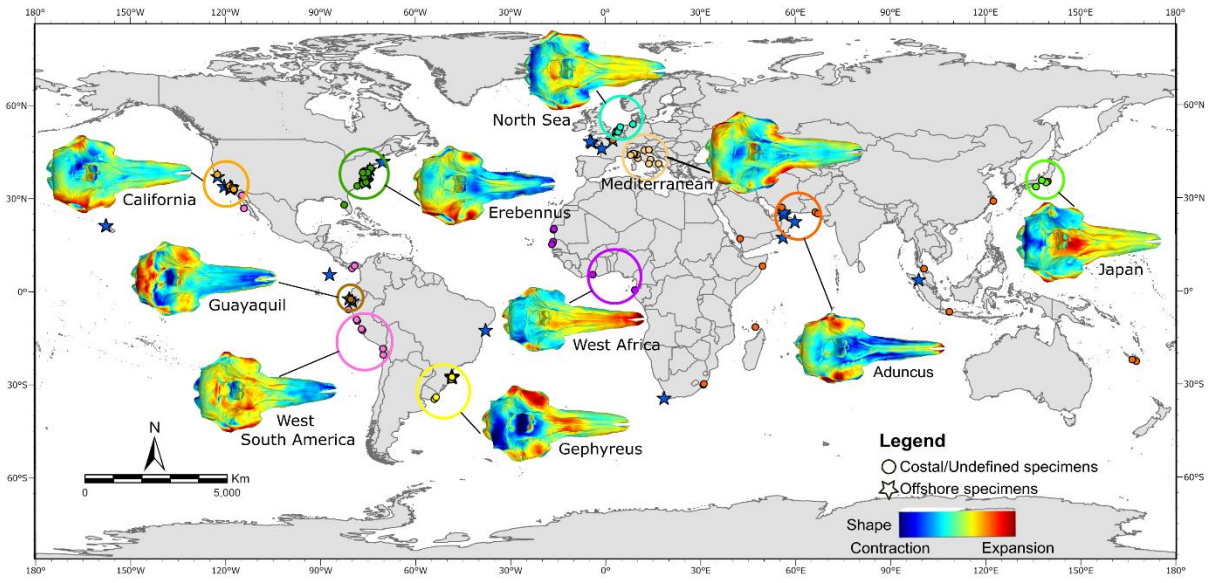

Figure 4.6. Map showing the distribution of bottlenose dolphin specimens analysed in this study, coloured based on a priori OTU classification. Skull images reflect 3D models characteristic of each OTU, warped from the mean skull shape determined by the PCA in Figure 4.4. The skull closest to the mean is represented by an offshore specimen from the North Atlantic. The colours on the skulls reflect the degree of difference from the mean, with blue representing a contraction and red representing an expansion.

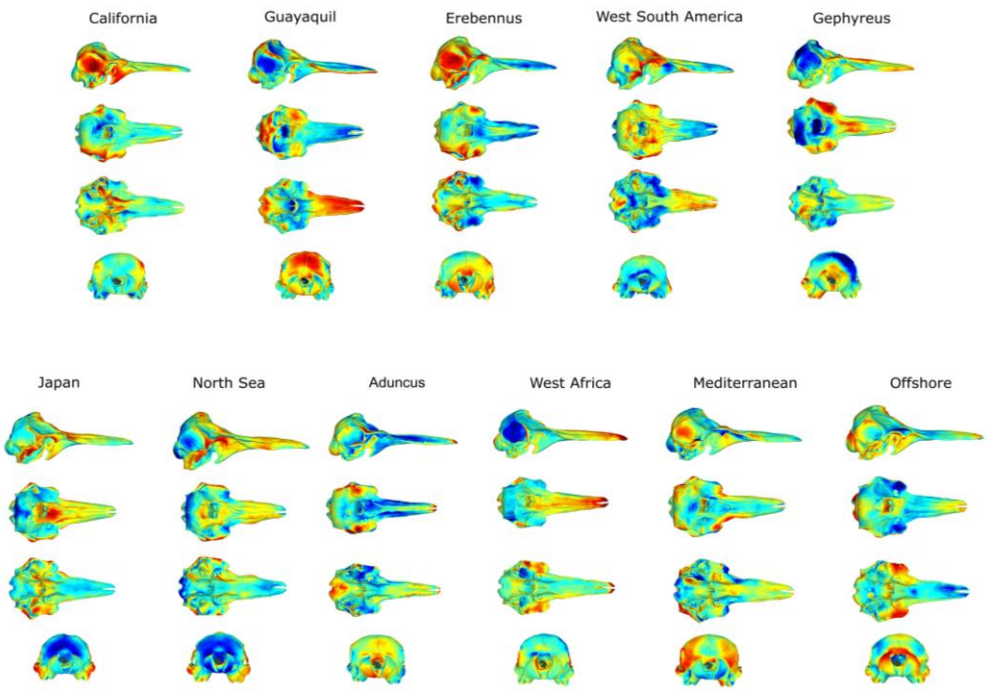

Figure 4.7. Skull images reflect 3D models characteristic of each OTU, warped from the mean skull shape determined by the PCA in Figure 4.4. The skull closest to the mean is represented by an offshore specimen from the North Atlantic. The colours on the skulls reflect the degree of difference from the mean, with blue representing a contraction and red representing an expansion.

Classification analysis

Random Forest

The Random Forest classified the skulls into their pre-defined OTUs with an accuracy of 72.65% (κ = 0.696; NIR = 0.15, *p*-value < 0.0001, CI: 0.665, 0.783; Table 4.2). All Aduncus and Gephyreus skulls (100%), and 89% of Erebennus skulls were correctly classified (Table 4.2). Additionally, over 75% of skulls from Guayaquil, Japan and the North Sea were correctly classified (76%, 86% and 79%, respectively; Table 4.4). Erebennus specimens were mostly misclassified into other coastal operational units from the American continent, namely California and Guayaquil. Similarly, most Guayaquil skulls were misclassified as Erebennus (3 out of 4), with one misclassified as West South America.

Interestingly, skulls from California and the Mediterranean were found to have lower correct classification rates (68%, and 67%, respectively; Table 4.4). Skulls from California were mainly misclassified into other coastal units from America, such as Erebennus, Guayaquil and West South America. The Mediterranean skulls were misclassified across four different units, including geographically close regions like the North Sea and West Africa.

West Africa, West South America, and the offshore operational units were found to have the highest misclassification rates (55%, 56% and 47%, respectively, Table 4.4). These units were most commonly misclassified into geographically proximate regions; for instance, West African skulls were often misclassified as Mediterranean (4 out of 5), and West South American skulls as California, Erebennus, and Offshore. However, it should be noted that the small sample sizes for both OTUs may have reduced the statistical power of the RF model. The offshore unit was found to have the highest diversity of misclassifications, being incorrectly assigned to eight groups, primarily California and the Mediterranean. This is consistent with the patterns observed in the PCA morphospace, where offshore skulls show closer morphological similarity to these groups.

Table 4.4 Confusion matrix from Random forest analysis classifying skulls to a priori groups.

	Predicted											
Real	Aduncus	California	Erebennus	Gephyreus	Guayaquil	Japan	Mediterranean	NorthSea	Offshore	WestAfrica	WsouthAmer	Total
Aduncus	28											28
California		13	2		1		1				2	19
Erebennus	1	1	25		1							28
Gephyreus				16								16
Guayaquil			3		13						1	17
Japan		1				12	1					14
Mediterranean		1	3				12	1		1		18
NorthSea							2	11		1		14
Offshore		7	2	1		3	10	1	25	3	1	53
WestAfrica							4		1	6		11
WSouthAmer		1	2			2		1	1		9	16
Total	29	24	37	17	15	17	30	14	27	11	13	234

Hierarchical Cluster Analysis:

The optimal number of clusters was determined using the gap statistic, which calculates within-cluster dispersion (how tightly the data points are grouped within each cluster) and compares it to the expected dispersion of a random dataset (null model). The gap, or difference between observed and expected dispersion, indicates the strength of the clustering structure, with a larger gap suggesting less likelihood that the structure is due to random variation. The gap statistic peaked at nine clusters with a value of 0.536, indicating that this configuration provides the greatest cluster separation relative to what would be expected by chance (See Supplementary Figure S4.3.1). In addition, the gap statistic plot showed a clear peak at nine clusters before stabilising. Therefore, the skulls were classified into nine clusters, as shown in the dendrogram (Figure 4.8; Supplementary Information Table S4.3.3 and S4.3.4).

Four clusters were primarily composed of a single operational unit, namely clusters 3, 7, 8 and 9, while the remaining clusters consisted of a combination of multiple units (Figure 4.8; Supplementary Information Table S4.3.4). Cluster 3 included 93.75% of all Gephyreus specimens, whose remaining skulls were part of the most diverse cluster (Cluster 2 - Figure 4.8; Supplementary Information Table S4.3.4). Cluster 9 was almost exclusively Aduncus, with 100% of its skulls included in this cluster, with the remaining portion being specimens from the Mediterranean. More than 75% of the skulls from Erebennus and Guayaquil are classified into their own distinct clusters (Figure 4.8; Supplementary Information Table S4.3.4). Cluster 8 is mainly composed of Erebennus (76.5%), with the remaining from California and to a lesser

extent Guayaquil and the Mediterranean. Similarly, cluster 7 is dominated by Guayaquil (76.5%), with the remaining consisting of Erebennus, California and West South America along with a smaller portion from the Mediterranean. The remaining skulls from these two operational units are mostly spread across Cluster 5 (Erebennus and Guayaquil) and Cluster 8 (Guayaquil), which also included specimens from California and West South America (Figure 4.8; Supplementary Information Table S4.3.4).

The skulls for the remaining operational units were more widely distributed. Mediterranean specimens were spread over seven clusters, while California skulls, were found in five clusters. Skulls from Japan and the North Sea were often classified together, in clusters that also included Offshore skulls (Clusters 1 and 6; Figure 4.8; supplementary Information Table S4.3.4). Clusters 2 and 4 were notable for consisting of specimens from nine and six different operational units, respectively and were mostly composed of Offshore skulls, along with smaller proportions from Japan, the North Sea, California, West Africa, West South America and the Mediterranean.

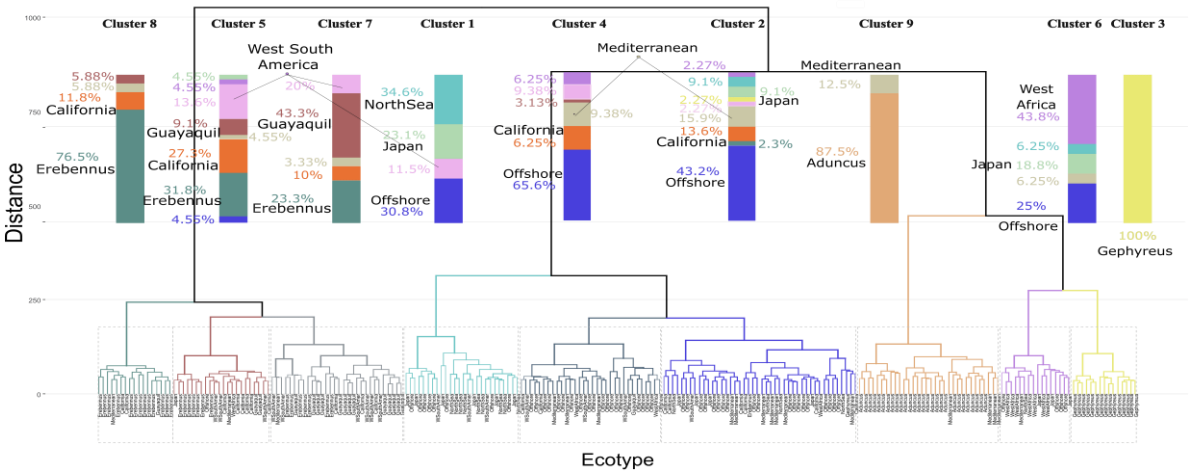

Figure 4.8. Hierarchical clustering analysis (HCA) was performed using Ward's distance metric on automated Procrustes aligned landmarks. The cluster R package was used to identify the most probable number of groups (i.e., K= 9). These groups are visually represented by different colours. The bar graphs illustrate the relative proportions of each OTU within each specific group, along with their corresponding proportion values. The colours match the OTUs on the PCA in Figure 4.4.

Comparison of Classification Results from the Two Landmarking Methods

The results from both Surface Semi-Landmarks (SSL) and Homologous Landmarks (HL) show consistent patterns of shape variation within the morphospace, with slight differences in

the extent of variation. A slightly greater proportion of total shape variation was explained by the first three PCs with HL, accounting for 58.6 % of total variation (PC1 = 26.8%, PC2 = 21.7%, PC3 = 10.1%). Both methods showed similar patterns of differentiation between offshore and coastal OTUs, with offshore units clustering centrally and coastal units spreading around them. However, HL provided a clearer distinction between Offshore and certain coastal units, such as West Africa, Gephyreus, Erebennus, and West South America (PERMANOVA *F*-values ranging from 3.62 to 31.82 and *p*-values ranging from 0.006 to 0.0825; See Supplementary Information Table S4.3.1. & S4.3.2.A). In contrast, the separation between North Sea and Japan, as well as between them and the Offshore, were less pronounced with HL (PERMANOVA *F*-values ranging from 3.53 to 5.97 and *p*-values ranging from 0.022 to 0.055; See Supplementary Information Table S4.3.1). Particularly, there was reduced intraspecific variation with HL for the North Sea.

RF model accuracy was similar for both methods (72.7% accuracy; CI: 0.665, 0.783; k = 0.694; NIR = 0.16; p-value < 0.0001), with slight variations in misclassification patterns (See Supplementary Information Table S4.3.2. and S4.3.3). Classification accuracy improved slightly by one or two specimens for most groups, except for California, North Sea, Japan and Offshore (1-2 specimens), where misclassifications mostly occurred into the Offshore OTU. Notably, Erebennus was misclassified into more operational units (e.g., Japan and West Africa), while Mediterranean specimens were predominantly misclassified as offshore or into Erebennus. Other units showed consistent misclassification patterns.

There were more discrepancies between the methods for the HCA analysis (See Supplementary Information Table S4.3.4. & Figure S4.3.4.). The gap statistics suggested eleven clusters with HL, resulting in more units separating into distinct clusters (e.g., Aduncus, Erebennus, California, North Sea, and West Africa) compared to SSL. Conversely, Guayaquil and Gephyreus were classified into fewer clusters, with all Gephyreus specimens grouped into a single cluster, while Guayaquil split into three. In the HL analysis, a higher proportion of Erebennus, California, West South America, and Japan specimens were classified into a single cluster. The opposite pattern was observed for Aduncus, Guayaquil, North Sea and West Africa, who had a lower percentage of classification into one group compared to SSL. Overall, HL increased the tendency for specimens from Erebennus, California, Guayaquil, and West South America to cluster together, while maintaining consistent classification patterns for most other units.

While HL results generally match those from SSL, more pronounced group separations tend to be shown in PCA and RF analyses, although only for certain units. By focusing on specific

anatomical similarities and localized structural changes, HL appears more sensitive to shape differences in the landmark areas, sometimes likely resulting in exaggerated separation of individual groups. Because SSL provides a broader and more balanced overview of shape across the entire skull, the results based on SSL are presented above and used in all downstream analyses. HL results are included in the supporting information for reference.

Environmental analysis

A significant correlation between shape and environmental variables was revealed by the 2b-PLS analysis (r = 0.538; p-value = 0.001). The shape vs environment plot shows a clear separation between Offshore and most other coastal OTUs, except for Aduncus and the Mediterranean (upper Figure 4.9). Coastal operational units are also well segregated from each other, with Erebennus being the most distinct, located at the opposite quarter of the plot relative to the Offshore unit. The North Sea was identified as the second most distinct coastal unit, although its separation was mostly driven by differences in their environment relative to other coastal units (upper Figure 4.9). Overall, clear differences in environmental characteristics of the habitats occupied by the various OTUs are suggested by the shape vs environment plot. Habitats occupied by coastal units can be as distinct from each other as the Offshore habitats are from coastal ones (based on the environmental variables used here). Coastal operational units from the American continent (except Erebennus) were clustered closely together, while units from Japan, the Mediterranean and West Africa were clustered closer to the Offshore and Aduncus operational units (upper Figure 4.9). This clustering pattern suggests that habitats from the American continent may be more similar to each other, while those in Japan, the Mediterranean and West Africa may share ecological characteristics with Offshore environments. Notably, Silicate Mean, Salinity Mean, Dissolved O2 Range, Chlorophyll Mean and Temperature Mean were identified as the main factors differentiating OTUs, contributing the most to the correlation between skull shape and environmental data. In contrast, Topographic position, Nitrate Mean and Ph Mean were found to contribute the least (lower Figure 4.9). It should be noted that these environmental factors are unlikely to directly influence skull shape but are instead proxies for broader biological processes.

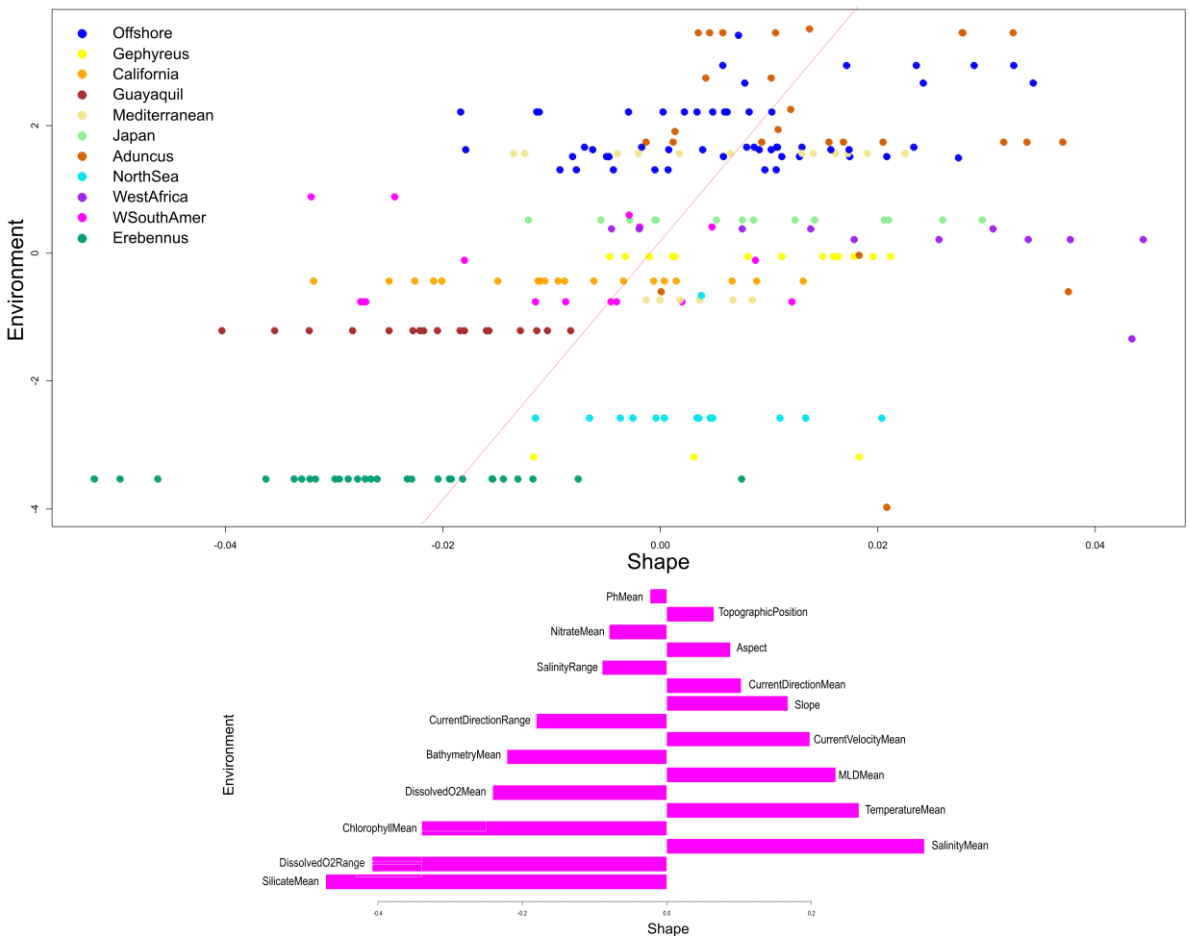

Figure 4.9. Upper - Results of the 2b-PLS analysis exploring the covariation between environmental variables and skull shape in bottlenose dolphins, with colours differentiating OTUs. Lower - Histogram giving the contributions of each environmental variable to the axis of covariation.

Significant associations between shape and environmental variables across the different OTUs were also revealed by the RDA analysis (F_{17}= 5.55, p-value = 0.001). Environmental variables were found to explain 30.58% of the total variance in skull shape. The first three constraint axes explain most of the variations, accounting for a total of 24.2% (RDA1 = 12.2%; RDA2 = 8.1%; RDA3 = 3.9%) of the variance in the shape data (ANOVA test: F_1=37.6, 24.9 and 11.9; *p*-value < 0.05; Table 4.5).

The Offshore OTU is observed to cluster at the negative end of RDA2, associated with MLD and bathymetry, reflecting its unique environmental conditions (Figure 4.10.A). Several other operational units were clustered near the Offshore OTU, including the North Sea, Japan, West South America, and West Africa (Figures 4.10.B & 4.10.D). While these units shared some associations with environmental variables, unique patterns were exhibited by each. For example, mean MLD and Bathymetry were associated with both the North Sea and Japan,

although the North Sea is strongly associated with mean O_2 and temperature. Mean salinity and, to a lesser extent, slope, mean silicate, and salinity range were associated with West Africa and West South America.

The coastal operational units are generally spread across the RDA biplot, suggesting greater variability in their patterns of association with environmental variables compared to the Offshore. At the positive ends of RD1 and RD2, specimens from the American continent (except Gephyreus) were clustered together (Figures 4.10.A & 4.10.D), showing strong associations with mean silicate and dissolved oxygen and to a lesser extent bathymetry and mean chlorophyll. On the other hand, West South America and California are associated with mean salinity, while Erebennus and Guayaquil have a small association with slopes. Aduncus spread mainly along the positive end of RD2 and negative end of RD1, showing a strong association with mean temperature and mean dissolved oxygen and a weaker association with mean current velocity (Figure 4.10.B & 4.10.D). In contrast, Gephyreus skulls cluster at the negative end of RD3, showing a strong association with salinity range (Figure 4.10A & 4.10.C).

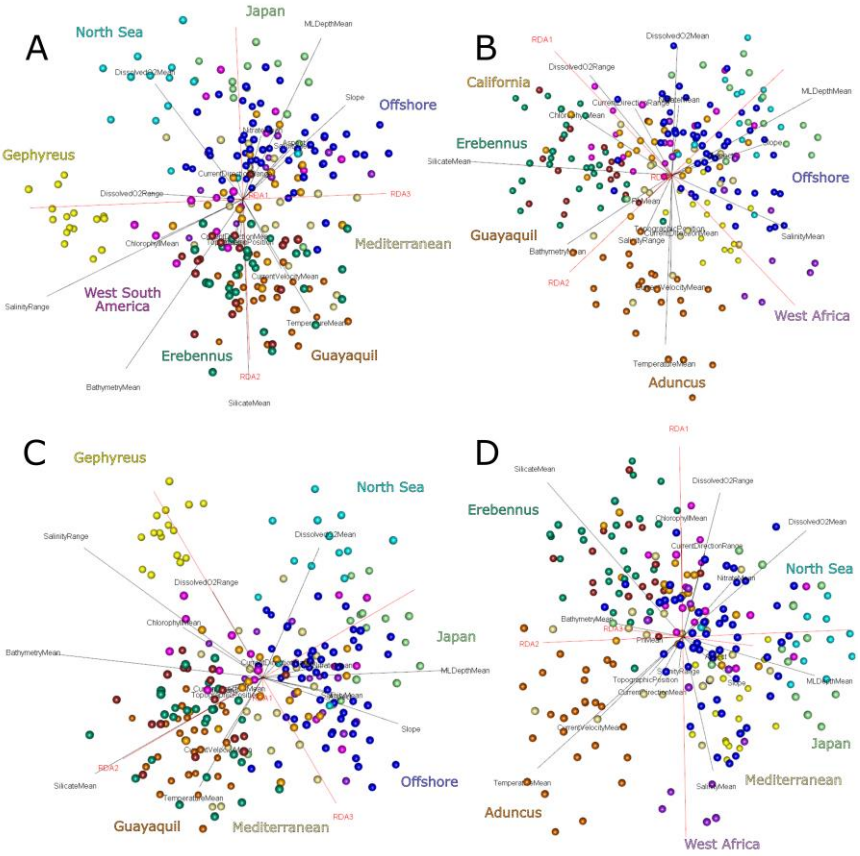

Figure 4.10. 3D plot of the RDA analysis exploring the association between environmental variables and skull shape in bottlenose dolphins along the three most important axes, with colours differentiating OTUs. The axes give the strength of association of skull shape with the corresponding environmental variable along RDA1 RDA2 and RDA3.

Table 4.5. Results from ANOVA on each RDA axis in the RDA model. Significance levels are indicated by stars: *: p < 0.05; **: p < 0.01; ***: p < 0.001.

	Df	Variance	F	Pr(>F)	
RDA1	1	0.00018434	37.6168	0.001	***
RDA2	1	0.00012211	24.9182	0.001	***
RDA3	1	0.00005824	11.8844	0.001	***
RDA4	1	0.00003325	6.7844	0.019	*
RDA5	1	0.00001616	3.2979	0.715	
RDA6	1	0.00000992	2.0246	0.99	
RDA7	1	0.00000919	1.8759	0.991	
RDA8	1	0.00000591	1.2066	1	
RDA9	1	0.00000494	1.0075	1	
RDA10	1	0.00000396	0.8077	1	
RDA11	1	0.00000338	0.6906	1	
RDA12	1	0.00000281	0.5737	1	
RDA13	1	0.0000021	0.4288	1	
RDA14	1	0.00000184	0.3761	1	
RDA15	1	0.00000158	0.3225	1	
RDA16	1	0.00000132	0.2702	1	
RDA17	1	0.00000094	0.1924	1	
Residual	214	0.00104868			

The strength of the association between each environmental variable and skull shape variability was tested with ANOVA analysis. Consistent with results from the 2b-PLS analysis, the strongest correlation values were shown by SilicateMean (ANOVA F_1= 16.74; *p*-value <0.001; Table 4.6.), accounting for 17.8% of the observed variation in skull shape. This was closely followed by SalinityMean and SalinityRange (ANOVA F_1= 11.15 and 13.54; *p*-value <0.001; Table 4.6), accounting for 11.8% and 14.36% of the variation, respectively. Strong correlation values were also exhibited by TemperatureMean (ANOVA F_1= 11.41; *p*-value <0.001; Table 4.6), accounting for 12.1% of the shape variation. The CurrentDirectionRange was found to contribute to 9.5% of skull shape variation (ANOVA F_1= 8.97; *p*-value <0.001; Table 4.6). In contrast, the least influence on skull shape variation was shown by NitrateMean, Slope, CurrentVelocityMean and TopographicPosition (ANOVA F_1= 0.747, 1.23; 1.58 and 0.607; *p*-values > 0.05; Table 4.6).

Table 4.6. Results from ANOVA on each environmental variable in the RDA model. Significance levels are indicated by stars: *: p < 0.05; **: p < 0.01; ***: p < 0.001.

	Df	Variance	F	Pvalue	
SalinityMean	1	0.000055	11.151	0.001	***
SalinityRange	1	0.000066	13.538	0.001	***
SilicateMean	1	0.000082	16.736	0.001	***
TemperatureMean	1	0.000056	11.406	0.001	***
Aspect	1	0.000028	5.655	0.001	***
MLDepthMean	1	0.000025	5.182	0.001	***
NitrateMean	1	0.000004	0.747	0.646	
PhMean	1	0.000012	2.394	0.015	*
Slope	1	0.000006	1.232	0.251	
ChlorophyllMean	1	0.000023	4.684	0.001	***
DissolvedO2Mean	1	0.000016	3.347	0.001	***
DissolvedO2Range	1	0.000010	2.027	0.044	*
CurrentDirectionMean	1	0.000012	2.533	0.017	*
CurrentDirectionRange	1	0.000044	8.972	0.001	***
CurrentVelocityMean	1	0.000008	1.583	0.115	
BathymetryMean	1	0.000012	2.487	0.01	**
TopographicPosition	1	0.000003	0.607	0.806	
Residual	214	0.001049			

Tooth count

The highest intra-unit variation in tooth count was shown by Aduncus, North Sea, West South America and West Africa (SD = 2.98, 3.67, 2.72 and 2.91, respectively; Figure 4.11), though the latter three had the smallest sample sizes (N= 10, 13 and 11, respectively). In contrast, the lowest intra-unit variation was shown by California, Gephyreus, Guayaquil and the Mediterranean (SD = 1.79, 1.44, 1.44, 1.79, respectively). Additionally, there were tooth count differences between groups, which were mostly driven by small differences in a few specific OTUs (Kruskal–Wallis test: H = 104.2; *p*-value <0.001; Figure 4.11 & Table 4.7). Aduncus was found to have significantly higher tooth counts (mean 48; range 42-52) compared to most other operational units (Dunn test: *p*-values range from <0.001 to 0.018; Table 4.7), except for Japan, North Sea, Erebennus, and West Africa (Dunn test: *p*-values > 0.05; Table 4.7). Significantly lower tooth counts were found for Guayaquil (mean 38; range 35 – 40), compared to most other units (Dunn test: *p*-values $\leq$ 0.005; Figure 4.11 & Table 4.7), except California, Gephyreus, Mediterranean, and West South America (Dunn test: *p*-value > 0.05; Table 4.7).

Table 4.7. Pairwise Dunn's test results for comparison between OTUs of teeth alveoli counts. Bonferroni corrected p-values are shown above the empty diagonal cells, while Z-statistic is shown below the empty diagonal cells. Significant comparisons are marked in bold.

	Aduncus	California	Gephyreus	Guayaquil	Japan	Mediterranean	North Sea	Offshore	West Africa	Erebennus	Wsouth America
Aduncus		**$5.30*10^{-8}$**	**$9.38*10^{-5}$**	**$3.23*10^{-12}$**	1	**$2.46*10^{-5}$**	0.443	**0.018**	1	1	**$8.92*10^{-08}$**
California	6.12		1	1	**0.006**	1	0.932	**0.013**	**0.024**	**0.001**	1
Gephyreus	4.79	0.706		0.732	0.145	1	1	0.938	0.465	0.129	1
Guayaquil	7.51	1.99	2.48		**$5.87*10^{-06}$**	0.334	**0.005**	**$2.29*10^{-6}$**	**$3.10*10^{-5}$**	**$1.98*10^{-7}$**	1
Japan	1.14	3.89	3.01	5.32		0.117	1	1	1	1	**0.003**
Mediterranean	5.05	0.881	0.108	2.74	3.07		1	0.682	0.399	0.079	1
North Sea	2.65	2.39	1.61	3.92	1.31	1.60		1	1	1	0.418
Offshore	3.59	3.69	2.39	5.48	1.49	2.50	0.198		1	1	**0.008**
West Africa	1.67	3.52	2.63	5.00	0.43	2.69	0.916	0.989		0.125	3.72
Erebennus	2.26	4.27	3.04	5.90	0.621	3.19	0.954	1.17	1		**0.001**
Wsouth America	6.03	0.527	1.13	1.34	4.06	1.31	2.67	3.80	0.011	4.35	

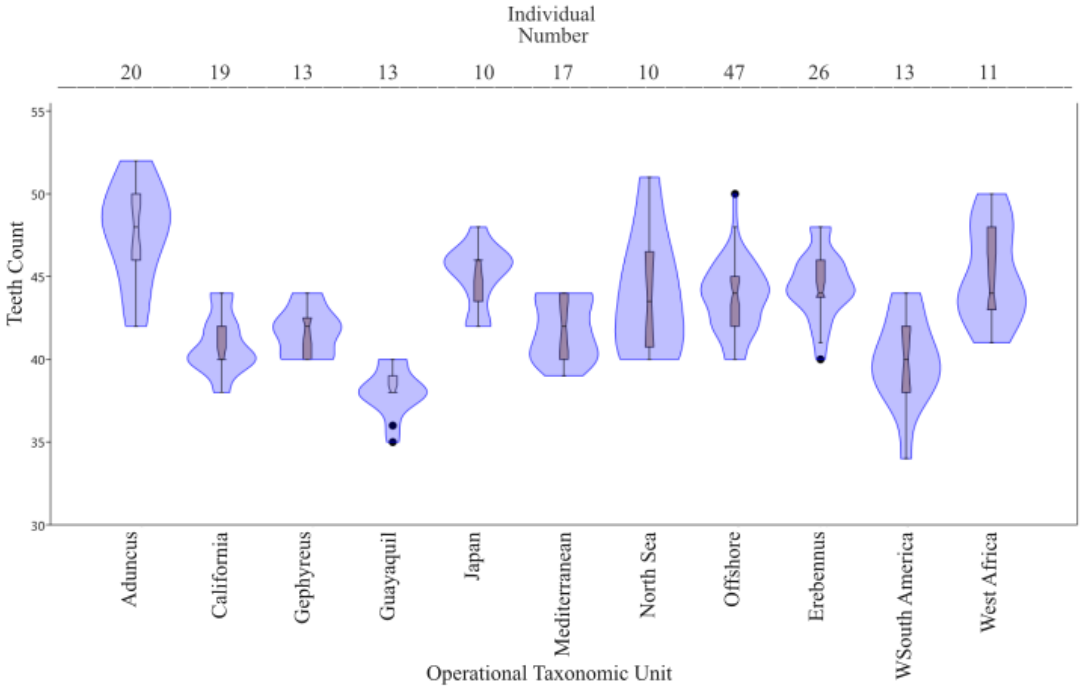

Figure 4.11. Violin plots showing the results of the teeth Count between a-priori OTUs. The boxes represent the interquartile range within each unit with the notches indicating the median value. The black dots represent the outliers.

4.4. Discussion

Shape patterns

A consistent pattern of skull-shape differentiation was identified across 10 operational taxonomic units (OTUs) of bottlenose dolphins, including coastal and offshore representatives from different locations worldwide. While substantial phenotypic diversity has been documented within the genus (Oxford-Smith et al., 2024), this study provides a more detailed description of these patterns across a broader geographic range, using higher resolution methods to detect and quantify morphological differentiation. The degree of inter-unit variation was found to differ between individual operational units. Specifically, Aduncus and Gephyreus, exhibited marked separation from other units in the morphospace, indicating clear differences in skull morphology. In these two cases, skull shape differences were consistent with previous genetic (Leduc et al., 1999; Wang et al., 1999; Möller & Beheregaray, 2001), osteological (Wang et al., 2000a; Costa et al., 2016) and morphological evidence (Wickert et al., 2016; Wang et al., 2000b) that led to their taxonomic distinctions. Contrastingly, less pronounced differentiation was detected in some coastal units, like California and the Mediterranean, particularly relative to the Offshore operational unit. Clear separation from the Offshores was also observed for well-known units such as Erebennus and Guayaquil, though some overlap with other coastal units from the American continent was also seen. Morphological differences were also identified in lesser-known units, consistent with previous studies that suggest unique coastal operational taxonomic units in these regions (as discussed in more detail below).

Most Offshore specimens clustered near the centre of the morphospace, a pattern consistent with previous studies comparing coastal and offshore OTUs (Dromby et al., 2023; Oxford-Smith et al., 2024). This suggests that the offshore skull shape represents the average morphology in our dataset and is largely independent of geographic location. Despite clear differentiation from well-described coastal operational units, the Offshores also overlapped with several coastal units. Our findings are thus consistent with previously reported patterns of clear skull shape differentiation between coastal and offshore OTUs (Wickert et al., 2016; Hohl et al., 2020; Costa et al., 2022) but also patterns of overlap among certain coastal units (Santillán et al., 2008; Dromby et al., 2023; Oxford-Smith et al., 2024). These overlaps possibly reflect intermediate or transitional shapes, as some individuals may not fit well into offshore or coastal categories. While ongoing gene flow between OTUs could create these patterns, previous studies indicate clear genetic differentiation among some of the units analysed here (e.g., Louis et al., 2014; Lowther-Thieleking et al., 2015; Bayas-Rea et al., 2018; Nykänen et al., 2019).

Coastal skull shapes, in contrast, were found to be unique to each geographic region, clustering in distinct regions of the morphospace. Even with overlap for some OTUs, clear distinctions from the Offshore unit were still observed for each coastal operational unit. However, variation in the degree of differentiation was observed and did not always reflect the inference from regional scale studies. For example, a high degree of differentiation was exhibited by Gephyreus, consistent with previous studies showing differentiation from offshore *Tursiops truncatus* in cranial structure, vertebrae count, and body size, along with a more restricted distribution (Wickert et al., 2016). Minimal genetic connectivity between the two OTUs has also been suggested by genetic markers (Fruet et al., 2017). In contrast, less pronounced skull shape differences were detected between offshore and coastal specimens for California and the Mediterranean, compared to those reported in individual studies (e.g., Perrin et al., 2011; Dromby et al., 2023). In the Mediterranean, a lower degree of differentiation is expected given previous research showing a mix of coastal and offshore individuals within the basin (Gaspari et al., 2015; Carnabuci et al., 2016). For California coastal specimens, however, this lower differentiation is somewhat unexpected, as a clear distinction from the offshore unit had been indicated in previous studies, including genetic differences (Perrin et al, 2011; Lowther-Thieleking et al., 2015).

Despite more limited ecological or genetic evidence, some locations show greater skull shape differentiations compared to other well-known coastal units, like California (Perrin et al., 2011). Therefore, the findings presented here support the existence of distinct coastal operational units in those regions, as suggested by previous studies in the Southeast Pacific (Santillán et al., 2008), the North Sea (Louis et al., 2014; 2023), and West Africa (Van Waerebeek et al., 2008). The West South America unit is mainly composed of individuals from Peru (10 out of 18), along with specimens from Chile, Mexico, and Panama. Previous studies have identified genetic (Sanino et al., 2005; Bayas-Rea et al., 2018) and morphological (Félix et al., 2018) distinctions between offshore and several coastal units in the Southeast Pacific, notably for individuals from Peru and Chile (Sanino et al., 2005; Santillán et al., 2008). In addition, there are also genetic differences between the different coastal units in this region (Sanino et al., 2005; Bayas-Rea et al., 2018). Our results support the existence of a distinct coastal operational unit in Peru but also the potential for other distinct units along the Southeast Pacific, although this study lacks the required resolution to identify them. Similar patterns have been observed in the West North Atlantic, where several coastal stocks are distinguished by their association with estuaries and gulfs (Rosel et al., 2009). Therefore, the presence of other coastal operational units in the southeast Pacific, distinct from both the Guayaquil and Offshore

units, is suggested by this study, further emphasizing the species diversity at a fine geographical scale.

Similarly, the North Sea operational unit was clustered on one side of the morphospace, with some degree of separation from the Offshore unit. These patterns are consistent with previous morphometric studies for these two coastal regions (Oxford-Smith et al., 2024), and genetic studies have also identified distinct resident groups in and around the North Sea, including those in East Scotland and West Scotland (Louis et al., 2014; Nykänen et al., 2019), with a low migration rate between these groups. In this study, most skulls were collected along the coasts of the Netherlands, however, movements of dolphins have been reported between East and West Scotland (Louis et al., 2014), and bottlenose dolphins in the Netherlands are thought to originate from areas throughout the North Sea including the Scottish coasts (Hoekendijk et al., 2021).

Evidence of distinct morphological structures is also shown in Japan, similar to the North Sea. A distinct coastal population has been suggested in East Japan, showing clear genetic differentiation from populations from the Western part of the island (Chen et al., 2017). Individuals in eastern Japan were also found to differ in body length and sexual maturity (Kasuya, 1997). Oceanographic features such as the Kuroshio Current may influence gene flow contributing to the formation of distinct groups in this region. In bottlenose dolphins, population structuring has been reported even in the absence of physical barriers (Natoli et al., 2005; Fruet et al., 2014; Pratt et al., 2018; Gray et al., 2021)

Individuals from West Africa are clearly identifiable as a distinct coastal OTU, despite a slight overlap with the Offshore unit. In the morphospace, they were clustered more closely to Gephyreus while remaining separate from other coastal units. Unlike previous studies (Oxford-Smith et al., 2024), this study shows that individuals from West Africa do not cluster closely with Aduncus, indicating that more distinct morphological traits may be present than previously identified. Specifically, longer rostrums and narrower craniums were observed, consistent with characteristics described in Senegal and Mauritania (Robineau & Vely, 1997). Thus, the results of this study support the presence of distinct coastal and offshore OTUs in the region, further supported by previously described differences in prey and feeding strategies (Van Waerebeek et al., 2016). These findings are especially significant given the limited resources for comprehensive studies in West Africa.

However, these regions were represented by relatively smaller sample sizes compared to other units, which may be biasing the apparent patterns of differentiation for this region. Furthermore, the lack of prior information on the ecology of those specimens in the area means that they cannot be correctly categorized as either offshore or coastal. Therefore, future research

is needed to clarify the diagnostic criteria for each operational unit in this region, making patterns of differentiations clearer.

Similarities in skull shape patterns were observed for the American continent OTUs, namely Erebennus, Guayaquil, West South America and California. While this overlap between specimens from the Pacific Ocean likely reflects a shared evolutionary history and closer genetic relationships, the similarity between Erebennus and the Pacific operational units is more difficult to interpret. One explanation is that similar environmental pressures between those regions may contribute to similar traits that serve similar functions. This is particularly likely given the low likelihood of modern genetic exchange between the Atlantic and Pacific Ocean populations, due to the closure of the Isthmus of Panama around 3 million years ago, which provided a known isolation barrier between Pacific and Atlantic marine species (O'Dea et al., 2016). Similarly, coastal areas of Japan and the North Sea are likely isolated by the large distances between these two regions. Although long-distance movement between these regions is possible, its likelihood can be considered low, particularly given that the longest documented journey by a bottlenose dolphin spans 4 200 km (Wells et al., 1999). Even then, this event involved an offshore form of the species, suggesting that such extensive migrations are rare and may not be representative of typical movement patterns within coastal units. Therefore, the morphological similarity between Japan and the North Sea is unlikely to reflect a recent shared evolutionary history.

Additionally, previous studies have indicated limited genetic mixing with adjacent populations in Erebennus (Hoelzel et al., 1998), Guayaquil (Bayas-Rea et al., 2018), the North Sea (Louis et al., 2014) and Japan (Chen et al., 2017). This is consistent with previous studies showing that coastal bottlenose dolphins exhibit strong site fidelity (Urian et al., 2009; Gonzalvo et al., 2014; Giacomo & Ott, 2016; Passadore et al., 2018a; Takeshita et al., 2021), which can contribute to pronounced genetic structuring even over short distances. These findings support the idea that gene exchange across the major barriers in our study is highly improbable. In contrast, the similarities between the North Sea and Japan could result from incomplete knowledge of ecological differentiation in those regions. Currently, no clear morphological criteria exist to clearly distinguish between coastal and offshore individuals in these regions, potentially misclassifying offshore individuals as coastal. Since offshore individuals are known to have similar skull shapes across different geographical areas, the overlap observed between the North Sea and Japan is likely to reflect these misclassifications.

The skull features differentiating coastal from offshore OTUs were found to vary between regions. For example, an expanded squamosal and parietal area with a slender rostrum was

observed in some coastal units (e.g., Erebennus), while a contracted parietal area and longer rostrums were found in others (e.g., West Africa). These combined traits are shown to contribute to the occurrence of unique skull shapes in each coastal region analysed in this study. Therefore, it is unlikely that shape variation is driven solely by adaptation to a coastal environment, as this would likely result in a more uniform skull shape across coastal operational units. Instead, historical demographic events in each coastal unit, associated with population isolation, likely played a significant role in shaping these patterns. Changes in ocean structuring and ecological conditions have been proposed as key drivers of differentiation in Delphinidae (e.g. Steeman et al., 2009; Morin et al., 2015; Segura-García et al., 2016; Amaral et al., 2017; do Amaral et al., 2018). Under such circumstances, coastal regions might have been recolonized repeatedly, increasing the chances of founder events, where specific traits from the initial colonisers become fixed due to limited genetic variation. Subsequently, genetic drift could have further emphasised morphological differences, because changes in allele frequencies are more pronounced in small, isolated populations (Kimura & Ohta, 1971). Genetic evidence from the North Sea (Louis et al., 2023) and the Mediterranean (Natoli et al., 2005; Moura et al., 2013; Gaspari et al., 2015), has suggested the recent divergence of coastal individuals from Atlantic sources, supporting the role of these processes.

Shape variations correspond to differences in the feeding apparatus and bones associated with the sound production system. Specifically, the anterior half of the rostrum and the temporal arches were often found to differ between OTUs. While Aduncus and West Africa showed a thin, elongated rostrum together with a contraction of the temporal arch and postorbital process, operational units such as Guayaquil and West South America displayed a shorter, wider rostrum and in South America an expanded temporal arch is noticeable. Additionally, in Gephyreus and Erebennus, the prenarial contraction coincided with an expansion around the rostral bump, possibly related to the melon attachment, which plays a role in sound production. Similarly, there were variations in the width of the bony nares and the length of the pterygoid between operational units. Generally, units from the North Sea, Japan, West Africa, and West South America were found to have wider bony nares, while Aduncus, Erebennus, Gephyreus, and Guayaquil were observed to have narrower nares. The pterygoid bone was typically expanded in California, Japan, and the North Sea but shorter in Aduncus and Guayaquil. Additionally, a ventral displacement of the occipital condyle was seen in Guayaquil, Erebennus, and Aduncus, while a dorsal displacement was seen in Gephyreus and an overall contraction of the condyle was observed in North Sea specimens.

Environmental Variables

Each skull shape typical of an OTU was correlated with several environmental variables. Most operational units were correlated with two or more variables, exhibiting distinct interaction patterns. Only Gephyreus and Aduncus showed strong associations with a single variable. These associations suggest that skull shape variations are influenced by multiple environmental factors, which collectively represent the complex ecological characteristics of an area. For example, a unit simultaneously correlated with silicate, dissolved oxygen, and chlorophyll, may reflect interconnected biological processes of nutrient cycling and primary production in marine environments (Jones, 1998). These variables typically indicate diverse, nutrient-rich coastal environments, where nutrient input from land mixes with ocean water. High silicate levels, for example, reflect higher diatom abundance, which forms the base of marine food webs (Ragueneau et al., 2002; Allen et al., 2005). Similarly, high chlorophyll levels serve as a proxy for phytoplankton abundance (Johnston & Brown, 2013). As a result, such waters often exhibit high levels of dissolved oxygen, indicative of active photosynthetic processes. This oxygen production is essential for sustaining fish and other marine organisms and is therefore characteristic of productive environments where a balance between oxygen generation and consumption is maintained. In contrast, an association with mixed layer depth (MLD) along with variables such as salinity, bathymetry and slopes, is more typical of nutrient-depleted environments. Elevated salinity levels may indicate limited freshwater input (Skliris et al., 2014), which is more pronounced in offshore waters. In addition, bathymetric features and gentle slopes contribute to reduced vertical mixing (Gille et al., 2022). These factors typically reflect lower primary productivity characteristics of the offshore environment. Considerable differences in patterns of environmental associations were observed between the offshore and remaining coastal units. Offshore individuals were mainly associated with bathymetry, mixed layer depth (MLD), slope, and salinity (both mean and range).

This is unlike coastal units, where associations with a broader range of variables were seen. Offshore regions exhibit more stable oceanographic conditions than coastal areas, although they tend to be more nutrient-limited (Webb, 2023). This environmental stability suggests that offshore individuals experience relatively consistent ecological pressures, even across their broad geographical ranges. While these pressures may seem subtle across large geographic extents, specific characteristics of the offshore environment, such as lower nutrient availability, and deeper waters, with associated steeper temperature gradients, are considered physiologically challenging. These extreme characteristics can contribute to strong selective pressures and influence skull shapes observed in this OTU. This may lead to more uniform skull

shapes, as individuals may be subject to selection pressures that promote traits favourable for survival in the open ocean. Coastal operational units are more strongly associated with environmental variables such as silicate, salinity, temperature, chlorophyll and dissolved O2. These hydrological features are typically used as proxies for nutrient concentration, primary productivity, and aggregation of biomass (Allen et al., 2005; Essington et al., 2022). The greater variability in coastal environments, due to factors like freshwater runoff, sediment deposition, nutrient inputs from rivers and streams, estuarine mixing, and seasonal fluctuations in temperature and salinity (Nixon et al., 1986) create diverse ecological conditions that directly impact biological productivity. This variability could contribute to selective pressure influencing skull shape, particularly structures related to functions such as feeding. Among these variables, dissolved oxygen in particular, can serve as a proxy for biological activity, with higher oxygen levels generally being associated with areas of greater fish abundance (Howell & Simpson, 1994).

Specific patterns of association were exhibited by Gephyreus and Aduncus. Salinity range was strongly associated with Gephyreus, while mean temperature was associated with Aduncus. Gephyreus is typically found in lagoon systems, bays and river mouths such as the Itajaí River, North Bay, Mampituba River, and Tramandaí River (Vermeulen et al., 2019). These environments exhibit high variability in salinity conditions like the Patos Lagoon estuary, where high temporal and spatial salinity fluctuations are experienced (Moller et al., 2001). Although these hydrological characteristics can influence broader ecological conditions, directly associating skull shape to biological processes driven by salinity range is challenging. Therefore, these results could primarily reflect the most distinctive variable for this specific habitat rather than the underlying processes driving adaptations. A similar conclusion applies to Aduncus, which inhabits shallow, complex coastal habitats in warmer tropical waters (John & Yang, 2009; Hammond et al., 2012). Aduncus has a wide distribution across the Indian Ocean (Braulik et al., 2019), indicating its presence in diverse environmental conditions. Shape variations in Aduncus are likely influenced by both biotic and abiotic factors, which may reflect adaptations to traits favourable for specific diets and varying oceanographic conditions. Nevertheless, despite its wide distribution and habitat variability, a particularly strong association with temperature, characteristic of the Indian Ocean is shown by Aduncus.

Biological Interpretation

Ecological Influences on Coastal and Offshore Skull Variation

Distinct skull shape patterns were displayed by each coastal OTU, unlike the more uniform shapes observed in the offshore operational unit. Coastal marine ecosystems are known for their high productivity and diverse habitats (Nixon et al., 1986), shaped by a complex interplay of biotic (e.g., prey availability) and abiotic factors (e.g., oceanographic conditions; McLean, 2001). These biotic and abiotic factors interact to create diverse ecological niches that contribute to the uniqueness of each coastal habitat. While certain features, such as abundant prey and shallow waters, are shared by coastal environments, they also differ in key aspects including prey composition, habitat complexity (e.g., kelp forest, seagrasses, estuaries) and oceanographic conditions (e.g., salinity, current velocity; Mann, 2000). These ecological differences may exert ecological pressures on skull shape, particularly in relation to feeding, communication, and swimming. As a result, unique skull shapes may have developed in coastal units. Supporting this idea, correlations between skull shape and factors like prey size have been shown in Delphinidae studies (McCurry et al., 2017), and potential associations with communication systems (Laeta et al., 2023). For example, cranial asymmetry and hypertrophy of the nasal apparatus are thought to be associated with the production of complex echolocation clicks and social vocalisations (Laeta et al., 2023). However, it is also important to consider that genetic drift in smaller coastal populations, may also contribute to the observed variation in skull shape (more detailed discussion below).

The consistent skull shape patterns observed in offshore individuals, regardless of their ocean of origin, suggest stabilising selection. Offshore habitats, characterized by deep waters, low prey abundance and limited ecological diversity (Webb, 2023), exhibit relatively stable and homogeneous ecological conditions. These consistent characteristics likely exert similar ecological pressures across the different offshore individuals worldwide, potentially maintaining skull shapes better suited for survival in these environments. In mammals, stabilising selection has been recognized as an important force driving evolution (Lemos et al., 2001; Schroeder & von Cramon-Taubadel, 2017; Machado et al., 2022). This evolutionary mechanism favours intermediate phenotypes, maintaining traits within beneficial adaptive zones (i.e., an ecological niche where organisms thrive by exploiting resources through specialised adaptations). For example, in cingulata (armadillos and their relatives), stabilising selection is thought to have preserved a consistent skull shape across most extant species (Machado et al., 2022). These species occupy what is called the "generalist-armadillo" adaptive zone, characterised by broad, non-specialised diets and ecological roles. As a result, their

overall skull shape remained stable over time, while other traits such as size have varied more readily in response to specific environmental pressures. Similarly, in bottlenose dolphins, offshore adaptations may include traits for long-distance travel to locate schooling fish or deep-diving capabilities for predation on pelagic fish.

Skull Morphology and Functional Implications

Within mammals, variations in skull shape, particularly in rostrum or snout size and shape, are well documented and often influence jaw mechanics (Slater et al., 2009; Slater & Van Valkenburgh, 2009; Damasceno et al., 2013). They can impact functional performance, including bite force, speed of jaw closure, and the range of jaw opening. For example, bite force can be enhanced by a shorter rostrum, which shortens the jaw out-lever distance, while a longer rostrum can facilitate faster jaw closing but typically reduces bite force (Radinsky, 1981). In mammalian carnivores, bite force is considered to play an important role in prey capture and processing (Rahmat & Koretsky, 2015; Campbell & Santana, 2017). Species that commonly crush or grind their food items (e.g., spotted hyenas, giant pandas) demonstrate higher bite forces due to specific morphological changes, whereas species with reduced bite force (e.g., Crabeater seals) exhibit alternative feeding strategies like suction or filter feeding (Rahmat & Koretsky, 2015).

Consequently, species with similar diets or using the same foraging techniques often exhibit comparable skull shapes, reflecting their shared bite force requirements (Figueirido et al., 2013). Conversely, different feeding habits can lead to distinct skull shapes (Santana et al., 2010; Kienle & Berta, 2016; 2018). These shape variations are often associated with muscles such as the masseter, temporalis, and pterygoid, which are directly connected to the rostrum. For example, in bats, a pronounced coronoid process and well-developed sagittal and nuchal crests, increase the surface area for temporalis muscle attachment while a broader zygomatic arch allows for a larger masseter muscle (Santana et al., 2010). In addition, the temporal arch provides attachment points for muscles such as the temporalis, masseter, and pterygoid (Cozzi et al., 2016). The temporalis is primarily involved in elevating and retracting the mandible, while the masseter contributes to jaw elevation and the pterygoids assist in lateral movements and additional stabilization (Franco-Moreno et al., 2021). In contrast, the preorbital process contributes to the overall rigidity and strength of the skull supporting the rostrum and withstanding the forces generated during swimming and prey capture (Cozzi et al., 2016). Variations in these structures appear closely related to rostrum variations, as they are both associated with muscles involved in biting. Biting is particularly important for dolphins, as their

feeding apparatus is the primary means for grasping and holding prey, compensating for limb reduction compared to terrestrial mammals. Therefore, significant changes in these skull structures are expected to result from dietary differences requiring varying bite forces.

Dietary, environmental, and vocal influences on skull shape in bottlenose dolphins

Although establishing direct relationships between cranial shape and feeding habits in such a generalist feeder such as the bottlenose dolphin might be challenging, some dietary studies suggest that bottlenose dolphins living in deep areas tend to consume small mesopelagic fish and squid (Barros et al., 2000), whereas those in coastal environments consume small to large nearshore fish (Barros, 1993; Gannon & Waples, 2004; McCabe et al., 2010), suggesting skull-shape adaptations to different feeding strategies. Furthermore, bottlenose dolphins have been observed using sponge-feeding in Shark Bay, Australia (Smolker et al., 1997; Krützen et al., 2005), mud ring feeding in the Gulf of Mexico (Ramos et al., 2022), beach hunting in the Colorado River, Mexico (Silber & Fertl, 1995) and fishermen cooperating in Brazil (Daura-Jorge et al., 2013). These regional strategies were also associated with different prey types; for example, mud ring feeders and beach hunters typically target schooling fish such as mullet or pinfish (Silber & Fertl, 1995; Ramos et al., 2022). In sponge feeders, dietary distinctions between sponge feeders and non-sponge feeders have been suggested through fatty acid analysis, suggesting that unique foraging niches are facilitated by sponge feeding (Krützen et al., 2014). Given that sponges are primarily used for foraging (Smolker et al., 1997), it is likely that sponge-feeding dolphins primarily consume benthic prey, including bottom-dwellers such as small fish, crustaceans, or cephalopods. Therefore, distinct skull shapes are likely influenced by the diversity in diet and foraging strategies among coastal operational units, with beach hunting requiring adaptations for navigating shallow waters, mud ring feeding for rapid swimming and sponge feeding for hard food biting.

Previous studies have suggested that different shape patterns could be related to different feeding habits between coastal and offshore OTUs. Key morphological differences previously observed between coastal and offshore bottlenose dolphins include: the width of the skull and the rostrum (Perrin et al., 2011; Costa et al., 2016; Jedensjö et al., 2017; Hohl et al., 2020; Costa et al., 2022; Dromby et al., 2023; Oxford-Smith et al., 2024), the width of the palate (Costa et al., 2022), and the length of the rostrum (Costa et al., 2016; 2022; Jedensjö et al., 2017; Dromby et al., 2023; Oxford-Smith et al., 2024). Coastal dolphins, like Aduncus or the WNA, tend to have longer rostrums and narrower skulls, which may improve foraging efficiency in shallow, complex environments (Jedensjö et al., 2017; Costa et al., 2022). In contrast, offshore dolphins

may exhibit adaptations related to a diet rich in squid. However, these patterns are not universally observed. For example, in California, more robust rostrums and skulls and larger temporal fossae, have been documented compared to their offshore counterpart (Perrin et al., 2011). By contrast, dolphins in the Gulf of Guayaquil possess robust skulls and shorter rostrums (Dromby et al., 2023). Coastal habitats in California are characterized by rocky shorelines, kelp forests, and varying water temperatures (Carr & Reed, 2016), which differ significantly from the murky mangroves of the Gulf of Guayaquil (Ortega-Pacheco et al., 2019). In this context, local environmental conditions, such as habitat complexity, may exert different ecological pressures on traits related to swimming and communication, thereby improving feeding strategies. Similar relationships between skull shape and feeding ecology have been observed in pinnipeds (Franco-Moreno et al., 2021). In this taxon, different species exhibit skull shapes and muscle efficiencies corresponding with their feeding strategies. For example, pelagic feeders like *Arctocephalus townsendi*, which prey on low resistance species such as pelagic red crab (*Pleuroncodes planes*) have streamlined skulls with less curved condyles and a less efficient mandibular lever system, resulting in lower bite force (Franco-Moreno et al., 2021). On the other side, generalist feeders such as *Mirounga angustirostris*, which consume a variety of prey with higher tissue resistance like Pacific hake develop more robust skulls with broad mandibular muscle insertions. Benthic feeders, such as *Phoca vitulina*, which process prey requiring significant chewing have less robust skulls with lower muscular efficiency, optimized to distribute bite force over a larger area (Franco-Moreno et al., 2021).

The premaxillae and maxillae**,** provide support and attachment points for the facial muscles (i.e. maxillo-nasolabial muscles). These muscles are themselves linked to the melon and are thought to modulate the melon's shape and stiffness, thereby influencing the production and direction of echolocation sounds (i.e., frequency, beam width; Harper et al., 2008). Previous studies have suggested that an expanded maxillae may be associated with a larger melon, potentially facilitating more powerful sound beams for deeper waters (Galatius & Goodall, 2016). Furthermore, the prenarial area, located in front of the nasal opening, is closely associated with cranial air sacs, which play a critical role in sound production. In dolphins, these air sacs facilitate a direct path for resonances, distinct from those produced by other cranial spaces or soft tissues (Foskolos et al., 2019)**.** This mechanism allows the production of echolocation clicks, with minimal air volume, even at great depths (Foskolos et al., 2019). Variations in the prenarial area have previously been observed in Gephyreus (Costa et al., 2016) and differentiate offshore porpoises from their coastal counterparts (Galatius et al., 2011), suggesting adaptations for sound production, particularly in deeper environments. While such

changes were most pronounced in the offshore unit, our study also observed greater cranial depth in some coastal units, particularly Aduncus, Erebennus, Japan, and West Africa. This finding challenges the conventional association of cranial depth exclusively with offshore environments. Although selective pressure in deeper environments may contribute to the development of this feature, its presence in coastal operational units suggests that other factors, such as communication systems related to foraging or social interactions, may also be important. This observation further supports the interpretation that stochastic processes could have played a role in shaping the morphological patterns observed in coastal units.

Several studies have demonstrated or suggested correlations between skull shapes and vocalisations in Delphinidae. Skull asymmetry (Del Castillo et al., 2016; Galatius & Goodall, 2016; Laeta et al., 2021) and elevated cranial vertex (Velez-Juarbe et al., 2015; Bianucci et al., 2016; Lambert et al., 2017) have often been suggested to be associated with vocalisation in odontocetes. Asymmetry has been described as involving a leftward shift in nasal bones and the right premaxilla, along with an enlargement of the right premaxilla and maxilla (Laeta et al., 2021; 2023) potentially reflecting the degree of asymmetry in sound-producing organs, such as the nasal apparatus and melon (Coombs et al., 2020). Similarly, deeper cranial concavity (Del Castillo et al., 2016; Galatius & Goodall, 2016; Laeta et al., 2021) and elevated cranial vertex (Velez-Juarbe et al., 2015; Lambert et al., 2017) may accommodate larger sound-producing structures. These variations are widespread across the Delphinidae family and often correlate with the ecological niches and vocalisation characteristics of different species (Galatius & Goodall, 2016; Coombs et al., 2020; Laeta et al., 2021; 2023). Pronounced asymmetry (Galatius & Goodall, 2016; Laeta et al., 2023), elevated cranial vertex (Bianucci et al., 2016), and deeper facial regions (Velez-Juarbe et al., 2015; Lambert et al., 2017) have frequently been documented in deep-diving species, requiring loud and far-reaching echolocations. Deeper frontal region concavity has also been associated with offshore habitat in Phocoenidae (Galatius et al., 2011).

Bottlenose dolphins are known to exhibit diverse vocalisation patterns, including a rich and diverse acoustic repertoire, often associated with social interactions (Luís et al., 2021). While certain signal types are commonly associated with feeding behaviours across populations, dolphins also produce specific clicks and vocalisations, such as whistles and bray series, more closely tied to social interactions (Janik & Slater, 1998; Janik, 2000; Janik et al., 2006). These vocal variations appear to correlate more with environmental conditions and social behaviours than with geographic distance, suggesting local functions (Luís et al., 2021). Previous studies suggest that bottlenose dolphins can adapt their vocalisations to different acoustic environments, potentially driving population differentiation over time (May-Collado &

Wartzok, 2008). Pronounced concave facial regions have also been observed in this study for some coastal OTUs. While these features might be related to vocalisation abilities, further research is needed to clarify the specific link between vocalisation, echolocation and skull morphology in bottlenose dolphins.

Conclusion

In this study, wider bony nares and larger pterygoids were observed in Offshore, Japan, and North Sea individuals compared to other operational units. In contrast, a ventro-dorsal displacement of the occipital condyle was displayed by coastal units like Aduncus, Erebennus and those from Guayaquil. Wider bony nares in offshore specimens have been previously observed and are suggested to enhance air exchange during diving or swimming (Mead & Potter, 1995; Perrin et al., 2011). The pterygoid bone, which anchors the pterygopharyngus muscle and connects the larynx to the nasal system (Cozzi et al., 2016), suggests potential differences in air exchange abilities among OTUs. For example, steep seabed gradients have been identified as a preferred foraging habitat for dolphins in the North Sea (Hastie et al., 2004). These features were also found to correlate with their associated environmental factors such as bathymetry, current velocity, MLD, and slope gradients, conditions that may require enhanced respiratory and locomotive functions. In contrast, the ventro-dorsal displacement of the occipital condyle in coastal operational units may provide benefits for manoeuvring in shallow waters, a characteristic observed in river dolphins. This displacement is thought to be associated with a more downward skull orientation relative to the body, potentially improving the dolphin's ability to scan the seabed for prey (De Araujo Monteiro-Filho et al., 2002). Such an adaptation could be particularly beneficial in coastal environments, which are characterized by more complex underwater seascapes.

4.5. Bibliography

Adams, D. C., Collyer, M., Kaliontzopoulou, A., & Baken, E. (2023). Geomorph: software for geometric morphometric analyses (R package version 4.0.6). *Comprehensive R Archive Network.*

Adams, D. C., Rohlf, F. J., & Slice, D. E. (2004). Geometric morphometrics: ten years of progress following the ‘revolution.’ Italian Journal of Zoology, 71(1), 5–16. doi: 10.1080/11250000409356545

Adams, D. C., Rohlf, F.J., & Slice, D. (2013). A field comes of age: geometric morphometrics in the 21st century. *Hystrix*, *24*, 7–14. doi: 10.4404/hystrix-24.1-6283

Alcantarilla, P. F., Nuevo, J., & Bartoli, A. (2011). Fast explicit diffusion for accelerated features in nonlinear scale spaces. *IEEE Transactions on Pattern Analysis and Machine Intelligence, 34*(7), 1281–1298. doi: bmvc/2013/Papers/paper0013

Allen, J. T., Brown, L., Sanders, R., Moore, C. M., Mustard, A., Fielding, S., Lucas, M., Rixen, M., Savidge, G., Henson, S., & Mayor, D. (2005). Diatom carbon export enhanced by silicate upwelling in the northeast Atlantic. *Nature*, *437*(7059), 728–732. doi: 10.1038/nature03948

Amaral, A. R., Smith, B. D., Mansur, R. M., Brownell, R. L., & Rosenbaum, H. C. (2017). Oceanographic drivers of population differentiation in Indo-Pacific bottlenose (*Tursiops aduncus*) and humpback (*Sousa* spp.) dolphins of the northern Bay of Bengal. *Conservation Genetics*, *18*(2), 371–381. doi: 10.1007/S10592-016-0913-7

Arbour, J. H., Curtis, A. A., & Santana, S. E. (2019). Signatures of echolocation and dietary ecology in the adaptive evolution of skull shape in bats. *Nature Communications*, *10*(1), 1–13. doi: 10.1038/s41467-019-09951-y

Assis, J., Fernández Bejarano, S. J., Salazar, V. W., Schepers, L., Gouvêa, L., Fragkopoulou, E., Leclercq, F., Vanhoorne, B., Tyberghein, L., Serrão, E. A., Verbruggen, H., & De Clerck, O. (2024). Bio-ORACLE v3.0. Pushing marine data layers to the CMIP6 Earth System Models of climate change research. *Global Ecology and Biogeography*, *33*(4), e13813. doi: 10.1111/GEB.13813

Baken, E. K., Collyer, M. L., Kaliontzopoulou, A., & Adams, D. C. (2021). Geomorph v4.0 and gmShiny: Enhanced analytics and a new graphical interface for a comprehensive morphometric experience. *Methods in Ecology and Evolution*, *12*(12), 2355–2363. doi: 10.1111/2041-210X.13723

Bardua, C., Felice, R. N., Watanabe, A., Fabre, A. C., & Goswami, A. (2019). A Practical Guide to Sliding and Surface Semilandmarks in Morphometric Analyses. *Integrative Organismal Biology*, *1*(1). doi: 10.1093/IOB/OBZ016

Barros, N. B. (1993). Feeding ecology and foraging strategies of bottlenose dolphins on the central east coast of Florida [*PhD Thesis*]. University of Miami.

Barros, N. B., Parsons, E. C. M., & Jefferson, T. A. (2000). Prey of offshore bottlenose dolphins from the South China Sea. *Aquatic Mammals*, *26*, 2–6.

Bayas-Rea, R., Félix, F., & Montufar, R. (2018). Genetic divergence and fine-scale population structure of the common bottlenose dolphin (*Tursiops truncatus*, Montagu) found in the Gulf of Guayaquil, Ecuador. *PeerJ*, *2018*(4), e4589. doi: 10.7717/peerj.4589

Bianucci, G., Di Celma, C., Urbina, M., & Lambert, O. (2016). New beaked whales from the late Miocene of Peru and evidence for convergent evolution in stem and crown Ziphiidae (Cetacea, Odontoceti). *PeerJ*, *2016*(9), e2479. doi: 10.7717/PEERJ.2479

Biau, G., & Scornet, E. (2016). A random forest guided tour. *Test*, *25*(2), 197–227. doi: 10.1007/S11749-016-0481-7

Bookstein, F. L. (1986). Size and Shape Spaces for Landmark Data in Two Dimensions. *Statistical Science*, *1*(2), 181–222. doi: 10.1214/SS/1177013696

Bookstein, FL. (1991). Morphometric tools for landmark data: geometry and biology (Issue 10). Cambridge University Press.

Braulik, G. , Natoli, A. , Kiszka, J. , Parra, G. , Plön, S. , & Smith, B. D. (2019). *Tursiops aduncus. The IUCN Red List of Threatened Species*. https://www.iucnredlist.org

Breiman, L. (2001). Random forests. *Machine Learning*, *45*(1), 5–32. doi: 10.1023/A:1010933404324

Cozzi, B., Huggenberger, S., & Oelschläger, H. A. (2016). Anatomy of Dolphins: Insights into Body Structure and Function. Academic Press.

Buser, T. J., Sidlauskas, B. L., & Summers, A. P. (2018). 2D or Not 2D? Testing the utility of 2D Vs. 3D landmark data in geometric morphometrics of the sculpin subfamily Oligocottinae (Pisces; Cottoidea). *The Anatomical Record*, *301*(5), 806–818. doi: 10.1002/AR.23752

Campbell, K. M., & Santana, S. E. (2017). Do differences in skull morphology and bite performance explain dietary specialization in sea otters? *Journal of Mammalogy*, *98*(5), 1408–1416. doi: 10.1093/jmammal/gyx091

Carnabuci, M., Schiavon, G., Bellingeri, M., Fossa, F., Paoli, C., Vassallo, P., & Gnone, G. (2016). Connectivity in the network macrostructure of *Tursiops truncatus* in the Pelagos Sanctuary (NW Mediterranean Sea): does landscape matter? *Population Ecology*, *58*(2), 249–264. doi: 10.1007/s10144-016-0540-7

Carr, M., & Reed, D. (2016). Shallow rocky reefs and kelp forests. *Ecosystems of California*, 311–336. doi: 10.1525/9780520962170-021

Chen, I., Nishida, S., Yang, W. C., Isobe, T., Tajima, Y., & Hoelzel, A. R. (2017). Genetic diversity of bottlenose dolphin (*Tursiops sp.)* populations in the western North Pacific and the conservation implications. *Marine Biology*, *164*(10), 1–17. doi: 10.1007/S00227-017-3232-8

Cignoni, P., Callieri, M., Corsini, M., Dellepiane, M., Ganovelli, F., & Ranzuglia, G. (2008). MeshLab: An open-source mesh processing tool. *Sixth Eurographics Italian Chapter Conference,* 129–136.

Committee on Taxonomy. (2023). List of Marine Mammal Species and Subspecies. *Society for Marine Mammalogy (consulted in 2024).*

Coombs, E. J., Clavel, J., Park, T., Churchill, M., & Goswami, A. (2020). Wonky whales: the evolution of cranial asymmetry in cetaceans. *BMC Biology*, *18*(1), 1–24. doi: 10.1186/s12915-020-00805-4

Correia, A. M., Sousa-Guedes, D., Gil, Á., Valente, R., Rosso, M., Sousa-Pinto, I., Sillero, N., & Pierce, G. J. (2021). Predicting cetacean distributions in the eastern north Atlantic to support marine management. *Frontiers in Marine Science*, *8*, 643569. doi: 10.3389/fmars.2021.643569

Costa, A. A., Mcfee, W., Wilcox, L. A., Archer, F. I., & Rosel, P. E. (2022). The common bottlenose dolphin (*Tursiops truncatus*) ecotypes of the western North Atlantic revisited: an integrative taxonomic investigation supports the presence of distinct species. *Zoological Journal of the Linnean Society*, *196*, 1608–1636. doi: 10.1093/zoolinnean/zlac025

Costa, A., Rosel, P., Daura-Jorge, F., & Simões-Lopes, P. (2016). Offshore and coastal common bottlenose dolphins of the western South Atlantic face-to-face: What the skull and the spine can tell us. *Marine Mammal Science*, *32*(4), 1433–1457. doi: 10.1111/mms.12342

Da Silva, F. O., Fabre, A. C., Savriama, Y., Ollonen, J., Mahlow, K., Herrel, A., Müller, J., & Di-Poï, N. (2018). The ecological origins of snakes as revealed by skull evolution. *Nature Communications 9*(1), 1–11. doi: 10.1038/s41467-017-02788-3

Damasceno, E. M., Hingst-Zaher, E., & Astúa, D. (2013). Bite force and encephalization in the Canidae (Mammalia: Carnivora). *Journal of Zoology*, *290*(4), 246–254. doi: 10.1111/JZO.12030

Daura-Jorge, F. G., Ingram, S. N., & Simões-Lopes, P. C. (2013). Seasonal abundance and adult survival of bottlenose dolphins (*Tursiops truncatus*) in a community that cooperatively forages with fishermen in southern Brazil. *Marine Mammal Science*, *29*(2), 293–311. doi: 10.1111/j.1748-7692.2012.00571.x

De Araujo Monteiro -Filho, E. L., Monteiro, L. R., & Dos Reis, S. F. (2002). Skull shape and size divergence in dolphins of the genus *Sotalia*: a tridimensional morphometric analysis. *Journal of Mammalogy*, *83*(1), 125–134. doi: 10.1644/1545-1542(2002)083<0125:SSASDI>2.0.CO;2

Del Castillo, D. L., Segura, V., Flores, D. A., & Cappozzo, H. L. (2016). Cranial development and directional asymmetry in Commerson's dolphin, *Cephalorhynchus commersonii commersonii* : 3D geometric morphometric approach. *Journal of Mammalogy*, *97*(5), 1345–1354. doi: 10.1093/jmammal/gyw101

Díaz López, B. (2020). When personality matters: personality and social structure in wild bottlenose dolphins, *Tursiops truncatus. Animal Behaviour*, *163*, 73–84. doi: 10.1016/J.anbehav.2020.03.001

Dinis, A., Molina, C., Tobeña, M., Sambolino, A., Hartman, K., Fernandez, M., Magalhães, S., dos Santos, R. P., Ritter, F., Martín, V., de Soto, N. A., & Alves, F. (2021). Large-scale movements of common bottlenose dolphins in the Atlantic: dolphins with an international courtyard. *PeerJ*, *9*, e11069. doi: 10.7717/peerj.11069

Do Amaral, K. B., Amaral, A. R., Ewan Fordyce, R., & Moreno, I. B. (2018). Historical biogeography of Delphininae dolphins and related taxa (Artiodactyla: Delphinidae). *Journal of Mammalian Evolution*, *25*(2), 241–259. doi: 10.1007/s10914-016-9376-3

Dormann, C. F., Elith, J., Bacher, S., Buchmann, C., Carl, G., Carré, G., Marquéz, J. R. G., Gruber, B., Lafourcade, B., Leitão, P. J., Münkemüller, T., Mcclean, C., Osborne, P. E., Reineking, B., Schröder, B., Skidmore, A. K., Zurell, D., & Lautenbach, S. (2013). Collinearity: a review of methods to deal with it and a simulation study evaluating their performance. *Ecography*, *36*(1), 27–46. doi: 10.1111/J.1600-0587.2012.07348.X

Dromby, M., Félix, F., Haase, B., Simões-Lopes, P. C., Costa, A. P. B., Lalis, A., Bens, C., Podestà, M., Doria, G., & Moura, A. E. (2023). Cranial variation between coastal and offshore bottlenose dolphins, *Tursiops truncatus* (Cetacea: Delphinidae) in Ecuador and the Mediterranean: a three-dimensional geometric morphometric study. *Zoological Journal of the Linnean Society*, *199*(1), 83–96. doi: 10.1093/zoolinnean/zlad022

Duffield, D. A., Ridgway, S. H., & Cornell, L. H. (1983). Hematology distinguishes coastal and offshore forms of dolphins (*Tursiops*). *Canadian Journal of Zoology*, *61*(4), 930–933. doi: 10.1139/Z83-123

Dumont, M., Wall, C. E., Botton-Divet, L., Goswami, A., Peigné, S., & Fabre, A. C. (2016). Do functional demands associated with locomotor habitat, diet, and activity patterns drive skull shape evolution in musteloid carnivorans? *Biological Journal of the Linnean Society*, *117*(4), 858–878. doi: 10.1111/BIJ.12719

Essington, T. E., Anderson, S. C., Barnett, L. A. K., Berger, H. M., Siedlecki, S. A., & Ward, E. J. (2022). Advancing statistical models to reveal the effect of dissolved oxygen on the spatial distribution of marine taxa using thresholds and a physiologically based index. *Ecography*, (8), e06249. doi: 10.1111/ECOG.06249

Esteves-Ponte, M. A., Aurioles-Gamboa, D., & García-Rodríguez, F. J. (2022). Skull morphometric variability related to offshore and inshore ecotypes of the common bottlenose dolphin (*Tursiops truncatus*) from northwestern Mexico. *Marine Mammal Science*, *38*(3), 1088–1103. doi: 10.1111/MMS.12914

Fagertun, J., Harder, S., Rosengren, A., Moeller, C., Werge, T., Paulsen, R. R., & Hansen, T. F. (2014). 3D facial landmarks: inter-operator variability of manual annotation. *BMC Medical Imaging*, *14*(1), 1–9. doi: 10.1186/1471-2342-14-35

Félix, F., Centeno, R., Romero, J., Zavala, M., & Vásconez, Ó. (2018). Prevalence of scars of anthropogenic origin in coastal bottlenose dolphin in Ecuador. *Journal of the Marine Biological Association of the United Kingdom*, *98*(5), 1177–1186. doi: 10.1017/S0025315417000686

Félix, F., Waerebeek, K. Van, Sanino, G. P., Castro, C., Bressem, M. F. Van, & Santillán, L. (2018). Variation in dorsal fin morphology in common bottlenose dolphin (*Tursiops truncatus*) populations from the southeast Pacific Ocean. *Pacific Science*, *72*(3), 307–320. doi: 10.2984/72.3.2

Figueirido, B., Tseng, Z. J., & Martín-Serra, A. (2013). Skull shape evolution in durophagous carnivorans. *Evolution*, *67*(7), 1975–1993. doi: 10.1111/EVO.12059

Foley, A., McGrath, D., Berrow, S., & Gerritsen, H. (2010). Social structure within the bottlenose dolphin (*Tursiops truncatus*) population in the Shannon Estuary, Ireland. *Aquatic Mammals*, *36*(4), 372–381. doi: 10.1578/AM.36.4.2010.372

Foskolos, I., Aguilar de Soto, N., Madsen, P. T., & Johnson, M. (2019). Deep-diving pilot whales make cheap but powerful, echolocation clicks with 50 µL of air. *Scientific Reports*, *9*(1), 1–9. doi: 10.1038/s41598-019-51619-6

Frainer, G., Huggenberger, S., Moreno, I. B., Plön, S., & Galatius, A. (2021). Head adaptation for sound production and feeding strategy in dolphins (Odontoceti: Delphinida). *Journal of Anatomy*, *238*(5), 1070–1081. doi: 10.1111/joa.13364

Franco-Moreno, R. A., Polly, P. D., Toro-Ibacache, V., Hernández-Carmona, G., Aguilar-Medrano, R., Marín-Enríquez, E., & Cruz-Escalona, V. H. (2021). Bite force in four pinniped species from the west coast of Baja California, Mexico, in relation to diet, feeding strategy, and niche differentiation. *Journal of Mammalian Evolution*, *28*(2), 307–321. doi: 10.1007/S10914-020-09524-7

Fruet, P. F., Secchi, E. R., Daura-Jorge, F., Vermeulen, E., Flores, P. A. C., Simões-Lopes, P. C., Genoves, R. C., Laporta, P., Di Tullio, J. C., Freitas, T. R. O., Rosa, L. D., Valiati, V. H., Beheregaray, L. B., & Möller, L. M. (2014). Remarkably low genetic diversity and strong population structure in common bottlenose dolphins (*Tursiops truncatus*) from coastal waters of the Southwestern Atlantic Ocean. *Conservation Genetics*, *15*(4), 879–895. doi: 10.1007/S10592-014-0586-Z

Fruet, P. F., Secchi, E. R., Di Tullio, J. C., Simões-Lopes, P. C., Daura-Jorge, F., Costa, A. P. B., Vermeulen, E., Flores, P. A. C., Genoves, R. C., Laporta, P., Beheregaray, L. B., & Möller, L. M. (2017). Genetic divergence between two phenotypically distinct bottlenose dolphin ecotypes suggests separate evolutionary trajectories. *Ecology and Evolution*, *7*(21), 9131–9143. doi: 10.1002/ece3.3335

Galatius, A., Berta, A., Frandsen, M. S., & Goodall, R. N. P. (2011). Interspecific variation of ontogeny and skull shape among porpoises (Phocoenidae). *Journal of Morphology*, *272*(2), 136–148. doi: 10.1002/jmor.10900

Galatius, A., & Goodall, R. N. P. (2016). Skull shapes of the Lissodelphininae: radiation, adaptation and asymmetry. *Journal of Morphology*, *277*(6), 776–785. doi: 10.1002/jmor.20535

Gannon, D. P., & Waples, D. M. (2004). Diets of coastal bottlenose dolphins from the U.S. mid-Atlantic coast differ by habitat. *Marine Mammal Science*, *20*(3), 527–545. doi: 10.1111/J.1748-7692.2004.TB01177.X

Gao, T., Kovalsky, S. Z., Boyer, D. M., & Daubechies, I. (2019). Gaussian Process Landmarking for Three-Dimensional Geometric Morphometrics. *SIAM Journal on Mathematics of Data Science*, *1*(1), 237–267. doi: 10.1137/18M1203481

Gao, T., Yapuncich, G. S., Daubechies, I., Mukherjee, S., & Boyer, D. M. (2018). Development and assessment of fully automated and globally transitive geometric morphometric methods, with application to a biological comparative dataset with high interspecific variation. *The Anatomical Record*, *301*(4), 636–658. doi: 10.1002/AR.23700

Gaspari, S., Holcer, D., Mackelworth, P., Fortuna, C., Frantzis, A., Genov, T., Vighi, M., Natali, C., Rako, N., Banchi, E., Chelazzi, G., & Ciofi, C. (2015). Population genetic structure of common bottlenose dolphins (*Tursiops truncatus*) in the Adriatic Sea and contiguous regions: implications for international conservation. *Aquatic Conservation: Marine and Freshwater Ecosystems*, *25*(2), 212–222. doi: 10.1002/AQC.2415

Gaspari, S., Scheinin, A., Holcer, D., Fortuna, C., Natali, C., Genov, T., Frantzis, A., Chelazzi, G., & Moura, A. E. (2015). Drivers of population structure of the bottlenose dolphin (*Tursiops truncatus*) in the Eastern Mediterranean Sea. *Evolutionary Biology*, *42*(2), 177–190. doi: 10.1007/S11692-015-9309-8

Gatis, D. (2020). *REMBG - A tool to remove images backgrounds*. Downloaded from https://github.com/danielgatis/rembg

Giacomini, G., Herrel, A., Chaverri, G., Brown, R., Russo, D., Scaravelli, D., & Meloro, C. (2022). Functional correlates of skull shape in Chiroptera: feeding and echolocation adaptations. *Integrative Zoology*, *17*(3), 430–442. doi: 10.1111/1749-4877.12564

Giacomo, A. B. Di, & Ott, P. H. (2016). Long-term site fidelity and residency patterns of bottlenose dolphins (*Tursiops truncatus*) in the Tramandaí Estuary, southern Brazil. *Latin American Journal of Aquatic Mammals*, *11*(1–2), 155–161. doi: 10.5597/00224

Gille, S. T., Sheen, K. L., Swart, S., & Thompson, A. F. (2022). Mixing in the Southern Ocean. In H. Simmons, K. Richards, & J. Mackinnon (Eds.), *Ocean mixing: Drivers, mechanisms and impacts* (pp. 301–327). Academic Press.

Paradell, O., Díaz López, B., & Methion, S. (2019). Modelling common dolphin (*Delphinus delphis*) coastal distribution and habitat use: insights for conservation. *Ocean & Coastal Management*, *179*, 104836. doi: 10.1016/J.ocecoaman.2019.104836

Gonzalvo, J., Forcada, J., Grau, E., & Aguilar, A. (2014). Strong site fidelity increases vulnerability of common bottlenose dolphins (*Tursiops truncatus*) in a mass tourism destination in the western Mediterranean Sea. *Journal of the Marine Biological Association of the United Kingdom*, *94*(6), 1227–1235. doi: 10.1017/S0025315413000866

Goodall, C. (1991). Procrustes methods in the statistical analysis of shape. *Journal of the Royal Statistical Society: Series B (Methodological)*, *53*(2), 285–321. doi: 10.1111/J.2517-6161.1991.TB01825.X

Gray, H. W. I., Chen, I., Moura, A. E., Natoli, A., Nishida, S., Tanabe, S., Minton, G., Ponnampalam, L. S., Kiani, M. S., Culloch, R., Gore, M., Särnblad, A., Amir, O., Berggren, P., Collins, T., Willson, A. J., Baldwin, R., & Hoelzel, A. R. (2021). Comparative biogeography and the evolution of population structure for bottlenose and common dolphins in the Indian Ocean. *Journal of Biogeography*, *48*(7), 1654–1668. doi: 10.1111/JBI.14102

Griwodz, C., Gasparini, S., Calvet, L., Gurdjos, P., Castan, F., Maujean, B., ... & Lanthony, Y. (2021). AliceVision Meshroom. An open-source 3D reconstruction pipeline. In *Proceedings of the 12th ACM multimedia systems conference*, 241–247. doi: 10.1145/3458305.3478443

Gunz, P., & Mitteroecker, P. (2013). Semilandmarks: a method for quantifying curves and surfaces. *Hystrix, the Italian Journal of Mammalogy*, *24*(1). doi: 10.4404/HYSTRIX-24.1-6292

Gunz, P., Mitteroecker, P., & Bookstein, F. L. (2005). Semilandmarks in three dimensions. In D. E. Slice (Ed.), *Modern morphometrics in physical anthropology* (pp. 73–98). Springer. doi: 10.1007/0-387-27614-9_3

Hammer, Ø., Harper, D. A. T., & Ryan, P. D. (2001). Past: Paleontological statistics software package for education and data analysis. *Palaeontologia Electronica, 4*(1), Article 4: 9pp.

Harper, C. J. J., McLellan, W. A. A., Rommel, S. A. A., Gay, D. M. M., Dillaman, R. M. M., & Pabst, D. A. A. (2008). Morphology of the melon and its tendinous connections to the facial muscles in bottlenose dolphins (*Tursiops truncatus*). *Journal of Morphology*, *269*(7), 820–839. doi: 10.1002/jmor.10628

Hastie, G. D., Wilson, B., Wilson, L. J., Parsons, K. M., & Thompson, P. M. (2004). Functional mechanisms underlying cetacean distribution patterns: hotspots for bottlenose dolphins are linked to foraging. *Marine Biology*, *144*(2), 397–403. doi: 10.1007/S00227-003-1195-4

Hendges, C. D., Bubadu E, J. M., & Aceres, N. C. C. (2016). Environment and space as drivers of variation in skull shape in two widely distributed South-American Tayassuidae, *Pecari tajacu* and *Tayassu pecari* (Mammalia: Cetartiodactyla). *Biological Journal of the Linnean Society*, *119*(4), 785-798. doi: 10.1111/bij.12859

Hersh, S. L., and D. A. Duffield. 1990. Distinction between northwest Atlantic offshore and coastal bottlenose dolphins based on hemoglobin profile and morphometry. Pages 129–139 in S. Leatherwood and R. R. Reeves, eds. The bottlenose dolphin. Academic Press, San Diego, CA .

Hoekendijk, J. P. A., Leopold, M. F., & Cheney, B. J. (2021). Bottlenose dolphins in the Netherlands come from two sides: across the North Sea and through the English Channel. *Journal of the Marine Biological Association of the United Kingdom*, *101*(5), 853–859. doi: 10.1017/S0025315421000679

Hoelzel, A. R. (1998). Genetic structure of cetacean populations in sympatry, parapatry, and mixed assemblages: implications for conservation policy. *Journal of Heredity, 89*(5), 451–458. doi: 10.1093/jhered/89.5.451

Hoelzel, A. R., Potter, C. W., & Best, P. B. (1998). Genetic differentiation between parapatric 'nearshore' and 'offshore' populations of the bottlenose dolphin. *Proceedings of the Royal Society of London. Series B: Biological Sciences*, *265*(1402), 1177–1183. doi: 10.1098/RSPB.1998.0416

Hohl, L. S. L., Sicuro, F. L., Wickert, J. C., Moreno, I. B., Rocha-Barbosa, O., & Barreto, A. S. (2020). Skull morphology of bottlenose dolphins from different ocean populations with emphasis on South America. *Journal of Morphology*, *281*(6), 564–577. doi: 10.1002/jmor.21121

Hornsby, F. E., McDonald, T. L., Balmer, B. C., Speakman, T. R., Mullin, K. D., Rosel, P. E., Wells, R. S., Telander, A. C., Marcy, P. W., Klaphake, K. C., & Schwacke, L. H. (2017). Using salinity to identify common bottlenose dolphin habitat in Barataria Bay, Louisiana, USA. *Endangered Species Research*, *33*(1), 181–192. doi: 10.3354/ESR00807

Howell, P., & Simpson, D. (1994). Abundance of marine resources in relation to dissolved oxygen in Long Island Sound. *Estuaries*, *17*(2), 394–402. doi: 10.2307/1352672

Janik, V. M. (2000). Food–related bray calls in wild bottlenose dolphins (*Tursiops truncatus*). *Proceedings of the Royal Society of London. Series B: Biological Sciences*, *267*(1446), 923–927. doi: 10.1098/RSPB.2000.1091

Janik, V. M., Sayigh, L. S., & Wells, R. S. (2006). Signature whistle shape conveys identity information to bottlenose dolphins. *Proceedings of the National Academy of Sciences*, *103*(21), 8293–8297. doi: 10.1073/PNAS.0509918103

Janik, V. M., & Slater, P. J. B. (1998). Context-specific use suggests that bottlenose dolphin signature whistles are cohesion calls. *Animal Behaviour*, *56*(4), 829–838. doi: 10.1006/ANBE.1998.0881

Jedensjö, M., Kemper, C., & Krützen, M. (2017). Cranial morphology and taxonomic resolution of some dolphin taxa (Delphinidae) in Australian waters, with a focus on the genus *Tursiops. Marine Mammal Science*, *33*(1), 187–205. doi: 10.1111/mms.12356

Johnston, C. A., & Brown, T. N. (2013). Water chemistry distinguishes wetland plant communities of the Great Lakes coast. *Aquatic Botany*, *104*, 111–120. doi: 10.1016/j.aquabot.2012.08.005

Jones, R. I. (1998). Phytoplankton, Primary Production and Nutrient Cycling. In D. Hessen & Tranvik LJ (Eds.), *Aquatic humic substances: Ecology and biogeochemistry* (pp.145-175). *Springer Berlin Heidelberg.* doi: 10.1007/978-3-642-95629-3_8

Kasuya, T. (1997). Life history parameters of bottlenose dolphins off Japan. *IBI Reports*, *7*, 71–107. doi: 10.1111/j.1748-7692.2004.tb01176.x

Kazhdan, M., & Hoppe, H. (2013). Screened Poisson surface reconstruction. *ACM Transactions on Graphics*, *32*(3). doi: 10.1145/2487228.2487237

Kienle, S. S., & Berta, A. (2016). The better to eat you with: the comparative feeding morphology of phocid seals (Pinnipedia, Phocidae). *Journal of Anatomy*, *228*(3), 396–413. doi: 10.1111/JOA.12410

Kienle, S. S., & Berta, A. (2018). The evolution of feeding strategies in phocid seals (Pinnipedia, Phocidae). *Journal of Vertebrate Paleontology*, *38*(6). doi: 10.1080/02724634.2018.1559172

Kimura, M., & Ohta, T. (2020). *Theoretical aspects of population genetics* (Vol. 4). Princeton University Press.

Krützen, M., Kreicker, S., MacLeod, C. D., Learmonth, J., Kopps, A. M., Walsham, P., & Allen, S. J. (2014). Cultural transmission of tool use by Indo-Pacific bottlenose dolphins (*Tursiops* sp.) provides access to a novel foraging niche. *Proceedings of the Royal Society B: Biological Sciences*, *281*(1784). doi: 10.1098/RSPB.2014.0374

Krützen, M., Mann, J., Heithaus, M. R., Connor, R. C., Bejder, L., & Sherwin, W. B. (2005). Cultural transmission of tool use in bottlenose dolphins. *Proceedings of the National Academy of Sciences*, *102*(25), 8939–8943. doi: 10.1073/PNAS.0500232102

La Manna, G., Rako-Gospić, N., Sarà, G., Gatti, F., Bonizzoni, S., & Ceccherelli, G. (2020). Whistle variation in Mediterranean common bottlenose dolphin: The role of geographical, anthropogenic, social, and behavioral factors. *Ecology and Evolution*, *10*(4), 1971–1987. doi: 10.1002/ece3.6029

La Manna, G., Ronchetti, F., Sarà, G., Ruiu, A., & Ceccherelli, G. (2020). Common bottlenose dolphin protection and sustainable boating: species distribution modeling for effective coastal planning. *Frontiers in Marine Science*, *7*, 542648. doi: 10.3389/fmars.2020.542648

Laeta, M., Oliveira, J. A., Siciliano, S., Lambert, O., Jensen, F. H., & Galatius, A. (2023). Cranial asymmetry in odontocetes: a facilitator of sonic exploration? *Zoology*, *160*, 126108. doi: 10.1016/j.zool.2023.126108

Laeta, M., Ruenes, G. F., Siciliano, S., Oliveira, J. A., & Galatius, A. (2021). Variation in cranial asymmetry among the Delphinoidea. *Biological Journal of the Linnean Society*, *132*(2), 414–430. doi: 10.1093/biolinnean/blaa161

Lambert, C., Authier, M., Blanchard, A., Dorémus, G., Laran, S., Van Canneyt, O., & Spitz, J. (2022). Delayed response to environmental conditions and infra-seasonal dynamics of the short-beaked common dolphin distribution. *Royal Society Open Science*, *9*(11). doi: 10.1098/RSOS.220379

Lambert, O., Bianucci, G., & De Muizon, C. (2017). Macroraptorial sperm whales (Cetacea, Odontoceti, Physeteroidea) from the Miocene of Peru. *Zoological Journal of the Linnean Society*, *179*(2), 404–474. doi: 10.1111/ZOJ.12456

Leduc, R. G., Perrin, W. F., & Dizon, A. E. (1999). Phylogenetic relationships among the delphinid cetaceans based on full cytochrome B sequences. *Marine Mammal Science*, *15*(3), 619–648. doi: 10.1111/j.1748-7692.1999.tb00833.x

Lemos, B., Marroig, G., & Cerqueira, R. (2001). Evolutionary rates and stabilizing selection in large-bodied opossum skulls (Didelphimorphia: Didelphidae). *Journal of Zoology*, *255*(2), 181–189. doi: 10.1017/S095283690100125X

Liaw, A., & Wiener, M. (2002). Classification and Regression by randomForest. *R news, 2*(3), 18-22.

Louis, M., Fontaine, M. C., Spitz, J., Schlund, E., Dabin, W., Deaville, R., Caurant, F., Cherel, Y., Guinet, C., & Simon-Bouhet, B. (2014). Ecological opportunities and specializations shaped genetic divergence in a highly mobile marine top predator. *Proceedings of the Royal Society B: Biological Sciences*, *281*(1795). doi: 10.1098/RSPB.2014.1558

Louis, M., Korlević, P., Nykänen, M., Archer, F., Berrow, S., Brownlow, A., Lorenzen, E. D., O'Brien, J., Post, K., Racimo, F., Rogan, E., Rosel, P. E., Sinding, M. H. S., van der Es, H., Wales, N., Fontaine, M. C., Gaggiotti, O. E., & Foote, A. D. (2023). Ancient dolphin genomes reveal rapid repeated adaptation to coastal waters. *Nature Communications*, *14*(1), 1–13. doi: 10.1038/s41467-023-39532-z

Louis, M., Viricel, A., Lucas, T., Peltier, H., Alfonsi, E., Berrow, S., Brownlow, A., Covelo, P., Dabin, W., Deaville, R., Stephanis, R. de, Gally, F., Gauffier, P., Penrose, R., Silva, M. A., Guinet, C., & Simon-Bouhet, B. (2014). Habitat-driven population structure of bottlenose dolphins, *Tursiops truncatus*, in the North-East Atlantic. *Molecular Ecology*, *23*(4), 857–874. doi: 10.1111/MEC.12653

Lowther-Thieleking, J. L., Archer, F. I., Lang, A. R., & Weller, D. W. (2015). Genetic differentiation among coastal and offshore common bottlenose dolphins, *Tursiops truncatus*, in the eastern North Pacific Ocean. *Marine Mammal Science*, *31*(1), 1–20. doi: 10.1111/MMS.12135

Luís, A. R., May-Collado, L. J., Rako-Gospić, N., Gridley, T., Papale, E., Azevedo, A., Silva, M. A., Buscaino, G., Herzing, D., & dos Santos, M. E. (2021). Vocal universals and geographic variations in the acoustic repertoire of the common bottlenose dolphin. *Scientific Reports, 11*(1), 1–9. doi: 10.1038/s41598-021-90710-9

Machado, F. A., Marroig, G., & Hubbe, A. (2022). The pre-eminent role of directional selection in generating extreme morphological change in glyptodonts (Cingulata; *Xenarthra*). *Proceedings of the Royal Society B*, *289*(1967). doi: 10.1098/RSPB.2021.2521

Macleod, C. D. D., Reidenberg, J. S. S., Weller, M., Santos, M. B. B., Herman, J., Goold, J., & Pierce, G. J. J. (2007). Breaking symmetry: the marine environment, prey size, and the evolution of asymmetry in

cetacean skulls. *The Anatomical Record: Advances in Integrative Anatomy and Evolutionary Biology*, *290*(6), 539–545. doi: 10.1002/ar.20539

Maechler, M. , Rousseeuw, P. , Struyf, A. , Hubert, M. , Hornik, K. , Studer, M. , & Gonzalez, J. (2013). *Package "cluster."*https://cran.r-project.org/web/packages/cluster/cluster.pdf.

Mann, K. H. (2000). *Ecology of coastal waters : with implications for management* (Vol. 8). John Wiley & Sons.

Manthey, L., & Ousley, S. D. (2020). Geometric morphometrics. *Statistics and Probability in Forensic Anthropology*, 289–298. doi: 10.1016/B978-0-12-815764-0.00023-X

May-Collado, L., & Wartzok, D. (2008). A comparison of bottlenose dolphin whistles in the Atlantic Ocean: factors promoting whistle variation. *Journal of Mammalogy*, *89*(5), 1229–1240. doi: 10.1644/07-MAMM-A-310.1

McCabe, E. J. B., Gannon, D. P., Barros, N. B., & Wells, R. S. (2010). Prey selection by resident common bottlenose dolphins (*Tursiops truncatus*) in Sarasota Bay, Florida. *Marine Biology*, *157*(5), 931–942. doi: 10.1007/S00227-009-1371-2

McCurry, M. R., Fitzgerald, E. M. G., Evans, A. R., Adams, J. W., & McHenry, C. R. (2017). Skull shape reflects prey size niche in toothed whales. *Biological Journal of the Linnean Society*, *121*(4), 936–946. doi: 10.1093/biolinnean/blx032

McCurry, M. R., Walmsley, C. W., Fitzgerald, E. M. G., & McHenry, C. R. (2017). The biomechanical consequences of longirostry in crocodilians and odontocetes. *Journal of Biomechanics*, *56*, 61–70. doi: 10.1016/j.jbiomech.2017.03.003

McLean, R., Tsyban, A., Burkett, V., Codignotto, J., Forbes, D., Mimura, N., & Ittekkot, V. (2001). Coastal zones and marine ecosystems. *Climate Change*, 343–379.

Mead, J., & Potter, C. (1995). Recognizing two populations of the bottlenose dolphin (*Tursiops truncatus*) of the Atlantic coast of North America-morphologic and ecologic considerations. *IBI Reports 5*, 51–44.

Meloro, C., & Tamagnini, D. (2022). Macroevolutionary ecomorphology of the Carnivora skull: adaptations and constraints in the extant species. *Zoological Journal of the Linnean Society*, *196*(3), 1054–1068. doi: 10.1093/zoolinnean/zlab075

Milani, C., Vella, A., Vidoris, P., Christidis, A., & Koutrakis, E. (2021). Abundance, distribution and diet of the common dolphin, *Delphinus delphis*, in the northern Aegean Sea (Greece). *Aquatic Conservation: Marine and Freshwater Ecosystems*, *31*(1), 76–86. doi: 10.1002/AQC.3081

Mitteroecker, P., & Schaefer, K. (2022). Thirty years of geometric morphometrics: achievements, challenges, and the ongoing quest for biological meaningfulness. *American Journal of Biological Anthropology*, *178*(S74), 181–210. doi: 10.1002/AJPA.24531

Möller, L. M., & Beheregaray, L. B. (2001). Coastal bottlenose dolphins from Southeastern Australia are *Tursiops aduncus* according to sequences of the mitochondrial DNA control region. *Marine Mammal Science*, *17*(2), 249–263. doi: 10.1111/J.1748-7692.2001.TB01269.X

Moller, O. O., Castaing, P., Salomon, J. C., & Lazure, P. (2001). The influence of local and non-local forcing effects on the subtidal circulation of Patos Lagoon. *Estuaries*, *24*(2), 297–311. doi: 10.2307/1352953

Moreno, K., & Acevedo-Gutierrez, A. (2016). The social structure of Golfo Dulce bottlenose dolphins (*Tursiops truncatus*) and the influence of behavioural state. *Royal Society Open Science*, *3*(8). doi: 10.1098/RSOS.160010

Morin, P. A., Parsons, K. M., Archer, F. I., Ávila-Arcos, M. C., Barrett-Lennard, L. G., Dalla Rosa, L., Duchêne, S., Durban, J. W., Ellis, G. M., Ferguson, S. H., Ford, J. K., Ford, M. J., Garilao, C., Gilbert, M. T. P., Kaschner, K., Matkin, C. O., Petersen, S. D., Robertson, K. M., Visser, I. N., … Foote, A. D. (2015). Geographic and temporal dynamics of a global radiation and diversification in the killer whale. *Molecular Ecology*, *24*(15), 3964–3979. doi: 10.1111/MEC.13284

Moura, A. E., Nielsen, S. C. A. A., Vilstrup, J. T., Moreno-Mayar, J. V., Gilbert, M. T. P., Gray, H. W. I., Natoli, A., Möller, L., & Hoelzel, A. R. (2013). Recent Diversification of a Marine Genus (*Tursiops* spp.) Tracks Habitat Preference and Environmental Change. *Systematic Biology*, *62*(6), 865–877. doi: 10.1093/sysbio/syt051

Muckenhirn, A., Bas, A. A., & Richard, F.J. (2021). Assessing the influence of environmental and physiographic parameters on common bottlenose dolphin (*Tursiops truncatus*) distribution in the southern Adriatic Sea. *Proceedings of the 1st International Electronic Conference on Biological Diversity, Ecology, and Evolution*, *65*. doi: 10.3390/bdee2021-09434

Murtagh, F., & Legendre, P. (2011). Ward's hierarchical clustering method: clustering criterion and agglomerative algorithm. *arXiv preprint arXiv:1111.6285.* doi: 10.1007/s00357-014-9161-z

Natoli, A., Birkun, A., Aguilar, A., Lopez, A., & Hoelzel, A. R. (2005). Habitat structure and the dispersal of male and female bottlenose dolphins (*Tursiops truncatus*). *Proceedings of the Royal Society B: Biological Sciences*, *272*(1569), 1217–1226. doi: 10.1098/RSPB.2005.3076

Natoli, A., Peddemors, V. M., & Hoelzel, R. A. (2004). Population structure and speciation in the genus *Tursiops* based on microsatellite and mitochondrial DNA analyses. *Journal of Evolutionary Biology*, *17*(2), 363–375. doi: 10.1046/j.1420-9101.2003.00672.x

Nixon, S. W., Oviatt, C. A., Frithsen, J., & Sullivan, B. (1986). Nutrients and the productivity of estuarine and coastal marine ecosystems. *Journal of the Limnological Society of Southern Africa*, *12*(1–2), 43–71. doi: 10.1080/03779688.1986.9639398

Nykänen, M., Kaschner, K., Dabin, W., Brownlow, A., Davison, N. J., Deaville, R., Garilao, C., Kesner-Reyes, K., Gilbert, M. T. P., Penrose, R., Islas-Villanueva, V., Wales, N., Ingram, S. N., Rogan, E., Louis, M., & Foote, A. D. (2019). Postglacial colonization of northern coastal habitat by bottlenose dolphins: a marine leading-edge expansion? *Journal of Heredity*, *110*(6), 662–674. doi: 10.1093/jhered/esz039

Nykänen, M., Louis, M., Dillane, E., Alfonsi, E., Berrow, S., O'Brien, J., Brownlow, A., Covelo, P., Dabin, W., Deaville, R., de Stephanis, R., Gally, F., Gauffier, P., Ingram, S. N., Lucas, T., Mirimin, L., Penrose, R., Rogan, E., Silva, M. A., … Gaggiotti, O. E. (2019). Fine-scale population structure and connectivity of bottlenose dolphins, *Tursiops truncatus*, in European waters and implications for conservation. *Aquatic Conservation: Marine and Freshwater Ecosystems*, *29*(S1), 197–211. doi: 10.1002/AQC.3139

O'Dea, A., Lessios, H. A., Coates, A. G., Eytan, R. I., Restrepo-Moreno, S. A., Cione, A. L., Collins, L. S., De Queiroz, A., Farris, D. W., Norris, R. D., Stallard, R. F., Woodburne, M. O., Aguilera, O., Aubry, M. P., Berggren, W. A., Budd, A. F., Cozzuol, M. A., Coppard, S. E., Duque-Caro, H., … Jackson, J. B. C. (2016). Formation of the Isthmus of Panama. *Science Advances*, *2*(8). doi: 10.1126/SCIADV.1600883

Ortega-Pacheco, D., Mendoza-Jimenez, M. J., & Herrera, P. (2019). Mangrove conservation policies in the Gulf of Guayaquil. *Climate Change Management*, 25–43. doi: 10.1007/978-3-319-98681-4_2

Otero, I. R., & Delbracio, M. (2014). Anatomy of the SIFT method, image processing. *Image Processing On Line*, *4*, 370–396.

Oxford-Smith, N., Ruta, M., Gao, A., Viaud-Martinez, K. A., Sabin, R., Herman, J., Ososky, J., Tajima, Y., Yamada, T. K., Kaliontzopoulou, A., & Moura, A. E. (2024). Skull morphology of bottlenose dolphins worldwide and patterns of adaptation between coastal and offshore environments. *Journal of Zoology*, *322*(1), 42–57. doi: 10.1111/jzo.13122

Passadore, C., Möller, L., Diaz-Aguirre, F., & Parra, G. J. (2018a). High site fidelity and restricted ranging patterns in southern Australian bottlenose dolphins. *Ecology and Evolution*, *8*(1), 242–256. doi: 10.1002/ECE3.3674

Passadore, C., Möller, L. M., Diaz-Aguirre, F., & Parra, G. J. (2018b). Modelling dolphin distribution to inform future spatial conservation decisions in a marine protected area. *Scientific Reports*, *8*(1), 1–14. doi: 10.1038/s41598-018-34095-2

Peres-Neto, P., Legendre, P., Dray, S., & Borcard, D. (2006). Variation partitioning of species data matrices: estimation and comparison of fractions. *Ecology*, *87*(10), 2614–2625. doi: 10.1890/0012-9658(2006)87[2614:vposdm]2.0.co;2

Perez, S. I., Bernal, V., & Gonzalez, P. N. (2006). Differences between sliding semi-landmark methods in geometric morphometrics, with an application to human craniofacial and dental variation. *Journal of Anatomy*, *208*(6), 769–784. doi: 10.1111/j.1469-7580.2006.00576.x

Perrin, W. F., & Heyning, J. E. (1993). Rostral fusion as a criterion of cranial maturity in the common dolphin, *Delphinus delphis*. *Marine Mammal Science*, *9*(2), 195–197. doi: 10.1111/J.1748-7692.1993.TB00444.X

Perrin, W. F., Thieleking, J. L., Walker, W. A., Archer, F. I., & Robertson, K. M. (2011). Common bottlenose dolphins (*Tursiops truncatus*) in California waters: cranial differentiation of coastal and offshore ecotypes. *Marine Mammal Science*, *27*(4), 769–792. doi: 10.1111/j.1748-7692.2010.00442.x

Porto, A., Rolfe, S., & Maga, A. M. (2021). ALPACA: a fast and accurate computer vision approach for automated landmarking of three-dimensional biological structures. *Methods in Ecology and Evolution*, *12*(11), 2129–2144. doi: 10.1111/2041-210X.13689

Pratt, E. A. L., Beheregaray, L. B., Bilgmann, K., Zanardo, N., Diaz-Aguirre, F., & Möller, L. M. (2018). Hierarchical metapopulation structure in a highly mobile marine predator: the southern Australian coastal bottlenose dolphin (*Tursiops cf. australis*). *Conservation Genetics*, *19*(3), 637–654. doi: 10.1007/S10592-017-1043-6

Radinsky, L. B. (1981). Evolution of skull shape in carnivores: 1. Representative modern carnivores. *Biological Journal of the Linnean Society*, *15*(4), 369–388. doi: 10.1111/J.1095-8312.1981.TB00770.X

Ragueneau, O., Chauvaud, L., Leynaert, A., Thouzeau, G., Paulet, Y. M., Bonnet, S., Lorrain, A., Grall, J., Corvaisier, R., Le Hir, M., Jean, F., & Clavier, J. (2002). Direct evidence of a biologically active coastal silicate pump: ecological implications. *Limnology and Oceanography*, *47*(6), 1849–1854. doi: 10.4319/LO.2002.47.6.1849

Rahmat, S. J., & Koretsky, I. A. (2015). Diversity of mandibular morphology in some carnivorans. *Vestnik zoologii*, 3(*49),* 267–284. doi: 10.1515/vzoo-2015-0028

Ramos, E. A., Santoya, L., Verde, J., Walker, Z., Castelblanco-Martínez, N., Kiszka, J. J., Rieucau, G., & Angel Ramos, E. (2022). Lords of the Rings: Mud ring feeding by bottlenose dolphins in a Caribbean estuary revealed from sea, air, and space. *Marine Mammal Science*, *38*(1). doi: 10.1111/mms.12854

Rice, D. W. (1998). Marine Mammals of the World: Systematics and Distribution. *Society for Marine Mammalogy Special Publication*, *4*, 1-231

Robineau, D., & Vely, M. (1997). Données préliminaires (taille corporelle, craniométrie) sur le grand dauphin *(Tursiops truncatus)* des côtes d'Afrique du nord-ouest (Mauritanie, Sénégal). *Mammalia*, *61*(3), 443-448. doi: 10.1515/mammalia-1997-610310

Rohlf, F. J., & Corti, M. (2000). Use of two-block partial least-squares to study covariation in shape. *Systematic Biology*, *49*(4), 740–753. doi: 10.1080/106351500750049806

Rohlf, F. J., & Slice, D. (1990). Extensions of the Procrustes method for the optimal superimposition of landmarks. *Systematic Biology*, *39*(1), 40–59. doi: 10.2307/2992207

Rohlf, F., & Marcus, L. (1993). A revolution morphometrics. *Trends in Ecology and Evolution*, *8*(4), 129–132. doi: 10.1016/0169-5347(93)90024-J

Rolfe, S., Davis, C., & Maga, A. M. (2021). Comparing semi-landmarking approaches for analyzing three-dimensional cranial morphology. *American Journal of Physical Anthropology*, *175*(1), 227–237. doi: 10.1002/AJPA.24214

Rolfe, S., Pieper, S., Porto, A., Diamond, K., Winchester, J., Shan, S., Kirveslahti, H., Boyer, D., Summers, A., & Maga, A. M. (2021). SlicerMorph: an open and extensible platform to retrieve, visualize and

analyse 3D morphology. *Methods in Ecology and Evolution*, *12*(10), 1816–1825. doi: 10.1111/2041-210X.13669

Rosel, P. E., Hansen, L., & Hohn, A. A. (2009). Restricted dispersal in a continuously distributed marine species: common bottlenose dolphins *Tursiops truncatus* in coastal waters of the western North Atlantic. *Molecular Ecology*, *18*(24), 5030–5045. doi: 10.1111/J.1365-294X.2009.04413.X

Russo, L. F., Meloro, C., De Silvestri, M., Chadwick, E. A., & Loy, A. (2022). Better sturdy or slender? Eurasian otter skull plasticity in response to feeding ecology. *PLOS ONE*, *17*(9), e0274893. doi: 10.1371/journal.pone.0274893

Sanino, G., Van Waerebeek, K., Van Bressem, M., & Pastene, L. (2005). A preliminary note on population structure in eastern South Pacific common bottlenose dolphins, *Tursiops truncatus*. *Journal of Cetacean Research and Management*, *7*(1), 65–70. doi: 10.1515/mammalia-1997-610310

Santana, S. E., Dumont, E. R., & Davis, J. L. (2010). Mechanics of bite force production and its relationship to diet in bats. *Functional Ecology*, *24*(4), 776–784. doi: 10.1111/J.1365-2435.2010.01703.X

Santillán, L., Félix, F., & Haase, B. (2008). A preliminary morphological comparison of skulls of common bottlenose dolphins *Tursiops truncatus* from Peru and Ecuador. Report of theIn IWC 60th Annual Meeting Santiago, Chile, document SC/60/SM10.

Schroeder, L., & von Cramon-Taubadel, N. (2017). The evolution of hominoid cranial diversity: a quantitative genetic approach. *Evolution*, *71*(11), 2634–2649. doi: 10.1111/EVO.13361

Segura-García, I., Gallo, J., Chivers, S., Díaz-Gamboa, R., & Hoelzel, A. (2016). Post-glacial habitat release and incipient speciation in the genus *Delphinus*. *Heredity*, *117*(6), 400–407. doi: 10.1038/hdy.2016.66

Silber, G., & Fertl, D. (1995). Intentional beaching by bottlenose dolphins *(Tursiops truncatus)* in the Colorado River Delta, Mexico. *Aquatic Mammals*. *21*, 183–186. Downloaded from https://www.researchgate.net/publication/230729883

Skliris, N., Marsh, R., Josey, S. A., Good, S. A., Liu, C., & Allan, R. P. (2014). Salinity changes in the World Ocean since 1950 in relation to changing surface freshwater fluxes. *Climate Dynamics*, *43*(3–4), 709–736. doi: 10.1007/S00382-014-2131-7

Slater, G. J., Dumont, E. R., & Van Valkenburgh, B. (2009). Implications of predatory specialization for cranial form and function in canids. *Journal of Zoology*, *278*(3), 181–188. doi: 10.1111/J.1469-7998.2009.00567.X

Slater, G. J., & Van Valkenburgh, B. (2009). Allometry and performance: the evolution of skull form and function in felids. *Journal of Evolutionary Biology*, *22*(11), 2278–2287. doi: 10.1111/J.1420-9101.2009.01845.X

Smolker, R., Richards, A., Connor, R., Mann, J., & Berggren, P. (1997). Sponge carrying by dolphins (Delphinidae, *Tursiops sp.*): a foraging specialization involving tool use? *Ethology*, *103*(6), 454–465. doi: 10.1111/J.1439-0310.1997.TB00160.X

Sprogis, K. R., Raudino, H. C., Rankin, R., Macleod, C. D., & Bejder, L. (2016). Home range size of adult Indo-Pacific bottlenose dolphins (*Tursiops aduncus*) in a coastal and estuarine system is habitat and sex-specific. *Marine Mammal Science*, *32*(1), 287–308. doi: 10.1111/MMS.12260

Steeman, M. E., Hebsgaard, M. B., Fordyce, R. E., Ho, S. Y. W. W., Rabosky, D. L., Nielsen, R., Rahbek, C., Glenner, H., Sørensen, M. V., & Willerslev, E. (2009). Radiation of extant cetaceans driven by restructuring of the oceans. *Systematic Biology*, *58*(6), 573–585. doi: 10.1093/SYSBIO/SYP060

Takeshita, R., Balmer, B. C., Messina, F., Zolman, E. S., Thomas, L., Wells, R. S., Smith, C. R., Rowles, T. K., & Schwacke, L. H. (2021). High site-fidelity in common bottlenose dolphins despite low salinity exposure and associated indicators of compromised health. *PLOS ONE*, *16*(9), e0258031. doi: 10.1371/Journal.pone.0258031

Tezanos-Pinto, G., Baker, C. S., Russell, K., Martien, K., Baird, R. W., Hutt, A., ... & Garrigue, C. (2009). A worldwide perspective on the population structure and genetic diversity of bottlenose dolphins (*Tursiops truncatus*) in New Zealand. *Journal of Heredity*, *100*(1), 11–24. doi: 10.1093/jhered/esn039

Torreblanca, E., Báez, J. C., Real, R., Macías, D., García-Barcelona, S., Ferri-Yañez, F., & Camiñas, J. A. (2022). Factors associated with the differential distribution of cetaceans linked with deep habitats in the Western Mediterranean Sea. *Scientific Reports 2022 12:1*, *12*(1), 1–16. doi: 10.1038/s41598-022-14369-6

Tyberghein, L., Verbruggen, H., Pauly, K., Troupin, C., Mineur, F., & De Clerck, O. (2012). Bio-ORACLE: a global environmental dataset for marine species distribution modelling. *Global Ecology and Biogeography*, *21*(2), 272–281. doi: 10.1111/J.1466-8238.2011.00656.X

Urian, K. W., Hofmann, S., Wells, R. S., & Read, A. J. (2009). Fine-scale population structure of bottlenose dolphins (*Tursiops truncatus*) in Tampa Bay, Florida. *Marine Mammal Science*, *25*(3), 619–638. doi: 10.1111/J.1748-7692.2009.00284.X

Van den Wollenberg, A. L. (1977). Redundancy analysis an alternative for canonical correlation analysis. *Psychometrika*, *42*(2), 207–219. doi: 10.1007/BF02294050

Van Waerebeek, K., Bamy Idrissa, L., Jiddou Amy, A. M., Sequeira, M., Diop, M., Ofori, D., Tchibozo, S., & Campredon, P. (2008). Indeterminate status of West African populations of inshore common bottlenose dolphins *Tursiops truncatus* cautions against opportunistic live-capture schemes. *Final report. Fondation Internationale du Banc 'Arguin*.

Van Waerebeek, K., Ofori-Danson, P. K., Debrah, J., Collins, T., Djiba, A., Samba, A., & Bilal, O. (2014). On the status of the common bottlenose dolphin *Tursiops truncatus* in western Africa, with emphasis on fisheries interactions*,* 1947-2015. *Document SC/66b/SM19 Presented to the International Whaling Commission*, Bled, 19.

Velez-Juarbe, J., Wood, A. R., De Gracia, C., & Hendy, A. J. W. (2015). Evolutionary patterns among living and fossil *Kogiid* sperm whales: evidence from the Neogene of Central America. *PLOS ONE*, *10*(4), e0123909. doi: 10.1371/journal.pone.0123909

Vermeulen, E. , Fruet, P. , Borges de Camargo Costa, A. , Coscarella, M. , & Laporta, P. (2019). The IUCN Red List of Threatened Species*.* doi: 10.2305/iucn.uk.2019-3.rlts.t134822416a135190824.en

Viaud-Martinez, K., Brownell Jr, R., Komnenou, A., & Bohonak, A. (2008). Genetic isolation and morphological divergence of Black Sea bottlenose dolphins. *Biological Conservation*, *141*(6), 1600–1611. doi: 10.1016/j.biocon.2008.04.004

Walker, W. A. (1981). Geographical variation in morphology and biology of Bottlenose dolphins (*Tursiops*) in the eastern North Pacific. NOAA Administrative Report LJ-81-03C.

Wang, J., Chou, L., & White, B. (2000a). Differences in the external morphology of two sympatric species of bottlenose dolphins (Genus *Tursiops*) in the waters of China. *Journal of Mammalogy*, *81*(4), 1157–1165. doi: 10.1644/1545-1542(2000)081<1157:DITEMO>2.0.CO;2

Wang, J., Chou, L., & White, B. (2000b). Osteological differences between two sympatric forms of bottlenose dolphins (Genus *Tursiops*) in Chinese waters. *Journal of Zoology*, *252*, 147–162. doi: 10.1111/j.1469-7998.2000.tb00611.x

Wang, J. Y., Chou, L. S., & White, B. N. (1999). Mitochondrial DNA analysis of sympatric morphotypes of bottlenose dolphins (genus: *Tursiops*) in Chinese waters. *Molecular Ecology*, *8*(10), 1603–1612. doi: 10.1046/J.1365-294X.1999.00741.X

Watanabe, A. (2018). How many landmarks are enough to characterize shape and size variation? *PLOS ONE*, *13*(6), e0198341. doi: 10.1371/journal.pone.0198341

Webb, P. (2021). Introduction to Oceanography. *Roger Williams University.*

Wells, R. S., Rhinehart, H. L., Cunningham, P., Whaley, J., Baran, M., Koberna, C., & Costa, D. P. (1999). Long distance offshore movements of bottlenose dolphins. *Marine Mammal Science*, *15*(4), 1098–1114. doi: 10.1111/J.1748-7692.1999.TB00879.X

Wells, R. S., & Scott, M. D. (2009). Common bottlenose dolphin: *Tursiops truncatus*. In *Encyclopedia of Marine Mammals* eds B. Würsig, J. G. M. Thewissen, and K. M. Kovacs (Amsterdam: Elsevier), 249–255. doi: 10.1016/B978-0-12-373553-9.00062-6

Wickert, J. C., Von Eye, S. M., Oliveira, L. R., & Moreno, I. B. (2016). Revalidation of *Tursiops gephyreus* Lahille, 1908 (Cetartiodactyla: Delphinidae) from the southwestern Atlantic Ocean. *Journal of Mammalogy*, *97*(6), 1728–1737. doi: 10.1093/jmammal/gyw139

Young, R., & Maga, A. M. (2015). Performance of single and multi-atlas based automated landmarking methods compared to expert annotations in volumetric microCT datasets of mouse mandibles. *Frontiers in Zoology*, *12*(1), 1–12. doi: 10.1186/S12983-015-0127-8

Zhang, C., Porto, A., Rolfe, S., Kocatulum, A., & Maga, A. M. (2022). Automated landmarking via multiple templates. *PLOS ONE*, *17*(12), e0278035. doi: 10.1371/journal.pone.0278035

Chapter 5 - Allometric Diversification of Skull Shape in Western North Atlantic Bottlenose Dolphins: Implications for Ecological Drivers of Population Structure

5.1. Introduction

Three-dimensional geometric morphometrics (3DGM) is a versatile methodology which is used to accurately capture the surface anatomy of complex biological structures (Adams et al., 2004; Mitteroecker & Gunz, 2009; Zelditch et al., 2012). This method is commonly used in comparative analyses to detect shape differentiation in wild organisms, including plants and animals, and infer their functional and evolutionary implications. The ability of 3DGM to detect subtle shape changes within species makes it particularly valuable. For example, in Peter's Earth Snake (*Rhinophis philippinus*), 3DGM was used to analyse skull and tail shield shape differences between sexes, to investigate potential sexual dimorphism (SD; Huntley et al., 2021). There was no evidence of SD, despite its prevalence in other snakes, suggesting that ecological pressures from head-first burrowing had a stronger influence on morphology than sexual selection (Huntley et al., 2021). Additionally, the study revealed that both cranial and tail-shield shapes likely serve functional roles in locomotion and predator avoidance, emphasising the impact of ecological factors on shaping morphology through functional demands. 3DGM is also valuable for studying long-term evolutionary dynamics, as it can be applied to both living and extinct species. In humans, the population history of South America was reconstructed through 3DGM, by comparing skulls from the early and late Holocene over a 9 000-year period, revealing potential migration events along the Pacific coast (Kuzminsky et al., 2018). Beyond shape, 3DGM can incorporate relative size into morphological data analysis (Klingenberg, 2016), allowing researchers to investigate how allometric relationships vary across taxa, sexes or age classes (Viacava et al., 2020, 2022, 2023).

In placental mammals, cranial shape evolution is strongly defined by allometry changes, with larger species tending to have proportionally longer faces, a pattern known as positive craniofacial allometry (CREA; Cardini & Polly, 2013; Cardini et al., 2015; Cardini, 2019). These allometric patterns can result from differences in growth rates and growth timing between organisms. Investigating these mechanisms is facilitated by GM, by comparing how shape and allometry differ across different life stages and between species, offering insights into the developmental processes shaping cranial diversity. For example, adult skull shape in catarrhine

primates derives from differences in allometric patterns during ontogeny (Simons & Frost, 2021). The developmental trajectories leading to adult cranial shapes have shown to vary independently in each clade over evolutionary time, likely reflecting a combination of size-related factors and clade-specific ecological or developmental context.

Intraspecific allometric patterns can also help differentiate and identify populations. Allometry studies the relationship between shape and size and can be applied to the comparison of different life stages (i.e. ontogenetic allometry), individuals at similar developmental stages (i.e. static allometry), or different evolutionary lineages (i.e. evolutionary allometry; Klingenberg & Zimmermann, 1992). Populations inhabiting different environments may exhibit distinct allometric trajectories, resulting in different shapes. For example, ants of the genus *Cataglyphis* were found to have different allometric patterns between populations in North Africa and Europe, with ants from North Africa having longer legs relative to body size than ants from Europe (Centorame et al., 2020). This trait was suggested to improve foraging efficiency in warmer North African conditions (Sommer & Wehner, 2012).

Size scaling relationships are especially influenced by feeding ecology. In some murid rodents, different feeding strategies are associated with modifications in skull shape and dental morphology that affect food processing efficiency. For large-bodied frugivores, these modifications are associated with faster rates of allometric evolution (Marcy et al., 2020). Conversely, similar environmental conditions or lifestyles can create convergent allometric patterns. Despite sexual dimorphism in some semi-fossorial snakes, head-shape allometric patterns converge as the snakes mature, which is likely driven by shared environmental conditions and similar ecological needs, such as diet, habitat use, and activity patterns (Abegg et al., 2020).

However, allometric relationships are complex and often influenced by both ecological conditions and life history traits. For example, female snakes tend to have proportionally more robust heads than males, potentially due to ontogenetic allometry: as females grow larger, their head shape becomes more robust (Abegg et al., 2020). This dimorphism is thought to be driven by differences in prey size. The more robust heads of females may allow them to consume larger prey, potentially improving their fecundity. On the contrary, adult males display stronger static allometry, where the relationship between head size and shape is more pronounced. This is possibly due to greater variability in head sizes among males, who engage in different behaviours during male competition, which may select for varied head morphologies (Abegg et al., 2020).

In Delphinidae, mosaic heterochrony, a process where different skull structures develop at different rates or times, is suggested to be an important driver of morphological diversity (Sydney et al., 2012). This phenomenon is often related to allometric processes, resulting in shape variation across dolphin species (Sydney et al., 2012; Guidarelli et al., 2014) and even among populations within the same species (Galatius & Gol'din, 2011). Skull shape changes between life stages in particular, are associated with different allometric growth patterns (Kurihara & Oda, 2009; De Francesco et al., 2016). For example, in the bottlenose dolphin (*Tursiops truncatus*), the rostral length and width of the temporal fossa exhibit positive allometry, growing proportionally faster than the rest of the skull. These differences were suggested to reflect adaptations to changes in feeding ecology throughout their life stages (Kurihara & Oda, 2009). Additionally, the time when an individual stops growing is considered an important factor in allometric processes. Variations in this timing within a species can affect the development of allometric shapes, leading to notable morphological differences (Galatius & Gol'din, 2011). For example, individuals experiencing delayed growth termination may attain larger sizes and exhibit distinct skull shapes. Larger individuals were found in environments with abundant but highly variable food sources, suggesting that larger sizes may enhance energy storage during periods of food scarcity (Galatius & Gol'din, 2011).

Morphological studies in the genus *Tursiops* have revealed recurring skull shape differentiation between coastal and offshore habitats (Oxford-Smith et al., 2024 and references therein). Recent studies comparing coastal and offshore operational taxonomic units (OTU) within individual regions have provided added detail on these patterns of shape changes (Hohl et al., 2020; Costa et al., 2022; Esteves-Ponte et al., 2022; Dromby et al., 2023) identifying region-specific skull shape changes between these environments (Oxford-Smith et al., 2024). Given its widespread distribution and recurrent ecotypic differentiation (Wells & Scott, 2009), *Tursiops* provides an interesting model organism for investigating fine-scale skull shape diversification and allometric patterns.

Substantial differentiation between geographically distant OTUs is also seen in other bottlenose dolphin traits. A wide range of feeding and foraging ecologies is observed worldwide, from sponge feeding (Smolker et al., 1997) to mud-ring feeding (Ramos et al., 2022). In some regions, feeding strategies are also different between sexes, (Rossman et al., 2015b) likely due to differences in habitat use (Secchi et al., 2017). Feeding behaviour can also change throughout their lives (Rossman et al., 2015b). Moreover, diverse acoustic patterns are observed worldwide (Luís et al., 2021), with finer-scale variations documented in certain areas such as the Mediterranean (La Manna et al., 2020). These acoustic patterns are closely

associated with the species' vocal learning capacity and plasticity (Janik, 2000) which are influenced by a complex interplay of social and environmental factors (La Manna et al., 2020).

Ecological differentiation is particularly pronounced in the Western North Atlantic (WNA), with clear spatial segregation between the coastal and offshore OTUs (Torres et al., 2003). Offshore dolphins have unique haematological profiles, likely associated with the demands of their deep-water environment (Duffield et al., 1983). This environment also exposes them to higher parasitic loads, as indicated by the increased presence of *Crassicauda* scars (Mead & Potter, 1990). In contrast, coastal individuals are found to be smaller and have fewer vertebrae (Costa et al., 2022), along with distinct cranial features such as smaller skulls and narrower internal nares (Mead & Potter, 1995; Costa et al., 2022). These traits likely reflect adaptations to nearshore environments and may influence air exchange and sound production. Additionally, coastal dolphins generally have shorter and more tapered rostrums relative to offshore dolphins (Costa et al., 2022), potentially reflecting different feeding strategies.

Both skull morphometric (Mead & Potter, 1995; Toledo, 2013) and genetics/genomics studies (Hoelzel et al., 1998; Torres et al., 2003; Rosel et al., 2009; Moura et al., 2013, 2020; Richards et al., 2013) have supported the designation of the WNA coastal dolphins as a separate OTU from the offshore animals. A clear genetic distinction between coastal and offshore dolphins in the WNA was initially identified through mitochondrial DNA analyses (Hoelzel et al., 1998; Torres et al., 2003). This differentiation was further supported by the distinct spatial distribution of the two OTUs (Torres et al., 2003). This divergence was confirmed by subsequent genetic analysis (Rosel et al., 2009), suggesting that the coastal unit evolved from the more genetically diverse offshore unit (Rosel et al., 2009; Richards et al., 2013). Recent molecular data have revealed that the genus *Tursiops* encompasses multiple species and several potential subspecies (Moura et al., 2020), with the formation of distinct coastal OTUs appearing to be driven by unit-specific drift and varying gene flow with the offshore (Louis et al., 2021). Furthermore, the WNA operational unit split from the offshore is considered relatively deep, representing the sister clade to other *Tursiops truncatus* (Moura et al., 2020). Consequently, a recent multidisciplinary study proposed classifying the WNA coastal OTU as a distinct species, *Tursiops erebennus* (Costa et al., 2022).

Genetic partitioning is also present between several coastal populations along the WNA coast (Rosel et al., 2009; Toth et al., 2012) and in the Gulf of Mexico and the Caribbean (Richards et al., 2013; Vollmer & Rosel, 2017). Five distinct populations from New Jersey to northern Florida (Rosel et al., 2009), inhabiting diverse environments, including nearshore coastal waters and estuaries have been identified through analysis of the mitochondrial control

region and microsatellite loci. Estuarine populations show particularly distinct genetics, characterised by lower genetic diversity (e.g., Charleston and Jacksonville) compared to more open coastal populations (Rosel et al., 2009). The WNA presents a particularly interesting case of genetic differentiation occurring in the absence of physical barriers (Rosel et al., 2009). This same pattern is observed in the Gulf of Mexico, where seven distinct populations of bottlenose dolphins have been recognised and classified as separate management stocks (Vollmer & Rosel, 2017). Accordingly, the Marine Mammal Protection Act defines the occurrence of multiple sub-populations along the WNA. These stocks are defined as a group of individuals "of the same species or smaller taxa in a common spatial arrangement, that interbreed when mature" (Marine Mammal Protection Act, 16 U.S. Code § 1361). This stock structure includes multiple recognised dolphin populations, usually associated with numerous bays, sounds, and estuaries (BSE; Hayes et al., 2020). Several lines of evidence suggest the occurrence of local-scale differentiation, including genetics (Rosel et al., 2009; Vollmer & Rosel, 2017; Litz et al., 2023) residency patterns (e.g. Bassos-Hull et al., 2023; Zolman, 2002), and spatiotemporal distribution (e.g. Balmer et al., 2018, 2019; Mazzoil et al., 2020; Wells et al., 2017). These have been reviewed by the National Marine Fisheries Service (NMFS), which is currently evaluating the stock status for 31 BSE-associated groups (Hayes et al., 2020).

Differences in allometric patterns between coastal and offshore OTUs have been identified in different geographic regions by recent studies (Costa et al., 2022; Esteves-Ponte et al., 2022). In the WNA, these are reflected by divergent allometric trajectories, slope vector lengths, and angular slopes (Costa et al., 2022). These findings suggest that skull differences between coastal and offshore OTUs may be influenced by size-scaling relationships. Such differences in allometric patterns may indicate underlying evolutionary processes such as phenotypic plasticity, the ability of an organism to alter its phenotype in response to environmental factors. In this case, the observed size and shape changes could be driven by differences in environmental conditions between coastal and offshore habitats.

Differentiating bottlenose dolphin populations in the WNA is challenging due to seasonal movements between locations (e.g. Hohn et al., 2022), which creates opportunities for genetic exchange. Accordingly, few studies have investigated skull shape changes across the different WNA populations. Investigating these variations can help define precise morphometric criteria for each stock, leading to more consistent stock classification. Furthermore, the ability of high-resolution skull shape analysis using 3DGM to identify discrete populations at a fine scale has not been fully tested. Three-dimensional geometric morphometrics is especially useful for investigating intraspecific skull shape changes, which are often subtle. The high-resolution data

captured across the entire skull surface allows 3DGM to detect these subtle shape differences that traditional methods might not capture as accurately. However, the potential of 3DGM to identify subtle shape differences between bottlenose populations living in close geographic proximity has not been extensively explored.

While allometry has often been investigated in populations with clear shape differences, such as coastal versus offshore OTUs (Costa et al., 2022), subtle variations within a single operational unit have yet to be explored. Investigating allometric patterns in this context could provide invaluable insights into population differentiation, particularly for species influenced by nuanced ecological, behavioural, or environmental factors. It could also deepen our understanding of how allometry contributes to skull shape changes in bottlenose dolphins.

In this study, skull shape variation among seven putative bottlenose dolphin sub-populations will be investigated, focusing on allometric contributions and ecological drivers of these allometric relationships. High-resolution 3DGM and surface semi-landmarks will be used for a precise mapping of the entire skull. Given that surface landmarking covers the entire skull, the detection of subtle variations will be facilitated without requiring prior knowledge of shape divergence, potentially revealing new diagnostic traits. Therefore, this approach aims to identify subtle shape differences and specific skull regions associated with population divergence and to explore their potential functional implications.

Broader-scale allometric patterns can serve as a reference point for evaluating finer-scale geographic differences. Allometry has been suggested as the main precursor of shape variation in some lineages (Alexander Pyron & Burbrink, 2009). These may initially appear as phenotypic plasticity in response to local environmental conditions, before becoming fixed within a population over time. Differences in allometric patterns between offshore and coastal habitats have been documented in the WNA. Given that these two OTUs reflect an advanced stage in the diversification of the genus, an allometric analysis within the coastal OTU will be performed and compared to the coastal vs offshore patterns to clarify allometry's role in shape diversification among these populations. Furthermore, since intraspecific shape changes are often subtle, especially in geographically proximate populations, understanding size-related shape divergence could be a powerful tool for distinguishing between different stocks along the WNA. Static allometric analysis (Cheverud, 1982) will be performed between regions, sexes and their interactions to investigate if size contributes to fine-scale skull shape variation in coastal bottlenose dolphins. Sex will be included as a factor, due to known patterns of SD in bottlenose dolphins in other regions, and differing allometric patterns between males and females could further contribute to observed shape differences. Finally, comparisons of skull

shape and allometric patterns between several coastal locations will be performed to evaluate whether coastal populations exhibit distinct shapes and allometric patterns, potentially indicating an early stage of diversification.

This comparison will help understand whether these fine-scale variations reflect adaptive changes or are instead driven by an interaction of local environmental factors and phenotypic plasticity. More pronounced differences in allometric patterns are anticipated between the offshore and coastal OTUs, than between coastal populations themselves. In conclusion, an integrated approach will be used, based on high-resolution 3DGM to provide critical insights into fine-scale morphological differentiation within the WNA coastal bottlenose dolphin OUT (currently classified as *T. erebennus*). By investigating these patterns, potential ecological drivers influencing differentiation will be identified. These findings will contribute to a deeper understanding of the evolutionary and ecological processes shaping bottlenose dolphin diversity in the region.

5.2. Material And Methods

Data collection

Skulls from 76 adult specimens of bottlenose dolphins (*Tursiops* spp.*)* were photographed at the Smithsonian National Museum of Natural History in Washington, USA. Only adult specimens were photographed, determined by their skull bones being fully fused. This analysis focused on investigating patterns of variation between different coastal populations along the West North Atlantic (WNA). To capture representative geographic diversity, skulls from several coastal locations were photographed and subsequently categorised based on the potential existence of local populations, as described in the literature (Rosel et al., 2009; Vollmer & Rosel, 2017; Litz et al., 2023). The populations were defined as follows: Chesapeake Bay (n= 14, including individuals collected in the inside of the estuary, along the coasts of Virginia and Maryland), Delaware Bay (n= 8, including individuals collected along the coasts of Delaware and New Jersey), Maryland (n= 4), North Carolina (n = 16), Georgia (n= 6), Florida (n= 5) and the Gulf of Mexico (n= 9, including individuals from Florida and the Mississippi) (See details in supplementary Table S5.2.2.). The precise origins of these samples are detailed in supplementary Table S5.2.1, and their approximate locations are shown in Figure 5.1. Additionally, offshore skulls collected along the WNA (Mead & Potter, 1995), exhibiting known differences in skull shape and allometric patterns compared to the coastal operational taxonomic unit (OTU), were also included. Their inclusion facilitated the classification of each

individual as either coastal or offshore and provided a reference point for analysing allometric patterns between the coastal populations.

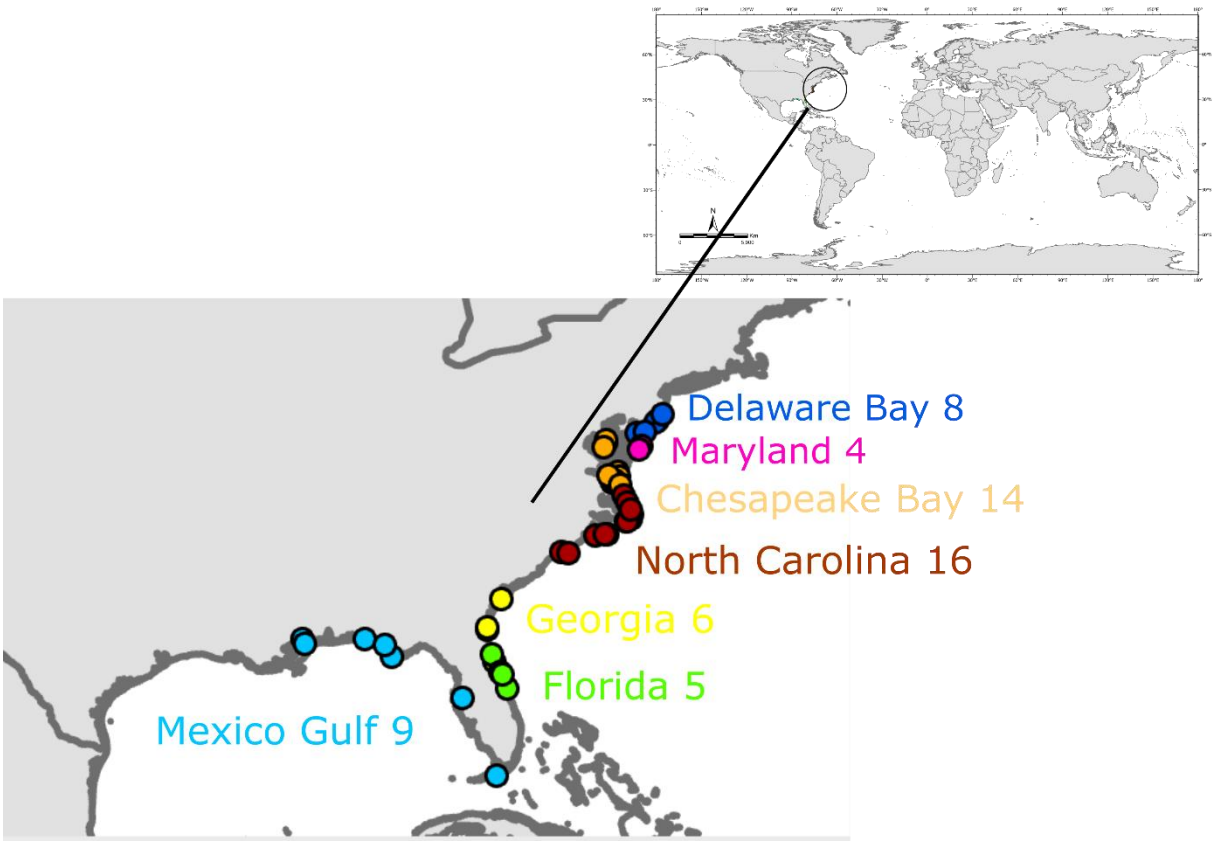

Figure 5.1. Map showing the distribution of bottlenose dolphin specimens analysed in this study, with colours representing their a priori geographic classification. The maps were sourced from the GADM project (version 3.6, gadm.org).

For each individual, 350 to 500 high-resolution photographs were taken with a DSLR camera (10.2 Megapixels, APS-C sized sensor). The camera was equipped with a Mecablitz 44AF-2 digital external flash unit, set to manual mode with the output manually adjusted between 1/2 and 1/8 power, depending on the room's lighting conditions. The flash was directed at the skull, using the integrated bounce diffuser to avoid strong light reflection on the pale surfaces of the skull. The camera was mounted on a tripod with adjustable height and a pivoting central column and set to a distance that centred and framed the skull in the camera view. The walls and floor were covered with a black sheet to minimize light reflections and background elements. Skulls were placed on a rotating table on the covered floor, with the rostrum facing the camera. For each skull, the tripod was adjusted between full turntable rotations, starting at a 0-degree angle relative to the turntable and then tilted to 25, 50, and 75 degrees. The turntable's rotation angle, speed, and stopping points were controlled with a remote and synchronized with the camera

using a remote trigger to ensure coordination between image capture and skull rotation. The remote trigger was set to capture photos with at least 60% lateral overlap and 80% frontal overlap between successive photos. To ensure complete coverage of the skull, the above workflow was repeated for both ventral and dorsal positions. Consistency was maintained throughout each photography session, by using a fixed focal length of 50 mm and setting the ISO to below 400 to minimize digital noise. Sharpness and depth of field were optimised by adjusting the aperture between f/16 and f/22 while using the highest possible shutter speed of 1/160 seconds. These settings were kept consistent for all the shots taken in the same museum.

Three-dimensional modelling

Three-dimensional (3D) models of each skull were constructed using photogrammetry, a technique that creates 3D representations from 2D images using the software Meshroom v.2019.2.0 (Griwodz et al., 2021). For most skulls (54 out of 78 individuals), backgrounds were first removed using the software REMBG (Gatis, 2020). The resulting pictures were then edited in Darktable (https://www.darktable.org), to enhance surface details by increasing local contrast and reducing global contrast. Specifically, the pictures were adjusted using the module's tone equalizer, black level correction, shadows and highlights, contrast equalizer, local contrast and sharpen. These adjustments were implemented to ensure even lighting across the luminance spectrum within each image. For 3D reconstruction, the “Sift” (Scale-Invariant Feature Transformation; Otero & Delbracio, 2014) and “sift_float” algorithms were used with the "Guided matching" option enabled in the "Feature Extraction" step, to improve matching accuracy. For individuals whose initial reconstruction was suboptimal, two to three meshes were created per individual by fine-tuning parameters during the “Meshing” step. The resulting meshes were then merged in Meshlab (Cignoni et al., 2008) using the "Flatten visible layers" option to produce the final model. A Poisson surface reconstruction (Kazhdan & Hoppe, 2013) was then performed with a depth of 13 and an interpolation weight of 0. Details for each individual can be found in the supplementary Table S5.2.3. The final 3D models were decimated to 1 000 000 faces using the “Simplification: Quadric Edge Collapse Decimation” option in Meshlab. This step reduced processing time while preserving the necessary details for morphometric analysis. Subsequently, the remaining zygomatic fragments were removed (if present) using the bisection tool in the open-source software Blender v.5.2.2 (Blender Development Team, 2022).

Landmarking

In 3DSlicer, a set of "Surface Semi-Landmarks" (SSL) was generated using the module PseudoLMGenerator from the extension SlicerMorph (Rolfe et al., 2021). This module places consistently spaced landmarks on a reference 3D object, which can then be projected onto the surfaces of other 3D objects through point registration. Point registration aligns landmarks with corresponding points on the targets, preserving their relative distances and positions, enabling consistent placement relative to the reference skull for a standardized representation of surface geometry. The SSLs were projected from the reference skull to the remaining skulls using the module ALPACA (Porto et al., 2021).

To select the optimal reference skull, a preliminary analysis was performed using an arbitrary well-preserved skull (see details in supplementary Figure S5.2.1), followed by a PCA using the R package geomorph in R (Adams & Otárola-Castillo, 2013). Individuals positioned near the centre of the PCA morphospace and with well-preserved skulls were considered as candidates, from which the individual with the least bilateral asymmetry (i.e., WA594515) was then selected.

A bilateral central plane was defined on the reference skull, allowing the pseudo-landmarks to be paired across each skull bilateral plane. This plane was positioned to be as close as possible to the following 4 skull points: the middle of the two maxilla edges at the tip of the rostrum; the central point between the occipital condyles, the central suture between the two pterygoid bones; the central line between the internal nares. PseudoLMGenerator was set with a "spacing tolerance" of 2.5 generating 719 pseudo-landmarks. These were visually inspected to ensure an accurate representation of skull shape and to prevent placement on non-informative surfaces, such as the internal surfaces of the skull. Non-informative landmarks, along with their corresponding pairs (17 landmarks in total) were excluded.

The final template landmarks were transferred to the remaining skulls using the Slicer extension ALPACA. In the Advanced Settings, the registration step was performed with a Point Density Adjustment of 0.5, Rigidity (alpha) of 2, and Motion coherence (beta) of 2; other parameters were kept at their default values. A GPA analysis was performed using the "GPA" module in Slicer and the landmark variance was then inspected to ensure correct landmark placement following the ALPACA. Any incorrectly placed landmarks were removed, resulting in a total of 701 pseudo-landmarks used for downstream statistical analyses (Figure 5.2).

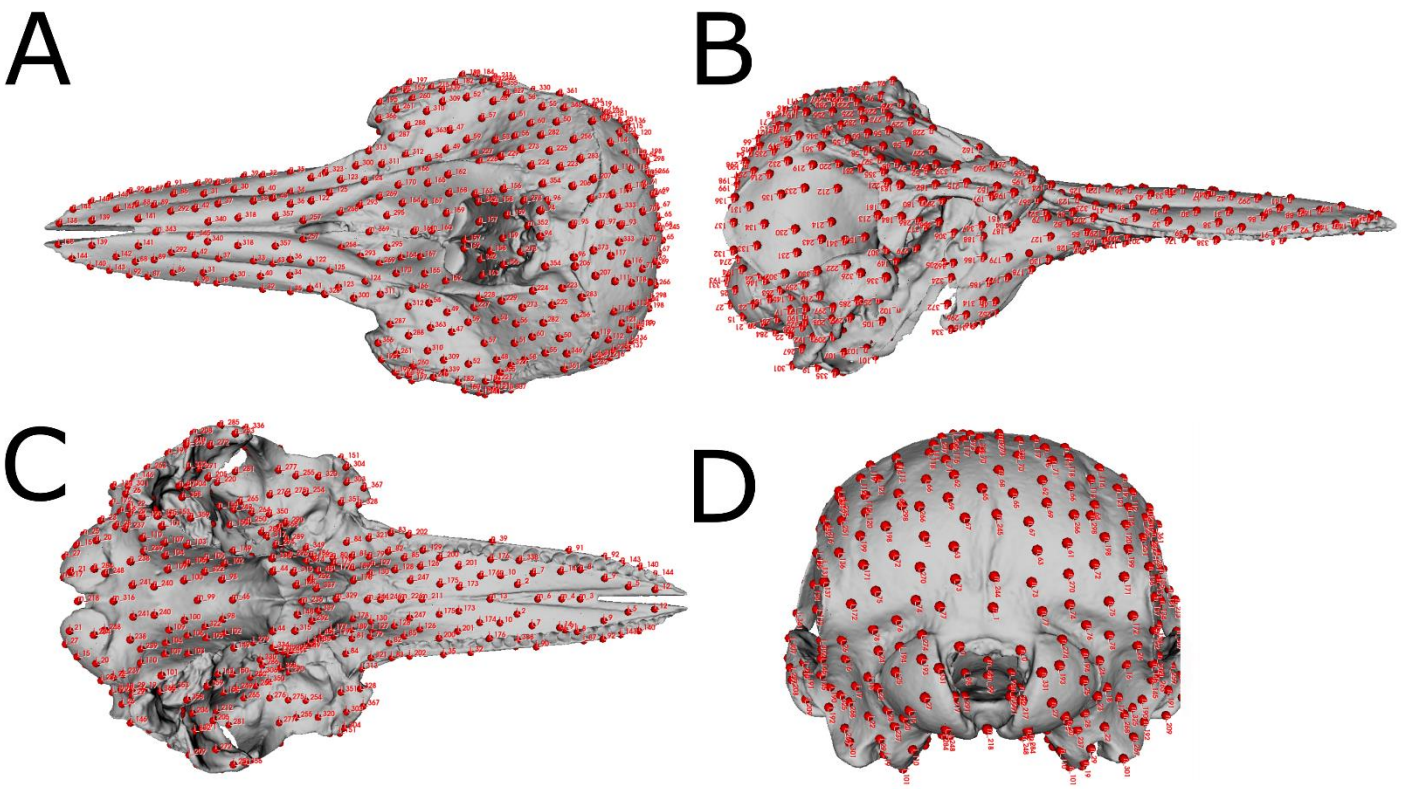

Figure 5.2. Three-dimensional landmarks from the semi-automatic landmarking shown in four views of the individual WA594515 skull: (A) Dorsal, (B) Lateral, (C) Ventral, and (D) Occipital.

Geometric morphometric shape analysis

Unless otherwise specified, all statistical analyses were performed using R Statistical Software (v4.3.0; R Core Team 2023). The sets of SSL generated in 3DSlicer were imported into R using the package SlicerMorphR(). A Generalized Procrustes Analysis (GPA) was performed using the gpagen() function implemented in the Geomorph package (Baken et al., 2021). This analysis aligned the shapes of each specimen within a common coordinate system by removing variations related to size, position and orientation (Rohlf & Slice, 1990). The placement of SSL on the skull surface was automated, and therefore it did not specifically target homologous anatomical features. As a result, geometric consistency was prioritised over biological relevance, implying that the landmarks may not correspond with anatomical features directly related to the skull's ecological functions (Zelditch et al., 2012). Therefore, during the GPA, pseudo-landmark positions were adjusted by sliding them along their tangent planes while maintaining the distances between corresponding landmarks (Bookstein, 1991; Bookstein, 1997; Gunz et al., 2005). This process ensures that the pseudo-landmark position between individuals approximates real homology (Mitteroecker & Schaefer, 2022).

The function bilat.symmetry() in the Geomorph package was used to remove the asymmetric component of shape variation. This was done by reflecting one side of the 3D skull shape to align with the opposite side and then calculating differences in position between the corresponding landmarks, which are then referred to as the asymmetric component. Asymmetry is then corrected by rotating, scaling, and aligning the landmarks on one side with those on the opposite side, producing a symmetrical component of skull shape used in subsequent analysis.

Principal Component Analysis (PCA) was performed on the symmetric components using the function gm.prcomp() in the Geomorph package, reducing the dimensionality of our dataset to a set of principal components (PCs), that account for most of the variance (James Rohlf & Marcus, 1993; Adams et al., 2004). Vector displacement graphs were generated for each PC using the function plotRefToTarget(), in the package geomorph. The method = "vector" was used, to visualise differences between shapes by showing vectors connecting a reference shape (i.e. the average shape of our dataset) to target shapes. Two target shapes were used, the first was a set of shapes corresponding to the minimum values of the components (e.g. comp1), while the second was a set of shapes corresponding to the maximum values of the same component. This setup provided insight into how shapes at the extreme values of a principal component differ from each other and the reference shape, therefore revealing the range of shape variation and the influence of different PCs on shape differences.

A Permutational Multivariate Analysis of Variance (PERMANOVA) was performed on all PCs to test for skull shape differentiation between pre-defined groups. The software PAST (Hammer et al., 2001) was used to calculate the distance matrix using the Euclidean method and significance was assessed through 10 000 permutations. The Bonferroni method was applied to adjust p-values for multiple pairwise comparisons.

Allometry Analysis

Allometry investigates how the size of an organism influences the proportions and scaling of its various morphological traits (Huxley & Teissier, 1936). This field is based on the principle that as an organism grows, different traits scale at different rates, leading to changes in their relative shape (Gould, 1966; Mosimann, 1970). Such scaling effects help describe how growth patterns and body size affect the form of biological structures. Understanding these relationships is essential, particularly when investigating fine-scale shape variations, which are often subtle and may not be sufficient to differentiate populations. Here, allometric analysis was used to investigate subtle morphological differences that may not be apparent from shape analyses alone and to determine whether incorporating size into morphological analysis reveals

more distinct patterns of population differentiation. This way, it can be assessed whether populations exhibit location-specific growth patterns, potentially reflecting differential ecology.

Inter-group differences in allometric patterns were investigated using three separate tests:

Test 1 - Allometric patterns between coastal locations were compared, using offshore individuals as a reference. Offshore individuals exhibit distinct allometric patterns compared to the coastal OTU from the WNA, demonstrating the expected differentiation patterns between genetically distinct groups. This provides a baseline for interpreting findings within coastal groups.

Test 2 - Differences in allometric patterns were tested between coastal locations, including sex as a factor.

Test 3 - Differences in allometric patterns were tested between sexes only (including only coastal specimens). Allometry can vary between sexes, as observed in some populations of bottlenose dolphins (e.g., the Gulf of Mexico), and therefore this test ensures that any allometric differences between locations are not attributed to sex differences but rather to true population differences. Individuals of unknown sex (n = 13) were excluded before performing tests that included sex as a covariate.

For each test, a model was defined and within-group regression analysis was performed between shape (Procrustes-aligned coordinates) and size (lnCS) data using the function procD.lm() in the geomorph package. A size-shape morphospace was generated using the function plotAllometry(method= “size.shape”) to visualise the relationship between size and shape variation in our data. This size-shape morphospace was produced using the results from the PCA performed on the shape data (Procrustes residuals) and incorporating the natural logarithm of centroid size in the calculation of the variance/covariance matrix (Mitteroecker et al., 2004).

Linear models were created using the function procD.lm to predict how different aspects of shape (PCs) change with size, generating predicted values for each PC. Then, these predictions were visualized with the function plotAllometry(method= “predline”), plotting the predicted PC1 values against size (Adams & Nistri, 2010). This produced regression lines showing the relationship between skull shape and size for PC1. By comparing the slopes of these lines across groups, the differences in their size-shape relationships were assessed.

Statistical differences in allometric patterns between groups were tested by applying two different multivariate linear regression models to each test’s size and shape data. The “common allometry” model (reduced hypothesis) considered regions as separate groups with different mean sizes but a common slope, while the “unique allometry” model (full hypothesis)

considered groups to have both different means and slopes (Mitteroecker et al., 2004; Adams et al., 2013). Each model was fitted using the procD.lm() function. An analysis of variance (ANOVA) was then performed on random permutations of each linear model using the function anova() to assess whether the models fit the data significantly better than expected by chance. Whether these relationships reflect true significant patterns rather than random variability, was determined by comparing the observed relationships between shape and predictors to those generated by random permutations. Model significance was assessed through 9 999 iterations and evaluated with Goodall's F-test (Goodall, 1991). For all tests except test 3 (see Paragraph 2 of the current section), pairwise comparisons (9 999 iterations) of the unique model against the common model were performed using the function pairwise() from the package geomorph. This analysis assessed differences in slope magnitude (i.e. amount of shape change per unit of lnCS) and orientation (i.e. direction of shape change per unit of lnCS) between groups.

5.3. Results

Principal Component Analysis

The first three principal component (PC) axes were shown to account for 51.8% of the total cranial shape variation in the coastal analysis (PC1 = 25.7%, PC2 = 16.2%, PC3 = 9.93%). The PCA morphospace including the complete dataset, shows that the offshore and coastal operational taxonomic units (OTUs) are clearly distinguished from each other (Figure 5.1.A). The PERMANOVA analysis confirms that the offshore OTU is significantly separated from all coastal populations collectively (all *F*-values ranging from 6.135 to 14.04 and *p*-values <0.005, see supplementary Table S5.3.1). This clear separation allows specimens without a clear OTU designation, to be unambiguously attributed to either the coastal or offshore unit.

The PCA morphospace including the coastal OTU only, shows subtle shape differentiation between coastal populations, despite considerable overall overlap. The Gulf of Mexico (N = 9) and Florida (N = 5) are noticeably separated in the morphospace, although the PERMANOVA comparisons are mostly non-significant (PERMANOVA *F*-values ranging from 0.46 to 3.679 and *p*-values ranging from 0.0042 to 1; Table 5.1). The Gulf of Mexico and North Carolina are the only populations showing significant differentiation (PERMANOVA – *F*-values = 3.679 and *p*-values = 0.0042, Table 5.1).

Delaware Bay (N = 8) appears separated from other locations mostly due to its narrow cloud dispersion, even when compared to locations with smaller sample sizes, such as Georgia (N = 6) and Maryland (N = 4). This visual separation was not, however, statistically significant

(PERMANOVA *F*-values ranging from 0.8416 to 2.813 and *p*-values = 0.0924 to 1, Table 5.1). Chesapeake Bay (N = 14) and North Carolina (N = 16) are widely dispersed throughout the morphospace and overlap with geographically close locations, namely Maryland (N = 4) and Georgia (N = 6). The relatively high sample sizes for Chesapeake Bay and North Carolina compared to other locations, may be contributing to their wider dispersions, potentially capturing more morphological variation. While these four locations overlap considerably, they also exhibit some separation along different PCs. Furthermore, part of the Maryland specimens, which in this case are represented by specimens sampled in the Atlantic coast of the state (as opposed to inside the Chesapeake Bay), are differentiated from Chesapeake Bay, North Carolina and Georgia, which occupy a more central position in the PCA. This separation is most noticeable along the positive values of PC2 and, to a lesser extent, PC3 (Figure 5.1.B - lower left plot). We therefore suggest regional associations with shape patterns along this coastline. However, it should be noted that these shape differences are identifiable only through a multi-dimensional differentiation in the morphospace. Regional separation is therefore subtle and most apparent when considering the first three PCs collectively, rather than any single PC alone. In contrast, offshore specimens are clearly differentiated from coastal ones along PC1, which explains the largest proportion of variation in the morphospace.

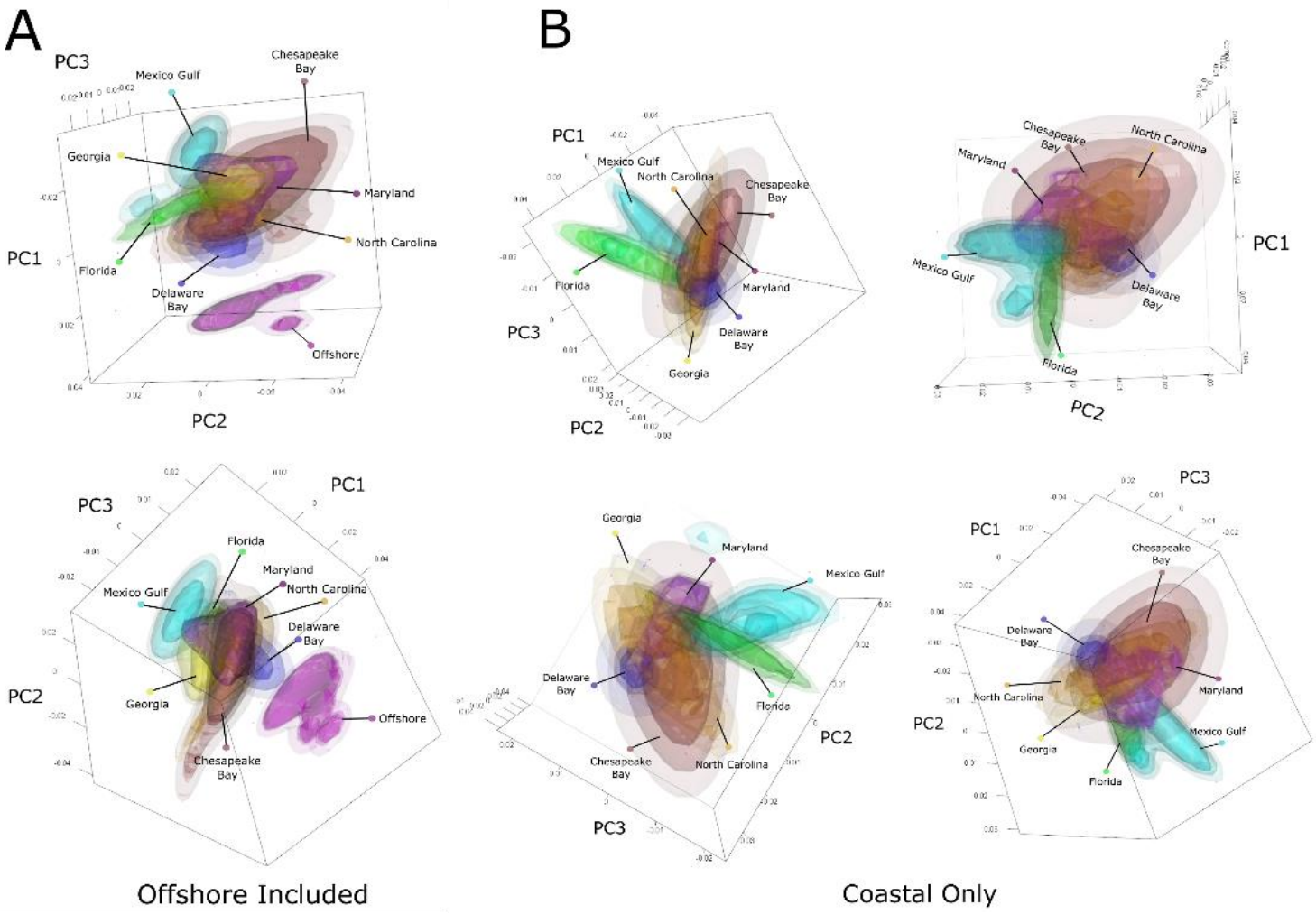

Figure 5.3. 3D PCA morphospace displays the three most important principal components, from different perspectives with the offshore OTU included (A) and with coastal populations only (B). The a priori populations are distinguished by colours. Kernel discriminant analysis clouds are calculated in the R package KS (Duong 2007).

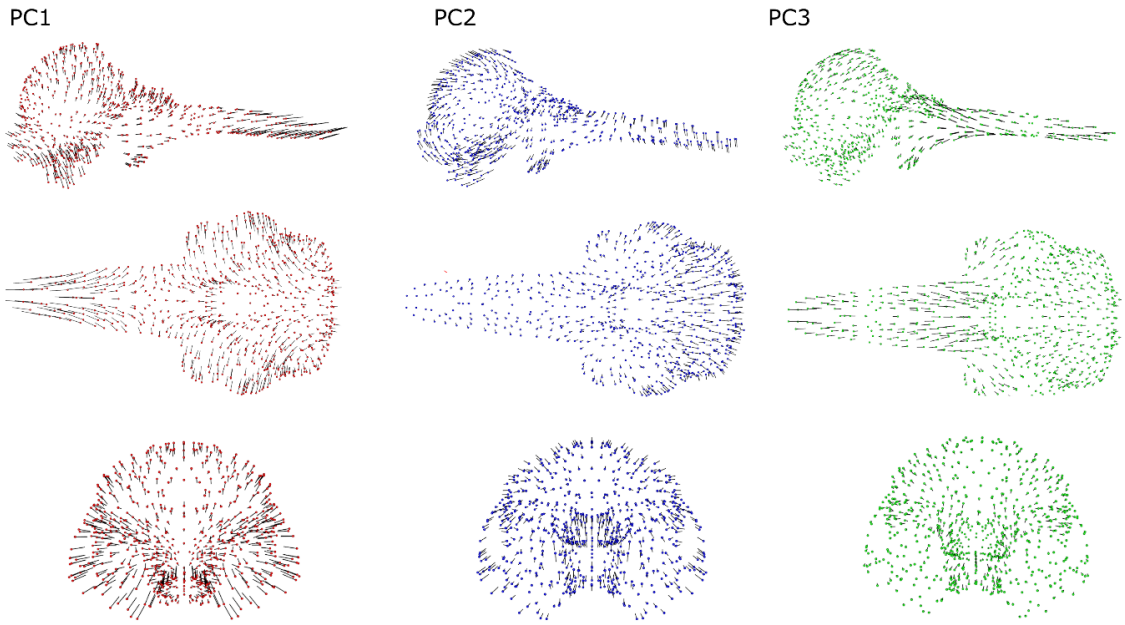

Figure 5.4. Vector displacement graph, representing differences in landmark position between the mean landmark configuration and specimens along the positive PC1, PC2 and PC3 axes from the PCA in Figure 5.1

Table 5.1. Pairwise PERMANOVA test results for the coastal locations, based on all Principal components retained from the PCA in Figure 5.1B. p-values are shown above the empty diagonal cells, while F-values are shown below the empty diagonal cells. Significant comparisons are marked in bold.

	ChesapeakeBay	NorthCarolina	DelawareBay	MexicoGulf	Florida	Maryland	Georgia
ChesapeakeBay (N =14)		1	1	0.315	1	1	1
NorthCarolina (N = 16)	0.7968		1	**0.0042**	1	1	1
DelawareBay (N = 8)	1.274	1.038		0.0924	1	1	1
MexicoGulf (N = 9)	2.456	3.679	2.813		1	1	1
Florida (N = 5)	1.551	1.782	1.121	1.064		1	1
Maryland (N = 4)	0.4726	0.9513	1.327	1.509	1.412		1
Georgia (N = 6)	0.9004	0.8709	0.8416	1.325	0.4588	0.8096	

Vector displacement plots

Along PC1, the vector displacement plot mainly captures shape changes in the rostrum, notably an elongation and a levelling of its anterior half, resulting in a flatter lateral profile. This is accompanied by a deepening of the ascending process of the maxillae and the most posterior section of the premaxillae, along with a downward shift of the nasal and ethmoid

bones (Figure 5.2), resulting in a more pronounced concavity in the naso-facial region. Additionally, the lateral part of the exoccipital bone and the zygomatic process is contracted upward, leading to a more dorsoventrally compact squamosal area. Lastly, the pterygoid bone is extended horizontally, broadening the pterygoid plate (Figure 5.2). Specimens from Florida, positioned towards the positive end of the PC1 axis, suggest a more streamlined and dorso-ventrally compact skull, with prominent concavity at the skull features surrounding the naso-facial region. In contrast, other populations clustered either near the centre (i.e., Delaware Bay and Georgia), displayed moderate deviations towards negative PC1 scores (i.e., Maryland), or overlapped considerably with each other along the negative scores of PC1. Therefore, skulls from these locations may appear stouter, with shorter rostrums and more expanded squamosal areas.

PC2 mainly captures shape changes involving a downward displacement of the anterior half of the rostrum, creating a more noticeable rostral bump in the midsection. Additionally, there is a posterior expansion of the frontal and supra-occipital regions, including the nasal bones. This is associated with a downward shift of the occipital condyles and an anteroventral shift of the lateral part of the occipital and temporal bones, while the tip of the pterygoid bone contracts anterodorsally (Figure 5.2). Specimens from the Gulf of Mexico, mostly separate along a combination of PC2 and PC3. Along PC2, these skulls would have a broader and more rounded cranium and ventrally deflected rostrum (see description of PC2 vector displacement graph). The frontal and supra-occipital regions are expanded posteriorly, with a downward shift of the occipital condyles and an anterodorsal displacement of the lateral part of the occipital and temporal bones. In contrast, specimens from North Carolina, Chesapeake Bay and Delaware Bay are mostly located along negative scores of PC2, suggesting opposite patterns of shape variation characterised by a more elliptical cranial case and flatter rostrums.

PC3 reflects shape changes involving a backward contraction of the anterior half of the rostrum and a forward expansion of the posterior half, resulting in a noticeably shorter rostrum. Additionally, the ascending process of the maxillae, palatal surface, and pterygoid bone are extended anteriorly, creating a more streamlined rostrum profile with a flattened naso-facial region (Figure 5.2). Delaware Bay, Georgia and Maryland are located along positive scores of PC3, suggesting their shape reflects those characteristics. Conversely, Florida and the Gulf of Mexico are clustered along the negative scores, suggesting opposite shape patterns, characterised by a longer and broader rostrum. Because most populations are differentiated along multiple PCs, their characteristic shapes require a combined interpretation of the vector displacement plots for all three PCs. Accordingly, Florida skulls are more streamlined and

dorsoventrally compact, with increased concavity of the dorsal area and an elongated rostrum. The Gulf of Mexico skulls exhibit a more rounded cranium and a robust, elongated and ventrally inclined rostrum. Delaware Bay skulls are characterised by an elliptical cranial case, a flatter, shorter and streamlined rostrum, and more horizontally oriented occipital condyles. Maryland skulls show, though to a milder extent, a more rounded cranial case and a slightly shorter rostrum with a ventrally deflected tip. Overall, other skulls tend to be relatively stouter, with shorter rostrums and expanded squamosal regions. For visual representations of typical skulls for each population see supplementary Figure S5.3.1.

Static allometry variability between coastal populations

Size-shape plots, allometric trajectory plots, and Procrustes ANOVA analysis were generated to test differences in allometric patterns between coastal locations. In the size-shape plots, PC1 mostly represents size-related changes in form, while shape changes independent of size are represented by the remaining PCs (Mitteroecker et al., 2004). The 3D PCA shape-size plot (Figure 5.3) shows that offshore and coastal OTUs are mainly separated along PC2 and PC3, while PC1 separates several other coastal populations. Therefore, our results suggest that shape is the main factor differentiating the offshore and coastal OTUs in this region, while size is an additional factor distinguishing between individual coastal locations. Namely, Delaware Bay, Maryland, the Gulf of Mexico and North Carolina locations show more pronounced differentiation on this PCA compared to the shape-only PCA results (Figure 5.3.B). For example, Delaware Bay and part of Maryland are more distinctly separated from other locations along PC1, while North Carolina and the other part of Maryland show greater separation along PC2, and the Gulf of Mexico along PC3. Interestingly, our shape analysis shows that there are intra-population differences when size was considered: Florida is divided into three distinct clusters, and Maryland into two, suggesting further morphological diversity within these populations, potentially driven by size differences. However, the small sample sizes in these populations may reduce the representation of morphological diversity within locations, potentially causing overemphasis on certain traits and thus leading to spurious differentiation patterns. However, these patterns could also suggest the existence of sub-populations or sex-related variations.

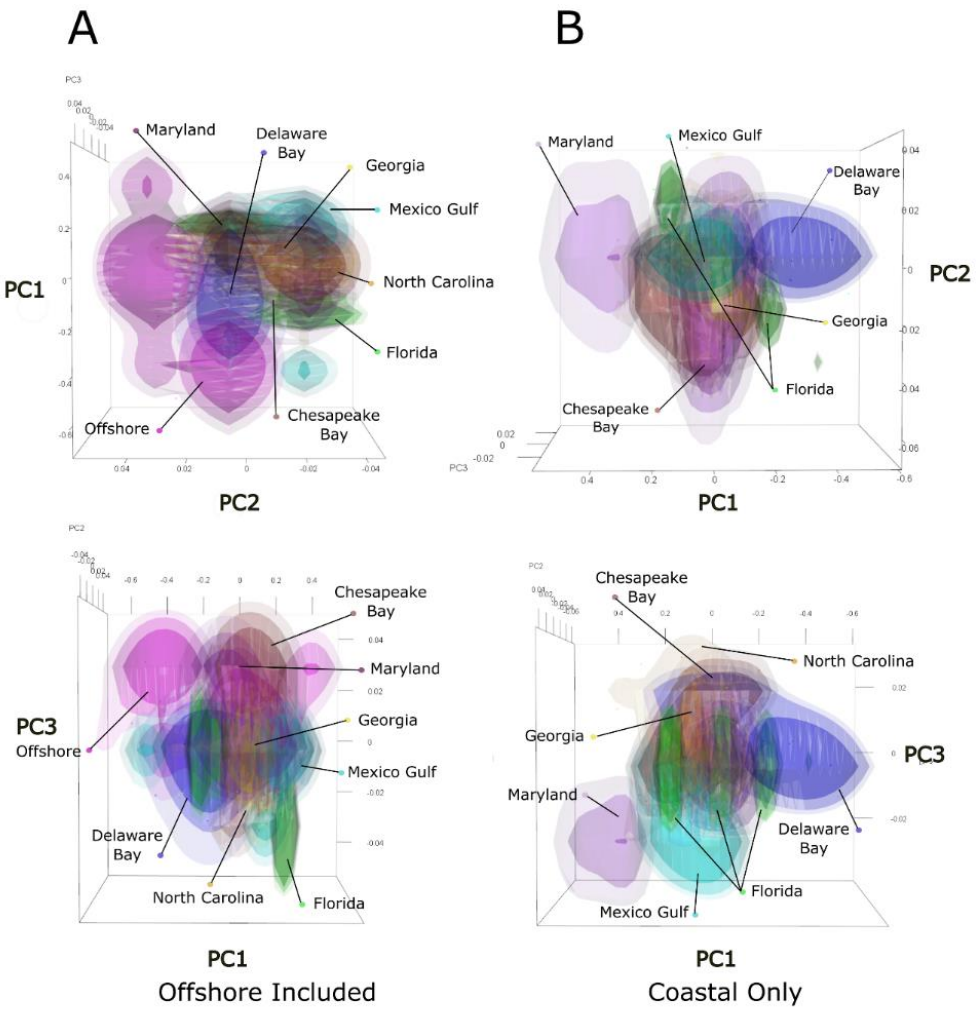

Figure 5.5. 3D PCA morphospace of the shape-size plot from the allometry analysis on the complete dataset (A) and coastal OTU only (B) displaying the three most important principal components, from three different perspectives. The locations are distinguished by colours. Kernel discriminant analysis clouds are calculated in the R package KS (Duong, 2007).

Differences in allometric patterns between coastal populations and sexes are illustrated by trajectory plots. In these plots, the x-axis represents the logarithm of centroid size, while the y-axis represents predicted shape values. Differences in slope length and/or direction between coastal populations and sex indicate varying size-shape relationships, with each having distinct allometric trajectories. Longer slopes (i.e. magnitude) reflect the greater magnitude of shape changes with varying size, while steeper slopes (i.e. direction) suggest larger shape changes with proportionally smaller size variation. The trajectory plots show visually distinct allometric trajectories for some coastal populations, although effect sizes are low (ANOVA F= 0.83, *p*-values = 0.878, Supporting information Table S5.3.2; Figure 5.4.A). North Carolina, Florida, Maryland, Georgia and the Gulf of Mexico regions show distinct slope directions from each

other (*z*-values ranging from -1.4 to -3.2, *p*-values ranging from 0.927 to 1, Supporting information Table S5.3.3), while Chesapeake and Delaware bays exhibit more similar allometric trajectories (*z*-value = -1.19, *p*-value = 0.879. Supporting information Table S5.3.3). North Carolina is unique compared to other coastal locations due to its negative slope (*z*-values from -1.4 to 3.0, *p*-values ranging from 0.927 to 1; Supporting information Table S5.3.3), while Maryland has the steepest slope (*z*-values ranging from -3.13 to -2.06, *p*-values ranging from 0.98 to 1; Supporting information Table S5.3.3), and Florida shows the shortest slope (*z*-values ranging from 0.43 to 1.0, *p*-values ranging from 0.348 to 0.970; Supporting information Table S5.3.3). The trajectory plots also show sex-specific differences in allometric slopes (F_1= 0.81, *p*-values = 0.662, Supporting information Table S5.3.2.; Figure 5.4.B). Females show a steep, positive and long slope, while males exhibit a slightly negative and short slope. The observed differences reflect population-specific patterns, with the most notable variations in North Carolina, Florida, Delaware Bay, the Gulf of Mexico, and Georgia. In North Carolina and Delaware Bay, males and females show strong, opposite slope directions, with females having a steep positive slope, while males show a steep negative slope, as observed in the sex-specific plots (Figure 5.4.C; Table S5.3.2).

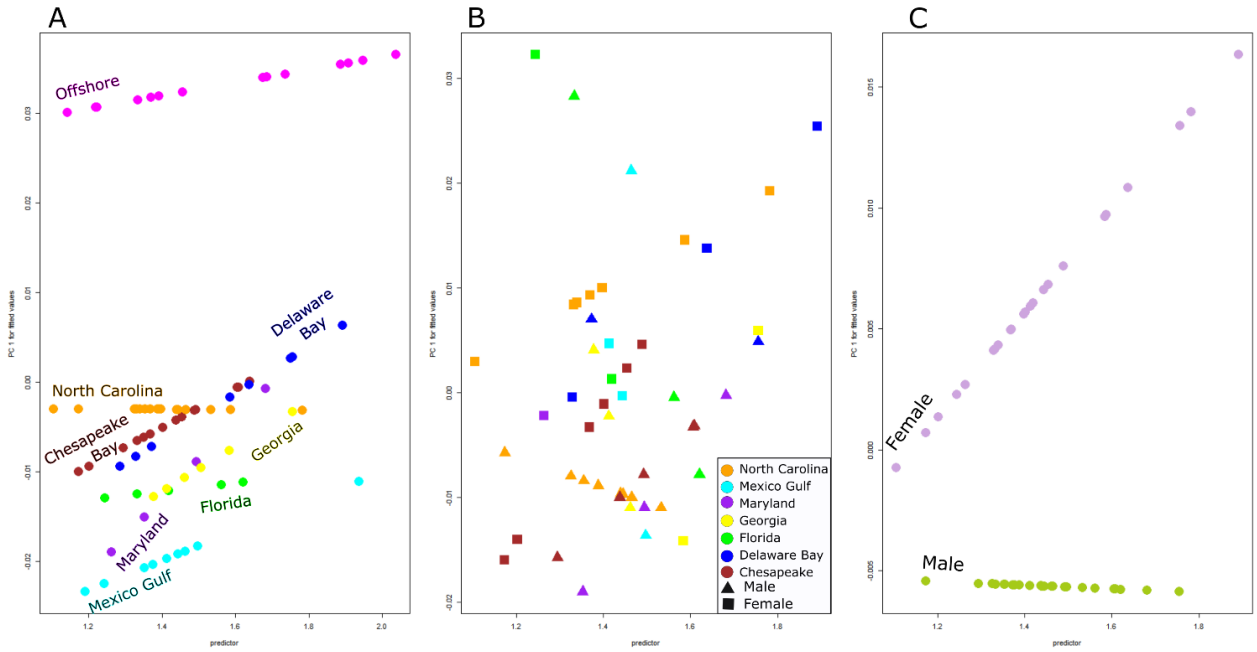

Figure 5.6. A) Allometric trajectories of the different coastal populations on the complete dataset (N = 76). B) Allometric trajectories of the different coastal populations with the offshore and individuals with unidentified sex removed (N = 49). C) Allometric trajectories between males and females with the offshore and individuals with unidentified sex removed (N = 49). The x-axis values are the log-transformed centroid sizes for each specimen; the y-axis values are the principal component 1 of the predicted values of a multivariate regression of shape on size.

Although visual inspection of the plots suggests potential distinct allometric patterns between coastal populations and sex, none of the tests is statistically significant (ANOVA coastal populations only - F_7= 0.83, *p*-values = 0.878; ANOVA Sex only – F_1= 0.81, *p*-values = 0.662; PERMANOVA Locations*Sex – F_5= 0.86, *p*-values= 0.693; Supporting information Table S5.3.2, S5.3.3, and S5.3.4; Figure 5.4). This analysis is focused on fine-scale differentiation, implying that variations are much subtler than those observed in broader-scale studies. This is especially evident when offshore individuals were included in the PCA morphospace allowing for a comparison between the well-known differentiation patterns of coastal versus offshore OTUs and the population level results. The shape and allometric differences between coastal populations are much subtler (Figure 5.1.B and Figure 5.4), and therefore low effect sizes from small sample sizes in some populations (like Maryland - N= 4, Florida - N= 5 and Georgia - N= 6) likely reduced statistical power. Despite these limitations, the results presented here are informative and useful within the context of the subtle intra-specific variations explored in this study, and therefore they can be considered as biologically meaningful.

5.4. Discussion

Shape patterns

The results of this study revealed distinct skull shape patterns between locations among coastal bottlenose dolphins along the Western North Atlantic (WNA). The populations from the Gulf of Mexico and Florida are markedly differentiated, as demonstrated by their clear separation along the first two principal components (PCs) of the morphospace (Figure 5.1.B). Interestingly, there is minimal morphological variation within the Delaware Bay population, which differentiates it from the other populations in our analysis (Figure 5.1.B). These findings corroborate genetic data indicating the presence of multiple stocks along the WNA (Rosel et al., 2009). Such differentiation may be influenced by factors including strong site fidelity, stable social structures, and limited dispersal among coastal bottlenose dolphin populations, which are suggested drivers of stock structure (Rosel et al., 2009). Genetic data suggests a potential demographically independent population of bottlenose dolphins in the Gulf of Mexico (Vollmer & Rosel, 2017) and in Florida (e.g. in Biscayne Bay and Florida Bay; Litz et al., 2012).

The first three principal components accounted for slightly over 50% of the total skull shape variations observed in our analysis. This suggests that the first three PCs are required to fully describe the variation patterns in this system. Intraspecific comparisons are usually subtler compared to interspecific ones, yet the variance explained by the first three PCs is similar to

that obtained including the offshore specimens. Furthermore, using a high number of landmarks also tends to reduce the proportion of variance explained by the first PCs. Therefore, the differentiation patterns identified by the PCA are likely to be statistically robust, even if the actual shape variations being described within the species are less pronounced compared to typical interspecific differences. Therefore, the identified PCs are informative in understanding skull shape variation within the dataset. North Carolina, Chesapeake Bay, Georgia and Maryland skull shape patterns appear as more central compared to other locations. These centrally located populations represent the more "average" or “typical” morphology within the dataset and therefore represent a baseline morphology that serves as the reference point to identify more differentiated skull shapes. Additionally, the observed overlap among these locations could reflect high levels of genetic exchange, which likely homogenises traits, reducing morphological differences between populations while also increasing the range of shape variation within the region.

Diagnostic skull shapes in Florida, the Gulf of Mexico and Delaware Bay were also identified. The populations from Florida and the Gulf of Mexico are primarily associated with the first two PCs and show the strongest separation in our analysis (Figure 5.1B). Similarities, such as a more convex lateral profile and a rounder cranium are shared by these populations, resulting from shifts in the occipital condyles, and the occipital and temporal bones (Figure 5.2). Despite these similarities, distinct traits are also displayed by each population. Florida skulls are notably slender, with a pronounced elongation of the rostrum, a strong ventro-dorsal contraction of the basioccipital bone and the zygomatic process (Figure 5.2). In contrast, the Delaware Bay population, primarily associated with the third PC, is characterized by a shortened rostrum and an elongated ascending process of the maxillae, palatal surface, and pterygoid bone (Figure 5.2).

Allometry

The incorporation of size into the shape data emphasised the distinctiveness of populations from Maryland, Delaware Bay and the Gulf of Mexico within the size-shape morphospace (Figure 5.3.B). This suggests that skull shape variations in these populations are accompanied by changes in size, a pattern commonly observed in other mammals, where size often correlates with environmental or dietary characteristics (Slater & Van Valkenburgh, 2009; Meloro et al., 2014a,b; Bubadué et al., 2021). Furthermore, the analysis of slope trajectories shows size-related differences in populations that initially appeared to have more similar skull shapes (Figure 5.4.A). While some core aspects of skull shape remain consistent across populations,

the way it scales with size was found to vary considerably by location, contributing to the observed overall morphological diversity. Therefore, it is suggested by these findings that size is a crucial factor influencing shape variation in the WNA, with local ecological factors influencing how skull shape changes with size.

Allometry, where size variations drive proportional changes in shape, is suggested to play a significant role in shaping skulls in some clades, such as primates (Frost et al., 2003; Marroig & Cheverud, 2005). For example, in Howler monkeys, allometry largely explains shape changes, with size-related skull shape changes being closely associated with a folivorous diet (Meloro et al., 2014). Across terrestrial mammals, it is described by the concept of craniofacial evolutionary allometry (CREA) that larger species typically have longer faces compared to their smaller relatives (Cardini, 2019). This craniofacial elongation pattern is observed across a wide range of placental mammals and is associated with skull shape changes both within and across species (Cardini & Polly, 2013; Cardini, 2019).

Differences in the length (magnitude) of allometric growth trajectories were revealed between coastal and offshore OTUs (Figure 5.1.A). These findings are somewhat comparable to those seen in previous studies comparing coastal and offshore bottlenose dolphins' OTUs along the WNA, where studies reported significantly longer (magnitude) and steeper (direction) vectors in the Offshore unit (Costa et al., 2022). The strong magnitude divergence between coastal and offshore OTUs, as reported in our study and others might reflect shape traits subject to stronger selective pressures. Within coastal populations, differences in the lengths and angles (direction) of the allometric vectors were also observed, with distinct patterns specific to each population (Figure 5.4.B). For instance, the population in North Carolina exhibited negative slope trajectories, while in Delaware Bay or Chesapeake Bay, populations had very steep positive slopes. In contrast, populations in Florida displayed shorter slopes compared to other coastal populations. Variations in slope direction at finer scales within coastal populations of the WNA may be linked to more localized ecological or developmental factors, influencing their allometric growth trajectories. Thus, the diversification of skull shape in WNA bottlenose dolphins appears to be driven not only by broad-scale ecological differences between coastal and offshore populations, but also by fine-scale allometric processes specific to local ecological conditions.

These findings support the idea that investigating allometric patterns can help differentiate between populations and provide insights into ecological processes such as dietary specializations or body size changes (Cardini & Polly, 2013). Moreover, the effectiveness of this approach at identifying fine-scale differentiation is demonstrated, as well as the role of

allometric processes in shaping population-specific traits. Although gene flow and other factors may sometimes obscure subtle local morphologies, this integrated approach remains useful in identifying and understanding these subtle variations. Deeper insights into population subdivisions along the WNA were provided, revealing previously unrecognized morphological differences that may have implications for understanding this species sub-structure. This method has previously shown to be useful in identifying cryptic diversity in other mammal species (Evin et al., 2008; Ferreira-Cardoso et al., 2020).

Distinct allometric patterns between males and females were observed in some populations, differing in both the magnitude and direction of their allometric growth trajectories (Figure 5.4.C). For example, in North Carolina and Delaware Bay, males show a negative allometric trajectory (where size increases more slowly than shape) while females display a more positive trajectory (where size and shape increase together). Some evidence of sexual dimorphism in skull shape patterns was observed in previous studies within each OTU (Costa et al., 2022), which corresponds with known instances of sexual dimorphism in bottlenose dolphins from other regions (De Francesco et al., 2016). Specifically, in the North Sea, males and females show different allometric growth in the ventral view, with males exhibiting more significant allometric growth in the palate and base of the braincase compared to females (De Francesco et al., 2016). The results of this study therefore reinforce that at a local scale, shape variations may occur through allometric processes. Local environmental conditions may influence how SD develops in dolphins, potentially due to different ecological requirements between the sexes.

In mammals, SD in skull shape is often explained by differences in allometric growth trajectories or relative growth rates (Flores & Casinos, 2011; Tarnawski et al., 2013, 2014). For example, males may exhibit either time hypermorphosis (longer growth periods) or rate hypermorphosis (faster growth rates), leading to larger facial and cranial structures, particularly those associated with mastication (Flores & Casinos, 2011). Relative growth rate, for example, is considered a key factor in SD in pinnipeds (Tarnawski et al., 2013, 2014). In species such as *Otaria byronia* and *Mirounga leonina*, skull length and braincase size are developed more rapidly in females than males, who show more rapid growth in canine width (Tarnawski et al., 2013, 2014). These sex-specific growth patterns are associated with the distinct ecological roles of each sex. Females tend to reach reproductive age earlier and allocate more energy to offspring, while males direct energy toward growth and the development of secondary sexual characteristics related to competition.

In the bottlenose dolphin, sexual dimorphism in skull shape has been observed in some populations within the Gulf of Mexico or on the east coast of Florida. For example, more teeth

and a slightly larger parietal width within the postemporal fossae are exhibited by males compared to females in the Indian/Banana River of Florida (Hersh et al., 1990). Similarly, in the Gulf of Mexico, skull measurements are different between sexes along the Texas coast, but not along Florida's Gulf Coast (Turner & Worthy, 2003). Interestingly, these changes appear to be mainly associated with females, with differences observed in the height of the braincase and width of the internal nares between females from Texas and Florida. In contrast, no significant differences were observed between males from the two populations (Turner & Worthy, 2003). In the North Sea, high interspecific competition is thought to promote sex-specific niche partitioning, where males and females adopt distinct feeding strategies to reduce direct competition for resources (De Francesco et al., 2016). Similar patterns have been observed across various mammalian and avian species (Condor, 1966; Earhart & Condor, 1970; Loy et al., 2004), suggesting that similar mechanisms may also be occurring in the Gulf of Mexico.

In the Gulf of Mexico, differences in foraging habits and other behaviours have been observed between the sexes. A study in Sarasota Bay showed that individual females tend to occupy smaller home ranges and demonstrate higher habitat specialization compared to males (Rossman et al., 2015b). This greater habitat specialization may allow females to exploit particular food sources with higher efficiency, enhancing their ability to meet the nutritional demands of reproduction. In contrast, larger home ranges and lower diversity in foraging habitat use are generally occupied by males (Rossman et al., 2015b), possibly to accommodate the social or mating behaviours that demand broader movement patterns. While males primarily feed on seagrass-associated fish prey, females are also likely foraging in more open waters on phytoplankton-based food webs (Rossman et al., 2015b). These differences in feeding behaviour are thought to also involve a component of social learning, as these foraging techniques are transmitted across generations (Rossman, et al., 2015a).

Ecological interpretation

While skull shape is commonly influenced by environmental factors like diet and habitat, the results of this study do not indicate strong regional selection pressures. Instead, the fine-scale variations in skull morphology observed here may be driven by a combination of subtle ecological pressures, gene flow between populations, and stochastic processes. Gene flow between coastal populations along the WNA likely contributes to the homogenisation of traits across regions, preventing the establishment of distinct morphologies despite ecological differences. However, in the Gulf of Mexico, gene flow is more restricted, with studies indicating low migration rates among the seven genetically distinct populations in the region

(Vollmer & Rosel, 2017), which may account for the more evident morphological differences observed there. Interestingly, greater diversity was observed with allometric patterns than skull shape data alone, with distinct patterns emerging between coastal populations and sexes. While skull shape changes are typically reflected by population-specific adaptations, they can also result from allometric processes that reflect shorter-term ecological responses. In this study, allometric patterns suggest that environmental pressures on coastal populations may have driven phenotypic plasticity, as discussed further below.

Variations in skull shape and allometric patterns are often associated with environmental factors such as climate, temperature regimes, seasonal fluctuations, and food availability, particularly in traits related to specific dietary needs (Cáceres et al., 2014; Meloro et al., 2014; Bubadué et al., 2021). For example, species living in colder climates with pronounced seasonal fluctuations in food resources may develop more robust skulls, which may provide mechanical advantages for processing tougher or more varied diets when food becomes scarcer (Bubadué et al., 2021). In contrast, species inhabiting warmer, more stable environments with year-long food supply might exhibit fewer variations both in terms of shape and allometric changes, since environment stability allows for the retention of more consistent traits over time (Bubadué et al., 2021). In such habitats, efficiency might be favoured over versatility, leading to more uniform skull shapes that match the consistency of available food sources.

Allometry in skull shape is often associated with functions such as bite force. Bite force allometry suggests that the demands of bite force requirements account for a considerable part of skull shape variation, while other factors like dietary shifts and evolutionary constraints may also play a role (Mitchell et al., 2024). According to this idea, larger species may have less robust skulls due to reduced relative bite force requirements, while animals with higher bite force demands tend to evolve more robust skulls as an adaptive response. This relationship is influenced by the scaling of cranial structures that optimize bite force generation. For example, in some bat species, significant allometric changes in skull shape and jaw muscle development occur during growth. Key adaptations include the outward growth of the zygomatic arches, expansion of the cranial dome and sagittal crest, and extensions of mandibular processes. Attachment areas for the temporalis and masseter muscles are enhanced by these modifications and therefore improve muscle function and joint stability, contributing to increased bite force (Stanchak et al., 2023). Similarly, the results presented here indicate that the most pronounced shape changes in the bottlenose dolphin occur in the rostrum and squamosal area. These structures are integral components of the feeding apparatus, and their variations between populations may reflect differences in biting capacities.

Specifically, in raptorial-like dolphin species, those with more elongated cranial shapes tend to target smaller and more agile prey (McCurry et al., 2017). In contrast, more generalized feeding strategies are often exhibited by larger dolphins, enabled by robust skulls and powerful jaws, which allow them to capture a wider range of prey species (McCurry et al., 2017). These variations are thought to be related to biomechanical factors, such as the leverage and force generated by different cranial and jaw structures. For instance, speed in jaw movements may be optimized by elongated skulls, while greater bite force and the ability to handle a wider range of prey sizes are provided by larger skulls (McCurry et al., 2017).

Different foraging behaviour along the WNA including specific echolocation abilities were suggested in previous studies. In the Gulf of Mexico, strong fidelity to shallow areas is exhibited in some resident populations of bottlenose dolphins, where they use learnt foraging strategies such as mud-ring (Torres & Read, 2009) or mud-plume (Lewis & Schroeder, 2003; Ramos et al., 2022). These techniques require high cooperation skills and the ability to move swiftly near the seafloor. In contrast, bottlenose dolphins along the East Coast of Florida target non-schooling, seagrass-associated prey, perhaps through the use of passive listening to detect fish (Barros, 1993). In North Carolina, dolphins are observed congregating in areas with pronounced slopes and channels (McBride-Kebert et al., 2019), suggesting that they may use different foraging strategies in this region. Although subtle, differences in skull structures identified in this study include a more concave ascending process of the maxillae, expansions of the supraoccipital, and a rostral bump at the mid-rostral region (Figure 5.2). These features are typically associated with the melon, a specialized fatty structure involved in echolocation. Muscles attached to these skull regions likely help control the melon's shape and function, modifying its ability to focus and project sound waves during vocalisation. Therefore, such variations could reflect functional differences in vocalisation, that could be associated with specific prey capture behaviours in different environments. As a result, these findings suggest that differences in skull shape across the WNA may be influenced by both dietary needs and vocalisation behaviours, which supports previous hypotheses in other bottlenose dolphin populations (Mead & Potter, 1995; Viaud-Martinez et al., 2008; Perrin et al., 2011).

A slight downward displacement of the occipital condyles is exhibited by bottlenose dolphins in the WNA, suggesting a more downward orientation of the skull relative to the body. This morphological variation has also been described in Phocoenidae species inhabiting coastal environments (Galatius et al., 2011) and is suggested to facilitate manoeuvrability in shallow waters in other Delphinidae species (De Araujo Montiero-Filho et al., 2002). Conversely, other populations may undergo less constraint related to the topographic specificity of their

environments. For example, in the Gulf of Mexico, mud-ring and mud-plum feeding behaviour (Lewis & Schroeder, 2003; Ramos et al., 2022) are used in some populations of bottlenose dolphins, suggesting that this downward orientation of the skull may provide a mechanical function related to these foraging strategies.

In this study, allometric differences between coastal populations of bottlenose dolphins and between sexes were observed, most often associated with shape changes. In the WNA, the contrasting habitats of coastal versus offshore OTUs are thought to play an essential role in driving morphological differentiations (Mead & Potter, 1995). Parallel processes may be occurring among coastal populations along the WNA, with each exhibiting behavioural adaptations that reflect specific local conditions. This could promote phenotypic plasticity, where different size-scaling relationships generate phenotypic variation that natural selection can then act upon (West-Eberhard, 2005). Over time, traits that initially develop as plastic responses to environmental conditions may become genetically fixed through a process known as "genetic assimilation" (Pigliucci et al., 2006). Notably, size-shape differences between sexes in bottlenose dolphins were also revealed in this study, consistent with existing literature on sexual niche partitioning (Rossman et al., 2015b). Therefore, the findings of this study suggest that variations in foraging strategies could be a primary driver of phenotypic plasticity among bottlenose dolphin populations.

5.5. Bibliography

Abegg, A. D., Passos, P., Mario-da-Rosa, C., Azevedo, W. dos S., Malta-Borges, L., & de Moura Bubadué, J. (2020). Sexual dimorphism, ontogeny and static allometry of a semi-fossorial snake (genus *Atractus*). *Zoologischer Anzeiger*, *287*, 95–104. doi: 10.1016/J.JCZ.2020.05.008

Adams, D. C., & Nistri, A. (2010). Ontogenetic convergence and evolution of foot morphology in European cave salamanders (Family: Plethodontidae). *BMC Evolutionary Biology*, *10*(1). doi: 10.1186/1471-2148-10-216

Adams, D. C., & Otárola-Castillo, E. (2013). Geomorph: an r package for the collection and analysis of geometric morphometric shape data. *Methods in Ecology and Evolution*, *4*(4), 393–399. doi: 10.1111/2041-210X.12035

Adams, D. C., Rohlf, F. J., & Slice, D. E. (2004). Geometric morphometrics: ten years of progress following the 'revolution.' *Italian Journal of Zoology*, *71*(1), 5–16. doi: 10.1080/11250000409356545

Adams D; Rohlf FJ; Slice D. (2013). A field comes of age: geometric morphometrics in the 21st century. *Hystrix*, *24*, 7–14.

Alexander Pyron, R., & Burbrink, F. T. (2009). Body size as a primary determinant of ecomorphological diversification and the evolution of mimicry in the lampropeltinine snakes (Serpentes: Colubridae). *Journal of Evolutionary Biology*, *22*(10), 2057–2067. doi: 10.1111/J.1420-9101.2009.01820.X

Baken, E. K., Collyer, M. L., Kaliontzopoulou, A., & Adams, D. C. (2021). Geomorph v4.0 and gmShiny: enhanced analytics and a new graphical interface for a comprehensive morphometric experience. *Methods in Ecology and Evolution*, *12*(12), 2355–2363. doi: 10.1111/2041-210X.13723

Balmer, B., Watwood, S., Quigley, B., Speakman, T., Barry, K., Mullin, K., Rosel, P., Sinclair, C., Zolman, E., & Schwacke, L. (2019). Common bottlenose dolphin (*Tursiops truncatus*) abundance and distribution patterns in St Andrew Bay, Florida, USA. *Aquatic Conservation: Marine and Freshwater Ecosystems*, *29*(3), 486–498. doi: 10.1002/AQC.3001

Balmer, B., Zolman, E., Rowles, T., Smith, C., Townsend, F., Fauquier, D., George, C., Goldstein, T., Hansen, L., Quigley, B., McFee, W., Morey, J., Rosel, P., Saliki, J., Speakman, T., & Schwacke, L. (2018). Ranging patterns, spatial overlap, and association with dolphin morbillivirus exposure in common bottlenose dolphins (*Tursiops truncatus*) along the Georgia, USA coast. *Ecology and Evolution*, *8*(24), 12890–12904. doi: 10.1002/ECE3.4727

Barros, N. B. (1993). Feeding ecology and foraging strategies of bottlenose dolphins on the central east coast of Florida [*Doctoral dissertation*]. University of Miami.

Bassos-Hull, K., Perrtree, R. M., Shepard, C. C., Schilling, S., Barleycorn, A. A., Allen, J. B., Balmer, B. C., Pine, W. E., & Wells, R. S. (2023). Long-term site fidelity and seasonal abundance estimates of common bottlenose dolphins (*Tursiops truncatus*) along the southwest coast of Florida and responses to natural perturbations. *Journal of Cetacean Research and Management*, *13*(1), 19–30. doi: 10.47536/jcrm.v13i1.551

Bookstein, F. L. (1997). Landmark methods for forms without landmarks: morphometrics of group differences in outline shape. *Medical Image Analysis*, *1*(3), 225–243. doi: 10.1016/S1361-8415(97)85012-8

Bookstein, FL. (1991). Morphometric tools for landmark data: geometry and biology (Issue 10). Cambridge University Press.

Bubadué, J., Meloro, C., Hendges, C., Battistella, T., Carvalho, R., & Cáceres, N. (2021). Clinal and allometric variation in the skull of sexually dimorphic opossums. *Journal of Mammalian Evolution*, *28*(2), 185–198. doi: 10.1007/S10914-020-09513-W

Cáceres, N., Meloro, C., Carotenuto, F., Passaro, F., Sponchiado, J., Melo, G. L., & Raia, P. (2014). Ecogeographical variation in skull shape of capuchin monkeys. *Journal of Biogeography*, *41*(3), 501–512. doi: 10.1111/JBI.12203

Cardini, A., Polly, D., Dawson, R., & Milne, N. (2015). Why the long face? Kangaroos and wallabies follow the same 'rule' of cranial evolutionary allometry (CREA) as placentals. *Evolutionary Biology*, *42*(2), 169–176. doi: 10.1007/S11692-015-9308-9

Cardini, A., & Polly, P. D. (2013). Larger mammals have longer faces because of size-related constraints on skull form. *Nature Communications*, *4*(1), 1–7. doi: 10.1038/ncomms3458

Cardini, Andrea. ,. (2019). Craniofacial allometry is a rule in evolutionary radiations of placentals.. *Evolutionary Biology*, *46*(3), 239–248. doi: 10.1007/S11692-019-09477-7

Centorame, M., Angelino, D., Bonanni, R., & Fanfani, A. (2020). Static and evolutionary allometry in the Italian endemic ant species *Cataglyphis italica* (Emery 1906). *Ethology Ecology & Evolution*, *32*(1), 16–28. doi: 10.1080/03949370.2019.1639080

Cheverud, J. M. (1982). Relationships among ontogenetic, static, and evolutionary allometry. *American Journal of Physical Anthropology*, *59*(2), 139–149. doi: 10.1002/AJPA.1330590204

Cignoni, P., Callieri, M., Corsini, M., Dellepiane, M., Ganovelli, F., & Ranzuglia, G. (2008). MeshLab: An open-source mesh processing tool. *Sixth Eurographics Italian Chapter Conference*, 129–136.

Condor, R. S. (1966). Sexual dimorphism and differential niche utilization in birds. *The Condor*, *68*(2), 113-151. doi: 10.2307/1365712

Costa, A. A., Mcfee, W., Wilcox, L. A., Archer, F. I., & Rosel, P. E. (2022). The common bottlenose dolphin (*Tursiops truncatus*) ecotypes of the western North Atlantic revisited: an integrative taxonomic investigation supports the presence of distinct species. *Zoological Journal of the Linnean Society*, *196*(4), 1608–1636. doi: 10.1093/zoolinnean/zlac025

De Araujo Monteiro-Filho, E. L., Monteiro, L. R., & Dos Reis, S. F. (2002). Skull shape and size divergence in dolphins of the genus *Sotalia*: a tridimensional morphometric analysis. *Journal of Mammalogy*, *83*(1), 125–134. doi: 10.1644/1545-1542(2002)083<0125:SSASDI>2.0.CO;2

De Francesco, M. C., Loy, A., Francesco, M. C. de, & Loy, A. (2016). Intra- and interspecific interactions as proximate determinants of sexual dimorphism and allometric trajectories in the bottlenose dolphin *Tursiops truncatus* (Cetacea, Odontoceti, Delphinidae). *PLoS One*, *11*(10), e0164287. doi: 10.1371/journal.pone.0164287

Dromby, M., Félix, F., Haase, B., Simões-Lopes, P. C., Costa, A. P. B., Lalis, A., Bens, C., Podestà, M., Doria, G., & Moura, A. E. (2023). Cranial variation between coastal and offshore bottlenose dolphins, *Tursiops truncatus* (Cetacea: Delphinidae) in Ecuador and the Mediterranean: a three-dimensional geometric morphometric study. *Zoological Journal of the Linnean Society*, *199*(1), 83–96. doi: 10.1093/ZOOLINNEAN/ZLAD022

Duffield, D. A., Ridgway, S. H., & Cornell, L. H. (1983). Hematology distinguishes coastal and offshore forms of dolphins (*Tursiops*). *Canadian Journal of Zoology*, *61*(4), 930–933. doi: 10.1139/Z83-123

Earhart, C., & Condor, N. J. (1970). Size dimorphism and food habits of North American owls. *The Condor*, *72*(3), 251–264. doi: 10.2307/1366002

Esteves-Ponte, M. A., Aurioles-Gamboa, D., & García-Rodríguez, F. J. (2022). Skull morphometric variability related to offshore and inshore ecotypes of the common bottlenose dolphin (*Tursiops truncatus*) from northwestern Mexico. *Marine Mammal Science*, *38*(3), 1088–1103. doi: 10.1111/MMS.12914

Evin, A., Baylac, M., Ruedi, M., Mucedda, M., & Pons, J. M. (2008). Taxonomy, skull diversity and evolution in a species complex of *Myotis* (Chiroptera: Vespertilionidae): a geometric morphometric appraisal. *Biological Journal of the Linnean Society*, *95*(3), 529–538. doi: 10.1111/J.1095-8312.2008.01076.X

Ferreira-Cardoso, S., Billet, G., Gaubert, P., Delsuc, F., & Hautier, L. (2020). Skull shape variation in extant pangolins (Pholidota: Manidae): allometric patterns and systematic implications. *Zoological Journal of the Linnean Society*, *188*, 255–275. doi: 10.1093/zoolinnean/zlz096

Flores, D., & Casinos, A. (2011). Cranial ontogeny and sexual dimorphism in two new world monkeys: *Alouatta caraya* (Atelidae) and *Cebus apella* (Cebidae). *Journal of Morphology*, *272*(6), 744–757. doi: 10.1002/jmor.10947

Frost, S. R., Marcus, L. F., Bookstein, F. L., Reddy, D. P., & Delson, E. (2003). Cranial allometry, phylogeography, and systematics of large-bodied papionins (primates: Cercopithecinae) inferred from geometric morphometric analysis of landmark data. *The Anatomical Record Part A: Discoveries in Molecular, Cellular, and Evolutionary Biology*, *275A*(2), 1048–1072. doi: 10.1002/AR.A.10112

Galatius, A., Berta, A., Frandsen, M. S., & Goodall, R. N. P. (2011). Interspecific variation of ontogeny and skull shape among porpoises (Phocoenidae). *Journal of Morphology*, *272*(2), 136–148. doi: 10.1002/jmor.10900

Galatius, A., & Gol'din, P. E. (2011). Geographic variation of skeletal ontogeny and skull shape in the harbour porpoise (*Phocoena phocoena*). *Canadian Journal of Zoology*, *89*(9), 869–879. doi: 10.1139/Z11-059

Gatis, D. (2020). *REMBG - A tool to remove images background*. Downloaded from https://github.com/danielgatis/rembg

Goodall, C. (1991). Procrustes Methods in the Statistical Analysis of Shape. *Journal of the Royal Statistical Society: Series B)*, *53*(2), 285–321. doi: 10.1111/J.2517-6161.1991.TB01825.X

Gould, S. J. (1966). Allometry and size in ontogeny and phylogeny. *Biological Reviews*, *41*(4), 587–638. doi: 10.1111/J.1469-185X.1966.TB01624.X

Griwodz, C., Gasparini, S., Calvet, L., Gurdjos, P., Castan, F., Maujean, B., ... & Lanthony, Y. (2021). AliceVision Meshroom. An open-source 3D reconstruction pipeline. In *Proceedings of the 12th ACM multimedia systems conference*, 241–247. doi: 10.1145/3458305.3478443

Guidarelli, G., Nicolosi, P., Fusco, G., de Francesco, M. C., & Loy, A. (2014). Morphological variation and modularity in the mandible of three Mediterranean dolphin species. *Italian Journal of Zoology*, *81*(3), 354–367. doi: 10.1080/11250003.2014.943685

Gunz, P., Mitteroecker, P., & Bookstein, F. L. (2005). Semilandmarks in three dimensions. In D. E. Slice (Ed.), *Modern morphometrics in physical anthropology* (pp. 73–98). Springer. https://doi.org/10.1007/0-387-27614-9_3

Hammer, Ø., Harper, D. A. T., & Ryan, P. D. (2001). Past: Paleontological statistics software package for education and data analysis. *Palaeontologia Electronica*, *4*(1), Article 4: 9pp.

Hayes, S. A., Josephson, E., Maze-Foley, K., Rosel, P. E., Byrd, B., Chavez-Rosales, S., Vn Cole, T., Garrison, L. P., Hatch, J., Henry, A., Horstman, S. C., Litz, J., Lyssikatos, M. C., Mullin, K. D., Orphanides, C., Pace, R. M., Palka, D. L., Powell, J., Wenzel, F. W., … Oliver, C. (2020). *U.S. Atlantic and Gulf of Mexico marine mammal stock assessments - 2019*. doi: 10.25923/NGSQ-QC69

Hersh, S. L., Odell, D. K., & Asper, E. D. (1990). Sexual dimorphism in bottlenose dolphins from the east coast of Florida. *Marine Mammal Science*, *6*(4), 305–315. doi: 10.1111/J.1748-7692.1990.TB00360.X

Hoelzel, A. R., Potter, C. W., & Best, P. B. (1998). Genetic differentiation between parapatric 'nearshore' and 'offshore' populations of the bottlenose dolphin. *Proceedings of the Royal Society of London. Series B: Biological Sciences*, *265*(1402), 1177–1183. doi: 10.1098/RSPB.1998.0416

Hohl, L. S. L., Sicuro, F. L., Wickert, J. C., Moreno, I. B., Rocha-Barbosa, O., & Barreto, A. S. (2020). Skull morphology of bottlenose dolphins from different ocean populations with emphasis on South America. *Journal of Morphology*, *281*(6), 564–577. doi: 10.1002/jmor.21121

Hohn, A. A., Gorgone, A. M., Byrd, B. L., Shertzer, K. W., & Eguchi, T. (2022). Patterns of association and distribution of estuarine-resident common bottlenose dolphins (*Tursiops truncatus*) in North Carolina, USA. *PLOS One*, *17*(8), e0270057. doi: 10.1371/JOURNAL.PONE.0270057

Huntley, L. C., Gower, D. J., Sampaio, F. L., Collins, E. S., Goswami, A., & Fabre, A. C. (2021). Intraspecific morphological variation in the shieldtail snake *Rhinophis philippinus* (Serpentes: Uropeltidae), with particular reference to tail-shield and cranial 3D geometric morphometrics. *Journal of Zoological Systematics and Evolutionary Research*, *59*(6), 1357–1370. doi: 10.1111/jzs.12505

Huxley, J. S., & Teissier, G. (1936). Terminology of Relative Growth. *Nature*. *137*(3471), 780–781. doi: 10.1038/137780b0

Janik, V. M. (2000). Food–related bray calls in wild bottlenose dolphins (*Tursiops truncatus*). *Proceedings of the Royal Society of London. Series B: Biological Sciences*, *267*(1446), 923–927. doi: 10.1098/RSPB.2000.1091

Kazhdan, M., & Hoppe, H. (2013). Screened Poisson surface reconstruction. *ACM Transactions on Graphics*, *32*(3). doi: 10.1145/2487228.2487237

Klingenberg, C. P. (2016). Size, shape, and form: concepts of allometry in geometric morphometrics. *Development Genes and Evolution*, *226*(3), 113–137. doi: 10.1007/S00427-016-0539-2

Klingenberg, C. P., & Zimmermann, M. (1992). Static, ontogenetic, and evolutionary allometry: a multivariate comparison in nine species of water striders. *The American Naturalist*, *140*(4), 601–620. doi: 10.1086/285430

Kurihara, N., & Oda, S. I. (2009). Effects of size on the skull shape of the bottlenose dolphin (*Tursiops truncatus*). *Mammal Study*, *34*(1), 19–32. doi: 10.3106/041.034.0104

Kuzminsky, S. C., Reyes Báez, O., Arriaza, B., Méndez, C., Standen, V. G., San Román, M., Muñoz, I., Durán Herrera, Á., & Hubbe, M. (2018). Investigating cranial morphological variation of early human skeletal remains from Chile: A 3D geometric morphometric approach. *American Journal of Physical Anthropology*, *165*(2), 223–237. doi: 10.1002/AJPA.23344

La Manna, G., Rako Gospić, N., Manghi, M., Picciulin, M., & Sarà, G. (2017). Assessing geographical variation on whistle acoustic structure of three Mediterranean populations of common bottlenose dolphin (*Tursiops truncatus*). *Behaviour*, *154*(5), 583–607. doi: 10.1163/1568539X-00003435

La Manna, G., Rako-Gospić, N., Sarà, G., Gatti, F., Bonizzoni, S., & Ceccherelli, G. (2020). Whistle variation in Mediterranean common bottlenose dolphin: The role of geographical, anthropogenic, social, and behavioral factors. *Ecology and Evolution*, *10*(4), 1971–1987. doi: 10.1002/ECE3.6029

Lewis, J. S., & Schroeder, W. W. (2003). Mud plume feeding, a unique foraging behavior of the bottlenose dolphin in the Florida Keys. *Gulf of Mexico Science*, *21*(1). doi: 10.18785/goms.2101.09

Litz, J. A., Hughes, C. R., Garrison, L. P., Fieber, L. A., & Rosel, P. E. (2023). Genetic structure of common bottlenose dolphins (*Tursiops truncatus*) inhabiting adjacent South Florida estuaries – Biscayne Bay and Florida Bay. *Journal of Cetacean Research and Management*, *12*(1), 107–117. doi: 10.47536/jcrm.v12i1.597

Louis, M., Galimberti, M., Archer, F., Berrow, S., Brownlow, A., Fallon, R., Nykänen, M., Roberston, K. M., Rosel, P. E., Simon-Bouhet, B., Wegmann, D., Fontaine, M. C., Foote, A. D., & Gaggiotti, O. E. (2021). Selection on ancestral genetic variation fuels repeated ecotype formation in bottlenose dolphins. *Science Advances*, 7(44), doi: 10.1126/sciadv.abg1245.

Loy, A., Spinosi, O., & Carlini, R. (2004). Cranial morphology of *Martes foina* and *M. martes* (Mammalia, Carnivora, Mustelidae): The role of size and shape in sexual dimorphism and interspecific differentiation. *Italian Journal of Zoology*, *71*(1), 27–34. doi: 10.1080/11250000409356547

Luís, A. R., May-Collado, L. J., Rako-Gospić, N., Gridley, T., Papale, E., Azevedo, A., Silva, M. A., Buscaino, G., Herzing, D., & dos Santos, M. E. (2021). Vocal universals and geographic variations in the acoustic repertoire of the common bottlenose dolphin. *Scientific Reports*, *11*(1), 1–9. doi: 10.1038/s41598-021-90710-9

Marcy, A. E., Guillerme, T., Sherratt, E., Rowe, K. C., Phillips, M. J., & Weisbecker, V. (2020). Australian rodents reveal conserved cranial evolutionary allometry across 10 million years of murid evolution. *The American Naturalist.*, *196*(6), 755–768. doi: 10.1086/711398

Marroig, G., & Cheverud, J. M. (2005). Size as a line of least evolutionary resistance: diet and adaptive morphological radiation in new world monkeys. *Evolution*, *59*(5), 1128–1142. doi: 10.1111/J.0014-3820.2005.TB01049.X

Mazzoil, M., Gibson, Q., Durden, W. N., Borkowski, R., Biedenbach, G., Mckenna, Z., Gordon, N., Brightwell, K., Denny, M., Howells, E., Jakush, J., Moreland, L., Perna, A., Pinto, G., & Caldwell, M. (2020). Spatiotemporal movements of common bottlenose dolphins (*Tursiops truncatus truncatus*) in Northeast Florida, USA. *Aquatic Mammals*, *46*(3), 285–300. doi: 10.1578/AM.46.3.2020.285

McCurry, M. R., Fitzgerald, E. M. G., Evans, A. R., Adams, J. W., & McHenry, C. R. (2017). Skull shape reflects prey size niche in toothed whales. *Biological Journal of the Linnean Society*, *121*(4), 936–946. doi: 10.1093/biolinnean/blx032

Mead, J. G., & Potter, C. W. (1990). Natural history of bottlenose dolphins along the central Atlantic coast of the United States. Pages 165–195 in S. Leatherwood and R. R. Reeves, eds.*The Bottlenose Dolphin*. Academic Press, San Diego, CA. doi: 10.1016/B978-0-12-440280-5.50013-5

Mead, J., & Potter, C. (1995). Recognizing two populations of the bottlenose dolphin (*Tursiops truncatus*) of the Atlantic coast of North America-morphologic and ecologic considerations.*IBI Reports*, *5*, 51–44.

Meloro, C., Cáceres, N., Carotenuto, F., Passaro, F., Sponchiado, J., Melo, G. L., & Raia, P. (2014). Ecogeographical variation in skull morphometry of howler monkeys (Primates: Atelidae). *Zoologischer Anzeiger - A Journal of Comparative Zoology*, *253*(4), 345–359. doi: 10.1016/J.JCZ.2013.11.002

Meloro, C., Cáceres, N., Carotenuto, F., Sponchiado, J., Melo, G. L., Passaro, F., & Raia, P. (2014). In and out the amazonia: evolutionary ecomorphology in howler and capuchin monkeys. *Evolutionary Biology*, *41*(1), 38–51. doi: 10.1007/S11692-013-9244-5

Mitchell, D. R., Sherratt, E., & Weisbecker, V. (2024). Facing the facts: adaptive trade-offs along body size ranges determine mammalian craniofacial scaling. *Biological Reviews*, *99*(2), 496–524. doi: 10.1111/BRV.13032

Mitteroecker, P., & Gunz, P. (2009). Advances in geometric morphometrics. *Evolutionary Biology*, *36*(2), 235–247. doi: 10.1007/S11692-009-9055-X

Mitteroecker, P., Gunz, P., Bernhard, M., Schaefer, K., & Bookstein, F. L. (2004). Comparison of cranial ontogenetic trajectories among great apes and humans. *Journal of Human Evolution*, *46*(6), 679–698. doi: 10.1016/j.jhevol.2004.03.006

Mitteroecker, P., & Schaefer, K. (2022). Thirty years of geometric morphometrics: achievements, challenges, and the ongoing quest for biological meaningfulness. *American Journal of Biological Anthropology*, *178*(S74), 181–210. doi: 10.1002/ajpa.24531

Mosimann, J. E. (1970). Size allometry: Size and shape variables with characterizations of the lognormal and generalized gamma distributions. *Journal of the American Statistical Association*, *65*(330), 930–945. doi: 10.1080/01621459.1970.10481136

Moura, A. E., Nielsen, S. C. A. A., Vilstrup, J. T., Moreno-Mayar, J. V., Gilbert, M. T. P., Gray, H. W. I., Natoli, A., Möller, L., & Hoelzel, A. R. (2013). Recent diversification of a marine genus (*Tursiops* spp.) tracks habitat preference and environmental change. *Systematic Biology*, *62*(6), 865–877. doi: 10.1093/sysbio/syt051

Moura, A. E., Shreves, K., Pilot, M., Andrews, K. R., Moore, D. M., Kishida, T., Möller, L., Natoli, A., Gaspari, S., McGowen, M., Chen, I., Gray, H., Gore, M., Culloch, R. M., Kiani, M. S., Willson, M. S., Bulushi, A., Collins, T., Baldwin, R., … Hoelzel, A. R. (2020). Phylogenomics of the genus Tursiops and closely related Delphininae reveals extensive reticulation among lineages and provides inference about eco-evolutionary drivers. *Molecular Phylogenetics and Evolution*, *146*, 106756. doi: 10.1016/j.ympev.2020.106756

Otero, I. R., & Delbracio, M. (2014). Anatomy of the SIFT method, image processing. *Image Processing On Line*, *4*, 370–396. doi: 10.5201/ipol.2014.82

Oxford-Smith, N., Ruta, M., Gao, A., Viaud-Martinez, K. A., Sabin, R., Herman, J., Ososky, J., Tajima, Y., Yamada, T. K., Kaliontzopoulou, A., & Moura, A. E. (2024a). Skull morphology of bottlenose dolphins worldwide and patterns of adaptation between coastal and offshore environments. *Journal of Zoology*, *322*(1), 42–57. doi: 10.1111/JZO.13122

Pigliucci, M., Murren, C. J., & Schlichting, C. D. (2006). Phenotypic plasticity and evolution by genetic assimilation. *Journal of Experimental Biology*, *209*(12), 2362–2367. doi: 10.1242/JEB.02070

Porto, A., Rolfe, S., & Maga, A. M. (2021). ALPACA: A fast and accurate computer vision approach for automated landmarking of three-dimensional biological structures. *Methods in Ecology and Evolution*, *12*(11), 2129–2144. doi: 10.1111/2041-210X.13689

Ramos, E. A., Santoya, L., Verde, J., Walker, Z., Castelblanco-Martínez, N., Kiszka, J. J., Rieucau, G., & Angel Ramos, E. (2022). Lords of the rings: mud ring feeding by bottlenose dolphins in a Caribbean estuary revealed from sea, air, and space. doi: 10.1111/mms.12854

Richards, V. P., Greig, T. W., Fair, P. A., Mcculloch, S. D., Politz, C., Natoli, A., Driscoll, C. A., Hoelzel, A. R., David, V., Bossart, G. D., & Lopez, J. V. (2013). Patterns of population structure for inshore bottlenose dolphins along the eastern United States. *Journal of Heredity*, *104*(6), 765–778. doi: 10.1093/jhered/EST070

Rohlf, F. J., & Slice, D. (1990). Extensions of the Procrustes method for the optimal superimposition of landmarks. *Systematic Biology*, *39*(1), 40–59. doi: 10.2307/2992207

Rohlf, F., & Marcus, L. (1993). A revolution morphometrics. *Trends in Ecology and Evolution*, *8*(4), 129–132. doi: 10.1016/0169-5347(93)90024-J

Rolfe, S., Pieper, S., Porto, A., Diamond, K., Winchester, J., Shan, S., Kirveslahti, H., Boyer, D., Summers, A., & Maga, A. M. (2021). SlicerMorph: An open and extensible platform to retrieve, visualize and analyse 3D morphology. *Methods in Ecology and Evolution*, *12*(10), 1816–1825. doi: 10.1111/2041-210X.13669

Rosel, P. E., Hansen, L., & Hohn, A. A. (2009). Restricted dispersal in a continuously distributed marine species: common bottlenose dolphins *Tursiops truncatus* in coastal waters of the western North Atlantic. *Molecular Ecology*, *18*(24), 5030–5045. doi: 10.1111/J.1365-294X.2009.04413.X

Rossman, S., Ostrom, P. H., Stolen, M., Barros, N. B., Gandhi, H., Stricker, C. A., & Wells, R. S. (2015a). Individual specialization in the foraging habits of female bottlenose dolphins living in a trophically diverse and habitat-rich estuary. *Oecologia*, *178*(2), 415–425. doi: 10.1007/S00442-015-3241-6

Rossman, S., Berens Mccabe, E., Barros, N. B., Gandhi, H., Ostrom, P. H., Stricker, C. A., & Wells, R. S. (2015b). Foraging habits in a generalist predator: Sex and age influence habitat selection and resource use among bottlenose dolphins (*Tursiops truncatus*). *Marine Mammal Science*, *31*(1), 155–168. doi: 10.1111/mms.12143

Secchi, E. R., Botta, S., Wiegand, M. M., Lopez, L. A., Fruet, P. F., Genoves, R. C., & Di Tullio, J. C. (2017). Long-term and gender-related variation in the feeding ecology of common bottlenose dolphins inhabiting a subtropical estuary and the adjacent marine coast in the western South Atlantic. *Marine Biology Research*, *13*(1), 121–134. doi: 10.1080/17451000.2016.1213398

Simons, E. A., & Frost, S. R. (2021). Ontogenetic allometry and scaling in catarrhine crania. *Journal of Anatomy*, *238*(3), 693–710. doi: 10.1111/joa.13331

Slater, G. J., & Van Valkenburgh, B. (2009). Allometry and performance: the evolution of skull form and function in felids. *Journal of Evolutionary Biology*, *22*(11), 2278–2287. doi: 10.1111/J.1420-9101.2009.01845.X

Smolker, R., Richards, A., Connor, R., Mann, J., & Berggren, P. (1997). Sponge carrying by dolphins (Delphinidae, *Tursiops* sp.): a foraging specialization involving tool use? *Ethology*, *103*(6), 454–465. doi: 10.1111/J.1439-0310.1997.TB00160.X

Sommer, S., & Wehner, R. (2012). Leg allometry in ants: extreme long-leggedness in thermophilic species. *Arthropod Structure & Development*, *41*(1), 71–77. doi: 10.1016/J.ASD.2011.08.002

Stanchak, K. E., Faure, P. A., & Santana, S. E. (2023). Ontogeny of cranial musculoskeletal anatomy and its relationship to allometric increase in bite force in an insectivorous bat (*Eptesicus fuscus*). *The Anatomical Record*, *306*(11), 2842–2852. doi: 10.1002/AR.25213

Sydney, N. V., Machado, F. A., & Hingst-Zaher, E. (2012). Timing of ontogenetic changes of two cranial regions in *Sotalia guianensis* (Delphinidae). *Mammalian Biology*, *77*(6), 397–403. doi: 10.1016/j.mambio.2012.04.007

Tarnawski, B. A., Cassini, G. H., & Flores, D. A. (2013). Skull allometry and sexual dimorphism in the ontogeny of the southern elephant seal (*Mirounga leonina*). *Canadian Journal of Zoology*, *92*(1), 19–31. doi: 10.1139/CJZ-2013-0106

Tarnawski, B. A., Cassini, G. H., & Flores, D. A. (2014). Allometry of the postnatal cranial ontogeny and sexual dimorphism in *Otaria byronia* (Otariidae). *Acta Theriologica*, *59*(1), 81–97. doi: 10.1007/S13364-012-0124-7

Toledo, G. A. C. (2013). Variação geográfica em crânios de golfinhos nariz-de-garrafa, Tursiops Gervais, 1855, no Atlântico Ocidental. [Ph.D. thesis]. Universidade Federal da Paraíba.

Torres, L. G., & Read, A. J. (2009). Where to catch a fish? the influence of foraging tactics on the ecology of bottlenose dolphins (*Tursiops truncatus*) in Florida Bay, Florida. *Marine Mammal Science*, *25*(4), 797–815. doi: 10.1111/j.1748-7692.2009.00297.x

Torres, L. G., Rosel, P. E., & Read, A. J. (2003). Improving management of overlapping bottlenose dolphin ecotypes through spatial analysis and genetics. *Marine Mammal Science*, *19*(3), 502–514. doi: 10.1111/j.1748-7692.2003.tb01317.x

Toth, J. L., Hohn, A. A., Able, K. W., & Gorgone, A. M. (2012). Defining bottlenose dolphin (*Tursiops truncatus*) stocks based on environmental, physical, and behavioral characteristics. *Marine Mammal Science*, *28*(3), 461–478. doi: 10.1111/J.1748-7692.2011.00497.X

Turner, J. P., & Worthy, G. A. J. (2003). Skull morphometry of bottlenose dolphins (*Tursiops truncatus*) from the Gulf of Mexico. *Journal of Mammalogy*, *84*(2), 665–672. doi: 10.1644/1545-1542

Viacava, P., Baker, A. M., Blomberg, S. P., Phillips, M. J., & Weisbecker, V. (2022). Using 3D geometric morphometrics to aid taxonomic and ecological understanding of a recent speciation event within a small Australian marsupial (*Antechinus*: Dasyuridae). *Zoological Journal of the Linnean Society*, *196*(3), 963–978. doi: 10.1093/zoolinnean/zlab048

Viacava, P., Blomberg, S. P., Sansalone, G., Phillips, M. J., Guillerme, T., Cameron, S. F., Wilson, R. S., & Weisbecker, V. (2020). Skull shape of a widely distributed, endangered marsupial reveals little evidence of local adaptation between fragmented populations. *Ecology and Evolution*, *10*(18), 9707–9720. doi: 10.1002/ece3.6593

Viacava, P., Blomberg, S. P., & Weisbecker, V. (2023). The relative performance of geometric morphometrics and linear-based methods in the taxonomic resolution of a mammalian species complex. *Ecology and Evolution*, *13*(3), e9698. doi: 10.1002/ECE3.9698

Vollmer, N. L., & Rosel, P. E. (2017). Fine-scale population structure of common bottlenose dolphins (*Tursiops truncatus*) in offshore and coastal waters of the US Gulf of Mexico. *Marine Biology*, *164*(8), 1–15. doi: 10.1007/S00227-017-3186-X

Wells, R. S., Schwacke, L. H., Rowles, T. K., Balmer, B. C., Zolman, E., Speakman, T., Townsend, F. I., Tumlin, M. C., Barleycorn, A., & Wilkinson, K. A. (2017). Ranging patterns of common bottlenose dolphins *Tursiops truncatus* in Barataria Bay, Louisiana, following the Deepwater Horizon oil spill. *Endangered Species Research*, *33*(1), 159–180. doi: 10.3354/ESR00732

Wells, R. S., & Scott, M. D. (2009). Common bottlenose dolphin: *Tursiops truncatus*, In *Encyclopedia of Marine Mammals*, eds B. Würsig, J. G. M. Thewissen, and K. M. Kovacs (Amsterdam: Elsevier), 249–255. doi: 10.1016/B978-0-12-373553-9.00062-6

West-Eberhard, M. J. (2005). Phenotypic accommodation: adaptive innovation due to developmental plasticity. *Journal of Experimental Zoology Part B: Molecular and Developmental Evolution*, *304B*(6), 610–618. doi: 10.1002/jez.b.21071

Zelditch, M., Swiderski, D. L., & Sheets, H. (2012). Geometric morphometrics for biologists : a primer. In *academic press.* (Academic Press.).

Zolman, E. S. (2002). Residence patterns of bottlenose dolphins (*Tursiops truncatus*) in the Stono River Estuary, Charleston County, South Carolina, U.S.A. *Marine Mammal Science*, *18*(4), 879–892. doi: 10.1111/J.1748-7692.2002.TB01079.X

Chapter 6 – Main Discussion

6.1. Processes Driving Differentiation Within *Tursiops*

In this study, each coastal unit displayed distinct skull shapes, with these variations being correlated with a range of environmental factors that are likely proxies for biological processes including prey abundance. Most observed shape changes could also be associated with functions such as feeding and vocalising, suggesting that morphological differences may reflect ecological functions. This is consistent with the genus well-known flexibility in foraging strategies (Pryor & Lindbergh, 1990; Krützen et al., 2005; Ramos et al., 2022) as well as diversity in whistle patterns (La Manna et al., 2020; Luís et al., 2021) worldwide. Furthermore, Offshore individuals exhibited more homogeneous skull shapes across their range and remained morphological distinct from those of all coastal units. This shape homogeneity within the Offshore operational unit may be maintained by stabilizing selection, as suggested by recent studies (Oxford-Smith et al., 2024). Offshore skulls are characterized by features such as widened nares and correlate with environmental variables suggestive of deep-water habitats, such as mixed layer depth (MLD) and bathymetry. This correlation suggests that the deep-water environment could exert selective pressures favouring a more uniform skull shape, thus reinforcing the differentiation between coastal and Offshore units.

However, the observed patterns cannot be fully explained by selection alone. Although common features are expected to be shared by populations inhabiting relatively similar habitats, each coastal operational taxonomic unit (OTU) exhibits distinct skull shapes, despite originating from coastal environments (characterized by shallow, productive environments). This suggests that non-adaptive processes must also play a role in shaping these variations. Overall, the findings presented here suggest that skull shape differentiation in bottlenose dolphins results from a multifactorial evolutionary process. While stabilizing selection and reduced genetic drift may constrain variation in more uniform offshore habitats, strong genetic drift is likely to drive diversification in coastal environments (as detailed below). Additionally, phenotypic plasticity may also contribute to subtle shape differences between neighbouring units, which could acquire selective value over time.

Genetic drift, a non-selective process, can result in the fixation of alleles over time, especially in small and isolated populations (Kimura & Ohta, 1971). While further research is needed to fully assess the worldwide patterns of population structure in coastal and offshore bottlenose dolphins, studies on individual coastal populations have revealed fine-scale

population structure with limited gene flow with outside areas (Parsons et al., 2006; Rosel et al., 2009; Mirimin et al., 2011; Fruet et al., 2014; Bayas-Rea et al., 2018; Nykänen et al., 2019), which likely increases the level of genetic drift. This effect can also result from founder effects, where a small group of individuals establishes a new population, often after colonising a new region. Founder effects create genetic bottlenecks by limiting the new population's genetic variation to the alleles carried by the founders, thus reducing overall genetic diversity (Nei et al., 1975). Indeed, repeated reductions in genetic diversity observed in coastal OTUs compared to their offshore counterparts have been attributed to such founder events (e.g. Hoelzel et al., 1998). For example, Mediterranean populations are thought to have originated from the Atlantic, with stochastic genetic variation resulting from a series of founder events during their recent invasion of the Mediterranean Sea (Gaspari et al., 2015). Notably, the lack of lineage sorting in the region suggests that as dolphins spread eastward, each new population was founded by a subset of the previous one, driving a directional (eastward) genetic pattern (Natoli et al., 2005). Similarly, North Sea populations likely colonized the region from the Atlantic via the English Channel after the submergence of Doggerland. This hypothesis is further supported by subfossil evidence of cetacean colonization in this area (Aaris-Sørensen et al., 2010).

Furthermore, substantial allometric differences were found between several coastal populations along the West North Atlantic (WNA), associated with shape changes in some regions. This suggests that morphological traits may initially vary through different size scaling relationships. Subsequently, these allometric differences may create shape variation which will ultimately turn into shape differentiation between habitats. In mammals, size is often a strong predictor of skull shape, even at the macroevolutionary scale. For example, in echolocating bats, species with greater muscle mass tend to have proportionally larger skulls (Giacomini et al., 2022)**.** Similarly, in felids, larger species tend to have longer jaws and ventrally displaced jaw joints, adaptations thought to allow for wider jaw gape distances which facilitates the capture and killing of large prey (Slater & Van Valkenburgh, 2009a). In toothed whales, skull size also correlates with brain mass and biosonar traits**,** both of which are influenced by body size (Vicari et al., 2023). This pattern of size-dependent echolocation frequency, with larger whales (like some bats; Giacomini et al., 2022) producing lower echolocation frequencies and smaller whales producing higher frequencies, highlights the functional role of size in driving skull shape variations via modifications to the biosonar system (Vicari et al., 2023).

In bottlenose dolphins, specific allometric relationships have also been observed. The temporal fossa, a depression on the side of the skull that serves as the attachment site for the temporalis muscle, follows a positive allometric scaling pattern during growth (Kurihara &

Oda, 2009). This scaling may allow the temporal fossa to expand proportionally with skull growth during maturation, accommodating larger temporalis and jaw muscles. A similar pattern of coordinated growth between skull size and temporal muscle development is observed in killer whales, where condylobasal length growth correlates with temporal muscle development (Takahashi et al., 2021). This suggests a broader trend in cetaceans for the skull to accommodate increasing muscle mass associated with size.

Phenotypic plasticity plays an important role in driving morphological variation, especially by influencing shape changes related to size. In such cases, environmental factors, rather than genetic divergence, are the likely primary drivers of shape variation. For example, in woolly opossums (*Caluromys* species), the degree to which skull shape is influenced by allometry differs between species, likely due to different seasonal environmental pressures. These pressures may require distinct feeding traits, such as larger temporal muscles and wider molars (Magnus et al., 2017). When groups exhibit distinct morphologies without corresponding genetic differences, environmental factors, rather than genetic divergence, are typically responsible for the observed variations (Holeski, 2007; Crispo, 2008; Schmid & Guillaume, 2017; Mazzochi et al., 2024).

In the present study, the size-shape differences observed between sexes in bottlenose dolphins are consistent with the hypothesis of phenotypic plasticity driving skull differentiation. Sexual dimorphism in bottlenose dolphins has been suggested to result from ecological and social factors. For example, differences in food resource partitioning in the North Sea (De Francesco et al., 2016) or feeding habits in Sarasota Bay (Gulf of Mexico; Rossman et al., 2015) between males and females, likely result in phenotypic plasticity at fine geographical scales. Over time, this process may facilitate "genetic assimilation", where traits initially shaped by plastic responses become genetically fixed (Pigliucci et al., 2006).

Phenotypic diversification has also likely happened through historical events. The radiation of modern delphinids began in the early Pliocene, as supported by molecular (McGowen et al., 2009; Steeman et al., 2009) and fossil data (Bianucci, 1996, 2013; Fordyce et al., 2002; Boessenecker, 2012). This diversification coincides with Pleistocene glacial-interglacial cycles, periods of substantial oceanic restructuring and changes in coastal topography (Steeman et al., 2009; Do Amaral et al., 2018). These cycles are considered important drivers of distribution and divergence in non-cetacean marine species (e.g. Wilson & Veraguth, 2010; Liu et al., 2011; Pardo-Gandarillas et al., 2018). Glacial cycles are known to have altered ocean conditions such as temperatures, currents, and upwelling patterns, which in turn influence prey availability and distribution. These environmental changes have impacted marine ecosystem diversity (Ludt &

Rocha, 2015). For example, the genetic distinction between western and eastern North Pacific herring populations are thought to have resulted from the isolation of Asia and North America during glacial cycles (Liu et al., 2011). Similarly, geographic isolation, such as that of island bat populations from the mainland, is believed to have led to skull morphology differences likely resulting from genetic drift and founder effects (Ikeda et al., 2020).

These glacial cycles also significantly impacted coastal habitats. During glacial periods, sea levels dropped, exposing previously submerged regions and creating new coastal areas. Conversely, interglacial periods saw rising sea levels, submerging previously exposed areas (Lambeck & Chappell, 2001). This process created new coastal habitats for marine species to colonise. This cycle of isolation and recolonisation is thought to have played a role in the evolution of cetaceans as well. For example, the freshwater species *Sotalia fluviatilis*, which inhabits the Amazon and Orinoco rivers is thought to have emerged as a result of isolation from the larger marine environments, after the flooding of the continental basins (Do Amaral et al., 2018). The influence of these glacial-interglacial cycles is also evident in the distribution of bottlenose dolphins. In the North East Atlantic (NEA), especially around the British Isles, bottlenose dolphins are hypothesised to have gradually expanded into the northernmost part of their range following the Last Glacial Maximum (LGM) through a leading-edge expansion (Nykänen et al., 2019). A similar pattern is seen in Australia, where post-LGM flooding is thought to have facilitated southward shifts of coastal populations as newly submerged regions created new ecological niches (Wittwer et al., 2023). Therefore, the skull shape changes observed in bottlenose dolphins in this study may have also resulted from the combined effects of genetic drift, influenced by founder events, as the species colonized and recolonized new coastal niches during and after the Last Glacial Maximum.

6.2. Bottlenose Dolphin Coastal Differentiation Mechanisms

The varying traits observed in this study are consistent with the early stages of cetacean skull shape diversification, such as nasal cavity reduction, rostrum elongation, and increased braincase size, all typical of early skull telescoping (Miller, 1923; Roston & Roth, 2019). These changes reflect functional demands associated with the transition from terrestrial habitats to a fully aquatic lifestyle. Modern cetacean skull morphology further exemplifies the link between shape and function, particularly concerning diverse feeding strategies. In the Delphinidae family, distinct skull traits are associated with suction and raptorial feeders, that appear beneficial for their respective feeding strategies. Suction feeders are typically characterized by

wider mandibular symphyses and broader nasal apertures, traits that are hypothesized to facilitate negative pressure generation during feeding (Galatius et al., 2020). In contrast, raptorial feeders tend to possess elongated rostra, which may be beneficial in capturing fast-moving prey (Galatius et al., 2020).

This study's findings reveal considerable variation in these key traits across bottlenose dolphin operational units, suggesting a potential link to specific ecological functions. For example, enlarged nasal cavities are observed in Offshore individuals and some coastal units, which could facilitate efficient air intake and minimise hydrodynamic disruption for surface breathing. Given that the naso-laryngeal system supports both respiration and echolocation (Green et al., 1980), these changes in nasal cavity morphology may also reflect differing echolocation demands across units.

Important role of feeding, communicating and potentially breathing.

Feeding related traits, including jaw shape, tooth morphology, or skull structure, are often under strong selective pressure due to their role in food acquisition (Pierce et al., 2009; Hendges et al., 2016; Maestri et al., 2016; Arbour et al., 2019). In mammals, these traits are often associated with variations in bone structures supporting the temporalis and masseter muscles, which in turn influence mechanical advantage and bite force (Christiansen & Adolfssen, 2005; Christiansen & Wroe, 2007; Hendges et al., 2016; Arbour et al., 2019). For example, shorter rostrums enhance bite force in canids (Slater et al., 2009), while a longer rostrum increases the maximum gape distance for capturing larger prey in felids (Slater et al., 2009). The findings shown here reveal considerable variation in these key feeding-related traits, particularly in the rostrum and region directly connected to jaw muscle attachment, including the squamosal, frontal, and parietal bones. These variations suggest a direct association with feeding strategies. This influence of diet on jaw morphology, particularly at the temporo-mandibular joint (the articulation between the posterior jaw and squamosal bone) is well documented across diverse mammalian clades, highlighting the convergent evolution of this trait (Grossnickle, 2020).

Communication related traits are also shown to vary, including differences in the concavity of the premaxillae and the presence of a rostral bump in some units, possibly indicating differences in melon size and shape. Given the role of the melon in focusing sound waves for signal transmission (Mckenna et al., 2012), these differences may reflect an ecological function for different vocalisation abilities related to aspects like social or environmental interactions. Features such as the size and shape of the nasal passages are often suggested to be linked to respiration (Mead & Potter, 1995; Perrin et al., 2011). However, they may also vary based on

communication needs. In cetaceans, communication plays an essential role in group coordination, mating, and hunting (Janik, 2000; Dudzinski & Hill, 2022). Smaller or isolated populations may rely more heavily on vocal clues for social cohesion and coordinated foraging, which could result in traits optimized for vocalisation. Indeed, variations in communication have been observed in distinct bottlenose dolphin populations (May-Collado & Wartzok, 2008; Papale et al., 2014; La Manna et al., 2017, 2020; Romeu et al., 2017), likely reflecting ecological pressures or functions related to social or foraging behaviours.

Finally, the structural integration of the skull must be considered. Mammalian skull components are highly interconnected, as evidenced by correlation and covariance patterns conserved across diverse taxa (Porto et al., 2009). Stabilizing selection is thought to preserve this structural cohesion, maintaining the skull's functionality and development during evolutionary changes (Porto et al., 2009). Therefore, traits related to feeding, communication, and breathing are likely interdependent, potentially creating structural trade-offs that influence skull shape evolution. For example, a skull optimised for efficient communication might differ structurally from one optimised for feeding or respiration. These trade-offs suggest that skull morphology reflects a balance of ecological functions, driven by the organism's broader survival strategies in different environments and may also result from structural integration rather than direct adaptation to a single factor.

Environmental demands and skull morphology

These traits are shaped by the ecological demands of different environments in many species. In mammals, habitat-specific conditions are often correlated with skull morphology, because they are often associated with key biological factors such as food availability and other vital demands. In this study, environmental variables were used as proxies for these ecological conditions. While these variables may not directly cause shape variations, they can reflect the ecological pressures that act on such traits. For example, in peccaries, skull shape is strongly associated with temperature and precipitation, which likely reflect food resources and feeding strategies (Hendges et al., 2016). In food-scarce environments with seasonal fluctuations, peccaries tend to exhibit traits suited to a varied diet to allow them to feed depending on availability. In contrast, in resource-rich areas, they show traits corresponding with a more specialized diet, reflecting consistent food sources year-round. Similarly, in carnivores from the Amazon rainforest, skull shape and size are related to variations in climatic conditions and feeding strategies (Bubadué et al., 2016). Hypercarnivores such as *Speothos venaticus,* display larger zygomatic arches and carnassials, along with thick, short muzzles for hunting large prey.

In contrast, termitophagous species such as *Leontopithecus vetulus* possess larger auditory bullae and thicker muzzles, as their feeding strategy requires less bite force (Bubadué et al., 2016). This principle is also evident in rodents, where distinct skull traits are closely associated with their lifestyles, (arboreal, terrestrial, or gliding), which are themselves related to feeding strategies (Lu et al., 2014). For example, flying squirrels have aspheric skulls and laterally expanded zygomatic arches that support larger orbits, enhancing visual field and depth perception to facilitate gliding (Jackson, 2000). This helps them locate food sources from a distance during gliding. In contrast, terrestrial squirrels have robust, triangular skulls, which is beneficial for foraging underground, along with large auditory bullae for effective underground communication and predator detection, which is essential for survival when searching for food in environments where visibility may be limited. Additionally, enhanced nasal bones in terrestrial species support olfactory abilities, essential for detecting food and moving in subterranean environments (Lu et al., 2014). The two subspecies of pilot whales, *Globicephala melas melas* (North Atlantic) and *Globicephala melas edwardii* (Southern Hemisphere), also exhibit distinct skull morphology, likely reflecting adaptations to different ecological pressures. *G. m. edwardii* features a longer skull, broader and larger rostrum, wider nares, and larger temporal fossa compared to *G. m. melas,* consistent with the hypothesis that skull morphology reflects functional demands like feeding, diving, and acoustic communication (Marina et al., 2018).

6.3. Habitat Characteristics and Differentiation

Environmental changes, especially those associated with founder events, can also influence feeding adaptations, by altering food type availability and therefore contributing to niche differentiation. This exerts pressure on feeding-related traits favouring those better suited to local prey types and foraging behaviours. In cetaceans, dietary shifts, such as squid specialization or predation on large marine mammals, have driven the evolution of larger body sizes (Slater et al., 2010), while skull shape in raptorial dolphins correlates with prey size (McCurry et al., 2017).

The strong differentiation of feeding-related traits suggests niche partitioning. Limited space and resources in coastal environments can intensify intraspecific competition. Coastal bottlenose dolphins often occupy restricted habitats including gulfs or estuaries, which limit opportunities for population expansion. Consequently, ecological strategies such as niche partitioning can help maintain population stability. For example, isotopic studies of bottlenose

dolphins in an insular region suggested different diets depending on group composition, which could reflect some form of niche partitioning (Dias et al., 2023).

Niche partitioning (Pianka, 1974) is common in cetaceans and may facilitate the exploitation of productive habitats (Giménez et al., 2018; García-Vernet et al., 2021; Tatsch et al., 2024). For example, in the northwestern Mediterranean, most cetacean species are thought to avoid competitive exclusion through trophic or spatial segregation (Borrell et al., 2021). Similarly, in the WNA, spatial analysis shows a clear separation in habitat use between the coastal Erebennus and Offshore OTUs, with individuals from the coastal operational unit found only within 7.5 km from the shoreline, while beyond 34 km from the shoreline only Offshore individuals are found (Torres et al., 2003). This suggests that the coastal unit relies on nearshore resources and shallow waters, whereas the Offshore unit exploits pelagic prey and navigates more dynamic and open ocean environments.

Allometry, Niche Partitioning, and Shape Diversification

Within the Erebennus operational unit, bottlenose dolphins from different locations exhibit variations in both skull shape and allometric pattern, suggesting a considerable role for allometry in driving skull shape differences over time. This hypothesis is further supported by the observed allometric sex differences within these locations and cases of niche partitioning between sexes in some locations within the Gulf of Mexico (Rossman et al., 2015). This suggests that niche partitioning may drive phenotypic plasticity, which, over time, can contribute to shape diversification, even among groups living in close proximity.

The link between niche partitioning and skull shape variation has been supported across diverse taxa (Figueirido et al., 2014; Hedrick, 2021; Nicholson & Clements, 2021). For example, although bamboo is the primary food item consumed by both giant pandas (*Ailuropoda melanoleuca*) and red pandas (*Ailurus fulgens*), a diet unusual among Carnivores, their feeding strategies are different. Red pandas strongly favour younger bamboo leaves and fruits, while giant pandas consume a wider range of plant traits such as peeled trunks and stems (Wei et al., 1999). While they share some skull shape similarities (Gittleman, 1994), these dietary differences may reflect subtle differences in skull morphology related to processing different bamboo parts. Biomechanical analysis suggests that, while both species exhibit comparable mechanical efficiency, it is concentrated in different parts of the cranium. In giant pandas, the length of the masseter input lever arms could enable high peak bite forces over short periods. In contrast, the red panda's mandible shape can support sub-maximal bite forces over longer periods. These differences in cranial biomechanics have been suggested to facilitate

resource partitioning within regions of shared habitat, thereby reducing competition between the two species (Figueirido et al., 2014).

Similarly, studies on the *Artibeus* bat species complex (Neotropical fruit bats), suggest that dietary differences may influence skull shape variation at both interspecific and intraspecific levels (Hedrick, 2021). Differences in size and skull shape between species were hypothesised to possess differing mechanical forces, enabling them to consume different types of fruits (e.g. hard versus soft), thereby facilitating resource partitioning. This adaptation would be particularly beneficial for food resources that are only available seasonally and may therefore be subject to intense competition when present. Sexual dimorphism in skull shape within some bat species (Hedrick, 2021) associated with distinct feeding behaviours between sexes (Morrison & Morrison, 1981), further supports this hypothesis.

Similar examples can be found in marine species. For example, parrotfishes exhibit cranial variations, suggested to reflect adaptations to the mechanical demands of feeding on substrates of varying hardness and density (Nicholson & Clements, 2021). Species with high adductor mandibular muscle mass (AMMM) values may be able to produce stronger bite force to process hard, calcareous substrata. Those with smaller AMMM residuals and higher maxillary kinematic transmission have weaker bite forces, therefore favouring softer, less dense or highly erodible substrates. These feeding specializations would allow parrotfish species to exploit different reef substrata at fine spatial scales, thereby reducing resource competition (Nicholson & Clements, 2021).

The Complexity of Adaptive Evolution and Stochastic Processes

While these skull traits may confer ecological advantages, they do not necessarily arise from direct selection pressures exclusively. Broader ecological function needs within a given environment can also influence trait development, making it difficult to disentangle adaptive evolution from other processes. For example, in founder events scenarios, colonising populations may carry traits that provide mechanical advantages related to feeding or communication in the new habitat. These traits may become rapidly fixed within isolated populations, promoting divergence in skull morphology relative to other populations or regions. Recent genomic studies of coastal bottlenose dolphin OTUs have shown that loci under selection associated with coastal habitats were already present in the genus ancestral genome before spreading into different coastal habitats (Louis et al., 2023). Additionally, neutral processes such as increased genetic drift in smaller populations also play a role in shaping morphological variation in coastal areas. Moreover, traits may also arise from linkage

disequilibrium, where a trait is linked to another trait under selection. Traits may also arise through pleiotropy, where the selection of an unrelated trait leads to the evolution of a linked trait. Finally, the adaptive value of a trait can vary across different environments. Traits that are advantageous in one environment may be neutral or even maladaptive in another (Frankenhuis & Del Giudice, 2012). In expanding populations that have occupied diverse coastal environments, traits may therefore reflect first historical events or processes rather than direct adaptation to current ecological conditions. Therefore, it is difficult to ascertain whether the changes observed in this study are a direct result of local adaptations to local ecological conditions through natural selection or simply reflect stochastic genetic processes such as genetic drift.

6.4. Potential Behavioural Reinforcement of Differentiation

Geographic variation in dolphin vocalisations is well documented, with distinct whistle types observed across populations (Luís et al., 2021), and vocalisations that vary in response to local conditions (La Manna et al., 2020). Local environmental factors, such as water depth, visibility, and the presence of coral reefs, create unique acoustic conditions that may shape dolphin vocal behaviour (Luís et al., 2021). While these environmental factors provide valuable insight into the drivers of vocal variation, the relationship between acoustic differences and physical traits such as skull morphology remains largely unexplored in dolphins. However, studies on other echolocating mammals, like bats, suggest that skull shape may be influenced by echolocation demands, especially in species relying heavily on this sensory modality for foraging (Giacomini et al., 2022). In these species, skull shape is thought to reflect a balance between dietary and echolocation needs. For example, insectivorous bats using low-frequency echolocation (better for long-range detection), are correlated with weaker bite forces, demonstrating a trade-off between feeding efficiency and sound emission (Giacomini et al., 2022). These findings suggest a potential parallel in the bottlenose dolphin, where observed skull shape variations may reflect an evolutionary balance between efficient echolocation and other functional demands. Unlike bats, dolphins also use sound for communication. Although a direct link between skull shape and communication mode has not been explored in dolphins, the fact that dolphin vocalisations can vary depending on local environments (La Manna et al., 2020), combined with studies showing a correlation between habitat type (coastal vs offshore) and premaxillary shape (Costa et al., 2016), suggests that such a mechanism may be possible.

Social Behaviour and Niche Partitioning

A combination of distinct social behaviours might be reinforcing niche partitioning mechanisms. Studies on bottlenose dolphin behaviour, show that individuals prefer to affiliate with others exhibiting similar foraging strategies (Methion & Díaz López, 2020), suggesting that social structure may reinforce ecological partitioning through behaviour. For example, in southern Brazil (*T. t. gephyreus;* Genoves et al., 2018) and Scotland's east coast, bottlenose dolphins form social units based on social preferences (Lusseau et al., 2006). These units are influenced by spatial and temporal dynamics, leading to distinct habitat use (Genoves et al., 2018). This social segregation may drive niche partitioning, a phenomenon also observed in other cetaceans. For example, Humpback whales along the north coast of British Columbia, exhibit social bonds and community structure mediated by site-specific habitat use strategies in their summer feeding ground (Wray et al., 2021). Territorial behaviours, though not extensively studied in bottlenose dolphins, may also contribute to this partitioning. In Guayaquil, "escorting behaviour" where resident dolphins coordinate to 'escort' non-residents out of the area, suggests a form of social territoriality (Felix, 2001). These social dynamics, coupled with resource specialisation, can reinforce ecological differences between populations and potentially contribute to morphological differentiation between coastal and Offshore OTUs. In other Delphinidae species, such as killer whales, behavioural innovation can spread within social groups through social learning (Whitehead & Ford, 2018). Over time, these behaviours can lead to morphological or physiological adaptations, ultimately contributing to the formation of distinct OTUs. Cultural specialisation, including learned feeding strategies, plays a significant role in shaping the killer whale ecology and adaptation to specific trophic environments.

The traits that showed strong selection in this study are likely to reflect common evolutionary pressures across other Delphinidae species, contributing to their widespread success in a variety of marine environments. Parallels can be drawn to other Delphinidae species where intraspecific skull shape variations are related to local environmental pressures. For example, Pacific killer whale (*Orcinus orca*) morphotypes specialized for either mammal-hunting or fish-eating show distinct cranial features, such as differences in cranial width or more hydrodynamic looking skulls (Fung, 2016). The more generalist 'offshore' killer whale ecotype, also exhibits longer tooth rows than 'resident' populations, indicating niche specialisation at a fine geographical. The dual role of selection and drift in shaping ecotypes is further highlighted by genomic evidence from killer whales, including genes involved in body development (Moura et al., 2014). Similar patterns of variations have been described in harbour porpoise (*Phocoena phocoena*), where intraspecific differences in ontogeny and adult shape were detected among

the four subspecies (Galatius & Gol'din, 2011). For example, Californian porpoises are generally larger and show more pronounced postnatal development of shape and skeletal fusion, likely due to their distinct habitat, characterised by inter-annual fluctuations in food availability (Galatius & Gol'din, 2011). Another key difference among porpoise subspecies is the orientation of the foramen magnum and rostrum, which affects skull alignment with the body and may facilitate scanning for benthic and demersal prey in shallow waters (a pattern also suggested in other Delphinidae species; Monteiro-Filho et al., 2002). In harbour porpoises, genetic differences between the putative North Sea and North Atlantic populations have also been associated with genetic drift, as evidenced by differentiation at neutral markers (De Luna et al., 2012). Similar to patterns shown in this study, sexual dimorphism is also notable in harbour porpoise populations, particularly in regions with strong interspecific competition (Galatius & Gol'din, 2011), supporting the hypothesis of niche partitioning. In such cases, females often grow larger than males, which is associated with different allometric scaling (Galatius, 2005) and earlier growth termination in males (Galatius & Gold'in, 2011). Collectively, these comparative studies provide evidence that skull shape variation in Delphinidae arises from the interplay of ecological pressures, genetic drift, and historical factors.

6.5. Implications for the Taxonomy of the Bottlenose Dolphin

This study revealed significant skull shape differences between multiple operational taxonomic units of bottlenose dolphins and can provide useful inferences in clarifying the taxonomy of the genus *Tursiops*. For example, the distinction of *T. aduncus* and *T. erebennus* as recognized species was confirmed through PCA and classification analysis, consistent with previous studies (Rice, 1998; Wang et al., 2000; Costa et al., 2022). Although the divergence between *T. t. gephyreus* and Offshore individuals appears more recent than other lineages (e.g. *T. aduncus* and *T. erebennus*; Moura et al., 2020; Pratt et al., 2023), the skull of *T. t. gephyreus* is considered more distinct than that of *T. erebennus*. This may be attributed to stronger genetic drift or larger differences in local environmental pressures.

The study findings also suggest the potential occurrence of further distinct coastal operational units. While these units may not yet be defined as separate lineages, evidence of divergence in their genetics and ecology has been reported (Santillán et al., 2008; Van Waerebeek et al., 2008; Louis et al., 2014, 2023). The ability to detect more pronounced morphological distinctions may have been constrained by limited samples from regions such as

West Africa and Western South America. Nonetheless, these regions showed patterns that suggest the occurrence of local coastal units differentiated from offshore dolphins. In some cases, less distinct skull shapes may be indicative of more recent divergence from the Offshore or challenges in separating coastal and Offshore OTUs during museum curation, which may have led to their misclassification.

Similar to the findings in the WNA, previous studies combining genetic, ecological, and morphometric evidence have suggested the existence of several distinct bottlenose dolphin populations in the Southeast Pacific (SEP; Sanino et al., 2005; Santillán et al., 2008; Bayas-Rea et al., 2018; Félix et al., 2018). Stronger skull shape differentiation between regions within the SEP than observed within the WNA was found in this study. This greater differentiation could reflect the greater ecological heterogeneity of West South America's coastlines. For example, the presence of both warm (Humboldt Current) and cold (Peru Current) waters creates a mosaic of habitats, particularly in terms of food web composition. In contrast, populations in the WNA are more interconnected due to continuous coastlines, shorter geographic distances, and less pronounced ecological barriers.

Most individuals from West South America analysed in this study were from Peru and Chile, areas previously suggested to host distinct coastal populations based on genetic and morphological evidence (Sanino et al., 2005; Bayas-Rea et al., 2018). However, comprehensive studies across the broader SEP are still lacking. Along the Wast coast of South America, the Guayaquil unit may have originated from a founder effect during the last interglacial period (Gutscher et al., 1999; Bayas-Rea et al., 2018). On the other hand, some operational units in Peru and Chile may have been established later, as evidenced by the higher levels of genetic exchange compared to the latter (Sanino et al., 2005; Bayas-Rea et al., 2018). This suggests that divergence processes in the SEP may still be ongoing.

6.1. Bibliography

Aaris-Sørensen, K., Rasmussen, K. L., Kinze, C., & Petersen, K. S. (2010). Late Pleistocene and Holocene whale remains (Cetacea) from Denmark and adjacent countries: species, distribution, chronology, and trace element concentrations. *Marine Mammal Science*, *26*(2), 253–281. doi: 10.1111/J.1748-7692.2009.00356.X

Arbour, J. H., Curtis, A. A., & Santana, S. E. (2019). Signatures of echolocation and dietary ecology in the adaptive evolution of skull shape in bats. *Nature Communications*, *10*(1), 1–13. doi: 10.1038/s41467-019-09951-y

Bayas-Rea, R. de los Á., Félix, F., & Montufar, R. (2018). Genetic divergence and fine-scale population structure of the common bottlenose dolphin (*Tursiops truncatus*, Montagu) found in the Gulf of Guayaquil, Ecuador. *PeerJ*, *2018*(4), e4589. doi: 10.7717/peerj.4589

Bianucci, G. (1996). The Odontoceti (Mammalia Cetacea) from Italian Pliocene. The Ziphiidae. *Palaeontographia Italica*, *83*, 73–167. Downloaded from https://www.researchgate.net/publication/285865674

Bianucci, G. (2005). *Arimidelphis sorbinii* a new small killer whale-like dolphin from the Pliocene of Marecchia River (central eastern Italy) and a phylogenetic analysis of the Orcininae (Cetacea: Odontoceti). *Rivista Italiana Di Paleontologia e Stratigrafia*, *111*(2). doi: 10.13130/2039-4942/6324

Bianucci, G. (2013). *Septidelphis morii*, n. gen. et sp., from the Pliocene of Italy: new evidence of the explosive radiation of true dolphins (Odontoceti, Delphinidae). *Journal of Vertebrate Paleontology*, *33*(3), 722–740. doi: 10.1080/02724634.2013.744757

Boessenecker, R. W. (2012). A new marine vertebrate assemblage from the late Neogene Purisima formation in central California, part II: pinnipeds and cetaceans. *Geodiversitas*, *35*(4), 815–940. doi: 10.5252/G2013N4A5

Borrell, A., Gazo, M., Aguilar, A., Raga, J. A., Degollada, E., Gozalbes, P., & García-Vernet, R. (2021). Niche partitioning amongst northwestern Mediterranean cetaceans using stable isotopes. *Progress in Oceanography*, *193*, 102559. doi: 10.1016/j.pocean.2021.102559

Christiansen, P., & Adolfssen, J. S. (2005). Bite forces, canine strength and skull allometry in carnivores (Mammalia, Carnivora). *Journal of Zoology*, *266*(2), 133–151. doi: 10.1017/S0952836905006643

Christiansen, P., & Wroe, S. (2007). Bite forces and evolutionary adaptations to feeding ecology in carnivores. *Ecology, 88*(2), 347-358. doi: 10.1890/0012-9658(2007)88[347:BFAEAT]2.0.CO;2

Costa, A. A., Mcfee, W., Wilcox, L. A., Archer, F. I., & Rosel, P. E. (2022). The common bottlenose dolphin (*Tursiops truncatus*) ecotypes of the western North Atlantic revisited: an integrative taxonomic investigation supports the presence of distinct species. *Zoological Journal of the Linnean Society*, *196*, 1608–1636. doi: 10.1093/zoolinnean/zlac025

Costa, A., Rosel, P., Daura-Jorge, F., & Simões-Lopes, P. (2016). Offshore and coastal common bottlenose dolphins of the western South Atlantic face-to-face: what the skull and the spine can tell us. *Marine Mammal Science*, *32*(4), 1433–1457. doi: 10.1111/mms.12342

Crispo, E. (2008). Modifying effects of phenotypic plasticity on interactions among natural selection, adaptation and gene flow. *Journal of Evolutionary Biology*, *21*(6), 1460–1469. doi: 10.1111/J.1420-9101.2008.01592.X

De Francesco, M. C., Loy, A., Francesco, M. C. de, & Loy, A. (2016). Intra- and interspecific interactions as proximate determinants of sexual dimorphism and allometric trajectories in the bottlenose dolphin *Tursiops truncatus* (Cetacea, Odontoceti, Delphinidae). *PLoS ONE*, *11*(10), e0164287. doi: 10.1371/journal.pone.0164287

De Luna, C. J., Goodman, S. J., Thatcher, O., Jepson, P. D., Andersen, L., Tolley, K., & Hoelzel, A. R. (2012). Phenotypic and genetic divergence among harbour porpoise populations associated with habitat regions in the North Sea and adjacent seas. *Journal of Evolutionary Biology*, *25*(4), 674–681. doi: 10.1111/J.1420-9101.2012.02461.X

Dias, E., Dromby, M., Ferreira, R., Gil, Á., Tejerina, R., Castro, L. F. C., Rosso, M., Sousa-Pinto, I., Hoffman, J. C., Teodósio, M. A., Dinis, A., & Alves, F. (2023). Trophic ecology of common bottlenose dolphins in a pelagic insular environment inferred by stable isotopes. *Hydrobiologia*, *850*(19), 4227–4241. doi: 10.1007/S10750-023-05294-4

Do Amaral, K. B., Amaral, A. R., Fordyce, R., & Moreno, I. B. (2018). Historical biogeography of Delphininae dolphins and related taxa (Artiodactyla: Delphinidae). *Journal of Mammalian Evolution*, *25*(2), 241–259. doi: 10.1007/s10914-016-9376-3

Dudzinski, K. M., & Hill, H. M. (2022). Cetacean communication. *Encyclopedia of Animal Cognition and Behavior*, 1223–1234. doi: 10.1007/978-3-319-55065-7_992

Felix, F. (2001). Escorting behaviour: a territorial manifestation in wild bottlenose dolphins? *Estudios Oceanológicos*, *20*, 67–72.

Félix, F., Waerebeek, K. Van, Sanino, G. P., Castro, C., Bressem, M. F. Van, & Santillán, L. (2018). Variation in dorsal fin morphology in common bottlenose dolphin (*Tursiops truncatus*) populations from the southeast Pacific Ocean. *Pacific Science*, *72*(3), 307–320. doi: 10.2984/72.3.2

Figueirido, B., Tseng, Z. J., Serrano-Alarcón, F. J., Martín-Serra, A., & Pastor, J. F. (2014). Three-dimensional computer simulations of feeding behaviour in red and giant pandas relate skull biomechanics with dietary niche partitioning. *Biology Letters*, *10*(4). doi: 10.1098/rsbl.2014.0196

Fordyce, R., Quilty, P. G., & Daniels, J. (2002). *Australodelphis mirus*, a bizarre new toothless ziphiid-like fossil dolphin (Cetacea: Delphinidae) from the Pliocene of Vestfold Hills, East Antarctica. *Antarctic Science*, *14*(1), 37–54. doi: 10.1017/S0954102002000561

Frankenhuis, W. E., & Del Giudice, M. (2012). When do adaptive developmental mechanisms yield maladaptive outcomes? *Developmental Psychology*, *48*(3), 628–642. doi: 10.1037/a0025629

Fruet, P. F., Secchi, E. R., Daura-Jorge, F., Vermeulen, E., Flores, P. A. C., Simões-Lopes, P. C., Genoves, R. C., Laporta, P., Di Tullio, J. C., Freitas, T. R. O., Rosa, L. D., Valiati, V. H., Beheregaray, L. B., & Möller, L. M. (2014). Remarkably low genetic diversity and strong population structure in common bottlenose dolphins (*Tursiops truncatus*) from coastal waters of the Southwestern Atlantic Ocean. *Conservation Genetics*, *15*(4), 879–895. doi: 10.1007/S10592-014-0586-Z

Fung, C. W. (2016). Cranial shape correlates with diet specialization in Northeast Pacific killer whale (*Orcinus orca*) ecotypes. [MSc thesis]. doi: 10.14288/1.0314137

Galatius, A. (2005). Sexually dimorphic proportions of the harbour porpoise (*Phocoena phocoena*) skeleton. *Journal of Anatomy*, *206*(2), 141-154. doi: 10.1111/j.1469-7580.2005.00381.x

Galatius, A., & Gol'din, P. E. (2011). Geographic variation of skeletal ontogeny and skull shape in the harbour porpoise (*Phocoena phocoena*). *Canadian Journal of Zoology*, *89*(9), 869–879. doi: 10.1139/z11-059

Galatius, A., Racicot, R., McGowen, M., & Olsen, M. T. (2020). Evolution and diversification of delphinid skull shapes. *IScience*, *23*(10), 101543. doi: 10.1016/j.isci.2020.101543

García-Vernet, R., Borrell, A., Víkingsson, G., Halldórsson, S. D., & Aguilar, A. (2021). Ecological niche partitioning between baleen whales inhabiting Icelandic waters. *Progress in Oceanography*, *199*, 102690. doi: 10.1016/j.pocean.2021.102690

Gaspari, S., Scheinin, A., Holcer, D., Fortuna, C., Natali, C., Genov, T., Frantzis, A., Chelazzi, G., & Moura, A. E. (2015). Drivers of population structure of the bottlenose dolphin (*Tursiops truncatus*) in the Eastern Mediterranean Sea. *Evolutionary Biology*, *42*(2), 177–190. doi: 10.1007/S11692-015-9309-8

Genoves, R. C., Fruet, P. F., Di Tullio, J. C., Möller, L. M., & Secchi, E. R. (2018). Spatiotemporal use predicts social partitioning of bottlenose dolphins with strong home range overlap. *Ecology and Evolution*, *8*(24), 12597–12614. doi: 10.1002/ece3.4681

Giacomini, G., Herrel, A., Chaverri, G., Brown, R., Russo, D., Scaravelli, D., & Meloro, C. (2022). Functional correlates of skull shape in Chiroptera: feeding and echolocation adaptations. *Integrative Zoology*, *17*(3), 430–442. doi: 10.1111/1749-4877.12564

Giménez, J., Cañadas, A., Ramírez, F., Afán, I., García-Tiscar, S., Fernández-Maldonado, C., Castillo, J. J., & de Stephanis, R. (2018). Living apart together: niche partitioning among Alboran Sea cetaceans. *Ecological Indicators*, *95*, 32–40. doi: 10.1016/j.ecolind.2018.07.020

Gittleman, J. L. (1994). Are the pandas successful specialists or evolutionary failures? *BioScience*, *44*(7), 456–464. doi: 10.2307/1312297

Green, R. F., Ridgway, S. H., & Evans, W. E. (1980). Functional and descriptive anatomy of the bottlenosed dolphin nasolaryngeal system with special reference to the musculature associated with sound production. In R.G. Busnel, & J.F. Fish (Eds.), *Animal sonar systems (pp. 199-238)*. Plenum Press. doi: 10.1007/978-1-4684-7254-7_8

Grossnickle, D. M. (2020). Feeding ecology has a stronger evolutionary influence on functional morphology than on body mass in mammals. *Evolution*, *74*(3), 610–628. doi: 10.1111/evo.13929

Gutscher, M. A., Malavieille, J., Lallemand, S., & Collot, J. Y. (1999). Tectonic segmentation of the North Andean margin: impact of the Carnegie Ridge collision. *Earth and Planetary Science Letters*, *168*(3–4), 255–270. doi: 10.1016/S0012-821X(99)00060-6

Hedrick, B. P. (2021). Inter- and intraspecific variation in the *Artibeus* species complex demonstrates size and shape partitioning among species. *PeerJ*, *9*, e11777. doi: 10.7717/peerj.11777

Hendges, C. D., Bubadu E, J. M., & Aceres, N. C. C. (2016). Environment and space as drivers of variation in skull shape in two widely distributed South-American Tayassuidae, *Pecari tajacu* and *Tayassu pecari* (Mammalia: Cetartiodactyla). *Biological Journal of the Linnean Society*, *119*(4), 785-798. doi: 10.1111/bij.12859

Hoelzel, A. R., Potter, C. W., & Best, P. B. (1998). Genetic differentiation between parapatric 'nearshore' and 'offshore' populations of the bottlenose dolphin. *Proceedings of the Royal Society of London. Series B: Biological Sciences*, *265*(1402), 1177–1183. doi: 10.1098/rspb.1998.0416

Holeski, L. M. (2007). Within and between generation phenotypic plasticity in trichome density of *Mimulus guttatus*. *Journal of Evolutionary Biology*, *20*(6), 2092–2100. doi: 10.1111/J.1420-9101.2007.01434.X

Ikeda, Y., Jiang, T., Oh, H., Csorba, G., & Motokawa, M. (2020). Geographic variations of skull morphology in the *Rhinolophus ferrumequinum* species complex (Mammalia: Chiroptera). *Zoologischer Anzeiger*, *288*, 125–138. doi: 10.1016/j.jcz.2020.08.004

Jackson, S. M. (2000). Glide angle in the genus *Petaurus* and a review of gliding in mammals. *Mammal Review*, *30*(1), 9–30. doi: 10.1046/J.1365-2907.2000.00056.X

Janik, V. M. (2000). Food–related bray calls in wild bottlenose dolphins (*Tursiops truncatus*). *Proceedings of the Royal Society of London. Series B: Biological Sciences*, *267*(1446), 923–927. doi: 10.1098/rspb.2000.1091

Kimura, M., (1971). Theoretical foundation of population genetics at the molecular level. *Theoretical population biology*, *2*(2), 174-208. doi: 10.1016/0040-5809(71)90014-1

Krützen, M., Mann, J., Heithaus, M. R., Connor, R. C., Bejder, L., & Sherwin, W. B. (2005). Cultural transmission of tool use in bottlenose dolphins. *Proceedings of the National Academy of Sciences*, *102*(25), 8939–8943. doi: 10.1073/pnas.0500232102

Kurihara, N., & Oda, S. I. (2009). Effects of size on the skull shape of the bottlenose dolphin (*Tursiops truncatus*). *Mammal Study*, *34*(1), 19–32. doi: 10.3106/041.034.0104

La Manna, G., Rako Gospić, N., Manghi, M., Picciulin, M., & Sarà, G. (2017). Assessing geographical variation on whistle acoustic structure of three Mediterranean populations of common bottlenose dolphin (*Tursiops truncatus*). *Behaviour*, *154*(5), 583–607. doi: 10.1163/1568539X-00003435

La Manna, G., Rako-Gospić, N., Sarà, G., Gatti, F., Bonizzoni, S., & Ceccherelli, G. (2020). Whistle variation in Mediterranean common bottlenose dolphin: the role of geographical, anthropogenic, social, and behavioral factors. *Ecology and Evolution*, *10*(4), 1971–1987. doi: 10.1002/ece3.6029

Lambeck, K., & Chappell, J. (2001). Sea level change through the last glacial cycle. *Science*, *292*(5517), 679–686. doi: 10.1126/science.1059549

Liu, J. X., Tatarenkov, A., Beacham, T. D., Gorbachev, V., Wildes, S., & Avise, J. C. (2011). Effects of Pleistocene climatic fluctuations on the phylogeographic and demographic histories of Pacific herring (*Clupea pallasii*). *Molecular Ecology*, *20*(18), 3879–3893. doi: 10.1111/J.1365-294X.2011.05213.X

Louis, M., Korlević, P., Nykänen, M., Archer, F., Berrow, S., Brownlow, A., Lorenzen, E. D., O'Brien, J., Post, K., Racimo, F., Rogan, E., Rosel, P. E., Sinding, M. H. S., van der Es, H., Wales, N., Fontaine, M. C., Gaggiotti, O. E., & Foote, A. D. (2023). Ancient dolphin genomes reveal rapid repeated adaptation to coastal waters. *Nature Communications*, *14*(1), 1–13. doi: 10.1038/s41467-023-39532-z

Louis, M., Viricel, A., Lucas, T., Peltier, H., Alfonsi, E., Berrow, S., Brownlow, A., Covelo, P., Dabin, W., Deaville, R., Stephanis, R. de, Gally, F., Gauffier, P., Penrose, R., Silva, M. A., Guinet, C., & Simon-Bouhet, B. (2014). Habitat-driven population structure of bottlenose dolphins, *Tursiops truncatus*, in the North-East Atlantic. *Molecular Ecology*, *23*(4), 857–874. doi: 10.1111/mec.12653

Lu, X., Ge, D., Xia, L., Huang, C., & Yang, Q. (2014). Geometric morphometric study of the skull shape diversification in Sciuridae (Mammalia, Rodentia). *Integrative Zoology*, *9*(3), 231–245. doi: 10.1111/1749-4877.12035

Ludt, W. B., & Rocha, L. A. (2015). Shifting seas: the impacts of Pleistocene sea-level fluctuations on the evolution of tropical marine taxa. *Journal of Biogeography*, *42*(1), 25–38. doi: 10.1111/jbi.12416

Luís, A. R., May-Collado, L. J., Rako-Gospić, N., Gridley, T., Papale, E., Azevedo, A., Silva, M. A., Buscaino, G., Herzing, D., & dos Santos, M. E. (2021). Vocal universals and geographic variations in the acoustic repertoire of the common bottlenose dolphin. *Scientific Reports*, *11*(1), 1–9. doi: 10.1038/s41598-021-90710-9

Lusseau, D., Wilson, B., Hammond, P., Grellier, K., Durban, J., Parsons, K., Barton, T., & Thompson, P. (2006). Quantifying the influence of sociality on population structure in bottlenose dolphins. *Journal of Animal Ecology*, *75*(1), 14–24. doi: stable/3505463

Maestri, R., Patterson, B. D., Fornel, R., Monteiro, L. R., & de Freitas, T. R. O. (2016). Diet, bite force and skull morphology in the generalist rodent morphotype. *Journal of Evolutionary Biology*, *29*(11), 2191–2204. doi: 10.1111/jeb.12937

Magnus, L. Z., Machado, R. F., & Cáceres, N. (2017). Comparative ecogeographical variation in skull size and shape of two species of woolly opossums (genus *Caluromys*). *Zoologischer Anzeiger*, *267*, 139–150. doi: 10.1016/j.jcz.2017.03.003

Marina, T. I., Marchesi, M. C., & Goodall, R. N. P. (2018). Long-finned pilot whale (*Globicephala melas*, Traill 1809) subspecies in the Atlantic Ocean: are there differences in their skulls? *Marine Mammal Science*, *35*(2), 660–676. doi: 10.1111/mms.12548

May-Collado, L., & Wartzok, D. (2008). A comparison of bottlenose dolphin whistles in the Atlantic Ocean: factors promoting whistle variation. *Journal of Mammalogy*, *89*(5), 1229–1240. doi: 10.1644/07-mamm-a-310.1

Mazzochi, M. S., Muraro, V., Fagundes, N. J. R., & Bugoni, L. (2024). Absence of genetic structure among ecologically diverse populations indicates high plasticity in a pantropical seabird. *Conservation Genetics*, *25*(4), 925–938. doi: 10.1007/S10592-024-01613-X

McCurry, M. R., Fitzgerald, E. M. G., Evans, A. R., Adams, J. W., & McHenry, C. R. (2017). Skull shape reflects prey size niche in toothed whales. *Biological Journal of the Linnean Society*, *121*(4), 936–946. doi: 10.1093/biolinnean/blx032

McGowen, M. R., Spaulding, M., & Gatesy, J. (2009). Divergence date estimation and a comprehensive molecular tree of extant cetaceans. *Molecular Phylogenetics and Evolution*, *53*(3), 891–906. doi: 10.1016/J.YMPEV.2009.08.018

Mckenna, M. F., Cranford, T. W., Berta, A., & Pyenson, N. D. (2012). Morphology of the odontocete melon and its implications for acoustic function. *Marine Mammal Science*, *28*(4), 690–713. doi: 10.1111/J.1748-7692.2011.00526.X

Mead, J., & Potter, C. (1995). Recognizing two populations of the bottlenose dolphin (*Tursiops truncatus*) of the Atlantic coast of North America morphologic and ecologic considerations. *IBI Reports*, *5*, 51–44.

Methion, S., & Díaz López, B. (2020). Individual foraging variation drives social organization in bottlenose dolphins. *Behavioral Ecology*, *31*(1), 97–106. doi: 10.1093/beheco/arz160

Miller, G. S. (1923). The telescoping of the cetacean skull (with eight plates). *Smithsonian Miscellaneous Collections*, *76*, 1-70.

Mirimin, L., Miller, R., Dillane, E., Berrow, S. D., Ingram, S., Cross, T. F., & Rogan, E. (2011). Fine-scale population genetic structuring of bottlenose dolphins in Irish coastal waters. *Animal Conservation*, *14*(4), 342–353. doi: 10.1111/J.1469-1795.2010.00432.X

Morrison, D. W., & Morrison, S. H. (1981). Economics of harem maintenance by a neotropical bat. *Ecology*, *62*(3), 864–866. doi: 10.2307/1937751

Moura, A. E., Kenny, J. G., Chaudhuri, R., Hughes, M. A., J. Welch, A., Reisinger, R. R., De Bruyn, P. J. N., Dahlheim, M. E., Hall, N., & Hoelzel, A. R. (2014). Population genomics of the killer whale indicates ecotype evolution in sympatry involving both selection and drift. *Molecular Ecology*, *23*(21), 5179–5192. doi: 10.1111/mec.12929

Moura, A. E., Shreves, K., Pilot, M., Andrews, K. R., Moore, D. M., Kishida, T., Möller, L., Natoli, A., Gaspari, S., McGowen, M., Chen, I., Gray, H., Gore, M., Culloch, R. M., Kiani, M. S., Willson, M. S., Bulushi, A., Collins, T., Baldwin, R., … Hoelzel, A. R. (2020). Phylogenomics of the genus *Tursiops* and closely related Delphininae reveals extensive reticulation among lineages and provides inference about eco-evolutionary drivers. *Molecular Phylogenetics and Evolution*, *146*, 106756. doi: 10.1016/j.ympev.2020.106756

Natoli, A., Birkun, A., Aguilar, A., Lopez, A., & Hoelzel, A. R. (2005). Habitat structure and the dispersal of male and female bottlenose dolphins (*Tursiops truncatus*). *Proceedings of the Royal Society B: Biological Sciences*, *272*(1569), 1217–1226. doi: 10.1098/rspb.2005.3076

Nei, M., Maruyama, T., & Chakraborty, R. (1975). The Bottleneck Effect and Genetic Variability in Populations. *Evolution*, *29*(1), 1–10. doi: 10.2307/2407137

Nicholson, G. M., & Clements, K. D. (2021). Ecomorphological divergence and trophic resource partitioning in 15 syntopic Indo-Pacific parrotfishes (Labridae: *Scarini*). *Biological Journal of the Linnean Society*, *132*(3), 590–611. doi: 10.1093/biolinnean/blaa210

Nykänen, M., Kaschner, K., Dabin, W., Brownlow, A., Davison, N. J., Deaville, R., & ... & Foote, A. D. (2019). Post-glacial colonization of northern coastal habitat by bottlenose dolphins: a marine leading-edge expansion? *Journal of Heredity*, *110*(6), 662–674. doi: 10.1093/jhered/esz039

Nykänen, M., Louis, M., Dillane, E., Alfonsi, E., Berrow, S., O'Brien, J., Brownlow, A., Covelo, P., Dabin, W., Deaville, R., de Stephanis, R., Gally, F., Gauffier, P., Ingram, S. N., Lucas, T., Mirimin, L., Penrose, R., Rogan, E., Silva, M. A., … Gaggiotti, O. E. (2019). Fine-scale population structure and connectivity of bottlenose dolphins, *Tursiops truncatus*, in European waters and implications for conservation. *Aquatic Conservation: Marine and Freshwater Ecosystems*, *29*(1), 197–211. doi: 10.1002/AQC.3139

Oxford-Smith, N., Ruta, M., Gao, A., Viaud-Martinez, K. A., Sabin, R., Herman, J., Ososky, J., Tajima, Y., Yamada, T. K., Kaliontzopoulou, A., & Moura, A. E. (2024). Skull morphology of bottlenose dolphins worldwide and patterns of adaptation between coastal and offshore environments. *Journal of Zoology*, *322*(1), 42–57. doi: 10.1111/jzo.13122

Papale, E., Azzolin, M., Cascão, I., Gannier, A., Lammers, M. O., Martin, V. M., Oswald, J., Perez-Gil, M., Prieto, R., Silva, M. A., & Giacoma, C. (2014). Acoustic divergence between bottlenose dolphin whistles from the Central–Eastern North Atlantic and Mediterranean Sea. *Acta Ethologica*, *17*(3), 155–165. doi: 10.1007/S10211-013-0172-2

Pardo-Gandarillas, M. C., Ibáñez, C. M., Torres, F. I., Sanhueza, V., Fabres, A., Escobar-Dodero, J., Mardones, F. O., & Méndez, M. A. (2018). Phylogeography and species distribution modelling reveal the effects of the Pleistocene ice ages on an intertidal limpet from the south-eastern Pacific. *Journal of Biogeography*, *45*(8), 1751–1767. doi: 10.1111/jbi.13362

Parsons, K. M., Durban, J. W., Claridge, D. E., Herzing, D. L., Balcomb, K. C., & Noble, L. R. (2006). Population genetic structure of coastal bottlenose dolphins (*Tursiops truncatus*) in the northern Bahamas. *Marine Mammal Science*, *22*(2), 276–298. doi: 10.1111/J.1748-7692.2006.00019.X

Perrin, W. F., Thieleking, J. L., Walker, W. A., Archer, F. I., & Robertson, K. M. (2011). Common bottlenose dolphins (*Tursiops truncatus*) in California waters: cranial differentiation of coastal and offshore ecotypes. *Marine Mammal Science*, *27*(4), 769–792. doi: 10.1111/j.1748-7692.2010.00442.x

Pianka, E. R. (1974). Niche overlap and diffuse competition. *Proceedings of the National Academy of Sciences*, *71*(5), 2141–2145. doi: 10.1073/pnas.71.5.2141

Pierce, S. E., Angielczyk, K. D., & Rayfield, E. J. (2009). Shape and mechanics in thalattosuchian (Crocodylomorpha) skulls: implications for feeding behaviour and niche partitioning. *Journal of Anatomy*, *215*(5), 555–576. doi: 10.1111/J.1469-7580.2009.01137.X

Pigliucci, M., Murren, C. J., & Schlichting, C. D. (2006). Phenotypic plasticity and evolution by genetic assimilation. *Journal of Experimental Biology*, *209*(12), 2362–2367. doi: 10.1242/jeb.02070

Porto, A., de Oliveira, F. B., Shirai, L. T., de Conto, V., & Marroig, G. (2009). The evolution of modularity in the mammalian skull I: morphological integration patterns and magnitudes. *Evolutionary Biology*, *36*(1), 118–135. doi: 10.1007/S11692-008-9038-3

Pratt, E. A. L., Beheregaray, L. B., Fruet, P., Tezanos-Pinto, G., Bilgmann, K., Zanardo, N., Diaz-Aguirre, F., Secchi, E. R., Freitas, T. R. O., & Möller, L. M. (2023). Genomic divergence and the evolution of ecotypes in bottlenose dolphins (Genus *Tursiops*). *Genome Biology and Evolution*, *15*(11). doi: 10.1093/gbe/evad199

Pryor, K., & Lindbergh, J. (1990). A dolphin-human fishing cooperative in Brazil. *Marine Mammal Science*, *6*(1), 77–82. doi: 10.1111/J.1748-7692.1990.TB00228.X

Ramos, E. A., Santoya, L., Verde, J., Walker, Z., Castelblanco-Martínez, N., Kiszka, J. J., Rieucau, G., & Angel Ramos, E. (2022). Lords of the rings: mud ring feeding by bottlenose dolphins in a Caribbean estuary revealed from sea, air, and space. *Marine Mammal Science*, *38*(1), 364–373. doi: 10.1111/mms.12854

Rice, D. W. (1998). *Marine mammals of the world: systematics and distribution*. Allen Press, Lawrence, Kansas, USA.

Romeu, B., Cantor, M., Bezamat, C., Simões-Lopes, P. C., & Daura-Jorge, F. G. (2017). Bottlenose dolphins that forage with artisanal fishermen whistle differently. *Ethology*, *123*(12), 906–915. doi: 10.1111/eth.12665

Rosel, P. E., Hansen, L., & Hohn, A. A. (2009). Restricted dispersal in a continuously distributed marine species: common bottlenose dolphins *Tursiops truncatus* in coastal waters of the western North Atlantic. *Molecular Ecology*, *18*(24), 5030–5045. doi: 10.1111/J.1365-294X.2009.04413.X

Rossman, S., Berens Mccabe, E., Barros, N. B., Gandhi, H., Ostrom, P. H., Stricker, C. A., & Wells, R. S. (2015). Foraging habits in a generalist predator: sex and age influence habitat selection and resource use among bottlenose dolphins (*Tursiops truncatus*). *Marine Mammal Science*, *31*(1), 155–168. doi: 10.1111/mms.12143

Roston, R. A., & Roth, V. L. (2019). Cetacean skull telescoping brings evolution of cranial sutures into focus. *The Anatomical Record*, *302*(7), 1055–1073. doi: 10.1002/ar.24079

Sanino, G., Van Waerebeek, K., Van Bressem, M., & Pastene, L. (2005). A preliminary note on population structure in eastern South Pacific common bottlenose dolphins, *Tursiops truncatus*. *Journal of Cetacean Research and Management*, *7*(1), 65–70. doi: 10.47536/jcrm.v7i1.759

Santillán, L., Félix, F., & Haase, B. (2008). A preliminary morphological comparison of skulls of common bottlenose dolphins *Tursiops truncatus* from Peru and Ecuador. In: *Document SC/60/SH10 presented to the Scientific Committee of the International Whaling Commission, Santiago, Chile, 2008*

Schmid, M., & Guillaume, F. (2017). The role of phenotypic plasticity on population differentiation. *Heredity*, *119*(4), 214–225. doi: 10.1038/hdy.2017.36

Slater, G. J., Dumont, E. R., & Van Valkenburgh, B. (2009). Implications of predatory specialization for cranial form and function in canids. *Journal of Zoology*, *278*(3), 181–188. doi: 10.1111/J.1469-7998.2009.00567.X

Slater, G. J., Price, S. A., Santini, F., & Alfaro, M. E. (2010). Diversity versus disparity and the radiation of modern cetaceans. *Proceedings of the Royal Society B: Biological Sciences*, *277*(1697), 3097–3104. doi: 10.1098/rspb.2010.0408

Slater, G. J., & Van Valkenburgh, B. (2009). Allometry and performance: the evolution of skull form and function in felids. *Journal of Evolutionary Biology*, *22*(11), 2278–2287. doi: 10.1111/J.1420-9101.2009.01845.X

Steeman, M. E., Hebsgaard, M. B., Fordyce, R. E., Ho, S. Y. W. W., Rabosky, D. L., Nielsen, R., Rahbek, C., Glenner, H., Sørensen, M. V., & Willerslev, E. (2009). Radiation of extant cetaceans driven by restructuring of the oceans. *Systematic Biology*, *58*(6), 573–585. doi: 10.1093/sysbio/syp060

Takahashi, M., Nakamura, G., & Kato, H. (2021). Growth-related cranial changes in Western North Pacific killer whales. *Cetacean Population Studies*, *3*, 175–188. doi: 10.34331/cpops.2020f009

Tatsch, A. C., de Lima, R. C., Secchi, E. R., & Botta, S. (2024). Niche partitioning among odontocetes in a marine biogeographic transition zone of the western South Atlantic Ocean. *Marine Biology*, *171*(1), 1–15. doi: 10.1007/S00227-023-04359-1

Torres, L. G., Rosel, P. E., & Read, A. J. (2003). Improving management of overlapping bottlenose dolphin ecotypes through spatial analysis and genetics. *Marine Mammal Science*, *19*(3), 502–514. doi: 10.1111/j.1748-7692.2003.tb01317.x

Van Waerebeek, K., Bamy Idrissa, L., Jiddou Amy, A. M., Sequeira, M., Diop, M., Ofori, D., Tchibozo, S., & Campredon, P. (2008). Indeterminate status of West African populations of inshore common bottlenose dolphins *Tursiops truncatus* cautions against opportunistic live-capture schemes. (Final report). *Fondation Internationale du Banc 'Arguin*.

Vicari, D., McGowen, M. R., Lambert, O., Brown, R. P., Bianucci, G., Sabin, R. C., & Meloro, C. (2023). Ecomorphology of toothed whales (Cetacea, Odontoceti) as revealed by 3D skull geometry. *Journal of Mammalian Evolution*, *30*(2), 475–491. doi: 10.1007/S10914-022-09642-4

Wang, J., Chou, L., & White, B. (2000). Differences in the external morphology of two sympatric species of bottlenose dolphins (Genus *Tursiops*) in the waters of China. *Journal of Mammalogy*, *81*(4), 1157–1165. doi: 10.1644/1545-1542(2000)081<1157:DITEMO>2.0.CO;2

Wei, F., Feng, Z., Wang, Z., & Li, M. (1999). Feeding strategy and resource partitioning between giant and red pandas. *Mammalia*, *63*(4), 417–430. doi: 10.1515/mamm.1999.63.4.417

Whitehead, H., & Ford, J. K. B. (2018). Consequences of culturally-driven ecological specialization: killer whales and beyond. *Journal of Theoretical Biology*, *456*, 279–294. doi: 10.1016/j.jtbi.2018.08.015

Wilson, A. B., & Eigenmann Veraguth, I. (2010). The impact of Pleistocene glaciation across the range of a widespread European coastal species. *Molecular Ecology*, *19*(20), 4535–4553. doi: 10.1111/J.1365-294X.2010.04811.X

Wray, J., Keen, E., & O'Mahony, E. N. (2021). Social survival: humpback whales (*Megaptera novaeangliae*) use social structure to partition ecological niches within proposed critical habitat. *PLOS ONE*, *16*(6), e0245409. doi: 10.1371/journal.pone.0245409

Supplementary Information

Supporting Materials for the PhD Thesis:

Adaptive skull shape changes in bottlenose dolphins (*Tursiops* spp.): inference from 3D morphological analyses

Author: Morgane Dromby
Institution: Uniwersytet Gdański
Year: 2025

Chapter 1

Table S1.2.1. Classification of studies using GM to study skull shape in odontocetes by field of study, species, and geographic location.

Articles	Field Study	Species	Location
(Laeta et al., 2021)	Functional Morphology, Interspecific	*Steno bredanensis, Grampus griseus, Pseudorca crassidens, Feresa attenuata, Peponocephala electra, Globicephala macrorhynchus, Globicephala melas, Sotalia guianensis, Sousa chinensis, Tursiops truncatus, Tursiops aduncus, Tursiops gephyreus, Stenella frontalis, Stenella attenuata, Stenella coeruleoalba, Stenella clymene, Stenella longirostris, Delphinus delphis, Delphinus capensis, Lagenodelphis hosei.*	Greenland, Baltic Sea, North sea, Indian Ocean, North Pacific, Berring Sea, South Atlantic
(Jedensjö et al., 2017)	Taxonomy, Interspecific	*Tursiops truncatus, Tursiops aduncus, Tursiops australis, Tursiops maugeanus, Delphinus catalania, Stenella attenuata, Stenella longirostris, Stenella coeruleoalba, Sousa sahulensis, Delphinus delphis, Steno bredanensis, Lagenodelphis hosei.*	South Pacific
(Gol'din & Vishnyakova, 2015)	Intraspecific, Evolutionary Ecology, Ontogeny, SD	*Phocoena phocoena*	Black Sea
(Gutstein et al., 2009)	Taxonomy, Interspecific, Ontogeny	*Brachydelphis hanseni*	South Pacific
(Higa et al., 2002)	SD, Evolutionary Ecology	*Pontoporia blainvillei*	South Atlantic
(Del Castillo et al., 2016)	Ontogeny, SD, Interspecific	*Cephalorhynchus commersonii*	South Atlantic, Indian Ocean
(Nicolosi & Loy, 2010)	Intraspecific, Evolutionary Ecology	*Delphinus delphis*	Mediterranean Sea, Atlantic, Indian, Pacific
(Amaral et al., 2009)	Interspecific, Taxonomy	*Delphinus delphis, Stenella coeruleoalba Tursiops truncatus*	North Atlantic
(Ngqulana et al., 2019)	Taxonomy, Intraspecific, Evolutionary Ecology	*Delphinus delphis, Delphinus capensis*	Indian Ocean, South Atlantic
(McCurry et al., 2017)	Evolutionary Ecology, Interspecific	*Berardius bairdii, Berardius arnuxii, Cephalorhynchus commersonii, Cephalorhynchus heavisidii, Cephalorhynchus hectori, Delphinus delphis, Delphinus capensis, Delphinus tropicalis, Delphinapterus leucas, Feresa attenuata, Grampus griseus, Globicephala melas, Globicephala macrorhynchus, Inia geoffrensis, Kogia breviceps, Kogia sima, Lagenorhynchus albirostris, Lagenorhynchus acutus, Lagenorhynchus australis, Lagenorhynchus cruciger, Lagenorhynchus obscurus, Lagenorhynchus obliquidens, Lissodelphis borealis, Lissodelphis peronii, Lipotes vexillifer, Mesoplodon bidens, Mesoplodon europaeus, Mesoplodon densirostris, Mesoplodon mirus, Mesoplodon peruvianus, Mesoplodon traversii, Monodon monoceros, Neophocaena phocaenoides, Neophocaena asiaeorientalis, Orcaella brevirostris, Orcaella heinsohni, Orcinus orca, Pontoporia blainvillei, Pseudorca crassidens, Phocoenoides dalli, Phocoena phocoena, Phocoena sinus, Phocoena spinipinnis, Phocoena dioptrica, Peponocephala electra, Platanista gangetica, Platanista minor, Stenella attenuata, Stenella clymene, Stenella coeruleoalba, Stenella frontalis, Stenella longirostris, Steno bredanensis, Sousa chinensis, Sousa plumbea, Sotalia fluviatilis,*	Global

		Sotalia guianensis, Tasmacetus shepherdi, Tursiops truncatus, Tursiops aduncus.	
(Frainer et al., 2021)	Interspecific, Ontogeny, Evolutionary Ecology	*Pontoporia blainvillei, Phocoena phocoena, Lagenorhynchus albirostris, Sousa plumbea, the Tursiops truncatus*	North Atlantic, North Pacific, South Atlantic, Indian Ocean
(Galatius et al., 2020)	Evolutionary Ecology, Interspecific	*Orcinus orca, Peponocephala electra, Pseudorca crassidens, Stenella attenuata, Stenella coeruleoalba, Globicephala melas, Lagenodelphis hosei, Stenella frontalis, Feresa attenuata, Leucopleurus acutus, Stenella clymene, Stenella longirostris, Delphinus delphis, Grampus griseus, Tursiops truncatus, Steno bredanensis, Globicephala macrorhynchus Lagenorhynchus albirostris*	Global
(Fung, 2016)	Intraspecific, Evolutionary Ecology	*Orcinus orca*	North Pacific
(Del Castillo et al., 2017)	Intraspecific, Evolutionary Ecology, Ontogeny	*Lagenorhynchus obscurus, Lagenorhynchus australis*	South Pacific
(Galatius & Goodall, 2016)	Interspecific, Evolutionary Ecology	*Lissodelphis borealis, Lissodelphis peronii, Lagenorhynchus obliquidens, Lagenorhynchus obscurus, Lagenorhynchus australis, Lagenorhynchus cruciger, Cephalorhynchus commersonii, Cephalorhynchus heavisidii, Cephalorhynchus hectori, Cephalorhynchus eutropia.*	South pacific, South Atlantic, North Pacific, Antarctic
(Guidarelli et al., 2014)	Interspecific, Taxonomy, Evolutionary Ecology	*Stenella coeruleoalba, Delphinus delphis, Tursiops truncatus*	Mediterranean Sea
(Parés-Casanova & Fabre, 2013)	Functional morphology, Intraspecific, Ontogeny	*Tursiops trucatus*	Global
(Galatius, 2010)	Ontogeny, Interspecific, Evolutionary Ecology	*Phocoena phocoena, Cephalorhynchus commersonii, Lagenorhynchus albirostris.*	North Sea, South Pacific
(Marina et al., 2018)	Intraspecific, Evolutionary Ecology	*Globicephala melas, Globicephala macrorhynchus*	North Atlantic, Southern Atlantic, South Pacific
(Page & Cooper, 2017)	Interspecific, Evolutionary Ecology	*Inia geoffrensis, Pontoporia blainvillei, Platanista gangetica, Lipotes vexillifer*	Amazon River
(De Francesco et al., 2016)	SD, Evolutionary Ecology, Ontogeny	*Tursiops truncatus*	Mediterranean Sea, North Sea
(De Araujo Montiero-Filho et al., 2002)	Intraspecific	*Sotalia fluviatilis, Sotalia guianensis.*	Amazon, South Atlantic
(Sydney et al., 2012)	Ontogeny	*Sotalia fluviatilis*	Amazon River
(Loy et al., 2011)	Intraspecific, Evolutionary Ecology	*Stenella coeruleoalba, Stenella frontalis, Stenella attenuata*	Mediterranean Sea, North Atlantic, North Sea.
(Jedensjö et al., 2020)	Intraspecific, Taxonomy	*Tursiops aduncus*	South Pacific
(Hohl et al., 2020)	Intraspecific, Evolutionary Ecology, Taxonomy	*Tursiops truncatus*	North Pacific, North Atlantic, South Pacific, South Atlantic
(Del Castillo et al., 2014)	Ontogeny, SD	*Pontoporia blainvillei*	South Atlantic
(Galatius et al., 2011)	Ontogeny, Interspecific, Evolutionary Ecology, Taxonomy	*Phocoena phocoena, Phocoenoides dalli, Phocoenoides dioptrica, Phocoenoides spinipinnis, Phocoenoides sinus, Neophocaena phocaenoides*	North Sea, North Pacific, South Pacific
(Galatius & Gol'din, 2011)	Population structrure	*Phocoena phocoena*	North Sea, Baltic Sea, Belt Sea
(Frandsen & Galatius, 2013)	SD, Interspecific	*Phocoena Phocoena, Phocoenoides dalli*	North Sea, North Pacific
(Conry et al., 2016)	SD, Intraspecific, Evolutionary Ecology	*Stenella coeruleoalba*	Indian Ocean
(Kurihara & Oda, 2009)	Ontogeny, Intraspecific	*Tursiops truncatus*	Pacific, Atlantic, Indian Oceans,

Chapter 3

Supplementary information to publication - Cranial variation between coastal and offshore bottlenose dolphins, *Tursiops truncatus* (Cetacea: Delphinidae) in Ecuador andthe Mediterranean: a three dimensional geometric morphometric study.

Morgane Dromby, Fernando Félix, Ben Haase, Paulo C. Simões-Lopes, Ana P.B. Costa, Aude Lalis, Celine Bens, Michela Podestà, Giuliano Doria, Andre E. Moura

Table S1. Accession numbers and details of the specimens used in the analysis.

Species	Museum Accession	Sex	Year	Location	Sea	Ecotype	Teeth
MUSEO DE BALLENAS (ECUADOR) N= 30							
T. truncatus	27	F	2007	MAR BRAVO	Southeast Pacific	OCEANIC	22
T. truncatus	29	M	2006	MAR BRAVO	Southeast Pacific	OCEANIC	22
T. truncatus	37	M	1995	MAR BRAVO	Southeast Pacific	OCEANIC	22
T. truncatus	40	M	1993	SAN PABLO	Southeast Pacific	COASTAL	22
T. truncatus	41	F	1997	MAR BRAVO	Southeast Pacific	OCEANIC	22
T. truncatus	43	Na	1990	JAMBELI ISLAND	Southeast Pacific	COASTAL	18
T. truncatus	48	M	1992	PUNTA CARNERO	Southeast Pacific	COASTAL	18
T. truncatus	51	M	1996	MAR BRAVO	Southeast Pacific	COASTAL	18
T. truncatus	58	Na	1991	PUNA ISLAND	Southeast Pacific	COASTAL	18
T. truncatus	59	Na	1991	PUNA ISLAND	Southeast Pacific	COASTAL	18
T. truncatus	60	Na	1991	PUNA ISLAND	Southeast Pacific	COASTAL	18
T. truncatus	61	Na	1991	PUNA ISLAND	Southeast Pacific	COASTAL	21
T. truncatus	62	M	1991	PUNA ISLAND	Southeast Pacific	COASTAL	21
T. truncatus	63	M	1992	PUNA ISLAND	Southeast Pacific	COASTAL	18
T. truncatus	64	F	1992	PUNA ISLAND	Southeast Pacific	COASTAL	18
T. truncatus	65	M	1993	PUNA ISLAND	Southeast Pacific	COASTAL	22
T. truncatus	66	Na	1993	JAMBELI ISLAND	Southeast Pacific	COASTAL	19
T. truncatus	69	M?	1994	PUNA ISLAND	Southeast Pacific	COASTAL	18
T. truncatus	70	Na	1994	Na	Southeast Pacific	COASTAL	19
T. truncatus	71	Na	1992	Na	Southeast Pacific	COASTAL	20
T. truncatus	72	Na	1994	Na	Southeast Pacific	COASTAL	18
T. truncatus	73	Na	1994	PUNA ISLAND	Southeast Pacific	COASTAL	18
T. truncatus	75	Na	1992	Na	Southeast Pacific	COASTAL	18
T. truncatus	76	Na	1994	PUNA ISLAND	Southeast Pacific	COASTAL	18
T. truncatus	77	Na	1996	PLAYAS	Southeast Pacific	COASTAL	20
T. truncatus	78	Na	2005	PUNTA CARNERO	Southeast Pacific	OCEANIC	22
T. truncatus	79	Na	1995	MAR BRAVO	Southeast Pacific	OCEANIC	21
T. truncatus	116	Na	2001	GALAPAGOS	Southeast Pacific	OCEANIC	18
T. truncatus	117	Na	Na	Na	Southeast Pacific	OCEANIC	23
T. truncatus	121	Na	2004	SUA	Southeast Pacific	COASTAL	18
THE FEDERAL UNIVERSITY OF SANTA CATARINA UFSC (BRAZIL) N= 6							
T. truncatus	UFSC 1011	Na			Southwest Atlantic	OCEANIC	22
T. truncatus	UFSC 1099	F			Southwest Atlantic	OCEANIC	21
T. truncatus	UFSC 1287	Na			Southwest Atlantic	OCEANIC	22

T. truncatus	UFSC 1322	Na			Southwest Atlantic	OCEANIC	22
T. truncatus	UFSC 1398	F			Southwest Atlantic	OCEANIC	22
T. truncatus	UFSC 1468	Na			Southwest Atlantic	OCEANIC	22
MUSEUM NATIONAL D'HISTOIRE NATURALLE MNHN (FRANCE) N= 4							
T. truncatus	MNHN-ZM-AC-1882-115	Na	1882	La rochelle	Northeast Atlantic	OCEANIC	22
T. truncatus	MNHN-ZM-AC-2012-1006	Na	2012	Puerto Casma	Southeast Pacific	OCEANIC	20
T. truncatus	MNHN-ZM-AC-1983-1157	Na	1983	Douarnenez	Northeast Atlantic	OCEANIC	22
T. truncatus	MNHN-ZM-AC-A3082	Na	Na	Cape of good hope	Northeast Atlantic	OCEANIC	Na
THE MUSEUM OF NATURAL HISTORY OF MILAN MSN (ITALY) N= 7							
T. truncatus	SMNS-Z-MAM-0078	Na	1952	GENOVA	Mediterranean	COASTAL	25
T. truncatus	SMNS-Z-MAM-0470	Na	1957	VENEZIA	Mediterranean	COASTAL	22
T. truncatus	SMNS-Z-MAM-4900	M	1988	BARI	Mediterranean	COASTAL	22
T. truncatus	SMNS-Z-MAM-4919	F	1989	BARI	Mediterranean	COASTAL	22
T. truncatus	SMNS-Z-MAM-6694	M	1988	BARI	Mediterranean	COASTAL	22
T. truncatus	SMNS-Z-MAM-7279	M	2001	IMPERIA	Mediterranean	COASTAL	22
T. truncatus	SMNS-Z-MAM-3968	M	2012	SAVONNA	Mediterranean	COASTAL	22
THE CIVIC MUSEUM OF NATURAL HISTORY "GIACOMO DORIA" MSNG (ITALY) N= 11							
T. truncatus	MSNG 36410	Na	1914	SARDEGNA	Mediterranean	COASTAL	Na
T. truncatus	MSNG 36413	Na	1915	TOSCANA	Mediterranean	COASTAL	22
T. truncatus	MSNG 46867	Na	Na	LIGURIA	Mediterranean	COASTAL	22
T. truncatus	MSNG 48545	M	1990	LIGURIA	Mediterranean	COASTAL	22
T. truncatus	MSNG 48564	F	1991	LIGURIA	Mediterranean	COASTAL	22
T. truncatus	MSNG 48568	F	1992	LIGURIA	Mediterranean	COASTAL	22
T. truncatus	MSNG 50246	M	1996	LIGURIA	Mediterranean	COASTAL	22
T. truncatus	MSNG 50249	F	1996	LIGURIA	Mediterranean	COASTAL	22
T. truncatus	MSNG 50250	F	1996	LIGURIA	Mediterranean	COASTAL	21
T. truncatus	MSNG 54766	F	2002	LIGURIA	Mediterranean	COASTAL	22
T. truncatus	MSNG 57160	M	2009	LIGURIA	Mediterranean	COASTAL	20

Table S2. The number of individuals per geographical area and habitat type.

Geography	**Habitat**	**N**
Gulf of Guayaquil	Coastal	22
Offshore Southeast Pacific (OSEP)	Offshore	9
Offshore South Atlantic (OSA)	Offshore	6
Offshore North Atlantic (ONA)	Offshore	3
Mediterranean	Coastal	18
Total		58

Table S3. Description of the parameters used for the 3D modelling in MESHROOM.

	Low number of pictures (<300 images)	**Adequate number of pictures (>300 images)**
Parameters		
Feature Extraction	Default + Sift_float + Akaze Preset = high	Default + Sift_float
Image matching	Max descriptor = 0 Number of matches = 0	Default
Feature matching	Default	Default
Structure from motion	Untick „Rig for constraint" Tick „Guided matching"	Untick „Rig for constraint" Tick „Guided matching"
Prepare dense scene	Default	Default
Depth map	Downscale = 1 Min consistency camera = 2 Min consistency camera similarity = 3	Default
Depth map filter	Default	Default
Mesh filtering	Keep the largest mesh	Keep the largest mesh

Table S4. Description of the manual LMs used in this study, as shown in Figure 2.

LANDMARKS	LANDMARK DESCRIPTION
	DORSAL VIEW
0	Right rostral tip
1	Left rostral tip
2	The most dorsal point of the rostrum on the midline at 1/6 of the distance between the anterior tip of the rostrum and the anterior orbit.
3	The most dorsal point of the rostrum on the midline at 1/3 of the distance between the anterior tip of the rostrum and the anterior orbit.
4	The most dorsal point of the rostrum on the midline at 1/2 of the distance between the anterior tip of the rostrum and the anterior orbit.
5	The most dorsal point rostrum and the anterior orbit.
6	The most dorsal point of the rostrum on the midline at 5/6 of the distance between the anterior tip of the rostrum and the anterior orbit.
7	The most dorsal point in line with the anterior orbit.
8	The most right lateral point at 1/6 of the distance between the anterior tip of the rostrum and the anterior point of the orbits.
9	The most left lateral point at 1/6 of the distance between the anterior tip of the rostrum and the anterior point of the orbits.
10	The most right lateral point at 1/3 of the distance between the anterior tip of the rostrum and the anterior point of the orbits.
11	The most left lateral point at 1/3 of the distance between the anterior tip of the rostrum and the anterior point of the orbits.
12	The most right lateral point at 1/2 of the distance between the anterior tip of the rostrum and the anterior point of the orbits.
13	The most left lateral point at 1/2 of the distance between the anterior tip of the rostrum and the anterior point of the orbits.
14	The most right lateral point at 2/3 of the distance between the anterior tip of the rostrum and the anterior point of the orbits.
15	The most left lateral point at 2/3 of the distance between the anterior tip of the rostrum and the anterior point of the orbits.
16	The most right lateral point in line with the anterior orbit.
17	The most left lateral point in line with the anterior orbit.
18	The left highest point of the rostrum (Melon attachment).
19	The right highest point of the rostrum (Melon attachment).
20	Right Antorbital notch
21	Left antorbital notch

22	Right premaxillary foramen
23	Left premaxillary foramen
24	The right upper tip of the premaxillary
25	Left upper tip of the premaxillary
26	Maximum deflection point of the right nasal opening
27	Maximum deflection point of the left nasal opening
28	The anterior midpoint of the suture between nasal points
29	Anteriormost point of the suture between the frontal and interparietal bones
30	Lateralmostextension of the left nasal bone.
31	Lateralmost extension of right nasal bone
32	Right Anterior margin of the posterior dorsal infraorbital foramen
33	Right posterior margin of anterior dorsal infraorbital foramen
34	Left Anterior margin of the posterior dorsal infraorbital foramen
35	Left posterior margin of the posterior dorsal infraorbital foramen
36	Left Tip of the antorbital process
37	Left ventral point of the postorbital process of the frontal
38	The left caudal most alveoli
39	Left upper Tip of the zygomatic process of the squamosal // Left correspondence to 49
40	Left lower Tip of the zygomatic process of the squamosal
41	Left anteroventralmost point of the retrotympanic
42	Left tip of the Pterygoid's protuberance// Left correspondence to 51
43	Left deep point of the Eustachian notch // Left correspondence to 52
44	The left posteriormost point on the pterygoid hamulus
45	Right tip of the antorbital process,
46	Right ventral point of the postorbital process of the frontal,
47	The right caudal most alveoli
48	The right lower tip of the zygomatic process of the squamosal.
49	The right upper tip of the zygomatic process of the squamosal.
50	The right anteroventralmost point of the retrotympanic;
51	Right tip of the Pterygoid's protuberance
52	Right deep point of the Eustachian notch

53	Left Posteriormost point of the basioccipital crest
54	Right Posteriormost point of the basioccipital crest
55	Left ventralmost point of the paraoccipital process

56	Right ventralmost point of the paraoccipital process
57	Left meeting of the anteriormost point of the paraoccipital process and the postglenoid process;
58	Right meeting of the anteriormost point of the paraoccipital process and the postglenoid process;
59	The right postero-medialmost point on the palatine surface of the pterygoid
60	Dorsalmost point of the foramen magnum
61	Left dorsalmost point of occipital condyle
62	Right dorsalmost point of occipital condyle
63	Left lateralmost point of occipital condyle
64	Right lateralmost point of occipital condyle
65	Right dorsal tip of occipital condyle,
66	Left dorsal tip of occipital condyle,
67	Left ventral most point of 6 occipital condyle
68	Right ventral most point of occipital condyle
69	The right posteriormost point on the pterygoid hamulus
70	The left postero-medialmost point on the palatine surface of the pterygoid
	LINES
C0	Right ascending process of the squamosal.
C1	Right descending process of the sphenoid
C2	Left descending process of the parietal
C3	Left ascending process of the sphenoid
C4	Left ascending process of the squamosal
C5	Right ascending process of the parietal
C6	Left descending process of the palate area
C7	Right descending process of the palate area
	PATCHES
P0	Left Maxillae area
P1	Right Maxillae area
P2	Occipital area

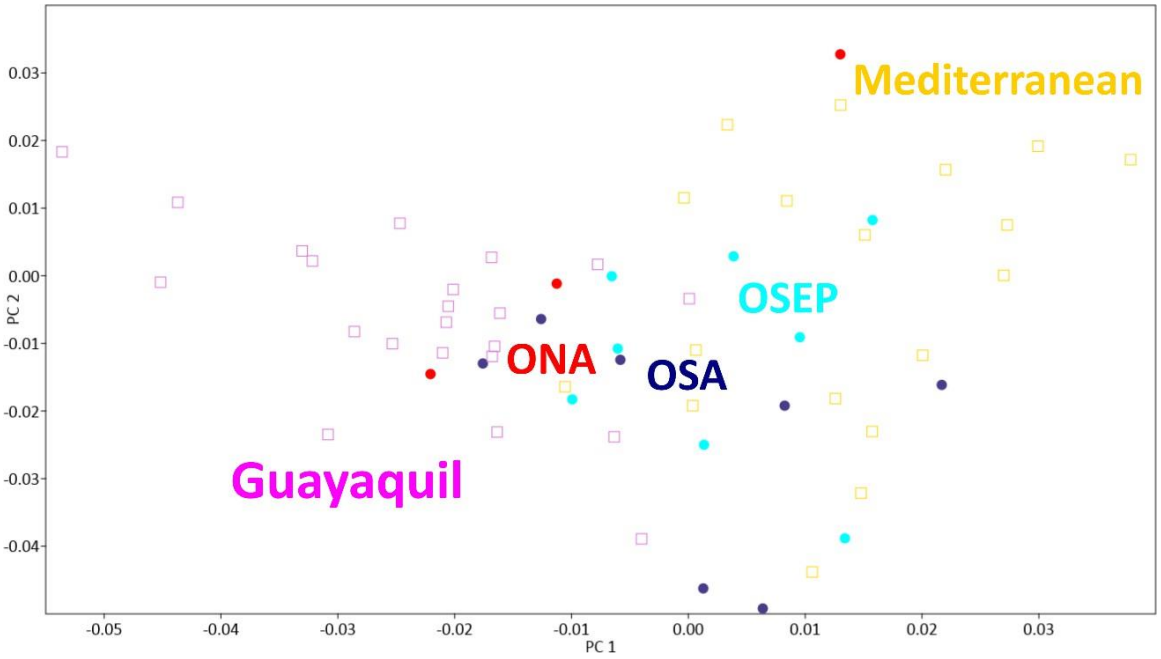

Figure S1. 2D PCA morphospace generated from the automatic landmarking procedure, with samples categorized by habitat and geographical area. Specimens from the Gulf of Guayaquil shown in magenta; Offshore from the Southeast Pacific in light blue (OSEP); Offshore from the South Atlantic in dark blue (OSA); Offshore from the North Atlantic in red (ONA); specimens from the Mediterranean Sea in orange.

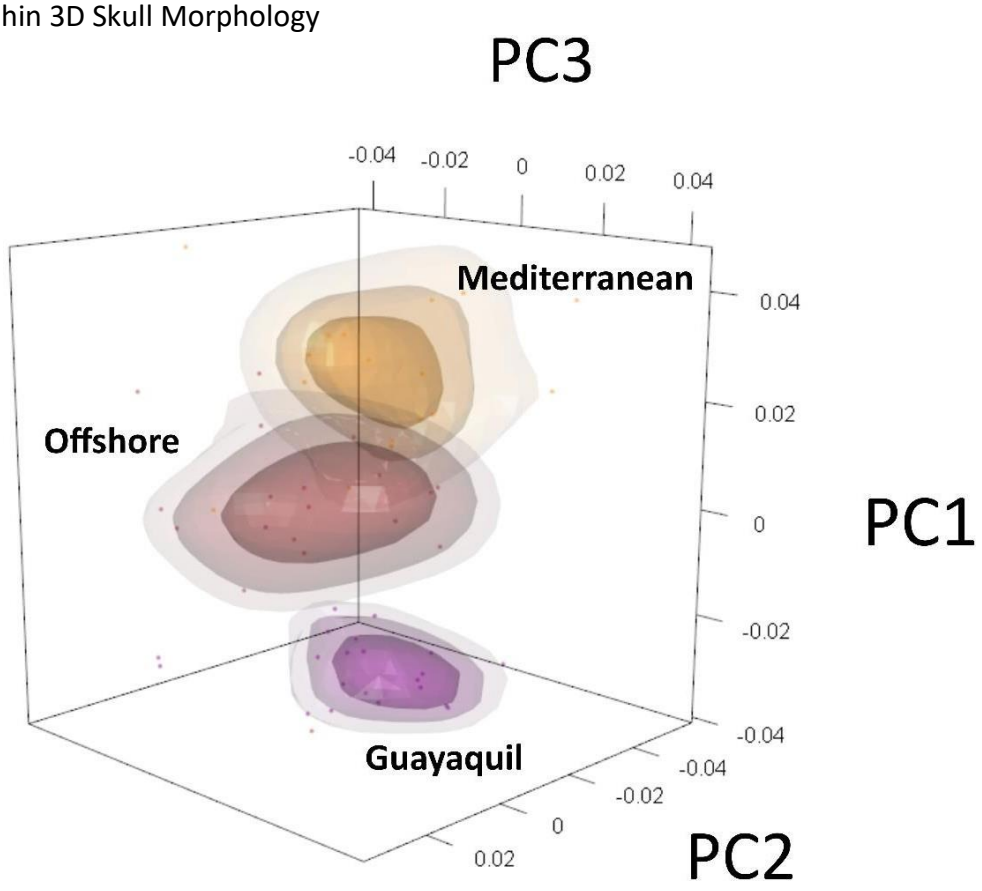

Figure S2. 3D PCA morphospace and kernel density cloud generated from the manual landmarking procedure, with samples categorized by habitat. Offshore populations in red, coastal populations from Guayaquil (Ecuador) in magenta, and from the Mediterranean in orange.

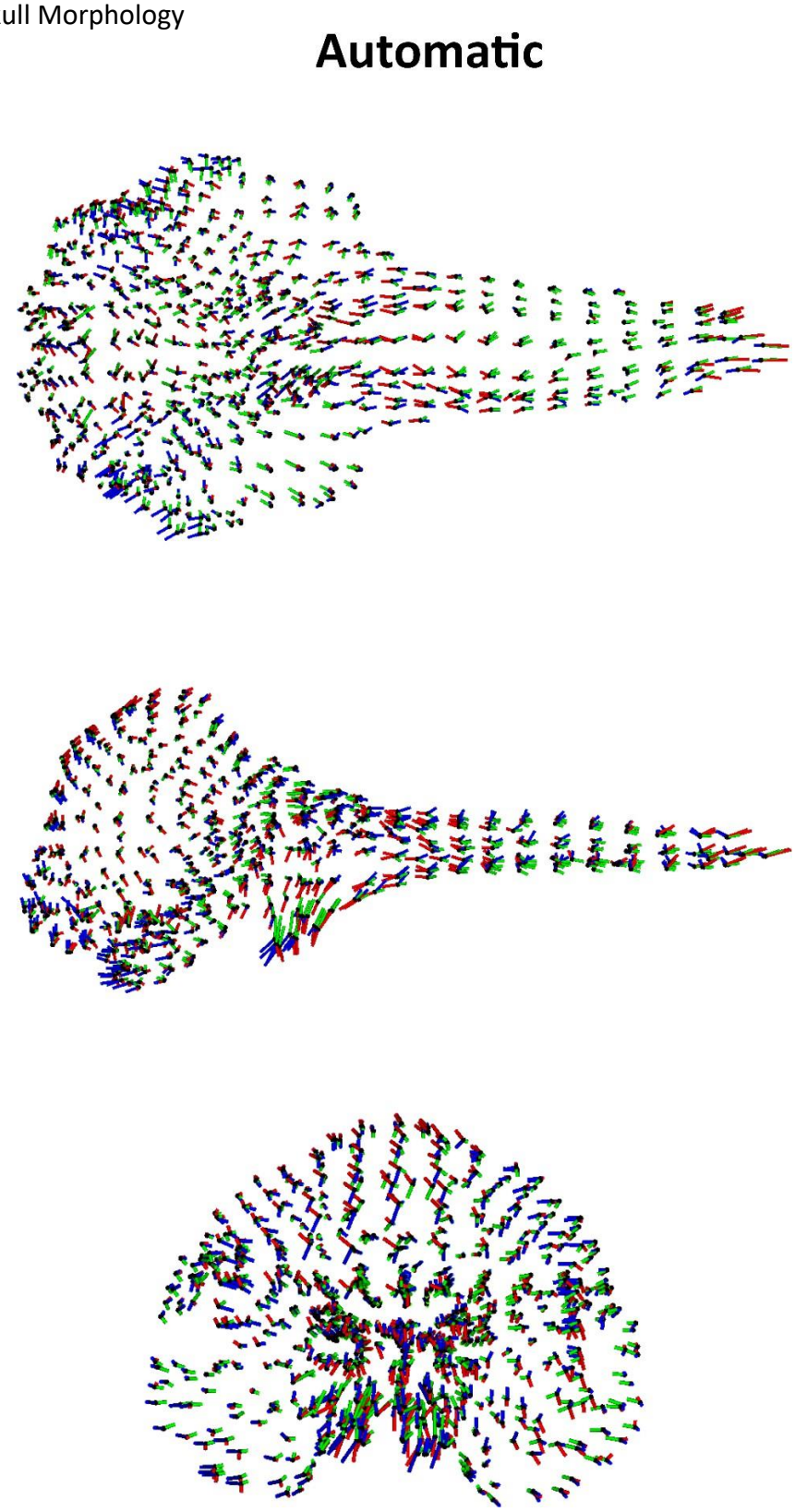

Figure S3. Landmark vector displacement plots (Lollipops) between the three ecotypes from the automatic landmarking. Lines represent the difference in landmark position between the mean landmark configuration (black dots) and specimens grouped along the positive PC axis. PC1 is represented in red, PC2 in green and PC3 in blue.

Manual

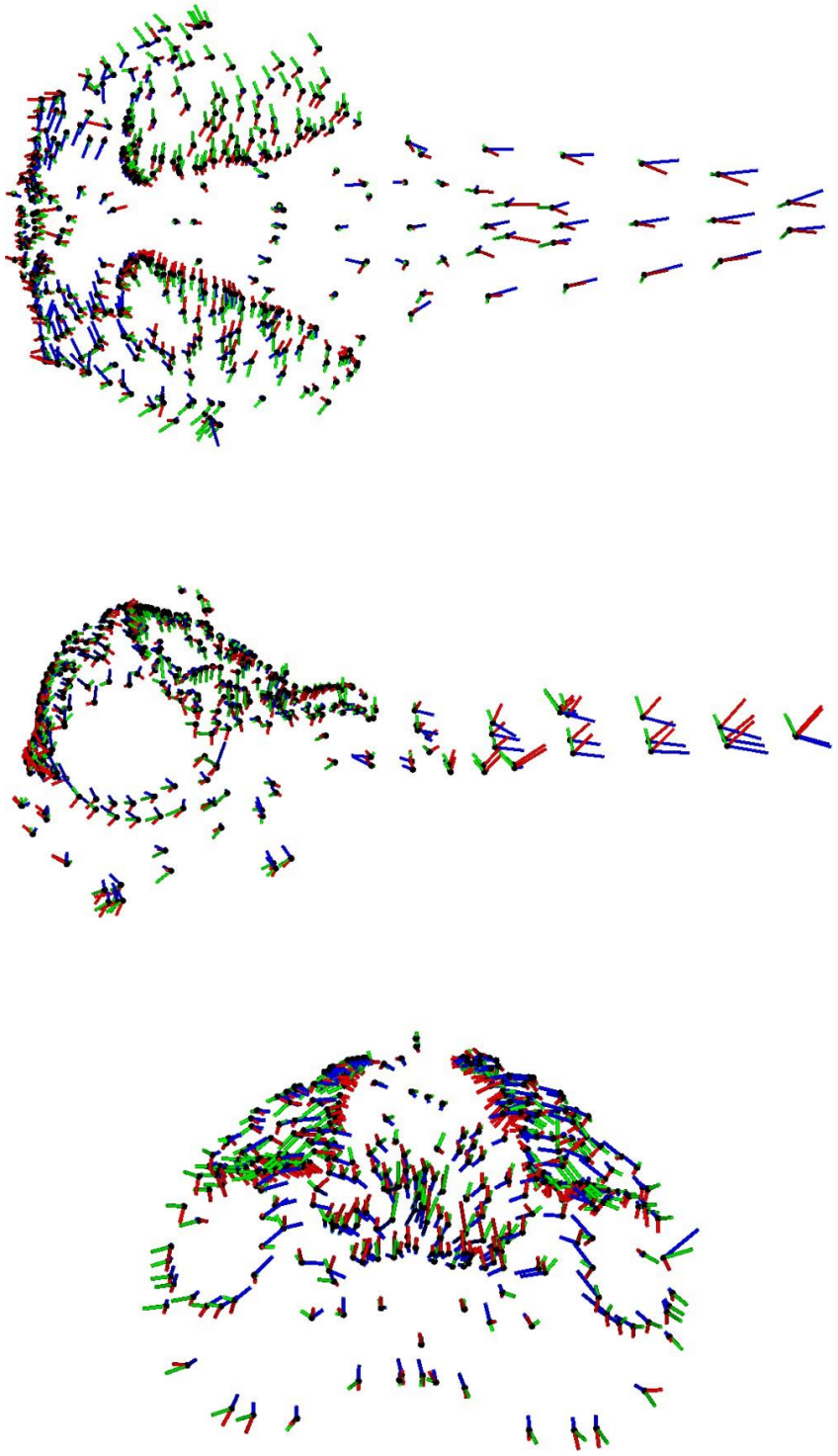

Figure S4. Landmark vector displacement plots (Lollipops) between the three ecotypes from the manual landmarking. Lines represent the difference in landmark position between the mean landmark configuration (black dots) and specimens grouped along the positive PC axis. PC1 is represented in red, PC2 in green and PC3 in blue.

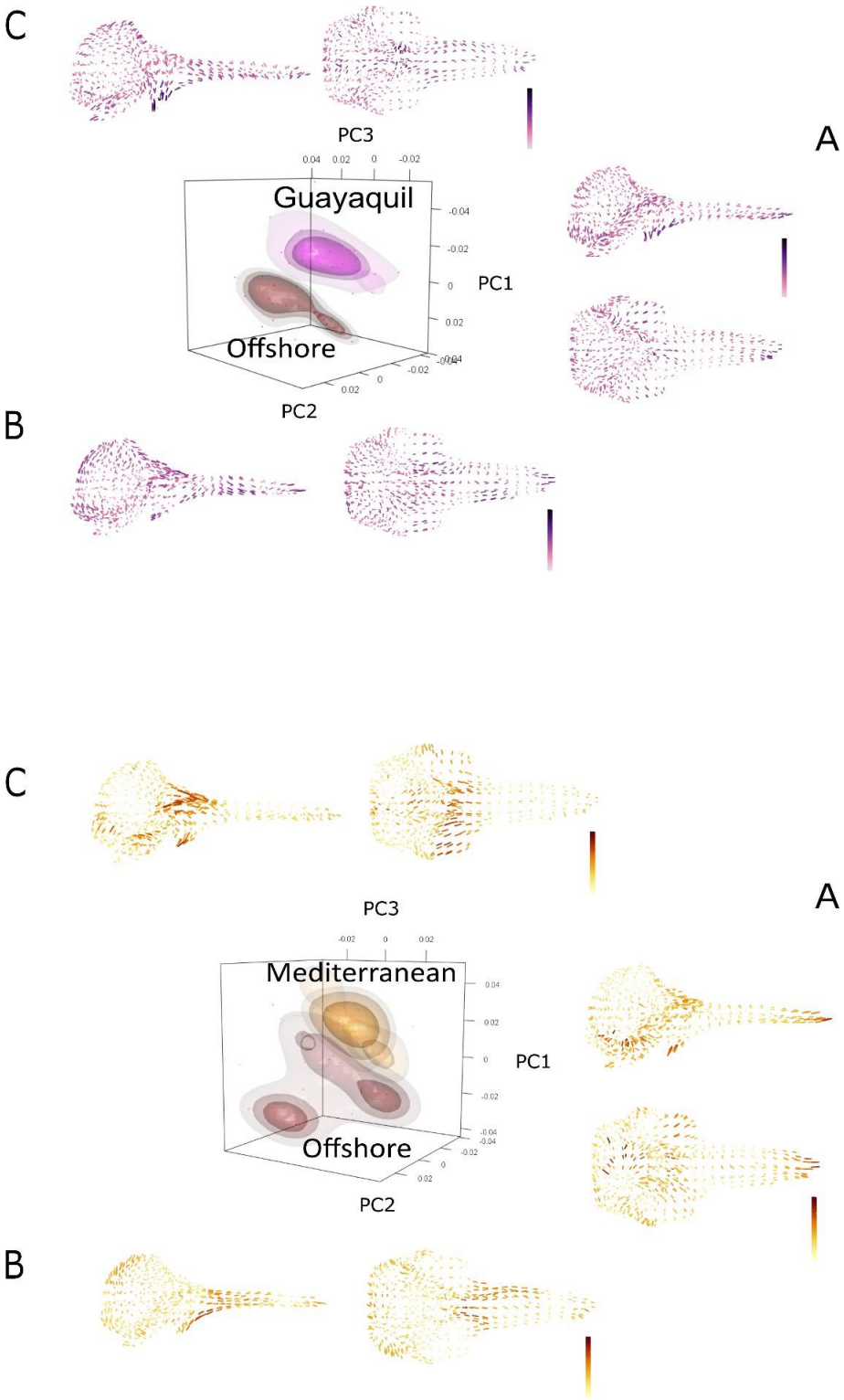

Figure S5. 3D PCA morphospace and kernel density cloud generated from the automatic landmarking procedure, comparing Guayaquil vs. offshore specimens only (top), and Mediterranean vs. offshore specimens only (bottom). Landmark vector displacement plots (lollipops) represent the difference in landmark position between the mean landmark configuration and specimens grouped along the positive PC1 (A), PC2 (B), and PC3 (C).

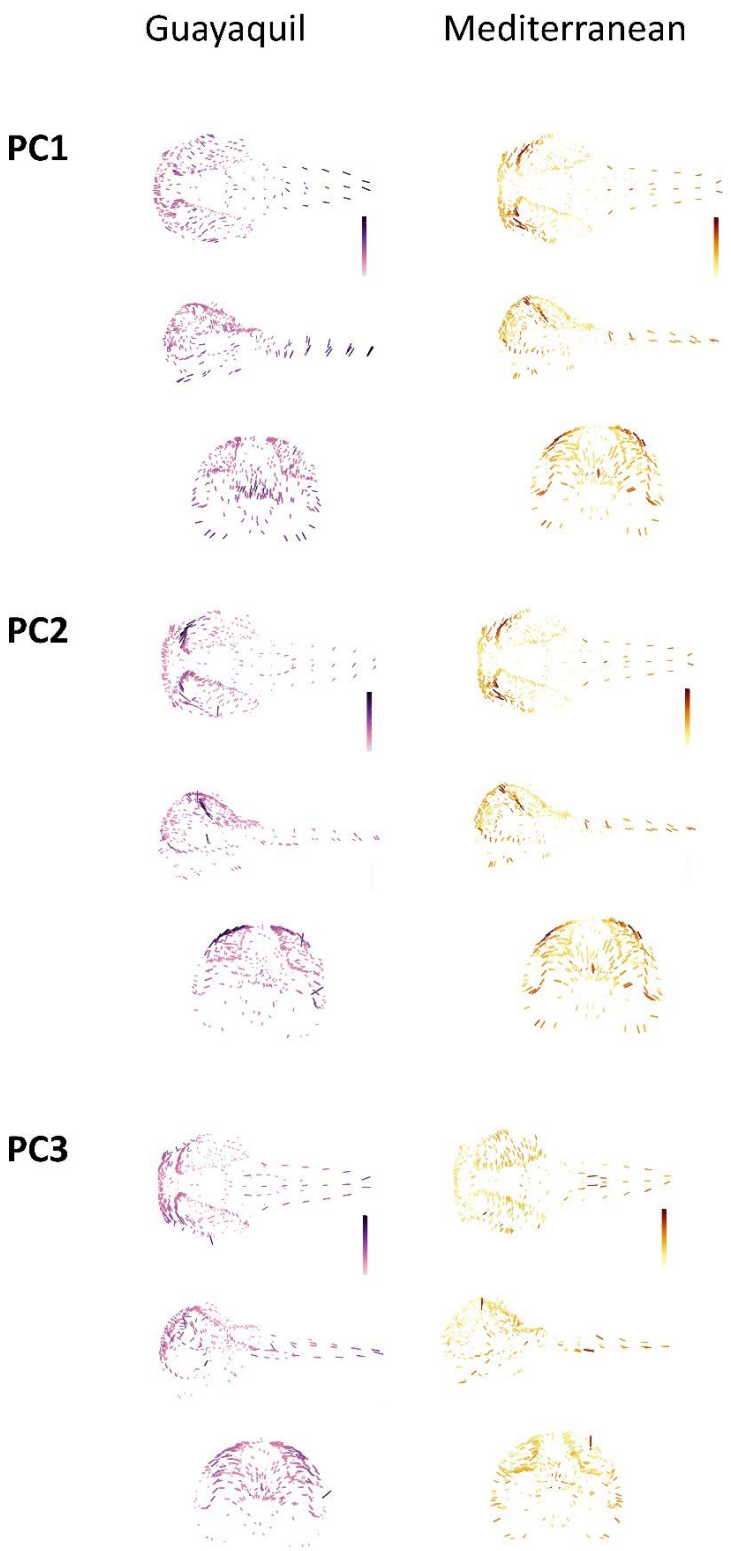

Figure S6. Landmark vector displacement plots (lollipops) for manual landmarking between offshore and Guayaquil specimens (left, magenta), and between offshore and Mediterranean (right, orange). Lines represent the difference in landmark position between the mean landmark configuration and specimens grouped along the positive PC axis.

Chapter 4

Table S4.2.1. Accession numbers and details of the specimens used in the analysis.

Lab_ID	Museum	Catalog Number	Species	OTU Label	OTU Given	Sex	Year	Country	Location
B1011	UFSC	1011	T. truncatus	Offshore	Offshore	Unknown	Unknown	Brazil	Pr.do Morro das Pedras
B1041	UFSC	1041	T. truncatus	Offshore	Offshore	Unknown	1986	Brazil	Porto Belo
B1077	UFSC	1077	T. gyphreus	Coastal	Gephyreus	Male	1989	Brazil	Pr. do pantano do sul
B1081	UFSC	1081	T. gyphreus	Coastal	Gephyreus	Female	1989	Brazil	Florianopolis
B1089	UFSC	1089	T. gyphreus	Coastal	Gephyreus	Female	1990	Brazil	Molhes Praia do mar grosso
B1099	UFSC	1099	T. truncatus	Offshore	Offshore	Female	1991	Brazil	Praia dos Ingleses
B1106	UFSC	1106	T. truncatus	Offshore	Offshore	Unknown	1991	Brazil	Pizaia da Joaquina
B1116	UFSC	1116	T. gyphreus	Coastal	Gephyreus	Female	1993	Brazil	Aterro Baia Sul, proximo Velairos
B1281	UFSC	1281	T. gyphreus	Coastal	Gephyreus	Female	2000	Brazil	Proc. Baia sul
B1287	UFSC	1287	T. truncatus	Offshore	Offshore	Unknown	2001	Brazil	Pr. da Joaquina
B1349	UFSC	1349	T. gyphreus	Coastal	Gephyreus	Female	2007	Brazil	Praia de Fora -Palhoca
B1350	UFSC	1350	T. gyphreus	Coastal	Gephyreus	Male	2007	Brazil	Itapiryba-Laguna
B1395	UFSC	1395	T. gyphreus	Coastal	Gephyreus	Male	2011	Brazil	Praia do Mocambique
B1398	UFSC	1398	T. truncatus	Offshore	Offshore	Female	2012	Brazil	Lamaq
B1415	UFSC	1415	T. truncatus	Offshore	Offshore	Male	2014	Brazil	Lamaq
B1420	UFSC	1420	T. gyphreus	Coastal	Gephyreus	Female	2014	Brazil	Lamaq
B1489	UFSC	1489	T. gyphreus	Coastal	Gephyreus	Unknown	2012	Brazil	Praia do Mocambique
B1501	UFSC	1501	T. gyphreus	Coastal	Gephyreus	Male	2017	Brazil	Baia Norte
B1506	UFSC	1506	T. gyphreus	Coastal	Gephyreus	Female	2017	Brazil	Ribeirao da ilha
B1631	UFSC	1631	T. truncatus	Offshore	Offshore	Female	2020	Brazil	Praia do forte
B1637	UFSC	1637	T. gyphreus	Coastal	Gephyreus	Female	2020	Brazil	Baia sul Ilha
C27401	LACM	27401	T. truncatus	Offshore	Offshore	Male	1966	USA	San Pedro channel, Palos verdes Peninsula, off long point
C54016	LACM	54016	T. truncatus	Unknown	Offshore	Male	1963	USA	Hawaian island, Offshore by Sea Life Park
C72169	LACM	72169	T. truncatus	Unknown	Offshore	Female	1963	USA	Hawaian island, Kaneohe Bay; Sampen Channel
C72294	LACM	72294	T. truncatus	Coastal	California	Female	1981	USA	North end of Bolsa Chica
C72295	LACM	72295	T. truncatus	Coastal	California	Male	1982	USA	Newport Beach, 34th St
C72493	LACM	72493	T. truncatus	Coastal	California	Male	1976	USA	Huntington Beach; end of Beach Blvd
C84029	LACM	84029	T. truncatus	Coastal	Offshore	Male	1971	USA	Santa Catalina Island; E end, 3 mi SE
C84034	LACM	84034	T. truncatus	Coastal	Offshore	Male	1982	USA	San Miguel Id; Simonton Cove
C84036	LACM	84036	T. truncatus	Coastal	California	Male	1970	USA	Rancho palos verdes; Pt Vicente, 16 mi S
C84055	LACM	84055	T. truncatus	Offshore	Offshore	Male	1972	USA	Catalina island, 3 miles S. Silver Canyon
C84056	LACM	84056	T. truncatus	Coastal	California	Female	1971	USA	Santa Catalina Id; West End, 1 mi off
C84058	LACM	84058	T. truncatus	Offshore	Offshore	Male	1970	USA	Pt Vicente, 16 mi S
C84059	LACM	84059	T. truncatus	Offshore	Offshore	Female	NA	USA	Unknown
C84065	LACM	84065	T. truncatus	Coastal	California	Male	1983	USA	Surfside
C84285	LACM	84285	T. truncatus	Coastal	California	Male	1990	USA	La Jolla Marine St Beach
C91862	LACM	91862	T. truncatus	Coastal	California	Male	1996	USA	Malibu
C91886	LACM	91886	T. truncatus	Coastal	California	Female	1993	USA	Silver Strand State Beach
C91913	LACM	91913	T. truncatus	Coastal	California	Female	1995	USA	South Torrey Pines State Beach
C95366	LACM	95366	T. truncatus	Coastal	California	Female	2003	USA	Coronado City Beach, N end
C95387	LACM	95387	T. truncatus	Offshore	Offshore	Male	2004	USA	Newport Beach, Prospect Street

C95459	LACM	95459	T. truncatus	Coastal	California	Male	2004	USA	Coronado; North Island (Naval Air Station)
C95471	LACM	95471	T. truncatus	Offshore	Offshore	Male	2006	USA	Dockweiler State Beach
E117	PAS	117	T. truncatus	Unknown	Offshore	Unknown	Unknown	Ecuador	Unknown
E27	PAS	27	T. truncatus	Offshore	Offshore	Female	2007	Ecuador	Mar Bravo
E29	PAS	29	T. truncatus	Offshore	Offshore	Male	2006	Ecuador	Mar Bravo
E37	PAS	37	T. truncatus	Offshore	Offshore	Male	1995	Ecuador	Mar Bravo
E40	PAS	40	T. truncatus	Coastal	Guayaquil	Male	1993	Ecuador	San Pablo
E41	PAS	41	T. truncatus	Offshore	Offshore	Female	1997	Ecuador	Mar Bravo
E43	PAS	43	T. truncatus	Coastal	Guayaquil	Unknown	1990	Ecuador	Jambeli Island
E48	PAS	48	T. truncatus	Coastal	Guayaquil	Male	1992	Ecuador	Punta Carnero
E58	PAS	58	T. truncatus	Coastal	Guayaquil	Unknown	1991	Ecuador	Puna Island
E60	PAS	60	T. truncatus	Coastal	Guayaquil	Unknown	1991	Ecuador	Puna Island
E61	PAS	61	T. truncatus	Coastal	Guayaquil	Unknown	1991	Ecuador	Puna Island
E63	PAS	63	T. truncatus	Coastal	Guayaquil	Male	1992	Ecuador	Puna Island
E64	PAS	64	T. truncatus	Coastal	Guayaquil	Female	1992	Ecuador	Puna Island
E65	PAS	65	T. truncatus	Coastal	Guayaquil	Male	1993	Ecuador	Puna Island
E66	PAS	66	T. truncatus	Coastal	Guayaquil	Unknown	1993	Ecuador	Jambeli Island
E69	PAS	69	T. truncatus	Coastal	Guayaquil	Male?	1994	Ecuador	Puna Island
E70	PAS	70	T. truncatus	Coastal	Guayaquil	Unknown	1994	Ecuador	Unknown
E71	PAS	71	T. truncatus	Coastal	Guayaquil	Unknown	1992	Ecuador	Unknown
E72	PAS	72	T. truncatus	Coastal	Guayaquil	Unknown	1994	Ecuador	Unknown
E73	PAS	73	T. truncatus	Coastal	Guayaquil	Unknown	1994	Ecuador	Puna Island
E75	PAS	75	T. truncatus	Coastal	Guayaquil	Unknown	1992	Ecuador	Unknown
E77	PAS	77	T. truncatus	Coastal	Guayaquil	Unknown	1996	Ecuador	Playas
E78	PAS	78	T. truncatus	Offshore	Offshore	Unknown	2005	Ecuador	Punta Carnero
E79	PAS	79	T. truncatus	Offshore	Offshore	Unknown	1995	Ecuador	Mar Bravo
G36413	MSNG	36413	T. truncatus	Unknown	Mediterranean	Unknown	1915	Italy	Bagno di Marciana
G46867	MSNG	46867	T. truncatus	Unknown	Mediterranean	Unknown	Unknown	Italy	Unknown
G48545	MSNG	48545	T. truncatus	Unknown	Mediterranean	Male	1990	Italy	Isola del Tino
G48564	MSNG	48564	T. truncatus	Unknown	Mediterranean	Female	1991	Italy	Spotorso
G48568	MSNG	48568	T. truncatus	Unknown	Mediterranean	Female	1992	Italy	Promontorio de Portofino
G50246	MSNG	50246	T. truncatus	Unknown	Mediterranean	Male	1996	Italy	Alassio
G50249	MSNG	50249	T. truncatus	Unknown	Mediterranean	Female	1996	Italy	Ameglia
G50250	MSNG	50250	T. truncatus	Unknown	Mediterranean	Female	1996	Italy	Santa Margherita
G54766	MSNG	54766	T. truncatus	Unknown	Mediterranean	Female	2002	Italy	Genova
J24unreg	NMNST	24unreg	T. truncatus	Unknown	Japan	Unknown	Unknown	Japan	Unknown
JM24788	NMNST	M24788	T. truncatus	Unknown	Japan	Male	Unknown	Japan	Ito-Shi
JM35127	NMNST	M35127	T. aduncus	Unknown	Aduncus	Female	Unknown	Japan	Yokosuka-shi
L14596	ZMA	14596	T. truncatus	Unknown	WestAfrica	Unknown	1971	Gabon	Unknown
L16455	RMNH	16455	T. truncatus	Unknown	NorthSea	Male	1957	Netherlands	Noordwijk
L19799	RMNH	19799	T. truncatus	Unknown	NorthSea	Male	1967	Netherlands	Westkapelle
L19837	RMNH	19837	T. truncatus	Unknown	NorthSea	Unknown	1967	Netherlands	Wassenaar
L20160	ZMA	20160	T. aduncus	Unknown	Aduncus	Unknown	1978	Saudi Arabia	Jizan
L20328	ZMA	20328	T. truncatus	Unknown	Offshore	Unknown	1978	Oman	Kuria Muria Islands, Alsawda Island
L20900	ZMA	20900	T. truncatus	Unknown	Offshore	Unknown	1979	Oman	Sib
L2113	RMNH	2113	T. truncatus	Unknown	NorthSea	Unknown	1932	Netherlands	Renesse
L21173	ZMA	21173	T. truncatus	Unknown	Offshore	Unknown	1980	Oman	Ras al Hadd
L21434	ZMA	21434	T. aduncus	Unknown	Offshore	Male	1980	Oman	Ra's Al Hadd
L21452	ZMA	21452	T. truncatus	Unknown	Offshore	Unknown	1981	Oman	Dibab

L2330	RMNH	2330	T. truncatus	Unknown	NorthSea	Male	1935	Netherlands	Cadzand
L24677	ZMA	24677	T. truncatus	Unknown	WSouthAmer	Male	1986	Peru	Pucusana
L24678	ZMA	24678	T. truncatus	Unknown	WSouthAmer	Male	1981	Peru	Pucusana
L24679	ZMA	24679	T. truncatus	Unknown	WSouthAmer	Unknown	Unknown	Peru	Pucusana
L24680	ZMA	24680	T. truncatus	Unknown	WSouthAmer	Male	1986	Peru	Pucusana
L26121	RMNH	26121	T. truncatus	Unknown	NorthSea	Unknown	1977	Netherlands	Domburg
L27044	RMNH	27044	T. truncatus	Unknown	NorthSea	Female	1978	Netherlands	Breskens
L28061	RMNH	28061	T. truncatus	Unknown	NorthSea	Male	1979	Netherlands	Vlissingen
L31148	RMNH	31148	T. truncatus	Unknown	NorthSea	Female	1982	Netherlands	NA
L31193	RMNH	31193	T. truncatus	Unknown	NorthSea	Male	1929	Netherlands	Hoek van Holland
L32350	RMNH	32350	T. truncatus	Unknown	Japan	Male	1978	Japan	Fage
L32352	RMNH	32352	T. truncatus	Unknown	Japan	Female	1978	Japan	Fage
L5000071	RMNH	5000071	T. truncatus	Unknown	NorthSea	Female	2013	Netherlands	Krabbendijke
L7964	ZMA	7964	T. aduncus	Unknown	Aduncus	Unknown	1890	Indonesia	Cheribon
L7965	ZMA	7965	T. aduncus	Unknown	Offshore	Unknown	1917	Indonesia	Deli
L8617	ZMA	8617	T. truncatus	Unknown	NorthSea	Unknown	1965	Netherlands	Julianadorp
M00470	MSN	470	T. truncatus	Unknown	Mediterranean	Unknown	1957	Italy	Venezia
M03968	MSN	3968	T. truncatus	Unknown	Mediterranean	Unknown	Unknown	Italy	Unknown
M04900	MSN	4900	T. truncatus	Unknown	Mediterranean	Male	1988	Italy	Bari
M04902	MSN	4902	T. truncatus	Unknown	Mediterranean	Unknown	1986	Italy	Pescara
M04919	MSN	4919	T. truncatus	Unknown	Mediterranean	Female	1989	Italy	Bari
M06694	MSN	6694	T. truncatus	Unknown	Mediterranean	Male	1988	Italy	Bari
M07279	MSN	7279	T. truncatus	Unknown	Mediterranean	Male	2001	Italy	Imperia
P014	MNHN	AC-1998-14	T. aduncus	Unknown	Aduncus	Unknown	1997	Madagascar	Ile Glorieuse, Ile du Lys
P1006	MNHN	2012-1006	T. truncatus	Lperonii	WSouthAmer	Unknown	1998	Peru	Puerto Casma
P115	MNHN	AC-1882-115	T. truncatus	Lperonii	Offshore	Unknown	Unknown	France	La rochelle
P1157	MNHN	MO-1983-1157	T. truncatus	Lperonii	Offshore	Unknown	1901	France	Baie de Douarnenez
P131	MNHN	AC-1982-131	T. truncatus	Lperonii	WestAfrica	Unknown	1980	Mauritania	Iwick
P138	MNHN	AC-1971-138	T. truncatus	Lperonii	Offshore	Unknown	Unknown	Unknown	Unknown
P1502	MNHN	MO-1992-1502	T. truncatus	Lperonii	WestAfrica	Unknown	1992	Mauritania	Cap Tafarit
P158	MNHN	AC-1971-158	T. truncatus	Lperonii	Offshore	Female	Unknown	France	Unknown
P161	MNHN	AC-1928-161	T. truncatus	Unknown	Offshore	Unknown	Unknown	Unknown	Unknown
P176	MNHN	AC-1971-176	T. truncatus	Lperonii	Offshore	Unknown	Unknown	France	Unknown
P198	MNHN	AC-1928-198	T. truncatus	Lperonii	Offshore	Unknown	Unknown	Unknown	Mers d'Europe
P199	MNHN	AC-1928-199	T. truncatus	Lperonii	Aduncus	Unknown	Unknown	Unknown	Unknown
P208	MNHN	AC-1965-208	T. aduncus	Sotalia	Aduncus	Unknown	Unknown	Unknown	Unknown
P304	MNHN	AC-1926-304	T. truncatus	Lperonii	Offshore	Unknown	Unknown	Unknown	Unknown
P67	MNHN	AC-1980-67bis	T. aduncus	Unknown	Aduncus	Unknown	1980	NCaledonia	Ile des Pins
P75	MNHN	AC-1979-75	T. aduncus	Unknown	Aduncus	Unknown	1977	NCaledonia	Baie de Gadji
PA3070	MNHN	AC-A3070	T. aduncus	Unknown	Aduncus	Unknown	Unknown	China	Unknown
PA3082	MNHN	AC-A3082	T. truncatus	Unknown	Offshore	Unknown	1882	South Africa	Cape of good hope
S045704	SMNS	45704	T. truncatus	Unknown	Mediterranean	Male	1968	Italy	Unknown
S045706	SMNS	45706	T. aduncus	Unknown	Aduncus	Male	Unknown	Pakistan	Unknown
S045707	SMNS	45707	T. aduncus	Unknown	Aduncus	Unknown	Unknown	Pakistan	Karachi
S045708	SMNS	45708	T. aduncus	Unknown	Aduncus	Unknown	1971	Pakistan	Karachi
S045709	SMNS	45709	T. aduncus	Unknown	Aduncus	Unknown	1972	Pakistan	Karachi
S045710	SMNS	45710	T. aduncus	Unknown	Aduncus	Unknown	1972	Pakistan	Unknown
S045711	SMNS	45711	T. aduncus	Unknown	Aduncus	Unknown	1973	Iran	Hormozgan

S045715	SMNS	45715	T. aduncus	Unknown	Aduncus	Unknown	1974	Pakistan	Unknown
S045716	SMNS	45716	T. aduncus	Unknown	Aduncus	Unknown	1974	Pakistan	Unknown
S045720	SMNS	45720	T. aduncus	Unknown	Aduncus	Unknown	1975	Pakistan	Unknown
S045722	SMNS	45722	T. aduncus	Unknown	Aduncus	Unknown	1979	Pakistan	Karachi
S046597	SMNS	46597	T. truncatus	Unknown	NorthSea	Unknown	1964	Germany	Cuxhaven
S046790	SMNS	46790	T. truncatus	Unknown	NorthSea	Unknown	Unknown	Denmark	Foroyar
S046791	SMNS	46791	T. truncatus	Unknown	Gephyreus	Unknown	1972	Uruguay	Rocha
S046792	SMNS	46792	T. truncatus	Unknown	Gephyreus	Unknown	1970	Uruguay	Rocha
S046793	SMNS	46793	T. aduncus	Unknown	Aduncus	Female	1973	Thailand	Songkhla
S050302	SMNS	50302	T. truncatus	Unknown	Mediterranean	Unknown	1956	Italy	Trieste
W12054	USNM	A12054	T. truncatus	Unknown	WSouthAmer	Unknown	Unknown	Mexico	Unknown
W16504	USNM	A16504	T. truncatus	Coastal	Erebennus	Male	1881	USA	Cherrystone Point
W16505	USNM	A16505	T. truncatus	Coastal	Erebennus	Female	1881	USA	Cherrystone Point
W176349	USNM	176349	T. truncatus	Coastal	Aduncus	Unknown	1912	South Africa	Durban
W176350	USNM	176350	T. truncatus	Coastal	Aduncus	Unknown	1912	South Africa	Durban
W176351	USNM	176351	T. truncatus	Coastal	Aduncus	Unknown	1912	South Africa	Durban
W176352	USNM	176352	T. truncatus	Coastal	Aduncus	Unknown	1912	South Africa	Durban
W176353	USNM	176353	T. truncatus	Coastal	Aduncus	Unknown	1912	South Africa	Durban
W254634	USNM	254634	T. aduncus	Offshore	Offshore	Female	1929	Coco's Island	500 Miles West Of Panama
W254910	USNM	254910	T. aduncus	Offshore	WSouthAmer	Male	1929	Panama	Cape Mala
W277170	USNM	277170	T. truncatus gillii	Unknown	WSouthAmer	Unknown	1944	Panama	San Jose Island
W298239	USNM	298239	T. truncatus	Offshore	California	Unknown	1953	USA	Pacific Beach
W395381	USNM	395381	T. truncatus	Unknown	WSouthAmer	Male	1968	Chile	Caleta Padillo
W395733	USNM	395733	T. truncatus	Unknown	WSouthAmer	Unknown	1969	Chile	Arica
W395924	USNM	395924	T. truncatus gillii	Unknown	California	Male	1970	USA	Torrey Pines State Park
W396165	USNM	396165	T. truncatus gillii	Unknown	WSouthAmer	Male	1965	Mexico	San Felipe
W470551	USNM	470551	T. truncatus	Unknown	WestAfrica	Unknown	Unknown	Ivory Coast	Abidjan
W470553	USNM	470553	T. truncatus	Unknown	WestAfrica	Female	1962	Ivory Coast	Abidjan
W470554	USNM	470554	T. truncatus	Unknown	WestAfrica	Unknown	Unknown	Ivory Coast	Abidjan
W470555	USNM	470555	T. truncatus	Offshore	WestAfrica	Unknown	Unknown	Ivory Coast	Abidjan
W470556	USNM	470556	T. truncatus	Unknown	WestAfrica	Unknown	Unknown	Ivory Coast	Abidjan
W501197	USNM	501197	T. truncatus	Unknown	Gephyreus	Unknown	Unknown	Uruguay	Punta Del Diablo
W504236	USNM	504236	T. truncatus gillii	Unknown	WSouthAmer	Unknown	1956	Mexico	San Felipe
W550021	USNM	550021	T. truncatus	Unknown	California	Female	1980	USA	San Clemente State Beach
W550097	USNM	550097	T. truncatus	Unknown	California	Male	1980	USA	Torrey Pines State Park
W550125	USNM	550125	T. truncatus	Unknown	California	Unknown	1981	USA	San Onofre
W550164	USNM	550164	T. truncatus	Unknown	Japan	Female	1982	Japan	Taiji
W550166	USNM	550166	T. truncatus	Unknown	Japan	Male	1982	Japan	Taiji
W550167	USNM	550167	T. truncatus	Unknown	Japan	Male	1982	Japan	Taiji
W550169	USNM	550169	T. truncatus	Unknown	Japan	Male	1982	Japan	Taiji
W550170	USNM	550170	T. truncatus	Unknown	Japan	Male	1982	Japan	Taiji
W550171	USNM	550171	T. truncatus	Unknown	Japan	Male	1982	Japan	Taiji
W550172	USNM	550172	T. truncatus	Unknown	Japan	Male	1982	Japan	Taiji
W550173	USNM	550173	T. truncatus	Unknown	Japan	Female	1982	Japan	Taiji
W550174	USNM	550174	T. truncatus	Unknown	Japan	Male	1982	Japan	Taiji
W550175	USNM	550175	T. truncatus	Unknown	Japan	Female	1982	Japan	Taiji

W550193	USNM	550193	T. truncatus gillii	Unknown	California	Unknown	1976	USA	Mussle Rock
W550194	USNM	550194	T. truncatus gillii	Unknown	California	Male	Unknown	USA	Cardiff By the Sea
W550265	USNM	550265	T. truncatus	Unknown	WSouthAmer	Unknown	1982	Peru	Chimbote
W550306	USNM	550306	T. truncatus	Unknown	WSouthAmer	Unknown	1982	Peru	Cerros De Illescas, Pipeline Camp
W550795	USNM	550795	T. truncatus	Unknown	WSouthAmer	Unknown	Unknown	Peru	Pucusana
W550798	USNM	550798	T. truncatus	Unknown	WSouthAmer	Unknown	Unknown	Peru	Unknown
W550942	USNM	550942	T. truncatus	Unknown	Aduncus	Female	1981	South Africa	Karriodere
W550947	USNM	550947	T. truncatus	Unknown	Aduncus	Male	1982	South Africa	Durban
W550969	USNM	550969	T. truncatus	Intermediate	Aduncus	Male	Unknown	Somalia	Eyl
W571388	USNM	571388	T. truncatus	Coastal	Erebennus	Female	1990	USA	Avon, North Carolina
W571477	USNM	571477	T. truncatus	Offshore	Offshore	Female	1991	USA	Cape Henlopen State Park
W571481	USNM	571481	T. truncatus	Offshore	Offshore	Female	1990	USA	Brigantine
W571624	USNM	571624	T. truncatus	Unknown	Erebennus	Unknown	1987	USA	Unknown
W572452	USNM	572452	T. truncatus	Unknown	Erebennus	Female	1999	USA	Norfolk, 986 West Ocean View
W572460	USNM	572460	T. truncatus	Unknown	Erebennus	Female	1999	USA	Hampton, 834 North 1st St, Buckroe Beach
W572560	USNM	572560	T. truncatus	Unknown	Erebennus	Unknown	2000	USA	Fisherman'S Island
W572600	USNM	572600	T. truncatus	Unknown	Erebennus	Male	2000	USA	Corolla, 1.7 Miles N of Albacore Street
W572605	USNM	572605	T. truncatus	Unknown	Offshore	Female	2001	USA	Buxton, 0.7 Miles South of the pooint, Hatteras
W572717	USNM	572717	T. truncatus	Unknown	Erebennus	Female	2000	USA	Frisco, 1 Mi N of Frisco Pier
W572740	USNM	572740	T. truncatus	Unknown	Erebennus	Male	1999	USA	South Core banks
W593398	USNM	593398	T. truncatus	Unknown	Erebennus	Female	2004	USA	Salvo, 0.2 Mi S of R23
W593404	USNM	593404	T. truncatus	Unknown	Erebennus	Male	2004	USA	Hatteras, 2.5 Mi S of R55
W593405	USNM	593405	T. truncatus	Unknown	Erebennus	Female	2004	USA	Harkers Island
W593749	USNM	593749	T. truncatus	Unknown	Erebennus	Male	2002	USA	South Nags Head, 4019 S. Virginia Dare Trail
W593783	USNM	593783	T. truncatus	Unknown	Erebennus	Male	2004	USA	Frisco, 0.3 Mi south of Frisco Pier
W593812	USNM	593812	T. truncatus	Unknown	Erebennus	Unknown	2002	USA	Emerald Isle
W593863	USNM	593863	T. truncatus	Unknown	Offshore	Male	2004	USA	Wachapreague
W594101	USNM	594101	T. truncatus	Unknown	Erebennus	Female	2002	USA	Shallotte Inlet, Hughes Marina, end of village Island road
W594117	USNM	594117	T. truncatus	Unknown	Erebennus	Male	2002	USA	Long Beach, end of 67th St, E
W594121	USNM	594121	T. truncatus	Unknown	Erebennus	Male	2002	USA	Hatteras Village
W594123	USNM	594123	T. truncatus	Unknown	Erebennus	Male	2003	USA	Harkers Island, S Core, Oceanside, Cape Point
W594195	USNM	594195	T. truncatus	Unknown	Erebennus	Female	2000	USA	Frisco, North Carolina
W594632	USNM	594632	T. truncatus	Unknown	WestAfrica	Unknown	2018	Senegal	Lompoul
W605143	USNM	605143	T. truncatus	Unknown	WestAfrica	Unknown	2018	Senegal	Grand Cote
W605144	USNM	605144	T. truncatus	Unknown	WestAfrica	Unknown	2018	Senegal	Near Mboro-sur-Mer
WA288084	USNM	288084	T. truncatus	Coastal	Erebennus	Unknown	1960	USA	Scientist Cliffs
WA395671	USNM	395671	T. truncatus	Intermediate	Erebennus	Unknown	1969	USA	Calvert Cliffs
WA49627	USNM	A49627	T. truncatus	Offshore	Erebennus	Unknown	Unknown	USA	Tampa Bay
WA504273	USNM	504273	T. truncatus	Offshore	Offshore	Female	1975	USA	Rodanthe, Koa Camp Ground
WA504766	USNM	504766	T. truncatus	Offshore	Offshore	Male	1971	USA	Nags head
WA550401	USNM	550401	T. truncatus	Coastal	Erebennus	Male	1984	USA	Norfolk, 9th Bay St, Ocean View
WA550447	USNM	550447	T. truncatus	Offshore	Offshore	Unknown	1985	USA	Truro, Beach point
WA550772	USNM	550772	T. truncatus	Offshore	Offshore	Female	1986	USA	Bodie Island, ramp 4
WA571013	USNM	571013	T. truncatus	Coastal	Erebennus	Female	1987	USA	Norfolk, Ocean view Beach
WA571027	USNM	571027	T. truncatus	Coastal	Erebennus	Male	1987	USA	Ocean City, 43rd St
WA571356	USNM	571356	T. truncatus	Offshore	Offshore	Female	1989	USA	Salvo, 200 M S Ramp 30

WA571557	USNM	571557	T. truncatus	Offshore	Offshore	Male	1992	USA	Cape Henlopen State Park
WA571618	USNM	571618	T. truncatus	Offshore	Offshore	Male	1992	USA	Unknown
WA572321	USNM	572321	T. truncatus	Offshore	Offshore	Male	1998	USA	South Bethany, end of south 9th st
WAA20767	USNM	A20767	T. truncatus	Coastal	Erebennus	Male	1882	USA	Point lookout

Table S4.2.2. Description of the parameters used for the 3D modelling in MESHROOM

	FeatureExtraction		**ImageMatching**			**FeatureMatching Guided matching ticked for all individuals**	**Structure From Motion Use Rig Constraint Unticked for all individuals**				**DepthMap**			**DepthMapFilter**		**Meshing**				**MeshFiltering**
Individuals	Describer Types	Describer Presets	Min number of images	Max descriptors	Number of matches	Describer Type	Describer Types	Minimum Input Track Lenght	Min Observation For Triangulation	Max Reprojection Error	Downscale	SGM:Nb Neighbour Cameras	Refine: Nb Neighbour Cameras	Min Consistent Cameras	Min Consistent Cameras Bad Similarity	Min Observations Angle For SFM Space Estimation	Max Input Points	Max Point	Max Point Per Voxel	Filter Large Triangles Factor
B1011	Sift - Sift_float	normal	80	0	0	Sift - Sift_float	Sift - Sift_float	2	2	4	1	5	6	2	3	10	50000000	5000000	1000000	50
B1041	Sift - Sift_float - akaze	high	80	0	0	Sift - Sift_float - akaze	Sift - Sift_float - akaze	3	1	4	1	5	6	2	3	10	50000000	5000000	1000000	48.5
B1077	Sift - Sift_float - akaze	high	80	0	0	Sift - Sift_float - akaze	Sift - Sift_float - akaze	3	1	4	1	5	6	2	3	10	25000000	2500000	500000	50
B1081	Sift - Sift_float	high	250	500	50	Sift - Sift_float	Sift - Sift_float	2	2	4	1	10	6	3	4	10	10000000	1000000	200000	60
B1089	Sift - Sift_float	normal	80	0	0	Sift - Sift_float	Sift - Sift_float	3	1	4	1	5	6	2	3	10	25000000	2500000	500000	48.5
B1099	Sift - Sift_float	normal	80	0	0	Sift - Sift_float	Sift - Sift_float	3	1	4	1	5	6	2	3	10	15000000	1500000	400000	48.5
B1106	Sift - Sift_float - akaze	normal	80	0	0	Sift - Sift_float - akaze	Sift - Sift_float - akaze	1	1	2	1	Mesh1 - 5 Mesh2 - 3	6	2	3	10	Mesh1 - 25000000 Mesh2 - 25000000	Mesh1 - 2500000 Mesh2- 2500000	Mesh1 - 500000 Mesh2 - 500000	50
B1116	Sift - Sift_float	normal	80	0	0	Sift - Sift_float	Sift - Sift_float	3	1	2	1	5	6	2	3	10	50000000	5000000	1000000	48.5
B1281	Sift - Sift_float	normal	80	0	0	Sift - Sift_float	Sift - Sift_float	3	1	4	1	5	6	2	3	10	50000000	5000000	1000000	48.5
B1287	Sift - Sift_float	normal	80	0	0	Sift - Sift_float	Sift - Sift_float	3	1	4	1	5	6	2	3	10	50000000	5000000	1000000	48.5
B1349	Sift - Sift_float	normal	80	0	0	Sift - Sift_float	Sift - Sift_float	3	1	2	1	5	6	2	3	10	50000000	5000000	1000000	48.5
B1350	Sift - Sift_float	normal	80	0	0	Sift - Sift_float	Sift - Sift_float	3	1	4	1	5	6	2	3	10	50000000	5000000	1000000	48.5
B1395	Sift - Sift_float - akaze	high	80	0	0	Sift - Sift_float - akaze	Sift - Sift_float - akaze	3	1	2	1	5	6	2	3	10	Mesh1 - 50000000 Mesh2 - 15000000	Mesh1 - 5000000 Mesh2 - 1500000	Mesh1 - 1000000 Mesh2 - 250000	48.5
B1398	Sift - Sift_float	normal	80	0	0	Sift - Sift_float	Sift - Sift_float	3	1	4	1	5	6	2	3	10	50000000	5000000	1000000	48.5
B1415	Sift - Sift_float	normal	80	0	0	Sift - Sift_float	Sift - Sift_float	2	2	4	1	5	6	2	3	10	50000000	5000000	1000000	30
B1420	Sift - Sift_float - akaze	high	80	0	0	Sift - Sift_float - akaze	Sift - Sift_float - akaze	3	1	2	1	5	6	2	3	Mesh1 - 60 Mesh2 - 90	Mesh1 - 10000000 Mesh2 - 70000000	Mesh1 - 1000000 Mesh1 - 7000000	Mesh1 - 200000 Mesh1 - 300000	Mesh1 - 48.5 Mesh2 - 48.5
B1489	Sift - Sift_float	normal	80	0	0	Sift - Sift_float	Sift - Sift_float	3	1	4	1	5	6	2	3	10	Mesh1 - 50000000	Mesh1 - 5000000	Mesh1 - 1000000	48.5
B1501	Sift - Sift_float	normal	80	0	0	Sift - Sift_float	Sift - Sift_float	3	1	4	1	5	6	2	3	10	50000000	5000000	1000000	48.5
B1506	Sift - Sift_float	high	200	500	50	Sift - Sift_float	Sift - Sift_float	2	2	4	1	10	6	3	4	Mesh1 - 10 Mesh2 - 5	Mesh1 - 25000000 Mesh2 - 10000000	Mesh1 - 2500000 Mesh2 - 1000000	Mesh1 - 500000 Mesh2 - 200000	Mesh1 - 48.5 Mesh2 - 60

B1631	Sift - Sift_float - akaze	normal	80	0	0	Sift - Sift_float - akaze	Sift - Sift_float - akaze	1	1	2	1	5	6	2	3	10	Mesh1 - 25000000 Mesh2 - 50000000	Mesh1 - 2500000 Mesh2 - 5000000	Mesh1 - 500000 Mesh2 - 1000000	48.5
B1637	Sift - Sift_float	normal	80	0	0	Sift - Sift_float	Sift - Sift_float	3	1	2	1	5	6	2	3	40	Mesh1 - 50000000 Mesh2 - 25000000	Mesh1 - 5000000 Mesh2 - 2500000	Mesh1 - 1000000 Mesh2 - 500000	Mesh1 - 48.5 Mesh2 - 60
C27401	Sift - Sift_float - akaze	normal	200	500	50	Sift - Sift_float - akaze	Sift - Sift_float - akaze	2	2	4	1	10	6	3	4	10	50000000	5000000	1000000	60
C54016	Sift - Sift_float	high	200	500	50	Sift - Sift_float	Sift - Sift_float	2	2	4	1	10	6	3	4	10	Mesh1 - 25000000 Mesh2 - 10000000	Mesh1 - 2500000 Mesh2 - 1000000	Mesh1 - 500000 Mesh2 - 500000	60
C72169	Sift - Sift_float - akaze	normal	200	500	50	Sift - Sift_float - akaze	Sift - Sift_float - akaze	2	2	4	1	10	6		4	10	50000000	5000000	1000000	60
C72294	Sift - Sift_float	high	200	500	50	Sift - Sift_float	Sift - Sift_float	2	2	4	1	10	6	3	4	10	10000000	1000000	500000	60
C72295	Sift - Sift_float	ultra	200	500	50	Sift - Sift_float	Sift - Sift_float	2	2	4	1	15	10	2	3	10	Mesh1 - 25000000 Mesh2 - 10000000	Mesh1 - 2500000 Mesh2 - 1000000	Mesh1 - 500000 Mesh2 - 500000	60
C72493	Sift - Sift_float - akaze	normal	200	500	50	Sift - Sift_float - akaze	Sift - Sift_float - akaze	2	2	4	1	10	6	3	4	10	Mesh1 - 25000000 Mesh2 - 10000000	Mesh1 - 2500000 Mesh2 - 1000000	Mesh1 - 500000 Mesh2 - 100000	60
C84029	Sift - Sift_float	high	200	500	50	Sift - Sift_float	Sift - Sift_float	2	2	4	1	10	6	3	4	10	50000000	5000000	1000000	60
C84034	Sift - Sift_float	high	200	0	0	Sift - Sift_float	Sift - Sift_float	2	2	4	1	10	6	2	3	10	Mesh1 - 50000000 Mesh2 - 10000000	Mesh1 - 5000000 Mesh2 - 1000000	Mesh1 - 1000000 Mesh2 - 100000	60
C84036	Sift - Sift_float	high	200	500	50	Sift - Sift_float	Sift - Sift_float	2	2	4	1	10	6	3	4	10	Mesh1 - 50000000 Mesh2 - 10000000	Mesh1 - 5000000 Mesh2 - 1000000	Mesh1 - 1000000 Mesh2 - 200000	60
C84055	Sift - Sift_float	normal	200	500	50	Sift - Sift_float	Sift - Sift_float	2	2	4	1	10	6	3	4	10	50000000	5000000	1000000	60
C84056	Sift - Sift_float	normal	200	500	50	Sift - Sift_float	Sift - Sift_float	2	2	4	1	10	6	3	4	10	50000000	5000000	1000000	60
C84058	Sift - Sift_float	normal	200	500	50	Sift - Sift_float	Sift - Sift_float	2	2	4	1	10	6	3	4	10	50000000	5000000	1000000	60
C84059	Sift - Sift_float	high	200	500	50	Sift - Sift_float	Sift - Sift_float	2	2	4	1	10	6	3	4	10	Mesh1 - 10000000 Mesh2 - 20000000	Mesh1 - 1000000 Mesh2 - 2000000	Mesh1 - 100000 Mesh2 - 400000	60
C84065	Sift - Sift_float	high	200	500	50	Sift - Sift_float	Sift - Sift_float	2	2	4	1	15	10	2	3	10	Mesh1 - 25000000 Mesh2 - 10000000	Mesh1 - 2500000 Mesh2 - 1000000	Mesh1 - 500000 Mesh2 - 200000	60
C84285	Sift - Sift_float	normal	200	500	50	Sift - Sift_float	Sift - Sift_float	2	2	4	1	10	6	3	4	10	50000000	5000000	1000000	60
C91862	Sift - Sift_float - akaze	normal	200	500	50	Sift - Sift_float - akaze	Sift - Sift_float - akaze	2	2	4	1	15	10	2	3	10	50000000	5000000	1000000	60
C91886	Sift - Sift_float	high	200	500	50	Sift - Sift_float	Sift - Sift_float	2	2	4	1	15	10	3	4	10	Mesh1 - 50000000 Mesh2 - 10000000	Mesh1 - 5000000 Mesh2 - 1000000	Mesh1 - 1000000 Mesh2 - 100000	60
C91913	Sift - Sift_float - akaze	normal	200	500	50	Sift - Sift_float - akaze	Sift - Sift_float - akaze	2	2	4	1	15	10	2	3	10	Mesh1 - 30000000 Mesh2 - 25000000 Mesh3 - 10000000	Mesh1 - 3000000 Mesh2 - 2500000 Mesh3 - 1000000	Mesh1 - 700000 Mesh2 - 500000 Mesh3 - 200000	60
C95366	Sift - Sift_float - akaze	normal	200	500	50	Sift - Sift_float - akaze	Sift - Sift_float - akaze	2	2	4	1	15	10	2	3	10	50000000	5000000	1000000	60
C95387	Sift - Sift_float	normal	200	500	50	Sift - Sift_float	Sift - Sift_float	2	2	4	1	15	10	3	4	10	50000000	5000000	1000000	60

C95459	Sift - Sift_float	high	200	500	50	Sift - Sift_float	Sift - Sift_float	2	2	4	1	10	6	3	4	10	Mesh1 - 50000000 Mesh2 - 25000000 Mesh3 - 10000000	Mesh1 - 5000000 Mesh2 - 2500000 Mesh3 - 1000000	Mesh1 - 1000000 Mesh2 - 500000 Mesh3 - 100000	60
C95471	Sift - Sift_float	high	200	500	50	Sift - Sift_float	Sift - Sift_float	2	2	4	1	10	6	2	3	10	Mesh1 - 25000000 Mesh2 - 50000000	Mesh1 - 2500000 Mesh2 - 5000000	Mesh1 - 500000 Mesh2 - 1000000	60
E117	Sift - Sift_float	normal	200	500	50	Sift - Sift_float	Sift - Sift_float	2	2	4	2	10	6	3	4	10	50000000	5000000	1000000	60
E27	Sift - Sift_float	normal	200	500	50	Sift - Sift_float	Sift - Sift_float	2	2	4	2	10	6	3	4	10	50000000	5000000	1000000	60
E29	Sift - Sift_float	normal	200	500	50	Sift - Sift_float	Sift - Sift_float	2	2	4	2	10	6	3	4	10	50000000	5000000	1000000	60
E37	Sift - Sift_float	normal	200	500	50	Sift - Sift_float	Sift - Sift_float	2	2	4	2	10	6	3	4	10	50000000	5000000	1000000	60
E40	Sift - Sift_float	normal	200	500	50	Sift - Sift_float	Sift - Sift_float	2	2	4	2	10	6	3	4	10	50000000	5000000	1000000	60
E41	Sift - Sift_float	high	200	500	50	Sift - Sift_float	Sift - Sift_float	2	2	4	1	10	6	3	4	80	25000000	2500000	500000	60
E43	Sift - Sift_float	normal	200	500	50	Sift - Sift_float	Sift - Sift_float	2	2	4	2	10	6	3	4	10	50000000	5000000	1000000	60
E48	Sift - Sift_float	normal	200	500	50	Sift - Sift_float	Sift - Sift_float	2	2	4	2	10	6	3	4	10	50000000	5000000	1000000	60
E58	Sift - Sift_float	normal	200	500	50	Sift - Sift_float	Sift - Sift_float	2	2	4	2	10	6	3	4	10	50000000	5000000	1000000	60
E60	Sift - Sift_float	normal	200	500	50	Sift - Sift_float	Sift - Sift_float	2	2	4	2	10	6	3	4	10	50000000	5000000	1000000	60
E61	Sift - Sift_float	normal	200	500	50	Sift - Sift_float	Sift - Sift_float	2	2	4	2	10	6	3	4	10	50000000	5000000	1000000	60
E63	Sift - Sift_float	normal	200	500	50	Sift - Sift_float	Sift - Sift_float	2	2	4	2	10	6	3	4	10	Mesh1 - 50000000 Mesh2 - 25000000	Mesh1 - 5000000 Mesh2 - 2500000	Mesh1 - 1000000 Mesh2 - 500000	60
E64	Sift - Sift_float	normal	200	500	50	Sift - Sift_float	Sift - Sift_float	2	2	4	2	10	6	3	4	10	50000000	5000000	1000000	60
E65	Sift - Sift_float	normal	200	500	50	Sift - Sift_float	Sift - Sift_float	2	2	4	2	10	6	3	4	10	50000000	5000000	1000000	60
E66	Sift - Sift_float	normal	200	500	50	Sift - Sift_float	Sift - Sift_float	2	2	4	2	10	6	3	4	10	50000000	5000000	1000000	60
E69	Sift - Sift_float	high	200	500	50	Sift - Sift_float	Sift - Sift_float	2	2	4	2	10	6	3	4	10	Mesh1 - 50000000 Mesh2 - 25000000	Mesh1 - 5000000 Mesh2 - 2500000	Mesh1 - 1000000 Mesh2 - 500000	60
E70	Sift - Sift_float	normal	200	500	50	Sift - Sift_float	Sift - Sift_float	2	2	4	2	10	6	3	4	10	50000000	5000000	1000000	60
E71	Sift - Sift_float	normal	200	500	50	Sift - Sift_float	Sift - Sift_float	2	2	4	2	10	6	3	4	10	50000000	5000000	1000000	60
E72	Sift - Sift_float	normal	200	500	50	Sift - Sift_float	Sift - Sift_float	2	2	4	2	10	6	3	4	10	50000000	5000000	1000000	60
E73	Sift - Sift_float	normal	200	500	50	Sift - Sift_float	Sift - Sift_float	2	2	4	2	10	6	3	4	10	50000000	5000000	1000000	60
E75	Sift - Sift_float	normal	200	500	50	Sift - Sift_float	Sift - Sift_float	2	2	4	2	10	6	3	4	10	50000000	5000000	1000000	60
E77	Sift - Sift_float	normal	200	500	50	Sift - Sift_float	Sift - Sift_float	2	2	4	2	10	6	3	4	10	50000000	5000000	1000000	60
E78	Sift - Sift_float	normal	200	500	50	Sift - Sift_float	Sift - Sift_float	2	2	4	2	10	6	3	4	10	50000000	5000000	1000000	60
E79	Sift - Sift_float	normal	200	500	50	Sift - Sift_float	Sift - Sift_float	2	2	4	2	10	6	3	4	10	50000000	5000000	1000000	60
G36413	Sift - Sift_float	normal	200	500	50	Sift - Sift_float	Sift - Sift_float	2	2	4	1	10	6	3	4	10	50000000	5000000	1000000	60
G46867	Sift - Sift_float	normal	200	500	50	Sift - Sift_float	Sift - Sift_float	2	2	4	1	10	6	3	4	10	50000000	5000000	1000000	60

G48545	Sift - Sift_float	normal	200	500	50	Sift - Sift_float	Sift - Sift_float	2	2	4	1	10	6	3	4	10	50000000	5000000	1000000	60
G48564	Sift - Sift_float	normal	200	500	50	Sift - Sift_float	Sift - Sift_float	2	2	4	1	10	6	3	4	10	50000000	5000000	1000000	60
G48568	Sift - Sift_float	normal	200	500	50	Sift - Sift_float	Sift - Sift_float	2	2	4	1	10	6	3	4	10	50000000	5000000	1000000	60
G50246	Sift - Sift_float	normal	200	500	50	Sift - Sift_float	Sift - Sift_float	2	2	4	1	10	6	3	4	10	Mesh1 - 50000000 Mesh2 - 10000000	Mesh1 - 5000000 Mesh2 - 1000000	Mesh1 - 1000000 Mesh2 - 200000	60
G50249	Sift - Sift_float	normal	200	500	50	Sift - Sift_float	Sift - Sift_float	2	2	4	1	10	6	3	4	10	50000000	5000000	1000000	60
G50250	Sift - Sift_float	normal	200	500	50	Sift - Sift_float	Sift - Sift_float	2	2	4	1	10	6	3	4	10	50000000	5000000	1000000	60
G54766	Sift - Sift_float	high	200	500	50	Sift - Sift_float	Sift - Sift_float	2	2	4	1	10	6	3	4	10	Mesh1 - 50000000 Mesh2 - 10000000	Mesh1 - 5000000 Mesh2 - 1000000	Mesh1 - 1000000 Mesh2 - 250000	60
JM24788	Sift - Sift_float	high	200	500	50	Sift - Sift_float	Sift - Sift_float	2	2	4	1	10	6	3	4	10	Mesh1 - 50000000 Mesh2 - 25000000	Mesh1 - 5000000 Mesh2 - 2500000	Mesh1 - 1000000 Mesh2 - 500000	60
J24unreg	Sift - Sift_float	high	200	500	50	Sift - Sift_float	Sift - Sift_float	2	2	4	1	10	6	3	4	10	25000000	2500000	500000	60
JM35127	Sift - Sift_float	high	200	500	50	Sift - Sift_float	Sift - Sift_float	2	2	4	1	10	6	3	4	10	Mesh1 - 25000000 Mesh2 - 10000000	Mesh1 - 2500000 Mesh2 - 1000000	Mesh1 - 500000 Mesh2 - 200000	60
L14596	Sift - Sift_float - akaze	normal	200	500	50	Sift - Sift_float - akaze	Sift - Sift_float - akaze	2	2	4	1	10	6	3	4	10	50000000	5000000	1000000	60
L16455	Sift - Sift_float	normal	200	500	50	Sift - Sift_float	Sift - Sift_float	2	2	4	1	10	6	3	4	10	50000000	5000000	1000000	60
L19799	Sift - Sift_float	normal	200	500	50	Sift - Sift_float	Sift - Sift_float	2	2	4	1	10	6	3	4	10	50000000	5000000	1000000	60
L19837	Sift - Sift_float	normal	200	500	50	Sift - Sift_float	Sift - Sift_float	2	2	4	1	10	6	3	4	10	50000000	5000000	1000000	60
L20160	Sift - Sift_float	normal	200	500	50	Sift - Sift_float	Sift - Sift_float	2	2	4	1	10	6	3	4	10	Mesh1 - 50000000 Mesh2 - 25000000	Mesh1 - 5000000 Mesh2 - 2500000	Mesh1 - 1000000 Mesh2 - 500000	60
L20328	Sift - Sift_float	normal	200	500	50	Sift - Sift_float	Sift - Sift_float	2	2	4	1	10	6	3	4	10	50000000	5000000	1000000	60
L20900	Sift - Sift_float	normal	200	500	50	Sift - Sift_float	Sift - Sift_float	2	2	4	1	10	6	3	4	10	Mesh1 - 50000000 Mesh2 - 30000000	Mesh1 - 5000000 Mesh2 - 3000000	Mesh1 - 1000000 Mesh2 - 602409	60
L2113	Sift - Sift_float	normal	200	500	50	Sift - Sift_float	Sift - Sift_float	2	2	4	1	10	6	3	4	10	50000000	5000000	1000000	60
L21173	Sift - Sift_float - akaze	normal	200	500	50	Sift - Sift_float - akaze	Sift - Sift_float - akaze	2	2	4	1	10	6	3	4	10	Mesh1 - 50000000 Mesh2 - 10000000	Mesh1 - 5000000 Mesh2 - 1000000	Mesh1 - 1000000 Mesh2 - 200000	60
L21434	Sift - Sift_float	high	200	500	50	Sift - Sift_float	Sift - Sift_float	2	2	4	1	10	6	3	4	Mesh1 - 10 Mesh2 - 10 Mesh3 - 2	Mesh1 - 50000000 Mesh2 - 10000000 Mesh3 - 50000000	Mesh1 - 5000000 Mesh2 - 1000000 Mesh3 - 5000000	Mesh1 - 1000000 Mesh2 - 100000 Mesh3 - 1000000	60
L21452	Sift - Sift_float	normal	200	500	50	Sift - Sift_float	Sift - Sift_float	2	2	4	1	10	6	3	4	10	50000000	5000000	1000000	60
L2330	Sift - Sift_float	normal	200	500	50	Sift - Sift_float	Sift - Sift_float	2	2	4	1	10	6	3	4	10	50000000	5000000	1000000	60
L24677	Sift - Sift_float	normal	200	500	50	Sift - Sift_float	Sift - Sift_float	2	2	4	1	10	6	3	4	10	50000000	5000000	1000000	60
L24678	Sift - Sift_float	normal	200	500	50	Sift - Sift_float	Sift - Sift_float	2	2	4	1	10	6	3	4	10	50000000	5000000	1000000	60
L24679	Sift - Sift_float	normal	200	500	50	Sift - Sift_float	Sift - Sift_float	2	2	4	1	10	6	3	4	10	50000000	5000000	1000000	60

L24680	Sift - Sift_float	normal	200	500	50	Sift - Sift_float	Sift - Sift_float	2	2	4	1	10	6	3	4	10	50000000	5000000	1000000	60
L26121	Sift - Sift_float	normal	200	500	50	Sift - Sift_float	Sift - Sift_float	2	2	4	1	10	6	3	4	10	50000000	5000000	1000000	60
L27044	Sift - Sift_float	normal	200	500	50	Sift - Sift_float	Sift - Sift_float	2	2	4	1	10	6	3	4	10	50000000	5000000	1000000	60
L28061	Sift - Sift_float	normal	200	500	50	Sift - Sift_float	Sift - Sift_float	2	2	4	1	10	6	3	4	10	50000000	5000000	1000000	60
L31148	Sift	normal	200	500	50	Sift	Sift	2	2	4	1	10	6	3	4	10	50000000	5000000	1000000	60
L31193	Sift - Sift_float	normal	200	500	50	Sift - Sift_float	Sift - Sift_float	2	2	4	1	10	6	3	4	10	50000000	5000000	1000000	60
L32350	Sift - Sift_float	normal	200	500	50	Sift - Sift_float	Sift - Sift_float	2	2	4	1	10	6	3	4	10	50000000	5000000	1000000	60
L32352	Sift - Sift_float - akaze	normal	200	500	50	Sift - Sift_float - akaze	Sift - Sift_float - akaze	2	2	4	1	10	6	3	4	10	25000000	2500000	500000	60
L5000071	Sift - Sift_float	high	200	500	50	Sift - Sift_float	Sift - Sift_float	2	2	4	1	10	6	3	4	10	25000000	2500000	500000	60
L7964	Sift - Sift_float	high	200	500	50	Sift - Sift_float	Sift - Sift_float	2	2	4	1	10	6	3	4	10	50000000	5000000	1000000	60
L7965	Sift - Sift_float - akaze	normal	200	500	50	Sift - Sift_float - akaze	Sift - Sift_float - akaze	2	2	4	1	10	6	3	4	10	50000000	5000000	1000000	60
L8617	Sift - Sift_float	normal	200	500	50	Sift - Sift_float	Sift - Sift_float	2	2	4	1	10	6	3	4	10	50000000	5000000	1000000	60
M00470	Sift - Sift_float	high	200	500	50	Sift - Sift_float	Sift - Sift_float	2	2	4	1	10	6	3	4	10	10000000	1000000	200000	60
M03968	Sift - Sift_float	normal	200	500	50	Sift - Sift_float	Sift - Sift_float	2	2	4	1	10	6	3	4	10	50000000	5000000	1000000	60
M04900	Sift - Sift_float	normal	200	500	50	Sift - Sift_float	Sift - Sift_float	2	2	4	1	10	6	3	4	10	50000000	5000000	1000000	60
M04902	Sift - Sift_float - akaze	high	200	500	50	Sift - Sift_float - akaze	Sift - Sift_float - akaze	2	2	4	1	10	6	3	4	10	Mesh1 - 50000000 Mesh2 - 25000000	Mesh1 - 5000000 Mesh2 - 2500000	Mesh1 - 1000000 Mesh2 - 500000	60
M04919	Sift - Sift_float	normal	200	500	50	Sift - Sift_float	Sift - Sift_float	2	2	4	1	10	6	3	4	10	50000000	5000000	1000000	60
M06694	Sift - Sift_float	normal	200	500	50	Sift - Sift_float	Sift - Sift_float	2	2	4	1	10	6	3	4	10	50000000	5000000	1000000	60
M07279	Sift - Sift_float	high	200	500	50	Sift - Sift_float	Sift - Sift_float	2	2	4	1	10	6	3	4	10	50000000	5000000	1000000	60
P014	Sift - Sift_float	normal	200	500	50	Sift - Sift_float	Sift - Sift_float	2	2	4	1	10	6	3	4	10	Mesh1 - 50000000 Mesh2 - 25000000 Mesh3 - 10000000	Mesh1 - 5000000 Mesh2 - 2500000 Mesh3 - 1000000	Mesh1 - 1000000 Mesh2 - 500000 Mesh3 - 250000	60
P1006	Sift - Sift_float	high	200	500	50	Sift - Sift_float	Sift - Sift_float	2	2	4	1	10	6	3	4	10	Mesh1 - 50000000 Mesh2 - 25000000	Mesh1 - 5000000 Mesh2 - 2500000	Mesh1 - 1000000 Mesh2 - 500000	60
P115	Sift - Sift_float	normal	200	500	50	Sift - Sift_float	Sift - Sift_float	2	2	4	1	10	6	3	4	10	50000000	5000000	1000000	60
P1157	Sift - Sift_float	normal	200	500	50	Sift - Sift_float	Sift - Sift_float	2	2	4	1	10	6	3	4	10	50000000	5000000	1000000	60
P131	Sift - Sift_float	normal	200	500	50	Sift - Sift_float	Sift - Sift_float	2	2	4	1	10	6	3	4	10	50000000	5000000	1000000	60
P138	Sift - Sift_float	normal	200	500	50	Sift - Sift_float	Sift - Sift_float	2	2	4	1	10	6	3	4	10	50000000	5000000	1000000	60
P1502	Sift - Sift_float	normal	200	500	50	Sift - Sift_float	Sift - Sift_float	2	2	4	1	10	6	3	4	10	50000000	5000000	1000000	60
P158	Sift - Sift_float	normal	200	500	50	Sift - Sift_float	Sift - Sift_float	2	2	4	1	10	6	3	4	10	50000000	5000000	1000000	60
P161	Sift - Sift_float	normal	200	500	50	Sift - Sift_float	Sift - Sift_float	2	2	4	1	10	6	3	4	10	50000000	5000000	1000000	60

P176	Sift - Sift_float	high	200	500	50	Sift - Sift_float	Sift - Sift_float	2	2	4	1	10	6	3	4	10	Mesh1 - 50000000 Mesh2 - 25000000 Mesh3 - 10000000	Mesh1 - 5000000 Mesh2 - 2500000 Mesh3 - 1000000	Mesh1 - 1000000 Mesh2 - 500000 Mesh3 - 200000	60
P198	Sift - Sift_float	normal	200	500	50	Sift - Sift_float	Sift - Sift_float	2	2	4	1	10	6	3	4	10	50000000	5000000	1000000	60
P199	Sift - Sift_float	normal	200	500	50	Sift - Sift_float	Sift - Sift_float	2	2	4	1	10	6	3	4	10	50000000	5000000	1000000	60
P208	Sift - Sift_float	normal	200	500	50	Sift - Sift_float	Sift - Sift_float	2	2	4	1	10	6	3	4	10	50000000	5000000	1000000	60
P304	Sift - Sift_float	normal	200	500	50	Sift - Sift_float	Sift - Sift_float	2	2	4	1	10	6	3	4	10	50000000	5000000	1000000	60
P67	Sift - Sift_float	high	200	500	50	Sift - Sift_float	Sift - Sift_float	2	2	4	1	10	6	3	4	10	25000000	2500000	500000	60
P75	Sift - Sift_float	normal	200	500	50	Sift - Sift_float	Sift - Sift_float	2	2	4	1	10	6	3	4	10	50000000	5000000	1000000	60
PA3070	Sift - Sift_float	high	80	0	0	Sift - Sift_float	Sift - Sift_float	3	1	4	1	10	6	3	4	10	Mesh1 - 50000000 Mesh2 - 25000000	Mesh1 - 5000000 Mesh2 - 2500000	Mesh1 - 1000000 Mesh2 - 500000	60
PA3082	Sift - Sift_float	normal	200	500	50	Sift - Sift_float	Sift - Sift_float	2	2	4	1	10	6	3	4	10	50000000	5000000	1000000	60
S045704	Sift - Sift_float - akaze	normal	200	500	50	Sift - Sift_float - akaze	Sift - Sift_float - akaze	2	2	4	1	10	6	3	4	10	Mesh1 - 50000000 Mesh2 - 25000000	Mesh1 - 6494000 Mesh2 - 2500000	Mesh1 - 1000000 Mesh2 - 500000	60
S045706	Sift - Sift_float	high	200	500	50	Sift - Sift_float	Sift - Sift_float	2	2	4	1	10	6	3	4	10	50000000	5000000	1000000	60
S045707	Sift - Sift_float	normal	200	500	50	Sift - Sift_float	Sift - Sift_float	2	2	4	1	10	6	3	4	10	50000000	5000000	1000000	60
S045708	Sift - Sift_float	high	200	500	50	Sift - Sift_float	Sift - Sift_float	2	2	4	1	10	6	3	4	10	Mesh1 - 50000000 Mesh2 - 25000000 Mesh3 - 10000000	Mesh1 - 5000000 Mesh2 - 2500000 Mesh3 - 1000000	Mesh1 - 1000000 Mesh2 - 500000 Mesh3 - 200000	60
S045709	Sift - Sift_float	normal	200	500	50	Sift - Sift_float	Sift - Sift_float	2	2	4	1	10	6	3	4	10	50000000	5000000	1000000	60
S045710	Sift - Sift_float	high	200	500	50	Sift - Sift_float	Sift - Sift_float	2	2	4	1	10	6	3	4	10	50000000	5000000	1000000	60
S045711	Sift - Sift_float	normal	200	500	50	Sift - Sift_float	Sift - Sift_float	2	2	4	1	10	6	3	4	10	50000000	5000000	1000000	60
S045715	Sift - Sift_float	high	200	500	50	Sift - Sift_float	Sift - Sift_float	2	2	4	1	10	6	3	4	10	Mesh1 - 25000000 Mesh2 - 10000000	Mesh1 - 2500000 Mesh2 - 1000000	Mesh1 - 500000 Mesh2 - 100000	60
S045716	Sift - Sift_float	high	200	500	50	Sift - Sift_float	Sift - Sift_float	2	2	4	1	10	6	3	4	10	Mesh1 - 50000000 Mesh2 - 30000000	Mesh1 - 5000000 Mesh2 - 3000000	Mesh1 - 1000000 Mesh2 - 700000	60
S045720	Sift - Sift_float - akaze	high	200	500	50	Sift - Sift_float - akaze	Sift - Sift_float - akaze	2	2	4	1	10	6	3	4	10	Mesh1 - 50000000 Mesh2 - 25000000 Mesh3 - 10000000	Mesh1 - 5000000 Mesh2 - 2500000 Mesh3 - 1000000	Mesh1 - 1000000 Mesh2 - 500000 Mesh3 - 200000	60
S045722	Sift - Sift_float	normal	200	500	50	Sift - Sift_float	Sift - Sift_float	2	2	4	1	10	6	3	4	10	50000000	5000000	1000000	60
S046597	Sift - Sift_float	normal	200	500	50	Sift - Sift_float	Sift - Sift_float	2	2	4	1	10	6	3	4	10	50000000	5000000	1000000	60
S046790	Sift - Sift_float	normal	200	500	50	Sift - Sift_float	Sift - Sift_float	2	2	4	1	10	6	3	4	10	50000000	5000000	1000000	60
S046791	Sift - Sift_float	normal	200	500	50	Sift - Sift_float	Sift - Sift_float	2	2	4	1	10	6	3	4	10	50000000	5000000	1000000	60
S046792	Sift - Sift_float	normal	200	500	50	Sift - Sift_float	Sift - Sift_float	2	2	4	1	10	6	3	4	10	50000000	5000000	1000000	60

Bottlenose Dolphin 3D Skull Morphology

S046793	Sift - Sift_float	high	200	500	50	Sift - Sift_float	Sift - Sift_float	2	2	4	1	10	6	3	4	10	Mesh1 - 10000000 Mesh2 - 25000000	Mesh1 - 1000000 Mesh2 - 2500000	Mesh1 - 200000 Mesh2 - 500000	60
S050302	Sift - Sift_float	normal	200	500	50	Sift - Sift_float	Sift - Sift_float	2	2	4	1	10	6	3	4	10	50000000	5000000	1000000	60
W12054	Sift - Sift_float	normal	200	500	50	Sift - Sift_float	Sift - Sift_float	2	2	4	1	10	6	3	4	10	50000000	5000000	1000000	60
W16504	Sift - Sift_float	normal	200	500	50	Sift - Sift_float	Sift - Sift_float	2	2	4	1	10	6	3	4	10	50000000	5000000	1000000	60
W16505	Sift - Sift_float	normal	200	500	50	Sift - Sift_float	Sift - Sift_float	2	2	4	1	10	6	3	4	10	50000000	5000000	1000000	60
W176349	Sift - Sift_float	normal	200	500	50	Sift - Sift_float	Sift - Sift_float	2	2	4	1	10	6	3	4	10	50000000	5000000	1000000	60
W176350	Sift - Sift_float	normal	200	500	50	Sift - Sift_float	Sift - Sift_float	2	2	4	1	10	6	3	4	10	50000000	5000000	1000000	60
W176351	Sift - Sift_float	normal	200	500	50	Sift - Sift_float	Sift - Sift_float	2	2	4	1	10	6	3	4	10	50000000	5000000	1000000	60
W176352	Sift - Sift_float	normal	200	500	50	Sift - Sift_float	Sift - Sift_float	2	2	4	1	10	6	3	4	10	50000000	5000000	1000000	60
W176353	Sift - Sift_float	normal	200	500	50	Sift - Sift_float	Sift - Sift_float	2	2	4	1	10	6	3	4	10	50000000	5000000	1000000	60
W254634	Sift - Sift_float	normal	200	500	50	Sift - Sift_float	Sift - Sift_float	2	2	4	1	10	6	3	4	10	50000000	5000000	1000000	60
W254910	Sift - Sift_float	normal	200	500	50	Sift - Sift_float	Sift - Sift_float	2	2	4	1	10	6	3	4	10	Mesh1 - 50000000 Mesh2 - 25000000	Mesh1 - 5000000 Mesh2 - 2500000	Mesh1 - 1000000 Mesh2 - 500000	60
W277170	Sift - Sift_float	normal	200	500	50	Sift - Sift_float	Sift - Sift_float	2	2	4	1	10	6	3	4	10	50000000	5000000	1000000	60
W298239	Sift - Sift_float	normal	200	500	50	Sift - Sift_float	Sift - Sift_float	2	2	4	1	10	6	3	4	10	50000000	5000000	1000000	60
W395381	Sift - Sift_float	normal	200	500	50	Sift - Sift_float	Sift - Sift_float	2	2	4	1	10	6	3	4	10	50000000	5000000	1000000	60
W395733	Sift - Sift_float	normal	200	500	50	Sift - Sift_float	Sift - Sift_float	2	2	4	1	10	6	3	4	10	50000000	5000000	1000000	60
W395924	Sift - Sift_float	normal	200	500	50	Sift - Sift_float	Sift - Sift_float	2	2	4	1	10	6	3	4	10	50000000	5000000	1000000	60
W396165	Sift - Sift_float	normal	200	500	50	Sift - Sift_float	Sift - Sift_float	2	2	4	1	10	6	3	4	10	50000000	5000000	1000000	60
W470551	Sift - Sift_float	normal	200	500	50	Sift - Sift_float	Sift - Sift_float	2	2	4	1	10	6	3	4	10	50000000	5000000	1000000	60
W470553	Sift - Sift_float	normal	200	500	50	Sift - Sift_float	Sift - Sift_float	2	2	4	1	10	6	3	4	10	50000000	5000000	1000000	60
W470554	Sift - Sift_float	normal	200	500	50	Sift - Sift_float	Sift - Sift_float	2	2	4	1	10	6	3	4	10	50000000	5000000	1000000	60
W470555	Sift - Sift_float	normal	200	500	50	Sift - Sift_float	Sift - Sift_float	2	2	4	1	10	6	3	4	10	50000000	5000000	1000000	60
W470556	Sift - Sift_float	normal	200	500	50	Sift - Sift_float	Sift - Sift_float	2	2	4	1	10	6	3	4	10	50000000	5000000	1000000	60
W501197	Sift - Sift_float	normal	200	500	50	Sift - Sift_float	Sift - Sift_float	2	2	4	1	10	6	3	4	10	50000000	5000000	1000000	60
W504236	Sift - Sift_float	normal	200	500	50	Sift - Sift_float	Sift - Sift_float	2	2	4	1	10	6	3	4	10	50000000	5000000	1000000	60
W550021	Sift - Sift_float	normal	200	500	50	Sift - Sift_float	Sift - Sift_float	2	2	4	1	10	6	3	4	10	50000000	5000000	1000000	60
W550097	Sift - Sift_float - akaze	normal	200	500	50	Sift - Sift_float - akaze	Sift - Sift_float - akaze	2	2	4	1	10	6	3	4	10	25000000	2500000	500000	60
W550125	Sift - Sift_float	normal	200	500	50	Sift - Sift_float	Sift - Sift_float	2	2	4	1	10	6	3	4	10	50000000	5000000	1000000	60
W550164	Sift - Sift_float	normal	200	500	50	Sift - Sift_float	Sift - Sift_float	2	2	4	1	10	6	3	4	10	50000000	5000000	1000000	60
W550166	Sift - Sift_float	normal	200	500	50	Sift - Sift_float	Sift - Sift_float	2	2	4	1	10	6	3	4	10	50000000	5000000	1000000	60
W550167	Sift - Sift_float	normal	200	500	50	Sift - Sift_float	Sift - Sift_float	2	2	4	1	10	6	3	4	10	50000000	5000000	1000000	60

W550169	Sift - Sift_float	normal	200	500	50	Sift - Sift_float	Sift - Sift_float	2	2	4	1	10	6	3	4	10	50000000	5000000	1000000	60
W550170	Sift - Sift_float	normal	200	500	50	Sift - Sift_float	Sift - Sift_float	2	2	4	1	10	6	3	4	10	Mesh1 - 50000000 Mesh2 - 25000000 Mesh3 - 90000000	Mesh1 - 5000000 Mesh2 - 2500000 Mesh3 - 9000000	Mesh1 - 1000000 Mesh2 - 500000 Mesh3 - 5000000	60
W550171	Sift - Sift_float	normal	200	500	50	Sift - Sift_float	Sift - Sift_float	2	2	4	1	10	6	3	4	10	50000000	5000000	1000000	60
W550172	Sift - Sift_float	normal	200	500	50	Sift - Sift_float	Sift - Sift_float	2	2	4	1	10	6	3	4	10	50000000	5000000	1000000	60
W550173	Sift - Sift_float	normal	200	500	50	Sift - Sift_float	Sift - Sift_float	2	2	4	1	10	6	3	4	10	50000000	5000000	1000000	60
W550174	Sift - Sift_float - akaze - akaze_liop	normal	200	500	50	Sift - Sift_float - akaze - akaze_liop	Sift - Sift_float - akaze - akaze_liop	2	2	4	1	10	6	3	4	10	Mesh1 - 50000000 Mesh2 - 25000000 Mesh3 - 90000000	Mesh1 - 5000000 Mesh2 - 2500000 Mesh3 - 9000000	Mesh1 - 1000000 Mesh2 - 500000 Mesh3 - 5000000	60
W550175	Sift - Sift_float	normal	200	500	50	Sift - Sift_float	Sift - Sift_float	2	2	4	1	10	6	3	4	10	50000000	5000000	1000000	60
W550193	Sift - Sift_float	normal	200	500	50	Sift - Sift_float	Sift - Sift_float	2	2	4	1	10	6	3	4	10	50000000	5000000	1000000	60
W550194	Sift - Sift_float	normal	200	500	50	Sift - Sift_float	Sift - Sift_float	2	2	4	1	10	6	3	4	10	50000000	5000000	1000000	60
W550265	Sift - Sift_float	normal	200	500	50	Sift - Sift_float	Sift - Sift_float	2	2	4	1	10	6	3	4	10	50000000	5000000	1000000	60
W550306	Sift - Sift_float	high	200	500	50	Sift - Sift_float	Sift - Sift_float	2	2	4	1	10	6	3	4	10	50000000	5000000	1000000	60
W550795	Sift - Sift_float	normal	200	500	50	Sift - Sift_float	Sift - Sift_float	2	2	4	1	10	6	3	4	10	50000000	5000000	1000000	60
W550798	Sift - Sift_float	normal	200	500	50	Sift - Sift_float	Sift - Sift_float	2	2	4	1	10	6	3	4	10	50000000	5000000	1000000	60
W550942	Sift - Sift_float	normal	200	500	50	Sift - Sift_float	Sift - Sift_float	2	2	4	1	10	6	3	4	10	50000000	5000000	1000000	60
W550947	Sift - Sift_float	normal	200	500	50	Sift - Sift_float	Sift - Sift_float	2	2	4	1	10	6	3	4	10	50000000	5000000	1000000	60
W550969	Sift - Sift_float	normal	200	500	50	Sift - Sift_float	Sift - Sift_float	2	2	4	1	10	6	3	4	10	50000000	5000000	1000000	60
W571388	Sift - Sift_float	high	200	500	50	Sift - Sift_float	Sift - Sift_float	2	2	4	1	10	6	3	4	10	Mesh1 - 50000000 Mesh2 - 25000000	Mesh1 - 5000000 Mesh2 - 2500000	Mesh1 - 1000000 Mesh2 - 500000	60
W571477	Sift - Sift_float	normal	200	500	50	Sift - Sift_float	Sift - Sift_float	2	2	4	1	10	6	3	4	10	50000000	5000000	1000000	60
W571481	Sift - Sift_float	normal	200	500	50	Sift - Sift_float	Sift - Sift_float	2	2	4	1	10	6	3	4	10	50000000	5000000	1000000	60
W571624	Sift - Sift_float	normal	200	500	50	Sift - Sift_float	Sift - Sift_float	2	2	4	1	10	6	3	4	10	50000000	5000000	1000000	60
W572452	Sift - Sift_float	normal	200	500	50	Sift - Sift_float	Sift - Sift_float	2	2	4	1	10	6	3	4	10	50000000	5000000	1000000	60
W572460	Sift - Sift_float	high	200	500	50	Sift - Sift_float	Sift - Sift_float	2	2	4	1	10	6	3	4	10	Mesh1 - 50000000 Mesh2 - 10000000	Mesh1 - 5000000 Mesh2 - 1000000	Mesh1 - 1000000 Mesh2 - 200000	60
W572560	Sift - Sift_float	high	200	500	50	Sift - Sift_float	Sift - Sift_float	2	2	4	1	10	6	3	4	10	50000000	5000000	1000000	60
W572600	Sift - Sift_float	normal	200	500	50	Sift - Sift_float	Sift - Sift_float	2	2	4	1	10	6	3	4	10	50000000	5000000	1000000	60
W572605	Sift - Sift_float	normal	200	500	50	Sift - Sift_float	Sift - Sift_float	2	2	4	1	10	6	3	4	10	50000000	5000000	1000000	60
W572717	Sift - Sift_float	normal	200	500	50	Sift - Sift_float	Sift - Sift_float	2	2	4	1	10	6	3	4	10	Mesh1 - 50000000 Mesh2 - 25000000	Mesh1 - 5000000 Mesh2 - 2500000	Mesh1 - 1000000 Mesh2 - 500000	60

W572740	Sift - Sift_float	normal	200	500	50	Sift - Sift_float	Sift - Sift_float	2	2	4	1	10	6	3	4	10	Mesh1 - 35000000 Mesh2 - 25000000	Mesh1 - 3500000 Mesh2 - 2500000	Mesh1 - 650000 Mesh2 - 500000	60
W593398	Sift - Sift_float	normal	250	500	50	Sift - Sift_float	Sift - Sift_float	2	2	4	1	10	6	3	4	10	30000000	3000000	700000	60
W593404	Sift - Sift_float	normal	200	500	50	Sift - Sift_float	Sift - Sift_float	2	2	4	1	10	6	3	4	10	50000000	5000000	1000000	60
W593405	Sift - Sift_float	high	200	500	50	Sift - Sift_float	Sift - Sift_float	2	2	4	1	10	6	3	4	10	50000000	5000000	1000000	60
W593749	Sift - Sift_float	normal	200	500	50	Sift - Sift_float	Sift - Sift_float	2	2	4	1	10	6	3	4	10	50000000	5000000	1000000	60
W593783	Sift - Sift_float	normal	200	500	50	Sift - Sift_float	Sift - Sift_float	2	2	4	1	10	6	3	4	10	Mesh1 - 50000000 Mesh2 - 30000000 Mesh3 - 10000000	Mesh1 - 5000000 Mesh2 - 3000000 Mesh3 - 1000000	Mesh1 - 1000000 Mesh2 - 800000 Mesh3 - 500000	60
W593812	Sift - Sift_float	normal	200	500	50	Sift - Sift_float	Sift - Sift_float	2	2	4	1	10	6	3	4	10	50000000	5000000	1000000	60
W593863	Sift - Sift_float	normal	200	500	50	Sift - Sift_float	Sift - Sift_float	2	2	4	1	10	6	3	4	10	50000000	5000000	1000000	60
W594101	Sift - Sift_float - akaze	normal	200	500	50	Sift - Sift_float - akaze	Sift - Sift_float - akaze	2	2	4	1	10	6	3	4	10	Mesh1 - 50000000 Mesh2 - 25000000	Mesh1 - 5000000 Mesh2 - 2500000	Mesh1 - 1000000 Mesh2 - 500000	60
W594117	Sift - Sift_float	normal	200	500	50	Sift - Sift_float	Sift - Sift_float	2	2	4	1	10	6	3	4	10	25000000	2500000	500000	60
W594121	Sift - Sift_float	normal	200	500	50	Sift - Sift_float	Sift - Sift_float	2	2	4	1	10	6	3	4	10	50000000	5000000	1000000	60
W594123	Sift - Sift_float	high	200	500	50	Sift - Sift_float	Sift - Sift_float	2	2	4	1	10	6	3	4	10	Mesh1 - 50000000 Mesh2 - 25000000	Mesh1 - 5000000 Mesh2 - 2500000	Mesh1 - 1000000 Mesh2 - 500000	60
W594195	Sift - Sift_float	normal	200	500	50	Sift - Sift_float	Sift - Sift_float	2	2	4	1	10	6	3	4	10	50000000	5000000	1000000	60
W594632	Sift - Sift_float - akaze	normal	200	500	50	Sift - Sift_float - akaze	Sift - Sift_float - akaze	2	2	4	1	10	6	3	4	10	Mesh1 - 50000000 Mesh2 - 25000000	Mesh1 - 5000000 Mesh2 - 2500000	Mesh1 - 1000000 Mesh2 - 2500000	60
W605143	Sift - Sift_float	normal	200	500	50	Sift - Sift_float	Sift - Sift_float	2	2	4	1	10	6	3	4	10	50000000	5000000	1000000	60
W605144	Sift - Sift_float	normal	200	500	50	Sift - Sift_float	Sift - Sift_float	2	2	4	1	10	6	3	4	10	50000000	5000000	1000000	60
WA288084	Sift - Sift_float	normal	200	500	50	Sift - Sift_float	Sift - Sift_float	2	2	4	1	10	6	3	4	10	50000000	5000000	1000000	60
WA395671	Sift - Sift_float	high	200	500	50	Sift - Sift_float	Sift - Sift_float	2	2	4	1	10	6	3	4	10	25000000	2500000	500000	60
WA49627	Sift - Sift_float	high	200	500	50	Sift - Sift_float	Sift - Sift_float	2	2	4	1	10	6	3	4	10	50000000	5000000	1000000	60
WA504273	Sift - Sift_float	normal	200	500	50	Sift - Sift_float	Sift - Sift_float	2	2	4	1	10	6	3	4	10	50000000	5000000	1000000	60
WA504766	Sift - Sift_float	normal	200	500	50	Sift - Sift_float	Sift - Sift_float	2	2	4	1	10	6	3	4	10	50000000	5000000	1000000	60
WA550401	Sift - Sift_float	high	200	500	50	Sift - Sift_float	Sift - Sift_float	2	2	4	1	10	6	3	4	10	50000000	5000000	1000000	60
WA550447	Sift - Sift_float	normal	200	500	50	Sift - Sift_float	Sift - Sift_float	2	2	4	1	10	6	3	4	10	50000000	5000000	1000000	60
WA550772	Sift - Sift_float	high	200	500	50	Sift - Sift_float	Sift - Sift_float	2	2	4	1	10	6	3	4	10	50000000	5000000	1000000	60
WA571013	Sift - Sift_float	high	200	500	50	Sift - Sift_float	Sift - Sift_float	2	2	4	1	10	6	3	4	10	Mesh1 - 50000000 Mesh2 - 25000000 Mesh3 - 10000000	Mesh1 - 5000000 Mesh2 - 2500000 Mesh3 - 1000000	Mesh1 - 1000000 Mesh2 - 500000 Mesh3 - 200000	60

WA571027	Sift - Sift_float	high	200	500	50	Sift - Sift_float	Sift - Sift_float	2	2	4	1	10	6	3	4	10	50000000	5000000	1000000	60
WA571356	Sift - Sift_float	high	200	500	50	Sift - Sift_float	Sift - Sift_float	2	2	4	1	10	6	3	4	10	50000000	5000000	1000000	60
WA571557	Sift - Sift_float	high	200	500	50	Sift - Sift_float	Sift - Sift_float	2	2	4	1	10	6	3	4	10	50000000	5000000	1000000	60
WA571618	Sift - Sift_float	normal	200	500	50	Sift - Sift_float	Sift - Sift_float	2	2	4	1	10	6		4	10	50000000	5000000	1000000	60
WA572321	Sift - Sift_float	high	200	500	50	Sift - Sift_float	Sift - Sift_float	2	2	4	1	10	6	3	4	10	50000000	5000000	1000000	60
WAA20767	Sift - Sift_float	high	200	500	50	Sift - Sift_float	Sift - Sift_float	2	2	4	1	10	6	3	4	10	50000000	5000000	1000000	60

Table S4.2.3. Settings for registration and landmark placement in 3D Slicer using PseudoLMGenerator and ALPACA for Surface semi-landmarking and MALPACA for Homologous Landmarking.

	Type of Landmarking		
Parameter	**SSL** (PseudoLMGenerator)	**HL** (MALPACA)	**SSL** (ALPACA)
Alpha	-	2	2
Beta	-	2	2
Point Density	-	**1**	**0.5**
Spacing Tolerance	**2.5**	0.001	0.001

Table S4.2.4. Description of the homologous landmarks (HL) used in this study, as shown in Figure 3 (Chapter 4)

LANDMARKS	LANDMARK DESCRIPTION
	DORSAL VIEW
S000	Right rostral tip
S001	Left rostral tip
S002	The most dorsal point of the rostrum on the midline at 1/6 of the distance between the anterior tip of the rostrum and the anterior orbit.
S003	The most dorsal point of the rostrum on the midline at 1/3 of the distance between the anterior tip of the rostrum and the anterior orbit.
S004	The most dorsal point of the rostrum on the midline at 1/2 of the distance between the anterior tip of the rostrum and the anterior orbit.
S005	The most dorsal point rostrum and the anterior orbit.
S006	The most dorsal point of the rostrum on the midline at 5/6 of the distance between the anterior tip of the rostrum and the anterior orbit.
S007	The most dorsal point in line with the anterior orbit.
S008	The most right lateral point at 1/6 of the distance between the anterior tip of the rostrum and the anterior point of the orbits.
S009	The most left lateral point at 1/6 of the distance between the anterior tip of the rostrum and the anterior point of the orbits.
S010	The most right lateral point at 1/3 of the distance between the anterior tip of the rostrum and the anterior point of the orbits.
S011	The most left lateral point at 1/3 of the distance between the anterior tip of the rostrum and the anterior point of the orbits.
S012	The most right lateral point at 1/2 of the distance between the anterior tip of the rostrum and the anterior point of the orbits.
S013	The most left lateral point at 1/2 of the distance between the anterior tip of the rostrum and the anterior point of the orbits.
S014	The most right lateral point at 2/3 of the distance between the anterior tip of the rostrum and the anterior point of the orbits.
S015	The most left lateral point at 2/3 of the distance between the anterior tip of the rostrum and the anterior point of the orbits.
S016	The most right lateral point in line with the anterior orbit.
S017	The most left lateral point in line with the anterior orbit.
S018	The left highest point of the rostrum (Melon attachment).
S019	The right highest point of the rostrum (Melon attachment).
S020	Right Antorbital notch

S021	Left antorbital notch
S022	Right premaxillary foramen
S023	Left premaxillary foramen
S024	Right upper tip of the premaxillary
S025	Left upper tip of the premaxillary
S026	Maximum deflection point of the right nasal opening
S027	Maximum deflection point of the left nasal opening
S028	The anterior midpoint of the suture between nasal points
S029	Anteriormost point of the suture between the frontal and interparietal bones
S030	Lateralmost extension of the right nasal bone.
S031	Lateralmost extension of left nasal bone
S032	Right Anterior margin of the posterior dorsal infraorbital foramen
S033	Left Anterior margin of the posterior dorsal infraorbital foramen
S034	Right posterior margin of the posterior dorsal infraorbital foramen
S035	Left posterior margin of the posterior dorsal infraorbital foramen
S036	Left Tip of the antorbital process
S037	Right Tip of the antorbital process
S038	The left caudal most alveoli
S039	The right caudal most alveoli
S040	Left lower Tip of the zygomatic process of the squamosal
S041	Right lower tip of the zygomatic process of the squamosal
S042	Left tip of the Pterygoid's protuberance
S043	Right tip of the Pterygoid's protuberance
S046	Right ventral point of the postorbital process of the frontal
S047	Left ventral point of the postorbital process of the frontal
S048	Left upper Tip of the zygomatic process of the squamosal
S049	Right upper tip of the zygomatic process of the squamosal.
S050	Right anteroventralmost point of the retrotympanic;
S051	Left anteroventralmost point of the retrotympanic
S052	Right deep point of the Eustachian notch
S053	Left deep point of the Eustachian notch
S054	Right Posteriormost point of the basioccipital crest
S055	Left Posteriormost point of the basioccipital crest
S056	Right ventralmost point of the paraoccipital process
S057	Left ventralmost point of the paraoccipital process
S059	Middle point of the Occipital region
S060	Ventralmost point of the foramen magnum
S061	Left dorsal tip of occipital condyle,
S062	Right dorsal tip of occipital condyle,
S063	Left lateralmost point of occipital condyle
S064	Right lateralmost point of occipital condyle
S065	Left lateral midpoint of occipital condyle
S066	Right lateral midpoint of occipital condyle
S067	Left ventralmost point of occipital condyle
S068	Right ventralmost point of occipital condyle
S069	Right tip of the antorbital process

S070	Left tip of the antorbital process
S071	Right point of intersection between the antorbital process and the occipital dorsal region
S072	Left point of intersection between the antorbital process and the occipital dorsal region
S073	Dorsal most point of the Occipital region
S074	Right fossa of the superior part of the occipital bone
S075	Left fossa of the superior part of the occipital bone

Table S4.2.5. Individuals included in the training dataset for the Random Forest model

Aduncus	California	Gephyreus	Guayaquil	Japan	Mediterranean	NorthSea	Offshore	WestAfrica	Erebennus	WSouthAmer
P014	C72295	B1081	E40	J24unreg	G50246	L16455	B1415	L14596	W16504	L24677
P208	C72493	B1089	E60	L32352	M00470	L19799	C84034	P131	W572600	L24679
S045706	C84056	B1349	E61	W550164	M03968	L19837	E37	P1502	W572717	P1006
S045709	C91862	B1350	E64	W550169	M04900	L2330	L20328	W470555	W593405	W12054
S045711	C95366	B1420	E65	W550172	M04919	L31148	L20900	W605143	W593749	W504236
S045715	C95459	B1489	E66	W550173	M06694	L31193	L7965	W605144	W594117	W550306
S045716	W550021	B1637	E71	W550174	M07279	L8617	WA504273	-	WA571013	W550795
S045720	W550194	W501197	E72	W550175	S045704	S046597	WA571356	-	WAA20767	W550798

Table S4.2.6. Summary of specimen distribution across polygons and associated Operational Taxonomic Unit

LabID	Operational Taxonomic Unit	Polygon
B1011	Offshore	SWA_OffshoreUruguay
B1041	Offshore	SWA_OffshoreUruguay
B1077	Gephyreus	Gephyreus
B1081	Gephyreus	Gephyreus
B1089	Gephyreus	Gephyreus
B1099	Offshore	SWA_OffshoreUruguay
B1106	Offshore	SWA_OffshoreUruguay
B1116	Gephyreus	Gephyreus
B1281	Gephyreus	Gephyreus
B1287	Offshore	SWA_OffshoreUruguay
B1349	Gephyreus	Gephyreus
B1350	Gephyreus	Gephyreus
B1395	Gephyreus	Gephyreus
B1398	Offshore	SWA_OffshoreUruguay
B1415	Offshore	SWA_OffshoreUruguay
B1420	Gephyreus	Gephyreus
B1489	Gephyreus	Gephyreus
B1501	Gephyreus	Gephyreus
B1506	Gephyreus	Gephyreus
B1631	Offshore	SWA_BrazilOffshore
B1637	Gephyreus	Gephyreus
C27401	Offshore	NEP_Offshore

C54016	Offshore	Hawaii
C72169	Offshore	Hawaii
C72294	California	California
C72295	California	California
C72493	California	California
C84029	Offshore	NEP_Offshore
C84034	Offshore	NEP_Offshore
C84036	California	California
C84055	Offshore	NEP_Offshore
C84056	California	California
C84058	Offshore	NEP_Offshore
C84059	Offshore	NEP_Offshore
C84065	California	California
C84285	California	California
C91862	California	California
C91886	California	California
C91913	California	California
C95366	California	California
C95387	Offshore	NEP_Offshore
C95459	California	California
C95471	Offshore	NEP_Offshore
E117	Offshore	SEP_Offshore
E27	Offshore	SEP_Offshore
E29	Offshore	SEP_Offshore
E37	Offshore	SEP_Offshore
E40	Guayaquil	Guayaquil
E41	Offshore	SEP_Offshore
E43	Guayaquil	Guayaquil
E48	Guayaquil	Guayaquil
E58	Guayaquil	Guayaquil
E60	Guayaquil	Guayaquil
E61	Guayaquil	Guayaquil
E63	Guayaquil	Guayaquil
E64	Guayaquil	Guayaquil
E65	Guayaquil	Guayaquil
E66	Guayaquil	Guayaquil
E69	Guayaquil	Guayaquil
E70	Guayaquil	Guayaquil
E71	Guayaquil	Guayaquil
E72	Guayaquil	Guayaquil
E73	Guayaquil	Guayaquil
E75	Guayaquil	Guayaquil
E77	Guayaquil	Guayaquil
E78	Offshore	SEP_Offshore
E79	Offshore	SEP_Offshore
G36413	Mediterranean	Ligurian

G46867	Mediterranean	Ligurian
G48545	Mediterranean	Ligurian
G48564	Mediterranean	Ligurian
G48568	Mediterranean	Ligurian
G50246	Mediterranean	Ligurian
G50249	Mediterranean	Ligurian
G50250	Mediterranean	Ligurian
G54766	Mediterranean	Ligurian
J24unreg	Japan	Japan
JM24788	Japan	Japan
JM35127	Aduncus	Japan_Offshore
L14596	WestAfrica	Gabon
L16455	NorthSea	NorthSea
L19799	NorthSea	NorthSea
L19837	NorthSea	NorthSea
L20160	Aduncus	Yemen
L20328	Offshore	IndianOcean_Offshore
L20900	Offshore	IndianOcean_Offshore
L2113	NorthSea	NorthSea
L21173	Offshore	IndianOcean_Offshore
L21434	Offshore	IndianOcean_Offshore
L21452	Offshore	IndianOcean_Offshore
L2330	NorthSea	NorthSea
L24677	WSouthAmer	Peru
L24678	WSouthAmer	Peru
L24679	WSouthAmer	Peru
L24680	WSouthAmer	Peru
L26121	NorthSea	NorthSea
L27044	NorthSea	NorthSea
L28061	NorthSea	NorthSea
L31148	NorthSea	NorthSea
L31193	NorthSea	NorthSea
L32350	Japan	Japan
L32352	Japan	Japan
L5000071	NorthSea	NorthSea
L7964	Aduncus	JavaSea
L7965	Offshore	Indonesia_Offshore
L8617	NorthSea	NorthSea
M00470	Mediterranean	Adriatic
M03968	Mediterranean	Ligurian
M04900	Mediterranean	Adriatic
M04902	Mediterranean	Adriatic
M04919	Mediterranean	Adriatic
M06694	Mediterranean	Adriatic
M07279	Mediterranean	Ligurian
P014	Aduncus	GrandeGlorieuseIsland

P1006	WSouthAmer	Peru
P115	Offshore	NEA_Offshore
P1157	Offshore	NEA_Offshore
P131	WestAfrica	Mauritania_Senegal
P138	Offshore	NEA_Offshore
P1502	WestAfrica	Mauritania_Senegal
P158	Offshore	NEA_Offshore
P161	Offshore	NEA_Offshore
P176	Offshore	NEA_Offshore
P198	Offshore	NEA_Offshore
P199	Aduncus	???
P208	Aduncus	???
P304	Offshore	NEA_Offshore
P67	Aduncus	NewCaledonia
P75	Aduncus	NewCaledonia
PA3070	Aduncus	ChinaSea
PA3082	Offshore	SEA_Offshore
S045704	Mediterranean	Ligurian
S045706	Aduncus	Pakistan
S045707	Aduncus	Pakistan
S045708	Aduncus	Pakistan
S045709	Aduncus	Pakistan
S045710	Aduncus	Pakistan
S045711	Aduncus	Iran
S045715	Aduncus	Pakistan
S045716	Aduncus	Pakistan
S045720	Aduncus	Pakistan
S045722	Aduncus	Pakistan
S046597	NorthSea	NorthSea
S046790	NorthSea	FaroeIslands
S046791	Gephyreus	Uruguay
S046792	Gephyreus	Uruguay
S046793	Aduncus	JavaSea
S050302	Mediterranean	Adriatic
W12054	WSouthAmer	BajaCalifornia
W16504	Erebennus	Erebennus
W16505	Erebennus	Erebennus
W176349	Aduncus	SouthAfrica
W176350	Aduncus	SouthAfrica
W176351	Aduncus	SouthAfrica
W176352	Aduncus	SouthAfrica
W176353	Aduncus	SouthAfrica
W254634	Offshore	SEP_Offshore
W254910	WSouthAmer	Panama
W277170	WSouthAmer	Panama
W298239	California	California

W395381	WSouthAmer	Chile
W395733	WSouthAmer	Chile
W395924	California	California
W396165	WSouthAmer	GulfCalifornia
W470551	WestAfrica	IvoryCoast
W470553	WestAfrica	IvoryCoast
W470554	WestAfrica	IvoryCoast
W470555	WestAfrica	IvoryCoast
W470556	WestAfrica	IvoryCoast
W501197	Gephyreus	Uruguay
W504236	WSouthAmer	GulfCalifornia
W550021	California	California
W550097	California	California
W550125	California	California
W550164	Japan	Japan
W550166	Japan	Japan
W550167	Japan	Japan
W550169	Japan	Japan
W550170	Japan	Japan
W550171	Japan	Japan
W550172	Japan	Japan
W550173	Japan	Japan
W550174	Japan	Japan
W550175	Japan	Japan
W550193	California	California
W550194	California	California
W550265	WSouthAmer	Peru
W550306	WSouthAmer	Peru
W550795	WSouthAmer	Peru
W550798	WSouthAmer	Peru
W550942	Aduncus	SouthAfrica
W550947	Aduncus	SouthAfrica
W550969	Aduncus	Somalia
W571388	Erebennus	Erebennus
W571477	Offshore	NWA_Offshore
W571481	Offshore	NWA_Offshore
W571624	Erebennus	Erebennus
W572452	Erebennus	Erebennus
W572460	Erebennus	Erebennus
W572560	Erebennus	Erebennus
W572600	Erebennus	Erebennus
W572605	Offshore	NWA_Offshore
W572717	Erebennus	Erebennus
W572740	Erebennus	Erebennus
W593398	Erebennus	Erebennus
W593404	Erebennus	Erebennus

W593405	Erebennus	Erebennus
W593749	Erebennus	Erebennus
W593783	Erebennus	Erebennus
W593812	Erebennus	Erebennus
W593863	Offshore	NWA_Offshore
W594101	Erebennus	Erebennus
W594117	Erebennus	Erebennus
W594121	Erebennus	Erebennus
W594123	Erebennus	Erebennus
W594195	Erebennus	Erebennus
W594632	WestAfrica	Mauritania_Senegal
W605143	WestAfrica	Mauritania_Senegal
W605144	WestAfrica	Mauritania_Senegal
WA288084	Erebennus	Erebennus
WA395671	Erebennus	Erebennus
WA49627	Erebennus	Erebennus
WA504273	Offshore	NWA_Offshore
WA504766	Offshore	NWA_Offshore
WA550401	Erebennus	Erebennus
WA550447	Offshore	NWA_Offshore
WA550772	Offshore	NWA_Offshore
WA571013	Erebennus	Erebennus
WA571027	Erebennus	Erebennus
WA571356	Offshore	NWA_Offshore
WA571557	Offshore	NWA_Offshore
WA571618	Offshore	NWA_Offshore
WA572321	Offshore	NWA_Offshore
WAA20767	Erebennus	Erebennus

Table S4.2.7. Correlation Matrix of the environmental variables, with multicollinearity indicators (Threshold: r > 0.7 with Pearson test).

	Salinity Mean	Salinity Range	Silicate Mean	Silicate Range	Temperature Mean	Temperature Range	Terrain Ruggedness	Aspect	PP Mean	PP Range	Phosphate Mean	Phosphate Range	MLD Mean	MLD Range	Nitrate Mean	Nitrate Range	Ph Mean	Ph Range	Slope	Chlorophyll Mean	Chlorophyll Range	Dissolved O2 Mean	Dissolved O2 Range	Iron_Mean	IronRange	CurrentDirection Mean	CurrentDirection Range	CurrentVelocity Mean	CurrentVelocity Range	Bathymetry Mean	Topographic Position
SalinityMean	1.000	-0.531	-0.613	-0.521	0.192	-0.309	0.243	0.299	-0.440	-0.373	-0.043	-0.086	0.546	0.668	-0.075	-0.128	-0.052	-0.279	0.265	-0.414	-0.377	-0.284	-0.458	-0.356	-0.090	0.312	0.045	0.034	-0.011	-0.370	0.007
SalinityRange	-0.531	1.000	0.413	0.307	0.072	0.429	-0.563	-0.362	0.205	0.061	-0.270	-0.189	-0.457	-0.389	-0.195	-0.136	0.267	0.326	-0.552	0.149	0.103	-0.020	0.320	0.498	0.292	-0.184	0.000	-0.146	-0.130	0.474	0.029
SilicateMean	-0.613	0.413	1.000	0.778	-0.125	0.580	-0.532	-0.285	0.337	0.127	-0.240	-0.189	-0.412	-0.379	-0.053	-0.027	0.281	0.659	-0.516	0.299	0.171	0.109	0.572	0.722	0.437	-0.329	0.093	-0.144	-0.161	0.458	0.021
SilicateRange	-0.521	0.307	0.778	1.000	-0.040	0.212	-0.340	0.159	0.666	0.492	0.184	0.276	-0.491	-0.454	0.287	0.388	-0.115	0.366	-0.331	0.637	0.531	0.040	0.323	0.504	0.507	-0.089	0.475	-0.146	-0.164	0.476	0.142
TemperatureMean	0.192	0.072	-0.125	-0.040	1.000	-0.478	0.044	0.097	-0.144	-0.166	-0.069	0.040	-0.199	-0.168	-0.194	-0.120	-0.174	-0.372	0.036	-0.192	-0.163	-0.942	-0.693	-0.071	0.080	0.278	0.167	0.289	0.270	-0.131	0.342
TemperatureRange	-0.309	0.429	0.580	0.212	-0.478	1.000	-0.395	-0.443	0.132	-0.011	-0.361	-0.342	-0.158	-0.037	-0.111	-0.151	0.508	0.894	-0.357	0.146	0.049	0.341	0.863	0.639	0.389	-0.506	-0.189	-0.234	-0.133	0.466	-0.234
Terrain_Ruggedness	0.243	-0.563	-0.532	-0.340	0.044	-0.395	1.000	0.113	-0.021	0.132	0.352	0.222	0.221	0.235	0.181	0.104	-0.217	-0.418	0.995	0.035	0.086	-0.105	-0.425	-0.599	-0.255	0.313	-0.088	0.304	0.388	-0.257	-0.062
Aspect	0.299	-0.362	-0.285	0.159	0.097	-0.443	0.113	1.000	0.346	0.364	0.509	0.586	-0.046	0.039	0.409	0.501	-0.607	-0.218	0.104	0.340	0.338	-0.060	-0.291	-0.129	0.260	0.264	0.676	-0.246	-0.301	-0.030	0.090
PrimaryProductivity Mean	-0.440	0.205	0.337	0.666	-0.144	0.132	-0.021	0.346	1.000	0.913	0.616	0.695	-0.652	-0.585	0.596	0.678	-0.502	0.284	-0.019	0.991	0.929	0.132	0.346	0.233	0.311	0.116	0.416	-0.032	-0.099	0.521	0.217
PrimaryProductivity Range	-0.373	0.061	0.127	0.492	-0.166	-0.011	0.132	0.364	0.913	1.000	0.620	0.785	-0.515	-0.490	0.572	0.728	-0.528	0.149	0.126	0.919	0.992	0.202	0.259	0.089	0.222	0.079	0.304	-0.009	-0.022	0.421	0.253
PhosphateMean	-0.043	-0.270	-0.240	0.184	-0.069	-0.361	0.352	0.509	0.616	0.620	1.000	0.865	-0.268	-0.291	0.829	0.738	-0.866	-0.170	0.317	0.631	0.577	0.010	-0.133	-0.401	-0.213	0.547	0.451	-0.026	-0.159	-0.043	0.061
PhosphateRange	-0.086	-0.189	-0.189	0.276	0.040	-0.342	0.222	0.586	0.695	0.785	0.865	1.000	-0.308	-0.337	0.787	0.875	-0.837	-0.103	0.198	0.712	0.754	-0.054	-0.077	-0.260	-0.026	0.355	0.478	0.012	-0.056	0.053	0.254
MLDepthMean	0.546	-0.457	-0.412	-0.491	-0.199	-0.158	0.221	-0.046	-0.652	-0.515	-0.268	-0.308	1.000	0.886	-0.158	-0.203	0.304	-0.278	0.229	-0.590	-0.534	0.113	-0.203	-0.521	-0.429	-0.056	-0.185	-0.080	0.006	-0.723	-0.202
MLDRange	0.668	-0.389	-0.379	-0.454	-0.168	-0.037	0.235	0.039	-0.585	-0.490	-0.291	-0.337	0.886	1.000	-0.176	-0.213	0.287	-0.087	0.259	-0.545	-0.501	0.067	-0.160	-0.347	-0.187	0.017	-0.060	-0.148	-0.085	-0.531	-0.217
NitrateMean	-0.075	-0.195	-0.053	0.287	-0.194	-0.111	0.181	0.409	0.596	0.572	0.829	0.787	-0.158	-0.176	1.000	0.916	-0.732	0.097	0.167	0.642	0.551	0.083	0.135	-0.230	-0.079	0.334	0.383	-0.023	-0.130	0.000	0.131
NitrateRange	-0.128	-0.136	-0.027	0.388	-0.120	-0.151	0.104	0.501	0.678	0.728	0.738	0.875	-0.203	-0.213	0.916	1.000	-0.723	0.092	0.093	0.718	0.718	0.073	0.138	-0.146	0.054	0.233	0.455	-0.012	-0.069	0.059	0.290
PhMean	-0.052	0.267	0.281	-0.115	-0.174	0.508	-0.217	-0.607	-0.502	-0.528	-0.866	-0.837	0.304	0.287	-0.732	-0.723	1.000	0.221	-0.181	-0.498	-0.483	0.178	0.244	0.322	0.156	-0.581	-0.515	-0.039	0.136	0.086	-0.353
PhRange	-0.279	0.326	0.659	0.366	-0.372	0.894	-0.418	-0.218	0.284	0.149	-0.170	-0.103	-0.278	-0.087	0.097	0.092	0.221	1.000	-0.385	0.281	0.194	0.247	0.838	0.721	0.516	-0.331	0.028	-0.271	-0.263	0.498	-0.046
Slope	0.265	-0.552	-0.516	-0.331	0.036	-0.357	0.995	0.104	-0.019	0.126	0.317	0.198	0.229	0.259	0.167	0.093	-0.181	-0.385	1.000	0.040	0.088	-0.109	-0.404	-0.559	-0.206	0.298	-0.107	0.336	0.420	-0.214	-0.041
ChlorophyllMean	-0.414	0.149	0.299	0.637	-0.192	0.146	0.035	0.340	0.991	0.919	0.631	0.712	-0.590	-0.545	0.642	0.718	-0.498	0.281	0.040	1.000	0.938	0.156	0.364	0.186	0.285	0.103	0.378	0.009	-0.040	0.490	0.199
ChlorophyllRange	-0.377	0.103	0.171	0.531	-0.163	0.049	0.086	0.338	0.929	0.992	0.577	0.754	-0.534	-0.501	0.551	0.718	-0.483	0.194	0.088	0.938	1.000	0.188	0.297	0.142	0.269	0.056	0.295	0.031	0.020	0.462	0.260
DissolvedO2Mean	-0.284	-0.020	0.109	0.040	-0.942	0.341	-0.105	-0.060	0.132	0.202	0.010	-0.054	0.113	0.067	0.083	0.073	0.178	0.247	-0.109	0.156	0.188	1.000	0.617	0.105	-0.080	-0.327	-0.184	-0.308	-0.295	0.162	-0.299
DissolvedO2Range	-0.458	0.320	0.572	0.323	-0.693	0.863	-0.425	-0.291	0.346	0.259	-0.133	-0.077	-0.203	-0.160	0.135	0.138	0.244	0.838	-0.404	0.364	0.297	0.617	1.000	0.579	0.274	-0.524	-0.112	-0.283	-0.241	0.439	-0.061
Iron_Mean	-0.356	0.498	0.722	0.504	-0.071	0.639	-0.599	-0.129	0.233	0.089	-0.401	-0.260	-0.521	-0.347	-0.230	-0.146	0.322	0.721	-0.559	0.186	0.142	0.105	0.579	1.000	0.809	-0.449	0.047	-0.211	-0.221	0.785	0.117
IronRange	-0.090	0.292	0.437	0.507	0.080	0.389	-0.255	0.260	0.311	0.222	-0.213	-0.026	-0.429	-0.187	-0.079	0.054	0.156	0.516	-0.206	0.285	0.269	-0.080	0.274	0.809	1.000	-0.299	0.307	-0.201	-0.139	0.753	0.133
CurrentDirection Mean	0.312	-0.184	-0.329	-0.089	0.278	-0.506	0.313	0.264	0.116	0.079	0.547	0.355	-0.056	0.017	0.334	0.233	-0.581	-0.331	0.298	0.103	0.056	-0.327	-0.524	-0.449	-0.299	1.000	0.275	0.262	-0.017	-0.210	0.059
CurrentDirection Range	0.045	0.000	0.093	0.475	0.167	-0.189	-0.088	0.676	0.416	0.304	0.451	0.478	-0.185	-0.060	0.383	0.455	-0.515	0.028	-0.107	0.378	0.295	-0.184	-0.112	0.047	0.307	0.275	1.000	-0.472	-0.487	0.034	0.108
CurrentVelocity Mean	0.034	-0.146	-0.144	-0.146	0.289	-0.234	0.304	-0.246	-0.032	-0.009	-0.026	0.012	-0.080	-0.148	-0.023	-0.012	-0.039	-0.271	0.336	0.009	0.031	-0.308	-0.283	-0.211	-0.201	0.262	-0.472	1.000	0.906	-0.011	0.282
CurrentVelocity Range	-0.011	-0.130	-0.161	-0.164	0.270	-0.133	0.388	-0.301	-0.099	-0.022	-0.159	-0.056	0.006	-0.085	-0.130	-0.069	0.136	-0.263	0.420	-0.040	0.020	-0.295	-0.241	-0.221	-0.139	-0.017	-0.487	0.906	1.000	-0.026	0.196
BathymetryMean	-0.370	0.474	0.458	0.476	-0.131	0.466	-0.257	-0.030	0.521	0.421	-0.043	0.053	-0.723	-0.531	0.000	0.059	0.086	0.498	-0.214	0.490	0.462	0.162	0.439	0.785	0.753	-0.210	0.034	-0.011	-0.026	1.000	0.095
TopographicPosition	0.007	0.029	0.021	0.142	0.342	-0.234	-0.062	0.090	0.217	0.253	0.061	0.254	-0.202	-0.217	0.131	0.290	-0.353	-0.046	-0.041	0.199	0.260	-0.299	-0.061	0.117	0.133	0.059	0.108	0.282	0.196	0.095	1.000

Table S4.3.1. Results from Pairwise PERMANOVA tests on all Principal components from the PCA analysis from Figure S4.3.2. for comparison between a priori groups. p-values are shown above the empty diagonal cells, while F-values are shown below the empty diagonal cells.

	Aduncus	**California**	**Gephyreus**	**Guayaquil**	**Japan**	**Mediterranean**	**North Sea**	**Offshore**	**West Africa**	**Erebennus**	**WSouth America**
Aduncus (N = 28)		**0.0055**	**0.0055**	**0.0055**	**0.0055**	**0.0055**	**0.0055**	**0.0055**	**0.0055**	**0.0055**	**0.0055**
California (N = 19)	23.26		**0.0055**	**0.0055**	**0.0055**	**0.0055**	**0.0055**	**0.0055**	**0.0055**	**0.0055**	1
Gephyreus (N = 16)	24.25	25.29		**0.0055**	**0.0055**	**0.0055**	**0.0055**	**0.0055**	**0.0055**	**0.0055**	**0.0055**
Guayaquil (N = 17)	18.35	8.106	28.38		**0.0055**	**0.0055**	**0.0055**	**0.0055**	**0.0055**	**0.0055**	**0.0165**
Japan (N = 14)	32.56	8.227	20.51	20.94		**0.0055**	**0.0055**	**0.022**	**0.0165**	**0.0055**	**0.022**
Mediterranean (N = 18)	8.945	5.977	15.58	9.976	11.07		**0.0055**	**0.0055**	0.132	**0.0055**	**0.0055**
North Sea (N = 14)	33.45	14.29	18.09	27.38	4.12	12.92		**0.0055**	**0.0055**	**0.0055**	**0.0055**
Offshore (N = 53)	38.08	7.363	21.97	21.27	3.534	7.833	5.973		0.0825	**0.0055**	**0.0055**
West Africa (N = 11)	10.92	7.647	10.12	12.92	5.526	3.084	6.234	3.617		**0.0055**	**0.011**
Erebennus (N = 28)	34.03	10.25	45.69	9.507	25.4	16.89	31.8	31.82	21.55		**0.0055**
Wsouth America (N = 16)	18.56	2.016	15.95	5.142	5.407	4.732	7.848	5.072	5.105	8.969	

Table S4.3.2. Result statistics from the Random forest analysis with the HL method.

```
Overall Statistics

               Accuracy : 0.7265
                 95% CI : (0.6646, 0.7825)
    No Information Rate : 0.1581
    P-Value [Acc > NIR] : < 2.2e-16

                  Kappa : 0.6938

 Mcnemar's Test P-Value : NA

Statistics by Class:

                     Class: Aduncus Class: California Class: Gephyreus Class: Guayaquil Class: Japan Class: Mediterranean Class: NorthSea Class: Offshore
Sensitivity              0.9333          0.44000          1.00000          0.93333       0.64706             0.73684        0.66667         0.6857
Specificity              1.0000          0.96172          1.00000          0.98630       0.98618             0.98140        0.98174         0.8543
Pos Pred Value           1.0000          0.57895          1.00000          0.82353       0.78571             0.77778        0.71429         0.4528
Neg Pred Value           0.9903          0.93488          1.00000          0.99539       0.97273             0.97685        0.97727         0.9392
Prevalence               0.1282          0.10684          0.06838          0.06410       0.07265             0.08120        0.06410         0.1496
Detection Rate           0.1197          0.04701          0.06838          0.05983       0.04701             0.05983        0.04274         0.1026
Detection Prevalence     0.1197          0.08120          0.06838          0.07265       0.05983             0.07692        0.05983         0.2265
Balanced Accuracy        0.9667          0.70086          1.00000          0.95982       0.81662             0.85912        0.82420         0.7700
                     Class: WestAfrica Class: WNAC Class: WSouthAmer
Sensitivity                0.53846       0.7027           0.75000
Specificity                0.98190       0.9898           0.96847
Pos Pred Value             0.63636       0.9286           0.56250
Neg Pred Value             0.97309       0.9466           0.98624
Prevalence                 0.05556       0.1581           0.05128
Detection Rate             0.02991       0.1111           0.03846
Detection Prevalence       0.04701       0.1197           0.06838
Balanced Accuracy          0.76018       0.8463           0.85923
```

Table S4.3.3. Confusion matrix from Random forest analysis classifying skulls to a priori OTUs using HL.

	Predicted											
Real	**Aduncus**	**California**	**Erebennus**	**Gephyreus**	**Guayaquil**	**Japan**	**Mediterranean**	**NorthSea**	**Offshore**	**WestAfrica**	**Wsouth Amer**	**Total**
Aduncus	28											28
California		11	5		1				1		1	19
Erebennus			26				2					28
Gephyreus				16								16
Guayaquil		1	2		14							17
Japan			1			11			2			14
Mediterranean	2						14	1		1		18
NorthSea								10	3	1		14
Offshore		12	1			4	3	4	24	4	1	53
WestAfrica			1						2	7	1	11
WSouthAmer		1	1			2			3		9	16

Table S4.3.4. Confusion matrix from HCA analysis with the HL landmarking method.

Cluster	Aduncus	California	Erebennus	Gephyreus	Guayaquil	Japan	Mediterranean	NorthSea	Offshore	West Africa	WSouth Amer	Total
1		3	1		1	8	1	2	19	2	4	41
2				16			1	1		1		19
3		1	2			1	7		5		1	17
4	1	2					2		13	6		24
5		11	7		4		1		2	1	5	31
6						1			5	1		7
7						4		6	9		3	22
8	1	1	3		12						3	20
9		1	15									16
10	26						5					31
11							1	5				6
Total	28	19	28	16	17	14	18	14	53	11	16	234

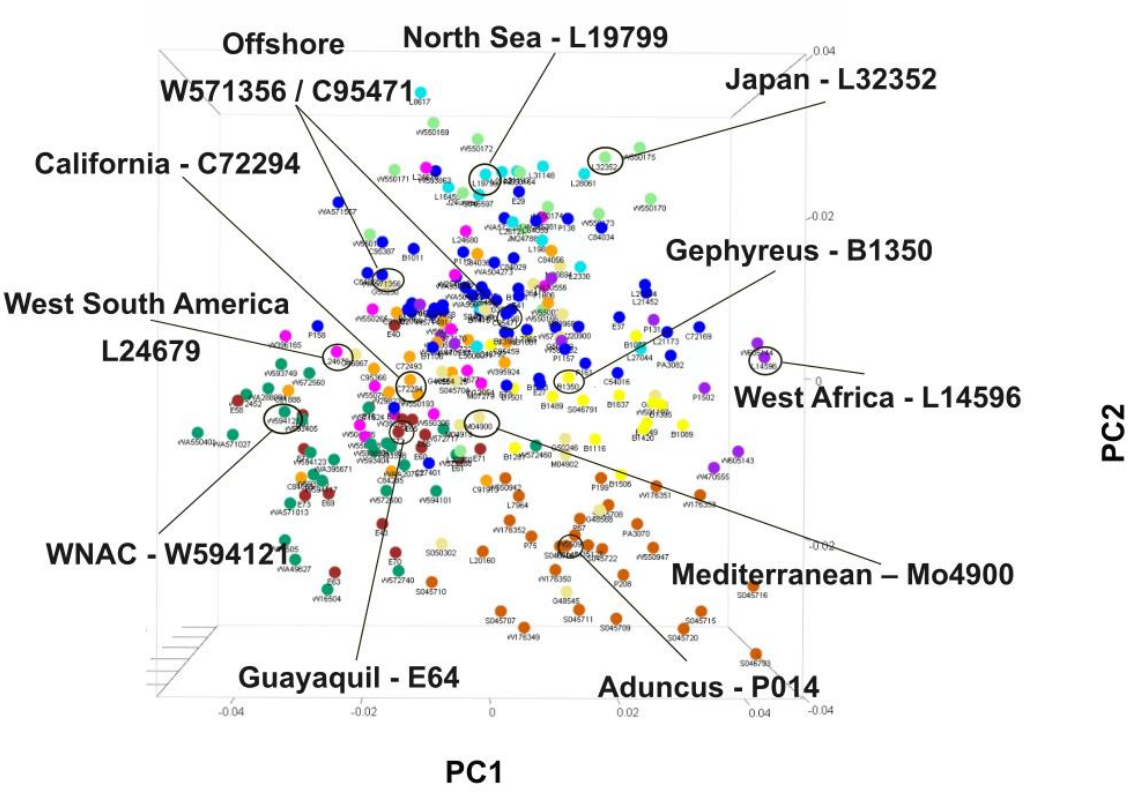

Figure S4.2.1. 3D PCA plot displaying the three most important principal components, with operational taxonomic unit distinguished by colours and individuals selected for MALPACA circled in black.

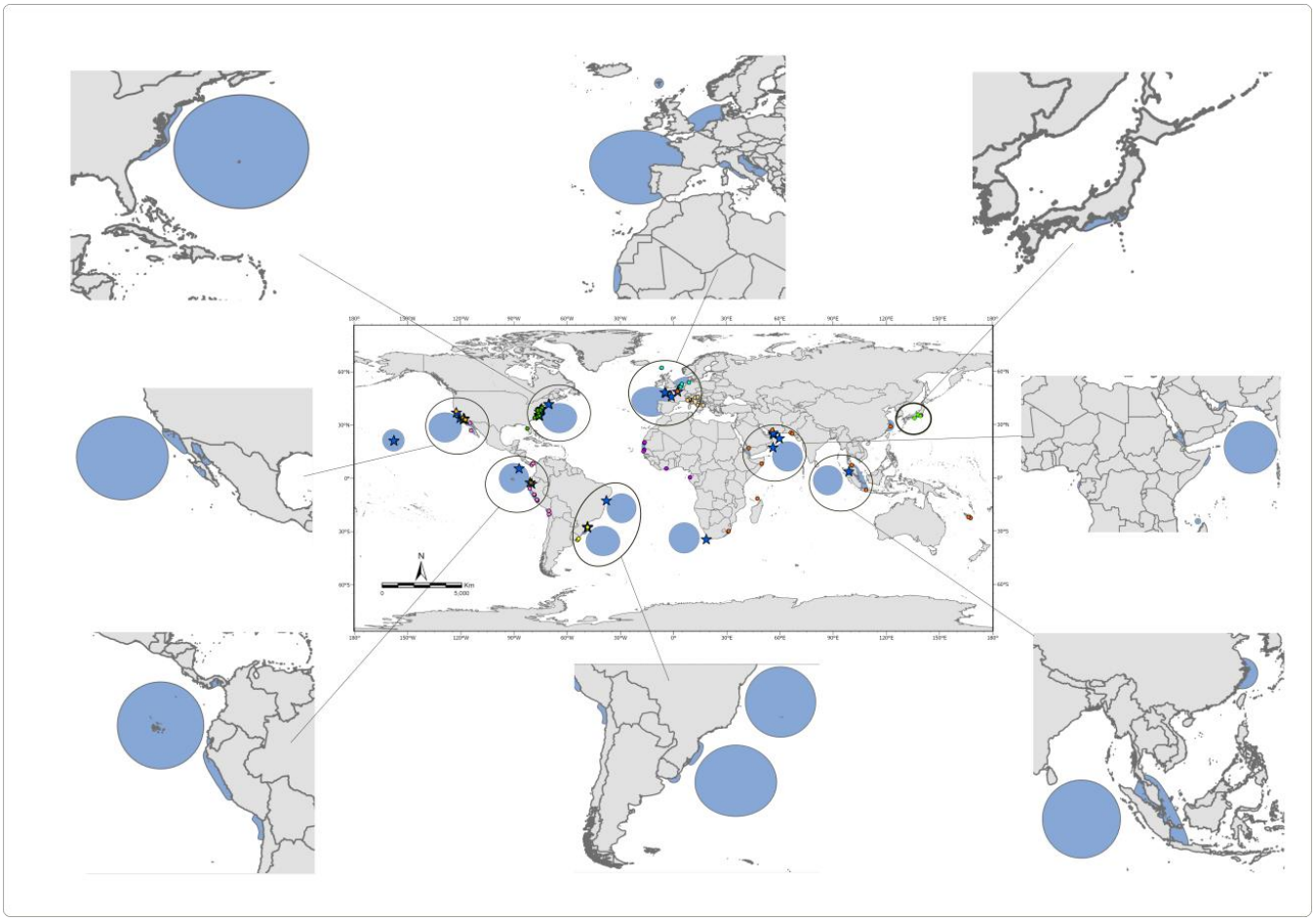

Figure S4.2.2. Map of the polygons representing core geographic areas for each operational taxonomic unit.

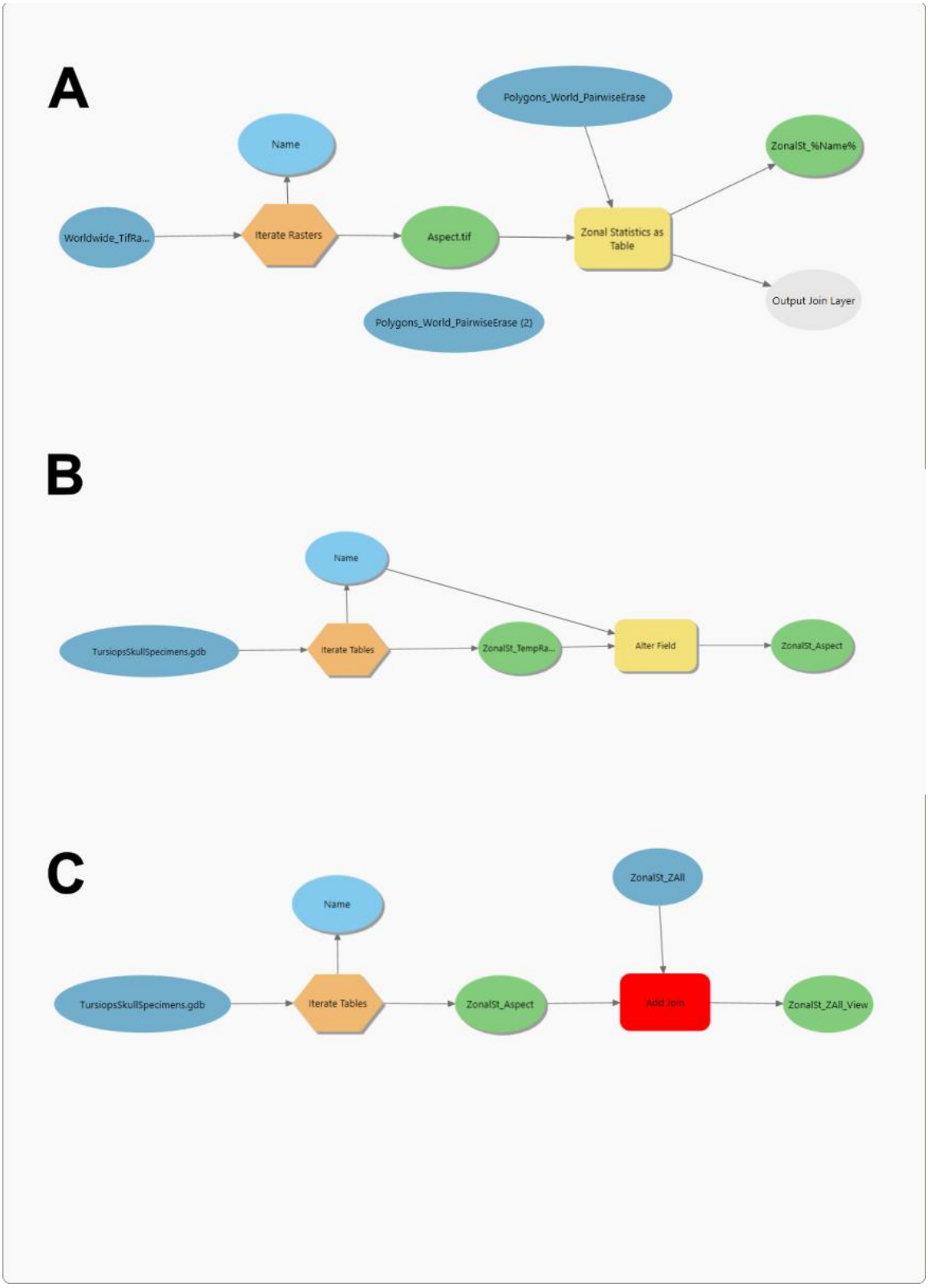

Figure S4.2.3. A) Model created in ArcGIS for automatic mean raster calculation for each polygon; B) Model created in ArcGIS Pro for renaming the generic field name "MEAN" to specific variable names; C) Model created in ArcGIS Pro to merge all individual.

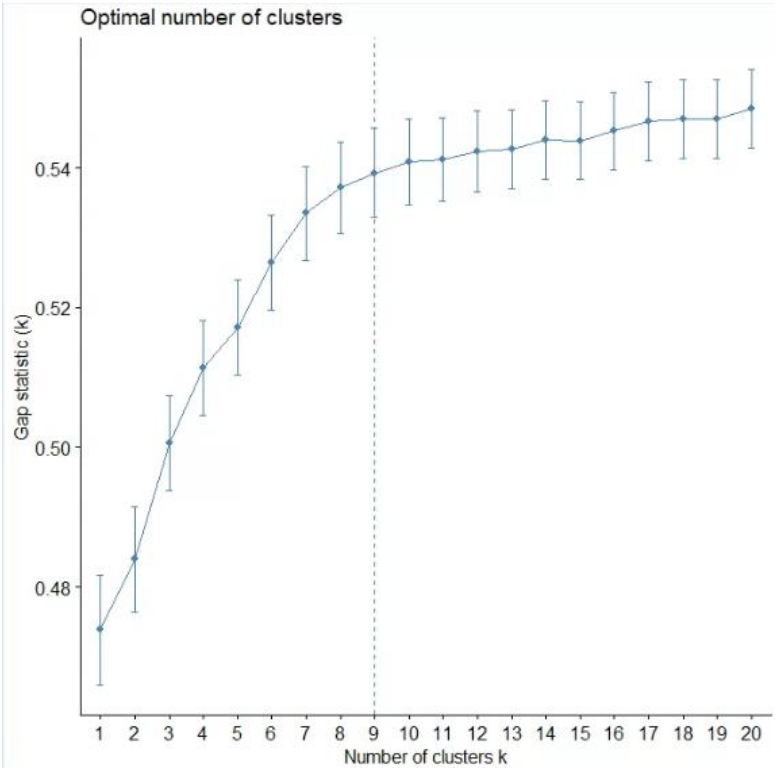

Figure S4.3.1. Gap statistic plot from the HCA analysis using the SSL landmarking method.

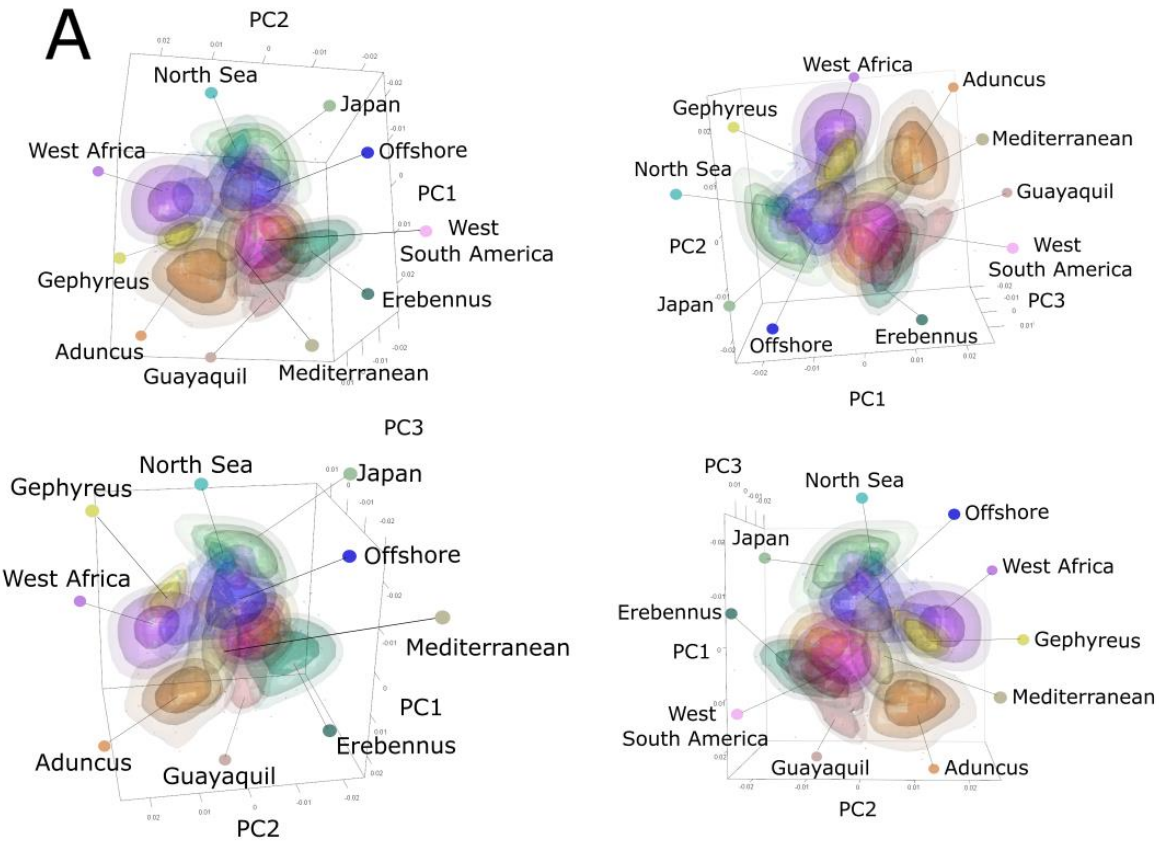

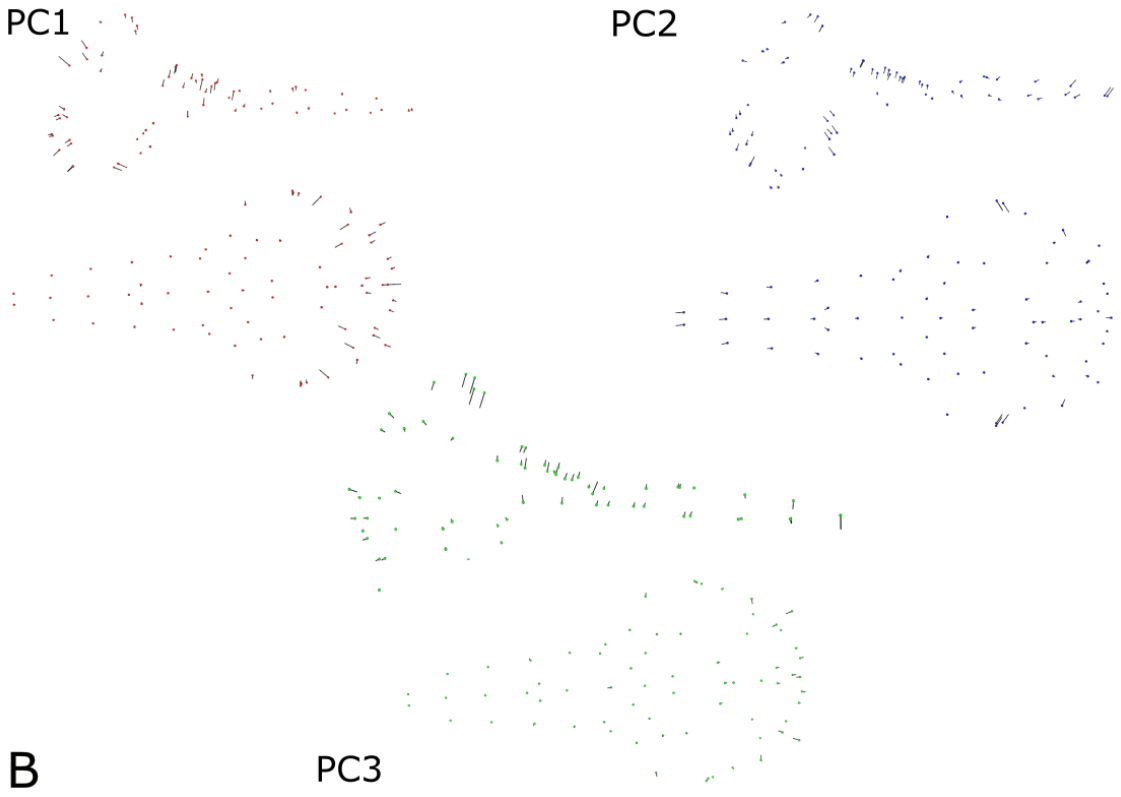

Figure S4.3.2. A) 3D PCA morphospace from the HL analysis displaying the three most important principal components, from five different perspectives, with operational taxonomic units distinguished by colours. Kernel discriminant analysis clouds are calculated in the R package KS (Duong, 2007). B) Vector displacement graph representing differences in landmark position between the mean landmark configuration and specimens along the positive PC1, PC2 and PC3 axes from the PCA produced in Figure S4.3.2.A.

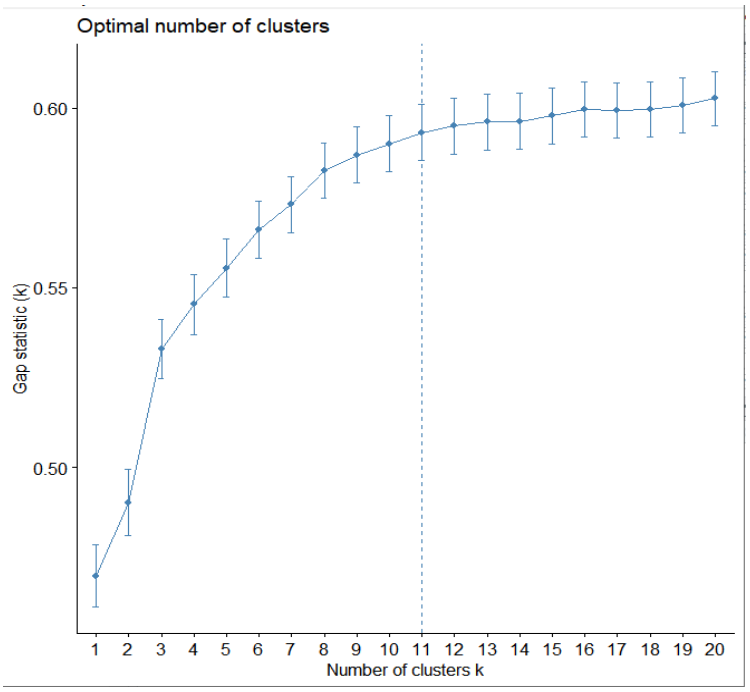

Figure S4.3.3. Gap statistic plot from the HCA analysis using the HL landmarking method.

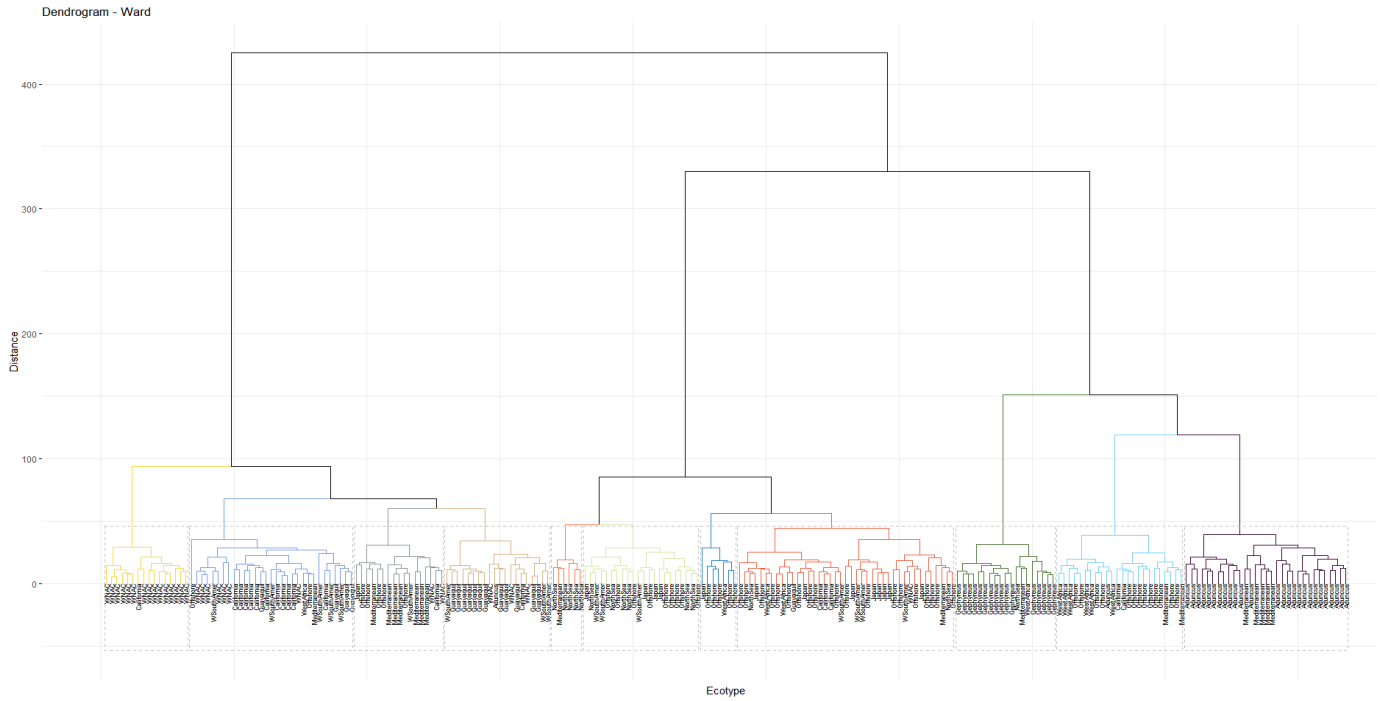

Figure S4.3.4. Dendrogram of the Hierarchical Clustering Analysis (HCA) performed using Ward's distance metric on HL Procrustes aligned landmarks. The cluster R package was used to identify the most probable number of groups (i.e., K= 11). These groups are visually represented by different colours.

Chapter 5

Table S5.2.1. Accession numbers and details of the specimens used in the analysis.

LabID	Museum	Catalog Number	Species	OTULabel	Sex	Year	Population	Location
W16504	USNM	A16504	T. truncatus	Coastal	Male	1881	Chesapeake	Cherrystone Point
W16505	USNM	A16505	T. truncatus	Coastal	Female	1881	Chesapeake	Cherrystone Point
W571388	USNM	571388	T. truncatus	Coastal	Female	1990	NorthCarolina	Avon
W571477	USNM	571477	T. truncatus	Offshore	Female	1991	Offshore	Cape Henlopen State Park
W571481	USNM	571481	T. truncatus	Offshore	Female	1990	Offshore	Brigantine
W571624	USNM	571624	T. truncatus	Unknown	Unknown	1987	DelawareBay	Unknown
W572452	USNM	572452	T. truncatus	Unknown	Female	1999	Chesapeake	Norfolk, 986 West Ocean View
W572460	USNM	572460	T. truncatus	Unknown	Female	1999	Chesapeake	Hampton, 834 North 1st St, Buckroe Beach
W572560	USNM	572560	T. truncatus	Unknown	Unknown	2000	Chesapeake	Fisherman'S Island
W572600	USNM	572600	T. truncatus	Unknown	Male	2000	NorthCarolina	Corolla, 1.7 Miles N of Albacore Street
W572605	USNM	572605	T. truncatus	Unknown	Female	2001	Offshore	Buxton, 0.7 Miles South of the pooint, Hatteras
W572717	USNM	572717	T. truncatus	Unknown	Female	2000	NorthCarolina	Frisco, 1 Mi N of Frisco Pier
W572740	USNM	572740	T. truncatus	Unknown	Male	1999	NorthCarolina	South Core banks
W593398	USNM	593398	T. truncatus	Unknown	Female	2004	NorthCarolina	Salvo, 0.2 Mi S of R23
W593404	USNM	593404	T. truncatus	Unknown	Male	2004	NorthCarolina	Hatteras, 2.5 Mi S of R55
W593405	USNM	593405	T. truncatus	Unknown	Female	2004	NorthCarolina	Harkers Island
W593749	USNM	593749	T. truncatus	Unknown	Male	2002	NorthCarolina	South Nags Head, 4019 S. Virginia Dare Trail
W593783	USNM	593783	T. truncatus	Unknown	Male	2004	NorthCarolina	Frisco, 0.3 Mi south of Frisco Pier
W593812	USNM	593812	T. truncatus	Unknown	Unknown	2002	NorthCarolina	Emerald Isle
W593863	USNM	593863	T. truncatus	Unknown	Male	2004	Offshore	Wachapreague
W594101	USNM	594101	T. truncatus	Unknown	Female	2002	NorthCarolina	Shallotte Inlet, Hughes Marina, end of village Island road
W594117	USNM	594117	T. truncatus	Unknown	Male	2002	NorthCarolina	Long Beach, end of 67th St, E
W594121	USNM	594121	T. truncatus	Unknown	Male	2002	NorthCarolina	Hatteras Village
W594123	USNM	594123	T. truncatus	Unknown	Male	2003	NorthCarolina	Harkers Island, S Core, Oceanside, Cape Point
W594195	USNM	594195	T. truncatus	Unknown	Female	2000	NorthCarolina	Frisco
WA49627	USNM	A49627	T. truncatus	Offshore	Unknown	Unknown	MexicoGulf	Tampa Bay
WA288084	USNM	288084	T. truncatus	Coastal	Unknown	1960	Chesapeake	Scientist Cliffs
WA291518	USNM	291518	T. truncatus	Offshore	Unknown	1928	Offshore	Frisco
WA364981	USNM	364981	T. truncatus	Intermediate	Male	1966	DelawareBay	Cape Henlopen
WA395671	USNM	395671	T. truncatus	Intermediate	Unknown	1969	Chesapeake	Calvert Cliffs
WA504291	USNM	504291	T. truncatus	Coastal	Male	1975	DelawareBay	Brigantine, 1225 Shore Drive
WA504766	USNM	504766	T. truncatus	Offshore	Male	1971	Offshore	Nags head
WA504935	USNM	504935	T. truncatus	Unknown	Female	1974	MexicoGulf	Gulfport
WA504936	USNM	504936	T. truncatus	Unknown	Female	1974	MexicoGulf	Gulfport
WA550198	USNM	550198	T. truncatus	Coastal	Male	1976	Florida	Flagler Beach
WA550315	USNM	550315	T. truncatus	Intermediate	Female	1983	NorthCarolina	300 Meters South Of Pea Island
WA550401	USNM	550401	T. truncatus	Coastal	Male	1984	Chesapeake	Norfolk, 9th Bay St, Ocean View
WA550439	USNM	550439	T. truncatus	Coastal	Female	1985	DelawareBay	Cape Henlopen
WA550447	USNM	550447	T. truncatus	Offshore	Unknown	1985	Offshore	Truro, Beach point
WA550772	USNM	550772	T. truncatus	Offshore	Female	1986	Offshore	Bodie Island, ramp 4
WA571013	USNM	571013	T. truncatus	Coastal	Female	1987	Chesapeake	Norfolk, Ocean view Beach
WA571025	USNM	571025	T. truncatus	Coastal	Female	1987	Maryland	Assateague Island
WA571027	USNM	571027	T. truncatus	Coastal	Male	1987	Maryland	Ocean City, 43rd St
WA571061	USNM	571061	T. truncatus	Coastal	Male	1987	Maryland	Ocean city, 125 St

WA571100	USNM	571100	T. truncatus	Coastal	Female	1987	Chesapeake	Little Creek
WA571152	USNM	571152	T. truncatus	Coastal	Female	1987	Chesapeake	Dam Neck
WA571239	USNM	571239	T. truncatus	Coastal	Male	1987	Maryland	Assateague Island
WA571248	USNM	571248	T. truncatus	Intermediate	Male	1987	Chesapeake	York River
WA571276	USNM	571276	T. truncatus	Coastal	Male	1988	Florida	Cocoa Beach, Ca 6 Km (4 Mi) S Sr520 And A1a
WA571289	USNM	571289	T. truncatus	Coastal	Male	1988	Florida	Marineland, Ocean side
WA571303	USNM	571303	T. truncatus	Intermediate	Female	1988	Florida	New Smyrna Beach, Canaveral Ns
WA571310	USNM	571310	T. truncatus	Coastal	Female	1988	Florida	Canaveral National Seashore
WA571341	USNM	571341	T. truncatus	Coastal	Unknown	1988	Georgia	Tybee Island, Ocean Beach at 8th St
WA571356	USNM	571356	T. truncatus	Offshore	Female	1989	Offshore	Salvo, 200 M S Ramp 30
WA571432	USNM	571432	T. truncatus	Coastal	Male	1990	Chesapeake	Dam Neck/Sandbridge Border.
WA571465	USNM	571465	T. truncatus	Coastal	Female	1991	DelawareBay	Ventnor, Summerset Ave
WA571468	USNM	571468	T. truncatus	Intermediate	Female	1991	DelawareBay	Surf City
WA571557	USNM	571557	T. truncatus	Offshore	Male	1992	Offshore	Cape Henlopen State Park
WA571618	USNM	571618	T. truncatus	Offshore	Male	1992	Offshore	Unknown
WA571624	USNM	571624	T. truncatus	Unknown	Unknown	1987	DelawareBay	Unknown
WA572321	USNM	572321	T. truncatus	Offshore	Male	1998	Offshore	South Bethany, end of south 9th st
WA572967	USNM	572967	T. truncatus	Coastal	Male	2003	Offshore	Duxbury, Bay Road
WA593974	USNM	593974	T. truncatus	Unknown	Male	2013	Offshore	Dennis, Crowe's Pasture
WA594105	USNM	594105	T. truncatus	Unknown	Male	1999	MexicoGulf	Destin, South shore of Choctawhatchee
WA594106	USNM	594106	T. truncatus	Unknown	Unknown	1999	MexicoGulf	Cape San Blas
WA594179	USNM	594179	T. truncatus	Unknown	Female	2001	Georgia	Unknown
WA594219	USNM	594219	T. truncatus	Unknown	Unknown	2001	MexicoGulf	Panama city
WA594233	USNM	594233	T. truncatus	Unknown	Male	2002	Georgia	Cumberland Island
WA594243	USNM	594243	T. truncatus	Unknown	Male	1999	Georgia	Cumberland Island
WA594250	USNM	594250	T. truncatus	Unknown	Male	1989	Georgia	Cumberland Island, North of Duckhouse
WA594515	USNM	594515	T. truncatus	Unknown	Female	1990	Georgia	Cumberland Island, Grave's house
WA594528	USNM	594528	T. truncatus	Unknown	Unknown	1991	MexicoGulf	Gulf side of East Ship island
WA594692	USNM	594692	T. truncatus	Unknown	Male	1962	MexicoGulf	Marathon
WAA20767	USNM	A20767	T. truncatus	Coastal	Male	1882	Chesapeake	Point lookout
WAA21536	USNM	A21536	T. truncatus	Coastal	Unknown	1884	DelawareBay	Cape May
WAA49577	USNM	A49577	T. truncatus	Coastal	Unknown	Unknown	MexicoGulf	Tampa Bay

Table S5.2.2. Number of individuals per geographical area.

Geography	**N**
Chesapeake Bay	14
Delaware Bay	8
Maryland	4
North Carolina	16
Georgia	6
Florida	5
Mexico Gulf	9
Offshore	14
Total	73

Table S5.2.3. Description of the parameters used for 3D modelling in MESHROOM.

	FeatureExtraction		**ImageMatching**			**FeatureMatching** Guided matching ticked for all individuals	**Structure From Motion** Use Rig Constraint Unticked for all individuals				**DepthMap**			**DepthMapFilter**		**Meshing**				**MeshFiltering**
Individuals	Describer Types	Describer Presets	Min number of images	Max descriptors	Number of matches	Describer Type	Describer Types	Minimum Input Track Lenght	Min Observation For Triangulation	Max Reprojection Error	Downscale	SGM:Nb Neighbour Cameras	Refine: Nb Neighbour Cameras	Min Consistent Cameras	Min Consistent Cameras Bad Similarity	Min Observations Angle For SFM Space Estimation	Max Input Points	Max Point	Max Point Per Voxel	Filter Large Triangles Factor
W16504	Sift - Sift_float	normal	200	500	50	Sift - Sift_float	Sift - Sift_float	2	2	4	1	10	6	3	4	10	50000000	5000000	1000000	60
W16505	Sift - Sift_float	normal	200	500	50	Sift - Sift_float	Sift - Sift_float	2	2	4	1	10	6	3	4	10	50000000	5000000	1000000	60
W571388	Sift - Sift_float	high	200	500	50	Sift - Sift_float	Sift - Sift_float	2	2	4	1	10	6	3	4	10	Mesh1 - 50000000 Mesh2 - 25000000	Mesh1 - 5000000 Mesh2 - 2500000	Mesh1 - 1000000 Mesh2 - 500000	60
W571477	Sift - Sift_float	normal	200	500	50	Sift - Sift_float	Sift - Sift_float	2	2	4	1	10	6	3	4	10	50000000	5000000	1000000	60
W571481	Sift - Sift_float	normal	200	500	50	Sift - Sift_float	Sift - Sift_float	2	2	4	1	10	6	3	4	10	50000000	5000000	1000000	60
W571624	Sift - Sift_float	normal	200	500	50	Sift - Sift_float	Sift - Sift_float	2	2	4	1	10	6	3	4	10	50000000	5000000	1000000	60
W572452	Sift - Sift_float	normal	200	500	50	Sift - Sift_float	Sift - Sift_float	2	2	4	1	10	6	3	4	10	50000000	5000000	1000000	60
W572460	Sift - Sift_float	high	200	500	50	Sift - Sift_float	Sift - Sift_float	2	2	4	1	10	6	3	4	10	Mesh1 - 50000000 Mesh2 - 10000000	Mesh1 - 5000000 Mesh2 - 1000000	Mesh1 - 1000000 Mesh2 - 200000	60
W572560	Sift - Sift_float	high	200	500	50	Sift - Sift_float	Sift - Sift_float	2	2	4	1	10	6	3	4	10	50000000	5000000	1000000	60
W572600	Sift - Sift_float	normal	200	500	50	Sift - Sift_float	Sift - Sift_float	2	2	4	1	10	6	3	4	10	50000000	5000000	1000000	60
W572605	Sift - Sift_float	normal	200	500	50	Sift - Sift_float	Sift - Sift_float	2	2	4	1	10	6	3	4	10	50000000	5000000	1000000	60
W572717	Sift - Sift_float	normal	200	500	50	Sift - Sift_float	Sift - Sift_float	2	2	4	1	10	6	3	4	10	Mesh1 - 50000000 Mesh2 - 25000000	Mesh1 - 5000000 Mesh2 - 2500000	Mesh1 - 1000000 Mesh2 - 500000	60
W572740	Sift - Sift_float	normal	200	500	50	Sift - Sift_float	Sift - Sift_float	2	2	4	1	10	6	3	4	10	Mesh1 - 35000000 Mesh2 - 25000000	Mesh1 - 3500000 Mesh2 - 2500000	Mesh1 - 650000 Mesh2 - 500000	60
W593398	Sift - Sift_float	normal	250	500	50	Sift - Sift_float	Sift - Sift_float	2	2	4	1	10	6	3	4	10	30000000	3000000	700000	60
W593404	Sift - Sift_float	normal	200	500	50	Sift - Sift_float	Sift - Sift_float	2	2	4	1	10	6	3	4	10	50000000	5000000	1000000	60
W593405	Sift - Sift_float	high	200	500	50	Sift - Sift_float	Sift - Sift_float	2	2	4	1	10	6	3	4	10	50000000	5000000	1000000	60
W593749	Sift - Sift_float	normal	200	500	50	Sift - Sift_float	Sift - Sift_float	2	2	4	1	10	6	3	4	10	50000000	5000000	1000000	60
W593783	Sift - Sift_float	normal	200	500	50	Sift - Sift_float	Sift - Sift_float	2	2	4	1	10	6	3	4	10	Mesh1 - 50000000 Mesh2 - 30000000 Mesh3 - 10000000	Mesh1 - 5000000 Mesh2 - 3000000 Mesh3 - 1000000	Mesh1 - 1000000 Mesh2 - 800000 Mesh3 - 500000	60
W593812	Sift - Sift_float	normal	200	500	50	Sift - Sift_float	Sift - Sift_float	2	2	4	1	10	6	3	4	10	50000000	5000000	1000000	60
W593863	Sift - Sift_float	normal	200	500	50	Sift - Sift_float	Sift - Sift_float	2	2	4	1	10	6	3	4	10	50000000	5000000	1000000	60

W594101	Sift - Sift_float - akaze	normal	200	500	50	Sift - Sift_float - akaze	Sift - Sift_float - akaze	2	2	4	1	10	6	3	4	10	Mesh1 - 50000000 Mesh2 - 25000000	Mesh1 - 5000000 Mesh2 - 2500000	Mesh1 - 1000000 Mesh2 - 500000	60
W594117	Sift - Sift_float	normal	200	500	50	Sift - Sift_float	Sift - Sift_float	2	2	4	1	10	6	3	4	10	25000000	2500000	500000	60
W594121	Sift - Sift_float	normal	200	500	50	Sift - Sift_float	Sift - Sift_float	2	2	4	1	10	6	3	4	10	50000000	5000000	1000000	60
W594123	Sift - Sift_float	high	200	500	50	Sift - Sift_float	Sift - Sift_float	2	2	4	1	10	6	3	4	10	Mesh1 - 50000000 Mesh2 - 25000000	Mesh1 - 5000000 Mesh2 - 2500000	Mesh1 - 1000000 Mesh2 - 500000	60
W594195	Sift - Sift_float	normal	200	500	50	Sift - Sift_float	Sift - Sift_float	2	2	4	1	10	6	3	4	10	50000000	5000000	1000000	60
WA288084	Sift - Sift_float	normal	200	500	50	Sift - Sift_float	Sift - Sift_float	2	2	4	1	10	6	3	4	10	50000000	5000000	1000000	60
WA291518	Sift - Sift_float	normal	200	500	50	Sift - Sift_float	Sift - Sift_float	2	2	4	1	10	6	3	4	10	50000000	5000000	1000000	60
WA364981	Sift - Sift_float	high	200	500	50	Sift - Sift_float	Sift - Sift_float	2	2	4	1	10	6	3	4	10	Mesh1 - 25000000 Mesh2 - 15000000	Mesh1 - 2500000 Mesh2 - 15000000	Mesh1 - 750000 Mesh2 - 550000	60
WA395671	Sift - Sift_float	high	200	500	50	Sift - Sift_float	Sift - Sift_float	2	2	4	1	10	6	3	4	10	25000000	2500000	500000	60
WA49627	Sift - Sift_float	high	200	500	50	Sift - Sift_float	Sift - Sift_float	2	2	4	1	10	6	3	4	10	50000000	5000000	1000000	60
WA504291	Sift - Sift_float	high	200	500	50	Sift - Sift_float	Sift - Sift_float	2	2	4	1	10	6	3	4	10	Mesh1 - 50000000 Mesh2 - 20000000	Mesh1 - 5000000 Mesh2 - 2000000	Mesh1 - 1000000 Mesh2 - 750000	60
WA504766	Sift - Sift_float	normal	200	500	50	Sift - Sift_float	Sift - Sift_float	2	2	4	1	10	6	3	4	10	50000000	5000000	1000000	60
WA504935	Sift - Sift_float - akaze	normal	200	500	50	Sift - Sift_float - akaze	Sift - Sift_float - akaze	2	2	4	1	10	6	3	4	10	50000000	5000000	1000000	60
WA504936	Sift - Sift_float	high	200	500	50	Sift - Sift_float - akaze	Sift - Sift_float - akaze	2	2	4	1	10	6	3	4	10	50000000	5000000	1000000	60
WA550198	Sift - Sift_float	high	200	500	50	Sift - Sift_float - akaze	Sift - Sift_float - akaze	2	2	4	1	10	6	3	4	10	50000000	5000000	1000000	60
WA550315	Sift - Sift_float	normal	200	500	50	Sift - Sift_float	Sift - Sift_float	2	2	4	1	10	6	3	4	10	50000000	5000000	1000000	60
WA550401	Sift - Sift_float	high	200	500	50	Sift - Sift_float	Sift - Sift_float	2	2	4	1	10	6	3	4	10	50000000	5000000	1000000	60
WA550439	Sift - Sift_float	high	200	500	50	Sift - Sift_float	Sift - Sift_float	2	2	4	1	10	6	3	4	10	Mesh1 - 50000000 Mesh2 - 70000000	Mesh1 - 5000000 Mesh2 - 7000000	Mesh1 - 1000000 Mesh2 - 3000000	
WA550447	Sift - Sift_float	normal	200	500	50	Sift - Sift_float	Sift - Sift_float	2	2	4	1	10	6	3	4	10	50000000	5000000	1000000	60
WA550772	Sift - Sift_float	high	200	500	50	Sift - Sift_float	Sift - Sift_float	2	2	4	1	10	6	3	4	10	50000000	5000000	1000000	60
WA571013	Sift - Sift_float	high	200	500	50	Sift - Sift_float	Sift - Sift_float	2	2	4	1	10	6	3	4	10	Mesh1 - 50000000 Mesh2 - 25000000 Mesh3 - 10000000	Mesh1 - 5000000 Mesh2 - 2500000 Mesh3 - 1000000	Mesh1 - 1000000 Mesh2 - 500000 Mesh3 - 200000	60
WA571025	Sift - Sift_float	high	200	500	50	Sift - Sift_float	Sift - Sift_float	2	2	4	1	10	6	3	4	10	20000000	2000000	750000	60
WA571027	Sift - Sift_float	high	200	500	50	Sift - Sift_float	Sift - Sift_float	2	2	4	1	10	6	3	4	10	50000000	5000000	1000000	60
WA571061	Sift - Sift_float	high	200	500	50	Sift - Sift_float	Sift - Sift_float	2	2	4	1	10	6	3	4	10	10000000	1000000	500000	60
WA571100	Sift - Sift_float	high	200	500	50	Sift - Sift_float	Sift - Sift_float	2	2	4	1	10	6	3	4	10	Mesh1 - 10000000 Mesh2 - 50000000	Mesh1 - 1000000 Mesh2 - 5000000	Mesh1 - 500000 Mesh2 - 1000000	60
WA571152	Sift - Sift_float	high	200	500	50	Sift - Sift_float	Sift - Sift_float	2	2	4	1	10	6	3	4	10	50000000	5000000	1000000	60

WA571239	Sift - Sift_float	high	200	500	50	Sift - Sift_float	Sift - Sift_float	2	2	4	1	10	6	3	4	10	Mesh1 - 25000000 Mesh2 - 12000000	Mesh1 - 2500000 Mesh2 - 1200000	Mesh1 - 500000 Mesh2 - 250000	60
WA571248	Sift - Sift_float	high	200	500	50	Sift - Sift_float	Sift - Sift_float	2	2	4	1	10	6	3	4	10	50000000	5000000	1000000	60
WA571276	Sift - Sift_float	high	200	500	50	Sift - Sift_float	Sift - Sift_float	2	2	4	1	10	6	3	4	10	50000000	5000000	1000000	60
WA571289	Sift - Sift_float	high	200	500	50	Sift - Sift_float	Sift - Sift_float	2	2	4	1	10	6	3	4	10	50000000	5000000	1000000	60
WA571303	Sift - Sift_float	high	200	500	50	Sift - Sift_float	Sift - Sift_float	2	2	4	1	10	6	3	4	10	50000000	5000000	1000000	60
WA571310	Sift - Sift_float	high	200	500	50	Sift - Sift_float	Sift - Sift_float	2	2	4	1	10	6	3	4	10	Mesh1 - 500000000 Mesh2 - 100000000	Mesh1 - 50000000 Mesh2 - 10000000	Mesh1 - 1000000 Mesh2 - 5000000	60
WA571341	Sift - Sift_float	high	200	500	50	Sift - Sift_float	Sift - Sift_float	2	2	4	1	10	6	3	4	10	50000000	5000000	1000000	60
WA571356	Sift - Sift_float	high	200	500	50	Sift - Sift_float	Sift - Sift_float	2	2	4	1	10	6	3	4	10	50000000	5000000	1000000	60
WA571432	Sift - Sift_float	high	200	500	50	Sift - Sift_float	Sift - Sift_float	2	2	4	1	10	6	3	4	10	50000000	5000000	1000000	60
WA571465	Sift - Sift_float	high	200	500	50	Sift - Sift_float	Sift - Sift_float	2	2	4	1	15	10	2	3	10	Mesh1 - 50000000 Mesh2 - 10000000	Mesh1 - 5000000 Mesh2 - 1000000	Mesh1 - 1000000 Mesh2 - 500000	60
WA571468	Sift - Sift_float	high	200	500	50	Sift - Sift_float	Sift - Sift_float	2	2	4	1	10	6	3	4	10	50000000	5000000	1000000	60
WA571557	Sift - Sift_float	high	200	500	50	Sift - Sift_float	Sift - Sift_float	2	2	4	1	10	6	3	4	10	50000000	5000000	1000000	60
WA571618	Sift - Sift_float	normal	200	500	50	Sift - Sift_float	Sift - Sift_float	2	2	4	1	10	6	NA	4	10	50000000	5000000	1000000	60
WA571624	Sift - Sift_float	high	200	500	50	Sift - Sift_float	Sift - Sift_float	2	2	4	1	10	6	NA	4	10	50000000	5000000	1000000	60
WA572321	Sift - Sift_float	high	200	500	50	Sift - Sift_float	Sift - Sift_float	2	2	4	1	10	6	3	4	10	50000000	5000000	1000000	60
WA572967	Sift - Sift_float	high	200	500	50	Sift - Sift_float	Sift - Sift_float	2	2	4	1	10	6	3	4	10	50000000	5000000	1000000	60
WA593974	Sift - Sift_float	high	200	500	50	Sift - Sift_float	Sift - Sift_float	2	2	4	1	10	6	3	4	10	50000000	5000000	1000000	60
WA594105	Sift - Sift_float	high	200	500	50	Sift - Sift_float	Sift - Sift_float	2	2	4	1	10	6	3	4	10	50000000	5000000	1000000	60
WA594106	Sift - Sift_float	high	200	500	50	Sift - Sift_float	Sift - Sift_float	2	2	4	1	10	6	3	4	10	50000000	5000000	1000000	60
WA594179	Sift - Sift_float	high	200	500	50	Sift - Sift_float	Sift - Sift_float	2	2	4	1	10	6	3	4	10	50000000	5000000	1000000	60
WA594219	Sift - Sift_float	high	200	500	50	Sift - Sift_float	Sift - Sift_float	2	2	4	1	10	6	3	4	10	Mesh1 - 50000000 Mesh2 - 10000000	Mesh1 - 5000000 Mesh2 - 1000000	Mesh1 - 1000000 Mesh2 - 200000	60
WA594233	Sift - Sift_float	high	200	500	50	Sift - Sift_float	Sift - Sift_float	2	2	4	1	10	6	3	4	10	50000000	5000000	1000000	60
WA594243	Sift - Sift_float	high	200	500	50	Sift - Sift_float	Sift - Sift_float	2	2	4	1	10	6	3	4	10	50000000	5000000	1000000	60
WA594250	Sift - Sift_float	high	200	500	50	Sift - Sift_float	Sift - Sift_float	2	2	4	1	10	6	3	4	10	50000000	5000000	1000000	60
WA594515	Sift - Sift_float	high	200	500	50	Sift - Sift_float	Sift - Sift_float	2	2	4	1	10	6	3	4	10	50000000	5000000	1000000	60
WA594528	Sift - Sift_float	high	200	500	50	Sift - Sift_float	Sift - Sift_float	2	2	4	1	10	Mesh1 - 10 Mesh2 -	Mesh1 - 3 Mesh2 - 2	Mesh1 - 4 Mesh2 - 3	10	Mesh1 - 50000000 Mesh2 - 300000000	Mesh1 - 5000000 Mesh2 - 10000000	Mesh1 - 1000000 Mesh2 - 6000000	60
WA594692	Sift - Sift_float	high	200	500	50	Sift - Sift_float	Sift - Sift_float	2	2	4	1	10	6	3	4	10	Mesh1 - 50000000 Mesh2 - 30000000 Mesh3 - 200000000	Mesh1 - 5000000 Mesh2 - 10000000 Mesh3 - 7000000	Mesh1 - 1000000 Mesh2 - 600000 Mesh3 - 5000000	60
WAA20767	Sift - Sift_float	high	200	500	50	Sift - Sift_float	Sift - Sift_float	2	2	4	1	10	6	3	4	10	50000000	5000000	1000000	60
WAA21536	Sift - Sift_float	high	200	500	50	Sift - Sift_float	Sift - Sift_float	2	2	4	1	10	6	3	4	10	50000000	5000000	1000000	60
WAA49577	Sift - Sift_float	high	200	500	50	Sift - Sift_float	Sift - Sift_float	2	2	4	1	10	6	3	4	10	50000000	5000000	1000000	60

Table S5.3.1. Pairwise PERMANOVA test results for the entire dataset, based on all the PCs from the PCA in Figure 1A (Chapter 5). p-values are shown above the empty diagonal cells, while F-values are shown below the empty diagonal cells. Significant comparisons are marked in bold.

	ChesapeakeBay	**NorthCarolina**	**Offshore**	**DelawareBay**	**MexicoGulf**	**Florida**	**Maryland**	**Georgia**
ChesapeakeBay (N= 14)		1	**0.0028**	1	0.4564	1	1	1
NorthCarolina (N= 16)	0.7968		**0.0028**	1	**0.0028**	1	1	1
Offshore (N= 14)	8.635	10.58		**0.0028**	**0.0028**	**0.0028**	**0.0028**	**0.0028**
DelawareBay (N= 8)	1.274	1.038	6.701		0.098	1	1	1
MexicoGulf (N= 9)	2.456	3.679	14.04	2.813		1	1	1
Florida (N= 5)	1.551	1.782	7.565	1.121	1.064		1	1
Maryland (N= 4)	0.4726	0.9513	6.135	1.327	1.509	1.412		1
Georgia (N= 6)	0.9004	0.8709	7.306	0.8416	1.325	0.4588	0.8096	

Table S5.3.2. ANOVA of shape (Procrustes coordinates) ~ log(Csize)*OTU shape (Procrustes coordinates) ~ log(Csize)*sex, shape (Procrustes coordinates) ~ log(Csize)*OTU+Sex. Significant results are written in bold. The randomized residual permutation procedure used 10 000 permutations.

Definitions of terms used in the table:
***DF**: Degrees of Freedom*
***SS**: Sum of Squares*
The total variation in the dataset, calculated by summing the squared differences between observed values and their respective means.
***MS**: Mean Square*
The average variability, calculated by dividing the Sum of Squares (SS) by the corresponding Degrees of Freedom (DF).
***Rsq (R-squared)**: Proportion of variance explained by the model.*
***F**: F-statistic*
The ratio of explained variance (between-group variance) to unexplained variance (within-group variance or error), used to test the significance of the model.
***Z**: Z-scores*
The score indicates how many standard deviations an element is from the mean.
***P**: P-value*
***ResDF**: Residual Degrees of Freedom*
The number of independent observations remaining after accounting for the degrees of freedom used by the model.
***RSS**: Residual Sum of Squares*
The sum of squared differences between the observed values and the predicted (fitted) values from the model. It quantifies the unexplained variation within the data.

	DF	SS	MS	Rsq	F	Z	P	ResDF	RSS
Hypothesis 1: shape ~ log(Csize) * OTU (N= 76)									
log(Csize)	1	0.003926	0.0039256	0.0324	2.8869	2.6311	**0.005**		
OTU	7	0.027763	0.0039661	0.22913	2.9167	6.3617	**0.001**		
log(Csize):OTU	7	0.007888	0.0011269	0.0651	0.8287	-1.1262	0.878		
Residuals	60	0.081589	0.0013598	0.67337					
Total	75	0.121166							
Anova(Reduced, Full)	7	0.0078882	0.0011269	0.065102	0.8287	-1.1262	0.878	60	0.081589
Hypothesis 2: shape ~ log(Csize) * sex + OTU (N= 49)									
log(Csize)	1	0.00164	0.0016398	0.02482	1.1954	0.63935	0.256		
sex	1	0.001545	0.0015448	0.02339	1.1261	0.5318	0.3		
OTU	6	0.009863	0.0016439	0.14931	1.1984	1.01394	0.164		
log(Csize):sex	1	0.001602	0.0016017	0.02425	1.1676	0.55495	0.29		
log(Csize):OTU	6	0.008541	0.0014234	0.12929	1.0377	0.24255	0.407		
sex:OTU	6	0.008289	0.0013815	0.12548	1.0071	0.09861	0.471		
log(Csize):sex:OTU	5	0.005883	0.0011766	0.08906	0.8577	-0.50303	0.693		
Residuals	22	0.030179	0.0013718	0.45686					
Total	48	0.066056							
Anova(Reduced, Full)	18	0.022686	0.0012603	0.34343	0.9188	-0.5964	0.729	22	0.030179
Hypothesis3:shape ~ log(Csize) * sex (N= 49)									
log(Csize)	1	0.001416	0.0014159	0.02143	1.0365	0.37854	0.342		
sex	1	0.002059	0.002059	0.03117	1.5072	1.33056	0.098		
log(Csize):sex	1	0.001108	0.0011081	0.01677	0.8111	-0.40772	0.662		
Residuals	45	0.061473	0.0013661	0.93062					
Total	48	0.066056							
Anova(Reduced, Full)	1	0.0011081	0.0011081	0.016775	0.8111	-0.40772	0.662	45	0.061473

Table S5.3.3. Pairwise comparisons of the allometric trajectory angles (VC), lengths (DL) and distance (Dist) for hypothesis 1. Significant results are written in bold.

Definitions of terms used in the table Dist:
d = Pairwise distances between means
UCL (95%) = Pairwise Upper Confidence Limits between means
Z = Pairwise effect sizes between means
Pr>d = Pairwise P-values between means
Definitions of terms used in the table VC:
r = Pairwise vector correlations between mean vectors
angle = Pairwise angles between mean vectors
UCL (95%) = Pairwise Upper Confidence Limits for angles between mean vectors
Z = Pairwise effect sizes for angles between mean vectors
Pr>d = Pairwise P-values for angles between mean vectors
Definitions of terms used in the table DL:
d = Pairwise absolute difference between mean vector lengths
UCL (95%) = Pairwise Upper Confidence Limits between mean vector lengths
Z = Pairwise effect sizes between mean vector lengths
Pr>d = Pairwise P-values between mean vector lengths

	Dist				**VC**					**DL**			
	d	UCL (95%)	Z	Pr > d	r	angle	UCL (95%)	Z	Pr > angle	d	UCL (95%)	Z	Pr > d
Chesapeake:DelawareBay	0.02078	0.03453	-1.18606	0.87900	0.9998	0.0208	0.0345	-1.1859	0.8790	0.000005	0.000165	-1.698603	0.946
Chesapeake:Florida	0.02338	0.03977	-2.09217	0.98200	0.9997	0.0234	0.0398	-2.0918	0.9820	0.000074	0.000327	-1.363018	0.91
Chesapeake:Georgia	0.02050	0.03393	-1.48002	0.92700	0.9998	0.0205	0.0339	-1.4798	0.9270	0.000035	0.000191	-0.881809	0.794
Chesapeake:Maryland	0.01781	0.03244	-3.13390	1.00000	0.9998	0.0178	0.0324	-3.1334	1.0000	0.000078	0.000390	-1.304998	0.914
Chesapeake:MexicoGulf	0.02620	0.03680	-0.96496	0.83700	0.9997	0.0262	0.0368	-0.9648	0.8370	0.000174	0.000338	-0.442136	0.679
Chesapeake:NorthCarolina	0.01432	0.02386	-1.76373	0.96200	0.9999	0.0143	0.0239	-1.7636	0.9620	0.000046	0.000126	0.131816	0.471
Chesapeake:Offshore	0.03987	0.04703	-0.54906	0.70500	0.9992	0.0399	0.0470	-0.5490	0.7050	0.000465	0.000570	0.188801	0.427
DelawareBay:Florida	0.01839	0.03456	-3.30116	1.00000	0.9998	0.0184	0.0345	-3.3007	1.0000	0.000069	0.000291	-0.801200	0.805
DelawareBay:Georgia	0.01850	0.03255	-2.72062	0.99500	0.9998	0.0185	0.0325	-2.7204	0.9950	0.000029	0.000163	-0.593186	0.715
DelawareBay:Maryland	0.02232	0.04130	-2.24029	0.99000	0.9998	0.0223	0.0413	-2.2399	0.9900	0.000073	0.000336	-0.812554	0.803
DelawareBay:MexicoGulf	0.02483	0.03749	-1.66947	0.95400	0.9997	0.0248	0.0375	-1.6692	0.9540	0.000169	0.000305	0.120754	0.452
DelawareBay:NorthCarolina	0.01485	0.02938	-3.03363	1.00000	0.9999	0.0148	0.0294	-3.0335	1.0000	0.000051	0.000204	-0.694741	0.775
DelawareBay:Offshore	0.03972	0.04690	-0.50042	0.69400	0.9992	0.0397	0.0469	-0.5002	0.6940	0.000460	0.000537	0.656500	0.246
Florida:Georgia	0.01396	0.03235	-6.39631	1.00000	0.9999	0.0140	0.0323	-6.3957	1.0000	0.000040	0.000265	-0.896913	0.805
Florida:Maryland	0.02387	0.04471	-2.89070	1.00000	0.9997	0.0239	0.0447	-2.8901	1.0000	0.000004	0.000235	-1.973221	0.97
Florida:MexicoGulf	0.02027	0.03491	-3.17494	1.00000	0.9998	0.0203	0.0349	-3.1743	1.0000	0.000100	0.000205	0.428262	0.348
Florida:NorthCarolina	0.01913	0.03495	-3.24793	0.99900	0.9998	0.0191	0.0349	-3.2477	0.9990	0.000120	0.000369	-1.552428	0.947
Florida:Offshore	0.04644	0.05529	-0.90572	0.82200	0.9989	0.0464	0.0553	-0.9053	0.8220	0.000390	0.000413	1.305841	0.089
Georgia:Maryland	0.02100	0.03833	-2.73695	0.99700	0.9998	0.0210	0.0383	-2.7365	0.9970	0.000043	0.000301	-0.896909	0.802
Georgia:MexicoGulf	0.02087	0.03407	-2.14577	0.98700	0.9998	0.0209	0.0341	-2.1455	0.9870	0.000139	0.000275	0.187551	0.449
Georgia:NorthCarolina	0.01638	0.02961	-2.67488	0.99900	0.9999	0.0164	0.0296	-2.6748	0.9990	0.000080	0.000224	-0.754067	0.789
Georgia:Offshore	0.04483	0.05259	-0.54940	0.68500	0.9990	0.0448	0.0526	-0.5491	0.6850	0.000430	0.000496	0.731694	0.231
Maryland:MexicoGulf	0.02533	0.04090	-2.06086	0.98000	0.9997	0.0253	0.0409	-2.0603	0.9800	0.000096	0.000231	0.346525	0.38
Maryland:NorthCarolina	0.01810	0.03430	-2.98483	0.99800	0.9998	0.0181	0.0343	-2.9847	0.9980	0.000124	0.000409	-1.537478	0.942
Maryland:Offshore	0.04615	0.05750	-0.94609	0.82500	0.9989	0.0461	0.0575	-0.9458	0.8240	0.000387	0.000411	1.321914	0.089
MexicoGulf:NorthCarolina	0.02497	0.03565	-1.43810	0.92700	0.9997	0.0250	0.0356	-1.4381	0.9270	0.000220	0.000381	-0.450453	0.682
MexicoGulf:Offshore	0.05220	0.05908	-0.51247	0.67400	0.9986	0.0522	0.0591	-0.5122	0.6740	0.000291	0.000378	0.562270	0.288
NorthCarolina:Offshore	0.03783	0.04369	-0.57735	0.71100	0.9993	0.0378	0.0437	-0.5773	0.7120	0.000511	0.000606	0.252524	0.413

Table S5.3.4. Pairwise comparisons of the allometric trajectory angles, lengths and distance for hypothesis 2. Significant results are written in bold and abbreviations are described in Table S5.3.3 legend.

	Dist				VC					DL			
	d	**UCL (95%)**	**Z**	**P Value**	**r**	**angle**	**UCL (95%)**	**Z**	**P Value**	**d**	**UCL (95%)**	**Z**	**P Value**
Chesapeake.Female:DelawareBay.Female	0.032	0.048	-0.581	0.725	1.000	0.032	0.048	-0.581	0.725	0.000	0.001	-0.497	0.708
Chesapeake.Female:Florida.Female	0.048	0.069	0.074	0.447	0.999	0.048	0.069	0.074	0.447	0.001	0.002	0.410	0.322
Chesapeake.Female:Georgia.Female	0.064	0.095	-0.223	0.578	0.998	0.064	0.095	-0.223	0.578	0.002	0.004	-0.135	0.56
Chesapeake.Female:Maryland.Female	0.050	0.070	-0.246	0.593	0.999	0.050	0.070	-0.245	0.593	0.001	0.002	-0.393	0.662
Chesapeake.Female:MexicoGulf.Female	0.059	0.069	0.929	0.178	0.998	0.059	0.068	0.930	0.178	0.001	0.002	0.616	0.271
Chesapeake.Female:NorthCarolina.Female	0.024	0.033	-0.241	0.584	1.000	0.024	0.033	-0.241	0.584	0.000	0.000	-0.299	0.617
Chesapeake.Female:Chesapeake.Male	0.027	0.036	0.260	0.407	1.000	0.027	0.036	0.260	0.407	0.000	0.000	-1.806	0.956
Chesapeake.Female:DelawareBay.Male	0.032	0.049	-0.774	0.781	0.999	0.032	0.049	-0.774	0.781	0.000	0.001	-0.196	0.591
Chesapeake.Female:Florida.Male	0.036	0.045	0.210	0.4	0.999	0.036	0.045	0.210	0.4	0.000	0.000	-0.064	0.546
Chesapeake.Female:Georgia.Male	0.031	0.050	-1.357	0.919	1.000	0.031	0.050	-1.357	0.919	0.000	0.001	-1.663	0.946
Chesapeake.Female:Maryland.Male	0.030	0.045	-0.581	0.724	1.000	0.030	0.045	-0.581	0.724	0.000	0.001	-0.143	0.567
Chesapeake.Female:MexicoGulf.Male	0.077	0.084	1.291	0.094	0.997	0.077	0.084	1.290	0.094	0.003	0.003	1.401	0.076
Chesapeake.Female:NorthCarolina.Male	0.024	0.034	-0.643	0.728	1.000	0.024	0.034	-0.643	0.728	0.000	0.000	-0.483	0.679
DelawareBay.Female:Florida.Female	0.043	0.068	-0.466	0.682	0.999	0.043	0.068	-0.467	0.682	0.001	0.001	0.592	0.275
DelawareBay.Female:Georgia.Female	0.068	0.101	-0.011	0.498	0.998	0.068	0.101	-0.010	0.498	0.002	0.004	-0.024	0.511
DelawareBay.Female:Maryland.Female	0.059	0.081	-0.102	0.528	0.998	0.059	0.081	-0.100	0.528	0.001	0.002	-0.151	0.561
DelawareBay.Female:MexicoGulf.Female	0.053	0.073	0.212	0.437	0.999	0.053	0.073	0.211	0.437	0.001	0.002	0.754	0.201
DelawareBay.Female:NorthCarolina.Female	0.029	0.044	-0.807	0.783	1.000	0.029	0.044	-0.807	0.782	0.000	0.001	-0.714	0.764
DelawareBay.Female:Chesapeake.Male	0.031	0.055	-1.211	0.88	1.000	0.031	0.055	-1.211	0.879	0.000	0.001	-0.276	0.623
DelawareBay.Female:DelawareBay.Male	0.031	0.052	-0.712	0.769	1.000	0.031	0.052	-0.712	0.769	0.000	0.001	-0.505	0.707
DelawareBay.Female:Florida.Male	0.032	0.049	-1.243	0.89	1.000	0.032	0.049	-1.243	0.89	0.000	0.000	-1.947	0.976
DelawareBay.Female:Georgia.Male	0.031	0.060	-2.105	0.985	1.000	0.031	0.060	-2.104	0.985	0.000	0.001	-0.669	0.743
DelawareBay.Female:Maryland.Male	0.031	0.059	-1.830	0.968	1.000	0.031	0.059	-1.830	0.968	0.000	0.000	-1.860	0.96
DelawareBay.Female:MexicoGulf.Male	0.075	0.091	0.864	0.184	0.997	0.075	0.091	0.861	0.184	0.003	0.003	1.470	0.074
DelawareBay.Female:NorthCarolina.Male	0.031	0.051	-1.035	0.844	1.000	0.031	0.051	-1.035	0.844	0.000	0.001	-0.645	0.751
Florida.Female:Georgia.Female	0.076	0.106	0.045	0.477	0.997	0.076	0.106	0.046	0.475	0.001	0.003	-0.294	0.638
Florida.Female:Maryland.Female	0.071	0.093	0.277	0.374	0.998	0.071	0.093	0.278	0.374	0.000	0.002	-1.279	0.894
Florida.Female:MexicoGulf.Female	0.060	0.082	0.156	0.437	0.998	0.060	0.082	0.156	0.437	0.000	0.002	-0.170	0.59
Florida.Female:NorthCarolina.Female	0.050	0.066	0.577	0.289	0.999	0.050	0.066	0.577	0.289	0.001	0.002	0.389	0.346
Florida.Female:Chesapeake.Male	0.046	0.073	-0.385	0.665	0.999	0.046	0.073	-0.386	0.665	0.001	0.002	0.459	0.302
Florida.Female:DelawareBay.Male	0.048	0.071	-0.270	0.613	0.999	0.048	0.071	-0.270	0.615	0.001	0.001	0.522	0.309
Florida.Female:Florida.Male	0.051	0.063	0.713	0.241	0.999	0.051	0.063	0.714	0.241	0.001	0.001	0.464	0.311
Florida.Female:Georgia.Male	0.043	0.077	-0.933	0.826	0.999	0.043	0.077	-0.934	0.827	0.001	0.001	0.854	0.175
Florida.Female:Maryland.Male	0.048	0.076	-0.406	0.648	0.999	0.048	0.075	-0.407	0.648	0.001	0.001	0.472	0.308
Florida.Female:MexicoGulf.Male	0.083	0.096	0.915	0.188	0.997	0.082	0.096	0.913	0.188	0.002	0.003	1.175	0.111
Florida.Female:NorthCarolina.Male	0.046	0.071	-0.146	0.56	0.999	0.046	0.071	-0.147	0.56	0.001	0.002	0.388	0.335
Georgia.Female:Maryland.Female	0.090	0.115	0.465	0.333	0.996	0.089	0.114	0.468	0.333	0.001	0.003	-0.085	0.546
Georgia.Female:MexicoGulf.Female	0.078	0.105	0.132	0.446	0.997	0.078	0.105	0.133	0.446	0.000	0.003	-0.568	0.718
Georgia.Female:NorthCarolina.Female	0.069	0.096	0.247	0.405	0.998	0.069	0.096	0.249	0.404	0.002	0.004	-0.163	0.572
Georgia.Female:Chesapeake.Male	0.061	0.094	-0.430	0.673	0.998	0.061	0.094	-0.430	0.673	0.002	0.004	-0.080	0.54
Georgia.Female:DelawareBay.Male	0.076	0.099	0.507	0.305	0.997	0.076	0.099	0.510	0.304	0.001	0.004	-0.060	0.531

Georgia.Female:Florida.Male	0.069	0.095	0.134	0.466		0.998	0.069	0.095	0.135	0.465		0.002	0.004	-0.118	0.542
Georgia.Female:Georgia.Male	0.057	0.095	-0.846	0.818		0.998	0.057	0.095	-0.848	0.818		0.002	0.004	0.139	0.434
Georgia.Female:Maryland.Male	0.055	0.096	-1.137	0.876		0.998	0.055	0.095	-1.139	0.877		0.002	0.004	-0.116	0.543
Georgia.Female:MexicoGulf.Male	0.109	0.116	1.338	0.095		0.994	0.109	0.116	1.340	0.095		0.001	0.003	0.420	0.322
Georgia.Female:NorthCarolina.Male	0.056	0.095	-0.855	0.808		0.998	0.056	0.094	-0.857	0.81		0.002	0.004	-0.151	0.575
Maryland.Female:MexicoGulf.Female	0.076	0.094	0.534	0.3		0.997	0.076	0.093	0.535	0.3		0.000	0.002	-0.797	0.776
Maryland.Female:NorthCarolina.Female	0.046	0.075	-1.178	0.886		0.999	0.046	0.075	-1.179	0.887		0.001	0.002	-0.457	0.687
Maryland.Female:Chesapeake.Male	0.051	0.075	-0.491	0.674		0.999	0.051	0.075	-0.491	0.674		0.001	0.002	-0.311	0.636
Maryland.Female:DelawareBay.Male	0.055	0.082	-0.689	0.761		0.999	0.055	0.082	-0.689	0.762		0.001	0.002	-0.219	0.604
Maryland.Female:Florida.Male	0.054	0.078	-0.626	0.735		0.999	0.054	0.078	-0.626	0.735		0.001	0.002	-0.324	0.637
Maryland.Female:Georgia.Male	0.059	0.083	-0.205	0.58		0.998	0.059	0.083	-0.204	0.579		0.001	0.002	0.141	0.444
Maryland.Female:Maryland.Male	0.062	0.083	0.199	0.431		0.998	0.062	0.083	0.200	0.431		0.001	0.002	-0.296	0.629
Maryland.Female:MexicoGulf.Male	0.103	0.104	1.586	0.058		0.995	0.103	0.104	1.588	0.058		0.002	0.002	1.343	0.085
Maryland.Female:NorthCarolina.Male	0.056	0.076	-0.044	0.52		0.998	0.056	0.076	-0.043	0.52		0.001	0.002	-0.432	0.667
MexicoGulf.Female:NorthCarolina.Female	0.058	0.069	0.756	0.2		0.998	0.058	0.069	0.757	0.2		0.001	0.002	0.600	0.301
MexicoGulf.Female:Chesapeake.Male	0.051	0.071	0.021	0.489		0.999	0.051	0.071	0.020	0.49		0.001	0.002	0.683	0.248
MexicoGulf.Female:DelawareBay.Male	0.063	0.072	0.923	0.167		0.998	0.062	0.071	0.924	0.167		0.001	0.001	0.668	0.252
MexicoGulf.Female:Florida.Male	0.054	0.068	0.411	0.33		0.999	0.054	0.068	0.411	0.33		0.001	0.002	0.620	0.253
MexicoGulf.Female:Georgia.Male	0.051	0.076	-0.439	0.666		0.999	0.051	0.076	-0.440	0.666		0.001	0.001	0.999	0.121
MexicoGulf.Female:Maryland.Male	0.055	0.075	0.140	0.439		0.998	0.055	0.075	0.139	0.439		0.001	0.002	0.650	0.246
MexicoGulf.Female:MexicoGulf.Male	0.085	0.087	1.506	0.064		0.996	0.085	0.087	1.506	0.063		0.002	0.002	1.109	0.122
MexicoGulf.Female:NorthCarolina.Male	0.053	0.071	0.074	0.492		0.999	0.053	0.071	0.072	0.492		0.001	0.002	0.600	0.289
NorthCarolina.Female:Chesapeake.Male	0.027	0.039	-0.295	0.607		1.000	0.027	0.039	-0.295	0.607		0.000	0.000	-0.775	0.769
NorthCarolina.Female:DelawareBay.Male	0.028	0.048	-1.359	0.908		1.000	0.028	0.048	-1.360	0.908		0.000	0.001	-0.369	0.633
NorthCarolina.Female:Florida.Male	0.026	0.041	-1.655	0.952		1.000	0.026	0.041	-1.655	0.952		0.000	0.001	-0.318	0.628
NorthCarolina.Female:Georgia.Male	0.031	0.051	-1.224	0.899		1.000	0.031	0.051	-1.224	0.899		0.000	0.001	-1.963	0.981
NorthCarolina.Female:Maryland.Male	0.034	0.044	0.196	0.422		0.999	0.034	0.044	0.196	0.422		0.000	0.001	-0.369	0.655
NorthCarolina.Female:MexicoGulf.Male	0.078	0.089	1.184	0.103		0.997	0.078	0.089	1.183	0.103		0.003	0.003	1.388	0.081
NorthCarolina.Female:NorthCarolina.Male	0.027	0.030	1.093	0.148		1.000	0.027	0.030	1.093	0.148		0.000	0.000	-0.510	0.706
Chesapeake.Male:DelawareBay.Male	0.032	0.051	-0.714	0.767		0.999	0.032	0.051	-0.714	0.767		0.000	0.001	0.025	0.506
Chesapeake.Male:Florida.Male	0.034	0.047	-0.134	0.555		0.999	0.034	0.047	-0.134	0.555		0.000	0.000	0.157	0.433
Chesapeake.Male:Georgia.Male	0.023	0.045	-2.913	0.997		1.000	0.023	0.045	-2.913	0.997		0.000	0.001	-1.402	0.921
Chesapeake.Male:Maryland.Male	0.024	0.038	-1.824	0.966		1.000	0.024	0.038	-1.824	0.966		0.000	0.000	0.109	0.459
Chesapeake.Male:MexicoGulf.Male	0.084	0.084	1.658	0.047		0.996	0.084	0.083	1.659	0.047		0.003	0.003	1.433	0.077
Chesapeake.Male:NorthCarolina.Male	0.018	0.032	-2.281	0.989		1.000	0.018	0.032	-2.281	0.989		0.000	0.000	-0.934	0.822
DelawareBay.Male:Florida.Male	0.034	0.051	-0.795	0.781		0.999	0.034	0.051	-0.795	0.781		0.000	0.001	-0.603	0.723
DelawareBay.Male:Georgia.Male	0.035	0.058	-0.913	0.824		0.999	0.035	0.058	-0.912	0.824		0.000	0.001	0.024	0.505
DelawareBay.Male:Maryland.Male	0.037	0.055	-0.341	0.65		0.999	0.037	0.055	-0.341	0.65		0.000	0.001	-0.587	0.722
DelawareBay.Male:MexicoGulf.Male	0.078	0.088	1.100	0.129		0.997	0.077	0.088	1.098	0.13		0.003	0.003	1.405	0.073
DelawareBay.Male:NorthCarolina.Male	0.036	0.048	0.058	0.468		0.999	0.036	0.048	0.058	0.468		0.000	0.001	-0.289	0.622
Florida.Male:Georgia.Male	0.032	0.053	-0.985	0.837		1.000	0.032	0.053	-0.984	0.837		0.000	0.001	-0.533	0.702
Florida.Male:Maryland.Male	0.038	0.051	0.058	0.47		0.999	0.038	0.051	0.058	0.47		0.000	0.000	-2.613	0.996
Florida.Male:MexicoGulf.Male	0.081	0.085	1.494	0.076		0.997	0.080	0.085	1.494	0.076		0.003	0.003	1.414	0.079
Florida.Male:NorthCarolina.Male	0.034	0.043	0.260	0.387		0.999	0.034	0.043	0.261	0.387		0.000	0.000	-0.237	0.614
Georgia.Male:Maryland.Male	0.026	0.048	-2.724	0.997		1.000	0.026	0.048	-2.724	0.997		0.000	0.001	-0.552	0.708
Georgia.Male:MexicoGulf.Male	0.080	0.086	1.298	0.102		0.997	0.080	0.086	1.298	0.102		0.003	0.003	1.605	0.063

Georgia.Male:NorthCarolina.Male	0.022	0.046	-2.779	0.998		1.000	0.022	0.046	-2.778	0.998		0.000	0.001	-1.754	0.967
Maryland.Male:MexicoGulf.Male	0.084	0.087	1.514	0.064		0.996	0.084	0.086	1.515	0.064		0.003	0.003	1.431	0.074
Maryland.Male:NorthCarolina.Male	0.021	0.039	-2.506	0.998		1.000	0.021	0.039	-2.506	0.998		0.000	0.001	-0.279	0.614
MexicoGulf.Male:NorthCarolina.Male	0.083	0.085	1.520	0.067		0.997	0.083	0.085	1.520	0.067		0.003	0.003	1.390	0.079

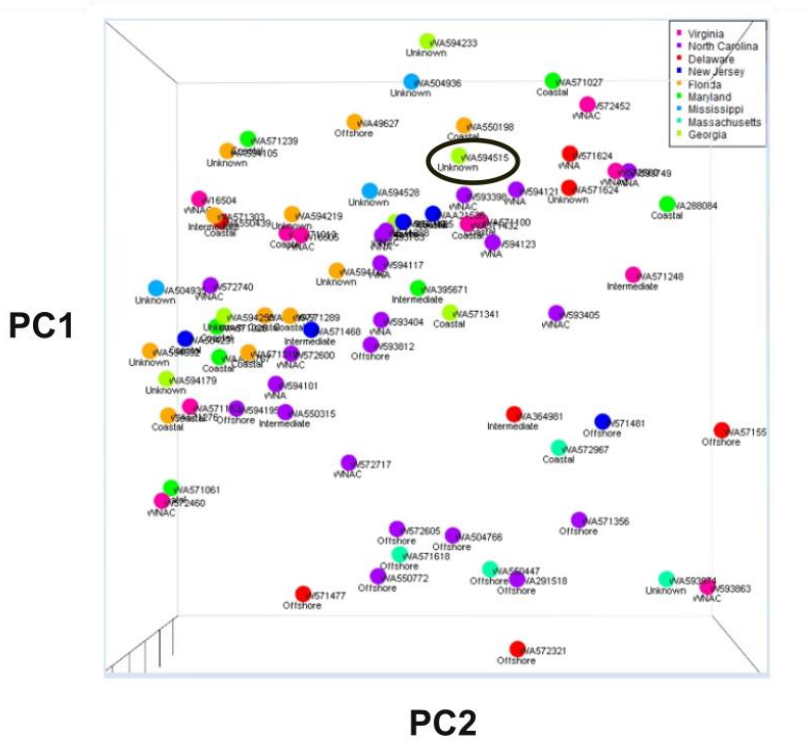

Figure S5.2.1. 3D PCA morphospace from the preliminary analysis with individuals used to set the bilateral symmetry plane circled in black.

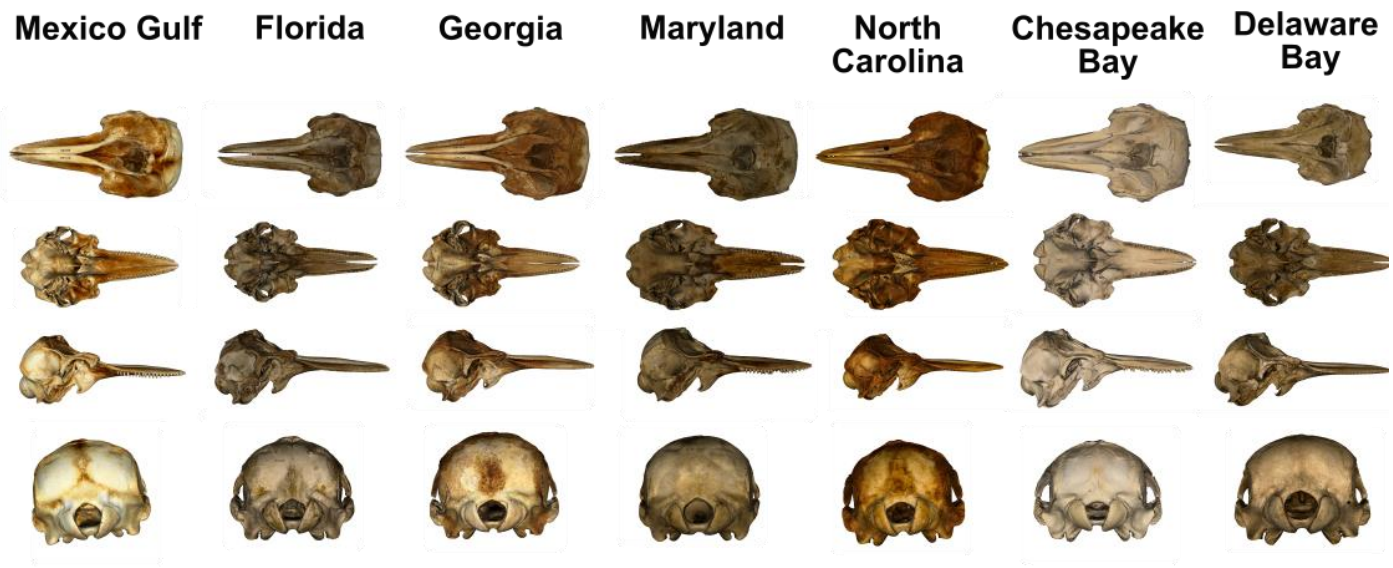

Figure S5.3.1. Visual representations of typical skulls for each WNA population with annotation of specific shape differences.

Bibliography

Amaral, A. R., Coelho, M. M., Marugán-Lobón, J., & James Rohlf, F. (2009). Cranial shape differentiation in three closely related delphinid cetacean species: Insights into evolutionary history. *Zoology*, *112*(1), 38–47.

Conry, D. S., Pistorius, P. A., Plön, S., & Hofmeyr, G. J. G. G. (2016). Sexual dimorphism in striped dolphin (*Stenella coeruleoalba*) crania from South Africa. *Marine Mammal Science*, *32*(4), 1254–1271.

De Araujo Montiero-Filho, E. L., Monteiro, L. R., & Dos Reis, S. F. (2002). Skull shape and size divergence in dolphins of the genus *Sotalia*: A tridimensional morphometric analysis. *Journal of Mammalogy*, *83*(1), 125–134.

De Francesco, M. C., Loy, A., Francesco, M. C. de, & Loy, A. (2016). Intra- and interspecific interactions as proximate determinants of sexual dimorphism and allometric trajectories in the bottlenose dolphin *Tursiops truncatus* (cetacea, odontoceti, delphinidae). *PLoS ONE*, *11*(10), e0164287.

Del Castillo, D. L., Flores, D. A., & Cappozzo, H. L. (2014). Ontogenetic development and sexual dimorphism of franciscana dolphin skull: A 3D geometric morphometric approach. *Journal of Morphology*, *275*(12), 1366–1375.

Del Castillo, D. L., Segura, V., Flores, D. A., & Cappozzo, H. L. (2016). Cranial development and directional asymmetry in Commerson's dolphin, *Cephalorhynchus commersonii commersonii* : 3D geometric morphometric approach. *Journal of Mammalogy*, *97*(5), 1345–1354.

Del Castillo, D. L., Viglino, M., Flores, D. A., & Cappozzo, H. L. (2017). Skull ontogeny and modularity in two species of *Lagenorhynchus*: Morphological and ecological implications. *Journal of Morphology*, *278*(2), 203–214.

Frainer, G., Huggenberger, S., Moreno, I. B., Plön, S., & Galatius, A. (2021). Head adaptation for sound production and feeding strategy in dolphins (Odontoceti: Delphinidae). *Journal of Anatomy*, *238*(5), 1070–1081.

Frandsen, M. S., & Galatius, A. (2013). Sexual dimorphism of Dall's porpoise and harbor porpoise skulls. *Mammalian Biology*, *78*(2), 153–156.

Fung, C. W. (2016). Cranial shape correlates with diet specialization in Northeast Pacific killer whale (*Orcinus Orca*) ecotypes. [Doctoral dissertation, University of British Columbia].

Galatius, A. (2010). Paedomorphosis in two small species of toothed whales (Odontoceti): How and why? *Biological Journal of the Linnean Society*, *99*(2), 278–295.

Galatius, A., Berta, A., Frandsen, M. S., & Goodall, R. N. P. (2011). Interspecific variation of ontogeny and skull shape among porpoises (Phocoenidae). *Journal of Morphology*, *272*(2), 136–148.

Galatius, A., & Gol'din, P. E. (2011). Geographic variation of skeletal ontogeny and skull shape in the harbour porpoise (*Phocoena phocoena*). *Canadian Journal of Zoology*, *89*(9), 869–879.

Galatius, A., & Goodall, R. N. P. (2016). Skull shapes of the Lissodelphininae: Radiation, adaptation and asymmetry. *Journal of Morphology*, *277*(6), 776–785.

Galatius, A., Racicot, R., McGowen, M., & Olsen, M. T. (2020). Evolution and diversification of delphinid skull shapes. *IScience*, *23*(10), 101543.

Gol'din, P. E., & Vishnyakova, K. A. (2015). Differences in skull size of harbour porpoises, *phocoena phocoena* (Cetacea), In the sea of azov and the black sea: Evidence for different morphotypes and populations. *Vestnik Zoologii*, *49*(2), 171–180.

Guidarelli, G., Nicolosi, P., Fusco, G., de Francesco, M. C., & Loy, A. (2014). Morphological variation and modularity in the mandible of three Mediterranean dolphin species. *Italian Journal of Zoology*, *81*(3), 354–367.

Gutstein, C. S., Cozzuol, M. A., Vargas, A. O., Suárez, M. E., Schultz, C. L., & Rubilar-Rogers, D. (2009). Patterns of skull variation of *brachydelphis* (Cetacea, Odontoceti) From the neogene of the southeastern pacific. *Journal of Mammalogy*, *90*(2), 504–519.

Higa, A., Hingst-Zaher, E., & Vivo, M. (2002). Size and shape variability in the skull of *Pontoporia blainvillei* (Cetacea: Pontoporiidae) from the Brazilian coast. *Latin American Journal of Aquatic Mammals*, *1*(1), 145–152.

Hohl, L. S. L., Sicuro, F. L., Wickert, J. C., Moreno, I. B., Rocha-Barbosa, O., & Barreto, A. S. (2020). Skull morphology of bottlenose dolphins from different ocean populations with emphasis on South America. *Journal of Morphology*, *281*(6), 564–577.

Jedensjö, M., Kemper, C., & Krützen, M. (2017). Cranial morphology and taxonomic resolution of some dolphin taxa (Delphinidae) in Australian waters, with a focus on the genus *Tursiops*. *Marine Mammal Science*, *33*(1), 187–205.

Jedensjö, M., Kemper, C. M. M., Milella, M., Willems, E. P. P., & Krützen, M. (2020). Taxonomy and distribution of bottlenose dolphins (genus *Tursiops*) in Australian waters: an osteological clarification. *Canadian Journal of Zoology*, *98*(7), 461–479.

Kurihara, N., & Oda, S. I. (2009). Effects of size on the skull shape of the bottlenose dolphin (*Tursiops truncatus*). *Mammal Study*, *34*(1), 19–32. https://doi.org/10.3106/041.034.0104

Laeta, M., Ruenes, G. F., Siciliano, S., Oliveira, J. A., & Galatius, A. (2021). Variation in cranial asymmetry among the Delphinoidea. *Biological Journal of the Linnean Society*, *132*(2), 414–430.

Loy, A., Tamburelli, A., Carlini, R., & Slice, D. E. (2011). Craniometric variation of some Mediterranean and Atlantic populations of *Stenella coeruleoalba* (Mammalia, Delphinidae): A three-dimensional geometric morphometric analysis. *Marine Mammal Science*, *27*(2), E65–E78.

Marina, T. I., Marchesi, M. C., & Goodall, R. N. P. (2018). Long-finned pilot whale (*Globicephala melas*, Traill 1809) subspecies in the Atlantic Ocean: Are there differences in their skulls? *Marine Mammal Science*, *35*(2), 660–676.

McCurry, M. R., Fitzgerald, E. M. G., Evans, A. R., Adams, J. W., & McHenry, C. R. (2017). Skull shape reflects prey size niche in toothed whales. *Biological Journal of the Linnean Society*, *121*(4), 936–946.

Ngqulana, S. G., Plön, S., Galatius, A., Pistorius, P., & Hofmeyr, G. J. G. (2019). Cranial variation in common dolphins *Delphinus spp*. off South Africa, with the inclusion of information from the holotype of *Delphinus capensis*. *African Journal of Marine Science*, *41*(3), 247–260.

Nicolosi, P., & Loy, A. (2010). Landmark based morphometric variation in Common dolphin (*Delphinus delphis* L.,1758). *Tools for Identifying Biodiversity: Progress and Problems*, 263–268.

Page, C. E., & Cooper, N. (2017). Morphological convergence in “river dolphin” skulls. *PeerJ 5:E4090;*

Parés-Casanova, P. M., & Fabre, L. (2013). Size and shape variability in the skull of the bottlenose dolphin, *Tursiops truncatus* (montagu, 1821). *Journal of Veterinary Medicine Series C: Anatomia Histologia Embryologia*, *42*(5), 379–383.

Sydney, N. V., Machado, F. A., & Hingst-Zaher, E. (2012). Timing of ontogenetic changes of two cranial regions in *Sotalia guianensis* (Delphinidae). *Mammalian Biology*, *77*(6), 397–

Uniwersytet Gdański | 55 LAT

The undersigned, as co-author of the article "Dromby M, Félix F, Haase B, Simões-Lopes PC, Costa APB, Lalis A, Bens C, Podestà M, Doria G, Moura AE (2023) Cranial variation between coastal and offshore bottlenose dolphins, *Tursiops truncatus* (Cetacea: Delphinidae) in Ecuador and the Mediterranean: a three-dimensional geometric morphometric study. Zoological Journal of the Linnean Society, 199:83–96. doi: 10.1093/ZOOLINNEAN/ZLAD022." approve of its use as part of the doctoral thesis entitled "Adaptive skull shape changes in bottlenose dolphins (*Tursiops* spp.): inference from 3D morphological analyses." authored by Morgane Dromby.

I state that I supported this manuscript by providing digital photographs of specimens housed at the Federal University of Santa Catarina (Brazil), provided support with specimen data curation, data analyses and expertise in local ecology, and revision of the final manuscript. The majority of the research work was done by Morgane Dromby, and the co-author declares that this article has not been part of any other doctoral thesis previously presented.

Ana Costa

Documento assinado digitalmente
PAULO CESAR DE AZEVEDO SIMOES LOPES
Data: 17/03/2025 11:02:30-0300
CPF: ***.281.620-**
Verifique as assinaturas em https://v.ufsc.br

Paulo Simões-Lopes

Wydział Biologii
Uniwersytet Gdański

ul. Wita Stwosza 59
80-308 Gdańsk

Uniwersytet Gdański | 55 LAT

The undersigned, as co-author of the article "Dromby M, Félix F, Haase B, Simões-Lopes PC, Costa APB, Lalis A, Bens C, Podestà M, Doria G, Moura AE (2023) Cranial variation between coastal and offshore bottlenose dolphins, *Tursiops truncatus* (Cetacea: Delphinidae) in Ecuador and the Mediterranean: a three-dimensional geometric morphometric study. Zoological Journal of the Linnean Society, 199:83–96. doi: 10.1093/ZOOLINNEAN/ZLAD022." approve of its use as part of the doctoral thesis entitled "Adaptive skull shape changes in bottlenose dolphins (*Tursiops* spp.): inference from 3D morphological analyses." authored by Morgane Dromby.

I state that supported this manuscript by providing access to specimens housed at the Museo Civico di Storia Naturale 'Giacomo Doria' in Genova (Italy), provided support with specimen data curation and expertise, and revision of the final manuscript. The majority of the research work was done by Morgane Dromby, and the co-author declares that this article has not been part of any other doctoral thesis previously presented.

Giuliano Doria

Wydział Biologii
Uniwersytet Gdański

ul. Wita Stwosza 59
80-308 Gdańsk

Uniwersytet Gdański | 55 LAT

The undersigned, as co-author of the article "Dromby M, Félix F, Haase B, Simões-Lopes PC, Costa APB, Lalis A, Bens C, Podestà M, Doria G, Moura AE (2023) Cranial variation between coastal and offshore bottlenose dolphins, *Tursiops truncatus* (Cetacea: Delphinidae) in Ecuador and the Mediterranean: a three-dimensional geometric morphometric study. Zoological Journal of the Linnean Society, 199:83–96. doi: 10.1093/ZOOLINNEAN/ZLAD022." approve of its use as part of the doctoral thesis entitled "Adaptive skull shape changes in bottlenose dolphins (*Tursiops* spp.): inference from 3D morphological analyses." authored by Morgane Dromby.

I state that supported this manuscript by providing access to specimens housed at the Museum of Natural History of Milan (Italy), provided support with specimen data curation and expertise, and revision of the final manuscript. The majority of the research work was done by Morgane Dromby, and the co-author declares that this article has not been part of any other doctoral thesis previously presented.

Michela Podestà

Wydział Biologii
Uniwersytet Gdański

ul. Wita Stwosza 59
80-308 Gdańsk

Uniwersytet Gdański | 55 LAT

The undersigned, as co-author of the article "Dromby M, Félix F, Haase B, Simões-Lopes PC, Costa APB, Lalis A, Bens C, Podestà M, Doria G, Moura AE (2023) Cranial variation between coastal and offshore bottlenose dolphins, *Tursiops truncatus* (Cetacea: Delphinidae) in Ecuador and the Mediterranean: a three-dimensional geometric morphometric study. Zoological Journal of the Linnean Society, 199:83–96. doi: 10.1093/ZOOLINNEAN/ZLAD022." approve of its use as part of the doctoral thesis entitled "Adaptive skull shape changes in bottlenose dolphins (*Tursiops* spp.): inference from 3D morphological analyses." authored by Morgane Dromby.

I state that supported this manuscript by providing acces to specimens housed at the Museum d'Histoire Naturelle in Paris (France), provided support with specimen data curation and expertise, and revision of the final manuscript. The majority of the research work was done by Morgane Dromby, and the co-author declares that this article has not been part of any other doctoral thesis previously presented.

Aude Lalis

Céline Bens

Wydział Biologii
Uniwersytet Gdański

ul. Wita Stwosza 59
80-308 Gdańsk

WYDZIAŁ BIOLOGII

Uniwersytet Gdański | 55 LAT

The undersigned, as co-author of the article "Dromby M, Félix F, Haase B, Simões-Lopes PC, Costa APB, Lalis A, Bens C, Podestà M, Doria G, Moura AE (2023) Cranial variation between coastal and offshore bottlenose dolphins, *Tursiops truncatus* (Cetacea: Delphinidae) in Ecuador and the Mediterranean: a three-dimensional geometric morphometric study. Zoological Journal of the Linnean Society, 199:83–96. doi: 10.1093/ZOOLINNEAN/ZLAD022." approve of its use as part of the doctoral thesis entitled "Adaptive skull shape changes in bottlenose dolphins (*Tursiops* spp.): inference from 3D morphological analyses." authored by Morgane Dromby.

I state that supported this manuscript by providing acces to specimens housed at the Museum d'Histoire Naturelle in Paris (France), provided support with specimen data curation and expertise, and revision of the final manuscript. The majority of the research work was done by Morgane Dromby, and the co-author declares that this article has not been part of any other doctoral thesis previously presented.

Aude Lalis

Céline Bens

Muséum National d'Histoire Naturelle
Direction des Collections
Mammifères et Oiseaux
55, rue Buffon - 75005 PARIS

Wydział Biologii
Uniwersytet Gdański

ul. Wita Stwosza 59
80-308 Gdańsk

Uniwersytet Gdański | 55 LAT

The undersigned, as co-author of the article "Dromby M, Félix F, Haase B, Simões-Lopes PC, Costa APB, Lalis A, Bens C, Podestà M, Doria G, Moura AE (2023) Cranial variation between coastal and offshore bottlenose dolphins, *Tursiops truncatus* (Cetacea: Delphinidae) in Ecuador and the Mediterranean: a three-dimensional geometric morphometric study. Zoological Journal of the Linnean Society, 199:83–96. doi: 10.1093/ZOOLINNEAN/ZLAD022." approve of its use as part of the doctoral thesis entitled "Adaptive skull shape changes in bottlenose dolphins (*Tursiops* spp.): inference from 3D morphological analyses." authored by Morgane Dromby.

I state that supported this manuscript by providing digital photographs of specimens housed at the Museo de Ballenas in Salinas (Ecuador), provided support with specimen data curation and expertise in local ecology, and revision of the final manuscript. The majority of the research work was done by Morgane Dromby, and the co-author declares that this article has not been part of any other doctoral thesis previously presented.

Fernando Félix

Ben Haase

Wydział Biologii
Uniwersytet Gdański

ul. Wita Stwosza 59
80-308 Gdańsk

Uniwersytet Gdański | 55 LAT

The undersigned, as co-author of the article "Dromby M, Félix F, Haase B, Simões-Lopes PC, Costa APB, Lalis A, Bens C, Podestà M, Doria G, Moura AE (2023) Cranial variation between coastal and offshore bottlenose dolphins, *Tursiops truncatus* (Cetacea: Delphinidae) in Ecuador and the Mediterranean: a three-dimensional geometric morphometric study. Zoological Journal of the Linnean Society, 199:83–96. doi: 10.1093/ZOOLINNEAN/ZLAD022." approve of its use as part of the doctoral thesis entitled "Adaptive skull shape changes in bottlenose dolphins (*Tursiops* spp.): inference from 3D morphological analyses." authored by Morgane Dromby.

I state that I was the main supervisor of the thesis, and the principal investigator of the research grant which funded the research. I supported Morgane through my expected duties as supervisor, including support with data collection logistics and protocols, data curation and analyses, interpretation of results and manuscript writing and submission. I certify that the majority of research work was done by Morgane Dromby, and the co-author declares that this article has not been part of any other doctoral thesis previously presented.

Andre Moura

Wydział Biologii
Uniwersytet Gdański

ul. Wita Stwosza 59
80-308 Gdańsk

Appendix

R codes For Chapter 4

Transferring Data from Slicer to R

```
# Load necessary libraries #
library(devtools)
library(SlicerMorphR)
library(rgl)
library(geomorph)
library(readxl)
library(ks)

###############################################
#   Load SlicerMorph Data and Preprocessing  #
###############################################

# Choose the Log File from Slicer
# (Ensure a line break is added at the end of the .log file before loading)
SM.log.file <- file.choose()
SM.log <- parser(SM.log.file, forceLPS = TRUE)

# Extract Landmark Data
Data <- SM.log$LM

# Create geomorph dataframe
datagdf <- geomorph.data.frame(landmarks = Data)

# Perform Procrustes Superimposition - PCoords stand for Procrustes coordinates
Pcoords <- gpagen(datagdf$landmarks)

# Save Procrustes Coordinates
save(Pcoords, file = "Pcoords.bin")

###############################################
#    Semi-Landmark Sliding (SSL vs HL)       #
###############################################

# Extract Semi-Landmarks Data
Data2 <- SM.log$semiLMs

# SSL: Sliding using **bending energy minimization**
```

```
PcoordsBent <- gpagen(A = Data, surfaces = as.numeric(Data2), ProcD = FALSE, print.progress = TR
UE)
save(PcoordsBent, file = "PcoordsBent.bin")


# HL: Sliding using **Procrustes distance minimization**
PcoordsProcDist <- gpagen(A = Data, surfaces = as.numeric(Data2), ProcD = TRUE, print.progress =
TRUE)
save(PcoordsProcDist, file = "PcoordsProcDist.bin")


# Extract and Save Centroid Size (Csize)
write.table(PcoordsBending$Csize, file = "PcoordsList_SSL.tsv", sep = "\t")
write.table(PcoordsProcDist$Csize, file = "PcoordsList_HL.tsv", sep = "\t")


##############################################
#       Merge with Master Dataset            #
##############################################


# Load Pcoords Lists
PcoordsList_SSL <- read.table(file = 'PcoordsList_SSL.tsv', sep = '\t', header = TRUE)
PcoordsList_HL <- read.table(file = 'PcoordsList_HL.tsv', sep = '\t', header = TRUE)


# Load Master Dataset
Masterfile <- read_excel("path/to/YourMasterfile.xlsx")


# Merge Pcoords with Master Dataset
Merge_SSL <- merge(PcoordsList_SSL, Masterfile, by = "LabID", sort = FALSE)
Merge_HL <- merge(PcoordsList_HL, Masterfile, by = "LabID", sort = FALSE)


# Save Merged Tables
write.csv(Table_SSL, file = "TursiopsSpec_SSL.csv", row.names = FALSE)
write.csv(Table_HL, file = "TursiopsSpec_HL.csv", row.names = FALSE)


##############################################
#   Create and Save Final Analysis Dataset   #
##############################################


# SSL Dataset
spec_SSL <- read.csv("TursiopsSpec_SSL.csv", header = TRUE)
tursiopsBent.dt <- list(gpa.sh = PcoordsBent$coords, cs = PcoordsBent$Csize, spec = spec_SSL)
save(tursiopsBent.dt, file = "tursiopsBent.dt.bin")


# HL Dataset
spec_HL <- read.csv("TursiopsSpec_HL.csv", header = TRUE)
```

```
tursiopsProcDist.dt <- list(gpa.sh = PcoordsProcDist$coords, cs = PcoordsProcDist$Csize, spec =
spec_HL)
save(tursiopsProcDist.dt, file = "tursiopsProcDist.dt.bin")


##############################################
#         Symmetry Analysis (SSL vs HL)      #
##############################################

## Define Landmark Pairs for Symmetry Analysis

# SSL: Surface Semi-Landmarks - Replace by your own landmarks
lm.pairs_SSL <- matrix(c(
  1:104, 106:109, 111:190, 192:195, 197, 198, 200:217, 219:236,
  238:287, 290:299, 301, 302, 304:403, 405:434, 436:445, 448:473,
  475, 476, 479:582, 584:621, 624, 625, 627:640, 642:661, 663:760
), ncol = 2, byrow = TRUE)

# HL: Homologous Landmarks - Replace by your own landmarks
lm.pairs_HL <- matrix(c(1:2, 9:28, 31:56, 59:70, 72:73), ncol = 2, byrow = TRUE)

## Perform Symmetry Analysis

# SSL
asym_SSL <- bilat.symmetry(PcoordsBent$coords, ind = dimnames(PcoordsBent$coords)[[3]],
                           object.sym = TRUE, land.pairs = lm.pairs_SSL, iter = 9)
symm.sh_SSL <- asym_SSL$symm.shape

# HL
asym_HL <- bilat.symmetry(PcoordsProcDist$coords, ind = dimnames(PcoordsProcDist$coords)[[3]],
                          object.sym = TRUE, land.pairs = lm.pairs_HL, iter = 9)
symm.sh_HL <- asym_HL$symm.shape

# Save Symmetry Data - sym stands for symmetry
YOURNAME_sym_SSL.dt <- list(gpa.sh = PcoordsBent$coords, cs = PcoordsBent$Csize,
                                    symm.sh = symm.sh_SSL, spec = spec_SSL)
save(YOURNAME_sym_SSL.dt, file = "YOURNAME_sym_SSL.dt.bin")

YOURNAME_sym_HL.dt <- list(gpa.sh = PcoordsProcDist$coords, cs = PcoordsProcDist$Csize,
                                   symm.sh = symm.sh_HL, spec = spec_HL)
save(YOURNAME_sym_HL.dt, file = "YOURNAME_sym_HL.dt.bin")
```

PCA SSL

```
# Load necessary libraries
```

```
library(geomorph)
library(readr)
library(ks)
library(rgl)

# Set working directory (modify as needed)
setwd("INSERT_PATH_HERE")

# Load dataset
load("YourName_sym.dt.bin")

#########################################################################
#                           PCA Analysis                                #
#########################################################################

# Perform Principal Component Analysis (PCA)
YourNamePCA <- gm.prcomp(YourName_sym.dt$symm.sh)

# Access eigenvalues
eigenvalues <- YourNamePCA$sdev^2

# Calculate proportion of variance explained by each principal component
variance_explained <- eigenvalues / sum(eigenvalues)

# Print proportion of variance explained by each principal component
print(variance_explained)

#########################################################################
#                           3D PCA Plot                                 #
#########################################################################

# Define colors based on Units
group_colors <- rainbow(length(unique(YourName_sym.dt$spec$YourGroup)))

# 3D scatter plot of first three PCs
plot3d(
  YourNamePCA$x[, 1:3],
  col = group_colors[as.factor(YourName_sym.dt$spec$YourGroup)],
  size = 20)

# Add legend
legend3d(
```

```
  "topright",
  legend = unique(as.factor(YourName_sym.dt$spec$YourGroup)),
  col = group_colors,
  pch = 10)

#########################################################################
#                          3D Cloud Plot                                #
#########################################################################

# Extract PCA scores
Score <- YourNamePCA$x[, 1:3]
Labels <- factor(x = YourNamePCA$YourGroup)

# Kernel density estimation for group classification
Hscv1.Bd <- Hkda(
  x = YourNamePCA$x[, 1:3],
  x.group = as.factor(YourName_sym.dt$spec$YourGroup),
  bw = "scv",
  pre = "sphere")

# Perform kernel discriminant analysis
Tt.kda3.Bd <- kda(
  x = YourNamePCA$x[, 1:3],
  x.group = as.factor(YourName_sym.dt$spec$YourGroup),
  Hs = Hscv1.Bd)

# Plot 3D Cloud
plot(
  Tt.kda3.Bd,
  colors = c("YourColou1","YourColou2","YourColou3","etc.."),
  drawpoints = TRUE,
  col.pt = c("YourColou1","YourColou2","YourColou3","etc.."),
  box = FALSE,
  display = "rgl")

#########################################################################
#                          PCA Lollipop Graphs                          #
#########################################################################

PC1 <- plotRefToTarget(
  YourNamePCA$shapes$shapes.comp1$min,
  YourNamePCA$shapes$shapes.comp1$max,
```

```
  method = "vector",
  mag = 1,
  gridPars = gridPar(pt.size = 0.25, pt.bg = "red"))

PC2 <- plotRefToTarget(
  YourNamePCA$shapes$shapes.comp2$min,
  YourNamePCA$shapes$shapes.comp2$max,
  method = "vector",
  mag = 1,
  gridPars = gridPar(pt.size = 0.25, pt.bg = "blue"))

PC3 <- plotRefToTarget(
  YourNamePCA$shapes$shapes.comp3$min,
  YourNamePCA$shapes$shapes.comp3$max,
  method = "vector",
  mag = 1,
  gridPars = gridPar(pt.size = 0.25, pt.bg = "green"))

#####################################################################
#                        PERMANOVA Analysis (PAST)                  #
#####################################################################

# Export PCA Scores for further analysis
write.table(YourNamePCA$x, file = "FileName1.tsv", sep = "\t")
```

PCA HL

```
# Load necessary libraries
library(geomorph)
library(readr)
library(readxl)
library(rgl)
library(ks)

#####################################################################
#             PCA on Symmetric Shape Component                      #
#####################################################################

# Perform PCA on symmetry-aligned data
YourNamePCA <- gm.prcomp(YourName_sym.dt$symm.sh)

# Define colors for visualization - Replace x by number of groups in categorical variable
cols <- rainbow(x)
```

```
# 3D scatter plot of PCA results
plot3d(
  YourNamePCA$x[, 1:3],
  col = cols[as.factor(YourName_sym.dt$spec$YourGroup)],
  size = 15)

# Add legend
legend3d(
  "topright",
  legend = unique(as.factor(YourName_sym.dt$spec$YourGroup)),
  col = unique(cols[as.factor(YourName_sym.dt$spec$YourGroup)]),
  pch = 10)

# Add text labels
text3d(YourNamePCA$x[, 1:3], texts = YourName_sym.dt$spec$YourGroup, pos = 1, cex = 0.6)

######################################################################
#                 Kernel Discriminant Analysis (KDA)                 #
######################################################################

# Perform PCA again for KDA analysis
YourNamePCA <- gm.prcomp(YourName_sym.dt$symm.sh)

# Extract PCA scores
Score <- YourNamePCA$x[, 1:3]
Labels <- factor(x = YourNamePCA$YOURGROUP)

# Kernel density estimation for classification
Hscv1.ProcD <- Hkda(
  x = YourNamePCA$x[, 1:3],
  x.group = as.factor(YOURNAME_sym.dt$spec$YOURGROUP),
  bw = "scv",
  pre = "sphere")

# Perform kernel discriminant analysis
Tt.kda3.ProcD <- kda(
  x = YourNamePCA$x[, 1:3],
  x.group = as.factor(YOURNAME_sym.dt$spec$YOURGROUP),
  Hs = Hscv1.ProcD)

# Plot 3D classification results
plot(
```

```
  Tt.kda3.ProcD,
  colors = c("YourColou1","YourColou2","YourColou3","etc"),
  drawpoints = TRUE,
  col.pt = c("YourColou1","YourColou2","YourColou3","etc"),
  box = FALSE,
  display = "rgl")

# Add text labels to classification plot
text3d(YourNamePCA$x[, 1:3], texts = YourName_sym.dt$spec$YourGroup, pos = 1, cex = 0.5)
```

Random Forest SSL

```
# Load required libraries
library(randomForest)
library(caret)
library(caTools)
library(ggplot2)

# Set working directory
setwd("INSERT_PATH_HERE")

##############################################
#              Data Preparation              #
##############################################

# Load training dataset

data<- read.csv("TrainingData.csv", sep=",", header= TRUE)

# Turn your categorical variable into factor (e.g., ecotype).
data<- transform(data,ecotype=as.factor(ecotype))
train= data

##############################################
#              Train the RF model            #
##############################################

# replace x by best mtry for your data - Replace xxxxx by the best ntree for your data
Model_Tunned <- randomForest(ecotype ~ ., data = train, mtry =x , importance=TRUE, ntree = xxxxx
, tuneLength = 5, metric = "ROC", trControl = ctrl,strata = data$ecotype)

# Display variable importance
importance(Model_Tunned)
varImpPlot(Model_Tunned)
```

```
##############################################
#              Test the RF Model             #
##############################################

# Load test dataset
dataTest<- read.csv("TestingData.csv", sep=",", header= TRUE)

# Make predictions
pred = predict(Model_Tunned, newdata=dataTest)

# Calculate accuracy
sum(pred==dataTest$ecotype) / nrow(dataTest)

# Create Confusion Matrix
cm = table(dataTest[,x], pred) # x correspond to the column where the ecotypes are.
conf_matrix_df <- confusionMatrix(cm, positive = NULL,prevalence = NULL)
conf_matrix_df
```

Random Forest HL

```
setwd("INSERT_PATH_HERE")

# Export Data From Slicer
Array <- two.d.array(YourName_sym.dt$symm.sh, sep = ".")
write.xlsx(Array, file="FileName2.xlsx")

# In Exel, open the file and write the "LabID" in the corresponding column

library(randomForest)
require(caTools)
library(caret)
library(ggplot2)

##############################################
#              Data Preparation              #
##############################################

# Prepare Testing DataSet - ProcDSym stands for Procrustes coordinates bent and corrected for as
ymmetry

VariableName <- read_excel("path/to/file.xlsx")
ProcDSym <- read_excel("path/to/FileName2.xlsx")
TestingData <- merge(VariableName, ProcDSym, by = "LabID", all = TRUE)
```

```
write.xlsx(TestingData, file="TestingData.xlsx") # Replace the columns names


# Prepare Training DataSet


VariableName_Training <- read_excel("path/to/file.xlsx")
Merge <- merge(VariableName_Training, ProcDSym, by = "LabID", all = TRUE)
TrainingData <- na.omit(Merge) # Removes the rows with Na values
write.xlsx(TrainingData, file="TrainingData.xlsx")


TrainingData<- transform(TrainingData, YourGroup=as.factor(YourGroup)) # YourGroup as factor
TestingData<- transform(TestingData, YourGroup=as.factor(YourGroup)) # YourGroup as factor


###############################################
#                Train RF Model               #
###############################################


# Replace xxxxx by the best ntree for your data
train= TrainingData
model <- randomForest(YourGroup ~ ., data = train, ntree=xxxxx)


# Find mtry
mtry <- tuneRF(train, train$YourGroup, ntreeTry=xxxxx,stepFactor=1.2,improve=0.01, trace=TRUE, p
lot=TRUE)
best.mtry <- mtry[mtry[, 2] == min(mtry[, 2]), 1]


# Results From Tunned Model - Replace x by best mtry for your model - Replace xxxxx by best ntre
e in your model
Model_Tunned <- randomForest(YourGroup ~ ., data = train, mtry =x , importance=TRUE, ntree = xxx
xx, tuneLength = 5,
                             metric = "ROC", trControl = ctrl, strata = TrainingData$YourGroup)


importance(Model_Tunned)
varImpPlot(Model_Tunned)


###############################################
#               Test RF Model                 #
###############################################


test=TestingData
pred = predict(Model_Tunned, newdata=test)


###############################################
```

```
#       Create the Confusion Matrix          #
##############################################

# Replca x where the columnwith variable is
cm = table(TestingData[,x], pred)
confusionMatrix(cm, positive = NULL,prevalence = NULL)

# Calculate the accuracy of the model
sum(pred==TestingData$YourGroup) / nrow(test)
```

HCA SSL

```
# Load required libraries
library(factoextra)
library(cluster)
library(ggdendro)
library(ggplot2)
library(ape)
library(dendextend)

##############################################
#              Data Preparation              #
##############################################

# Load dataset (Ensure the CSV file is in the working directory)
data<- read.csv("PCoordBentSym.csv", sep=",", header= TRUE)

# Convert Your categorical variable to a factor
data <- transform(data,YourGroup=as.factor(YourGroup))

##############################################
#                Data Scaling                #
##############################################

# Standardize the data
data.scaled <- scale(data)

# Compute Euclidean distance matrix
d <- dist(data.scaled, method = "euclidean")

##############################################
# Optimal Cluster Number Selection
        (Gap Statistic)                      #
##############################################
```

```
gap_stat <- clusGap(scaled_data, FUN = hcut, nstart = 25, K.max = 20, B = 200)

# Visualize the gap statistic
fviz_gap_stat(gap_stat)

# ---------------------------------------
# Hierarchical Clustering
# ---------------------------------------
############################################
#           Hierarchical Clustering        #
############################################

# Compute hierarchical clustering using Ward's method
final_clust <- hclust(d, method = "ward.D2" )

# Cut tree into predefined clusters (replace x with the determined optimal number)
groups <- cutree(final_clust, k=x)

############################################
#            Save Cluster Results          #
############################################

YourGroup<- c(data$YourGroup)
LabID<- c(data$LabID)

# Combine LabID, assigned cluster groups, and original Ecotype
results<-cbind(LabID, CLUSTER, YourGroup)

# Convert into a data Frame
results1<-as.data.frame(results)
colnames(results1)<-c("LabID",'CLUSTER','YourGroup')

# Export results to CSV
write.table(results1, file="PredictedClusters.csv", row.names = FALSE)

############################################
#          Dendrogram Visualization        #
############################################

# Assign labels to the dendrogram
final_clust$labels <- data$YourGroup
```

```
# Create dendrogram plot - Replace x by determines k number
dend_plot<- fviz_dend(final_clust, rect = TRUE, cex = 0.5, k = x,
main = "YourName",
xlab = "YourGroup", ylab = "Distance", sub = "",
ggtheme = theme_minimal(), k_colors = "simpsons",
color_labels_by_k = FALSE, type = "rectangle")

# Display the dendrogram
dend_plot

# Save the dendrogram as an image
ggsave("dendrogram.png", plot = dend_plot)
```

HCA HL

```
# Set working directory (modify as needed)
setwd("INSERT_PATH_HERE")

# Load required libraries
library(factoextra)
library(ggdendro)
library(cluster)
library(ggplot2)
library(ape)
library(dendextend)
library(readxl)

##############################################
#              Data Preparation              #
##############################################

# Load dataset (ensure the file is in the working directory)
data <- read_excel("TestingData.xlsx")

# Convert categorical variable column to a factor
data$YourGroup <- as.factor(data$YourGroup)

##############################################
#                Data Scaling                #
##############################################

# Standardize the data
scaled_data <- scale(data)
```

```
# Compute Euclidean distance matrix
d <- dist(scaled_data, method = "euclidean")

##############################################
# Optimal Cluster Number Selection
        (Gap Statistic)                     #
##############################################

gap_stat <- clusGap(scaled_data, FUN = hcut, nstart = 25, K.max = 20, B = 200)

# Visualize the gap statistic
fviz_gap_stat(gap_stat)

##############################################
#          Hierarchical Clustering           #
##############################################

# Compute hierarchical clustering using Ward's method
final_clust <- hclust(dist(scaled_data, method = "euclidean"), method = "ward.D")

# Cut tree into predefined clusters (replace x with the determined optimal number)
groups <- cutree(final_clust, k = x)

##############################################
#           Save Cluster Results             #
##############################################

# Combine LabID, assigned cluster groups, and original Ecotype
YourGroup<- c(Data$YourGroup)
YourGroup <- as.character(YourGroup)
LabID<- c(Data$LabID)

results<-cbind(LabID, cluster, YourGroup)

# Export results to CSV
write.table(results, file = "PredictedClusters.csv", row.names = FALSE, sep = ",")

##############################################
#        Dendrogram Visualization            #
##############################################
```

```
# Assign labels to the dendrogram
final_clust$labels <- data$YourGroup

# Create dendrogram plot
dend_plot <- fviz_dend( final_clust,
  rect = TRUE, cex = 0.5, k = x,
  main = "YourName",
  xlab = "YourVariable",
  ylab = "Distance",
  ggtheme = theme_minimal(),
  k_colors = "simpsons",
  color_labels_by_k = FALSE, type = "rectangle")

# Display the dendrogram
print(dend_plot)

# Save the dendrogram as an image
ggsave("dendrogram.png", plot = dend_plot)
```

2B-PLS

```
# Set working directory (modify as needed)
setwd("INSERT_PATH_HERE")

# Load required libraries
library(readxl)
library(geomorph)

##############################################
#                  Load Data                 #
##############################################

# Load the shape data (symmetry-adjusted)

load("YourName_sym.dt.bin")
Shape <- YourName_sym.dt$symm.sh

# Load environmental and Polygon data
Polygon <- read_excel("path/to/polygon.xlsx")
Env_Variable <- read_excel("path/to/Environmental_Var.xlsx")

##############################################
#              Data Preparation              #
##############################################
```

```
# Convert environmental variables to numeric
X1 <- Shape
Y1 <- as.data.frame(lapply(Env_Variable, as.numeric))

##############################################
#                Data Scaling                #
##############################################

scaled_Y1 <- scale(Y1)

##############################################
#                PLS Analysis                #
##############################################

PLS1 <-two.b.pls(X1,scaled_Y1,iter=999, seed=NULL, print.progress = TRUE)

# Display summary statistics
summary(PLS1)

# Cumulative variance explained
cumsum(explvar(PLS1))

##############################################
#              PLS Scatter Plot              #
##############################################

# Define color palette
cols <- c("YourColour1", "YourColour2", "YourColour3", "etc")

# Generate PLS plot
P <- plot(PLS1, col = cols[as.factor(YourGroup$YourGroup)], pch = 19, cex = 1.5)

# Add legend
legend("topleft", legend = unique(as.factor(YourGroup$YourGroup)),
       col=c(unique(cols[as.factor(YourGroup$YourGroup)])),
       pt.cex = 2, cex = 1, pch = 19)

##############################################
#           PLS Loadings Barplot             #
##############################################
```

```
# Extract and sort loadings
loadings_X <- PLS1$right.pls.vectors[,1]
sorted_indices <- order(abs(loadings_X), decreasing = TRUE)
sorted_loadings <- loadings_X[sorted_indices]

# Create a sorted environmental variable names vector
sorted_env_variables <- colnames(Env_Variable)[sorted_indices]

# Generate barplot
barplot(sorted_loadings, beside = TRUE,
        main = "YourName",
        xlab = "Shape", ylab = "Environment",
        names.arg = sorted_env_variables,
        col = "magenta", border = "white", space = 0.2, horiz = TRUE, las = 2)
```

RDA

```
# Set working directory (modify as needed)
setwd("INSERT_PATH_HERE")

# Load required libraries
library(vegan)
library(geomorph)
library(readxl)
library(ggvegan)
library(ggplot2)
library(vegan3d)

############################################
#                 Load Data                #
############################################

# Load shape data
load("YourName_sym.dt.bin")
Shape <- YourName_sym.dt$symm.sh

# Convert shape data to a 2D array
ShapesData <- two.d.array(Shape, sep = ".")

# Load environmental and regional data
Polygon <- read_excel("path/to/polygon.xlsx")
Env_Variable <- read_excel("path/to/Environmental_Var.xlsx")

############################################
```

```
#              Data Preparation              #
##############################################

Ecotype <- Ecotype

# Convert environmental variables to numeric - Replace numbers by your column
Env_variable_Numeric <- sapply(Env_Variable[1:17], as.numeric)

##############################################
#                Data Scaling                #
##############################################

Scaled_Env_Variable <- scale(Env_variable_Numeric)

# Convert to dataframe if necessary
if (!is.data.frame(Scaled_Env_Variable)) {
  Scaled_Env_Variable <- as.data.frame(Scaled_Env_Variable)}

##############################################
#                RDA Analysis                #
##############################################

rda_result <- rda(ShapesData ~ ., data = Scaled_Env_Variable)

# Display summary statistics
summary(rda_result)

##############################################
#           Significance Testing             #
##############################################

Anova.RDA.Overall <- anova.cca(rda_result)  # Overall significance
Anova.RDA.terms <- anova.cca(rda_result, by = "terms")  # Individual predictor significance
Anova.RDA.margin <- anova.cca(rda_result, by = "margin")  # Overall contribution of terms
Anova.RDA.onedf <- anova.cca(rda_result, by = "onedf")  # Collective explanatory power
Anova.RDA.axis <- anova.cca(rda_result, by = "axis")  # Axis significance

##############################################
# Variance Explained by Each Environmental Variable #
##############################################

# Define variances - Replace values by your values
```

```
variances <- c(
  SalinityMean = 0.00005464, SalinityRange = 0.00006634, SilicateMean = 0.00008201,
  TemperatureMean = 0.00005589, Aspect = 0.00002771, MLDepthMean = 0.00002539,
  NitrateMean = 0.00000366, PhMean = 0.00001173, Slope = 0.00000604,
  ChlorophyllMean = 0.00002295, DissolvedO2Mean = 0.0000164, DissolvedO2Range = 0.00000993,
  CurrentDirectionMean = 0.00001241, CurrentDirectionRange = 0.00004396,
  CurrentVelocityMean = 0.00000776, BathymetryMean = 0.00001218, TopographicPosition = 0.0000029
7)

# Calculate total variance
total_variance <- sum(variances)

# Calculate percentage of variance explained by each variable
percent_variance <- (variances / total_variance) * 100

# Display the results
percent_variance

##############################################
#               RDA Biplots                  #
##############################################

# Standard 2D biplot
autoplot(rda_result, arrows = TRUE, geom = "text", legend = "none")

# 3D biplot using vegan3d
cols <- c("YourColour1","YourColour2","YourColour3", "etc")

ordirgl(rda_result, display = "site", cex = 0.5, choices = 1:3,
        ax.col = "red", arr.len = 0.05, arr.col = "blue", pch = 16,
        col = cols[as.factor(Ecotype$Ecotype)])

# Alternative 3D plot
ordiplot3d(rda_result, display = "site", choices = 1:3, ax.col = "black",
           arr.len = 0.1, arr.col = "green", col = cols[as.factor(Ecotype$Ecotype)], pch = 20)

##############################################
#       Statistical Tests on Covariates      #
##############################################

# Permutation test for axis significance
permutation_test <- anova.cca(rda_result)
```

```
# Extract p-values for each axis
axis_pvalues <- permutation_test$CCA$pvals

# Permutation test for individual variable significance
variable_pvalues <- anova.cca(rda_result, by = "terms")$CCA$pvals

############################################
# Correlation Between Environmental Variables #
############################################

Correlation <- cor(Env_Variable)

# Save correlation matrix
write.table(Correlation, file = "Env_Variable_Correlation.tsv", sep = "\t")

# Identify variables with high correlation (≥ 0.6)
high_correlation_variables <- which(Correlation >= 0.6 & Correlation < 1, arr.ind = TRUE)

# Display results
print(high_correlation_variables)
```

R codes For Chapter 5

Transferring Data from Slicer to R

```
# Load necessary libraries #
library(devtools)
library(SlicerMorphR)
library(rgl)
library(geomorph)
library(readxl)
library(ks)

#  Set your working directory
setwd("INSERT_PATH_HERE")

############################################
#   Load SlicerMorph Data and Preprocessing  #
############################################

# Choose the Log File from Slicer
# (Ensure a line break is added at the end of the .log file before loading)
```

```
# Choose the SlicerMorph .log file
SM.log.file <- file.choose()
SM.log <- parser(SM.log.file, forceLPS = TRUE)

# Extract Landmark Data
Data <- SM.log$LM

# Create geomorph dataframe
datagdf <- geomorph.data.frame(landmarks = Data)

# Perform Procrustes Superimposition
Pcoords <- gpagen(datagdf$landmarks)

# Save Procrustes Coordinates
save(Pcoords, file = "filename.bin")

##############################################
#          Semi-Landmark Sliding             #
##############################################

# Extract Semi-Landmarks Data
Data2 <- SM.log$semiLMs

# Sliding using **bending energy minimization**
PcoordsSlid <- gpagen(A = Data, surfaces = as.numeric(Data2), ProcD = FALSE, print.progress = TR
UE)
save(PcoordsSlid, file = "filenameSlidLandmarks.bin")

# Extract and Save Centroid Size (Csize)
write.table(PcoordsSlid$Csize, file = "FileName1.tsv", sep = "\t")

##############################################
#       Merge with Master Dataset            #
##############################################

# Load Pcoords Lists
PcoordsList <- read.table(file = 'FileName1.tsv', sep = '\t', header = TRUE)

# Load Master Dataset
Masterfile <- read_excel("path/to/YourMasterfile.xlsx")
```

```
# Merge Pcoords with Master Dataset
Table_SSL <- merge(PcoordsList, Masterfile, by = "LabID", sort = FALSE)

# Save Merged Tables
write.csv(Table_SSL, file = "FileName2.csv", row.names = FALSE)

##############################################
#   Create and Save Final Analysis Dataset   #
##############################################

# SSL Dataset
spec <- read.csv("FileName2.csv", header = TRUE)
YourName.dt <- list(gpa.sh = PcoordsSlid$coords, cs = PcoordsSlid$Csize, spec = spec)
save(YourName.dt, file = "filename.dt.bin")

##############################################
#            Symmetry Analysis               #
##############################################

## Define Landmark Pairs for Symmetry Analysis - Replace by your own paired landmarks
lm.pairs <- matrix(c(1, 2, 4, 5, 8, 9, 11:20, 22:85, 87:128, 130:177, 179, 180, 182, 183, 185, 1
86, 188:301, 304:399, 401:412, 414:427, 429:446, 448:461, 465:600, 602:625, 627:652, 656:665, 66
7:694, 696:701), ncol = 2, byrow = T)

## Perform Symmetry Analysis
asym <- bilat.symmetry(PcoordsSlid$coords, ind = dimnames(PcoordsSlid$coords)[[3]],
                           object.sym = TRUE, land.pairs = lm.pairs, iter = 9)
symm.sh <- asym$symm.shape

# Save Symmetry Data
YourNewName.dt <- list(gpa.sh = PcoordsSlid$coords, cs = PcoordsSlid$Csize,
                                    symm.sh = symm.sh, spec = spec)
save(YourNewName.dt, file = "YourNewfilename.dt.bin")
```

PCA

```
# Load necessary libraries
library(geomorph)
library(readr)
library(ks)
library(rgl)

# Set working directory (modify as needed)
setwd("INSERT_PATH_HERE")
```

```
# Load dataset
load("YourNewfilename.dt.bin")

######################################################################
#                          PCA Analysis                              #
######################################################################

# Perform Principal Component Analysis (PCA)
YourNamePCA <- gm.prcomp(YourNewfileName.dt$symm.sh)

# Access eigenvalues
eigenvalues <- YourNamePCA$sdev^2

# Calculate proportion of variance explained by each principal component
variance_explained <- eigenvalues / sum(eigenvalues)

# Print proportion of variance explained by each principal component
print(variance_explained)

######################################################################
#                          3D PCA Plot                               #
######################################################################

# Plot - Replace x by your number of groups in the categorical variable
cols <- rainbow(x)
plot3d(YourNamePCA$x[,1:3], col = cols[as.factor(YourNewfileName.dt$spec$YourGroup)], size = 20)

# Add legend
legend3d("topright", legend = unique(as.factor(YourNewfileName.dt$spec$YourGroup)), col=c(unique
(cols[as.factor(YourNewfileName.dt$spec$YourGroup)])), pch = 10)
# Add text
text3d(YourNamePCA$x[,1:3], texts = YourNewfileName.dt$spec$LabID, pos = 1, cex = 0.8)

######################################################################
#                        3D Cloud Plot                               #
######################################################################

# Extract PCA scores
Score <- YourNamePCA$x[,1:3]
Labels <- factor(x=YourNamePCA$YourGroup)

# Kernel density estimation for group classification
```

```
Hscv1.Bd <- Hkda(x = YourNamePCA$x[,1:3], x.group = as.factor(YourNewfileName.dt$spec$YourGroup)
, bw = "scv", pre = "sphere")


# Perform kernel discriminant analysis

Tt.kda3.Bd <- kda(x = YourNamePCA$x[,1:3], x.group = as.factor(YourNewfileName.dt$spec$YourGroup
), Hs = Hscv1.Bd)


# Plot 3D Cloud

plot(Tt.kda3.Bd, colors = c("YourColour","YourColour","YourColour", "etc"), drawpoints=TRUE, col
.pt=c("YourColour","YourColour","YourColour", "etc"), box=FALSE, display="rgl")


# Add text

text3d(YourNamePCA$x[,1:3], texts = YourNewfileName.dt$spec$LabID, pos = 1, cex = 0.8)


# Perform PERMANOVA IN PAST

# Export the Pc Scores #

write.table(YourNamePCA$x, file="FileName3.tsv", sep="\t") # tsv because of space


######################################################################

#                           Plot 3D Coastal Only                     #

######################################################################


# Filter out group of specimens (e.g., filter out offshore)

# Identify indices for specimens we want to keep

Indice <- YourNewfileName.dt$spec$YourGroup != "offshore"


# Subset the dataset based on offshore specimens

YourNewfileName.dt$symm.sh <- YourNewfileName.dt$symm.sh[, , Indice, drop = FALSE]

YourNewfileName.dt$cs <- YourNewfileName.dt$cs[Indice, drop = FALSE]

YourNewfileName.dt$spec <- YourNewfileName.dt$spec[Indice, ]


# Create Geomorph Data Frame (GDF) without offshore specimens

gdfNoOffshore <- geomorph.data.frame(

  shape = YourNewfileName.dt$symm.sh,

  ecotype = YourNewfileName.dt$spec$YourGroup,

  ind = YourNewfileName.dt$spec$LabID,

  Csize = YourNewfileName.dt$cs)


# Perform PCA

YourNamePCA <- gm.prcomp(YourNewfileName.dt$symm.sh)


######################################################################

#                           3D PCA Plot                              #
```

```
######################################################################


# Replace x by your number of group in the categorical variable

cols <- rainbow(x)

plot3d(YourNamePCA$x[,1:3], col = cols[as.factor(YourNewfileName.dt$spec$YourGroup)], size = 20)


# Add a legend

legend3d("topright", legend = unique(as.factor(YourNewfileName.dt$spec$YourGroup)), col=c(unique
(cols[as.factor(YourNewfileName.dt$spec$YourGroup)])), pch = 10)


# Add text

text3d(YourNamePCA$x[,1:3], texts = YourNewfileName.dt$spec$LabID, pos = 1, cex = 0.8)


######################################################################
#                          3D Cloud Plot                             #
######################################################################


# Extract PCA scores

Score <- YourNamePCA$x[,1:3]

Labels <- factor(x=YourNamePCA$YourGroup)


# Kernel density estimation for group classification

Hscv1.Bd <- Hkda(x = YourNamePCA$x[,1:3], x.group = as.factor(YourNewfileName.dt$spec$YourGroup)
, bw = "scv", pre = "sphere")


# Perform kernel discriminant analysis

Tt.kda3.Bd <- kda(x = YourNamePCA$x[,1:3], x.group = as.factor(YourNewfileName.dt$spec$YourGroup
), Hs = Hscv1.Bd)


# Plot 3D plot

plot(Tt.kda3.Bd, colors = c("YourColour","YourColour","YourColour", "etc"), drawpoints=TRUE, col
.pt=c("YourColour","YourColour","YourColour", "etc"), box=FALSE, display="rgl")


# Add text

text3d(YourNamePCA$x[,1:3], texts = YourNewfileName.dt$spec$LabID, pos = 1, cex = 0.8)


######################################################################
#              Plot lollipop graphs for PCA components               #
######################################################################


PC1 <- plotRefToTarget(

  YourNamePCA$shapes$shapes.comp1$min,

 YourNamePCA$shapes$shapes.comp1$max,

  method = "vector",
```

```
  mag = 1,
  gridPars = gridPar(pt.size = 0.25, pt.bg = "red"))

PC2 <- plotRefToTarget(
  YourNamePCA$shapes$shapes.comp2$min,
 YourNamePCA$shapes$shapes.comp2$max,
  method = "vector",
  mag = 1,
  gridPars = gridPar(pt.size = 0.25, pt.bg = "blue"))

PC3 <- plotRefToTarget(
  YourNamePCA$shapes$shapes.comp3$min,
  YourNamePCA$shapes$shapes.comp3$max,
  method = "vector",
  mag = 1,
  gridPars = gridPar(pt.size = 0.25, pt.bg = "green"))

######################################################################
#              Export PCA scores for external analysis               #
######################################################################

# Export PCA scores for external analysis
write.table(YourNamePCA$x, file = "FileName4.tsv", sep = "\t")
```

Allometry analysis

```
# Set working directory
setwd("INSERT_PATH_HERE")

# Load necessary libraries
library(geomorph)

# Load data
load("filenameSlidLandmarks.bin")
load("YourNewfilename.dt.bin")

########################################
# HYPOTHESIS 1: ECOLOGICAL ALLOMETRY TEST #
########################################

## Create Geomorph Data Frame (GDF) ##
gdf <- geomorph.data.frame(
  shape = filenameSlidLandmarks$coords,
  YourGroup = filename.dt$spec$YourGroup,
```

```
  ind = filename.dt$spec$LabID,
  Csize = filenameSlidLandmarks$Csize)


# Reduced (Null Hypothesis)
YourName_Reduced <- procD.lm(shape ~ log(Csize) + YourGroup, data = gdf, SS.type = "I", iter = 9
99)
anova(YourName_Reduced)


# Full Model (Alternative Hypothesis)
YourName_Full <- procD.lm(shape ~ log(Csize) * YourGroup, data = gdf, SS.type = "I", iter = 999)
anova(YourName_Full)


# Model Comparison
anova(YourName_Reduced, YourName_Full)


# Pairwise Comparisons
YourName_Pairwise <- pairwise(fit = YourName_Full, fit.null = YourName_Reduced, groups = gdf$You
rGroup)
summary.pairwise(YourName_Pairwise, test.type = "dist", stat.table=TRUE)
summary.pairwise(YourName_Pairwise, test.type = "VC", stat.table=TRUE)
summary.pairwise(YourName_Pairwise, test.type = "DL", stat.table=TRUE)


# Plot Allometry with Prediction Line
# Set colors
color <- c("YourColour","YourColour","YourColour", "etc")
e<-as.factor(gdf$YourGroup)
color <- color[as.numeric(as.factor(e))]


# Plot allometry
plotAllometry(YourName_Full, size = gdf$Csize, logsz = TRUE, method = "PredLine", pch = 16, col
= color, cex=1.5)


# Add legend
legend(x = "bottomright", legend = c("YourGroupName1", "YourGroupName2", "YourGroupName3", "etc"
), cex=0.8, fill=c("YourColour","YourColour","YourColour", "etc"))


##############################################
# HYPOTHESIS 2: SEX AND ECOLOGICAL INTERACTION #
##############################################


## Filter Data for different groups (e.g., Remove Unknown Sex and Offshore groups) ##
Indices <- filenameSlidLandmarks.dt$spec$Sex != "Unknown" & filenameSlidLandmarks.dt$spec$YourGr
oup != "Offshore"
filenameSlidLandmarks.dt$gpa.sh <- filenameSlidLandmarks.dt$gpa.sh[, , indices, drop = FALSE]
```

```
filenameSlidLandmarks.dt$cs <- filenameSlidLandmarks.dt$cs[indices, drop = FALSE]

filtered_spec <- filenameSlidLandmarks.dt$spec[filenameSlidLandmarks.dt$spec$Sex != "Unknown" &
filenameSlidLandmarks.dt$spec$YourGroup != "Offshore", ]

filenameSlidLandmarks.dt$spec <- filtered_spec


gdfCleaned <- geomorph.data.frame(

  shape = filenameSlidLandmarks.dt$gpa.sh,

  sex = filenameSlidLandmarks.dt$spec$Sex,

  YourGroup = filenameSlidLandmarks.dt$spec$YourGroup,

  ind = filenameSlidLandmarks.dt$spec$LabID,

  Csize = filenameSlidLandmarks.dt$cs)


# Reduced Model (Common Allometry)

YourName_Reduced_Interaction <- procD.lm(shape ~ log(Csize) + YourGroup + sex, data = gdfCleaned
, SS.type = "II", iter = 999)

anova(YourName_Reduced_Interaction)


# Full Model (Unique Allometry)

YourName_Full_Interaction <- procD.lm(shape ~ log(Csize) * sex * YourGroup, data = gdfCleaned, S
S.type = "II", iter = 999)

anova(YourName_Full_Interaction)


# Model Comparison

anova(YourName_Reduced_Interaction, YourName_Full_Interaction)


# Pairwise Comparisons

YourName_Pairwise_Interaction <- pairwise(fit = YourName_Full_Interaction, fit.null = YourName_R
educed_Interaction, groups = interaction(gdfCleaned$YourGroup, gdfCleaned$sex))

summary.pairwise(YourName_Pairwise_Interaction, test.type = "dist", stat.table=TRUE)

summary.pairwise(YourName_Pairwise_Interaction, test.type = "VC", stat.table=TRUE)

summary.pairwise(YourName_Pairwise_Interaction, test.type = "DL", stat.table=TRUE)


# Plot Allometry

# Set color

color2 <- c("YourColour","YourColour","YourColour", "etc")

e<-as.factor(gdfCleaned$YourGroup)

color2 <- color2[as.numeric(as.factor(e))]


Pch1 <- c(15, 17)

f <- as.factor(gdfCleaned$sex)

Pch1 <- Pch1[as.numeric(as.factor(f))]


# Plot
```

```
plotAllometry(YourName_Full_Interaction, size = gdfCleaned$Csize, logsz = TRUE, method = "PredLi
ne", pch = Pch1, col = color2, cex=1.5)


# Add legend

legend(x = "bottomright", legend = c("YourGroupName1", "YourGroupName2", "YourGroupName3", "etc"
), cex=0.8, fill=c("YourColour","YourColour","YourColour", "etc"))


###################################

# HYPOTHESIS 3: SEXUAL ALLOMETRY #

###################################


# Reduced Model

YourName_Reduced_Sex <- procD.lm(shape ~ log(Csize) + sex, data = gdfCleaned, SS.type = "I", ite
r = 999)

anova(YourName_Reduced_Sex)


# Full Model

YourName_Full_Sex <- procD.lm(shape ~ log(Csize) * sex, data = gdfCleaned, SS.type = "I", iter =
999)

anova(Allometry.Sex)


# Model Comparison

anova(YourName_Reduced_Sex, YourName_Full_Sex)


# Plot Allometry

color3 <- c("YourColour","YourColour")

e<-as.factor(gdfCleaned$sex)

color3 <- color3[as.numeric(as.factor(e))]


plotAllometry(YourName_Full_Sex, size = gdfCleaned$Csize, logsz = TRUE, method = "PredLine",

              pch = 16, col = color3, cex=1.5)


###############################

# COMBINE ALL PLOTS IN ONE FIGURE

###############################


par(mfrow=c(1, 3)) # 1 row, 3 columns

plotAllometry(YourName_Full, size = gdf$Csize, logsz = TRUE, method = "PredLine", pch = 16, col
= color, cex=3)

plotAllometry(YourName_Full_Interaction, size = gdfCleaned$Csize, logsz = TRUE, method = "PredLi
ne", pch = 16, col = color2, cex=3)

plotAllometry(YourName_Full_Sex, size = gdfCleaned$Csize, logsz = TRUE, method = "PredLine", pch
= 16, col = color3, cex=3)


############ 3D Clouds, with Offshore ##########
```

```
# Load required libraries

library(readr)

library(ks)

library(rgl)


YourName_Full <- procD.lm(shape ~ log(Csize)*YourGroup,

                          data = gdf, SS.type = "I", print.progress = FALSE, iter = 999)


color <- c("YourColour","YourColour","YourColour", "etc")

e<-as.factor(gdf$YourGroup)

color <- color[as.numeric(as.factor(e))]


PlotName <- plotAllometry(YourName_Full, size = gdf$Csize, logsz = TRUE, method = "size.shape",
pch = 16, col = color, cex=1.5)

legend(x = "bottomright", legend = c("YourGroupName1", "YourGroupName2", "YourGroupName3", "etc"
), cex=0.8, fill=c("YourColour","YourColour","YourColour", "etc"))


# Create density clouds for the first 3 PCs of the above PCA plot

Score <- PlotName$size.shape.PCA$x[,1:3]

Labels <- factor(x=filenameSlidLandmarks.dt$spec$YourGroup)


Hscv1.GM2 <- Hkda(x = PlotName$size.shape.PCA$x[,1:3], x.group = as.factor(filenameSlidLandmarks
.dt$spec$YourGroup), bw = "scv", pre = "sphere")

Tt.kda3.GM2 <- kda(x = PlotName$size.shape.PCA$x[,1:3], x.group = as.factor(filenameSlidLandmark
s.dt$spec$YourGroup), Hs = Hscv1.GM2)


plot(Tt.kda3.GM2, colors = c("YourColour","YourColour","YourColour", "etc"), drawpoints=TRUE, co
l.pt=c("YourColour","YourColour","YourColour", "etc"), box=FALSE, display="rgl")


text3d(PlotName$size.shape.PCA$x[,1:3], texts = filenameSlidLandmarks.dt$spec$YourGroup, pos = 1
, cex = 0.5)


############ 3D Clouds, excluding a group (e.g., Plot Coastal Only and remove the group offshore
) ##########


## Filter Data (e.g, Remove Offshore Group) ##


Indice <- filenameSlidLandmarks.dt$spec$YourGroup != "Offshore"

filenameSlidLandmarks.dt$gpa.sh <- filenameSlidLandmarks.dt$gpa.sh[, , Indice, drop = FALSE]

filenameSlidLandmarks.dt$cs <- filenameSlidLandmarks.dt$cs[Indice, drop = FALSE]

filtered_spec <- filenameSlidLandmarks.dt$spec[filenameSlidLandmarks.dt$spec$YourGroup != "Offsh
ore", ]

filenameSlidLandmarks.dt$spec <- filtered_spec
```

```
# Updated gdf

gdfNoOffshore <- geomorph.data.frame(shape = filenameSlidLandmarks.dt$gpa.sh, YourGroup = filena
meSlidLandmarks.dt$spec$YourGroup, ind = filenameSlidLandmarks.dt$spec$LabID, Csize=filenameSlid
Landmarks.dt$cs)


# Allometry

YourName_Full <- procD.lm(shape ~ log(Csize)*YourGroup,

                                          data = gdfNoOffshore, SS.type = "I", print.progress =
FALSE, iter = 999)


# 3D plot #

color4 <- c("YourColour","YourColour","YourColour", "etc")

ee<-as.factor(gdfNoOffshore$YourGroup)

color4 <- color4[as.numeric(as.factor(ee))]


PlotName <- plotAllometry(YourName_Full, size = gdfNoOffshore$Csize, logsz = TRUE, method = "siz
e.shape", pch = 16, col = color4, cex=1.5)

legend(x = "bottomright", legend = c("YourGroupName1", "YourGroupName2", "YourGroupName3", "etc"
), cex=0.8, fill=c("YourColour","YourColour","YourColour", "etc"))


# 3D CLoud plot

Score <- PlotName$size.shape.PCA$x[,1:3]

Labels <- factor(x=dt.pca.bending$YourGroup)


Hscv1.GM <- Hkda(x = PlotName$size.shape.PCA$x[,1:3], x.group = as.factor(filtered_spec$YourGrou
p), bw = "scv", pre = "sphere")

Tt.kda3.GM <- kda(x = PlotName$size.shape.PCA$x[,1:3], x.group = as.factor(filtered_spec$YourGro
up), Hs = Hscv1.GM)


plot(Tt.kda3.GM, colors = c("YourColour","YourColour","YourColour", "etc"), drawpoints=TRUE, col
.pt=c("YourColour","YourColour","YourColour", "etc"), box=FALSE, display="rgl")


text3d(PlotName$size.shape.PCA$x[,1:3], texts = filtered_spec$YourGroup, pos = 1, cex = 0.5)
```